AFCRL 438

Sidney Teweles

GRD RESEARCH NOTES

No. 36

CONTRIBUTIONS TO SATELLITE METEOROLOGY

Volume II

Edited by

Francis R. Valovcin

April 1961

GRD

GEOPHYSICS RESEARCH DIRECTORATE
AF CAMBRIDGE RESEARCH LABORATORIES
OFFICE OF AEROSPACE RESEARCH
UNITED STATES AIR FORCE
BEDFORD, MASSACHUSETTS

earch Notes are published
ı for disseminating, in a
ıpid and informal way,
esearch results obtained
of a broader investigation,
formation pending comple-
ɔr research effort."

116 032

Requ
Depa
gover

Armed
Arling
Arling

Depart
for AS
fied b
or cont

All oth

U. S. D
OFFICE
WASHIN

AFCRL 438

U.S. Air Force. Cambridge Research Center. Geophysics Research Directorate.

GRD Research Notes

No. 36

CONTRIBUTIONS TO SATELLITE METEOROLOGY

VOLUME II

J. A. Leese, F. R. Valovcin, W. K. Widger, Jr.
Geophysics Research Directorate

R. J. Boucher, R. C. Copeland, G. Cooper, C. Dean
A. H. Glaser, R. J. Newcomb, R. B. Smith, R. Wexler
Allied Research Associates, Inc.

J. London, K. Ooyama, H. Viebrock
New York University

R. H. Blackmer, K. L. Coulson, P. M. Furukawa
M. M. Holl, M. G. H. Ligda, F. L. Ludwig, R. E. Nagle
Stanford Research Institute

H. M. Johnson
University of Hawaii

QC
801
.U55
no.36
v.2

Edited by

Francis R. Valovcin

LIBRARY
OCT 11 1961
WEATHER BUREAU

April 1961

LIBRARY
N.O.A.A
U S Dept. of Commerce

Projects 4982 and 6698

Atmospheric Circulations Laboratory
GEOPHYSICS RESEARCH DIRECTORATE
AF CAMBRIDGE RESEARCH LABORATORIES
OFFICE OF AEROSPACE RESEARCH
UNITED STATES AIR FORCE
Bedford, Massachusetts

116 032

National Oceanic and Atmospheric Administration
TIROS Satellites and Satellite Meteorology

ERRATA NOTICE

One or more conditions of the original document may affect the quality of the image, such as:

Discolored pages
Faded or light ink
Binding intrudes into the text

This has been a co-operative project between the NOAA Central Library and the Climate Database Modernization Program, National Climate Data Center (NCDC). To view the original document contact the NOAA Central Library in Silver Spring, MD at (301) 713-2607 x124 or Library.Reference@noaa.gov.

HOV Services
Imaging Contractor
12200 Kiln Court
Beltsville, MD 20704-1387
January 26, 2009

FOREWORD

TIROS I, the first truly meteorological satellite, was an unqualified success in determining the capability of acquiring excellent pictorial data of cloud and weather systems from satellite altitudes.

The utility and future role of such data in the science of meteorology can well be judged by the enthusiasm of those experienced meteorologists who have had the opportunity to participate in this first experiment. The initial reactions and preliminary studies of some of these workers are presented in this Research Note.

This Research Note is a logical extension to GRD Research Note No. 36, "Contributions to Satellite Meteorology", and therefore has the notation of Volume II in the series.

As this document is being written, TIROS II is providing, in addition to pictorial cloud data, what appears to be excellent atmospheric radiation data. It is hoped, and expected, that Volume III of this series will be able to document the success of this equipment with the same enthusiasm afforded the pictorial data.

JAMES C. SADLER
Major, USAF

ABSTRACT

This Second Volume of "Contributions to Satellite Meteorology" contains some preliminary results using photographs from TIROS I and some possible meteorological satellite applications of cloud and radiation data. A detailed abstract will be found at the beginning of each chapter.

Chapter I presents an operational evaluation of TIROS I. It includes a general discussion of scientific results of the TIROS I operational-use program, the role of future TV weather satellites in synoptic meteorology and research and problems that require immediate study so that optimum use can be made of future satellite observations.

Chapter II contains atmospheric radiation studies which have possible satellite applications. These include radiation regimes, development of and experimentation with dynamical-numerical models containing a heating term suitable for use in the study of radiational heating effects, the problem of radiation geometry, and finally, an analysis of theoretical and experimental results on atmospheric transmission and emmission of infrared.

Cloud studies are reported in Chapter III. The first

Section discusses the relationship between composite radarscope pictures and cloud patterns with the objective of identifying regions of precipitation in satellite cloud photographs. Next, the use of satellite data in tropical meteorology is commented on briefly. Finally, a frontal system is followed for a period of nine days in its movement across the Pacific Ocean through the use of cloud photographs from TIROS I.

Chapter IV is concerned with meteorological satellite system analyses. The subjects discussed in this chapter include an analysis of the effect of satellite height on the quantity and quality of optical coverage, satellite data processing and interpretation, and an experiment for studying the optimum interval between satellite meteorological observations.

TABLE OF CONTENTS

		Page
FOREWORD		ii
ABSTRACT		iii
LIST OF ILLUSTRATIONS		xiii
Chapter 1.	TIROS I: AN OPERATIONAL EVALUATION OF A NEW METEOROLOGICAL TOOL	
	ABSTRACT	1
Section 1.	INTRODUCTION	3
Section 2.	SOME SCIENTIFIC RESULTS OF THE TIROS I OPERATIONAL USE PROGRAM	6
2.1	Introduction	6
2.2	Meteorological Information Immediately Available	8
2.3	Additional Meteorological Information Derivable by Inference	67
Section 3.	THE ROLE OF FUTURE TV WEATHER SATELLITES IN SYNOPTIC METEOROLOGY AND RESEARCH	78
3.1	Introduction	78
3.2	The Use of Satellite Data in Global Weather Analysis	79
3.3	The Use of Satellite Data for Operational Problems	88
3.4	The Use of Satellite Data for Geophysical Research	92

			Page
Section 4.		PROBLEMS REQUIRING IMMEDIATE STUDY FOR OPTIMUM USE OF FUTURE SATELLITE OBSERVATIONS	96
	4.1	Introduction	96
	4.2	Optical Properties of the Field of View	98
	4.3	Cloud Identification	110
	4.4	Analysis Techniques	123
	4.5	Data Processing and Presentation	135
	4.6	Application Survey	136
	4.7	Conclusion	138
Chapter II.		ATMOSPHERIC RADIATION STUDIES	
		ABSTRACT	139
Section 1.		SYNOPTIC SCALE RADIATION PROCESSES	141
	1.1	Introduction	141
	1.2	Terrestrial Radiation Regime	144
		1.2.1. General	144
		1.2.2. Upward Flux	145
		1.2.3. Emergent Upward Flux	146
		1.2.4. Downward Flux	146
		1.2.5. Flux Divergence	148
		1.2.6. Effect of Water Vapor	149
		1.2.7. Effect of Ground Surface Temperature	150

		Page
1.3	Solar Radiation Regime	152
1.3.1.	General	152
1.3.2.	Molecular Scattering and Surface Reflection	153
1.3.2.1.	Variation with Wave length	153
1.3.2.2.	Effect of Surface Reflection	154
1.3.2.3.	Significance for Satellite Measurements	155
1.3.3.	Absorption by Ozone	156
1.3.4.	Absorption by Water Vapor	157
1.3.5.	Absorption by Liquid Water and the Effects of Haze	158
1.3.6.	Net Solar Energy Balance for Omaha	158
Section 2.	DYNAMICAL-NUMERICAL EXPERIMENTATION	159
2.1	The Need for Test Integrations	159
2.2	The Dynamical-Numerical Model Selected	161
2.3	Progress to Date	164
2.4	Experiments Planned	169
Section 3.	STUDIES OF ATMOSPHERIC RADIATION AS OBSERVED FROM SATELLITES	171
3.1	Introduction	171
3.2	The Geometrical Problem	172
3.3	The Non-Collimated Flux	179
3.4	Some Simulated Observations	183

		Page
Section 4.	SATELLITE OBSERVATIONS OF INFRARED RADIATION	191
4.1	Introduction	191
4.2	Rotational Water	192
4.2.1.	Temperature Dependence	192
4.2.2.	Maps of Rotational Water for 6 March 1959	196
4.3	Temperature Dependence for 6.3 μ H_2O	198
4.3.1.	Absorption at 50 cm^{-1} Intervals	198
4.3.2.	Temperature Dependence at 50 cm^{-1} Intervals	202
4.3.3.	Temperature Dependence for Entire Band	205
4.4	Temperature Dependence for 15 μ CO_2	206
4.4.1.	General	206
4.4.2.	Theoretical Transmission	206
4.4.3.	Comparison of Theoretical with Empirical Transmissions	207
4.4.4.	Variation of Theoretical Transmission with Temperature	208
4.5	Comparison of Theory with Observation	213
4.5.1.	General	213
4.5.2.	Comparison with Strong's Measurements	214

		Page
4.6	Infrared Maps for 9, 10 and 11 February 1959	218
	4.6.1. General	218
	4.6.2. Maps for 9 February 1959	219
	4.6.3. Maps for 10 February 1959	223
	4.6.4. Maps for 11 February 1959	226
	4.6.5. Characteristic Circulation Patterns	229
4,7	Summary and Conclusion	231
Chapter III.	CLOUD STUDIES	
	ABSTRACT	237
Section 1.	CLOUD SHIELD AND RADAR PRECIPITATION ECHO RELATIONSHIPS WITH SATELLITE APPLICATIONS	239
1.1	Introduction	239
1.2	Data sources	239
	1.2.1. Radarscope Photographs	240
	1.2.2. Cloud Data	240
	1.2.3. Frontal Analyses	241
1.3	Methods of Analyses	246
	1.3.1. Continental Data	246
	1.3.1.1. Radar Composites	246
	1.3.1.2. Cloud Analyses	246

Page

1.3.2. Reconnaissance Flight Oceanic Data 249

1.3.2.1. Radar Strip Composites 249

1.3.2.2. Cloud Analyses 250

1.4 Discussion of a Continental Storm 253

1.4.1. 17-19 November 1957 Storm 253

1.5 Discussion of Airborne Radarscope Storm Study 272

1.5.1. Lark Uniform Flight of 10 December 1959 272

1.5.2. Loon Hotel Flight of 12 December 1959 276

1.5.3. Evolution of Synoptic Situation During the Period from 0000Z, 13 December to 18 December 1959 281

1.5.4. Stork India Flight of 17 December 1959 282

1.6 Conclusions 306

Section 2. USE OF SATELLITE DATA IN TROPICAL METEOROLOGY 312

2.1 Introduction 312

2.2 Cloud Pattern Analysis 314

2.3 Picture and Cloud Pattern Orientation 320

2.4 Data Collection 321

2.4.1. Synoptic Data 321

2.5 Analysis and Use of Satellite Data in Tropical Meteorology 325

		Page
Section 3.	THE LIFE-CYCLE OF A PACIFIC FRONTAL SYSTEM	328
3.1	Introduction	328
3.2	Discussion and TIROS Rectification of a Pacific Frontal System	329
3.3	Conclusion	338
Chapter IV.	METEOROLOGICAL SATELLITE SYSTEM ANALYSES	
	ABSTRACT	349
Section 1.	ORBITAL SAMPLING CHARACTERISTICS	
1.1	The Effect of Satellite Height on Optical Coverage	351
1.1.1.	Introduction	351
1.1.2.	Total Coverage - Grazing Angle Parameter	353
1.1.3.	Total Coverage - Scale Factor Parameter	355
1.1.4.	Specific Coverage	362
1.1.5.	Conclusion	367
Section 2.	DATA PROCESSING AND INTERPRETATION	368
2.1	Photographic Rectifiers for Satellite Applications	369
2.1.1.	Introduction	369
2.1.2.	The Nature of the Coordinate Transformation Equations	370

		Page
	2.1.3. A Possible Electromechanical Photographic Rectifier	374
	2.1.4. Other Applications and Configurations	382
	2.1.5. Summary	383
Section 3.	AN EXPERIMENT FOR STUDYING THE OPTIMUM INTERVAL BETWEEN SATELLITE METEOROLOGICAL OBSERVATIONS	385
3.1	Introduction	385
3.2	Experiment Description	385
APPENDIX A.	ATTITUDE DETERMINATION FROM PICTURE DATA	391
APPENDIX B.	IMMEDIATE OPERATIONAL USE (IOU) PROGRAM OF TIROS I	407
APPENDIX C.	RADARSCOPE PHOTOGRAPHY PROGRAM FOR TIROS I	419
APPENDIX D.	THE PHOTOGRAPHIC AND PHOTOGRAMMETRIC ASPECTS OF TIROS I	441
APPENDIX E.	WHOLE SKY CAMERA PROGRAM OF TIROS I	447
APPENDIX F.	METEOROLOGICAL SUMMARIES OF TIROS I--NORTHERN HEMISPHERE	451
REFERENCES		551

LIST OF ILLUSTRATIONS

Figure No.		Page
Chapter I - 1.	Cyclone over South Indian Ocean 0420Z 30 April 1960 Readout on Orbit (Hereafter R/O) 417.	11
2.	Cyclone over South Indian Ocean 0600Z 30 April 1960 R/O 418.	12
3a.	Occluded cyclone over South Atlantic Ocean 1425Z 30 April 1960 R/O 423.	13
3b.	Example of isentropic analysis.	13
4.	Mature low over Pacific Ocean about 2200Z 4 April 1960 R/O 50.	16
5a.	Sea level analysis 0000Z 5 April 1960.	17
5b.	500 mb analysis 0000Z 5 April 1960.	17
6.	Typhoon over South Pacific Ocean 0300Z 10 April 1960 R/O 128.	19
7.	Facsimile map of typhoon 0300Z 10 April 1960.	20
8.	Vortex north of Caspian Sea 1240Z 16 May 1960 R/O 657.	22
9a.	Sea level analysis 1200Z 16 May 1960.	23
9b.	500 mb analysis 1200Z 16 May 1960.	23
10.	Facsimile map for 1200Z 16 May 1960.	24
11.	Vortex southwest of Bermuda 2200Z 7 May 1960 R/O 529.	26
12.	Facsimile map of vortex 2200Z 7 May 1960.	27

Figure No.		Page
Chapter I - 13a.	Sea level analysis 0000Z 8 May 1960.	28
13b.	500 mb analysis 0000Z 8 May 1960.	28
14.	Vortex southwest of Bermuda 2105Z 8 May 1960 R/O 543.	29
15.	Facsimile map of vortex 2105Z 8 May 1960.	31
16a.	Sea level analysis 0000Z 9 May 1960.	32
16b.	500 mb analysis 0000Z 9 May 1960.	32
17a.	Sea level analysis 2100Z 11 May 1960 with superimposed TIROS nephanalysis.	34
17b.	500 mb analysis 0000Z 12 May 1960 with superimposed TIROS nephanalysis.	34
18.	Vortex over northern Louisiana 2155Z 11 May 1960 R/O 587.	36
19a.	Sea level analysis 0000Z 13 May 1960.	37
19b.	500 mb analysis 0000Z 13 May 1960.	37
20.	Facsimile map of vortex 2245Z 12 May 1960.	38
21.	Vortex over Michigan 2245Z 12 May 1960 R/O 602.	39
22.	Intertropical convergence clouds over Atlantic Ocean 1525Z 9 April 1960 R/O 119.	42
23.	Cloud bands over Indian Ocean 0335Z 23 April 1960 R/O 315.	43
24.	Facsimile map of small scale organization over North Pacific Ocean 2040Z 16 May 1960.	45

Figure No.		Page
Chapter I - 25.	Cloud streets over Pacific Ocean 2040Z 16 May 1960 R/O 659.	47
26.	Transverse waves over Indian Ocean about 0840Z 23 April 1960 R/O 317.	48
27.	Annular cloud near Africa 1740Z 8 May 1960 R/O 543.	51
28.	Facsimile map of annular cloud 1740Z 8 May 1960.	52
29.	Clouds depicting vertical development at sunset over Atlantic Ocean 4 May 1960 R/O 486.	53
30.	Clouds over Alps 1115Z 2 April 1960 R/O 15.	56
31.	Clouds over Alps 1015Z 7 April 1960 R/O 86.	57
32.	Facsimile map of Mediterranean area 1015Z 7 April 1960.	58
33.	Atolls of Tuamotu Archipelago	60
33a.	2225Z 10 May 1960 R/O 573.	60
33b.	Portion of an enlarged to map scale.	60
33c.	Map of atolls visible in photograph.	60
34.	Snow on Himalayas and Karakorums	62
34a.	1705Z 9 May 1960 R/O 552.	62
34b.	Portion of an enlarged to map scale.	62
34c.	Map of terrain visible in photograph.	62
35.	Cloud Pattern over eastern United States about 1700Z 5 April 1960 R/O 61.	65

Figure No.		Page
Chapter I - 36.	Similar pattern to Figure 35 off east coast of United States 1610Z 6 April 1960 R/O 75.	66
37.	Atlas missile photo showing island generated cloud streamers.	69
38.	Sunglint on the open ocean sequence illustrates the relative brightness of ocean, clouds, and sunglint R/O 704.	106
39a.	Sunglint on the ocean just outside San Francisco Bay	107
39b.	Sunglint with the principal reflections from San Francisco Bay R/O 703.	107
40.	Resolution examples a wide angle, b narrow angle R/O 602.	112
41.	Line of presumed cumulonimbus activity over western Australia 0746Z 6 May 1960 R/O 505.	113
42.	Apparent large scale band of cirrus over the Gulf of Aden 1156Z 9 May 1960 R/O 552.	115
43.	Suggested schematic representation of surface cloud observation.	119
Chapter II - 1.	Geometrical Relationships showing the Radiation received by the Satellite Sensor.	174
2.	The intensity in the 900-1000 cm^{-1} spectral interval for different atmospheric models.	188
3.	Temperature correction for rotational water	195
4.	Outgoing radiation in the 250 - 310 cm^{-1} region for 0000Z, 6 March 1959.	199

Figure No.			Page
Chapter II -	5.	Precipitable Water w_o(cm) for a Transmission of 50% in the 6.3μ H_2O Band.	201
	6.	Temperature Correction in 6.3μ H_2O Band.	204
	7.	Theoretical Transmission from 1000 to 100 mb for $T_o = 273^o$, k = 1/6 in 15μ CO_2 Region.	210
	8.	Theoretical Transmissions for 15μ CO_2 Band as a Function of a Weighted Temperature $\overline{T}$.	211
	9.	Theoretical Transmissions as a Function of $\overline{T}$ for 5 cm^{-1} Intervals Centered at the Indicated Wave Number.	212
	10.	Variation of Upward Minus Downward Radiation with Altitude.	215
	11.	Surface Map 1200Z, 9 February 1959.	220
	12.	Window Map 1200 Z, 9 February 1959.	222
	13.	Surface Map 1200Z, 10 February 1959.	224
	14.	Window Map 1200Z, 10 February 1959.	225
	15.	Surface Map 1200Z, 11 February 1959.	227
	16.	Window Map 1200Z, 11 February 1959.	228
Chapter III -	1.	Radar Station Network.	242
	2.	Reconnaissance Flight Tracks and Radar Coverage.	243
	3.	Cloud Data Network.	244
	4.	Cloud Data Network used in Analysis of 17-19 November 1957 Storm.	245

Figure No.		Page
Chapter III - 5.	Schematic Representation of Cloud Shield.	252
6.	Radar Composite, Fronts, and Cloud Distributions for 17 November 1957, 1200Z.	262
7.	Radar Composites, Fronts, and Cloud Distributions for 17 November 1957, 1800Z.	263
8.	Radar Composite, Fronts, and Cloud Distributions for 18 November 1957, 0000Z.	264
9.	Radar Echo Pattern and Fronts for 18 November 1957, 0600Z.	265
10.	Radar Composite, Fronts, and Cloud Distribution for 18 November 1957, 1200Z.	266
11.	Radar Composite, Fronts, and Cloud Distribution for 18 November 1957, 1800Z.	267
12.	Radar Composite, Fronts, and Cloud Distribution for 19 November 1957, 0000Z.	268
13.	Radar Echo Pattern and Fronts for 19 November 1957, 0600Z.	269
14.	Radar Composite, Fronts, and Cloud Distributions for 19 November 1957, 1200Z.	270
15.	Radar Composite, Fronts, and Cloud Distributions for 19 November 1957, 1800Z.	271
16.	Eastern Pacific Surface Chart, 11 December 1959, 0000Z.	286
17.	Radarscope Strip Composite for Lark Uniform Flight of 10 December 1959.	287
18.	Low Cloud Distribution and Type Over Eastern Pacific on 10 December 1959.	288

Figure No.		Page
Chapter III - 19.	Middle Cloud Distribution and Type over Eastern Pacific on 10 December 1959.	289
20.	High Cloud Distribution and Type over Eastern Pacific on 10 December 1959.	290
21.	Total "Top View" Cloud Distribution and Type over Eastern Pacific on 10 December 1959.	291
22.	Eastern Pacific Surface Chart, 13 December 1959, 0000Z.	292
23.	Radarscope Strip Composite for Loon Hotel Flight of 12 December 1959.	293
24.	Low Cloud Distribution and Type over Eastern Pacific on 12 December 1959.	294
25.	Middle Cloud Distribution and Type Over Eastern Pacific on 12 December 1959.	295
26.	High Cloud Distribution and Type over Eastern Pacific on 12 December 1959.	296
27.	Total "Top View" Distribution and Type over Eastern Pacific on 12 December 1959.	297
28.	Eastern Pacific Surface Chart, 15 December 1959, 0000Z.	298
29.	Eastern Pacific Surface Chart, 17 December 1959, 0000Z.	299
30.	Eastern Pacific Surface Chart, 18 December 1959, 0000Z.	300
31.	Radarscope Strip Composite for Stork India Flight of 17 December 1959.	301
32.	Low Cloud Distribution and Type over Eastern Pacific on 17 December 1959.	302

Figure No.		Page
Chapter III - 33.	Middle Cloud Distribution and Type over Eastern Pacific on 17 December 1959.	303
34.	High Cloud Distribution and Type over Eastern Pacific on 17 December 1959.	304
35.	Total "Top View" Cloud Distribution and Type over Eastern Pacific on 17 December 1959.	305
36A.	Surface Analysis 0000Z May 18, 1960.	339
36B.	Orbit 677 0230Z May 18, 1960.	339
37A.	Surface Analysis 0000Z May 19, 1960.	340
37B.	ORBIT 691 0145Z May 19, 1960.	340
38A.	Surface Analysis 0000Z May 20, 1960.	341
38B.	ORBIT 705 0100Z May 20, 1960.	341
39A.	Surface Analysis 0000Z May 21, 1960.	342
39B.	ORBIT 720 0145Z May 21, 1960.	342
40A.	Surface Analysis 0000Z May 22, 1960.	343
40B.	ORBITS 733 and 734 0000Z May 22, 1960.	343
41A.	Surface Analysis 0000Z May 23, 1960.	344
41B.	ORBITS 747 and 748 2300Z May 22, 1960.	344
42A.	Surface Analysis 0000Z May 24, 1960.	345
42B.	ORBITS 762 and 763 0000Z May24, 1960.	345
43A.	Surface Analysis 0000Z May 25, 1960.	346
43B.	ORBITS 775 and 776 2200Z May 24, 1960.	346
44A.	Surface Analysis 0000Z May 26, 1960.	347
44B.	ORBIT 791 2300Z May 25, 1960.	347

Figure No.		Page
Chapter IV - 1.	Geometry Pertinent to Grazing Angle Computations.	354
2.	Radius of Coverage vs. Satellite Height (Grazing Angle as Parameter).	356
3.	Geometry Pertinent to Scale Factor Computation.	357
4.	Scale Factor vs. Distance from Subpoint.	359
5.	Radius of Coverage vs. Satellite Height (Scale Factor as Parameter).	360
6.	Coverage Figure of Merit vs. Satellite Height.	363
7.	Scale Factor vs. Satellite Height.	364
8.	Optimum Scale Factor at Given Distance from Subpoint.	366
9.	The Resolver and its Operation.	376
10.	An Electromechanical Computer for Mapping of the Earth on a Mercator Projection.	379

CHAPTER I

TIROS I: AN OPERATIONAL EVALUATION OF A NEW METEOROLOGICAL TOOL*

ABSTRACT

TIROS I has demonstrated that Meteorology has at its disposal in the television satellite a tool which will be capable of: 1) providing cloud analyses on as small or grand a scale as the meteorological consumer demands, 2) broadening the knowledge of the dynamics of the atmosphere and 3) contributing to improvement in forecasting, both through more observational coverage and through new techniques.

The photographs from TIROS contain a wealth of detailed information, much of it revealing large scale organization never before suspected, as well as possibly new types of systems. The wide angle photographs, or their earth-surface rectifications, occasionally permit recognition of cloud types, often indicate cloud families, sometimes show small scale organization such as cloud streets, and usually demonstrate massive and persistent cloud organization including large frontal bands and cyclonic circulations. The "built-in" similarities and discrepancies between these and conventionally

---

* Originally prepared as a Semi-Annual Technical Summary Report under Contract No. AF19(604)-5581, ARPA Order No. 26-59 and GRD-TN-60-600, 30 June 1960. This Chapter was written by A. H. Glaser, Allied Research Associates, Inc.

conceived isobaric analyses are both notable. A critical review of the operational methods used to retrieve these cloud analyses suggests improvements for future TIROS-type satellites.

While TIROS I provided a vast amount of a new kind of data which encourages investigation into atmospheric processes, it also posed a number of new questions about the nature of the atmosphere, answers to which will be required for the design of more advanced systems and for more effective utilization of the data they provide. The optical properties of clouds and the atmosphere are at best imperfectly known. The features by which clouds and cloud systems may be recognized have not been identified. The significance of cloud manifestations of various scales and types to meteorological analyses and forecasting has yet to be established.

These problems with all the sub-studies they imply, must be at least partially solved before the full potential of TIROS and its successors can be realized.

SECTION 1

INTRODUCTION

TIROS I was launched from Cape Canaveral on 1 April 1960. Its prime function, that of telemetering back to earth pictures of cloud cover in the earth's atmosphere, was carried out with eminent success. It transmitted about 23,000 pictures during its useful life of 78 days. At the two data acquisition stations, Belmar, N. J. and Kaena Point, Hawaii, teams of meteorologists worked with the pictorial information as it came down from the satellite, learning to abstract from the pictures meteorologically significant information that might be used for practical operation purposes, and passing on the information to operational centers.

While this "Immediate Operational Use" (hereafter I. O. U.) program was originally set up as an experiment to evaluate the operational problem posed by later satellites, it quickly became apparent that the TIROS I pictorial material was immediately useful. Instances occurred where conventional weather map analyses were altered when TIROS presented clear evidence

of erroneous interpretation of conventional data. Use was made of TIROS information for missile range control. It is a tribute to the imagination of the operational meteorologist that these and many other utilizations occurred in spite of the fragmentary unscheduled data disseminations that occurred.

The cold objective words called for in an evaluation cannot transmit to the reader the thrill experienced by the meteorologists as they saw the pictures from the first orbits and realized the tremendous impact that the new technology would have on their science and profession. The report can at best give a sketchy resume of the revelations contained in each individual picture of the grand organization of the world's weather as exhibited by the clouds, of the structure of atmospheric systems, and of the meteorological curiosities revealed for the first time. Hopefully the report will present some indication of the types of useful information contained in the TIROS pictures.

As expected, TIROS has posed many more questions that it has answered. In this report we can only begin to explore the avenues of meteorological research which have been

abruptly opened. We do, however, point out a few problems that appear to be capable of at least partial solutions that will readily enhance the utilization of satellite meteorological pictures. These are the problems that we feel must be attacked promptly and effectively to capitalize on this remarkable new source of meteorological information.

A practical consideration lends special urgency to research on these problems. The TIROS experiment is intended to guide the design of later Satellite TV systems for both research and operational applications. Evaluation of the TIROS system performance is in progress, of course, but evaluation of the suitability of the design parameters for the various meteorological applications cannot be complete without these research studies on the information that is contained in the pictures.

Coming as rapidly as it does after the launch of TIROS I, this evaluation must necessarily be somewhat fragmentary and tentative. If it induces in the reader our enthusiasm for this new observational tool and the branch of meteorology that it has so dramatically opened, this evaluation will have served its purpose.

CHAPTER I (Continued)

SECTION 2

SOME SCIENTIFIC RESULTS OF THE TIROS OPERATIONAL USE PROGRAM

2.1 Introduction

With each picture taking sequence, TIROS I depicts in detail the cloud cover of millions of square miles of the earth's surface. The cloud cover displays a broad spectrum of organization ranging from the lower limit of picture resolution (3 to 5 miles) to systems a thousand miles or more in diameter.

This section will concern itself with the meteorological information available from the TIROS pictures, obtainable without recourse to synoptic maps or other conventional meteorological analyses. Furthermore, mostly organized clouds will be discussed, since their meteorological significance is best understood.

Meteorological features recognized have included cyclones in various stages of development, intertropical convergence zones and frontal clouds, cloud streets, small waves, cloud

forms, and, frequently but not regularly, some cloud types or genera.

Prints made from copies of original TIROS negatives are used in the text to illustrate points under discussion. Unfortunately, these prints often show less detail than the positive films used for the I. O. U. analyses. This stems from the necessity of making copies of the original films in such long reels that control of quality could not be adjusted for individual orbits.

The pictures telemetered back to earth were obtained through two separate systems. A narrow angle (40mm) lens was employed in one system, while the other used a wide angle (5.3mm) lens. The I. O. U. program was primarily concerned with pictorial information supplied by the latter, since the area coverage is so much greater. Thus, the following discussions are almost exclusively confined to the wide angle camera data.

Copies of facsimile transmissions of rectified TIROS pictures (TIROS nephanalyses hereafter) originating from the Belmar, N. J. I. O. U. site and portions of conventional meteorological analyses for sea level and 500 mb are presented for comparison with TIROS photographs. The TIROS nephanalyses have been reduced in scale from the originals and are presented with standardized cloud cover symbolism.

The distribution of cloudiness is immediately obvious from the TIROS pictures. Clear, "scattered", "broken" and overcast areas may be readily delineated from a series of frames of an orbit. However, some of these terms, as used by TIROS analysts, especially "scattered" and "broken", have a somewhat different meaning from that conventionally associated with them, because of the vast difference in the scale of view of TIROS and that of a ground observer. Similarly, areas designated as "broken" or "scattered" by a TIROS analyst might be considered more or less cloudy from the ground. On the other hand, thin clouds, hardly noticeable from TIROS pictures, may be reported as broken or overcast by ground observers. The significance of these differences in the use of cloudiness terminology will be reduced as the recipients of the TIROS analyses become familiar with the capabilities of the I. O. U. system.

2.2 Meteorological Information Immediately Available*

2.2.1 Large-Scale Features

2.2.1.1 Cyclones

Cyclonic circulation patterns have been among the

* This Section was written by R. B. Smith and R. C. Copeland, Allied Research Associates, Inc.

most frequent and outstanding large-scale features found in the TIROS photographs. While the cyclones observed do not often display the classical textbook cloud model in their development, patterns have been observed which can be linked to the progressive phases of a cyclonic system such as: the open wave, occluding, and mature or dissipating stages.

2.2.1.2 Open Waves

The first stage of a nascent cyclonic storm is generally referred to by synopticians as an "open wave". This term signifies that the cold front of the disturbance has not yet begun to overtake or "occlude" the warm front. Unfortunately the TIROS photographs identified as illustrative of the cloud distribution accompanying such a system have been taken at high nadir angles and hence are unsuitable for presentation here. Nevertheless an inspection of the positive films so far available and rectifications thereof reveal that at this stage no evidence of a vortex is present. The position of the wave may be revealed merely as a broadening of the frontal cloud band. Also, if the wave is developing and actively producing precipitation, the cloudiness over the most active

central portion may appear most dense and highly reflective. This description however is based on a very small sample and may be subject to future modification.

2.2.1.3 Occluding Cyclones

After examining a relatively large number of TIROS pictures of cyclonic vortices, two facts become apparent: the patterns are amazingly similar regardless of their location over the globe; there is a gradual evolution of vortical pattern which appears to correspond to successive stages of the cyclonic development or degree of frontal occlusion. Obviously it is not possible to determine the precise stage of a storm from a picture of its cloud pattern. However, this pattern does appear to follow a logical development from that of the unpatterned "open wave" to one exhibiting a vortex. A recurrent feature of a stage of these cyclonic vortices is the appearance of a clear sector, usually parallel to the cold front. This clear zone may be located on either side of the front. A cyclone, evidently undergoing occlusion, is shown in Figures 1 and 2, TIROS photographs from successive orbits in the Southern Hemisphere. The characteristic clear "tongue" is evident, as well as the vortex pattern

Fig. 1 CYCLONE OVER SOUTH INDIAN OCEAN 0420Z 30 APRIL 1960 READOUT ON ORBIT (HEREAFTER R/O) 417.

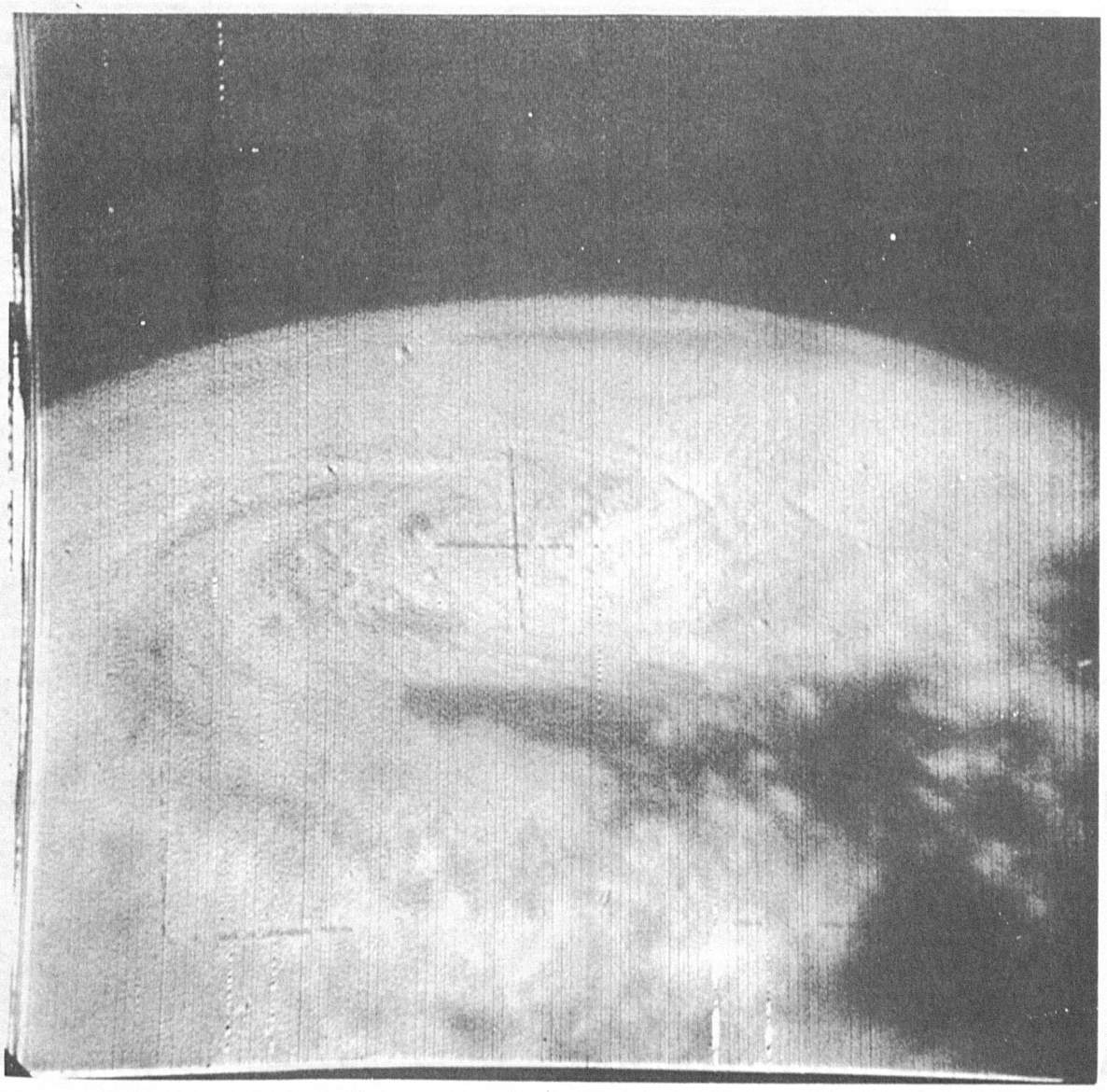

Fig. 2 CYCLONE OVER SOUTH INDIAN OCEAN 0600Z
30 APRIL 1960 R/O 418

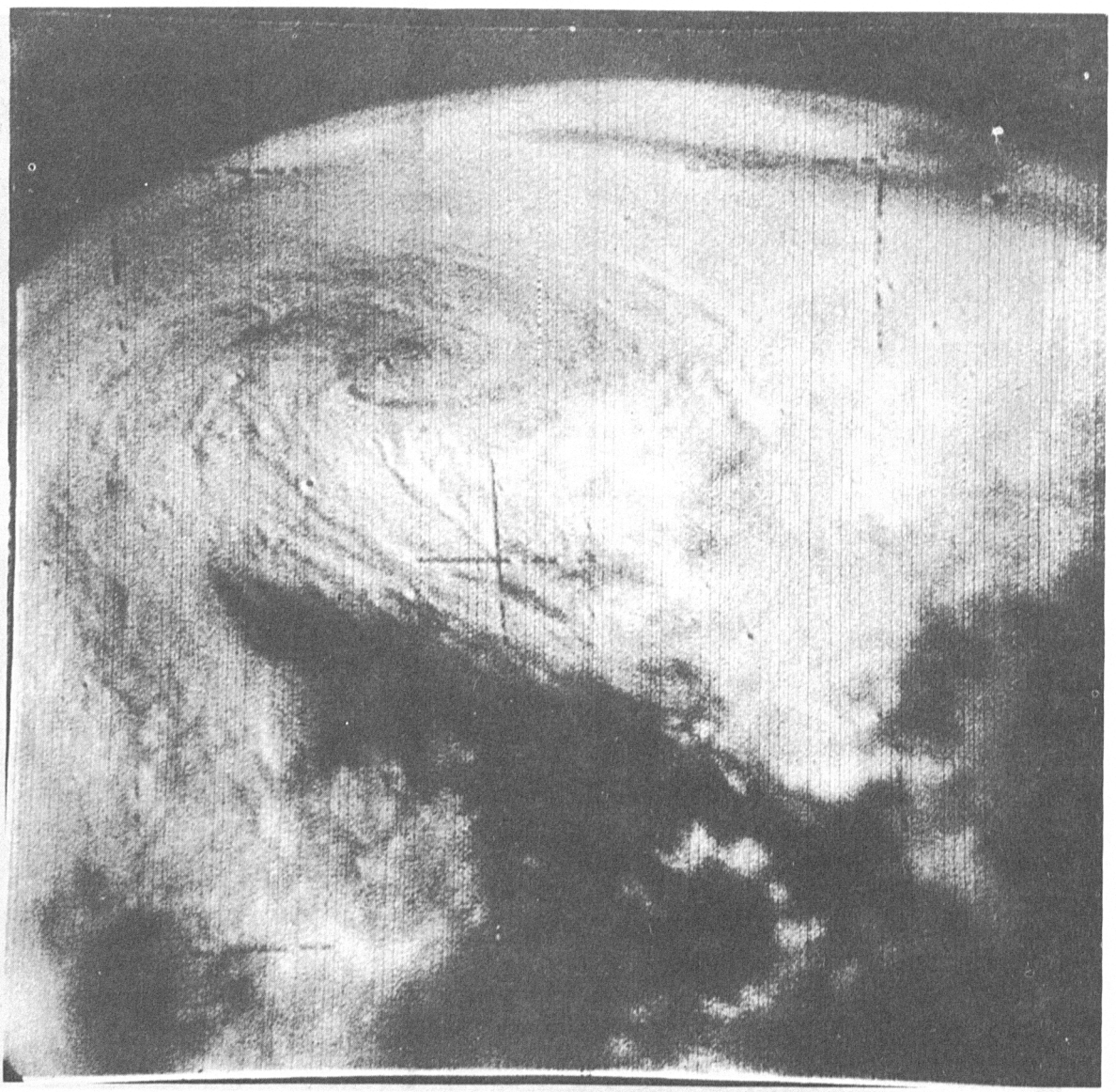

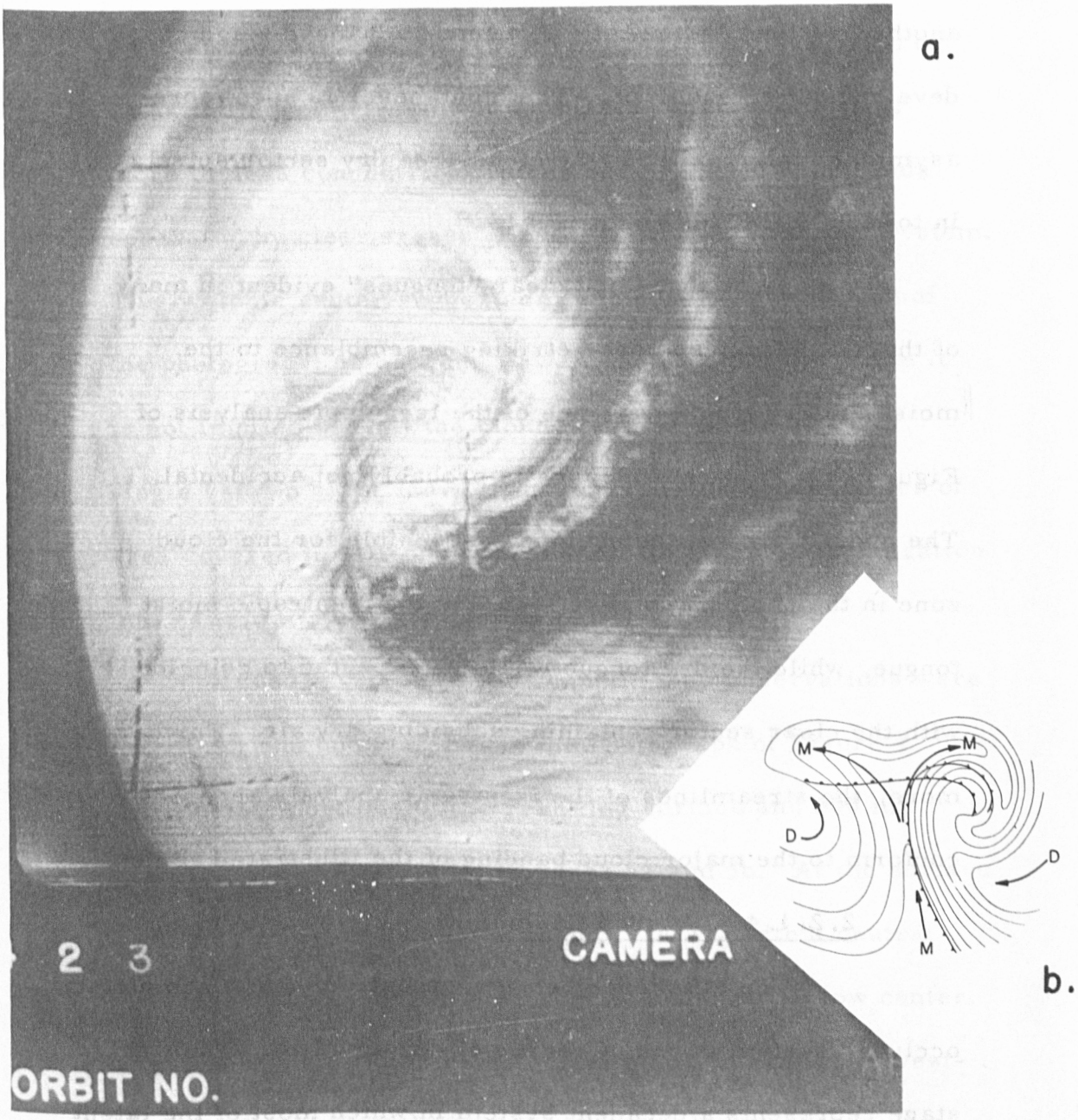

Fig. 3 a. OCCLUDED CYCLONE OVER SOUTH ATLANTIC OCEAN
1425Z 30 APRIL 1960 R/O 423
b. EXAMPLE OF ISENTROPIC ANALYSIS

embedded in the dense cloud cover. Figure 3a illustrates another cyclone, apparently in a more advanced stage of development or occlusion. The cloud cover is even more asymmetrical, as the nearly cloud-free dry sector spirals in toward the vortex center.

The cloud patterns and clear "tongues" evident in many of the TIROS pictures bear striking resemblance to the moist and dry tongue patterns of the isentropic analysis of Figure 3b. This resemblance is probably not accidental. The updraft area of the cyclone responsible for the cloud zone in the photograph is reflected in the isentropic moist tongue, while the dry tongue would be expected to coincide with the clear sector containing subsiding dry air. Furthermore, the streamlines of the isentropic analysis apparently conform to the major cloud banding of the illustrated vortex.

2.2.1.4 Occluded Cyclone

The difference between an occluding and completely occluded system is one of degree of development. The final stage represents a decadent system in which most of the latent energy has been realized and the cyclonic system is starting to "run down". This period of "free wheeling" may last several

days, especially in the case of a large intense ocean cyclone. At this stage the cloud distribution appears to lose much of its initial asymmetry and resolves itself into a series of more or less concentric, rather homogeneous wide bands separated by clear areas. Figure 4 illustrates such a system. The cyclonic center suggested in the upper right portion of the photograph, is between Hawaii and California. While it is not implied that all the clouds seen here are part of a single "storm", the more than 1-1/2 million square miles of area covered in this photograph indicate massive organization into essentially one circulation pattern.

The 0000Z, 5 April 1960 synoptic map observations were taken just one hour later than the photograph of Figure 4. Appropriate portions of the resulting surface and 500 mb analyses are reproduced in Figures 5a and 5b. At the surface a weak cold low is located near 34N, 141W, with a central pressure of about 1004 mb. South and east of the low center, a frontal system is indicated on the map and continues westward until it eventually joins another cyclonic system. Assuming the analyses to be reasonably accurate, the lower continuous cloud band in Figure 4 may be identified as the

Fig. 4 MATURE LOW OVER PACIFIC OCEAN ABOUT 2200Z
4 APRIL 1960 R/O 50

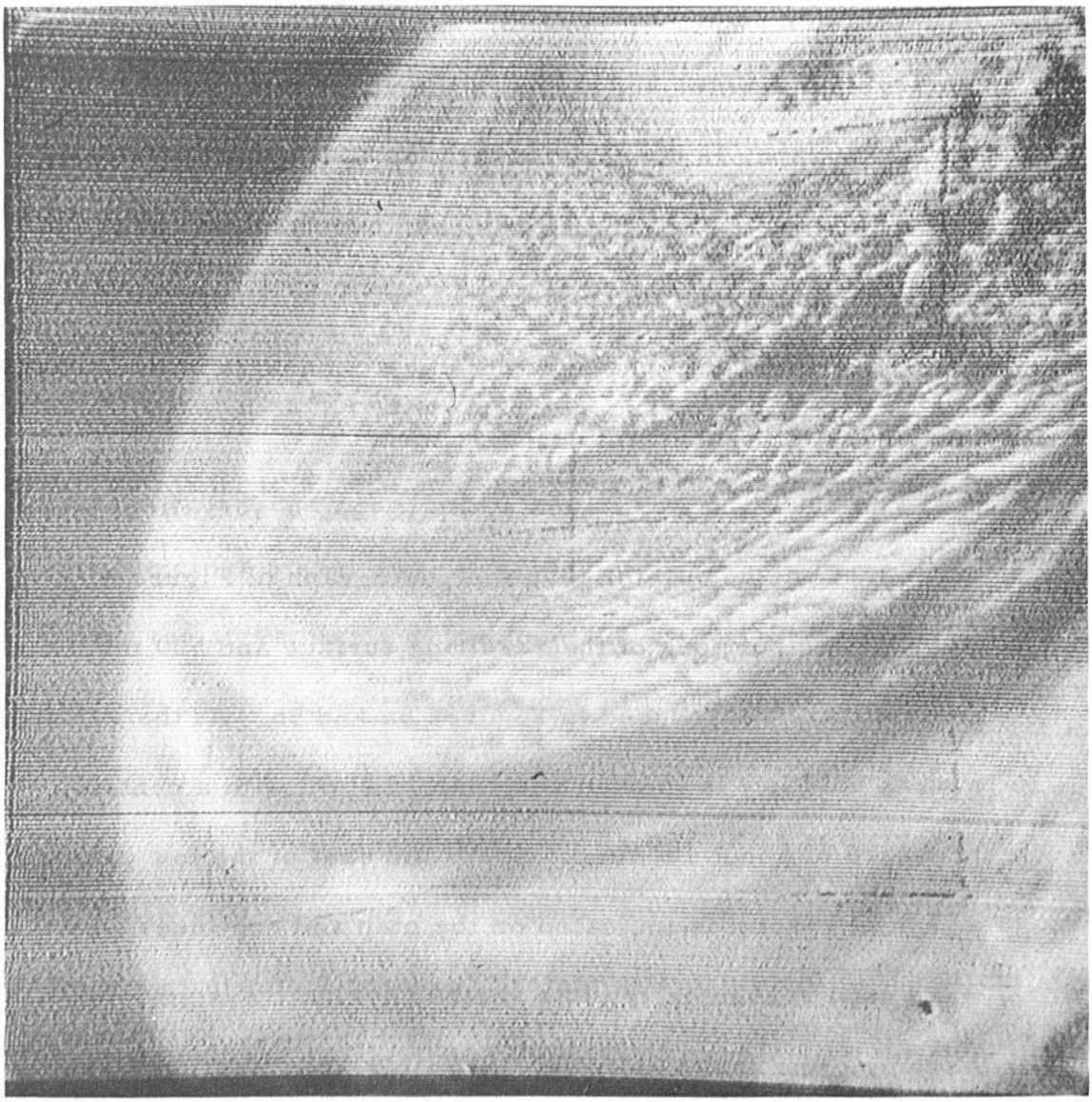

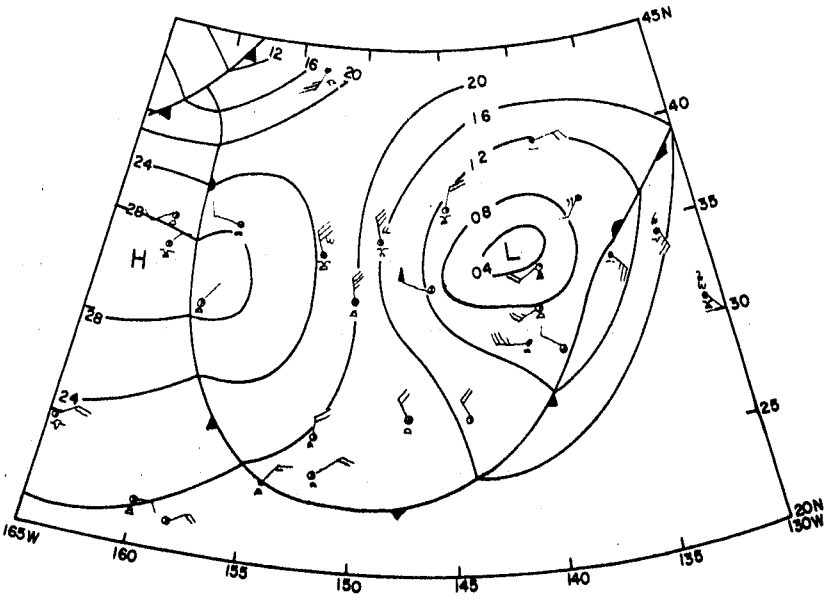

Fig. 5a. SEA LEVEL ANALYSIS 0000Z 5 APRIL 1960

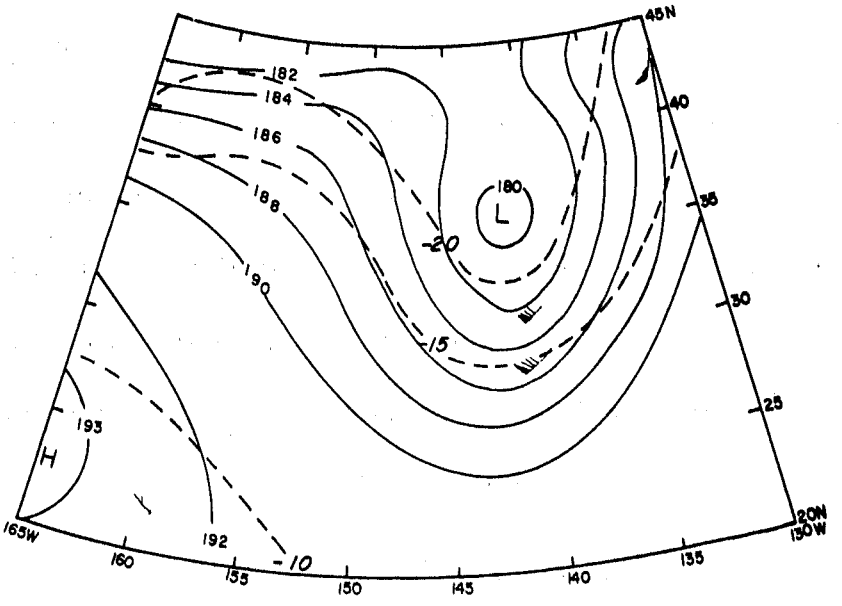

Fig. 5b. 500mb ANALYSIS 0000Z 5 APRIL 1960

frontal clouds; the heavier band to the north and west may be an unanalyzed "secondary" cold front. At 500 mb (Fig. 5b) and at 300 mb (not shown) a pronounced, though filling, cold low exists essentially vertically over the surface center.

2.2.1.5 Additional Case Studies of Vortical Cloud Distribution

10 April 1960--South Pacific Typhoon

A small but rather intense circulation is exemplified by a typhoon over the South Pacific Ocean north of New Zealand on 10 April 1960, shown in Figure 6. Unfortunately, the quality of the duplicate negative was poor, and some of the circulation features evident in the original positive transparency were lost. For example, many more clouds, mostly banded, were visible in the now dark foreground area. A copy of the TIROS nephanalysis of this typhoon region, originally prepared at the Belmar readout station, is presented in Figure 7.

16 May 1960--Caspian Sea Low

Another example of a vortex, well documented by conventional data, was initially observed on 16 May 1960,

Fig. 6 TYPHOON OVER SOUTH PACIFIC OCEAN 0300Z
10 APRIL 1960 R/0128

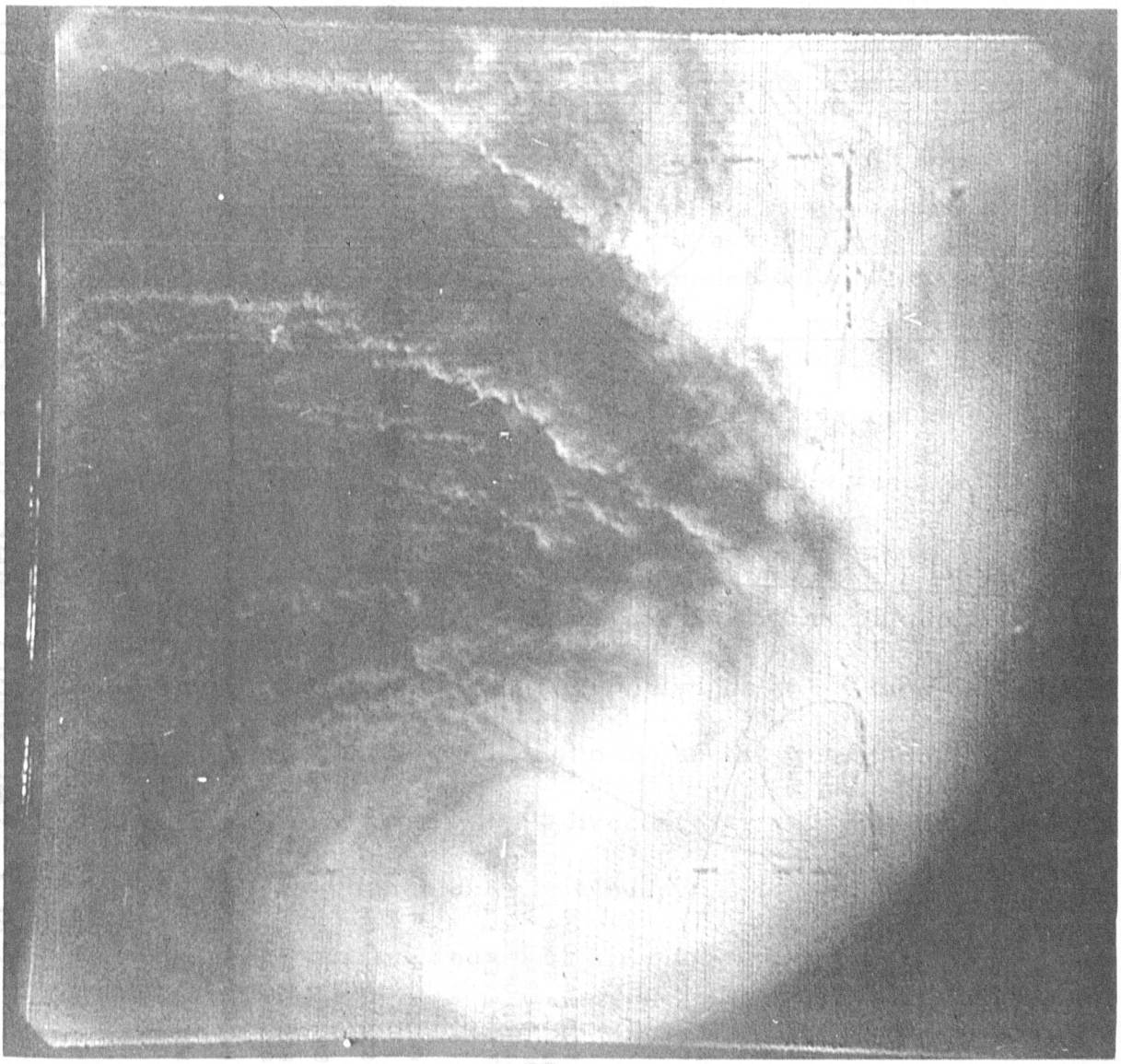

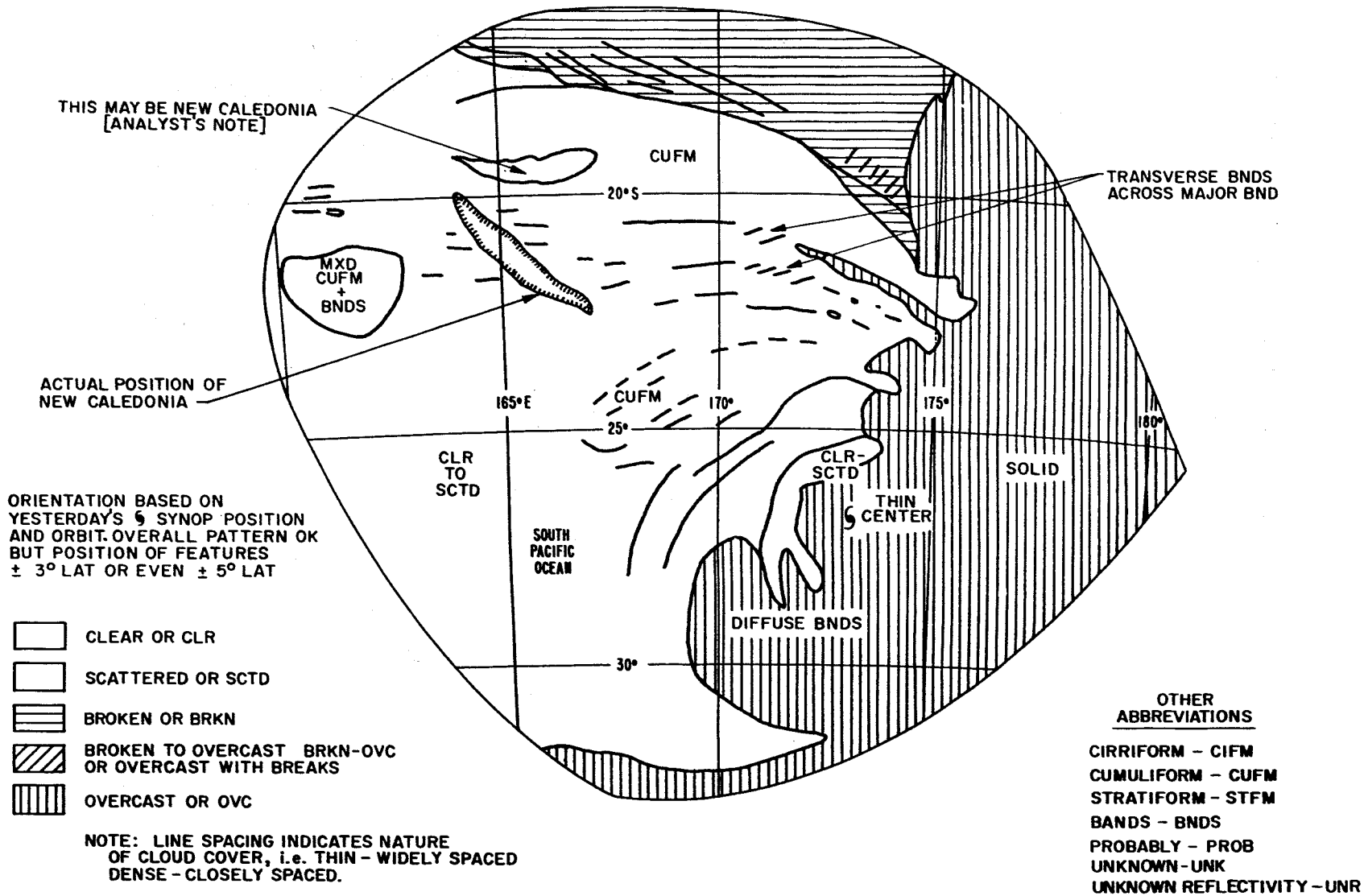

Fig. 7 FACSIMILE MAP OF TYPHOON 0300Z 10 APRIL 1960

and monitored by TIROS for three successive days. Figure 8 displays the gross features of the circulation pattern although the more delicate spiral banding has been lost in reproduction. Portions of well-defined cumuliform bands are clearly visible at the upper right.

Figure 9 shows sections of the sea level and 500 mb maps in the vicinity of this cyclone at 1200Z. The surface map indicates a well-developed wave cyclone centered at 49N, 52E. The 500 mb map shows a moderately intense closed low southwest of the surface center.

In Figure 10, a copy of the TIROS nephanalysis of this orbit, the cloud cover distribution is shown from western Africa to north of the Caspian Sea. The cloud spiral is centered near 48N, 48E, or at the position of the 500 mb low and in the region of light variable winds at 300 mb. While this position is displaced to the southwest of the surface pressure center, it is directly over a circulation center indicated by the surface winds.

Since the surface and upper air maps indicate northerly flow across the Black Sea, orographic lifting over the mountains could be the cause of the heavy cloud cover observed over northern Turkey.

Fig. 8 VORTEX NORTH OF CASPIAN SEA 1240Z
16 MAY 1960 R/O 657

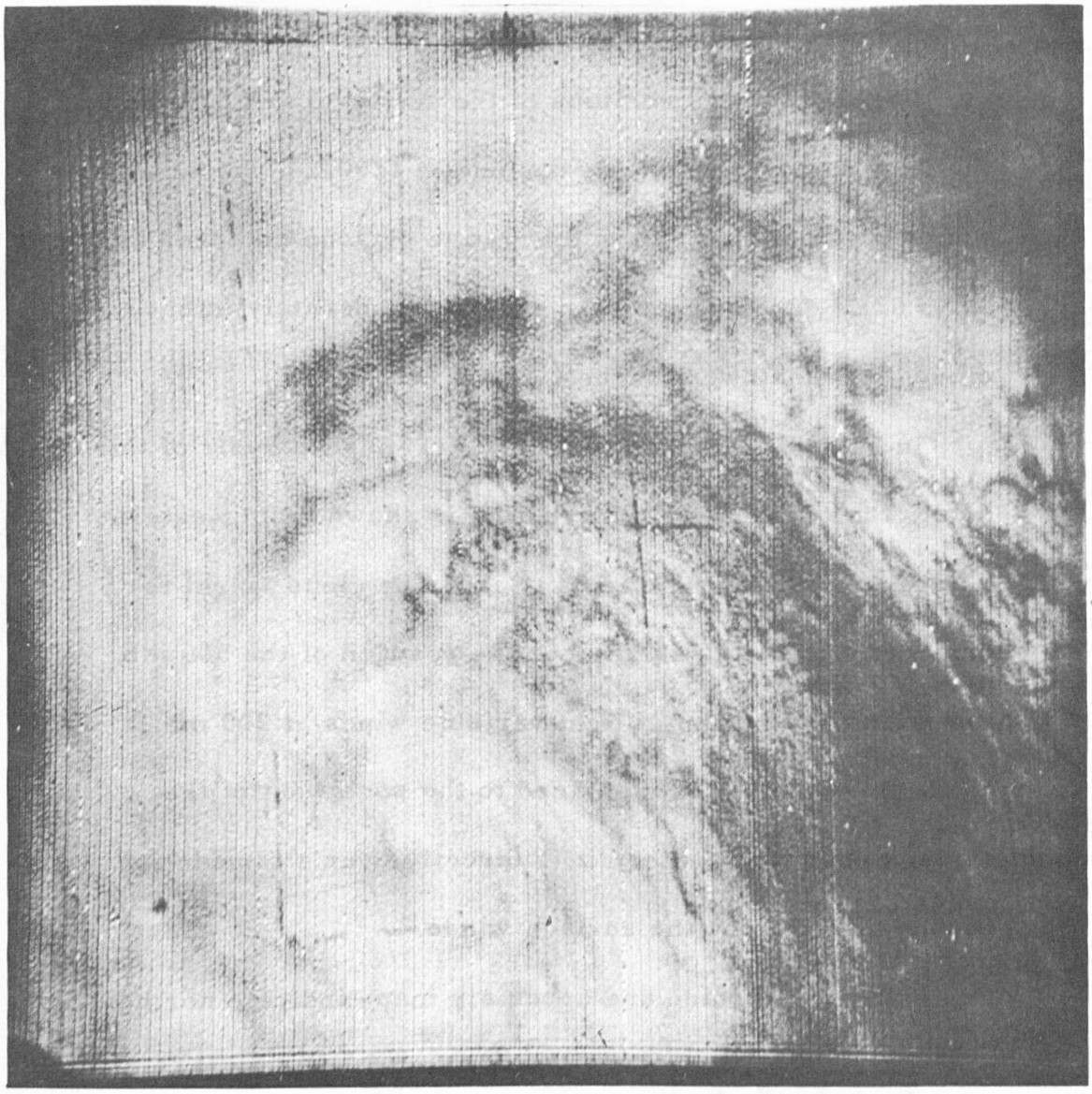

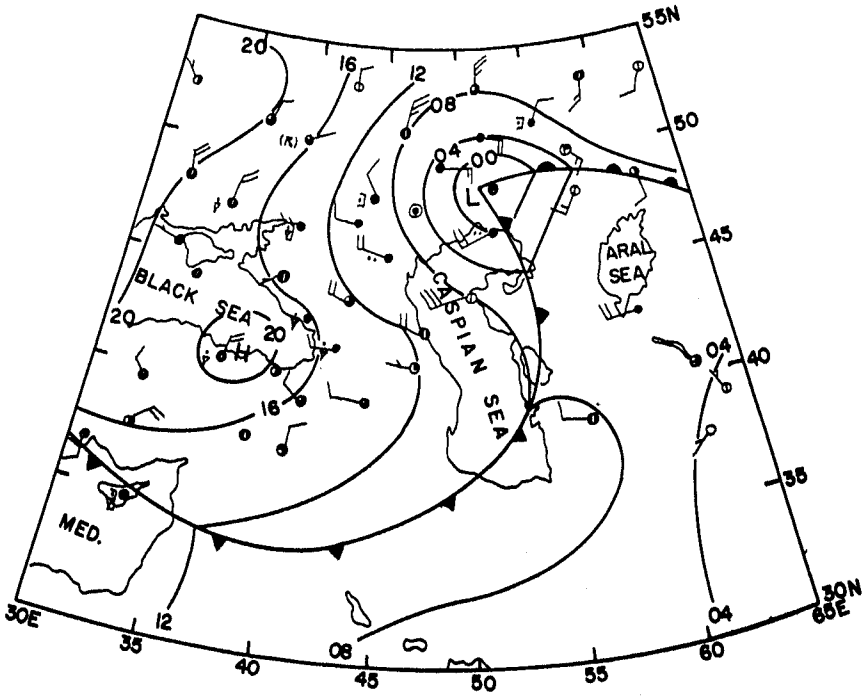

Fig. 9a SEA LEVEL ANALYSIS 1200Z 16 MAY 1960

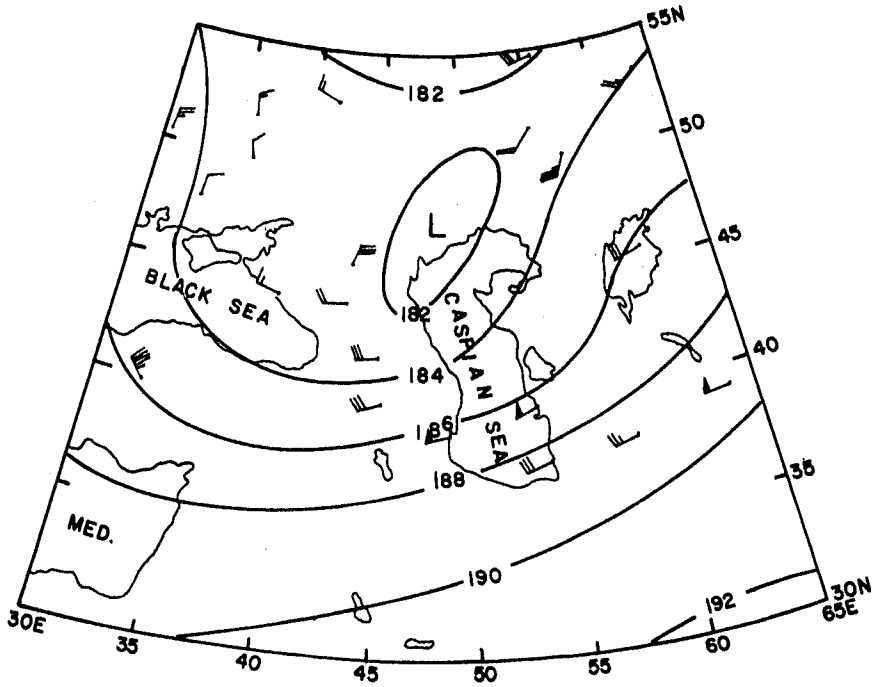

Fig. 9b 500 mb ANALYSIS 1200Z 16 MAY 1960

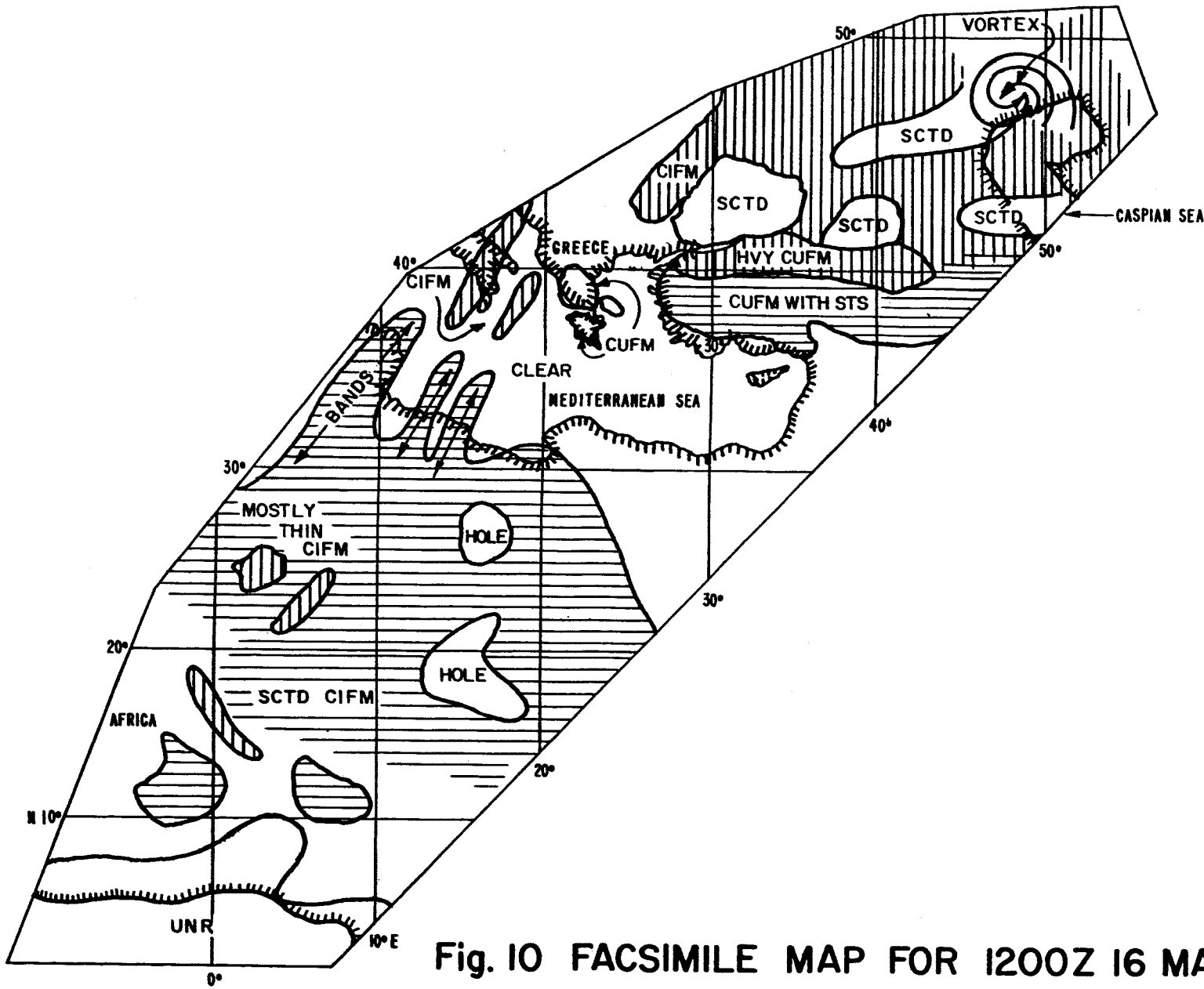

Fig. 10 FACSIMILE MAP FOR 1200Z 16 MAY 1960

In North Africa, the surface weather map (not reproduced) shows broken or overcast cirrus cloudiness in the area indicated as "broken" by TIROS. It is of interest to note here that the cirrus, though thin enough to allow land features to be discerned beneath it, was nevertheless distinguishable from the highly reflective sandy desert, although for its identification, the analyst relied heavily on the fact that the cirrus was clearly visible where it projected into the Mediterranean.

7 - 8 May 1960--"Bermuda Low"

Figure 11 is a TIROS photo taken on 7 May 1960 at about 2200Z, off the southeast coast of the United States. It shows a well-defined spiral with many cumuliform cloud bands but with very little area of solid cloud visible, indicating that this system is in a decadent stage. A nephanalysis prepared from this pass is shown in Figure 12. In this analysis, the organization of the spiral circulation is the outstanding feature.

The maps for 0000Z 8 May, Figure 13 show the "Bermuda Low", east of Florida, to be typical of such slow-moving systems, blocked by the Atlantic high to the northeast. There is no evidence of a front in the cyclone, and the surface cloud reports give no hint of the organization which is so striking in the TIROS picture.

Fig. 11 VORTEX SOUTHWEST OF BERMUDA 2200Z
7 MAY 1960 R/O 529

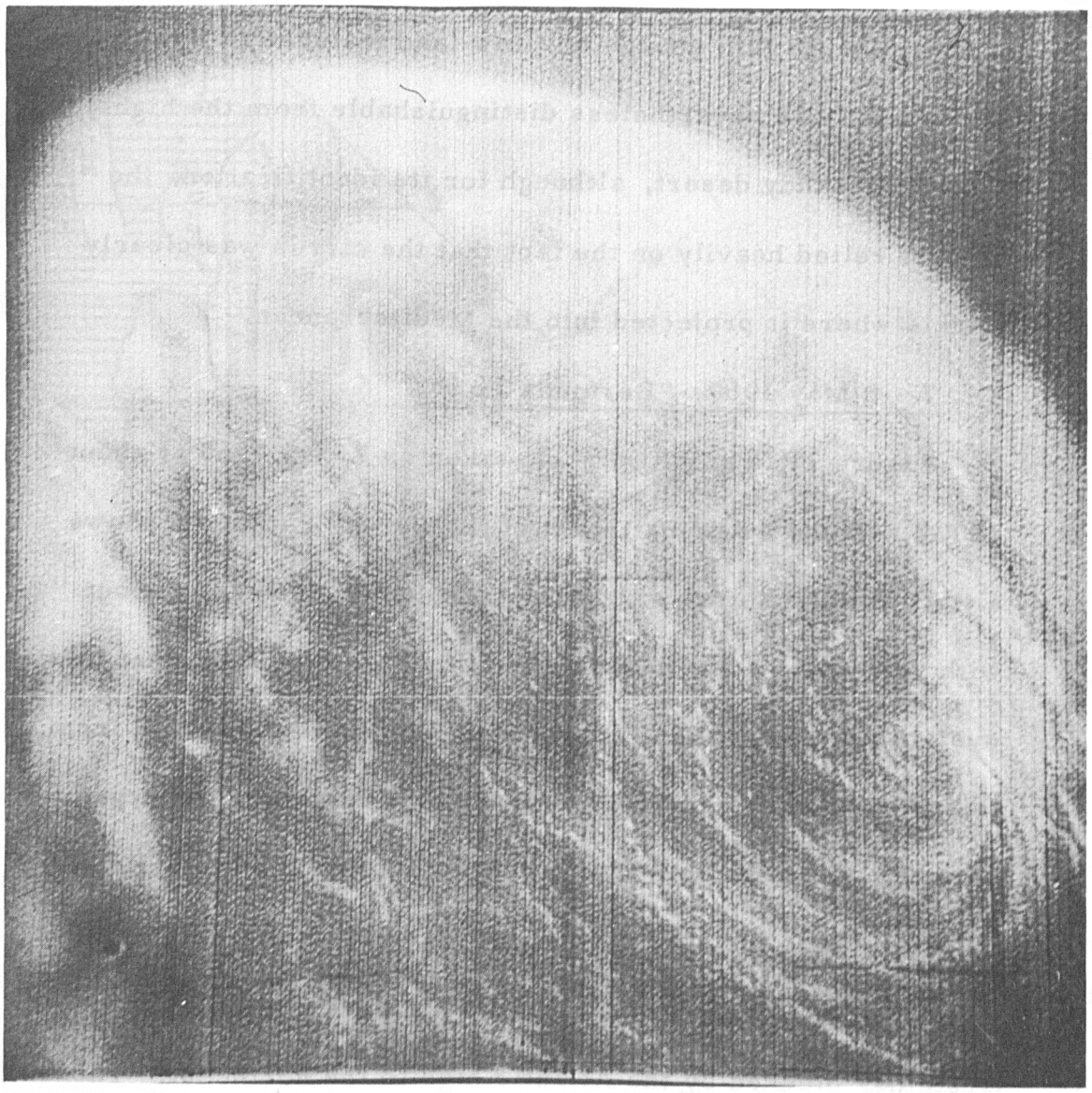

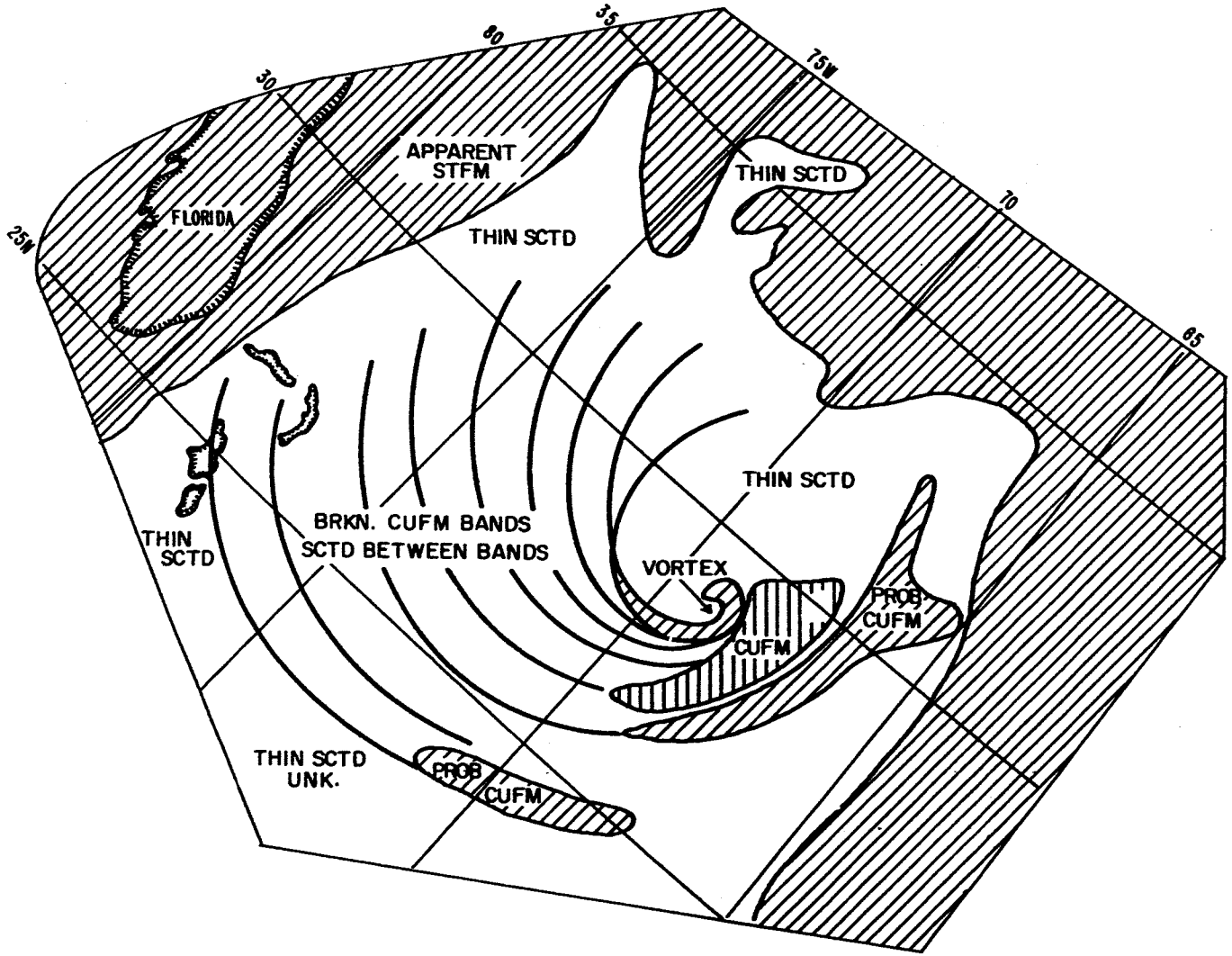

Fig.12 FACSIMILE MAP OF VORTEX 2200Z 7 MAY 1960

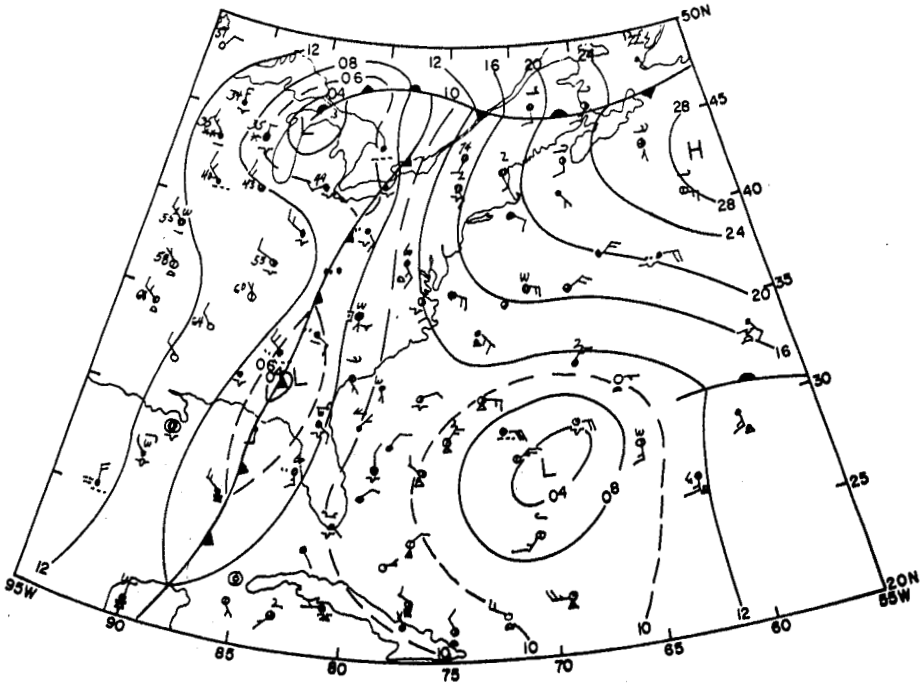

Fig. 13a SEA LEVEL ANALYSIS 0000Z 8 MAY 1960

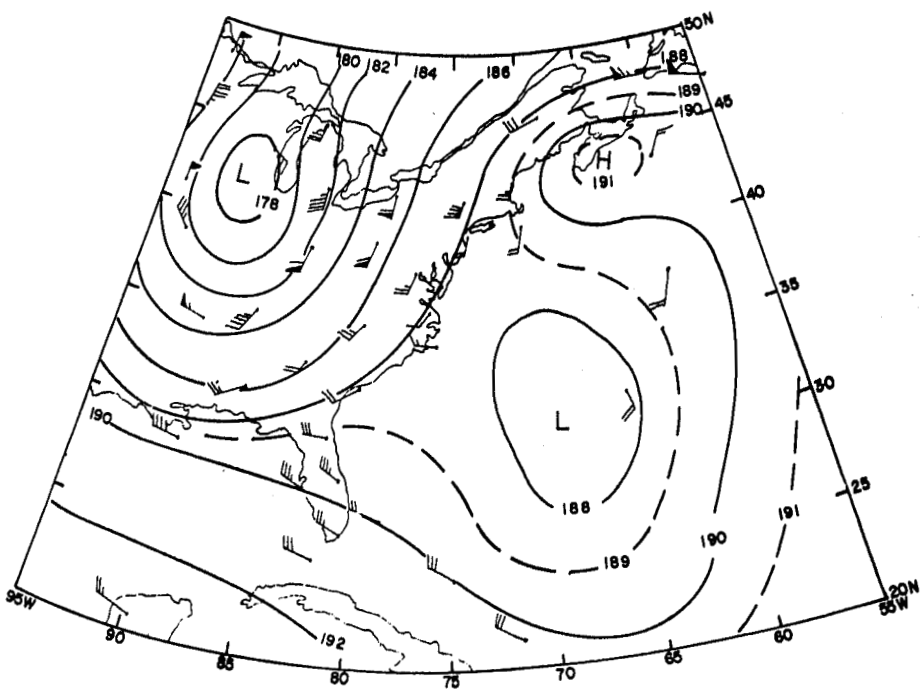

Fig. 13b 500mb ANALYSIS 0000Z 8 MAY 1960

Fig. 14 VORTEX SOUTHWEST OF BERMUDA 2105Z
8 MAY 1960 R/O 543

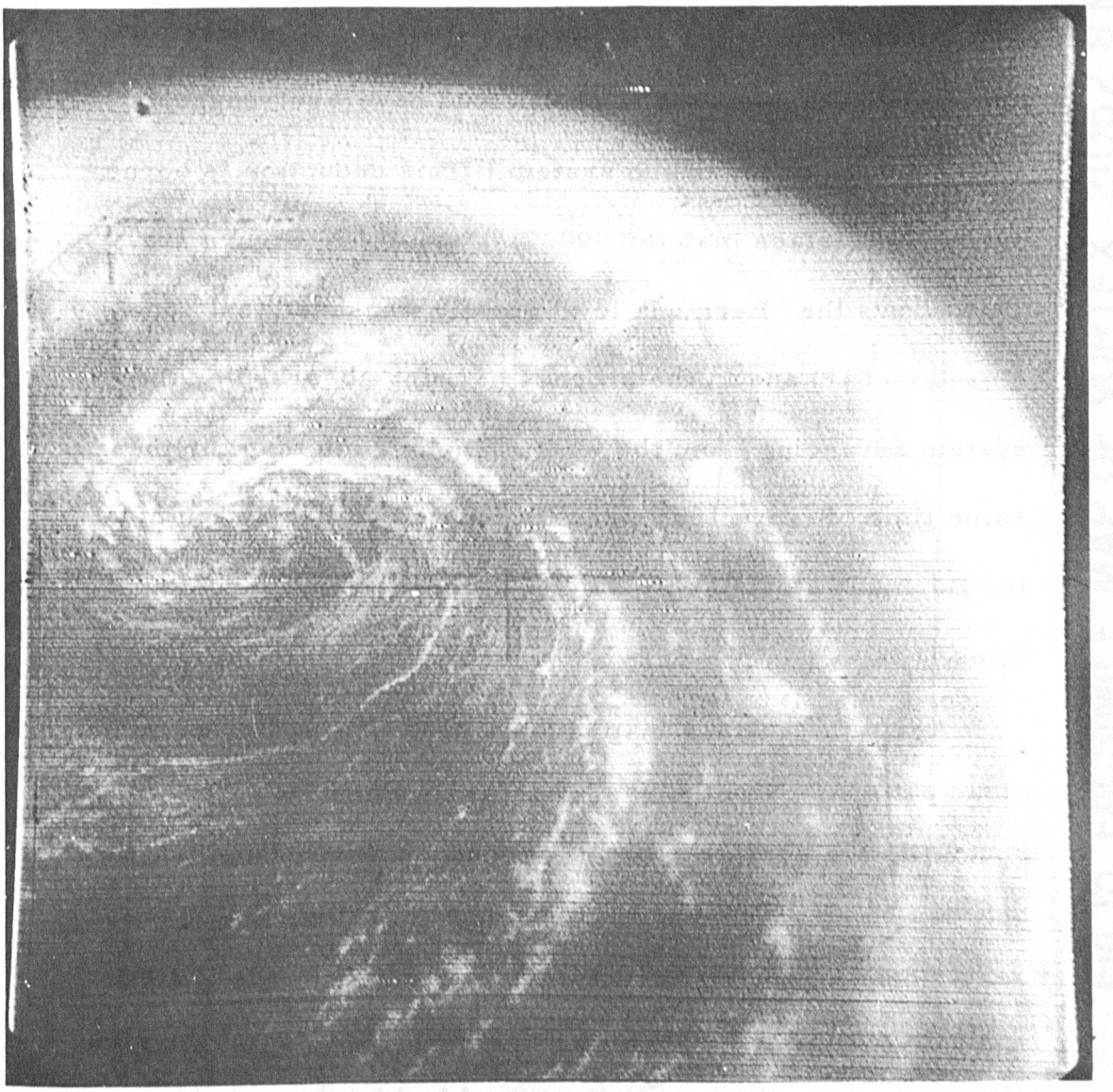

Figures 14 and 15 are the TIROS photograph and the mapped nephanalysis of the same area 24 hours later or about 2105Z 8 May 1960. The general impression is that the cloud patterns are similar to those seen 24 hours earlier. The bands are spaced further apart and this, together with the apparent decrease in overall cloud coverage, suggests a further weakening of the system. This deduction is borne out by the surface map for 0000Z 9 May 1960, Figure 16a. This shows the "Bermuda low" greatly weakened (only one closed isobar) and in the process of being absorbed by the system advancing from the west. The 500 mb map for the same time, Figure 16b, likewise shows the dissolution of the Bermuda storm, only a bulge remaining in the contour lines.

Again the surface map gives a poor impression of the cloud pattern. Nonetheless, the TIROS observed cloud cover fits the surface reports well except along longitude 74W between 25 and 29 N where cloudiness reported by surface observations is greater than indicated by TIROS. The TIROS analysis may have been faulty in locating the edge of the cloud sheet seen near the horizon of Fig. 14 which is probably a cloud band ahead of the cold front.

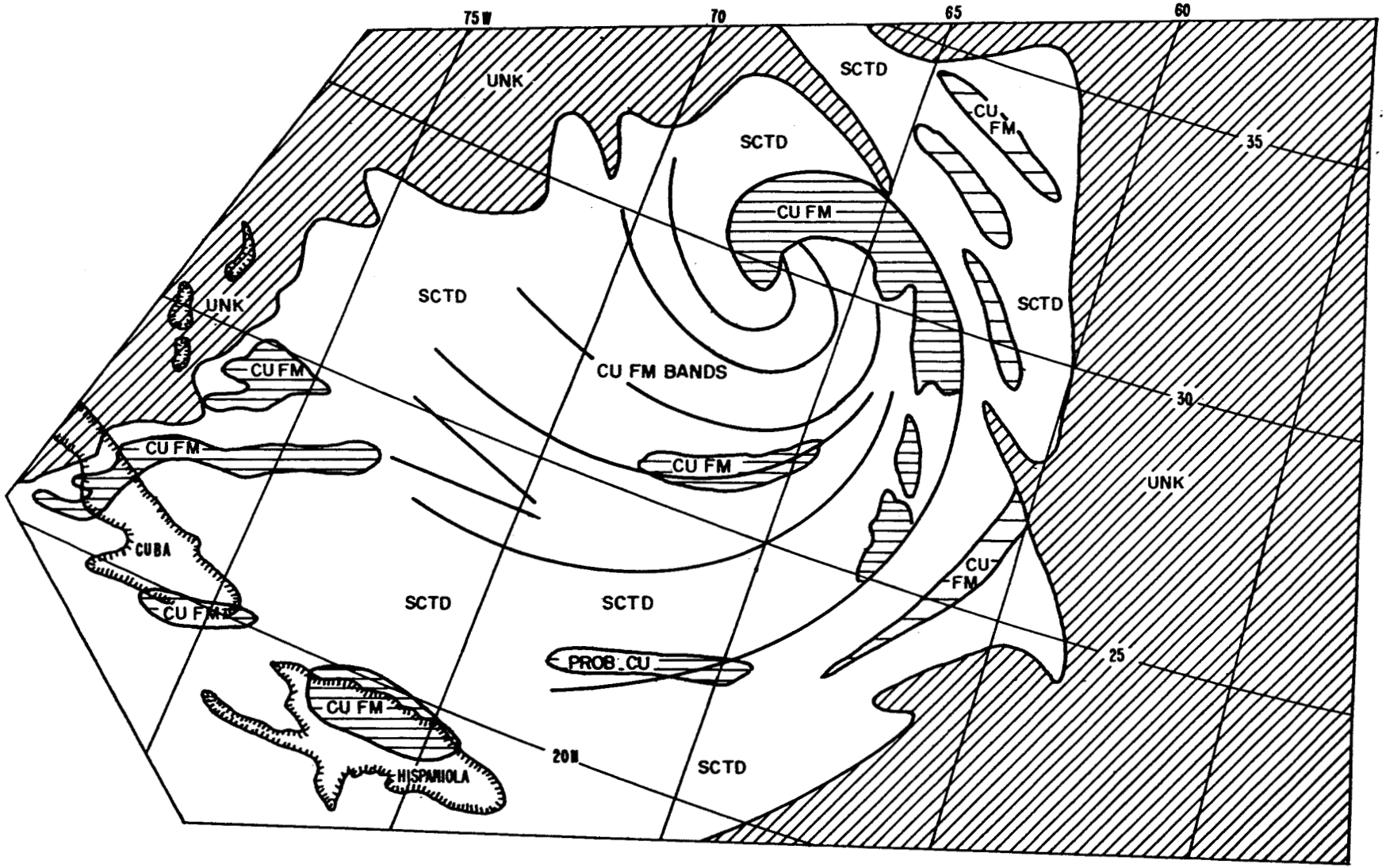

Fig. 15 FACSIMILE MAP OF VORTEX 2105Z 8 MAY 1960

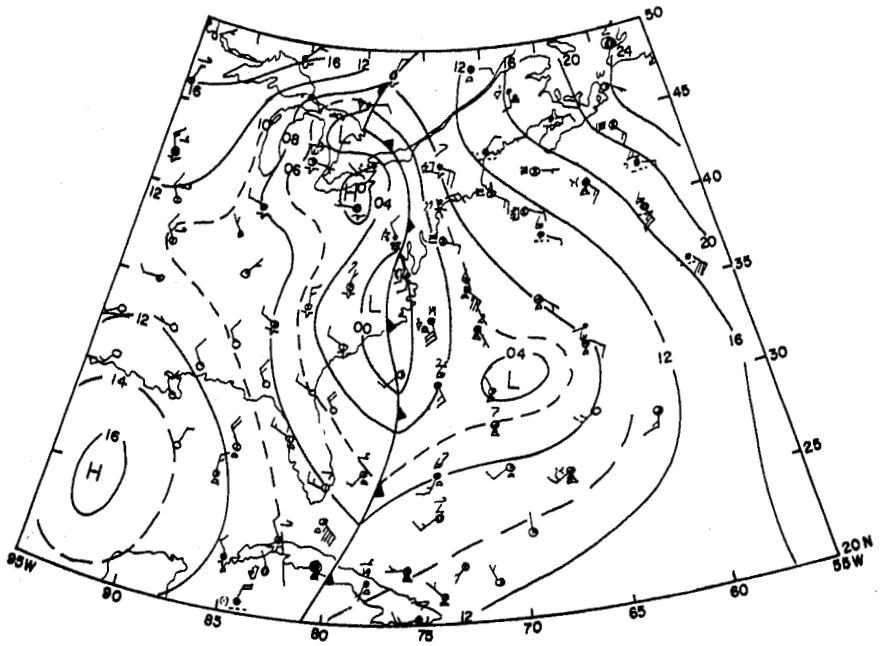

Fig. 16a. SEA LEVEL ANALYSIS 0000Z 9 MAY 1960

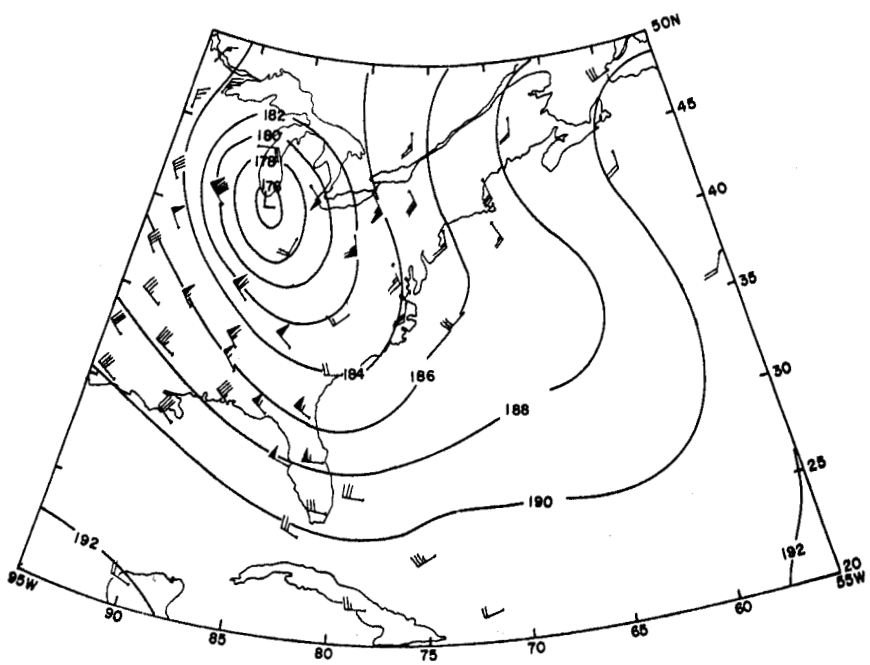

Fig. 16b. 500mb ANALYSIS 0000Z 9 MAY 1960

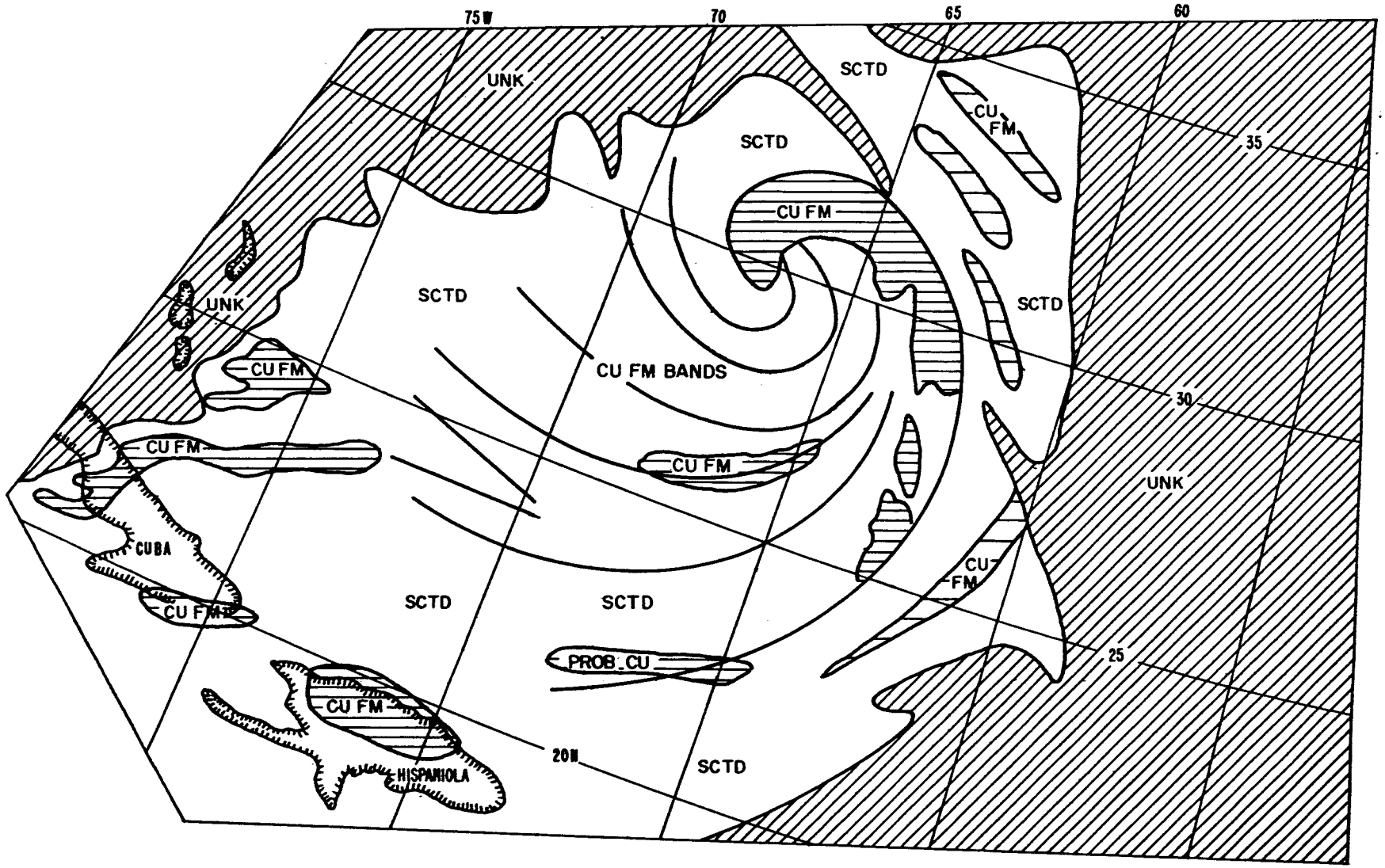

Fig. 15 FACSIMILE MAP OF VORTEX 2105Z 8 MAY 1960

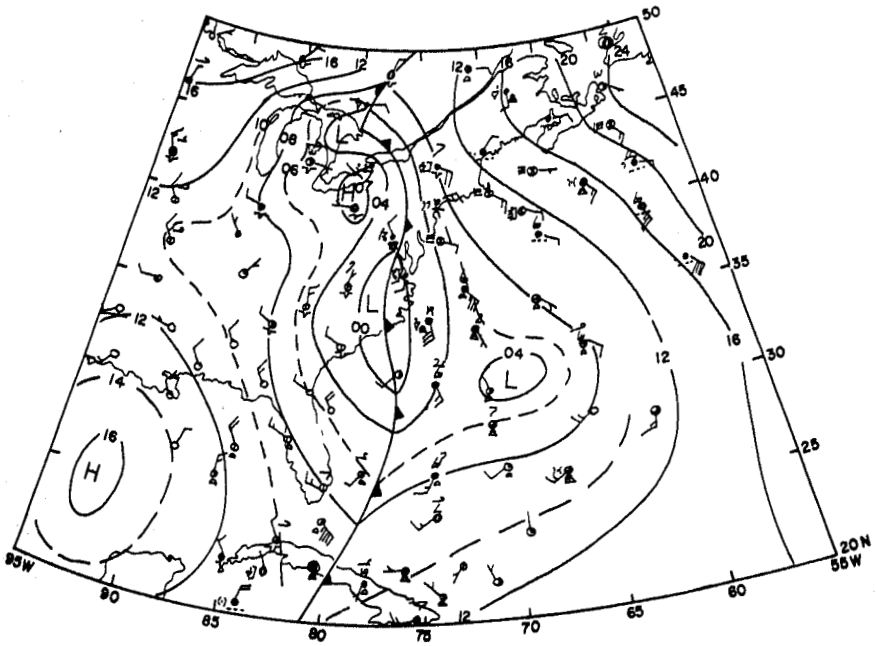

Fig. 16a. SEA LEVEL ANALYSIS 0000Z 9 MAY 1960

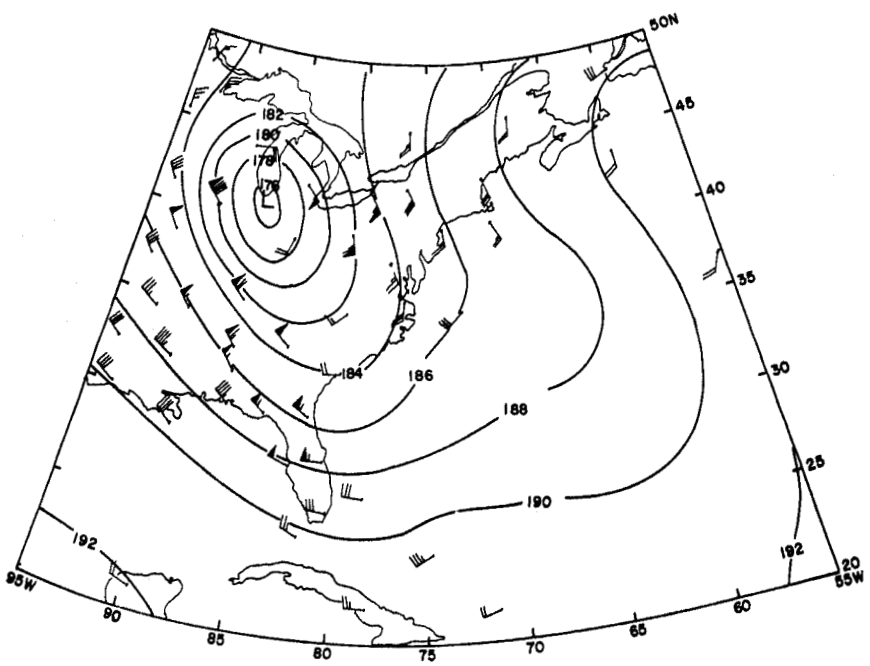

Fig. 16b. 500mb ANALYSIS 0000Z 9 MAY 1960

Lows over the United States--11 and 12 May 1960

TIROS passes over the United States late on 11 and 12 May 1960 revealed a complex circulation pattern which included several vortices. These cloud patterns can be documented reasonably well from conventional analyses on these dates. The 2155Z, 11 May 1960 nephanalysis has been superimposed on the surface and upper air charts for the 11th to illustrate the agreement.

The 2100Z surface map for 11 May (Fig. 17a) indicates an old occluded low in the eastern Great Lakes region with an open wave of sorts in the Carolinas, and another circulation center in the lower Mississippi Valley. A deep cold low is indicated over Lake Erie on the 12 May, 0000Z 500 mb map (Fig. 17b) with another circulation center in the trough over Louisiana. Figure 18 shows a TIROS photograph of the southern Mississippi Valley region, taken at about 2200Z, 11 May. In this picture, the cloud vortex center agrees well with locations of the surface and upper level circulations shown on the conventional maps. Apparent overrunning, with a cirrus band superposed on lower clouds of different orientation, is visible. On the 2155Z nephanalysis (Fig. 17b) for this

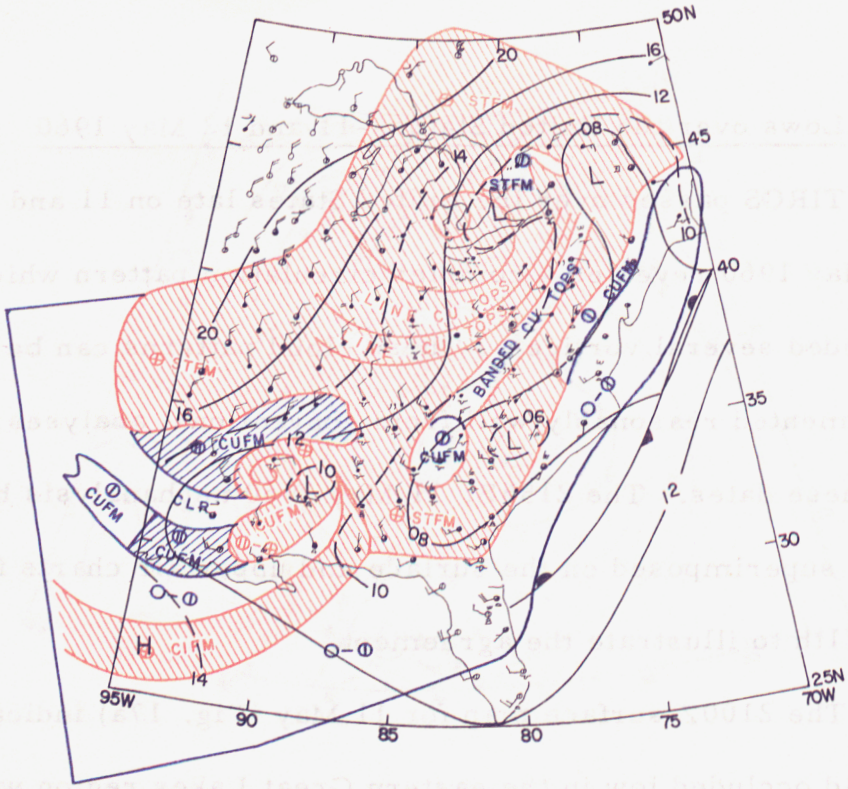

Fig.17a SEA LEVEL ANALYSIS 2100Z 11 MAY 1960
WITH SUPERIMPOSED TIROS NEPHANALYSIS

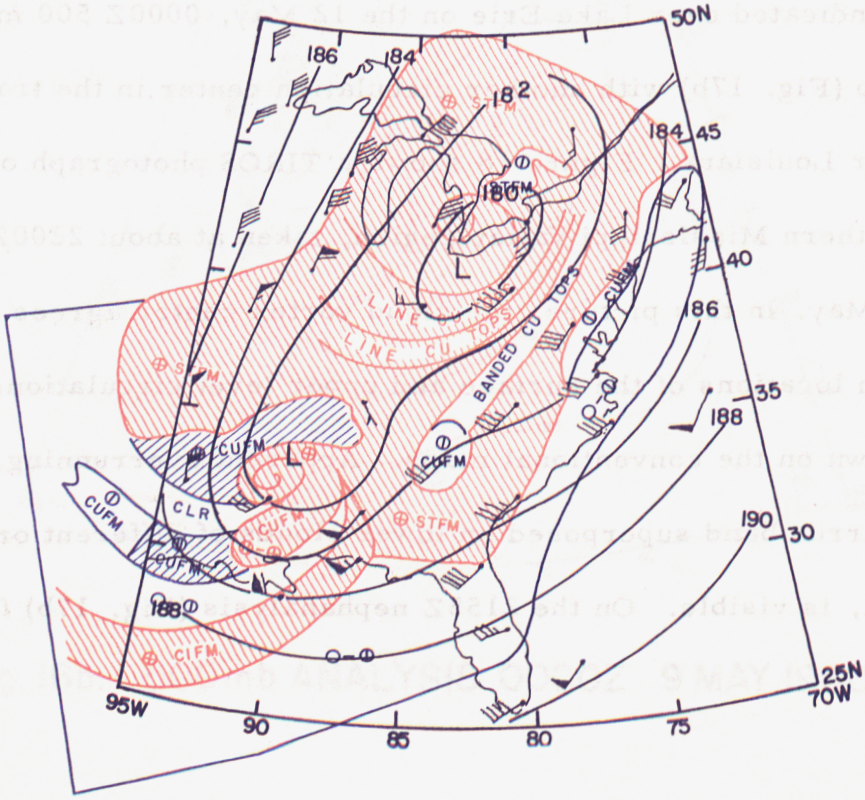

Fig.17b 500mb ANALYSIS 0000Z 12 MAY 1960
WITH SUPERIMPOSED TIROS NEPHANALYSIS

date, considerable stratiform overcast is also apparent in the area corresponding to that portion of the 500 mb trough generally associated with rising motion. While the locations and cloud configurations surrounding the vortices agree well with the surface and 500 mb circulation centers, it is interesting to note the lack of a vortical cloud pattern or of a spiral wind circulation in the vicinity of the Carolina wave. Instead, the clear or scattered cloud areas conform well to the region behind the wind shift line on the surface map, as though a front followed by subsiding air could have been analyzed along the wind shift line. It is suggested that an open wave early in its development maysometimes have this characteristic "text book" cloud distribution, which soon develops into the more frequently observed spiral circulation as the occlusion process continues.

A set of illustrations for 12 May shows that circulation centers at the surface (Fig. 19a) and at 500 mb (Fig. 19b) are again in good agreement with the vortex location on the nephanalysis, Figure 20. Note also the sharp western edge on the clouds of the vortex near Lake Michigan, apparent in the photograph of Figure 21. This discontinuity is also apparent in the surface data of the 0000Z map for 13 May, Figure 19a. (A nephanalysis of the previous pass, not included here, indicates

Fig. 18 VORTEX OVER NORTHERN LOUISIANA 2155Z
11 MAY 1960 R/O 587

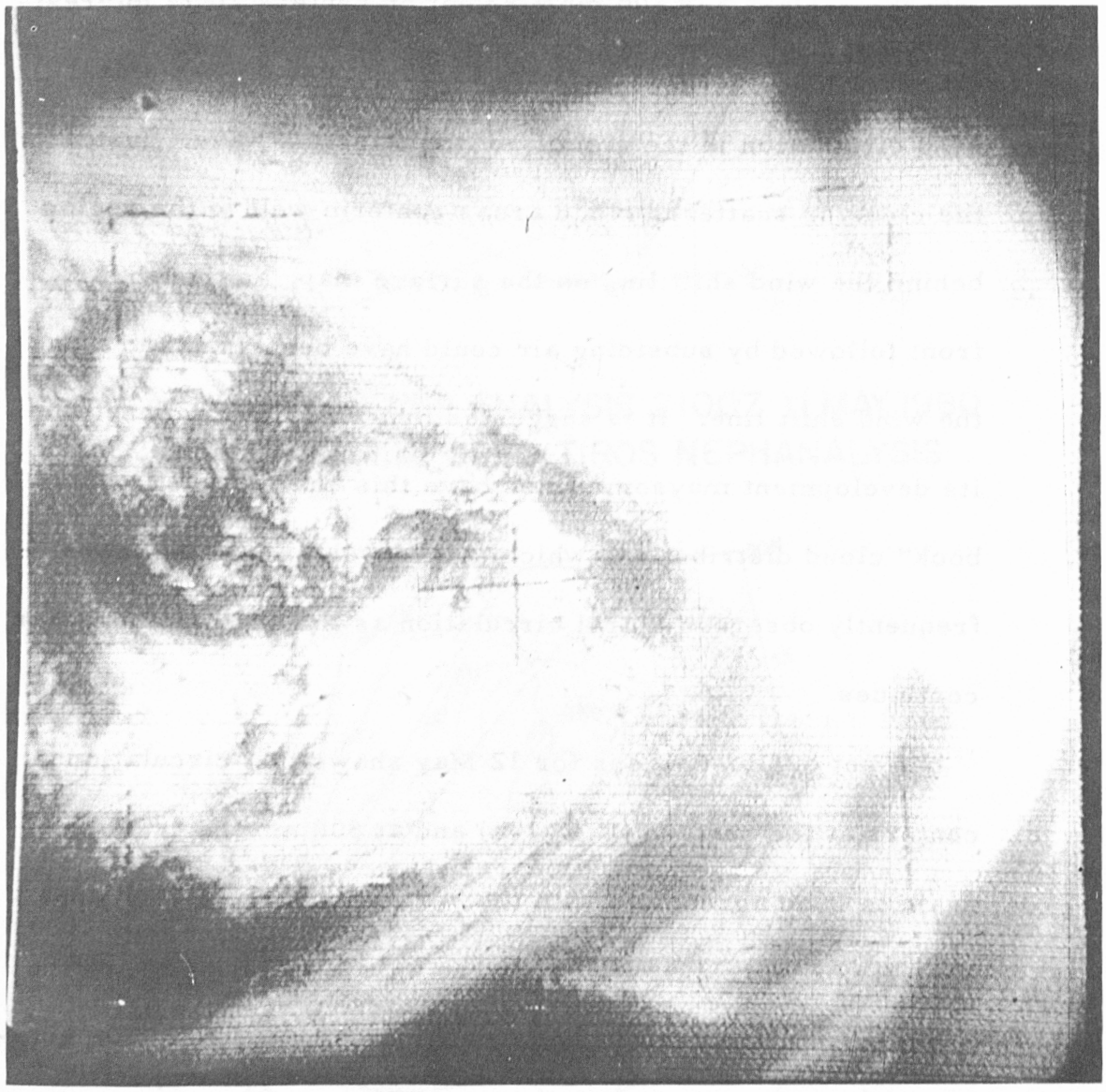

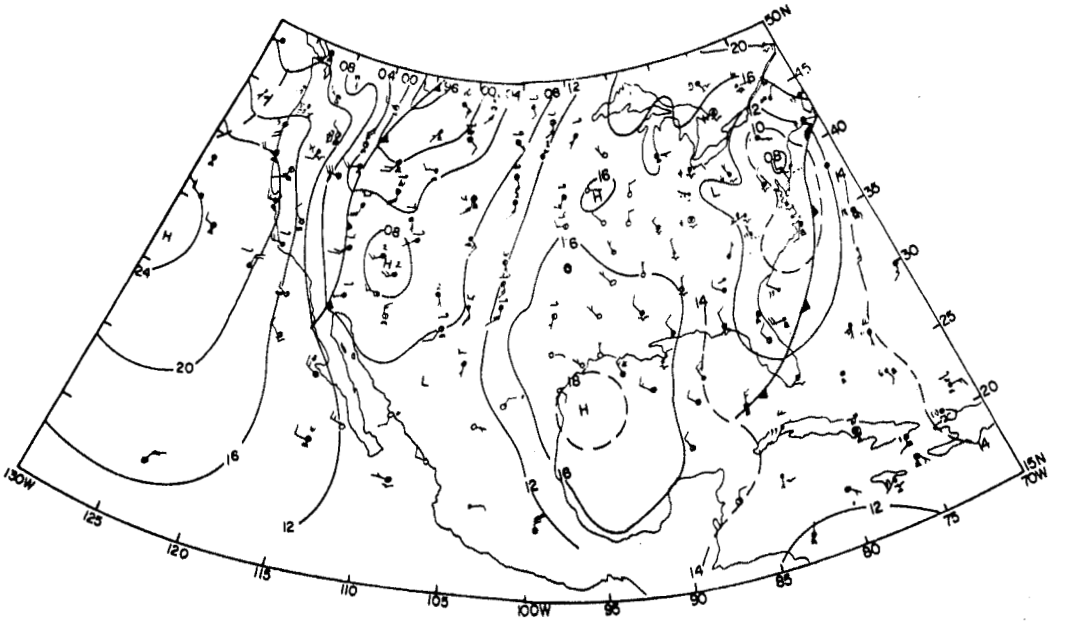

Fig. 19a. SEA LEVEL ANALYSIS 0000Z 13 MAY 1960

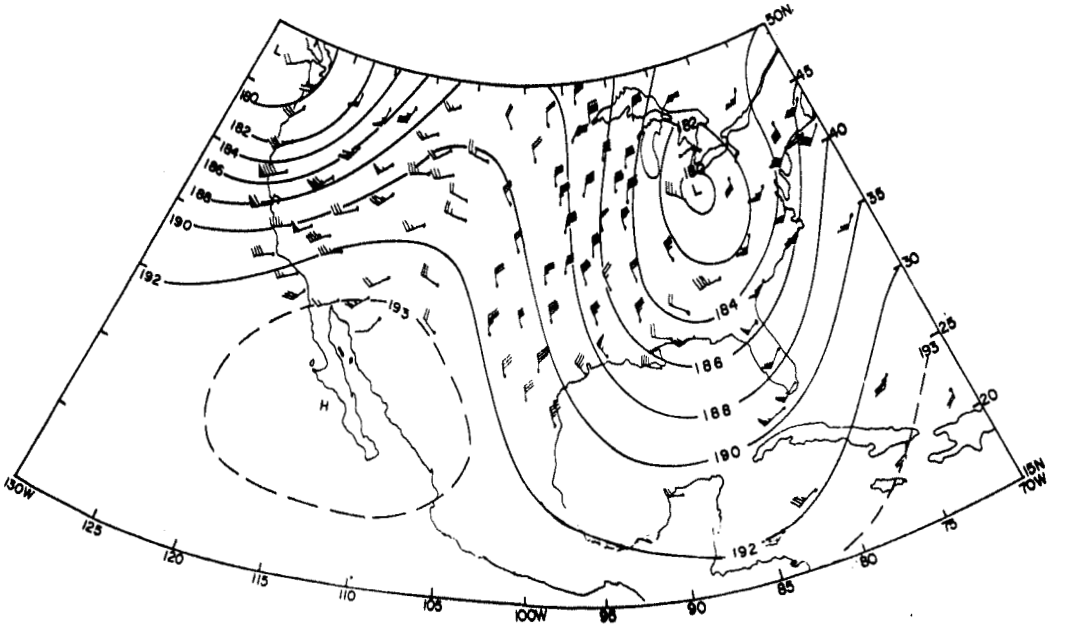

Fig. 19b. 500mb ANALYSIS 0000Z 13 MAY 1960

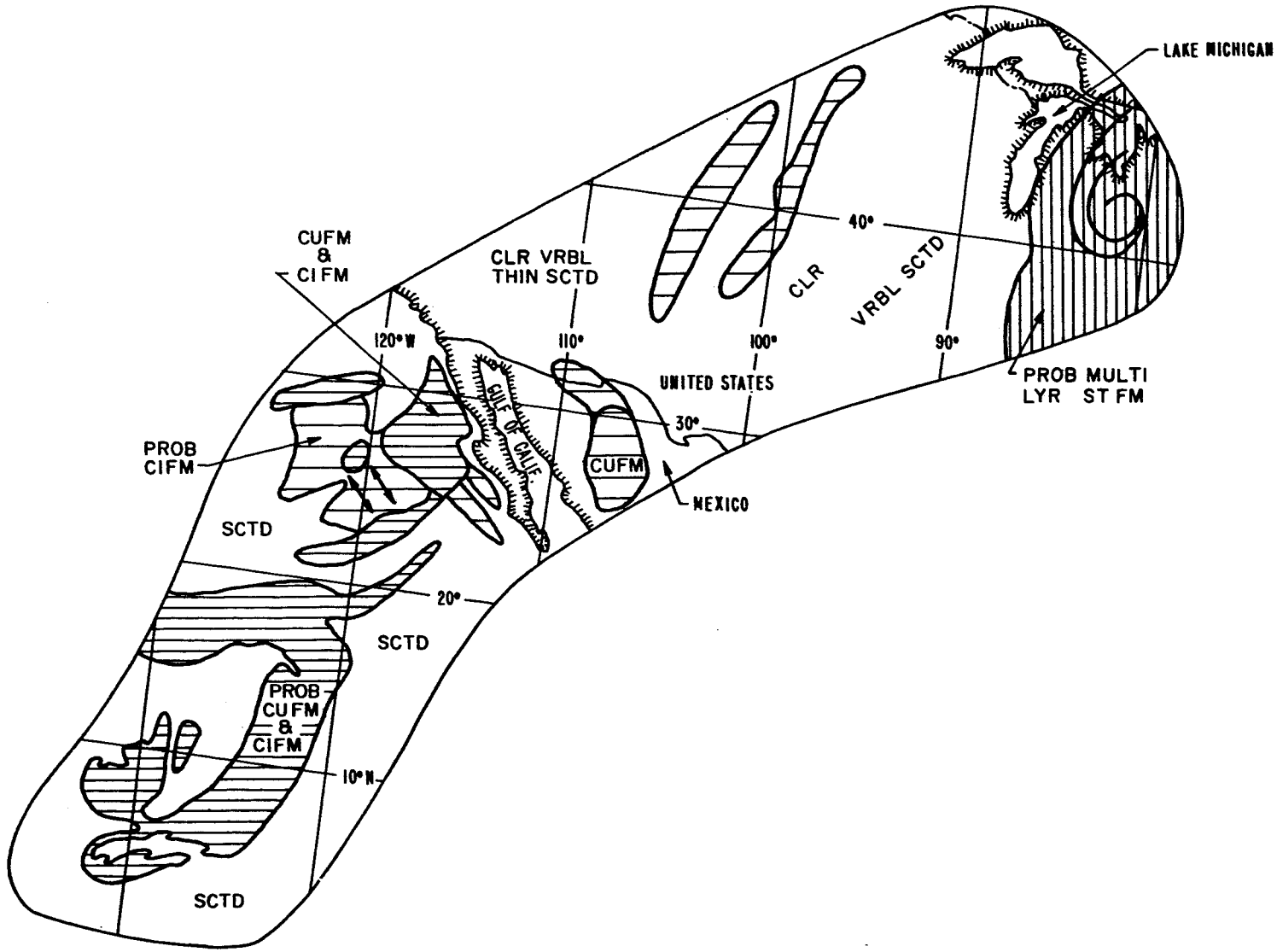

Fig. 20 FACSIMILE MAP OF VORTEX 2245Z 12 MAY 1960

Fig. 21 VORTEX OVER MICHIGAN 2245Z
12 MAY 1960 R/O 602

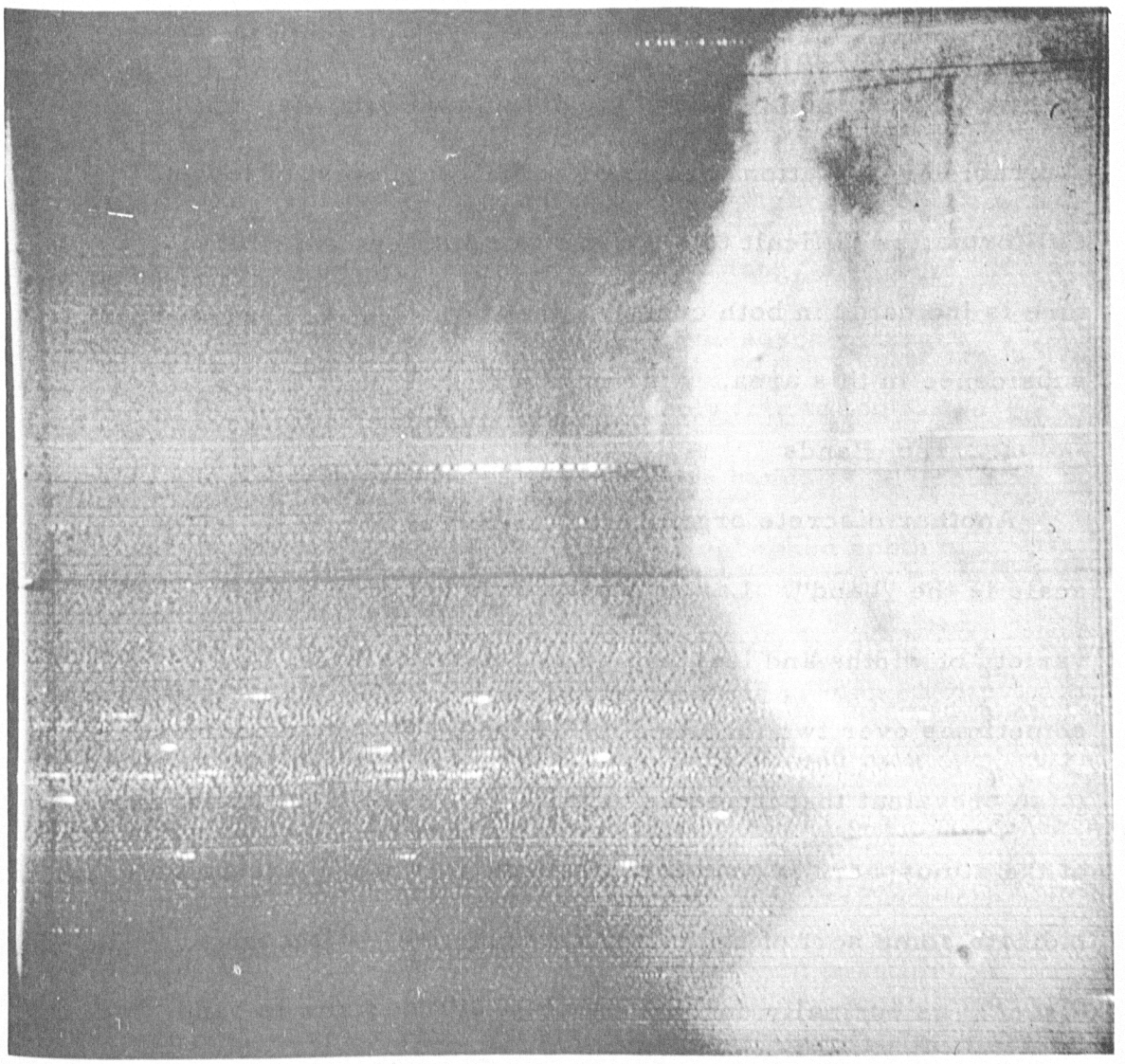

that the southernmost vortex dissipated, as did its corresponding wind circulation center, while the Carolina wave developed the typical vortical cloud distribution.) The cloudiness indicated over the central plains in the nephanalysis may be associated with weak north-to-south jet stream in the region. The cloud distribution showing considerable organization over the Pacific, southwest of lower California, is difficult to explain since anti-cyclonic curvature is indicated in both constant pressure charts, suggesting subsidence in this area.

2.2.1.6 Bands

Another discrete organization of cloudiness on the large scale is the "band". Large-scale bands occur in a wide variety of widths and lengths, up to 200 miles wide, and sometimes over two thousand miles long. Banded cloudiness is so prevalent that it seems to indicate a dynamical preference of the atmosphere to manifest itself in lines which presumably indicate some sort of organized convergence. Although a "front", as normally defined, is not a prerequisite to band development, the largest and most important bands weather-wise are usually observed in regions of marked convergence of surface

winds. A prominent example of often-observed large-scale banded cloudiness is the intertropical convergence zone (Fig. 22) which does not separate different air masses in the usual frontal sense.

Figure 23 is a photographic example of naturally occurring bands in a variety of sizes. The largest band is 150 miles wide and 750 miles of it are visible in this photograph. The two smaller bands to the right of the fiducial crossmark are at least 400 miles long, and from 20 to 40 miles wide. Qualifying for the mesoscale range are the thinnest bands in the picture, only five to ten miles wide. No synoptic interpretation of these bands is possible since conventional data for the area photographed south of Australia were unavailable for study.

Banded cloudiness, usually of the cirrus genus, sometimes occurs in the vicinity of the jet stream, and may delineate the edge of the jet on its equatorward side (Conover, 1959).

Such cloudiness has been observed by TIROS (Fig. 42), but identification as jet-stream cirrus has been possible only through comparison with the conventional analyses. At the present stage, certainly the jet stream cloud bands

Fig. 22 INTERTROPICAL CONVERGENCE CLOUDS
OVER ATLANTIC OCEAN 1525 Z
9 APRIL 1960 R/O 119

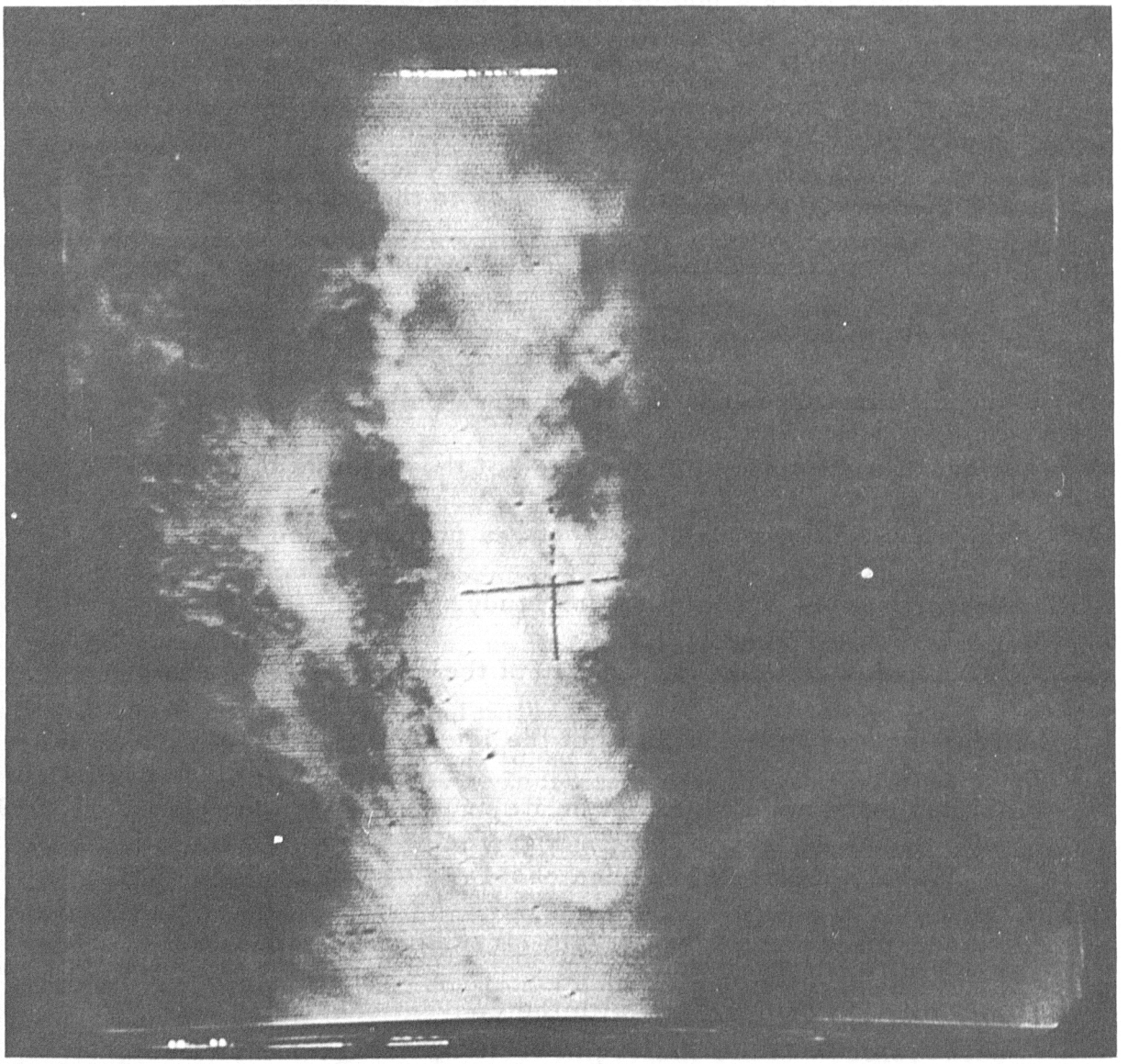

Fig. 23 CLOUD BANDS OVER INDIAN OCEAN 0335Z
23 APRIL 1960 R/O 315

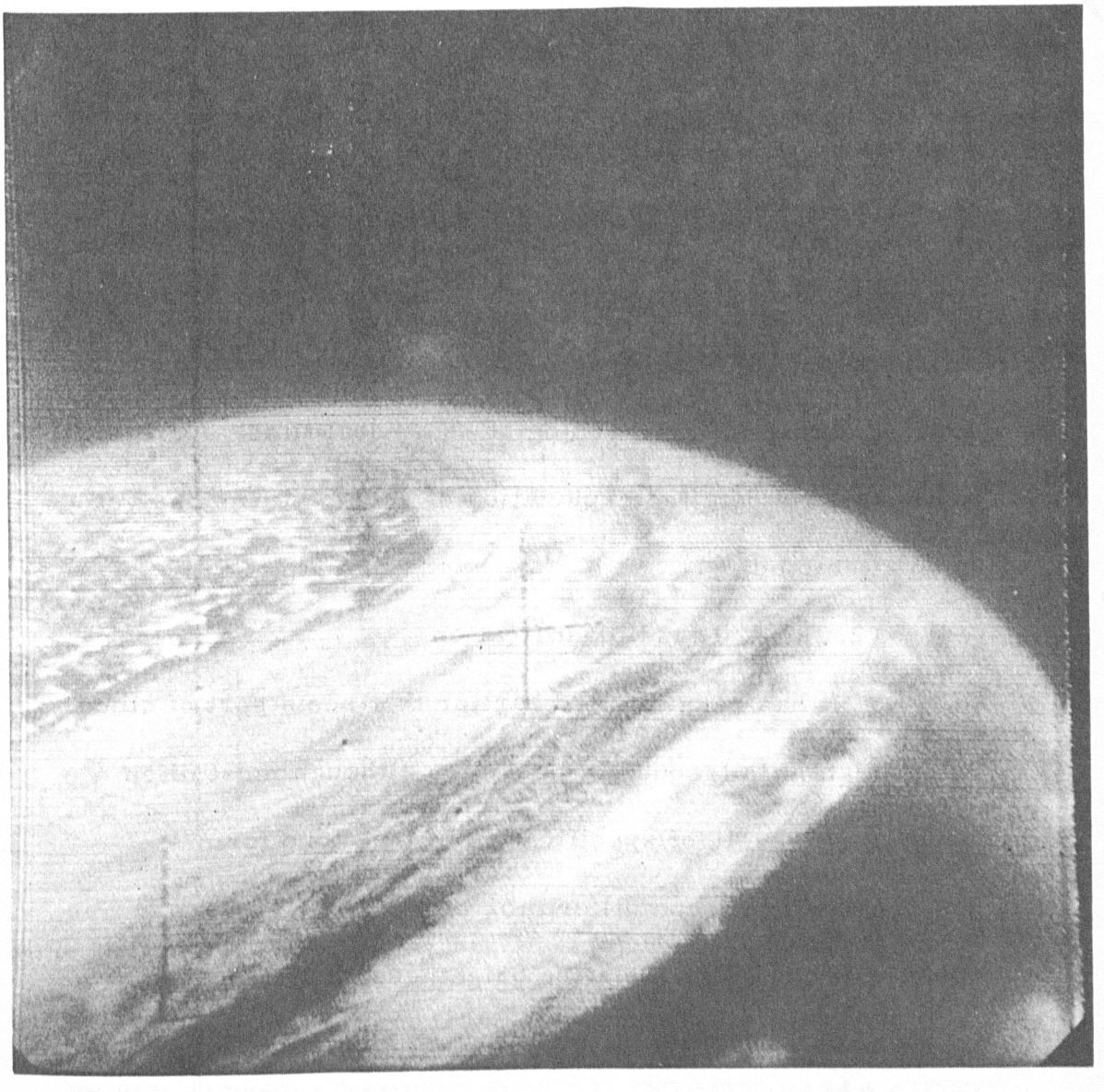

cannot be identified exclusively from TIROS photographs.

2.2.2 Small-Scale Features

Probably the main meteorological surprises TIROS has presented are the extent to which clouds are organized into patterns and the extent to which patterns tend to persist. Many examples of large-scale patterns have been presented. Examples of small-scale organization will now be shown.

Figure 24 is an example of the amount of small-scale organization in clouds which can be derived from a careful analysis of TIROS pictures. This analysis was performed by an experienced meteorologist as a "real time" operational analysis. No detailed explanation of such patterns has yet been attempted.

2.2.2.1 Cloud Identification

It has been implied earlier that some sort of cloud identification is frequently possible, although most often consisting merely of specification of the cloud form--i.e., stratiform, cumuliform or cirriform. Texture, density of coverage, relative brightness, and degree of organization all serve as aids in such identification, as they do on occasions in identifying cloud genera.

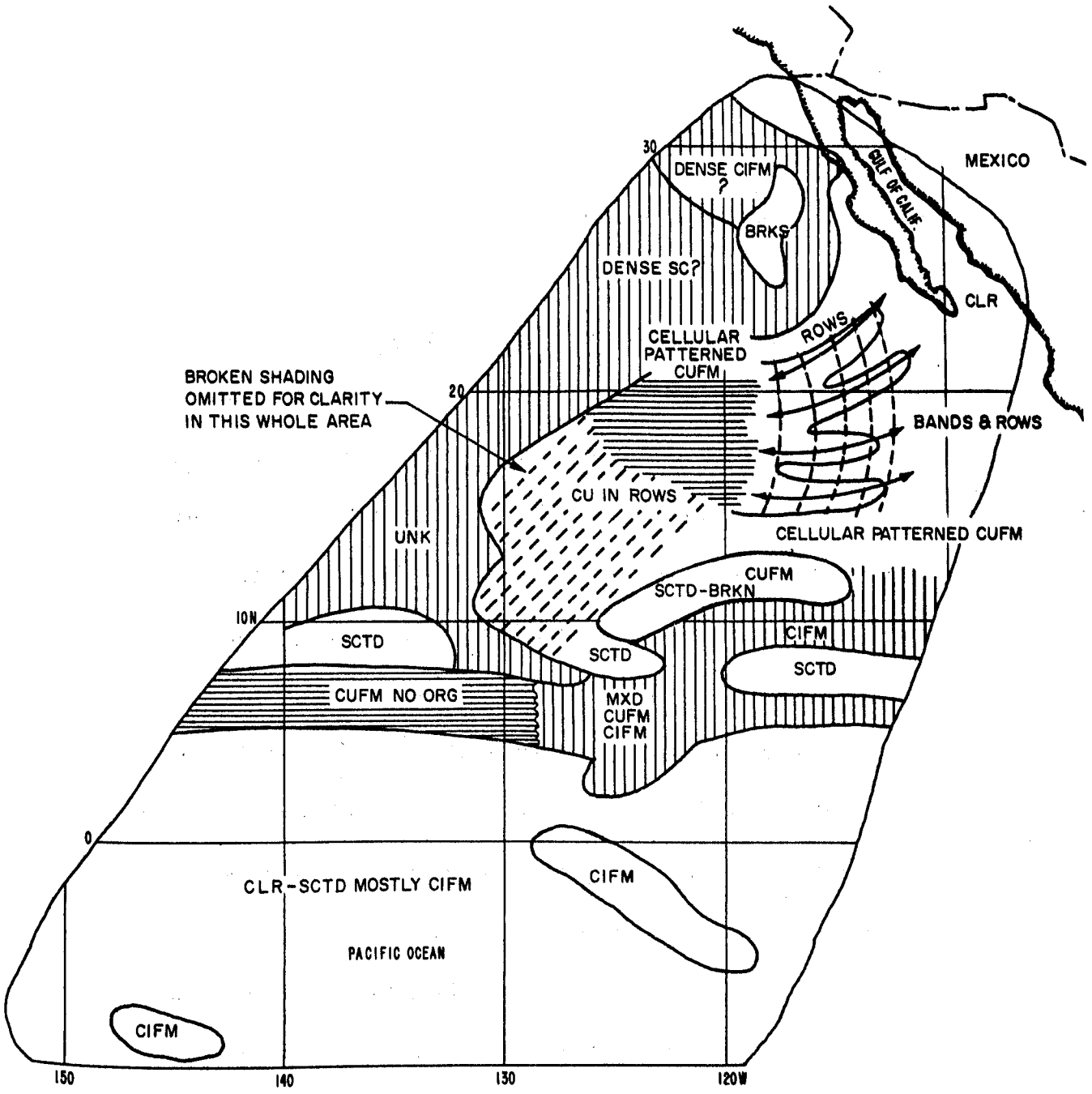

Fig. 24 FACSIMILE MAP OF SMALL SCALE ORGANIZATION OVER NORTH PACIFIC OCEAN 2040Z 16 MAY 1960

The identification of cloud genera is in general more difficult but the difficulty varies with the genera. Of the low clouds, cumulus, cumulonimbus, stratocumulus and once or twice, stratus have been tentatively identified. The TIROS wide angle pictures rarely resolve single cloud elements, except perhaps for giant cumulonimbi, but even these consist of an agglomeration of many individual cells. Recognition is usually done indirectly, cumulus in general being recognized by its "pebbled" pattern and its organization into streets. Examples of cumulus clouds may be seen in Figures 23 and 26 of this section.

The distinction between stratocumulus and cumulus is a rather difficult one to make and has seldom been attempted with TIROS. This is not surprising because of the frequency with which both types are found together.

The middle cloud genera are probably the most difficult to identify and few attempts have been made so far to do so. One factor to be considered is that these clouds very frequently are part of a multi-layered system and are overlain by dense cirrus clouds.

Of the high clouds, only the cirrus genus has been

Fig. 25 CLOUD STREETS OVER PACIFIC OCEAN 2040Z
16 MAY 1960 R/O 659

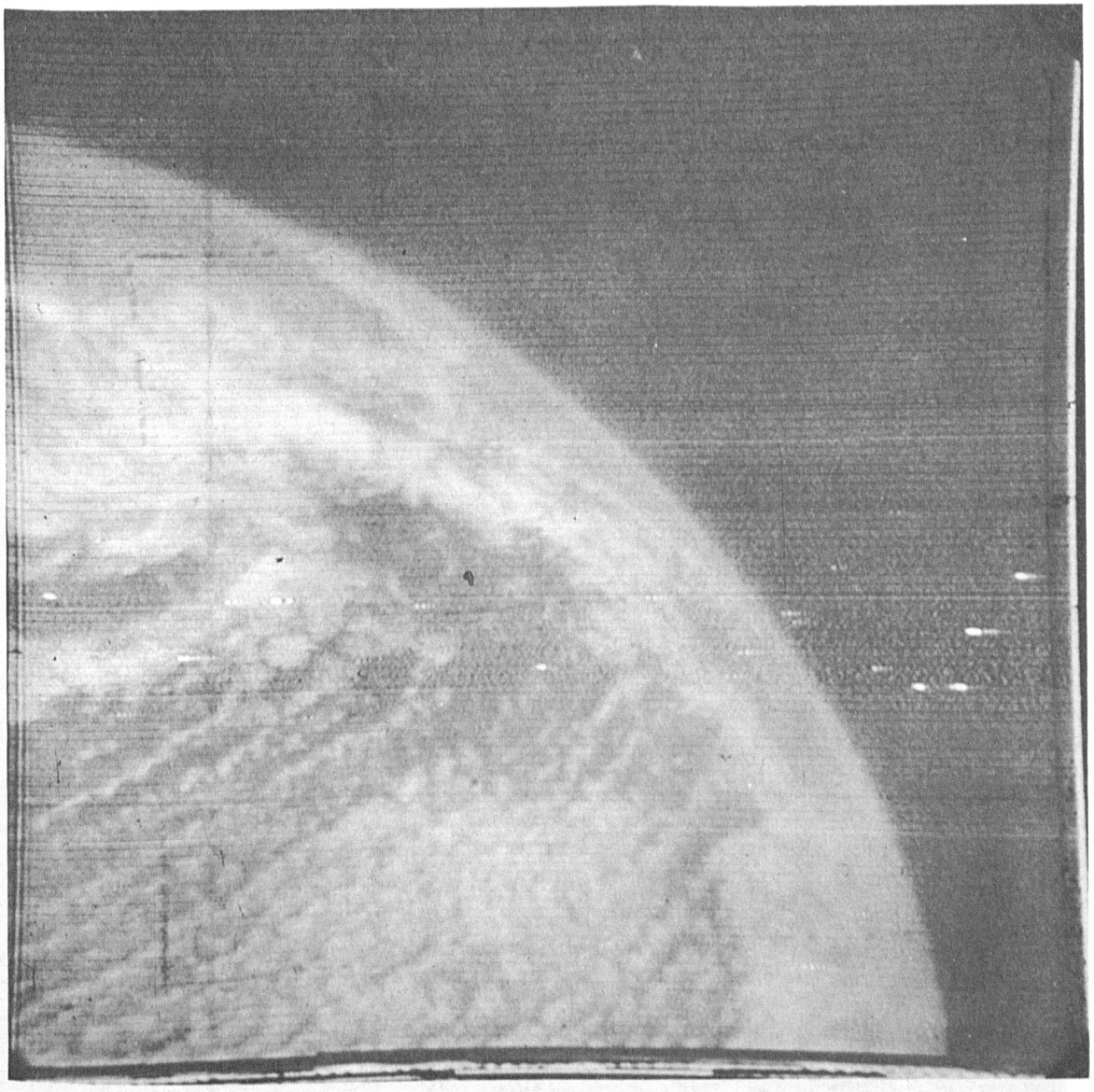

Fig. 26 TRANSVERSE WAVES OVER INDIAN OCEAN
ABOUT 0840Z
23 APRIL 1960 R/O 317

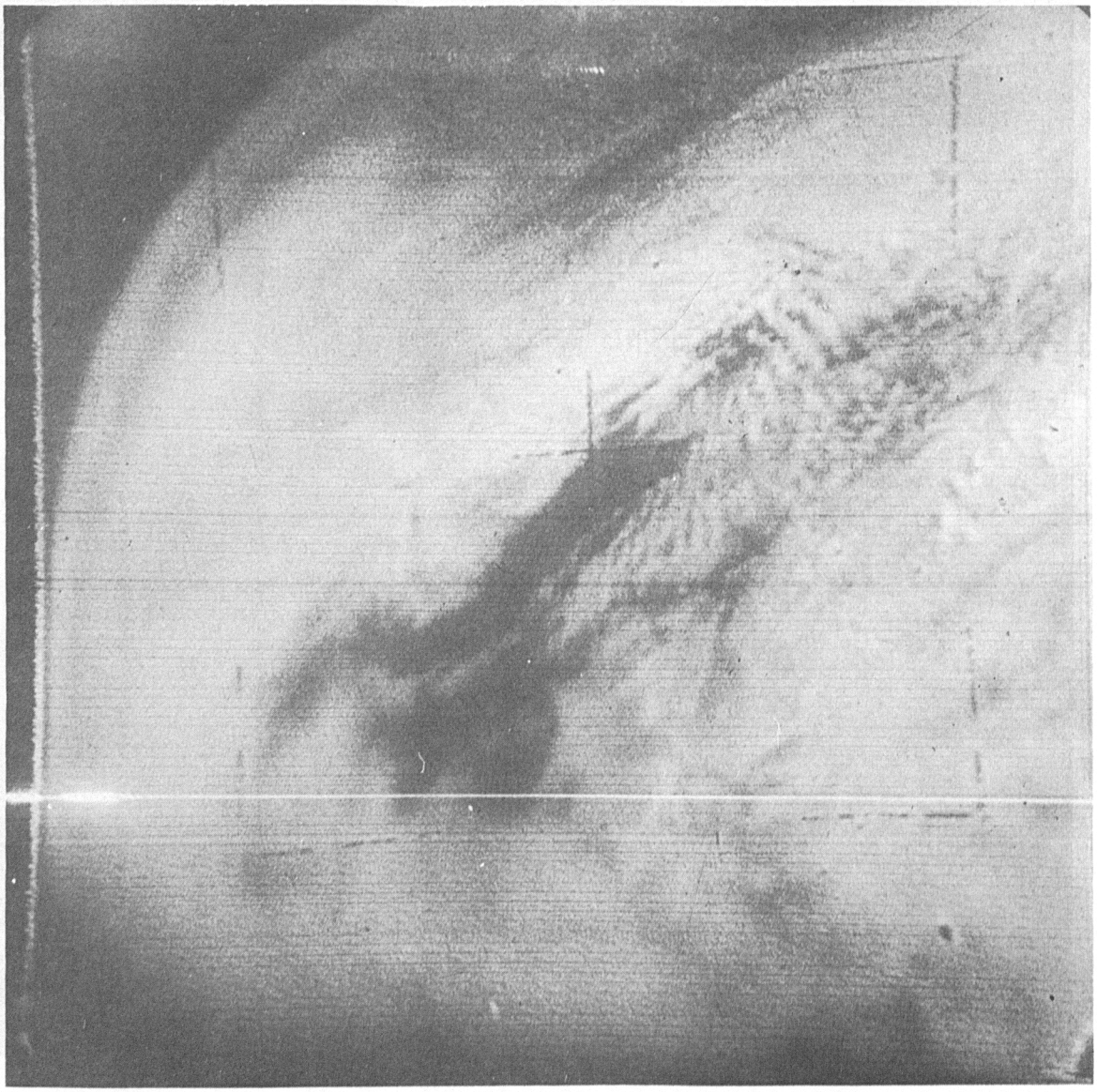

tentatively identified. Such identification has leaned heavily on such features as smoothness of texture, high reflectivity, wispy edges. Some of the examples undoubtedly belong to either the cirrostratus or cirrocumulus genera, so that here again the label "cirriform" is probably the only one justifiable until some positive technique of cloud identification has been developed.

2.2.2.2 Organization

Cloud Streets

The phenomenon of the organization of clouds into streets appears repeatedly in the TIROS pictures. Several examples have already been pointed out as in Figures 11 and 14. Figure 25 shown here is perhaps one of the outstanding examples of this sort of organization. This picture was taken over the eastern Pacific, and displays rows of large cumuli, some of them on the order of 5 to 10 miles in diameter spaced 30 to 40 miles apart. Whether streets can be spaced so closely together as to be unresolvable by TIROS I wide angle camera is uncertain at present.

Transverse Waves

Waves across a cloud band are illustrated in Figure 26 over the South Indian Ocean near Kerguelen Island. Wave length

from crest to crest is about 20 miles. Near the waves, bright clouds which are probably cumulonimbi, can be seen. Close inspection reveals that shadows are visible, indicating apparent vertical development.

Rings and Annular Clouds

From time to time clouds are organized into rings which last for at least 1-1/2 hours (see Figures 1 and 2 lower right). On at least two occasions, TIROS has observed a very interesting large annular cloud. Figure 27 is a photograph of such a cloud off the west coast of Africa; the same cloud was noted by the analyst on the TIROS nephanalysis map, reproduced as Figure 28. Explanations for these clouds cannot be offered with confidence at this time.

2.2.2.3 Vertical Development

Since the TIROS pictures have a resolution of three to five miles horizontally (for the wide angle lens) it is reasonable that cumulonimbi or other clouds having extensive vertical development should be resolvable, particularly in oblique views. Vertical development can be seen in Figure 2 between the vortex and the center cross, as well as elsewhere in the photograph. Vertical development can be deduced in Figure 29

Fig. 27 ANNULAR CLOUD NEAR AFRICA 1740Z
8 MAY 1960 R/O 543

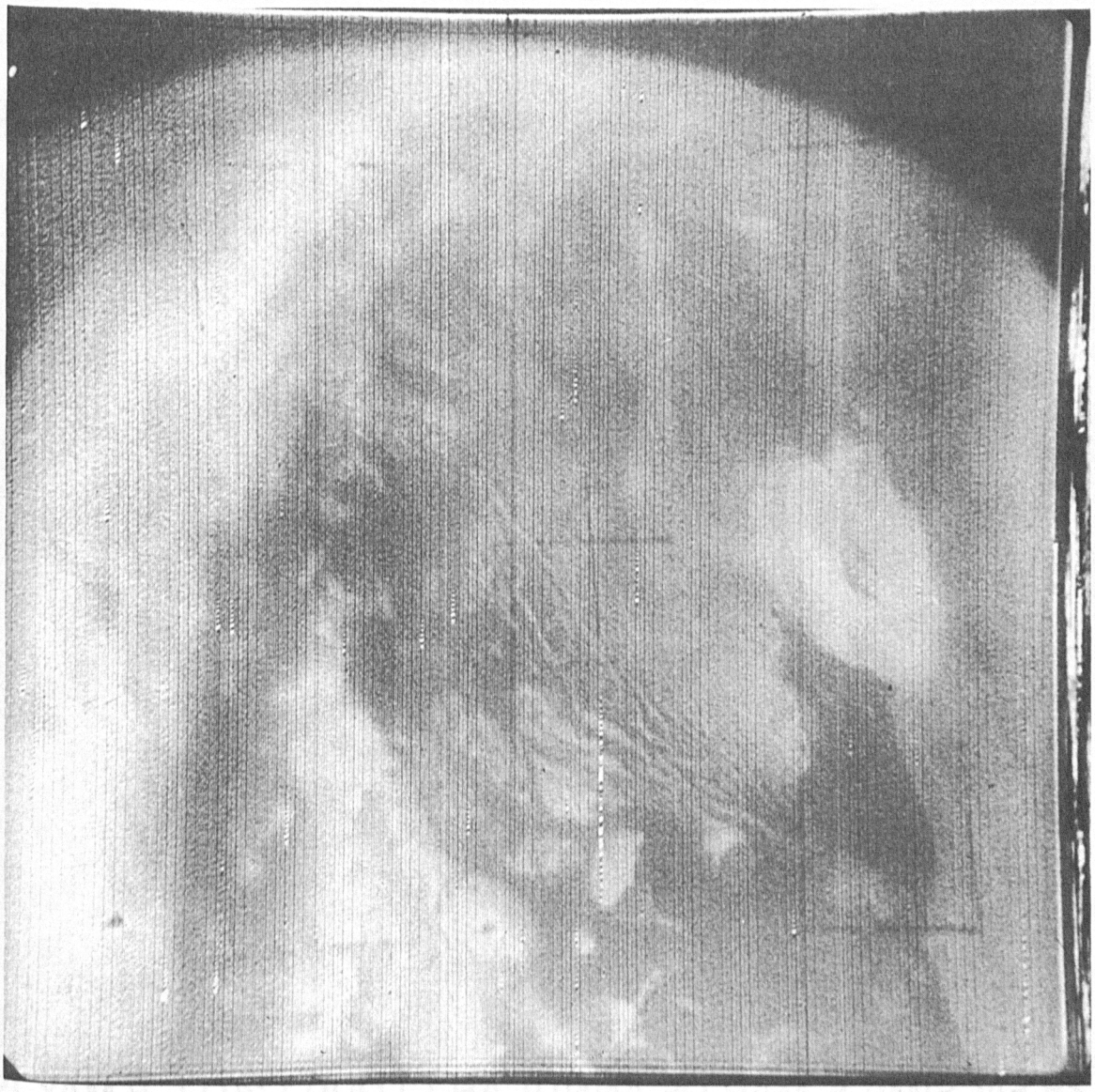

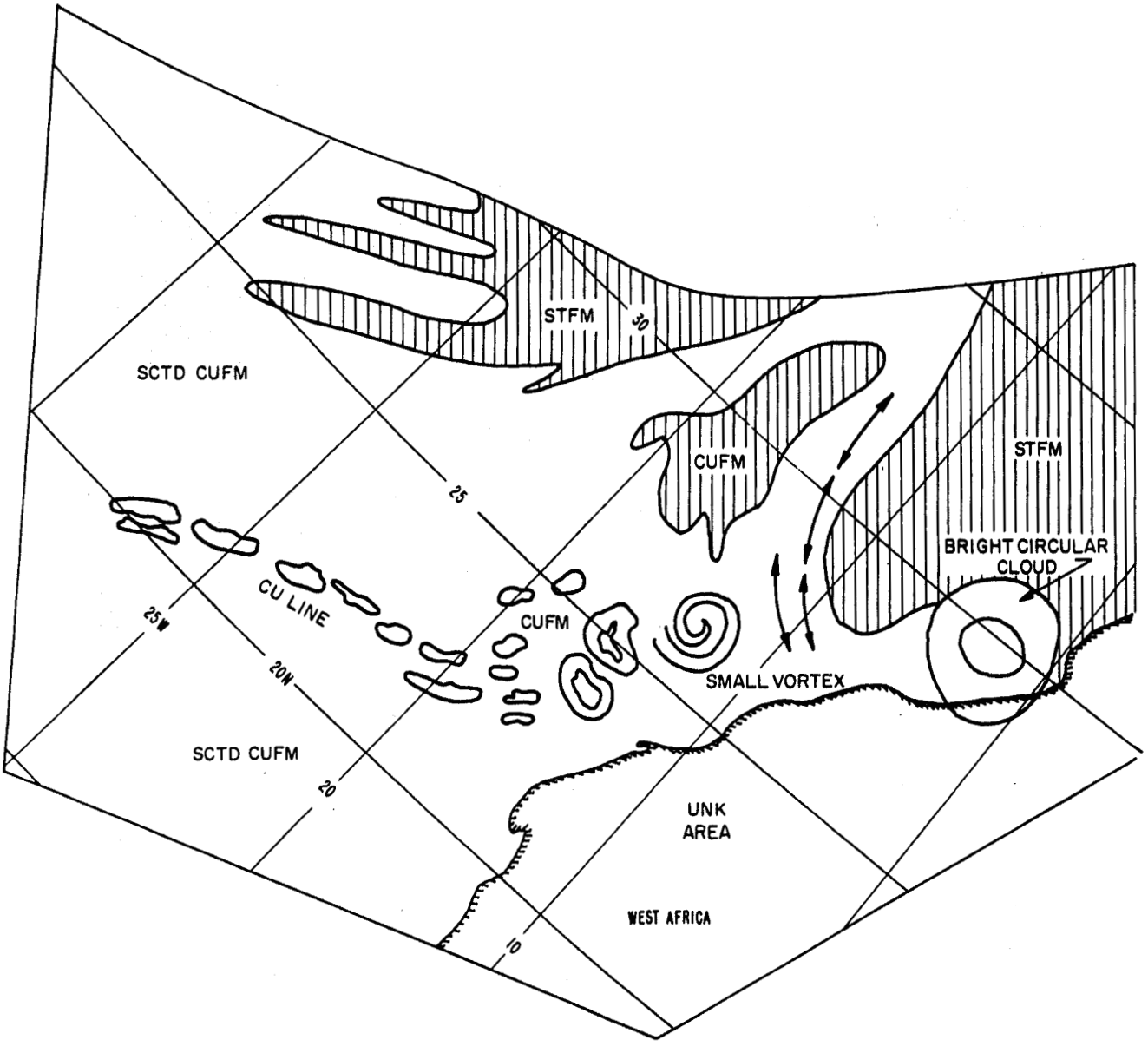

Fig. 28 FACSIMILE MAP OF ANNULAR CLOUD 1740Z 8 MAY 1960

Fig. 29 CLOUD DEPICTING VERTICAL DEVELOPMENT AT SUNSET OVER ATLANTIC OCEAN 4 MAY 1960 R/O 486

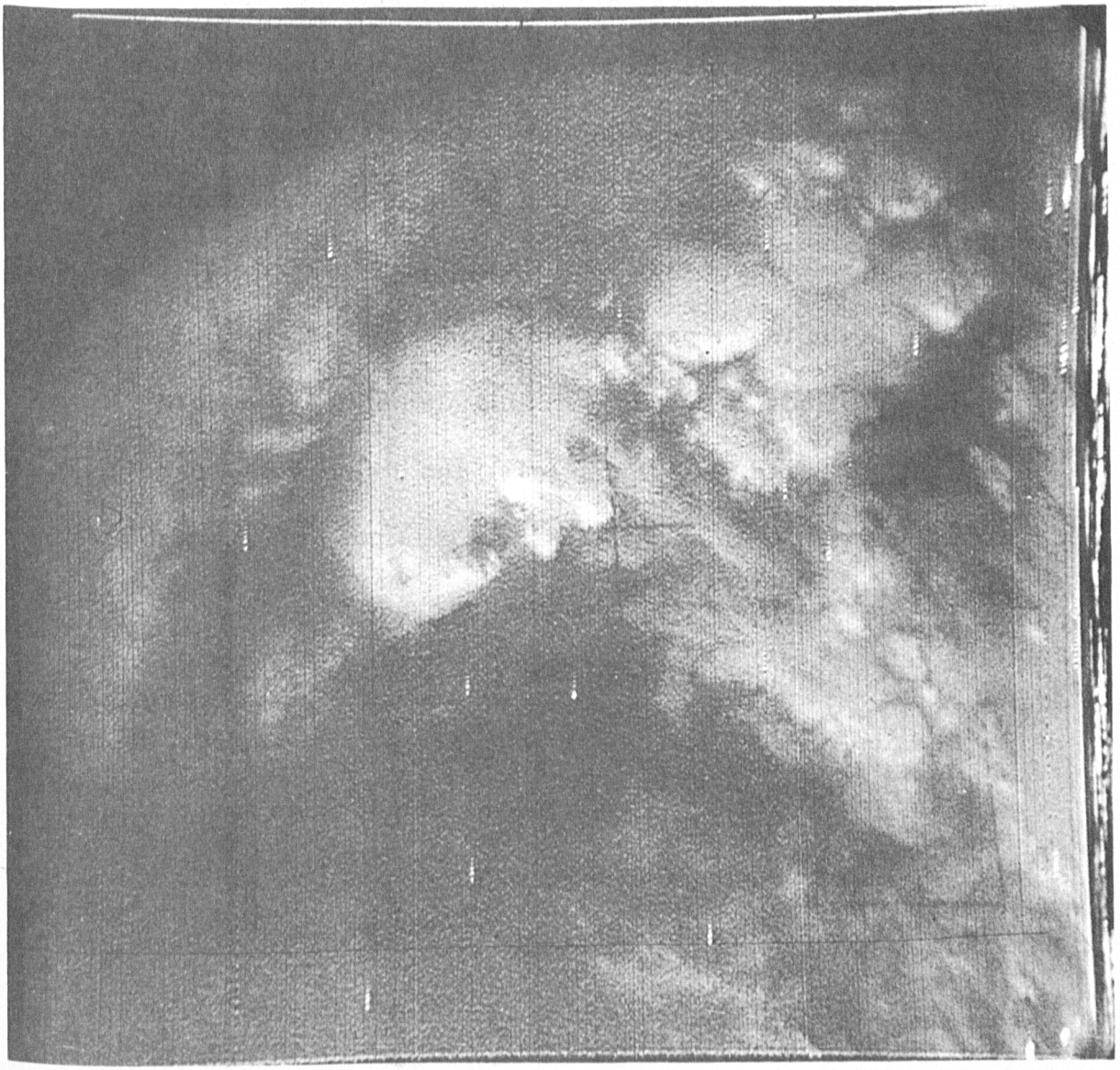

from the lighting of clouds over the South Atlantic Ocean, and it is apparent in Figure 40.

If TIROS is programmed to take pictures as it moves from daylight to darkness across the sunset line, the typical situation is for the clouds to become darker and darker, with the contrast diminishing until cloud features or cloud-earth contrasts cannot be distinguished. Clouds with substantial vertical development may have their higher portions in sunlight while the lower parts are in the dark. In Figure 29 the western portions of the higher cloud elements are still in sunlight. Toward the horizon (east) the clouds disappear into darkness. Thus, in some situations it is possible to estimate extent of vertical development near the sunset line.

Stereo pictures can be taken with TIROS to obtain an impression of depth for clouds possessing great vertical depth or in an attempt to distinguish higher clouds from lower clouds or the ground. Such an attempt was made by Dr. H. K. Weickmann, SRDL, using both 10 and 15 second picture intervals, but the results of this experiment are not presently available (but see Section 4.3.5.1).

2.2.2.4 Orographic Clouds

Outstanding among small-scale features are orographic clouds. They have been seen in many areas over the Pyrenees, the Caucasus, Lebanon, and, particularly the Alps, where a hook-shaped cloud was observed for a week during April 1960. Figures 30 and 31 show this "hook" on 2 and 7 April. The cloud shape conforms to the shape of the highlands very well. In Figure 30 the Mediterranean Sea is visible to the left of the Alp cloud (along with part of Corsica), the upper Italian peninsula lies below it, and the Adriatic Sea is in the lower right corner. In Figure 31 the cloud appears to have a slightly longer hook. The negative from which the print was made is very poor, but the whole Italian peninsula is faintly visible, as is Sicily and the Mediterranean westward to Gibraltar.

In Figure 30 structure is evident in the "Alp cloud." This, together with apparent slight changes of shape from day to day, strengthens the conclusion that the phenomenon is indeed mostly cloud, and not snow, which has also been suggested.

Figure 32 shows the Alp cloud of Figure 30 on a

Fig. 30 CLOUDS OVER ALPS 1115Z
2 APRIL 1960 R/015

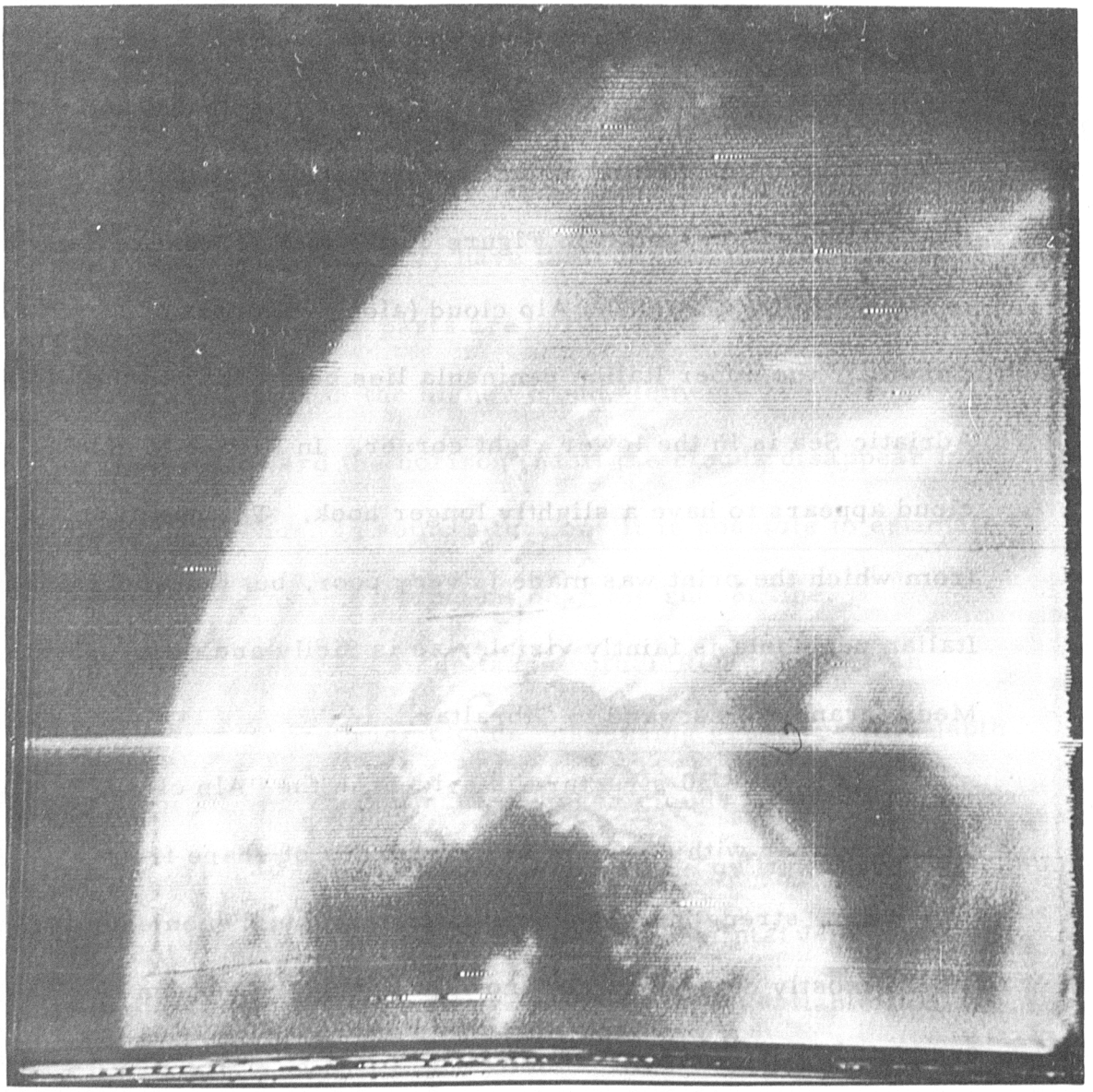

Fig. 31 CLOUDS OVER ALPS 1015Z
7 APRIL 1960 R/087

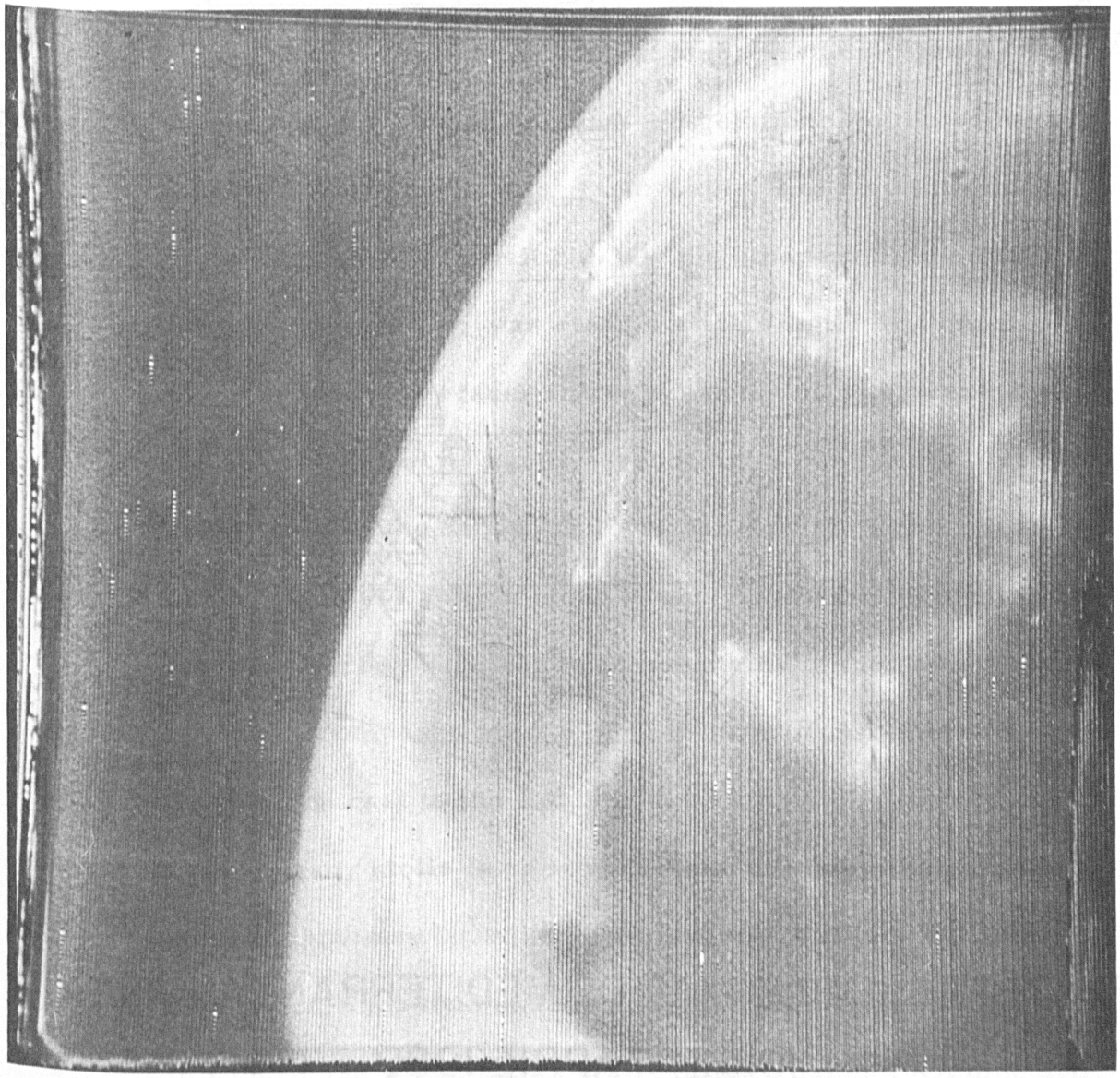

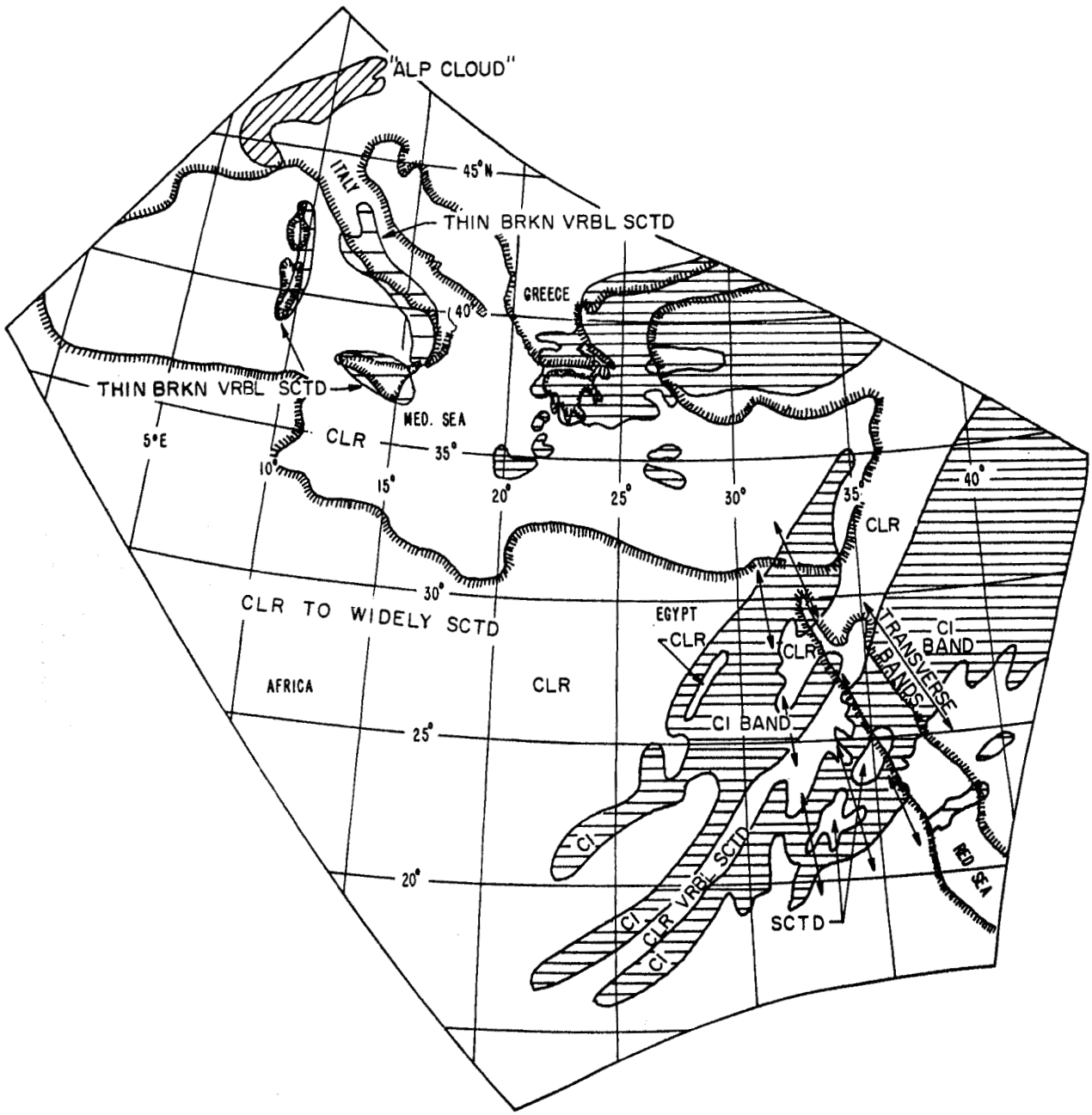

Fig. 32 FACSIMILE MAP OF MEDITERRANEAN AREA
1015Z 7APRIL 1960

nephanalysis map. The map also shows considerable cloudiness over the upper Red Sea, which had been clear 24 hours previously.

2.2.2.5 Characteristics of Land

When TIROS is looking at land, surface characteristics may sometimes be seen. Vegetation is often so dark it is difficult to distinguish from water, and may thus mask the ocean-to-land transition. On the other hand, the Nile River, for example, was clearly visible in the wide angle pictures, partly because the vegetation along its banks stood out in contrast to its sandy surroundings. In general, desert areas such as the Sahara and Arabian deserts appear very bright, almost like thin cloud, when viewed from certain angles. Certain highlands and mountains in the same area, however, composed mostly of rock formations, are very dark in contrast to the sand.

Many atolls have so little land breaking the ocean surface they may be mistaken for wisps of cloud, but their regular outlines tend to reveal them. This effect is illustrated in Figure 33a which shows atolls of the Tuamotu Archipelago in the South Pacific Ocean seen by the narrow angle camera

a. 2225Z 10 MAY 1960
R/O 573

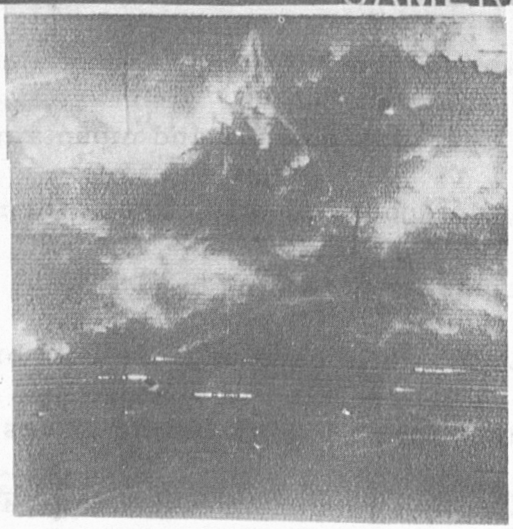

16°
SOUTH

143.5°
WEST

b. PORTION OF a. ENLARGED TO MAP SCALE

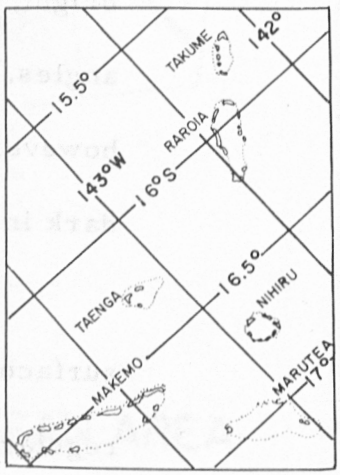

c. MAP OF ATOLLS VISIBLE IN PHOTOGRAPH

Fig. 33 ATOLLS OF TUAMOTU ARCHIPELAGO

at a nadir angle of 45°. (The raft Kon Tiki landed on Raroia atoll of this group after an historic voyage from Peru). A portion of the photograph (Fig. 33b) has been enlarged to show more detail. The accompanying map (Fig. 33c), to roughly the same scale, gives the names and locations of the atolls. Some of the atolls and clouds visible in the enlargement are difficult to distinguish from each other. The relatively poor agreement between map and photograph in places could be due to lens distortion, map error, etc.; we might expect poor agreement, however, since the photograph may be revealing underwater coral reefs not indicated on the map. Portions of the barrier reef off the Australian coast have also been observed, with identifiable features similar to those of the atolls.

Snow or ice cover may sometimes be distinguished. Meteorologically, this is useful information for temperature, cloudiness, and development forecasts. Frozen lakes were visible over Canada in early April. Snow on the Himalayas and Karokorums of Kashmir, an hour and a half before sunset, on 9 May 1960 is shown in Figure 34a, where lower regions are almost dark in contrast to the snow. A portion of the

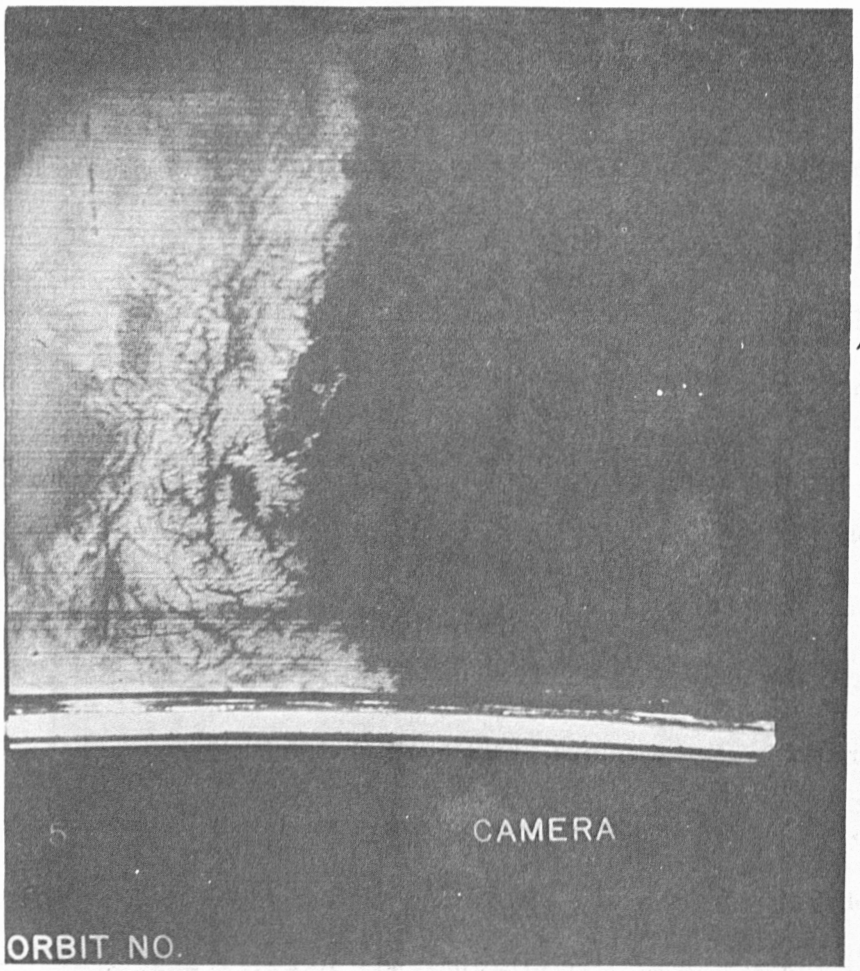

a. 1705Z 9 MAY 1960
R/O 552

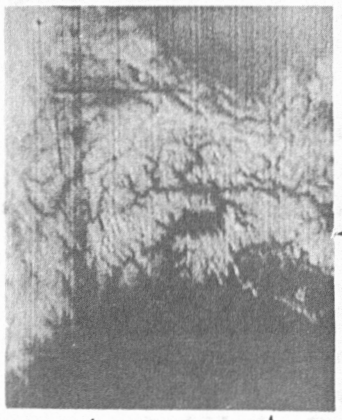

35°
EAST

75°
NORTH

ON OF a. ENLARGED TO MAP SCALE

35°
EAST

75°
NORTH

c. MAP OF TERRAIN VISIBLE IN PHOTOGRAPH

Fig. 34 SNOW ON HIMALAYAS AND KARAKORUMS

photograph has been enlarged (Fig. 34b) and presented for comparison with a portion of a map (Fig. 34c) on the same scale. The latter is from Goode's School Atlas; areas above 10,000 feet are white, areas between 5,000 and 10,000 feet are gray, while lower levels are hatched. The valley of the Indus River can be clearly distinguished in the photograph as a dark area penetrating into the white. From the comparatively good agreement between the contours and the photograph, the conclusion seems warranted that the snow line was generally between 5,000 and 10,000 feet at this time. Although certain especially bright areas in the mountains could be cloud, it is believed the pattern of brightness indicates that mostly snow and not cloud is being observed.

2.2.2.6 Persistence

Cyclones may exist for days or even weeks, so it is not surprising that TIROS is able to see the clouds associated with them for days at a time. A low in the Indian Ocean off Madagascar was observed for five or six days. Orographic clouds also can be persistent. The "Alp Cloud," for instance, was seen for seven days.

The persistence of smaller scale patterns has been

surprising. Patterns in lows often last for 24 hours and the low can be recognized from day to day by its pattern. Figures 11 and 14 illustrate this point.

Unusual patterns can be recalled. A jagged cloud-free area (the "Christmas Tree") seen over the United States on 5 April, lasted at least 24 hours while moving northeastward several hundred miles into the Atlantic (Figs. 35 and 36). In the two figures, the pattern one day appears almost like a mirror image of that on the next. Undoubtedly, many other examples of persistence could be found from the TIROS photographs.

2.2.2.7 Summary

Meteorological phenomena which can be immediately recognized from TIROS have been illustrated by photographs and drafts of facsimile maps prepared operationally on the basis of such photographs. For some cyclones, portions of standard weather maps have been presented to document the photographs and facsimile maps. Phenomena immediately identifiable include cyclones, bands, waves, rings and orographic clouds. Deserts, river valleys, snow cover and other cloud features and characteristics are observable.

Fig. 35 CLOUD PATTERN OVER EASTERN UNITED STATES
ABOUT 1700Z 5 APRIL 1960 R/O 61

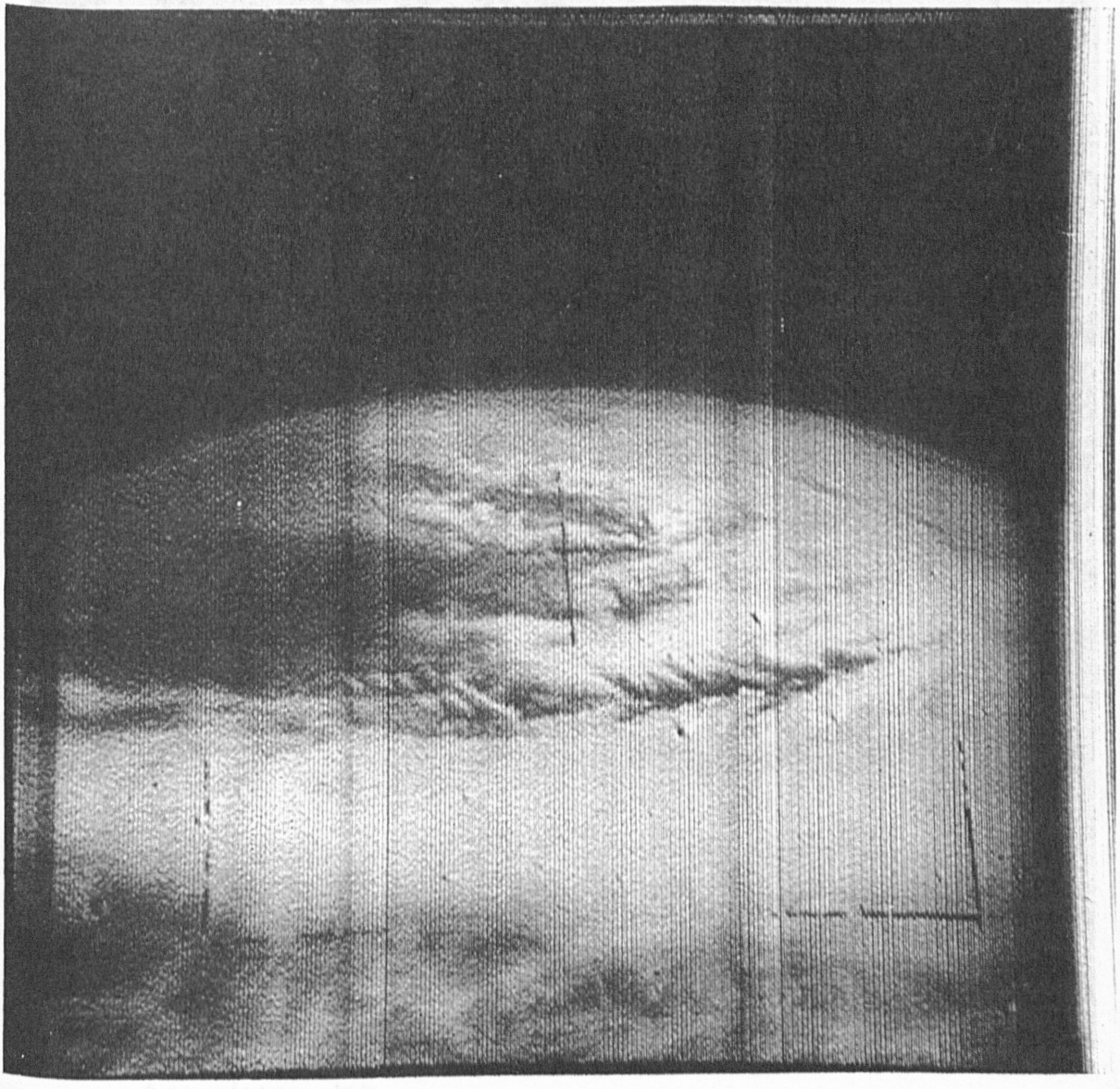

Fig. 36 SIMILAR PATTERN TO Fig. 35 OFF EAST COAST OF UNITED STATES 1610Z 6 APRIL 1960 R/O 75

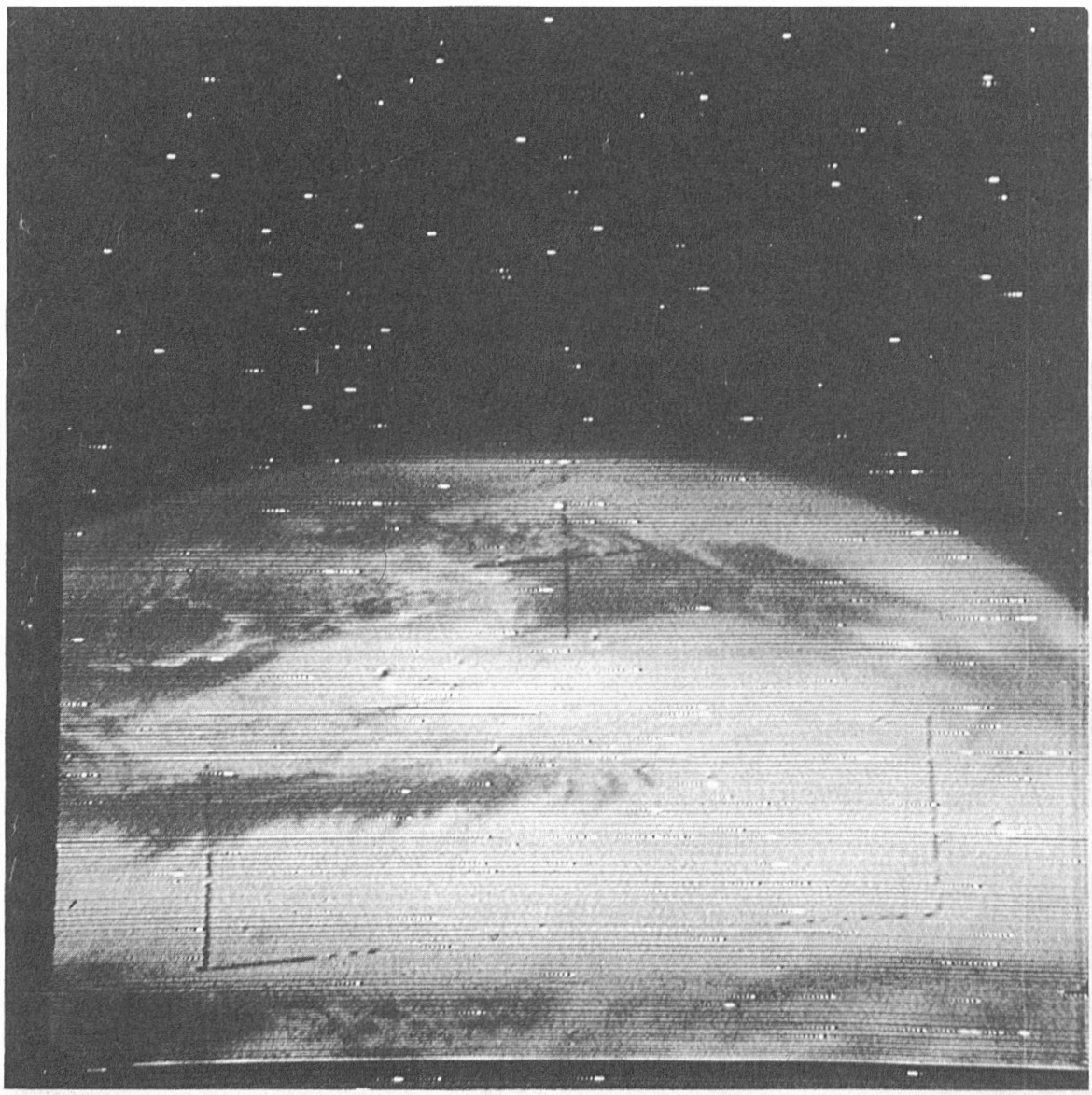

2.3 Additional Meteorological Information Derivable by Inference*

In addition to the meteorological information, more or less directly available from the TIROS pictures as exemplified in the preceding pages, a certain amount of additional, useful information appears derivable. This can be subdivided into: 1) conventional type data which may be used to supplement direct observations in sparse data areas, and 2) diagnostic information which furnishes useful clues to the synoptic analyst and forecaster regarding the weather processes at work, enabling him to make a more accurate diagnosis of the weather situation.

2.3.1 Conventional Data

2.3.1.1 Wind Information

One of the most easily obtained and obvious bits of information is the direction of the low-level flow or streamline flow which may be obtained from the direction of cloud streamers originating at small islands, particularly in the

---

* This Section was written by R. J. Boucher, Allied Research Associates, Inc.

tropical or semi-tropical oceans; see Figure 37. Assuming the islands from which these streamers originate can be identified, they provide an unambiguous indication of the resultant direction of the low-level wind.

It is known from several studies that cloud rows, or "streets" as they are called, usually align themselves parallel to the wind. TIROS cloud photos do not always reveal the individual streets but lines of cloud organization are visible in the TIROS pictures (see Fig. 25) and, presumably, are also aligned with the wind. Here, however, there is ambiguity present since the wind may be in one of two directions, 180° apart. If land masses and/or coastlines are present, this ambiguity may resolve itself since the clouds will generally be displaced inland with an onshore wind, and vice versa. Since the motion vector of any cloud is due to the horizontal components integrated over the cloud's vertical extent, it is not possible to establish a "level" in the atmosphere that corresponds to the indicated wind.

It has been established by several investigators that the narrow belt of high-speed winds at jet aircraft cruising altitudes, usually referred to as the "jet stream," is often accompanied by

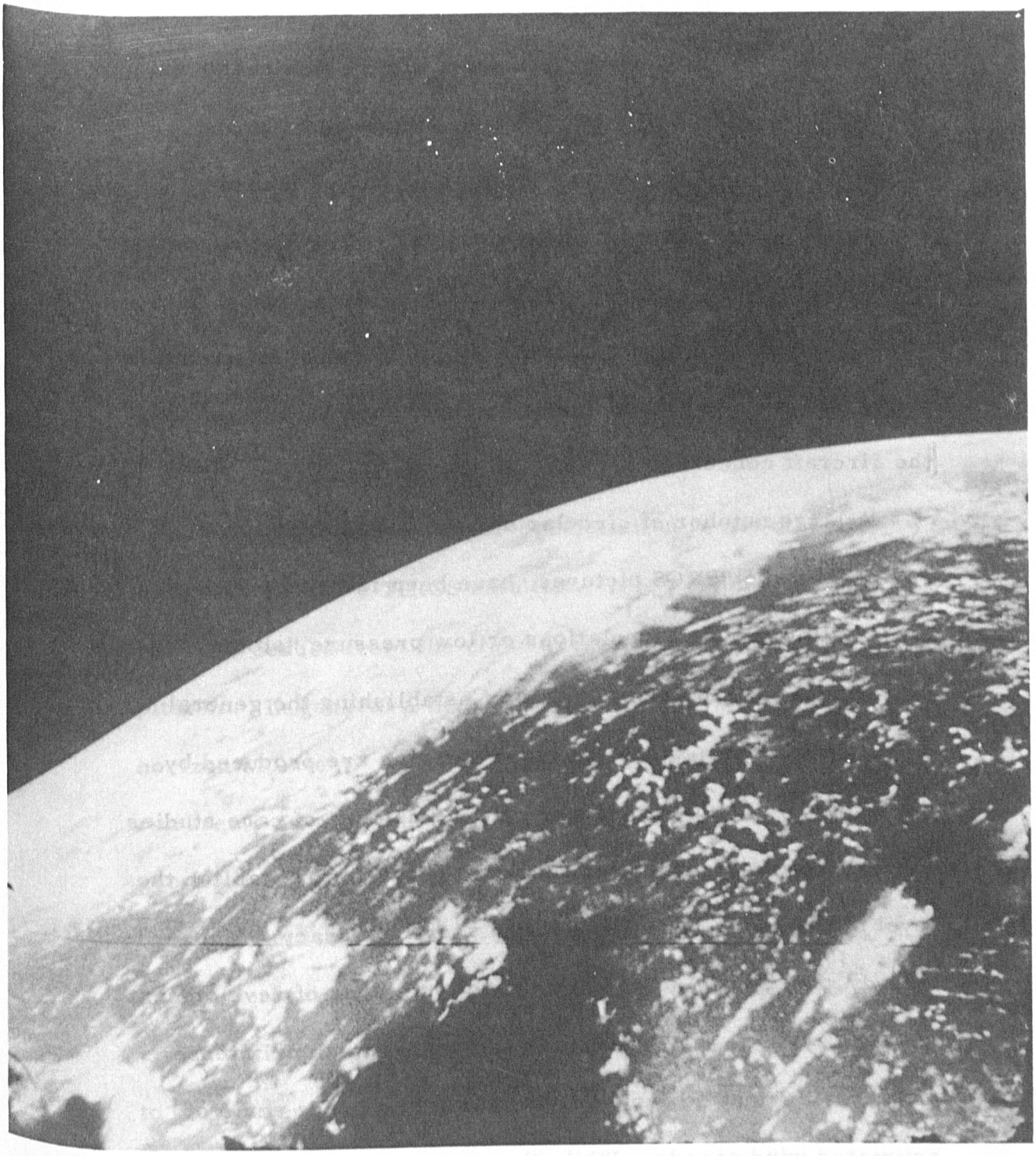

Fig. 37 ATLAS MISSILE PHOTO SHOWING ISLAND GENERATED CLOUD STREAMERS

characteristic bands of cirrus clouds. There is already evidence from the TIROS pictures that these cloud bands can be identified (Fig. 42). We may thus have a means of locating jet streams in areas where the network of upper wind observations is deficient. Location of the jet is of obvious economic and strategic importance since jet stream flying can provide a tremendous ground speed advantage to the aircraft concerned.

A large number of circular and spiral cloud patterns, revealed in the TIROS pictures, have been identified with closed atmospheric circulations or low pressure "storm" centers. This provides a means of establishing the general direction of winds, since the cloud patterns are produced by the wind. With experience and a minor number of case studies and associated research, it should be possible to establish the level of the winds represented with useful accuracy. It is already possible to differentiate between stages of development of these systems, i.e., whether a storm is weak or intense, and this information can be converted into a crude scale of estimated wind speeds. While these procedures will probably never provide a complete substitute for direct observations,

they will certainly be a valuable gap-filler.

To the extent that weather fronts can be identified on the pictures, so can regions of wind shifts be located. The latter may in turn be related to wind patterns on either side of the frontal area, derived as suggested in the preceding paragraphs, to form an integrated representation of the general wind flow over a sizeable area.

2.3.1.2 Precipitation

For obvious reasons, precipitation is not directly observable from a TIROS satellite. It is possible in some cases to deduce from the cloud areas of substantial precipitation. In general a dense cloud mass of considerable horizontal extent, without breaks and of high reflectivity represents an area where precipitation is occurring at the ground in measurable quantity. Where the cloudiness is broken or scattered, areas of precipitation are more difficult to determine except in the case of outstanding thunderstorm activity. In other cases, a probability statement as to the presence of showers or perhaps a percentage of the area likely to be experiencing precipitation would be feasible. Some research is indicated to attain this objective.

2.3.2 Diagnostic Information

2.3.2.1 Vertical Motion

The motion of the atmosphere is generally considered in terms of the horizontal wind produced by horizontal gradients of atmospheric pressure. While the vertical component of the wind is generally small in comparison to the horizontal component, it is very important, since it is the upward vertical motion which produces most of the clouds and all of the precipitation.

With the exception of fogs and low-level stratus, products of cooling from below, clouds then indicate the presence of upward vertical motion. This may take place in restricted areas, giving rise to clouds that only partially cover the surface. This will occur with weak circulation systems producing small cloud elements. Strong local circulations (thunderstorms, squall lines, etc.) give rise to larger elements, exhibiting greater or lesser organization among themselves.

Well-organized storm systems will have rather large areas of nearly uniform upward motion which characteristically produce large areas of solid cloud. Since recognition

of such areas of cloud and differentiation between solid, broken and scattered cloud masses is one of the simpler forms of analysis from TIROS pictures, the upward vertical motion fields can thus be recognized. However, it must be realized that some cloud forms, especially cirrus, will persist in a neutral atmosphere (neither rising nor sinking) for some time and can therefore be transported a considerable distance downwind from the region of active vertical motion where they were produced.

Thus, a qualitative method is available for the definition of areas of upward vertical motion. Any quantitative interpretation will remain difficult, although the recognition of cloud density, and reflectivity do suggest degrees of lift.

Conversely, areas where clouds are absent indicate the presence of downward vertical motion. Again these areas may consist of relatively small but definite "holes" surrounded by cloud, or large areas covering a major portion of a continent or ocean. On the one hand the downward motion is on a small scale, possibly even smaller than the grid size used in numerical prediction techniques. On the other hand, the larger clear areas indicate downward motion

on a scale comparable with that delineated in charts of vertical motion produced by numerical prediction methods.

Thus, TIROS type pictures correctly interpreted, can be used to indicate the areas of vertical motion, the direction (up or down), and a rough scale of magnitude. These data should provide a valuable diagnostic tool to the forecaster and serve to check on vertical motion values derived numerically from analyzed charts.

2.3.2.2 Cyclonic Development

The TIROS pictures have revealed unexpectedly large numbers of vortices which in most cases turn out to be visible evidence of the existence of cyclonic circulations or organized storm areas at some level in the atmosphere. One of the most interesting features is that there appears to be a close connection between the stage of development of the system as presented in a conventional analysis, and its appearance in the TIROS pictures.

In the early stages of a cyclonic (storm) development, the cloud areas are not too well organized although in the tropics the spiral clouds seem to be present from the start. If the system is intensifying, then there will be an area of

dense, highly reflective cloud usually north of the low pressure center. This is the area of continuous and substantial precipitation. A vortex may or may not be in evidence at this point, but as the storm deepens the vortex pattern becomes more evident in the pictures. The dense cloud shield becomes displaced to the east and north of the low pressure center where the steady precipitation is found at the ground while to the west and southwest may appear clear areas or rows of cloud masses or "streets."

The final stage of a cyclonic storm, the decaying stage, occurs after the energy source has become cut off or dissipated. Precipitation then becomes more or less disorganized and there appears to be no nucleus to the storm. Over the oceans a deep storm in this state may take several days to "run down." This decadent condition appears to produce a characteristic pattern in the TIROS pictures consisting of concentric, more or less circular alternating bands of broken cloud and clear spaces (see Fig. 4).

Thus it appears quite feasible to deduce from the

TIROS pictures the stage of a cyclonic development. This is particularly true if the storm can be observed on successive days. The recognizable features appear to change gradually, each storm pattern retaining its identity from one day to the next.

2.3.2.3 Cloud Anomalies

Pictures of the type produced by TIROS I lend themselves to the formulation of a world cloud climatology. In fact such a climatology should indeed be compiled as rapidly as possible in order to obtain a "normal" distribution of clouds, cloud forms and cloud patterns over the world. From the limited amount of data already available, it is becoming very apparent that some areas almost invariably display the same cloud forms and patterns. In others there is greater variability but one or two patterns predominate. In still other regions there appears, so far, to be an almost constant change in cloud form and pattern.

Knowing beforehand the normal type, pattern and distribution of clouds to be expected in a certain region would enable a meteorological diagnostician to readily discern anomalies in those infrequently disturbed areas. A significant

change from one weather regime to another which ordinarily heralds a large scale hemispherical reshuffling of key weather systems should become immediately discernable in the cloud patterns. This would be particularly true following a period of relatively stagnant weather (low index) where the large-scale cloud patterns would tend to show little day-to-day change. The denouement of such a situation should reveal itself by significant changes in the cloud patterns which could furnish useful clues to the impending changes before these become apparent in the conventional analyses, since the latter tend to present a somewhat time-integrated picture rather than completely instantaneous representation of the state of the atmosphere.

SECTION 3

THE ROLE OF FUTURE TV WEATHER SATELLITES IN SYNOPTIC METEOROLOGY AND RESEARCH*

3.1 Introduction

The pictures from TIROS I have already provided a completely new store of information about the atmosphere, as described in the preceding section, and research is expected to increase both the precision and the variety of the data which will be extracted from them. The routine construction of nephanalyses and their experimental dissemination to operational forecast centers have combined to give a clear outline of many of the characteristics and capabilities of these new resources for synoptic meteorology. This section draws on that experience to describe what we consider possible and desirable to work toward in planning the use of the meteorological TV satellite systems that will become available in the next few years.

---

* This Section was written by Dr. C. Dean, Allied Research Associates, Inc.

3.2 The Use of Satellite Data in Global Weather Analysis

A fundamental characteristic of the satellite cloud pictures is their ability to make the main features of large-scale cloud systems apparent to the most casual observer. In effect each picture can be used as a supplementary weather map which is already analyzed. The initial work with the TIROS I pictures has verified that these cloud systems correspond qualitatively to the systems of atmospheric structure which are important in the dynamics of the atmosphere and the pictures themselves now make the research possible to determine the full extent of this relationship. Therefore, it is certain that a major objective of a fully operational meteorological satellite system will be to provide an integrated synopsis of the distribution of weather systems on a global scale, with sufficient frequency to provide what amounts to continuous coverage in time. It seems unlikely at present that satellite photographs will ever provide conventional numerical data of enough precision and detail to replace conventional observing techniques. It is also unlikely that the pictures will lessen the importance of the conventional analyses which require

numerical data. The real contribution of the pictures will be to eliminate the major uncertainties which the analyst now faces every day in dealing with data collected at widely separated points by providing a clear outline of the analysis to which the numerical data must be fitted.

Complete global analyses have long been recognized as a necessity for the development of long range forecasting techniques, and the TIROS I pictures have already shown the ease with which satellite observations permit the extension of accurate analyses through regions for which the conventional data are very sparse. The surprising thing has been the amount of important new detail which the pictures have revealed in the cloud systems over areas with relatively dense networks of conventional observing stations. The value of this new detail is such that satellite surveillance of the weather in these areas will be nearly as important as for unpopulated regions.

Besides increasing the accuracy of the analyses, the satellite observations should increase the area which an individual analyst can study thoroughly in a facility such as the National Weather Analysis Center. This will reduce the

artificial fragmentation of the total synoptic picture which necessarily accompanies to some extent any division of labors, in spite of the care taken to insure close contact between the cooperating analysts. The additional detail contained in the pictures might seem to increase the task of the man who must analyze and explain what he sees, but the ready-made structural framework which the pictures also provide more than compensates for this factor.

The future system will present a unified view of the satellite data for the complete area which an analyst is considering, and preferably for the contiguous areas also. His basic task is to understand his area as a single unit of interrelated weather systems. Any serious fragmentation of the data forces him to spend extra time in synthesis, and any such delay diminishes the operational usefulness of the final weather analysis. An ideal method, although fanciful, might be to print the complete rectified satellite nephanalysis lightly on the synoptic base map by some rapid reproduction process, taking care to insure accurate geographical alignment and location. With the conventional synoptic data plotted on the same map, an accurate and rapid analysis would be assured.

The timing and the frequency of the satellite observations needed to maintain an adequate surveillance of a given area cannot be specified accurately at this time. Part of the research suggested in Section 4 is intended to provide a better understanding of this problem. What is involved includes the amount of persistence shown by the distinctive features in the cloud systems, which determines our ability to recognize the continuity between two sets of pictures separated by a given time lapse, as well as the extent to which the pictures must be synchronous with the conventional data in order to permit a reasonably coherent unified analysis. The early results from TIROS I have suggested that one full view of an area each day might suffice, and that the systems develop slowly enough on the scale that we are considering to permit assembling that view from a mosaic of pictures with a timing discrepancy of several hours. Obviously research on this meteorological problem is needed to insure, for example, that the satellite system design is not unduly complicated by unnecessarily stringent requirements.

It is instructive to list some of the principal specifications that will be met by satellite picture data for use in the

analysis of large areas:

(1) A unified view will be given as much as possible of the area under analysis,

(2) The various parts of the view of a given area will be as nearly synchronous as possible,

(3) The data will be presented very quickly, with a minimum amount of preliminary processing and interpretation,

(4) The data will contain as much of the original picture information as possible, since the significance of many details cannot be assessed fully prior to the combined analysis,

(5) The resolution of the original photographs may be lower than that of TIROS, however, since it is the large-scale cloud organization that is important; and

(6) A single good view of a given area each day may well suffice.

It is not easy to visualize the system that will be finally adopted to meet these specifications. With TIROS I, all large area nephanalyses require synthesis from many

individual pictures. In the I. O. U. experiment this is accomplished in the hand-drawn rectification sketches, a time-consuming process which necessarily suppresses a tremendous amount of qualitative information concerning texture, intricate patterns and shadings of cloud cover, all of which contribute vitally to the total information in the pictures. Elaborate optical or electronic methods may be used to rectify the pictures, so as to allow mosaics to be assembled for large areas. Thus, the future system may be designed with the high precision location and aspect data and with the minimum distortion optics and electronics that would be required for automatic real-time construction of high quality mosaic syntheses.

Although the processing of the photographic data is necessarily rather complex for a satellite at a few hundred miles elevation, it should be realized that comparable coverage is virtually impossible with observations from any appreciably lower elevation. Although the resolution may be so low that each data bit is an average for several square miles of earth surface, we are considering a complete set of such data bits for the entire earth. To obtain such coverage

from an airplane flying at 20 miles, for example, viewing a strip 60 miles wide (a wider field of view than was found fully useful in TIROS I), somewhat over three million miles of flying per day would be needed to provide a one-per-day view of the earth's surface. To obtain an equivalent density of data from surface observations, allowing a radius of view of roughly 20 miles for each station, would require about 150,000 observing stations. Aside from the problem of assembling and analyzing the bits of data, a function which is essentially performed automatically by each TIROS I picture for an area of nearly a million square miles, it would seem that the cost of any such lower altitude system would be orders of magnitude greater than for a satellite system.

On the other hand, it is interesting to notice that the individual photographs as received from a high-altitude satellite, with very little further interpretation, would seem to meet the specifications for large area analysis surprisingly well. According to an analysis of meteorological systems (Cooper, 1959) the optimum altitude would be roughly 4000 miles above the earth's surface, on the basis of a reasonable

compromise between maximum useful area per picture and the increased difficulty of achieving higher altitude. The cost of providing this specialized satellite might be partly offset by simplified communications and drastically simplified preparation of the large-area nephanalyses. The increased speed with which the nephanalyses could be presented to the weather analysis center by itself might justify a considerable expense.

Even for a complete meteorological system a single 4000 mile satellite might suffice. With one orbit about every four hours and with a camera angle of view of about 60°, approximately six pictures per orbit could provide complete global coverage each day with ample overlap between pictures. A polar orbit is not essential for this complete coverage. Long telemetering paths are possible because of the great elevation, permitting considerably more latitude in locating the telemetering sites than is possible for a lower level satellite.

For an early experimental system one might consider a lightweight and somewhat simplified version of TIROS which perhaps could be placed in a 4000 mile orbit in the fairly near

future. Although a circular orbit is distinctly preferable, an elliptical orbit might be acceptable if the camera were aimed downward at apogee. A single 60° camera would suffice and the tape recorder could be omitted, since the high altitude would permit adequate area coverage on direct sequence pictures for the initial experimental purposes. With this angle of view adequate resolution for large-scale cloud system analysis might be furnished by the TIROS camera design. In this application the spin-stabilized vehicle has the distinct advantage that the camera axis direction relative to the earth progresses smoothly according to simple rules, so that the pictures themselves provide enough data for altitude determinations (see Appendix A). Since reasonable pictures would be needed for success of the experiment in any event, the special altitude sensors might be omitted, further lightening the vehicle.

To provide some measure of attitude control for a spin-stabilized vehicle one might consider the use of small reaction motors to reorient the spin axis from time to time on command from the ground station, provided the nutation dampers could work effectively at the slow spin rate needed

for the camera. For the experimental vehicle this control could be quite crude, as it is needed only to insure that the camera will see the earth's surface during a reasonable fraction of the vehicle's orbit over the sunlit hemisphere. Judging from the performance of TIROS I, the control might be needed as infrequently as once in a hundred orbits or more. A reference direction for this operation might be provided by the direction of arrival of the command signal, for example, or simply by the sun.

3.3 The Use of Satellite Data for Operational Problems

The individual features in the TIROS I pictures, which account for the textures of the cloud masses on a gross scale, correspond roughly to the details of a mesoanalysis on closer inspection. Part of the research suggested elsewhere in this report is intended to make the interpretations precise on just this scale. In spite of the detail that was necessarily suppressed in the TIROS I. O. U. rectification sketches, many of the favorable comments that have been received about their use in operational forecast centers pertain to this aspect of the satellite TV data, and it is certain that future meteorological satellite systems will include provisions for the full use of this potential.

The many different questions that can be answered by detailed analyses of satellite cloud pictures have been discussed in Section 2 of this Chapter. The obvious requirements for this new information include a variety of local cloud cover problems for different aircraft and naval operations, many other local details of the existence of possibly troublesome weather for such operations, and the thorough monitoring of meteorological developments in areas of potentially severe storms.

Common to all of these applications are the need for good resolution in the photographs and the need for views of specific and relatively restricted areas on specified occasions, requirements distinctly different from those for global analysis. The areas of interest to most of the operations in which these weather details are important are still expanding rapidly, and it would be prudent to plan the future meteorological satellite system on the assumption of an essentially global interest. The global analysis program described in the preceding paragraphs is motivated by this consideration, in addition to the need for global data in analyzing and forecasting the dynamics of the atmosphere. These analyses will provide the continual surveillance of the world's weather which must be furnished to the

operational forecast centers. These analyses, together with the current operational requirements, will determine which local regions should be inspected by mesoscale satellite photography at any given time.

Although the resolution of the narrow-angle camera is preferable for fine details, the relevance of the TIROS I wide-angle data to mesoanalysis as well as to large-scale cloud systems analysis is one of the most impressive outcomes of the TIROS experiment. This fact could lead to a meteorological system in which the basic data consist of frequent high resolution pictures for the whole earth, from which syntheses would provide the global analyses as described above, and detailed inspections would provide the chosen mesoanalyses. To really meet the operational requirements for mesoscale data, the operations centers would probably need to receive in effect the original pictures. The routine transmission of all the pictures to all of the operations centers, for each to use as it sees fit, seems ridiculous so that presumably only specific pictures would be transmitted upon request.

An alternative might rely on a separate system in which special satellites would be ready to provide operational mesoscale

data on command. If these instruments were sufficiently flexible, they could be used for a variety of research purposes at other times, as discussed in the following paragraphs. The satellite instruments could be made available for local pictures on direct command from the nearest of a selected group of operational centers, although centralized coordination would be required. In a slightly different system there might be a centralized control center which would program the pictures according to specific requests from the operational centers and then transmit the selected pictures to the appropriate centers by high speed facsimile. Certainly it will be necessary to provide for remote pictures, perhaps tape-recorded like those from TIROS, to provide mesoscale information from inaccessible or perhaps unfriendly areas.

As already mentioned in connection with the 4000 mile satellite suggestion, even economics might favor a system built around two or more specialized types of satellite instruments. The combination of operational and research requirements must be met somehow, and certainly it is most economical to be able to control the selection, type, and scale of the data at

the source, rather than to attempt to measure everything everywhere all the time and to maintain a vast data processing center to reduce it to the various forms required for the various purposes.

3.4 The Use of Satellite Data for Geophysical Research

The meteorological TV satellite system which serves the weather analysis and forecast functions described above will also serve many purposes in geophysical research. With the chosen operational functions provided, the instruments will have the maximum additional flexibility permitted by power and weight requirements, in order to facilitate whatever specialized additonal observations the scheduling may allow. One might anticipate, for instance, provision for calibration of the absolute light intensity, a selection of optical filters, polarizers, and perhaps a lens system with a selection of fields of view to vary the resolution of the transmitted pictures for special purposes.

It is only natural that many of the research purposes will be strictly meteorological as illustrated by the range of topics discussed in Sections 2 and 4 of this Chapter. An important additional field of meteorological research is that of accurate

albedo measurements, for which a well calibrated instrument is required, and for which the selection of optical filters would be extremely valuable. In addition to the reflected light intensities from the various types of surfaces, the albedo depends on the average cloud cover over the earth, and on the distribution of the clouds relative to water and land surfaces. The systematic global nephanalyses will provide the first accurate means of evaluating both the long-term average and the possibly significant short period fluctuations in this factor.

A new cloud climatology will gradually be derived from the satellite observations. It will not be limited to considerations of average cover, since high-resolution studies can be used as needed to furnish the finer details of cloud type. An interesting prospect is climatology of high clouds, freed from the bias that local or essentially surface-generated cloudiness gives to ground-based observations. This subject, important both for numerous aeronautical applications and for studies of atmospheric dynamics, should be opened up by the studies to be made on identifying cloud types from the satellite photographs.

The pictures of the earth's surface in clear regions can be

used for a variety of geophysical observations. Important to both meteorology and hydrography will be the indication of snow cover. It also may be possible to observe regions of extensive floods, since the amounts of light reflected by land and water are typically quite different. Other studies are possible, since the shading of land areas in a number of TIROS I photographs show nuances which appear to be related to the terrain.

A separate area of research concerns the sun-glint which can be seen on water when the camera is oriented to receive specularly reflected sunlight. The overall geometry of the sun-glint, the distribution of light intensity through it, and its degree of polarization may be of interest. From this research may come a useful means of measuring the state of the sea over wide areas. A related possibility is a study of the appearance of shallow ocean waters, which may well depend on the state of the sea. Still other oceanographic information which may be accessible to satellite photography includes the location of icepacks, and perhaps the delineation of the major ocean currents which may be distinguishable by color. For such studies as these the flexibility of the satellite

instrument will be important, since the standard meteorological observations would only occasionally involve the right instrumental parameters for the oceanographic work.

Observation of the earth's surface by the meteorological satellites might be valuable from a completely different standpoint. Such questions as snow cover, flooding, drought and perhaps the details of gross appearance such as color, could possibly contribute useful bits of information to our intelligence of foreign territories to supplement the output of the regular surveillance systems if necessary.

SECTION 4

PROBLEMS REQUIRING IMMEDIATE STUDY FOR OPTIMUM USE OF FUTURE SATELLITE OBSERVATIONS

4.1 Introduction

The extreme utility of the pictures obtained from TIROS I, for both practical and for research purposes is apparent to the most casual on-looker. For a few applications the TIROS pictures are useable without any particular study being required. But for many of the potential, more sophisticated uses, various studies and research endeavors are required to answer outstanding questions, to provide effective techniques, and to furnish a firm basis for the practical applications.

It is the purpose of this section of the report to review, in more or less orderly fashion, a number of the studies which we believe are required to continue the growth of the infant science and technology of satellite meteorology. Little attempt is made to evaluate the magnitude of the various tasks. In each case, it is probable that an optimum application of both

imagination and brute force will yield the most useful results.

Characteristically, many of the problems lie on the interfaces between meteorology and other disciplines. Thus, the work can best be approached by integrated groups containing specialists in the various fields required. It affords an excellent opportunity for scientists from other areas to be brought into the meteorological field and at the same time provides an opportunity for the broadening of the sometimes seriously restricted backgrounds of meteorological specialists.

A number of the problems represent somewhat thorny questions that have been sidestepped by meteorological investigators of the past. With the availability of TIROS data and the incentive of more thorough scientific and practical utilization of satellite meteorology data, these problems may be now solved.

4.2 Optical Properties of the Field of View*

4.2.1 Specification of the Cloud Field

4.2.1.1 General

The clouds in the field of view of the television satellite form the primary information source for the relatively complex communications chain that terminates with the operational use of the satellite data. Between this source of information and the consumer of the information there are inserted a number of processes that may be treated as logical filters. These filters restrict the amount of information which can be made available to the eventual user. Sophisticated design would arrange the filters in such fashion that the maximum amount of wanted information would be presented to the consumer, along with as little as possible of unnecessary information, which may be regarded as "noise."

In the TIROS I Immediate Operational Use experiment at least three filters existed between the primary information field in the atmosphere and the consumers in Washington. The first of these was the restricted resolution of the television

---

* This Section was written by Dr. A. Glaser, Allied Research Associates, Inc.

system, which did not permit seeing features of size 3.0 miles or less. The second filter, one of relatively complex nature, was the human link between the picture received on the ground and the message, either coded or facsimile, sent to the operational users.

Analysis of this human filtering process would be most interesting. In a gross sense, the human filter cuts the resolution of the system to a very poor figure, perhaps 50 miles, but on a separate "channel" adds a representation of the texture of the large regions treated. In addition, pattern recognition permits a consolidated description of complicated features which repeat themselves in nature. Commentary on the performance of the human filters indicated that they were usually somewhat "opaque."

A third, somewhat unavoidable, source of information loss was the position uncertainty of the identified information elements. This is another area that may be of considerable interest to study, as the accuracy required in the location of features in the field of view is by no means immediately apparent. It is obviously dependent upon the intended use of the information, or the nature of the information.

A number of investigations are called for to provide sufficient information about the nature of the field of view of the meteorological satellite to permit future system designs. Suggestions as to the means of approach are contained in the following sections.

4.2.1.2 Informational Specification of the Field of View

The field of view may be treated as a two dimensional continuum composed of a number of discrete unit areas. The size of the unit areas can be left arbitrary, since resolution of the system is one of the parameters to be investigated. Each unit area is characterized by a level of brightness. In order to simplify the analysis, it will be convenient to assume a uniform level of illumination for the given picture and reduce the brightness to somewhat more manageable units of reflectance. It may be convenient to quantize the reflectance according to some grey-scale.

The first question that might be asked of a field thus specified is the nature of the Fourier spectrum represented. For a scanning system, it might be sufficient to consider a simple one-dimensional spectrum. However, the obvious patterning and orientation of patterns makes it desirable to

conduct a two-dimensional analysis with appropriate co-spectrum terms.

The results of such an analysis must be studied with some care. It will be necessary to conduct the analysis itself over regions of reasonable cloud homogeneity to permit visual identification of the features that show up as characteristic wave numbers of the analysis. Once this has been done, it will be possible to compare the spectral contributions of various manifestations in the field of view with the utility of the knowledge of these manifestations to the consumer of the information. This, of course, requires detailed knowledge of the requirements of the various potential consumers of the information, a separate investigation.

The availability of the fundamental spectral information will permit a relatively sophisticated analysis of the communications requirements of the system and of savings in communications capacity that may be effected by elimination of extreme redundancy.

Another by-product would be an indication of the feasibility of some form of on-board analysis. This possibility has already been explored (Glaser, 1957) but no actual data were available to perform

116 032

the necessary conclusive evaluation. It may be added parenthetically that, while advances in communication capability may make on-board analysis unnecessary, a similar form of data reduction may be required at some point on the ground to assure the maximum utilization of the hard-won data without burying the consumer under piles of finely detailed pictures.

In addition to its obvious application in the design of future satellite systems, a documentation of the spatial spectrum of the cloud field should be of considerable interest to meteorologists concerned with the motions of the atmosphere. While it can not be claimed that the spectrum of cloud manifestations matches the spectrum of vertical motion, the correlation is quite obvious.

4.2.2 Cloud Composition and Reflectivity

A problem that arises constantly in the interpretation of TIROS pictures is the interpretation of variations in cloud brightness. Elementary reasoning would indicate that the brightest clouds are the thickest. However, it is also obvious that to a certain extent the brightness of the cloud is controlled by the relative position of sun, cloud, and camera. It is not

known, except perhaps in a very general way, what the effect of dropsize distribution or the presence of ice crystals is upon directional reflectivity. A good understanding of these effects is required before successful cloud identification can be possible. Future satellite meteorological systems of higher resolution capability will not eliminate the need for cloud identification by brightness.

Several different approaches might be used to amass the required data. A purely empirical approach would consist in matching up the observed brightness as seen by TIROS with as good a description of cloud characteristic as is available from conventional observation. This will require a somewhat greater level of location accuracy than is currently present in most TIROS data. Hopefully, future TIROS satellites will be better documented. The use of TIROS has the distinct advantage that actual brightnesses are well documented by the calibration and standardization procedures that have been used. As a result, the use of a microdensitometer on film records reproduced from the TIROS magnetic tapes can be expected to give excellent

results. The same cannot be said to be true of most aircraft and rocket photography to date. No grey-scale documentation is available for these pictures, and overexposure seems to be the general rule.

Wherever possible, special high altitude aircraft flights should be made carrying camera equipment of a type well suited to photometric measurement. Extreme care must be taken to assure brightness calibration of the film records and to assure an adequate range of exposure. The use of wide angle or trimetrogon cameras will permit documentation of the relative effects of sun, cloud, and camera positions. If such photographic flights could be made in conjunction with cloud physics type flights, it would be possible to provide full documentation of the internal structure of the clouds to provide a guide for theoretical studies of the relation between cloud composition and reflectivity.

The observational program should be supported by a strong theoretical program, as it will manifestly be impossible to take a sufficient number of observations to cover all contingencies. The problem of scattering from a polydisperse aerosol

is a rather complex one. No general solutions are known to exist. A practical approach would probably involve the establishment of acceptable simplifying assumptions and of suitable approximate methods of solution.

The ice crystal problem is one requiring special attention, particularly for the frequent case of more or less monodisperse and uniformly oriented crystals.

It is quite apparent that a great deal of work must be done on cloud optics to provide useable results. The magnitude of the task should not, however, be permitted to discourage an early approach.

4.2.3 The Sun Glint as an Oceanographic Tool

Specular reflection of sunlight from water surfaces has been seen clearly in many TIROS I pictures. With a perfectly smooth water surface the camera would see an image of the sun very slightly reduced in size by the curvature of the earth. Waves on the water surface provide a distribution of angles of reflection which break up the central image and reduce its intensity, but which also provide specularly reflected image components from a large additonal area of the sea. Thus the sun-glint, i.e., the total pattern of specularly reflected

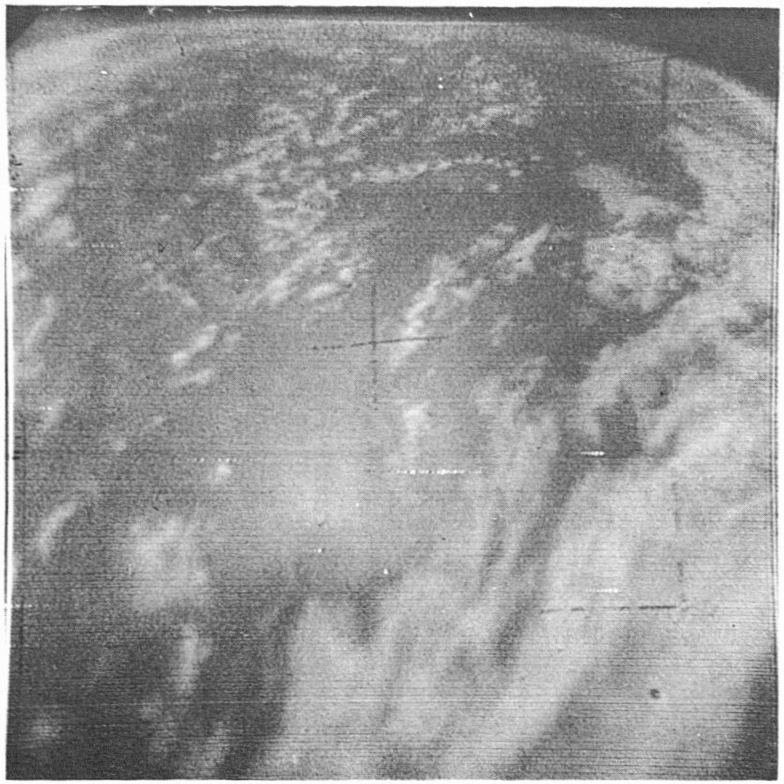

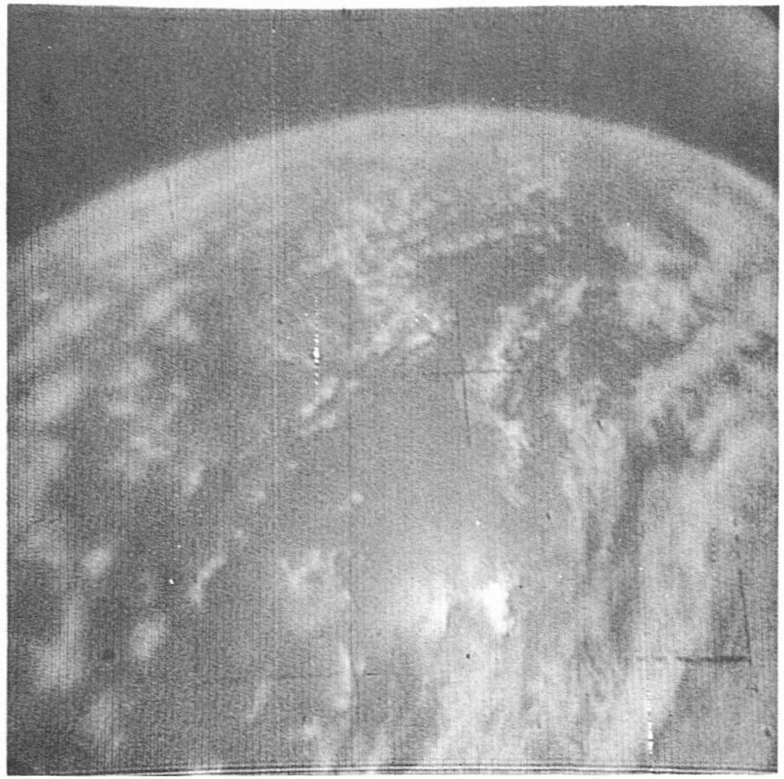

Fig. 38 SUNGLINT ON THE OPEN OCEAN
ON SUCCESSIVE FRAMES
R/O 704

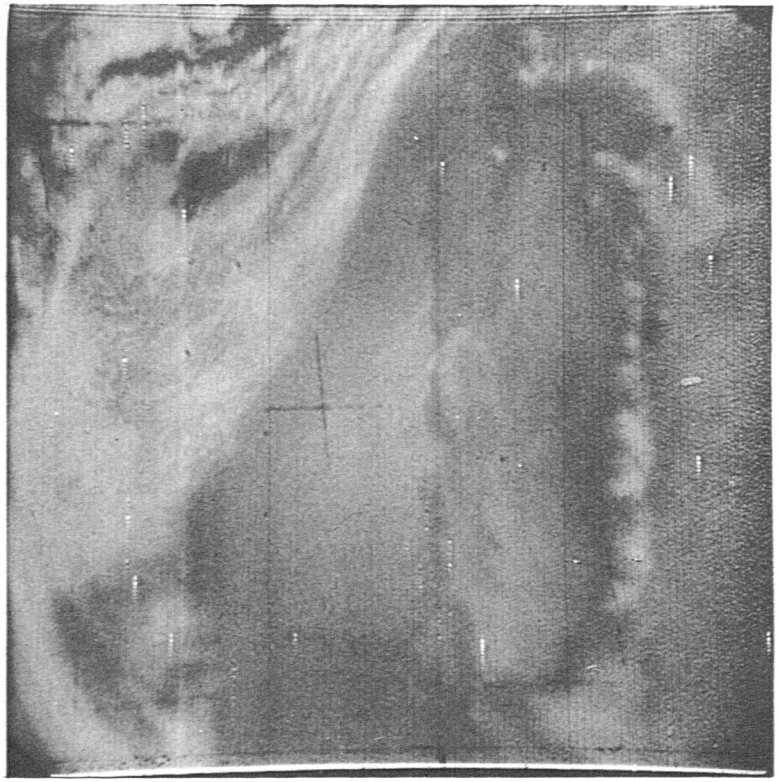

Fig. 39a SUNGLINT ON THE OCEAN JUST OUTSIDE SAN FRANCISCO BAY.

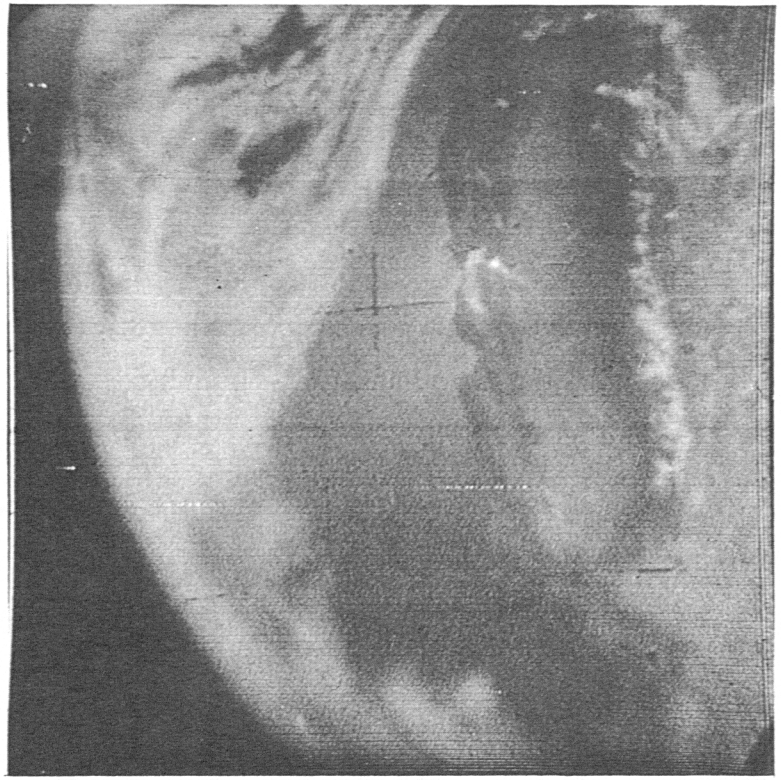

Fig. 39b SUNGLINT WITH PRINCIPAL REFLECTION FROM SAN FRANCISCO BAY

R/O 703

sunlight as imaged by the camera, has a distribution of light intensity and polarization which depends on the state of the sea as well as on the basic geometrical relations between earth, sun, and satellite.

Figures 38 and 39 show examples of sun-glint to illustrate the range of variation that is encountered. Of particular interest is the difference in brightness between the reflections from San Francisco Bay and from the open ocean just outside the Golden Gate. (Fig. 39 near center), it appears from the surface reports that both areas were essentially clear, so that the difference in brightness may be due to the difference between relatively calm and relatively rough water.

The derivation of state-of-the-sea information from sun-glint data has been studied in considerable detail (Cox and Munk, 1954). However such information from satellite photographs would appear unique in the vast areas of the oceans which would be brought under relatively direct observation. For this reason it would be useful to specialize the earlier work on sun-glint for the case of an observation point at the elevation of TIROS I, and to analyze the sun-glints seen in TIROS pictures as fully as possible.

A second objective of this work would be to consider what specifications for future satellites might provide the most useful pictures for oceanographic studies. Elsewhere in this report it has been pointed out that future meteorological satellite systems may be sufficiently flexible to permit scheduling a certain number of special purpose pictures in addition to the presumably standardized cloud pictures. It would be useful to determine what special instrumentation or characteristics might be included to facilitate oceanographic observations.

This research, therefore, would include a review of sun-glint calculations and their specialization to the particular case of TIROS I pictures. TIROS pictures showing sun-glint would be tabulated along with the relevant geometry, and the sun-glints would be analyzed as completely as possible and compared with oceanographic records as available. The purpose would be to determine the usefulness of the technique, list any satellite modifications that would be helpful, and suggest procedures for routine analysis if deemed feasible.

4.3 Cloud Identification*

4.3.1 Introduction

Historically, the identification and classification of cloud forms far outdistanced the early science of meteorology, much as anatomy outran medicine for many years. Experience has shown that cloud studies, of themselves, are rather fruitless endeavors--it is only when clouds are used as indicators of atmospheric processes that cloud analysis acquires significance. As our knowledge of atmospheric processes has increased, a renewed interest in clouds as processes has occurred. It is against this background that the techniques of cloud form recognition from satellite data and their potential utility must be considered.

In the attempts at immediate utilization of TIROS wide angle pictures, positive cloud identification was impossible in most cases. Even the determination of cloud family (high, middle or low) by analysis was quite difficult. But certainly something more sophisticated than merely the identification of bands, vortices or general cloud cover is desirable for the future.

---

* This Section was written by R. J. Newcomb, Allied Research Associates, Inc.

The principal obstacle to cloud recognition seems to be the resolution restriction of the satellite image system. The best resolution of the TIROS wide-angle camera is in principle about 1.6 miles. Under operating conditions, it appears to be only slightly poorer; a value of approximately 3.0 miles looking straight down has been estimated using small islands as reference. An example of the resolution is presented in Figure 40a, a wide-angle photo of the Gulf of California and 40b, a narrow angle photo of a smaller portion of the gulf. The larger island visible in both photographs is Tiburon. The smaller circular island, San Sebastian, is approximately 3.4 miles in diameter. At this resolution, most cloud genera are unrecognizable.

However, despite the resolution restriction, tentative identification of certain cloud genera has been accomplished. Groups of cumulonimbus clouds are often deemed recognizable because of their brightness, vertical development and overall size. An illustration of a line of these suspected cumulonimbus groups is found in Figure 41, taken over western Australia on 6 May 1960. Occasionally identifiable are long bands of apparent cirrus, probably related to the proximity of the jet

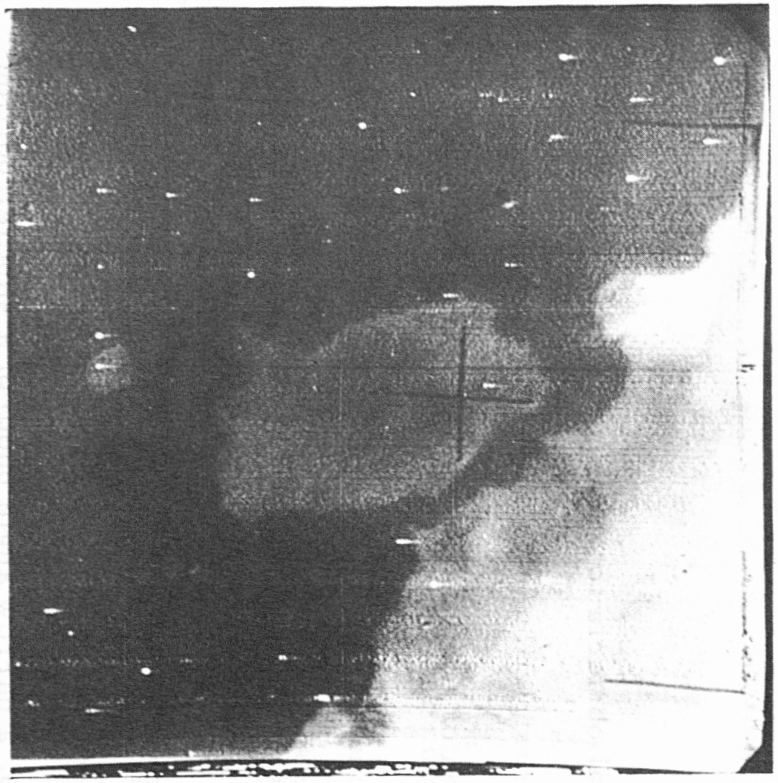

Fig. 40 RESOLUTION EXAMPLES

a. WIDE ANGLE

b. NARROW ANGLE

R/0602

Fig. 41 LINE OF PRESUMED CUMULONIMBUS ACTIVITY OVER WESTERN AUSTRALIA 0746Z 6 MAY 1960 R/O 505

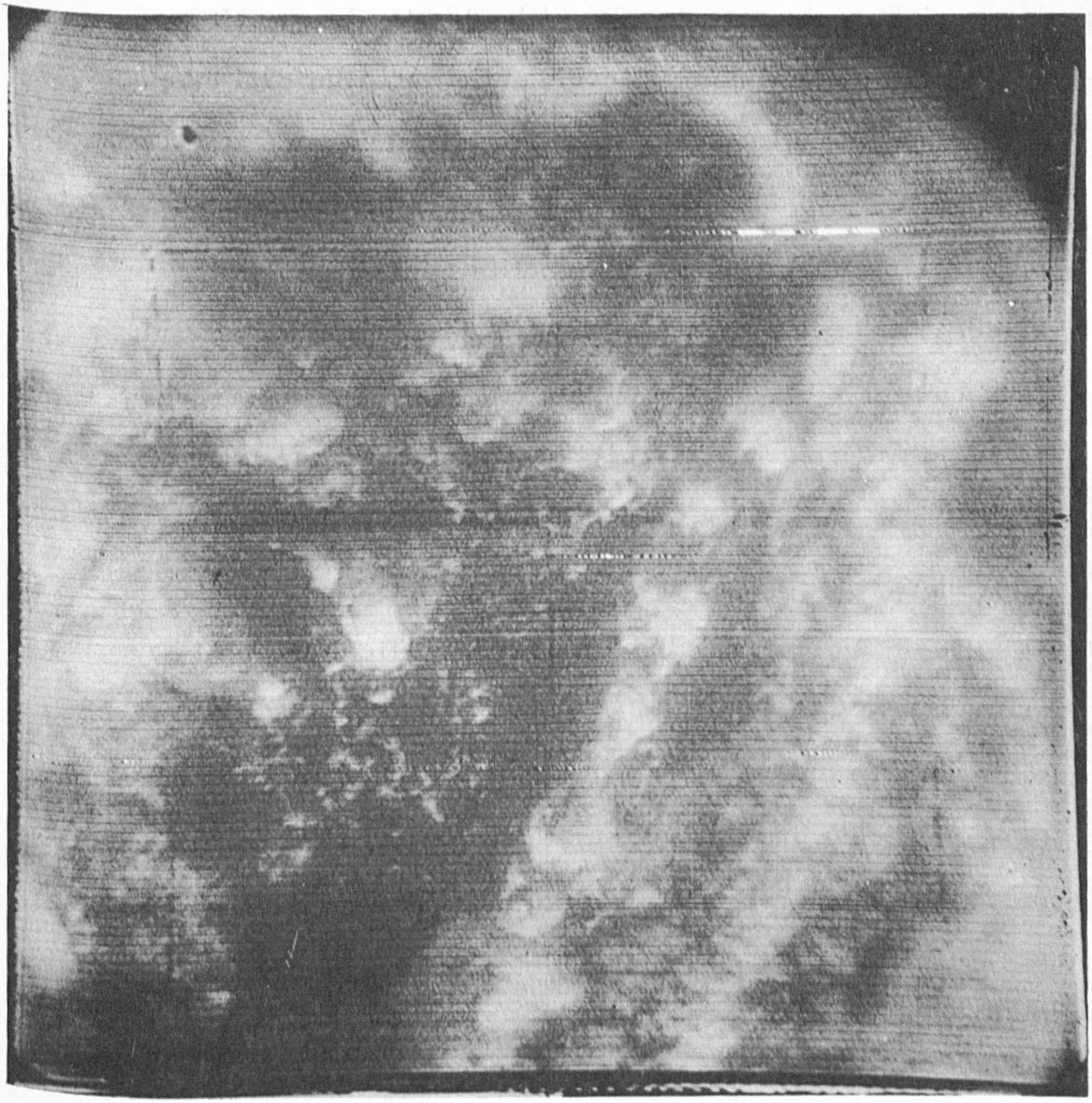

stream (Conover, 1959). An example of one of these bands is found in Figure 42, taken from an orbit over the Indian Ocean on 9 May 1960. A band of cirrus, some 600 miles long and 50 miles wide, is seen to stretch almost the entire length of the Gulf of Aden. Socotra Island is visible at the lower right of the picture, Somaliland in the lower left foreground and the Arabian peninsula at the top. Uniform cirrus was successfully identified over North Africa on 16 May 1960, Figure 10.

A fair number of similar identifications have been made. Frequent major errors occur, however, as a result of attempts to "stretch" the state of the art. These errors stem from erroneous interpretation of the size of cloud elements, from interesting interactions between the scan lines and cloud lines, and from blurring of unresolved elements. As an example of the latter, a field of small cumulus, far too small to be resolved individually, may take on the appearance of a cirrus veil.

Significant progress in cloud recognition can be achieved only with the appropriate expenditure of research effort. The following are suggested methods of approach to some of the

Fig. 42 APPARENT LARGE SCALE BAND OF CIRRUS OVER THE GULF OF ADEN 1156Z 9 MAY 1960 R/O 552

identification problems. A careful integration of the resulting techniques should prove rewarding.

4.3.2 Comparison to Conventional Observations

The most obvious method of learning cloud identification involves the intercomparison of the TIROS Satellite data and conventional cloud data, including the extremely valuable pilot reports. This type of effort will prove to be rather time consuming but fairly productive. It maintains the advantage of utilizing readily available conventional information.

A number of practical difficulties will be encountered, familiar to those who have practiced nephanalysis. In particular, regularly recorded cloud observations at ground stations seldom reflect the pertinent information required for accurate analysis and correlation with satellite data. A listing of the most desirable information might include: the distance and direction of observed cloud forms, an estimation of cloud thickness, the existence of significant bands, and the estimated amount of cloud cover in the upper layers. In some cases pilot reports in the vicinity of the surface cloud observations help to clarify the situation.

At least a partial solution to the lack of detail in the hourly cloud observations could be achieved by the construction of schematic diagrams of cloud cover at each station during periods when the satellite is known to be in the vicinity. It would be desirable to select these stations in coherent groups for the purpose of maintaining continuity from one to another. Three or four of these diagrams per day constitute the maximum requirement for a weather station in the case of a single TIROS type satellite. An example of the suggested schematic representation of a cloud observation is shown in Figure 43. This scheme would establish much of the vital information now lacking in cloud reports.

A program organized around the intercomparison of satellite and ground observations must be well documented so that personnel other than the researchers may obtain the benefit of the experience. It must be recognized that satellite cloud recognition is—and probably will continue to be—something of an art, proficiency in which can only be gained through sufficient experience, the acquisition of which can be facilitated by the preparation of manuals, documented examples, etc. In the long run, however, there is no substitute for long term

experience with a continuous verification program maintaining "quality control."

It may be argued that the increasing resolution capabilities of future satellites will make specialized training and experience in cloud recognition unnecessary. There can be little doubt that the process will be facilitated by better resolution, as evidenced by the narrow angle pictures of TIROS. But these pictures also demonstrate that interpretive skill is still required in many—if not in most—cases.

4.3.3 Comparison to Photographic Cloud Observations

To enhance the utility of the comparison of satellite data to conventional data, more tangible cloud information in the form of photographs offers many advantages. Two distinct methods are available for obtaining this type of data.

High altitude aerial cloud photography would provide excellent resolution pictures from above, approaching the type of information provided by the satellite. The fact that the pictures would be taken from above the clouds is helpful, but does not insure ease of identification. Past experience has demonstrated that even with high resolution aerial

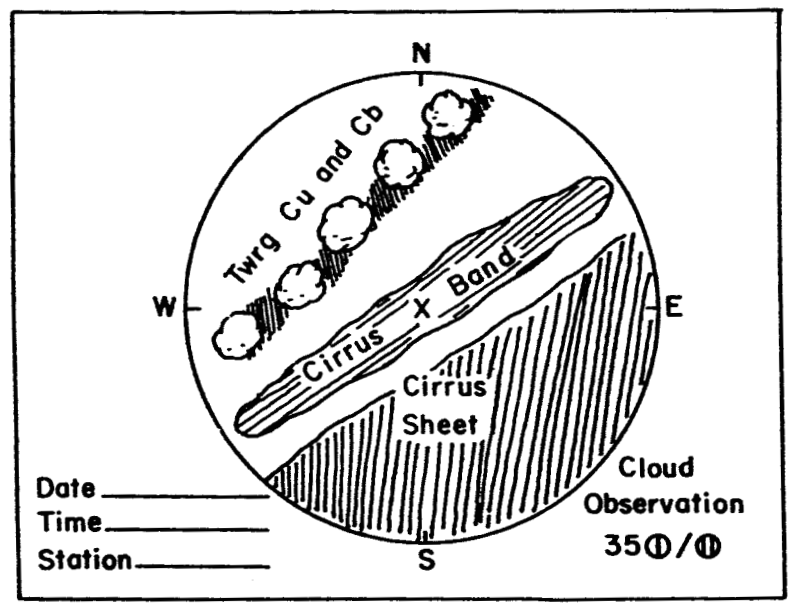

REMARKS:

Cu & Cb 10 Mi. NW
Est Tops 450
Ci Sheet Est
Base 270, Tops
310. Ci Band
About 5 Mi. Wide.

Fig. 43 SUGGESTED SCHEMATIC REPRESENTATION OF SURFACE CLOUD OBSERVATION

photographs, positive cloud identification still requires a certain amount of comparison to conventional data. The principal deterrent to this method, other than the prohibitive cost of routine flights, is the problem of correlating satellite data to aircraft flight data.

A more desirable alternate method is the use of one or more networks of ground based cameras capable of photographing the entire sky. This technique is essentially a more positive form of the cloud schematic method discussed earlier. Here the problem is encountered that the clouds are viewed from below, a definite disadvantage when several cloud layers are present. However, this should present no great problem with the proper selection of sequences for study.

The "whole sky camera" method has the distinct advantage of being much more economical than aerial photography. It should be pointed out here that this type of identification program is currently being pursued on a small scale by the Satellite Meteorology Branch of the Geophysics Research Directorate, United States Air Force. (See Appendix E)

4.3.4 Identification by Inference from Patterns

Even the most casual inspection of the TIROS data

provides an indication of very extensive organization of the clouds into definite patterns. Admittedly present knowledge of the significance of these large scale patterns is limited since their existence had only been suspected prior to recent verification by missile and satellite observations. An outstanding example of cloud organization is illustrated in Figure 2 over the Indian Ocean, depicting an area of large scale cyclonic circulation.

The recurrence of specific patterns has been frequently observed. It is suspected that many less obvious patterns also exist, but have passed unnoticed. There appears to be sufficient evidence to support the concept that cloud forms which constitute these repetitive patterns may be quite similar from one situation to another. Once this relationship has been established it may be possible to bypass the stringent cloud identification requirements to a large extent. This should certainly be thoroughly investigated since it would provide an extremely useful meteorological analysis tool.

4.3.5 Additional Identification Aids

4.3.5.1 Stereo

The application of stereo viewing techniques would provide a most useful implement to aid cloud identification.

This type of information would enable the analyst to distinguish cloud layers one from another and also extract at least approximate estimates of cloud thickness. An initial attempt has been made by Allied Research Associates, Inc., to determine whether or not this is feasible, using a limited number of TIROS wide angle photographs. Some mild evidence of stereo was observed, but it was apparent that more elaborate techniques are required for proper utility of this information. Investigations along these lines are currently being undertaken by Allied Research.

4.3.5.2 Brightness Variation

Variations in brightness of the cloud field are also quite helpful in distinguishing cloud type. With reasonably uniform lighting of the field of view—i.e., relatively high solar angle—clouds of the greatest vertical development appear brighter than other forms. This fact becomes quite apparent when one views presumed areas of cumulonimbus development (see Fig. 41). In contrast to this, areas of limited vertical development take on a greyish cast. Cloud identification through brightness and brightness variation should be greatly facilitated by pursuit of the studies recommended in Section 4.2.

4.3.5.3 Cloud Shadows

Cloud shadows are clearly evident in many of the TIROS narrow angle photographs, and are present in the wide angle pictures. Recognition of shadows is dependent upon the relative brightness of the surface on which they are cast, the sun and satellite positions, and the cloud composition and thickness. When cloud shadows are present, reasonably accurate determinations of cloud height are possible.

Techniques are required to permit ready use of shadows for cloud height determination, taking account of the variations of solar elevation, camera position, and perspective (Glaser, 1957). The mathematical complexity of these relationships makes essential the construction of nomograms or other computational aids.

4.4 Analysis Techniques*

4.4.1 The Self-analyzing Weather Map

The feature of the TIROS pictures that first strikes the meteorological observer is the tendency of cloud elements to group themselves into straight or smoothly curved lines that outline major systems in much the same

* This Section was written by R. C. Copeland, Allied Research Associates, Inc.

way that the isobaric patterns of the conventional map analysis delineate circulation systems. In addition, major fronts are clearly indicated by heavy cloud lines; cyclonic centers become vortex centers; major anticyclones are marked by substantial blank areas limited by the encroaching cyclonic clouds on the one side and on the other by a fan of clouds organized into fractured lines that clearly show the divergent anticyclonic flow. This striking portrayal of basic atmospheric processes has led more than one TIROS worker to call the pictorial presentation a "self-analyzing weather map."

Unfortunately, the full import of this feature had not been fully appreciated when the Immediate Operational Use system of data abstraction was set up by Allied Research meteorologists, even though the Atlas 11C pictures provided a beautiful example. No adequate provision was made for transmitting the "self analysis" from the data acquisition sites to the operational users, who thus obtained the analysis in a form severely limited by the artistic capabilities (for facsimile) or topological skill (for code) of the data abstractor.

Attempts to equate the self-analysis to more conventional analyses (e.g., Conover and Sadler, 1960) show that it is difficult to account for the cloud features on the basis of a horizontal conventional analysis at any single level, although it is probable that most major cloud features will be seen as a synoptic feature at some level in the atmosphere. Thus, it would be difficult to reproduce a constant pressure chart from cloud information.

This suggests that the cloud picture self-analysis, if it is to be used at all, must be treated as a separate form of analysis. Before it can be properly exploited, it must be understood, both from a theoretical and a practical point of view. Programs are required to clarify the nature of the cloud streams that point out definite directions. Are these directions of flow, of shear, or of some more complex vector quantity?

Empirical work is required to derive methods of analysis of the cloud field, methods which will lend themselves to forecast purposes. If forecasting from these analyses proves to be possible—and surely it must be—then forecast techniques and rules must be evolved.

It would appear that the pictorial self-analyzing map will provide the greatest benefits in the tropical and middle latitude oceanic regions. Here the greatest clarity is attained, and it is also in these regions that conventional analysis techniques provide the poorest service. It should be in these under-observed areas that the greatest benefits of the meteorological satellite occur.

4.4.2 Cloud Systems

The meteorologist in dealing with weather data of the past has been accustomed to dealing with identifiable entities that he refers to generically as "systems." When called upon to define "system," he may grow somewhat vague, but still insists on the legitimacy of dividing the atmosphere into a number of identifiable regions of indefinite boundaries, each of which contains a grouping of features that can be manipulated as a mental symbol.

These "systems" can occur on any scale of analysis. Thus, "systems," for the long range forecaster are likely to consist of entire waves in the westerlies. For a meso-meteorologist a "system" becomes a single identifiable cloud complex of a few miles size.

Regardless of the presence or absence of any theoretical justification, the satellite meteorologist also finds himself dealing in systems. In many cases, cloud systems are nicely defined and reasonably well bounded. The characteristics displayed in the region permit recognition of the system as belonging to a definite class and also permit day to day recognition of the same system. Unfortunately, at the present state of the art, a number of situations arise in which the clouds present a confused pattern that does not permit any ready recognition of the central nucleus of a system. It may very well be that after a sufficient amount of experience has been acquired in interpretation of satellite pictures, even these situations will become manageable.

The first step in the use of the cloud system concept as a logical tool in the use of satellite pictures is identification of the various types of cloud system. The most obvious method of approach would be to equate cloud systems with conventional synoptic systems. Thus, the cloud system associated with a surface cyclone would be termed a cyclonic cloud system.

This method of approach seems artificial, as cloud

systems have already been identified with recurring patterns which seem to have no counterpart in regular synoptic systems. Most noticeable of these is the "annular" cloud system, which has been observed in various forms in several areas. Inspection of TIROS pictures has revealed many cloud complexes on a moderate to large scale that exhibit the type of coherence that would make it possible to dignify them with the name of "system."

Accordingly, it is probable that the isolation of types of cloud systems will require a great deal of independent analysis of TIROS pictures. The experience of radar meteorology suggests that some time may go by before a useful systematization can be accomplished, but this should not discourage a vigorous attack.

4.4.3 Continuity of Cloud Pattern

The concept of distinct large-scale cloud systems implies some measure of continuity in time, in addition to the possibility of distinguishing regularly recurring families of similar structures as outlined above. A useful study can take the form of empirical research in which the large-scale cloud distributions are viewed as the independent observable

entities. In this approach one inquires into the time scales over which one can recognize the evolution and motion of the cloud distributions. Such a study can be relatively independent of the attempt to define useful categories of cloud systems, and thus it provides a relatively unbiased test of the concept itself.

This research would have some bearing on the relationship between cloud organizations and synoptic systems. Certainly the clouds should reflect to some extent the day-to-day continuity of the dynamic (synoptic) systems with which they are associated. Conversely, therefore, it would be valuable to determine what cloud features do show strong continuity, for presumably these features would be the ones with the most fundamental connections to the dynamic systems.

Operational forecast purposes would also be served by empirical research into the continuity of cloud distributions. Although each operational problem demands an assessment of many different weather factors, common to each seems to be the fundamental need to establish quickly the location and extent of areas of unfavorable weather. According to the response of a number of operational centers to the TIROS

nephanalyses, the large-scale organization of the cloud systems as seen in the TIROS pictures apparently describes the distribution of this crude binary function in a way which is immediately useful for all applications. Thus the results of the study would relate directly to an operationally significant concept, and they could be applied directly to guide nephanalysis extrapolations in operational forecasting.

Among the many purposes of the TIROS experiment is that of obtaining evidence on whichto base the specifications of future operational weather satellite systems. Here again the question of the continuity of cloud systems is important, for it bears directly on the frequency with which the nephanalyses will be needed in order to provide adequate meteorological surveillance of any given area.

The empirical study by no means implies an artificial attempt to analyze the TIROS I pictures without regard to available synoptic analyses. The intention is rather to insure that a portion of the overall program of research in satellite meteorology will be directed toward an important specific question which the pictorial data are ready to answer directly, and for which the synoptic data can be regarded as merely a

useful supplement. That the problem of cloud system behavior is indeed such a question is shown by the fact that it required the TIROS I pictures themselves to demonstrate to us the majestic scale on which the cloud systems are really organized.

Following a listing of the geographical areas covered by the available sequences of TIROS I pictures, cases would be selected which permit as many days of essentially continuous coverage of an area as possible. Rectified nephanalyses for these cases would be progressively refined to include all details that appear relevant to the problem of continuity. These nephanalyses would be compared with analyzed synoptic maps and conventional nephanalyses when available, and diurnal effects would be considered and taken into account when possible. The presentation of results would necessarily depend on the outcome of the investigation. At a minimum the completed analyses would be valuable as individual case studies. Beyond this, however, it is anticipated that empirical cloud forecast rules could be formulated, and the work should certainly assist other research projects in the classification of cloud systems and in the study of their relations to dynamic systems.

4.4.4 Integrated Analysis Techniques

It is apparent that one of the largest problems in the use of satellite meteorological data will be the effective integration of material observed by the satellite with that collected through conventional sources. A number of difficulties are apparent with casual inspection. Let us review some of these.

Conventional meteorological data are essentially point data taken at one of a number of points on an irregular grid. The satellite information, on the other hand, is continuous in the horizontal plane. This continuum may be regarded as a series of point data but the spacing is very much finer than that available with conventional observations. Most of the information available from the conventional observations is quantitative; that from the satellite is notoriously qualitative. These differences in fundamental nature of the data make integration a knotty problem.

The first reaction of most meteorologists of TIROS is that they would like to see a rectified projection of actual cloud pictures superposed on a conventional macroscale weather map. This would then serve as a guide in performing

the conventional analysis. The weakness of this approach is that it does not take full advantage of the wealth of material contained in the satellite pictures. It is difficult to find the appropriate level in the atmosphere to which the clouds must be assigned; thus, clouds delineating high level circulations will add little to the understanding of the analytical features of a surface weather chart. Somewhat modified analytical techniques must be found which will give appropriate weight to the satellite observations.

A number of analytical situations may be considered. The first, already discussed in the previous section, would occur where only satellite information is available and the eventual application of the analysis would be directed toward forecasts of material similar to that contained in the pictures. If on the other hand, it is desired to forecast the meteorological variables more accessible to conventional analysis, it will be necessary to convert the cloud analysis to something approximating a conventional analysis, possibly with the aid of whatever scattered conventional observations are available. While it is probable that some success would be attained even now at such an endeavor, it is obviously required that systematic techniques

be evolved for performing this transformation.

Where ample quantities of both conventional and satellite information are available, the form of analysis may be dictated by the eventual utilization of the analysis. If it is intended for forecasting of variables well represented in the satellite pictures, the analysis probably should take the form of a nephanalysis supported by conventional information. Techniques are completely lacking here.

If the analysis is to be used for forecasting of winds or temperatures, conventional analysis techniques are probably preferred. Here the problem becomes one of devising appropriate techniques of presentation of the satellite material in a form permitting ready use. It is probable that initial development will be along these lines, if for no other reason than this route requires least modification of analytical procedures and concepts.

It is difficult to prescribe a plan of attack at this time. Initial attempts at analysis will serve to indicate problem areas and may suggest techniques. A sample "first approach" appears as Figure 17, showing an analysis for 11 May 1960.

4.5 Data Processing and Presentation*

The experience of the I. O. U. program of TIROS I has sharply pointed up the necessity for the streamlining of data handling and processing procedures. Two somewhat interrelated problems exist--that of satisfactorily locating features seen in the pictures, and that of making a satisfactory map presentation of the features seen. While each of these is essentially a geometrical problem,methods of solution cannot be divorced from the meteorological context. It is suggested, therefore, that an investigation be performed to establish the most effective means of presentation of information to the operational user. This may be performed on a more or less empirical or even a trial and error basis. Once the general principles of data presentation have been established on a rational basis, it will then be easier to establish the data locating and data abstracting parts of the overall data-handling system.

It has been suggested by some observers that the operational user could best use rectified and assembled

* This Section was written by R. C. Copeland, Allied Research Associates, Inc.

mosaics covering large areas. This assumes that the user is qualified to interpret the raw pictorial material to the best advantage. However, following the present-day trend of the treatment of conventional meteorological data, it may be found more convenient for abstractions and analyses to be performed by extremely skilled centralized personnel, with pertinent abstractions sent to the operational users, possibly along with a sufficient amount of degraded pictorial material to permit the user to reach the necessary decisions.

It should be re-emphasized that the design of equipment for rectification and data presentation should only be undertaken when a clear evaluation of the meteorological aspects of the problem is available.

4.6 Application Survey

The previous paragraphs point up the obvious fact that it is most difficult to design a general-purpose system for processing and presenting satellite pictorial data. The various applications that suggest themselves require a variety of types of abstraction and of presentation. Before any intelligent approach to these problems can be made, clear outlines of the nature of the applications must be available.

Accordingly, one of the first steps in the design of the "system" must be a systematic survey of probable eventual applications and their data requirements. Cursory surveys have already been made, mostly in the form of questionnaires of interviews with operational activities. While these have had an encouraging response, they can best serve as a starting point for a more organized analysis.

Operational personnel are wont to consider application in terms of supplement to their current operating procedures, which may take their form largely because of lack of information similar to that available from the satellite. Accordingly, it may be necessary for an investigator to delve rather deeply into the operational procedures of the consumers of meteorological information as well as of the meteorologists themselves.

The results of any application survey must be presented in as finite terms as possible, to implement the eventual organization of a satellite meteorological system that will satisfy the greatest number of requirements.

4.7 Conclusion

The preceding paragraphs have indicated a few of the problems that must find partial solution before operational satellite meteorology comes of age. Fortunately, the satellite camera is so powerful a tool that fair use of its capabilities can be made even though much knowledge and most techniques are still lacking.

The investment in TIROS, its predecessor photographic rockets, and in future meteorological satellites has been and will continue to be heavy. The return on this investment will be determined in large measure by the effectiveness of use of the hard-won data. It is hoped that the future will see an appropriate investment in the necessary research to realize the vast potential of the successors to TIROS.

CHAPTER II

ATMOSPHERIC RADIATION STUDIES

ABSTRACT

This chapter on atmospheric radiation studies is divided into four sections. The first section is concerned with the radiation regimes and processes in the atmosphere. It is a study of the relationships of observations of the upward radiation flux from the atmosphere with the radiative processes within the atmosphere and the synoptic state. The next section is concerned with a discussion of a numerical experiment with dynamical-numerical models containing the heating term.

In order to interpret satellite infrared observations in terms of atmospheric radiation parameters, the problem of radiation geometry is considered in Section 3. It is shown that in general the radiation flux leaving the atmosphere cannot be derived simply from total radiation flux observations from a satellite. Specific intensity observations, however, can yield sufficient information so that the flux could be determined. Some intensity computations are carried out for the infrared

transparent region (900-1000 cm^{-1}) to show the dependence on surface temperature, water vapor, and aspect angle of the observation.

In Section 4 an analysis of theoretical and experimental results on atmospheric transmission and emission of infrared is continued in order to determine the amount of radiation in small spectral intervals that would be measured by a satellite with various atmospheric conditions. For rotational water, at wave numbers 250-560 cm^{-1}, atmospheric transmission increases with temperature. For the 6.3μ H_2O band, at 1200-2000 cm^{-1}, transmission decreases with increasing temperatures in the highly absorbing central region of width about 100 cm^{-1}, but increases with temperature outside this region. The entire band shows small dependence on temperature. Transmissions at 5 cm^{-1} intervals in the 15μ CO_2 band, as computed theoretically by Kaplan for model atmospheres, are analyzed. Outside of the central highly absorbing region, an approximately linear relation is found between transmission and a pressure weighted mean temperature of a layer. Over the entire 15μ CO_2 band theoretical absorptions are about 6% lower than Howard's experimental values. Patterns of infrared radiations, computed for different days over the United States and southern Canada, reveal the macroscale field of vertical motion not readily apparent from surface or upper air weather maps.

SECTION 1

SYNOPTIC SCALE RADIATION PROCESSES*

1.1 Introduction

The necessity of knowing the time and space variations of radiative processes and energy distribution within the atmosphere during changes of synoptic state led to the choice of a time-section study at a given station as an appropriate means of investigation. The selection of a station for the case study required that the station have (1) sufficient meteorological data to facilitate computations of radiation fluxes, (2) a cyclone or frontal passage to bring about changes in the state of the atmosphere, (3) clear sky conditions before and after the passage of the disturbance as "references," and (4) a location preferably on flat continental terrain.

The station selected as meeting these requirements was Omaha, which experienced a cyclone-frontal passage during the period of 12-16 March 1957. At the beginning of the period (12 March 1957) almost the entire Midwest, including Omaha, was under a weak high-pressure system and except for a few

---

* This section was written by K. L. Coulson and P. M. Furukawa, Stanford Research Institute. The work was sponsored under Contract No. AF19(604)-5965, under ARPA Order No. 26-59.

scattered cirrus, clear skies predominated throughout most of the area. On the 13th of March, a weak low situated on the leeside of the Rocky Mountains initiated a regeneration with an accompanying frontogenesis. This continued to develop on the 14th, the center of the low and the polar front with its associated weather passing through Omaha at about 03Z on this date. This was followed on the 15th and 16th by the outbreak of cold continental polar air behind the front, and a build-up of a high-pressure cell with clear skies over Omaha and much of the Midwest.

The time-section analysis of the synoptic situation, as well as the analyses of the radiation fields with supplementary computations, were based on the usual meteorological data (pressure, temperature, humidity) as published in the U. S. Weather Bureau's Northern Hemisphere Data Tabulation and on synoptic data obtained from the National Weather Records Center. Lack of data on the moisture distribution above 400mb made it necessary to extrapolate the moisture curve to the tropopause level in all cases. The procedure used here was to extend the dew point sounding upward from the point of its termination with a curve that paralleled the mean meridional

moisture distribution given by J. London in 1957.

The most difficult phase in the analyses of the time sections was encountered in the determination of the cloud effects on the radiation field. This was partly due to the lack of data on the heights of the cloud bases and tops but more to the complicated physical parameters of clouds. The limitations of the study compelled gross simplifications to be made as follows: (1) all clouds were assumed to be black bodies and only radiation from their tops and bases was considered, (2) all amounts of cloudiness were considered as moving over the station as one smooth-surfaced cloud body, (3) the period for the radiation field to go from clear sky condition to cloudy condition was assumed to be two hours for all amounts of cloudiness, (4) a discontinuity in the flux distribution was considered to occur at the leading and trailing edges of the cloud layers, (5) heavy continuous precipitation was also assumed to be black body and was considered together with the accompanying cloud as such, and (6) multi-layered clouds were assumed continuous in the vertical in such a way as to form a single layer. In the case of partial cloudiness the fluxes were determined by proportionately

weighting the calculation for a clear-sky condition and that for an overcast condition.

Although the simplifications are considerable, it is felt that the important features of the synoptic situation are sufficiently retained in the modelling to produce a reasonable estimate and the main details of the cloud effects on the radiation field.

The net contribution to the tropospheric radiative cooling or heating by the long-wave absorption or emission by carbon dioxide is generally very small compared to that of water vapor. For our purposes it was considered to be insignificant, and the effects of carbon dioxide on terrestrial radiation were entirely neglected.

1.2 Terrestrial Radiation Regime

1.2.1 General

The present study of the long-wave terrestrial radiation was primarily directed towards gaining an appreciation of its role in the radiative energy balance (cooling and heating) of the atmosphere, the variations in the distribution during changes in synoptic states, and its contribution to the radiation flux emerging from the top of the atmosphere. Elsasser's graphical

method was employed in the computations of the upward flux and downward flux and from these two, the net flux and the flux divergence were determined. While it is recognized that later improved methods of computing fluxes of long-wave radiation are available, the use of Elsasser's earlier technique is justified because (1) it is convenient, (2) the values obtained are thought to be sufficiently accurate to give a valid pattern and the essential changes of the distribution of the radiation parameters, and (3) the precise magnitude of the parameters is not the main concern of the study.

1.2.2 Upward Flux

The time-section analysis of the upward flux of terrestrial radiation reveals definite patterns of distribution. The essential features of these patterns show, first of all, marked diurnal variations of the upward flux, with the maximum amount occurring at the time of the midday maximum of the ground surface temperature. The effect of clouds is to decrease the upward flux of clear sky conditions in the region of the atmosphere above the cloud tops. The black body assumption for the cloud surfaces results in the vertical distribution of the upward flux approaching cloudless sky

conditions with decreasing height of the cloud tops. For clear skies, the upward flux decreases with height and the largest changes take place in the lower part of the troposphere.

There does not appear to be any consistent trend in the flux distribution through inversion layers. Results of the analysis show both increases and decreases from the bases to the tops of inversions, the dependence being attributable to the strength (temperature gradient) and the moisture distribution through the stable layer.

1.2.3 Emergent Upward Flux

The long-wave radiation flux emanating from the top of the atmosphere gives the expected result that the largest values are to be found in clear skies during the period of the diurnal maximum of the ground surface temperature. In areas of cloudiness, a sharp decrease of upward flux from clear sky conditions occurs at the periphery of the cloud layers, with a more or less uniform distribution of reduced flux throughout the region above the cloud top proper.

1.2.4 Downward Flux

Changes in the distribution of the downward flux are not as obvious as the ones depicted by the distribution patterns

of the upward flux. An examination of the field shows that there is no regular diurnal variation of the downward flux and that the variations in the downward flux distribution throughout the day are small compared to the diurnal changes of upward flux. At the very high levels, the isopleths of flux values appear to parallel the tropopause, but this undoubtedly reflects the restrictions of the computational method rather than a reliable display of physical distribution.

The presence of a cloud produces an increase, relative to a cloudless condition, of the downward flux below the cloud layer. Horizontally, the greatest change from clear sky conditions occurs at the cloud edges, while vertically, the increase is largest just below the cloud base and decreases with increasing distance toward the earth's surface. The downward flux that reaches the surface is affected more by clouds with low bases than by those with bases at higher elevations.

The gradients of the downward flux in the vertical direction are again larger in the lower atmosphere where the water vapor content is greater. In addition, the vertical distribution of the downward flux shows less decrease with

height (weaker gradient) in the cold, dry air behind the polar front than in the relatively warmer and more moist air ahead of it. The computed values of the downward flux decrease from the bases to the tops of inversions, but the decrease is not noticeable on the scale of the time-section analysis since the magnitude of the change is small.

1.2.5 Flux Divergence

The field of flux divergence or rate of cooling displays more cellular patterns than does the analysis of the upward or the downward flux. The outstanding feature is the relatively greater cooling that takes place above the cloud layers and at or above inversion tops; less cooling occurs below clouds and at the bottom surfaces of inversions. In cases of clouds with low bases, the analysis shows radiative heating in the region below the clouds. Centers of maximum cooling occur near and above the cloud edges, but whether this is the consequence of the assumptions used with regard to clouds or whether it is physically valid requires further study.

There is no definite or consistent pattern of radiative cooling in the cloudless sky. In a very general sense, and in the absence of an inversion in the lower levels, the rate of

cooling appears to decrease with height and then increase to the tropopause level. In the presence of a low-level inversion, the rate of cooling increases to and above the inversion top, decreases to mid-tropospheric levels, and then increases again.

1.2.6 Effect of Water Vapor

The most important radiative mechanism involving the long-wave terrestrial radiation is the absorption and re-emission by the water vapor in the troposphere. The processes involved here provide the well-known greenhouse effect which contributes to the overall radiative budget by reducing the flux passing through the atmosphere and being lost in space. By this mechanism some of the radiant energy absorbed by the water vapor is returned to the ground surface where it is again absorbed, thereby decreasing the net loss of energy by the earth.

The absorption and emission of long-wave radiation by water vapor takes place mainly in the lower levels of the atmosphere where most of the water vapor is concentrated. The analyses of the upward and downward flux mentioned earlier showed stronger vertical variation in the lower half of the troposphere than in the upper half.

Accounting for the effects of the water vapor distribution in the interpolation of the radiant flux field was difficult because radiation emanating from a mass of air depends on both its temperature and pressure, as well as on its water vapor content. The detailed analysis necessary to delineate the separate effects is outside the scope of the present study.

1.2.7 Effect of Ground Surface Temperature

The effect of the ground surface temperature is most noticeable in the diurnal variation of the upward flux within the atmosphere and in the upward flux leaving the top of the atmosphere for cloudless conditions. In both cases, the magnitude of the upward flux rises and falls in phase with the variations of the surface temperature. The diurnal variations at all levels are much less pronounced for overcast conditions.

Although it is known from observations that the temperature of the earth's surface can differ appreciably from the temperature of the air layer next to it, the radiative temperature of the surface was taken here as the air temperature given in the regular meteorological observation.

This has two consequences. First, the amount of energy computed for a given time may have been in error and, second, the assumption may introduce a phase displacement of the diurnal oscillation. Computations of fluxes were made to determine the probable error that may result from neglecting any air-ground temperature differences. The results show that if the ground temperature is greater than the reported air temperature, the radiant flux emitted by the earth's surface is increased by approximately eight percent for each 5°C difference in the temperatures. The flux is decreased by very nearly the same amount when the ground temperature is less than the air temperature. Thus, in taking for the radiating surface the temperature of the air, an error is introduced which can be significant and may be quite large. These considerations also emphasize the need of regular soil surface temperature data for radiational studies in the atmosphere.

The phase difference between the diurnal variations of the two temperatures is only of the order of an hour or so, corresponding to a shift of the patterns by a like amount in the time section representation. The distribution patterns themselves are otherwise unaffected by the shift.

1.3 Solar Radiation Regime

1.3.1 General

The main processes effecting the distribution of solar radiant energy in the atmosphere are (1) scattering by the molecules of the air, (2) reflection from ground or clouds, (3) absorption by atmospheric constituents such as ozone, water vapor, and liquid water, and (4) scattering and absorption by particles such as haze and dust. The first two of these have been studied by the use of the exact theory of radiative transfer, as originally derived by Chandrasekhar and extensively applied by Sekera and collaborators. The latest information on the distribution of ozone has been used to determine the rate of heating by ultraviolet absorption by ozone, and an empirical method derived by Korb, et al, was applied for determining water vapor absorption. Still to be studied are the effects of liquid water absorption and of absorption and scattering by haze particles.

In order to provide one example of the significance of the various processes in the atmospheric energy balance, quantitative values are being computed for the synoptic situation described above. Both the total contribution and the diurnal variation of each process are being included.

1.3.2 Molecular Scattering and Surface Reflection

The Rayleigh-Chandrasekhar theory of light scattering was used for computing the flux of radiation emerging from the top of the atmosphere as a function of wavelength and of sun elevation. Since this is an exact theory and the atmospheric model is a realistic one, the results obtained in these computations are of basic importance and form an underlying foundation to which the other processes can be added. Because of its fundamental nature, somewhat more emphasis has been placed on this work than on the phases for which only approximative or empirical methods of attack are available.

1.3.2.1 Variation with Wavelength

According to the original Rayleigh theory the amount of scattering by an air molecule is inversely proportional to the fourth power of the wavelength. Thus, short waves are scattered much more strongly than are long waves, a fact which is responsible for the blue color of the sunlit sky. The scattered light which escapes to space from the top of the atmosphere is similarly rich in short wavelengths, being even "bluer" than the skylight. In this work the separate contributions of ultraviolet, visible, and infrared spectral

regions are computed, for the incident radiation corresponding to that from the sun. The results can be summarized by saying that for energy considerations Rayleigh scattering of the infrared is completely negligible in comparison to that of the visible and ultraviolet. For the short wavelengths, on the other hand, Rayleigh scattering is the controlling factor in determining the energy distribution in a clear atmosphere.

1.3.2.2 Effect of Surface Reflection

Only by the method used here has it been found possible to evaluate exactly the effects introduced by radiation reflected from the underlying surface, be it soil, snow surface, cloud droplets, or other diffusely reflecting material. The computations show that surface reflectivity largely determines the characteristics of the solar radiation which emerges from the top of the atmosphere, especially for the solar infrared region. Practical consequences at long wavelengths are already well known, but these computations emphasize the very important influence of surface reflectivity on the energy budget.

Because of the method by which the optical thickness of the atmosphere is defined by Chandrasekhar, it is possible

to determine the effects introduced by the reflecting surface being located at different heights in the atmosphere. This means that we can determine the characteristics of the radiation upward from the top of the atmosphere for the case of the top of a uniform cloud deck of known reflectivity being located at various heights in the atmosphere. A cloud reflectivity of 0.50 has been taken as reasonable, and computations of the upward flux have been made for the cloud top at sea level, 2 km, 5 km, 10 km, 20 km, and at the top of the atmosphere.

1.3.2.3 Significance for Satellite Measurements

The results of the above computations suggest the possibility of determining the height of cloud tops by measurements of the solar radiation emerging from the top of the atmosphere. Briefly, because of the negative fourth-power dependence of molecular scattering on wavelength, the intensity of the scattered radiation in the short wavelengths is much more sensitive to the thickness of the molecular scattering medium than is that in the longer wavelengths, while the cloud-reflected radiation appears to have little

wavelength dependence. Thus the ratio of the intensities of the escaping radiation at, say, 3200 Å and 15,000 Å, could be used as a measure of the amount of molecular scattering which occurs in the clear air above a cloud top, and hence yields the height of the cloud top. Integration of the intensities over the downward hemisphere has been accomplished in the present case, and the results show the cloud-height dependence very well. Considering the sun's position and the dependence of scattering on angle, these measurements might be made more sensitive by confining measurements to a small solid angle in a given direction.

The degree of polarization is likewise sensitive to the amount of molecular scattering in the overlying clear air and is, therefore, sensitive to cloud-top height. But this is outside the scope of the present investigation.

1.3.3 Absorption by Ozone

The absorption of ultraviolet radiation by atmospheric ozone has been determined by the method derived by Craig. The data of Dütsch from Arosa on the vertical distribution of ozone have been altered slightly to be applicable to the synoptic situation during March at Omaha. As expected,

the magnitude and height of the heating maximum is a function of sun elevation, the noon value for Omaha being 1.3°C/hour at 46-48 kilometers. The integrated temperature change for the whole sunrise-to-sunset period was over 12°C at 50 kilometers, decreasing to about 2°C at 70 kilometers and less than 1°C at 30 kilometers.

1.3.4 Absorption by Water Vapor

An empirical method given by Korb, Michalowski, and Möller was applied to the data of the synoptic case for determining the total solar energy absorbed by the water vapor at Omaha, from both the incident parallel radiation and the radiation diffusely reflected from the soil or snow surface or cloud tops. Fortunately the water vapor absorption bands are in the infrared region, where molecular scattering is minor. Only small errors are introduced therefore, in considering the two processes independently, as was done here. Energy absorption values of from 57 to 78 langleys/day were obtained, corresponding to about 9% to 12% of the solar energy incident at the top of the atmosphere.

1.3.5 Absorption by Liquid Water and the Effects of Haze

These factors in the short wave radiation regime will be studied. It is known beforehand that any results obtained must be very approximate. So far the theory of radiative transfer in a turbid atmosphere has not been developed to the point at which a rigorous approach is feasible. It is probable, however, that existing methods can be applied to give reasonably satisfactory results.

1.3.6 Net Solar Energy Balance for Omaha

Still to be accomplished, also, is an integration of the various effects, to arrive at a net solar energy input for the selected synoptic situation of March, 1957, at Omaha.

CHAPTER II (Continued)

SECTION 2

DYNAMICAL-NUMERICAL EXPERIMENTATION*

2.1 The Need for Test Integrations

Our goal is the realization of heating formulations—either of physical heating processes or of relationships which are more empirical—in the improvement of dynamical-numerical models used in the study and prediction of the evolution of atmospheric motions. However, there are many difficulties involved and it is wise to take these on singly, as far as possible. In the first set of experiments planned (and discussed here), the heating will be directly prescribed, by choice, in space and time—that is, the heating will not be coupled to any of the evolving parameters.

Although radiative heating processes are being emphasized in the present study, the first set of experiments

---

* This Section was written by M. M. Holl, Stanford Research Institute. The work was sponsored under Contract No. AF19(604)-5965, under ARPA Order No. 26-59.

is more general. The independent heating distributions may be prescribed and attributed to other processes as well, such as the release of latent heat. Later experiments would attempt dependent formulations of the heating.

Experiments are wanted which will reveal some of the influences of heating on the basic dynamics of air motion. Understanding is desired of the effectiveness of heating, (1) in creating thermally-driven circulations, (2) in modifying the evolution of circulation systems, and (3) in triggering dynamic instabilities. The heating is differentiated as regards to magnitude and distribution. Distributions are of significance geographically, and relative to motion systems. Of special interest are the effects of heating at high levels.

There are also numerical analogue and integration difficulties to be explored. Recent reports from researches in dynamical-numerical experimentation indicate increasing success in the use of the basic system of dynamic equations. However, every somewhat-different model permits new difficulties to arise. Of particular interest here is the problem of the generation of compression-gravity waves versus abruptness of change in the heating.

2.2 The Dynamical-Numerical Model Selected

Considerations which led to the choice of the meridional-plane model (independent of longitude) were indicated in the Technical Progress Report No. 1, (Holl, 1960). The pertinent system of differential equations presented in that report is:

$$\frac{\partial u}{\partial t} = -\frac{v}{\cos\phi}\frac{\partial}{\partial y}(u\cos\phi) - w\frac{\partial u}{\partial z} + 2\Omega\sin\phi\, v \tag{1}$$

$$\frac{\partial v}{\partial t} = -u^2\frac{\tan\phi}{a} - v\frac{\partial v}{\partial y} - w\frac{\partial v}{\partial z} - 2\,u\Omega\sin\phi - \frac{1}{\rho}\frac{\partial p}{\partial y} \tag{2}$$

$$\frac{\partial \rho}{\partial t} = -\frac{1}{\cos\phi}\frac{\partial}{\partial y}(\rho\, v\cos\phi) - \frac{\partial}{\partial z}(\rho\, w) \tag{3}$$

$$\frac{\partial w}{\partial z} = \frac{g}{Kp}\int_z^\infty \frac{1}{\cos\phi}\frac{\partial}{\partial y}(\rho\, v\cos\phi)\, dz$$

$$- \frac{1}{\rho}\frac{1}{\cos\phi}\frac{\partial}{\partial y}(\rho\, v\cos\phi)$$

$$- v\left(\frac{1}{Kp}\frac{\partial p}{\partial y} - \frac{1}{\rho}\frac{\partial \rho}{\partial y}\right) + \frac{R}{C_p}\frac{\rho}{p}\dot{Q} \tag{4}$$

$$p = g\int_z^\infty \rho\, dz \tag{5}$$

where $K = C_p/C_v$, ϕ is the latitude, "a" is the earth's radius, and Q is the rate of heating per unit mass. The northward coordinate is $y = a\phi$. At sea-level, $w = o$.

The main reasons for deciding on experiments with a hemispheric longitude-independent model are: (1) the task is smaller, with fewer difficulties than with full three-dimensional variability in space. It was decided to forego horizontal variability in preference to considerable detail in the vertical. (2) In this model, noise-free initial distributions may readily be prescribed. These are arbitrary zonal flows <u>in balance</u>, which are then unbalanced by the commencement of heating.

The model falls short for some types of investigations. Compression-gravity waves and surface-type waves should exhibit other sensitivities and characteristics when full variability is allowed. Also, the dynamic instability of zonal motions subject to longitudinal perturbations, which results in the breakdown of the zonal motion and the growth of horizontal eddies, cannot be manifested. This means that we cannot get such limit cycles of the type demonstrated by

general circulation model integrations having full horizontal variability.

Because we have not included a limiting form of friction, the total energy should keep increasing as long as net heat energy is supplied. However, heating and cooling distributions may also be prescribed which, over the volume, integrate to a net energy-input rate of zero. For the latter, it may be possible to asymptotically reach a steady state. Assuming that a steady state can be reached, friction formulations may be added in a repetition of the experiment to investigate the modified asymptotic behavior.

Heating distributions, as a function of latitude and altitude, over the hemisphere, will result in pure thermally-driven planetary circulations because the development of horizontal eddies is excluded. The heat energy is transported without the effect of cyclones, etc. Such results are of interest in understanding the general circulation, and cannot be determined from observational data because the transport due to eddies does not average out.

The choice of many levels in the vertical makes the model particularly attractive in the study of the propagation

of influences in the vertical. Also, compression-gravity and surface-type wave disturbances need many degrees of freedom in the vertical for their portrayal.

2.3 Progress to Date

The equation system was first transformed into a more suitable form. As absolute angular rotation, Ω_a was introduced:

$$\Omega_a = \Omega + \frac{u}{a \cos \phi} \quad . \tag{6}$$

Also introduced were λ as the angular momentum of a zonal ring of unit cross section, and η as the mass in a zonal ring of unit cross section:

$$\lambda = \rho \Omega_a \cos^3 \phi \; \cancel{(2\pi a^3)} \tag{7}$$

$$\eta = \rho \cos \phi \; \cancel{(2\pi a)} \tag{8}$$

The constants in parentheses were dropped from these definitions. With these substitutions, Eqs. (1), (2), and (3) of the system are replaced by

$$\frac{\partial}{\partial t}\eta = -\frac{\partial}{\partial y}(v\eta) - \frac{\partial}{\partial z}(w\eta) \tag{9}$$

$$\frac{\partial}{\partial t}\lambda = -\frac{\partial}{\partial y}(v\lambda) - \frac{\partial}{\partial z}(w\lambda) \tag{10}$$

$$\frac{\partial w}{\partial t} = -v\frac{\partial v}{\partial y} - w\frac{\partial v}{\partial z} - \frac{1}{\rho}\frac{\partial p}{\partial y} - a\cos\phi \quad \sin\phi(\Omega_a^2 - \Omega^2). \tag{11}$$

These reveal the conservation of mass and angular momentum in a more useful form for the development of a numerical analogue for the system.

The hemisphere, as represented by distributions in a representative meridional plane, was divided by lines $y = y_m$ and $z = z_n$ which create zonal rings as volume modules. The m, nth volume module consists, in the meridional plane, of one corner, two sides, and the interior. All parameters belonging to the m, n module are subscripted by m, n and are located as shown in the following figure:

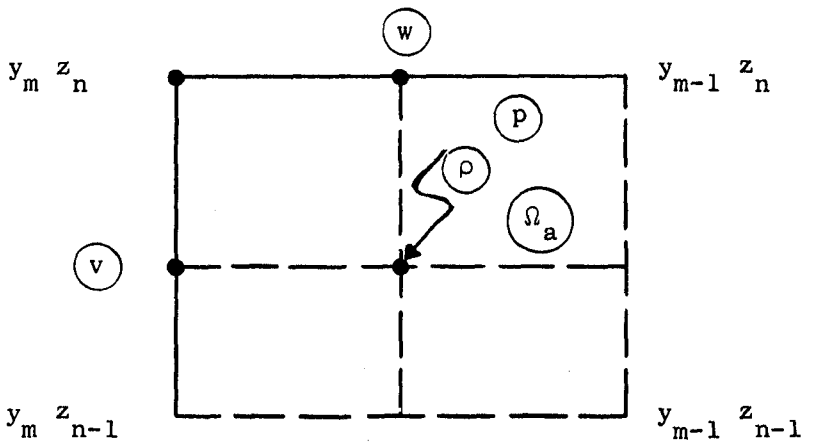

The y_m increase in regular increments from $y_o = 0$ at the equator to $y_{49} = a\pi/2$ at the pole. Levels were selected in irregular increments, according to variability considerations, from $z_o = 0$ at sea level to $z_{18} = 55$ km.

For the formulation of boundary conditions at the top, there is little difference between extending the upper layer of volume modules from 55 km to $z = \infty$ or terminating them at, say, $z = 100$ km (where ρ is taken as zero), although the former is somewhat more appealing. A heating rate is prescribed for each volume module.

The development of the numerical analogue will be detailed in a scientific report. However, some comments are in order here.

Equations (9) and (10) were analogued in such a way as to conserve total mass, and total angular momentum about the polar axis. So-called truncation errors in these two distributions cancel internally. The analogues are based on the pertinent fluxes through module walls, and on one-to-one correspondences between the mass in a volume module and the density at a chosen interior position, and between the absolute angular momentum in a volume module and the value of $\mathcal{F}\Omega_a$ at the interior position. These correspondences are based on the geometry and the standard atmosphere and are fixed except for the following exception: The ratio between the mass in the module of the <u>uppermost layer</u> and the density at an interior position in that module may be idealized into a pressure-density relationship and is tantamount to stating the temperature. It is through this relationship that heat is introduced into the uppermost layer of volume modules. It is done in this way because heat cannot be introduced there via Eq. (4). Equation (4) is used to determine

the vertical motion at the top of the module, given w at the bottom, but since we are not having any outflow through the top of the uppermost modules, Eq. (4) is ineffective there.

The numerical-analogue for the system was completed by the end of February and work was started on programming the analogue for SRI's Burroughs 220 computer. Considerable work went into code-checking and developing data transfer and output routines. The first results were achieved during late June.

The first results have been examined. These are of a test integration for an atmosphere at rest, with the equilibrium being upset by heating one column of latitude-ring volume-modules, at the rate of $10^{\circ}C$ per day. The integration was taken in one-hour increments to hour five. Results agreed with independent calculations prepared for the first two time-steps.

The chain of events is as follows: Heating the column results in its upward expansion. At an upper level, then, mass from below moves above and raises the pressure at that level. This sets up a horizontal pressure gradient which accelerates mass out of the column. The disturbance thus begins its northward

and southward propagation from the heated latitude.

This abrupt heating was chosen to help determine the maximum time increment which might be used in the integrations. As expected, the one-hour time-step is considerably too large. The mass divergence for the upper three volume modules of the heated column was large enough at hour three to evacuate them if held steady for so long a time interval. Recalculation at shorter intervals would gradually reduce the mass divergence as the pressure drops accordingly. We shall next try a considerably reduced time-step in order to determine the propagation speed of the compression-gravity waves which are set up by the abrupt heating.

Eight hours of computing time on the Burroughs 220 have been used to date, largely for code checking.

2.4 Experiments Planned

The first experiment in which one vertical column of modules at mid-latitude is heated should indicate the time increment which may be used and also should give some insight into the compression-gravity and surface-type waves. This experiment might also produce some computational

difficulties which will require analogue modifications.

This experiment will be followed by another in which the atmosphere is initially at rest but with its equilibrium disturbed by a complete meridional heating and cooling distribution corresponding somewhat to winter and adjusted so that the net heating rate is zero. An attempt will be made to reach an asymptotic state. Results will lead to later experiments.

CHAPTER II (Continued)

SECTION 3

STUDIES OF ATMOSPHERIC RADIATION AS OBSERVED FROM SATELLITES*

3.1 Introduction

One of the basic objectives of the meteorological satellite program is to obtain continuous observations of atmospheric radiation over all regions of the world. It has been suggested that these observations can provide useful information in determining the vertical structure of the atmosphere (see, for instance, Kaplan, 1959). Satellite observations of cloudiness, short and long wave radiation would also be of prime importance in dynamic forecasting techniques (Holl, 1960). When sufficient observations are available, it will be possible to determine the various components of the mean atmospheric radiation budget from considerations other than purely theoretical. This latter

---

* This Section was written by J. London, K. Ooyama, and H. Viebrock, New York University. The work was sponsored under Contract No. AF19(604)-5955, under ARPA Order No. 26-59.

problem is of course fundamental to our understanding of the large scale circulation of the atmosphere and the planetary climate of the earth.

As has been pointed out (London, 1959) the determination of radiative flux in the atmosphere has, until recently, been carried out largely by theoretical means. However, in the past few years there have been many attempts, moderately successful, in instrumenting airborne apparatus to observe atmospheric radiation under various conditions. One major problem, however, has been the interpretation of these observations in terms of the desired radiation parameters. The following report deals with a preliminary discussion of the geometrical problem, and an attempt to simulate such observations as would be taken from a satellite equipped with suitable filters for limited regions of the infrared spectrum.

3.2 The Geometrical Problem

The total long wave radiation from the earth-atmosphere to space can be observed by a satellite equipped with a non-collimated infrared sensor. However, what is important in application of these observations is the differential distribution

of the radiative heat balance with latitude (and eventually longitude). If the upwelling beam is collimated through the detecting unit and can view at all angles, this problem can be solved in a relatively straightforward albeit tedious manner. However, if the radiative flux as received at satellite levels is not collimated, there are additional geometric difficulties which prevent the unique determination of the atmospheric flux as a function of latitude without some simplifying assumptions. In order to avoid a great deal of mathematical manipulation, we consider a two-dimensional case where the earth is a thin circular plate with its atmosphere around the rim. For practical application, of course, these results must be extended to the spherical case. However, the essence of the problem can be treated with the above assumption.

Consider a thin circular plate including the polar axis as diameter. All the radiation is assumed to lie in the plane of the circular plate. The part of the atmosphere which contributes significantly to the radiative budget is a relatively thin layer of only a few tens of kilometers thick. Therefore the effective top of the atmosphere may be assumed to have

a radius r, which is almost equal to the earth's radius. The orbit of the satellite is assumed to be circular with a radius R. It is also assumed that the receiving surface of the satellite sensor is flat and always faced toward the earth's center. The total (outgoing) flux, $G(\theta)R\ d\theta$ at the co-latitude θ, crossing a segment of the satellite orbit $R\ d\theta$ from all possible directions is then given by

$$G(\theta)R\ d\theta = \left[\int_{-\phi_m}^{\phi_n} I_s(\theta, \phi)\cos\phi\ d\phi \right] R\ d\theta$$

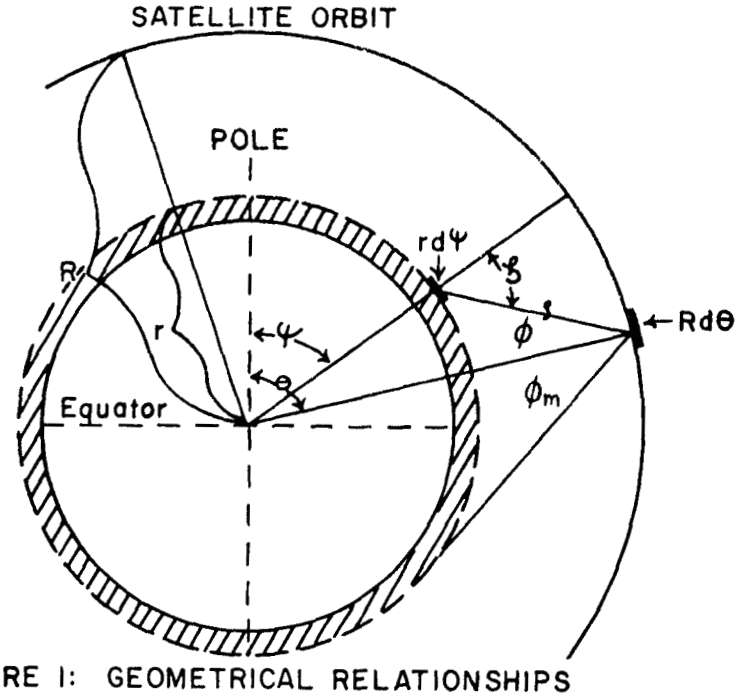

FIGURE I: GEOMETRICAL RELATIONSHIPS SHOWING THE RADIATION RECEIVED BY THE SATELLITE SENSOR

where $I_s(\theta, \phi)$ is the intensity of the flux in the direction ϕ from the normal of the orbit at the point of the co-latitude θ on the orbit. The angle ϕ_m is the maximum value for ϕ for which I_s does not vanish. Then (see Fig. 1)

$$\sin \phi_m = r/R$$

(for a satellite orbiting at 700 km above the earth's surface ϕ_m is approximately 64°).

We suppose that the satellite observation is such that $G(\theta)$ can be obtained as a function of θ. In practice, $G(\theta)$ is not observed simultaneously for different values of θ. Further, in the three-dimensional case, a considerable time interval would be required for a satellite to cover the entire earth for a sufficiently dense net of observations. $G(\theta)$ is therefore obtained as a certain average over a long period of observations. We simply here assume that $G(\theta)$ is everywhere known from the satellite observations.

The quantity of particular meteorological interest is not $G(\theta)$ but the radiative energy loss per unit volume for all points within the atmosphere (shaded area in Fig. 1). It is not however possible to determine the three-dimensional radiative flux

divergence from the observations of $G(\theta)$ alone. We will here consider only the problem of the upward radiative flux as a function of the horizontal coordinates (in this case θ) from the (effective) top of the atmosphere.

If we denote the outgoing total flux from a small segment $(r\, d\psi)$ of the effective top of the atmosphere, at the co-latitude ψ, by $F(\psi) r\, d\psi$, then we may write

$$F(\psi) r\, d\psi = \left[\int_{-\pi/2}^{\pi/2} I(\psi, \zeta) \cos \zeta \, d\zeta \right] r\, d\psi \tag{2}$$

where $I(\psi, \zeta)$ is the intensity of the outgoing flux in the direction ζ from zenith, at the co-latitude ψ.

Our problem, then, is to obtain $F(\psi)$ from $G(\theta)$. $F(\psi) \equiv F(\theta) \equiv G(\theta)$ only if $R = r$.

When $R \gtrsim r$ we have the following relationship

$$I_s(\theta, \phi) = I(\psi, \zeta) \tag{3}$$

where from fig. 1 the four angles satisfy the following:

$$\frac{\sin \phi}{r} = \frac{\sin \zeta}{R} = \frac{\sin (\theta - \psi)}{\rho} \tag{4}$$

and

$$\rho = R \cos \phi - r \cos \zeta \tag{5}$$

Then from (4) we have

$$\sin\phi = \frac{r}{R}\sin\zeta$$
$$= \sin\phi_m \sin\zeta \qquad (6)$$

and

$$\cos\phi\,\frac{d\phi}{d\zeta} = \sin\phi_m \cos\zeta \qquad (6')$$

Also, from (4) and (5)

$$\sin(\theta - \psi) = \frac{\zeta}{R}\sin\zeta$$
$$= (\cos\phi - \sin\phi_m\cos\zeta)\sin\zeta$$
$$= \left[\sqrt{1 - \sin^2\phi_m\sin^2} - \sin\phi_m\cos\zeta\right]\sin\zeta$$

Since for a particular satellite altitude, the right hand side is a function of ζ alone, we may write

$$\theta - \psi = a(\zeta) \qquad (7)$$

where

$$a(\zeta) \equiv \arcsin\left[\left(\sqrt{1 - \sin^2\phi_m\sin^2\zeta} - \sin\phi_m\cos\zeta\right)\sin\zeta\right]$$

From (3), (6') and (7) we have

$$I_s(\theta,\phi)\cos\phi\, d\phi = \sin\phi_m\, I(\theta - a(\zeta), \zeta)\cos\zeta\, d\zeta$$

and the expression for $G(\theta)$ is now

$$G(\theta) = \sin\phi_m \int_{-\pi/2}^{\pi/2} I(\theta - a(\zeta), \zeta)\cos\zeta\, d\zeta\,. \qquad (8)$$

The expression for F at a point at the effective top of the atmosphere is

$$F(\theta) = \int_{-\pi/2}^{\pi/2} I(\theta, \xi) \cos \xi \, d\xi \tag{9}$$

The exchange here of the symbols ψ and θ should not introduce any confusion, since both angles are co-latitude and we are interested in obtaining the functional form of F from the observed function G.

The flux intensity function $I(\theta, \xi)$ is not observed. However, since its integral value given by (8) is observed, G and F can be related in terms of I as given above.

If the satellite radiation measurements are made on a collimated beam for every possible angle ψ and at each co-latitude θ, the total flux $F(\psi)$ can be calculated directly for each co-latitude ψ. In the case, however, where the satellite orbit is non-polar, there are restrictions to the calculation of $F(\psi)$ since it would then be necessary to assume that $I(\psi, \xi)$ can be neglected for large values of ξ. Sample calculations of $I_s(\theta, \phi)$ and $G(\theta)$ are given at the end of this report.

3.3 The Non-collimated Flux

Since $I(\theta,\xi)$ is a function of two independent variables, in general it is impossible to eliminate I between (8) and (9) in order to obtain a unique functional relationship between the observed flux G and the desired flux F.

Because $I(\theta,\xi)$ is a periodic function of θ, we can expand I into a Fourier series.

$$I(\theta,\xi) = a_0(\xi) + \sum_{n=1}^{\infty} \left[a_n(\xi)\cos n\theta + b_n(\xi) \sin n\theta\right] \qquad (10)$$

Substituting (10) into (8) gives

$$\frac{G(\theta)}{\sin\phi_m} = \int_{-\pi/2}^{\pi/2} \left\{ a_0(\xi) + \sum^{\infty} \left[a_n(\xi)\cos n(\theta-\alpha(\xi))+b_n(\xi)\sin n(\theta-\alpha(\xi))\right]\right\} \cos\xi \, d\xi \qquad (11)$$

$$= g_o + \sum_{n=1}^{\infty} (g_n \cos n\theta + h_n \sin n\theta) \qquad (12)$$

where

$$g_o = \int_{-\pi/2}^{\pi/2} a_o(\xi) \cos\xi \, d\xi$$

$$g_n = \int_{-\pi/2}^{\pi/2} \left\{a_n(\xi) \cos n\alpha(\xi) - b_n(\xi) \sin n\alpha(\xi)\right\} \cos\xi \, d\xi \qquad (13)$$

and

$$h_n = \int_{-\pi/2}^{\pi/2} \left\{ a_n(\xi) \sin n\alpha(\xi) + b_n(\xi) \cos n\alpha(\xi) \right\} \cos\xi \, d\xi$$

for $n = 1, 2, 3, \cdots$.

The coefficients of g and h can be determined by expanding the observations of $G(\theta)$ into a Fourier series. Thus,

$$g_o = \frac{1}{2\pi} \int_{-\pi}^{\pi} G(\theta) \, d\theta$$

$$g_n = \frac{1}{\pi} \int_{-\pi}^{\pi} G(\theta) \cos n\theta \, d\theta \tag{14}$$

and

$$h_n = \frac{1}{\pi} \int_{-\pi}^{\pi} G(\theta) \sin n\theta \, d\theta$$

The desired function $F(\theta)$ can also be expanded in Fourier series giving

$$F(\theta) = A_o + \sum_{n=1}^{\infty} (A_n \cos n\theta + B_n \sin n\theta) \tag{15}$$

and from (9) and (10) we can write

$$A_o = \int_{-\pi/2}^{\pi/2} a_o(\xi) \cos\xi \, d\xi$$

$$A_n = \int_{-\pi/2}^{\pi/2} a_n(\xi) \cos\xi \, d\xi \qquad (16)$$

$$B_n = \int_{-\pi/2}^{\pi/2} b_n(\xi) \cos\xi \, d\xi$$

The problem now is to determine the A's and B's from the known values of the g's and h's. By comparing (13) and (16), we have

$$A_o = g_o \, .$$

That is, the coefficient A_o is uniquely determined from the observed value g_o. It is obvious, however, that all other coefficients A_n and B_n cannot be so determined from g_n and h_n <u>unless</u> $\alpha(\xi)$ is constant for all values of ξ. This last condition is possible if and only if

$$\sin \phi_m = \frac{r}{R} = 1 \, .$$

Then $\alpha(\xi) \equiv 0$ and the solutions are

$$A_n = g_n, \; B_n = h_n \, .$$

In other words, if the satellite orbits the earth at the height of the effective top of the atmosphere (R=r), we then have the trivial case

$$F(\theta) \equiv G(\theta) .$$

For R larger than r, $\alpha(\xi)$ varies within the range

$$|\alpha(\xi)| \leq (\frac{\pi}{2} - \phi_m) \quad \text{or}$$

$$|\sin \alpha(\xi)| \leq \sqrt{1 - r^2/R^2}$$

Thus if R is only slightly larger than r, the variation of $\cos n\alpha(\xi)$ and $\sin n\alpha(\xi)$ is small if n is small. Thus the coefficients A_n and B_n for small n can be determined to a <u>lesser degree of uncertainty</u> than is the case for large n. That is, if the orbital radius of the satellite is increased, only a broad distribution of $F(\theta)$ can be obtained and details of the variation of $F(\theta)$ with respect to θ become lost and unrecoverable from the observations of $G(\theta)$.

It is possible that information of the form and

variation of $F(\theta)$ can be derived from the observations of $G(\theta)$ with additional restrictions. For instance, we may introduce an assumption restricting the functional behavior of $I(\theta, \xi)$ in such a way that $I(\theta, \xi)$ will be a function of only one independent variable. This functional relationship, however, must be derived from the empirical relationships between the parameters studied.

3.4 Some Simulated Observations

The intensity of a collimated beam arriving at the top of the atmosphere (level of the satellite) at some angle from the vertical, is

$$I_s = \int_{\nu} I_o \, \tau(0, u_s) \, d\nu + \int_{\nu} \int_0^{u_s} I_b \, k\tau(u, u_s) \, du \, d\nu \qquad (18)$$

where u is the optical thickness of the gas in the direction of the beam ξ and τ represents the specific transmission function for the gas and spectral interval involved. The intensity of radiation reaching the sensor then originates in part at the earth's surface (or at a cloud top) and in part from the atmosphere itself. If the sensor can view at all angles, the flux of radiation observed across a horizontal surface at the

satellite level can be computed since, for the three dimensional case

$$G = \int_0^{2\pi} \int_0^{\phi_m} I_s \cdot \cos\phi \quad \sin\phi \, d\phi \, d\lambda \tag{19}$$

In order to simplify the present calculations, we will deal with the spectral interval 10-11μ (wave numbers 900-100 cm^{-1}). This is a region that is free from the numerous atmospheric absorption bands which cover the remainder of the infrared spectrum. The major portion of the 900-1000 cm^{-1} region is occupied by an absorption continuum whose origin lies in the rotational band of water vapor. The average water vapor absorption coefficient at STP for the so-called 'transparent' region is approximately $\bar{k}_o = 0.27$ (see, for instance, Yamamoto and Onishi, 1949). In this interval $\bar{k}$ is a linear function of half-width and therefore of pressure.

We assume that the satellite is overhead at 45°N at a height of 700 km. The maximum aspect angle of the collimated beam is then 64°16' corresponding to a zenith angle of $\pi/2$ at latitudes 70°44' and 19°16'N. For this satellite elevation, we also have from Eq. (4)

$$\sin \zeta = 1.11 \sin\phi,$$

and from Fig. 1 $\psi = \theta + \phi - \zeta$.

The following table gives the zenith angle and co-latitude from which the surface beam originates for each ten degrees of aspect angle, for $\theta = 45^{\circ}$N. ψ_N and ψ_S refer to positive and negative values of ϕ (i.e., looking north and south from the satellite respectively).

ϕ	ζ	ψ_N	ψ_S
0°	0°	45°	45°
10	11.1	43.9	46.1
20	22.4	42.6	47.4
30	33.7	41.3	48.7
40	45.7	39.3	50.7
50	58.3	36.7	53.3
60	75.0	30.0	60.0
$64^{\circ}16'$	90	19.3	70.7

A satellite in an inclined orbit of 60° north and south would eventually receive all radiation leaving the earth's surface within the latitude belt $\sim 35^{\circ}$N and S.

For the purpose of these sample calculations, different models of temperature and water vapor distribution were adopted. In each case circular symmetry was assumed.

These models were:

1) Temperature and specific humidity increasing outward from the sub-satellite point.

2) Temperature and specific humidity constant over the sub-satellite area.

3) Temperature and specific humidity decreasing outward.

In addition, in order to test the effect of temperature and water vapor separately,

4) Temperature increasing but specific humidity decreasing outward.

5) Temperature decreasing but specific humidity increasing outward.

(Note: Sub-satellite surface temperature for models 4, 5 was assumed slightly higher than for models 1, 2, 3.)

The computed intensity of the collimated beam which would be observed by the detector as a function of the aspect angle is shown in figure 2(a) for the first three atmospheric models, and figure 2(b) for the last two models assumed.

As can be seen from the diagrams, in all cases the total intensity decreases with increasing aspect angle. This, of course, results from the fact that with increasing aspect angle, the surface beam is depleted to a larger extent and more of the radiation originates from the atmosphere (colder than the ground). Comparison of the three curves in figure 2(a) indicates again that the effect of atmospheric moisture is to lift the effective radiating surfaces.

Variations of the surface temperature and water vapor distribution have some effect on the radiation intensity received, as seen in figure 2(b). At small aspect angles the temperature and humidity values are nearly the same in both models. At large angles, however, the radiation conditions are quite different. Most of the radiation reaching the satellite comes from an area close to the sub-satellite point. As a result, so long as the surface conditions remain relatively the same, the observed radiation flux in this spectral interval will depend largely on the sub-satellite surface meteorological conditions. The computed flux for the spectral interval 900-1000 cm^{-1} reaching a satellite at 700 km and 45°North, is

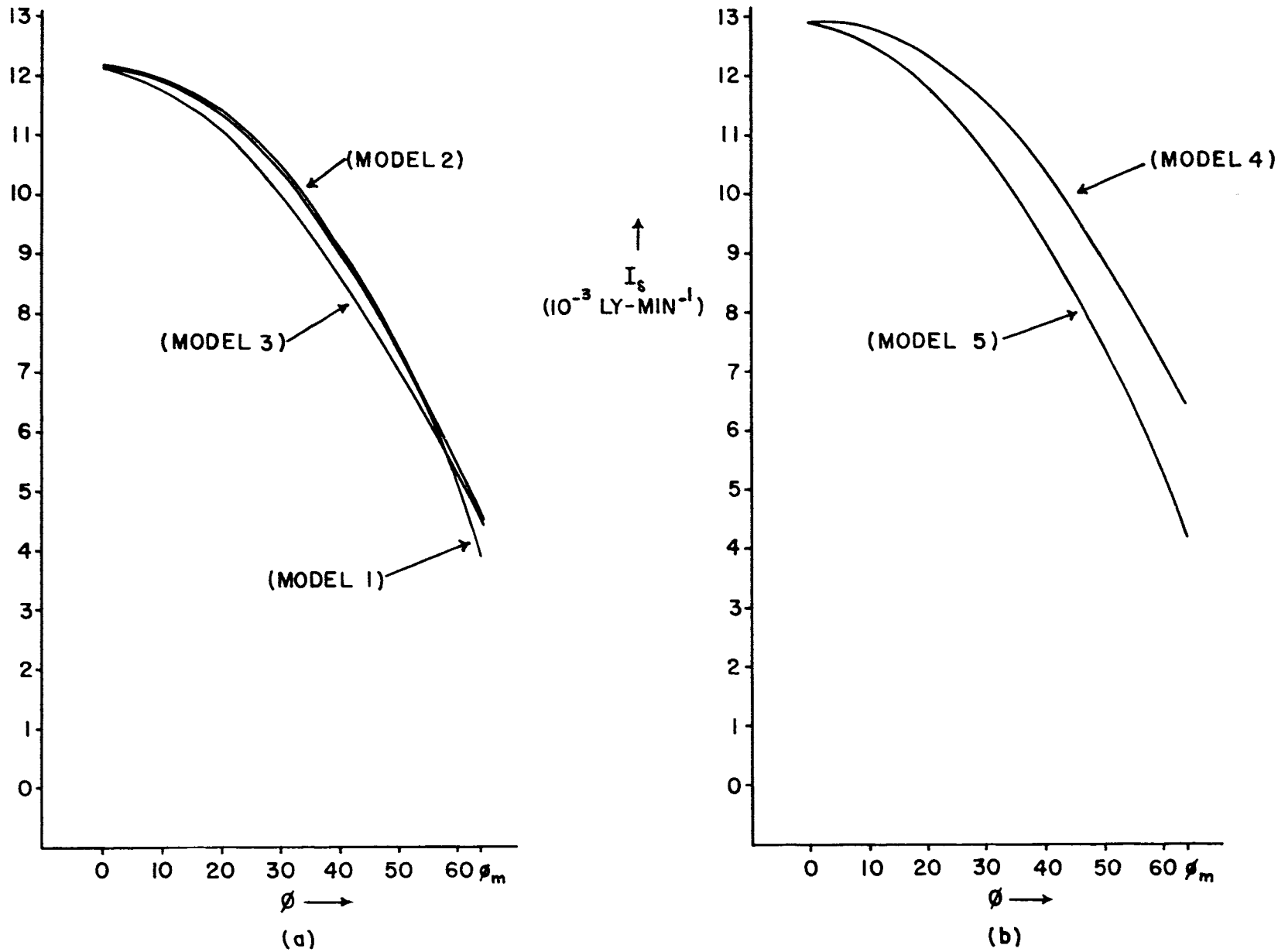

FIGURE 2: THE INTENSITY IN THE 900 - 1000 cm^{-1} SPECTRAL INTERVAL FOR DIFFERENT ATMOSPHERIC MODELS

given below for each of the five models evaluated.

	$G(45^{o}N)\ 10^{-3}$ ly min^{-1}
Model 1.	22.4
Model 2.	22.5
Model 3.	21.8
Model 4.	24.5
Model 5.	21.9

The maximum difference in the flux is only about 10 percent. This is because the sub-satellite surface conditions were assumed similar in all five cases. Calculations were made only for clear skies since the effect of cloudiness would simply be to decrease the surface (emitting) temperature and thereby decrease the intensity and the radiation flux as observed by the satellite detector.

Finally, it should be pointed out that in the so-called 'transparent' spectral interval, although only slightly more than half of the upwelling radiation comes from the surface of the earth, the remaining portion is emitted by the lowest three kilometers of the atmosphere. Thus the computations of the outgoing radiation as a function of latitude can be made in a relatively straightforward manner provided that the

satellite observations are collimated, the aspect angle for each observation is known (all aspect angles $\phi \leq \phi_m$ must be observed), and the satellite is at or near a polar orbit.

SECTION 4

SATELLITE OBSERVATIONS OF INFRARED RADIATION *

4.1 Introduction

The photographic observations of TIROS I have shown a termendous organization of cloud patterns which may extend over large areas of the earth's surface. A future TIROS may map patterns of infrared radiation which will provide additional information.

It was shown in GRD Research Note No. 36 [1] that a computed infrared map (6 March 1959) gave a pattern which could be interpreted in terms of the motion field associated with a deep storm. Greatest intensity constrast was obtained in the "window" regions of the infrared spectrum between 8.3 - 9.1 μ and 10 - 12.5 μ, in which the outgoing radiation is closely related to the temperatures of the radiating surface

---

* Originally prepared as a Semi-Annual Technical Summary Report under Contract No. AF19(604)-5968, under ARPA Order No. 26-59 and GRD-TN-60-493, 30 June 1960. This Section was written by R. Wexler, Allied Research Associates, Inc.

[1] "Contributions to Satellite Meteorology, " Vol. I, Hereafter referred to as Volume I.

(ground or cloud). The use of other broad spectral regions gave similar patterns but with reduced contrast. This reduction in contrast is a function of the amount and distribution of the intervening absorbing gas between the radiation surface and the satellite, with dependence on both pressure and temperature.

In Volume I, calculation of the infrared radiation that would be emitted from the atmosphere was made by neglecting temperature dependence. In the present report the effect of temperature dependence is considered from the viewpoint of determining empirical relations which can be used operationally whenever satellite observations of the infrared are made. Comparisons of the outgoing radiation for different portions of the spectrum are made with balloon measurements of the infrared in New Mexico.

This Section also discusses other cases of "window" maps in an effort to determine the association of infrared patterns with synoptic weather.

4.2 Rotational Water

4.2.1 Temperature Dependence

In Volume I it was shown that the empirical transmissions for rotational water through large layers may be represented

quite well as a function of mP only, where m is the optical depth and P is the pressure. For transmission through the atmosphere from a level p to the top of the atmosphere the pressure P should be defined by the Curtis-Godson approximations.

$$mP = \int_{p}^{o} p \, dm \tag{1}$$

It was found that the transmission τ, from Palmer's data for rotational water, fitted a relation

$$\tau = e^{-K\sqrt{mP}} \tag{2}$$

where K is a constant. This equation is valid in narrow spectral regions for relatively large absorption in a gas having absorption lines randomly distributed. Values of K were derived from Palmer's data for 60 to 70 cm^{-1} intervals and are repeated in Table 1 below (Section 4.2.2). These values of K were based on measurements made at a temperature of about 17°C and may be expected to vary with temperature. Theoretically K is related to the intensities S_i and half widths γ_i

of the absorption lines in the following manner:

$$K \sim \left(\sum_i S_i \gamma_i\right)^{1/2} \tag{3}$$

the product $S_i \gamma_i$ is proportional to the pressure and some function of the temperature. Where (3) is valid, correction for both pressure and temperature can be made by modifying the Curtis approximation as follows:

$$mP = \int_p^o yp \, dm \tag{4}$$

where

$$y = \frac{\left(\sum_i S_i \gamma_i\right)^{1/2}}{\left(\sum_i S_{io} \gamma_{io}\right)^{1/2}} \tag{5}$$

where the subscript o refers to the value at 17°C at which the measurements were made. The function y may be computed from unpublished computations of $S_i \gamma_i$ made by Benedict and Kaplan which are given as a function of the wave number from the band center. Figure 3 shows a plot of y as a function of temperature for the different rotational water bands. It is

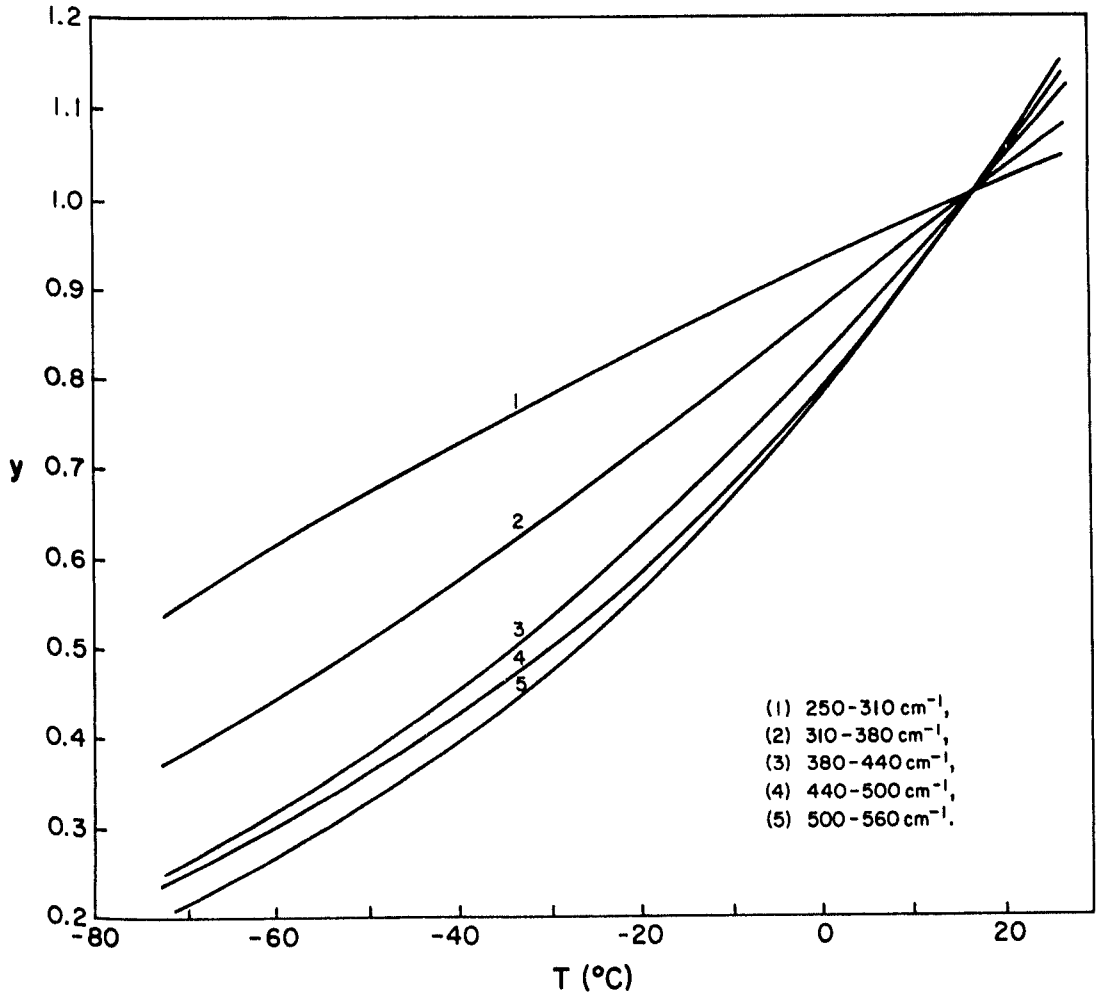

FIG. 3 TEMPERATURE CORRECTION FOR ROTATIONAL WATER.

seen that $y = 1$ at $17^{\circ}C$ (by definition) but may be appreciably lower at cold temperatures. The temperature correction is relatively large for the 500-560 cm^{-1} region, where absorption is relatively small; in the region of high absorption 250-310 cm^{-1} temperature dependence is less important.

4.2.2 Maps of Rotational Water for 6 March 1959

Calculations of the amount of radiation in the rotational water region leaving the top of the atmosphere for air masses 1, 2 and 3 have been computed for 6 March 1959 at 0000Z. This case was discussed at length in Volume I for other spectral regions of the infrared. Maps for the rotational water region show essentially the same pattern as the other regions. The contrast between the warm areas (generally at or near the surface) and the cold areas (generally high cirrus) of the map is greatest where absorption is relatively small (500 - 560 cm^{-1}) and becomes progressively smaller as the absorption increases with decreasing wave number. A sample map plotted in terms of radiation amounts is shown in Figure 4 for the 250 - 310 cm^{-1} region, where absorption is relatively high. The contrast for the different bands may

be made by comparing the equivalent black body temperatures (T_E) of the outgoing radiation of Miami, with clear conditions and a surface temperature of 24°C, with those of Pittsburgh with a cirrus cloud top temperature of -65°C. Table 1 shows the values of T_E for Miami at air masses 1, 2 and 3 for the different bands. Because of the small amounts of water vapor above the cirrus clouds, the T_E for all bands and for all three air masses over Pittsburgh may be considered as equal to -65°C.

TABLE 1

EQUIVALENT TEMPERATURES (°C) FOR ROTATIONAL WATER AT MIAMI 0000Z, 6 MARCH 1959

Wave No. (cm^{-1})	K ($cm^{-1/2}mb^{-1/2}$)	Air Mass 1	2	3
500 - 560	.046	3	-2	-5
440 - 500	.080	-5	-10	-12
380 - 440	.145	-13	-18	-20
310 - 380	.31	-24	-29	-31
250 - 310	.51	-32	-37	-40

It is evident that the contrast in T_E between warmest and coldest areas for air mass 1 is almost $70^{\circ}C$ in the region of low absorption (500 - 560 cm^{-1}) and only about $30^{\circ}C$ in the region of high absorption (250 - 310 cm^{-1}). The reduction in contrast is $5^{\circ}C$ for air mass 2, and 7 to $8^{\circ}C$ for air mass 3.

4.3 Temperature Dependence for 6.3 μ H_2O

4.3.1 Absorption at 50 cm^{-1} Intervals

Absorption tends to decrease with temperature in the central portion of the band but to increase in the wings. In order to correct for temperature in the 6.3 μ H_2O band it is desirable to separate the band into intervals of about 50 cm^{-1}. Unfortunately, experimental data on the absorption at such intervals is not available. However, by assuming an equation of the form (2), it is possible to utilize Howard's data to determine values of K for these smaller intervals. The assumption should be valid for 50 cm^{-1} intervals since for the entire band a straight line relation exists between log τ and P (at high absorption--see Volume I) and since (2) holds for intervals of 60 cm^{-1} in the rotational H_2O region.

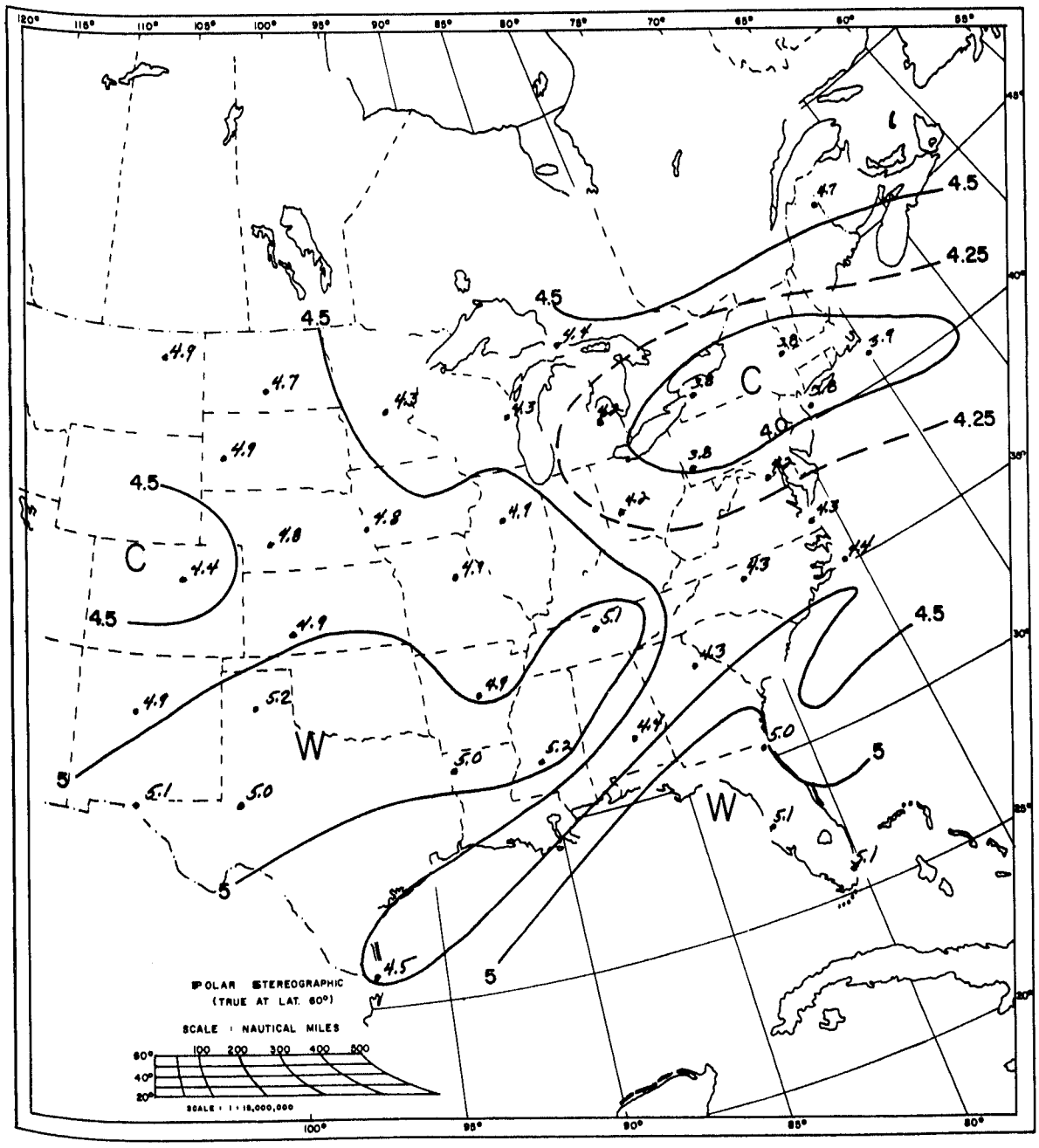

FIG. 4 OUTGOING RADIATION (10^{-3} CAL MIN^{-1} CM^{-2} $STER^{-1}$) IN THE 250-310 CM^{-1} REGION FOR 0000Z, 6 MARCH 1959.

Figure 5 from Howard, (1955) shows the amount of precipitable water w_o for a transmission of 50% as a function of wave number for the 6.3 μ H_2O band. The mean w_o for 50 cm^{-1} intervals from 1200 to 2000 cm^{-1} was obtained from the 125 mm H_g curves. Assuming now that Equation (2) is valid for each 50 cm^{-1} interval, the constant K was computed and is listed in Table 2.

TABLE 2

VALUES OF K IN 6.3 μ H_2O BAND

Wave Number (cm^{-1})	K ($cm^{-1/2}mb^{-1/2}$)	Wave Number (cm^{-1})	K ($cm^{-1/2}mb^{-1/2}$)
1200 - 1250	0.018	1600 - 1650	0.33
1250 - 1300	0.034	1650 - 1700	0.49
1300 - 1350	0.065	1700 - 1750	0.34
1350 - 1400	0.130	1750 - 1800	0.19
1400 - 1450	0.25	1800 - 1850	0.10
1450 - 1500	0.42	1850 - 1900	0.058
1500 - 1550	0.60	1900 - 1950	0.035
1550 - 1600	0.33	1950 - 2000	0.023

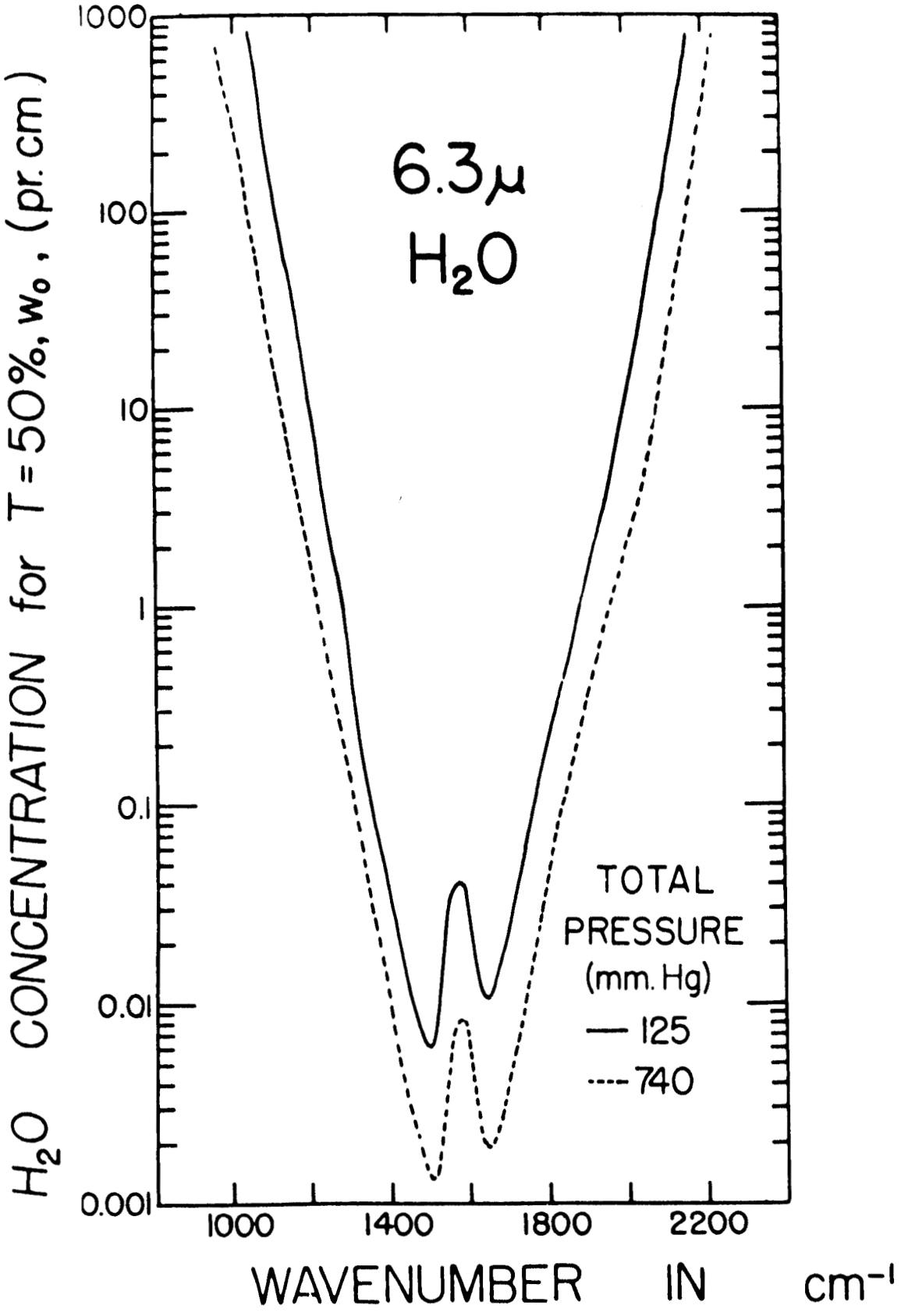

FIG. 5 PRECIPITABLE WATER W_0 (CM) FOR A TRANSMISSION OF 50% IN THE 6.3μ H_2O BAND (AFTER HOWARD).

In order to test the accuracy of the K values, the average transmissions for $\sqrt{mP} = 5$ was calculated over the entire band 1200 - 2000 cm^{-1} and the result was compared with the formula derived in Volume I.

$$= 0.665\, e^{-0.0715\sqrt{mP}} \qquad \sqrt{mP} \geq 5 \qquad (6)$$

The calculations by the two methods gave almost identical results, indicating that the K values in Table 2 are reasonably accurate.

4.3.2 Temperature Dependence at 50 cm^{-1} Intervals

The formula (6) and the derived values of K in Table 2 may be considered valid for a temperature of about 22°C at which the measurements were made. For other temperatures, a correction may be made by the use of a factor y similar to that made for rotational water; y is computed in the same manner, using 1600 cm^{1} as the center of the band, and multiplying by a factor

$$\frac{1 - e^{-\frac{1.4388\nu}{T_o}}}{1 - e^{-\frac{1.4388\nu}{T}}} \qquad (7)$$

where ν is the difference between the central wave number (e.g., of the intervals in Table 2) and 1600 cm^{-1}, T is the temperature and T_o the experimental temperature of 295°K. In the rotational water region the factor (7) is the ratio of the induced emissions at the two temperatures, and is included in the calculations of $\sum_i S_i \nu_i$ by Kaplan. For 6.3 μ H_2O, because of the higher wave number, the exponential term is negligible so that the value of (7) is unity. Therefore, by taking ν as the departure from the central wave number, this term is eliminated from the calculations of y in the 6.3 μ H_2O band.

The corrected factor y is shown in Figure 6 as a function of temperature for mean wave number differences from 1600 cm^{-1}, the band center. Thus, a $\Delta\nu$ of 25 refers to the interval between 1550 and 1600 or 1650 and 1600 cm^{-1}. It is seen that at cold temperatures y is greater than 1 for a spectral region within 100 cm^{-1} of the band center. Thus, the transmission in this central region increases with increasing temperature but beyond 100 cm^{-1} it decreases with temperature. Figure 6 shows that y generally decreases with increasing $\Delta\nu$. The anomalous

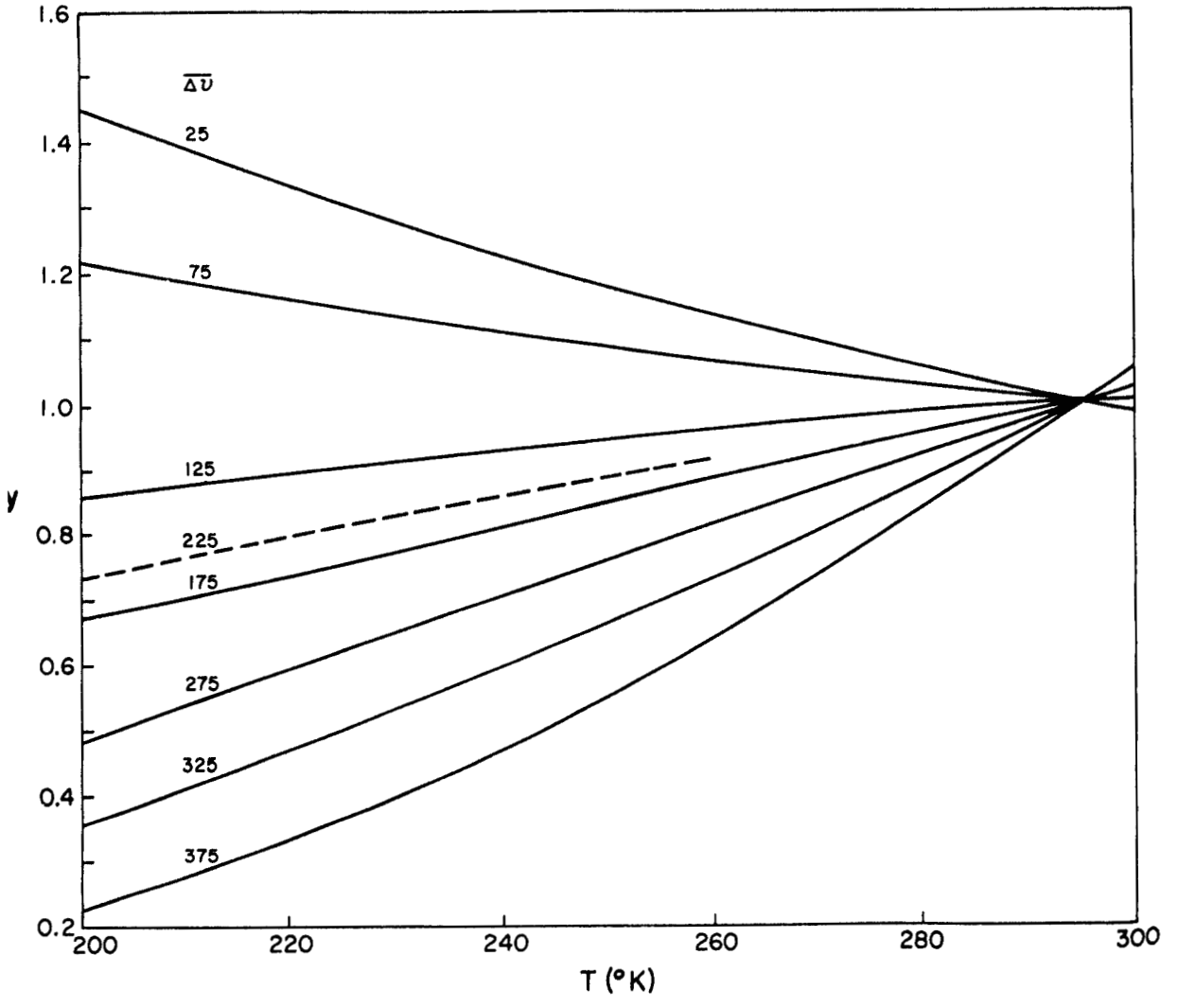

FIG. 6 TEMPERATURE CORRECTION IN 6.3μ H_2O BAND.

behavior of y for $\Delta\nu$ = 175 and 225 cm^{-1} is difficult to explain but appears related to the presence of relatively strong absorption lines in the region 200 to 205 cm^{-1} and 245 to 250 cm^{-1}.

4.3.3 Temperature Dependence for Entire Band

In order to determine the effect of temperature dependence for the entire 6.3 μ band the calculations using the y factor in Figure 6 were made for $\sqrt{mP}$ = 5 and 10 $cm^{1/2}mb^{1/2}$ at temperatures of 200, 250, and 295°K. The results are shown in Table 3.

TABLE 3

TRANSMISSIONS (%) FOR 6.3 μ H_2O BAND

Temperature	$\sqrt{mP}$	
(°K)	5	10
295	46	30
250	48	32.5
200	50	36.5

These results indicate that the temperature effect on transmissions over the entire 6.3 μ H_2O band is relatively small. The effect of temperature on the wings causes the transmission for the whole band to decrease with increasing temperature.

4.4 Temperature Dependence for 15μ CO_2

4.4.1 General

The 15μ CO_2 band is similar to the 6.3μ H_2O band in that absorption in the wings increases with temperature, while at the center it decreases. However, the central portion of the band is opaque for transmission through a layer of atmosphere only 100 mb in thickness. The result is that absorption over the entire CO_2 band increases with temperature.

4.4.2 Theoretical Transmission

Kaplan (unpublished, but see Kaplan, 1959) has computed the theoretical mean transmissions over 5 cm^{-1} intervals of the 15μ CO_2 band in four different model atmospheres for uniformly distributed CO_2 with a surface value of 260 cm NTP. He assumed a temperature structure in accordance with the equation

$$\frac{T}{T_o} = \left(\frac{p}{p_o}\right)^k \tag{8}$$

Transmissions were computed for T_o = 313 and 273^oK (at p_o = 1000 mb) and for k = 1/6 and 1/3. These values

of k are approximately equivalent to lapse rates of 5.5 and 11°C km^{-1}, respectively. Transmissions were computed for various small layers (50 mb at lower levels); finally the transmissions from various levels to 100 mb were determined. A sample curve for the transmissions from 1000 to 100 mb for $T_o = 273°K$ and $k = 1/6$ is shown in Figure 7. The atmosphere is essentially opaque in the central region between 630 and 710 cm^{-1}.

4.4.3 Comparison of Theoretical with Empirical Transmissions

To determine whether Kaplan's theoretical transmissions over the entire $15\mu CO_2$ band agree with Howard's experimental values, comparisons were made for 50 mb layers of the model atmosphere in which the mean temperature of the layers were close to the temperature of Howard's experiments (approximately 17°C). The results for two 50 mb layers containing a normal atmospheric amount of CO_2 (13 cm, NTP) and for one layer containing only 1/2 the normal amount are shown below.

TABLE 4

COMPARISON OF THEORETICAL (KAPLAN) AND EMPIRICAL (HOWARD) TRANSMISSIONS FOR ENTIRE 15 CO_2 BAND

Layer (mb)	CO_2 (cm)	Transmissions (%) Kaplan	Howard
600 - 650	13	58	56
600 - 650	6.5	64.5	61
800 - 850	13	55.5	52

These results indicate that Kaplan's theoretical absorptions are consistently about 5% smaller than Howard's empirical values. According to a private communication from Howard the theoretical values appear to be within the range of experimental error.

4.4.4 Variation of Theoretical Transmission with Temperature

In order to be able to correct for temperature in the 15 μ CO_2 band in satellite or balloon observation it would be desirable to calculate transmissions similar to those of Figure 7 for any lapse rate and for layers of different pressures. Such calculation can be made with Kaplan's methods, involving

the use of an electronic computer. However, several tests with the results for his four model atmospheres indicate that an empirical correction for temperature may be made. For a layer extending from pressure p to 100 mb, transmissions for the four model atmospheres were plotted as a function of the temperature at the mean pressure of the layer. An approximately linear relation was found. A better linear relation was obtained by using a temperature T at a pressure of 0.65 p + 0.35 X 100 mb, thus in effect using a temperature at a level closer to the level p. The result is shown in Figure 8, in which the transmissions between the indicated pressure p and 100 mb are plotted as a function of T. The straight lines drawn by eye fit the plotted points very well. Thus, temperature correction for the entire 15 μ CO_2 band is obtained by simple graphical methods.

The same procedure was attempted for 5 cm^{-1} intervals of the CO_2 band (Figure 9). A good linear relation is evident in the 5 cm^{-1} intervals centered at 600 and 730 cm^{-1}. However, the linear relation does not hold in the central highly absorbing region as characterized by the interval centered at 700 cm^{-1} in Figure 9.

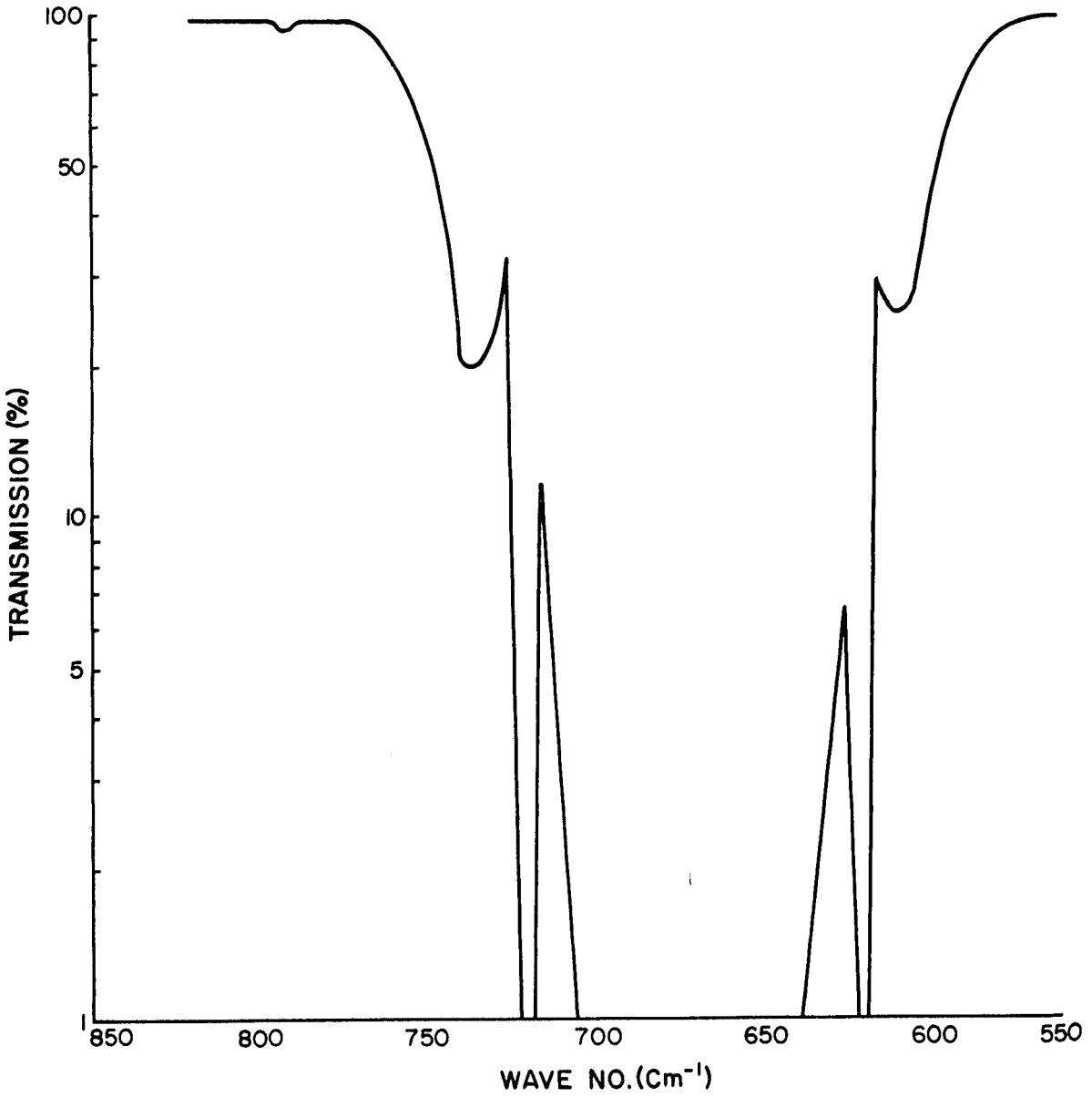

FIG. 7 THEORETICAL TRANSMISSION FROM 1000 TO 100MB FOR $T_0 = 273^\circ$, $K = 1/6$ IN 15μ CO_2 REGION.

(BASED ON CALCULATIONS BY KAPLAN).

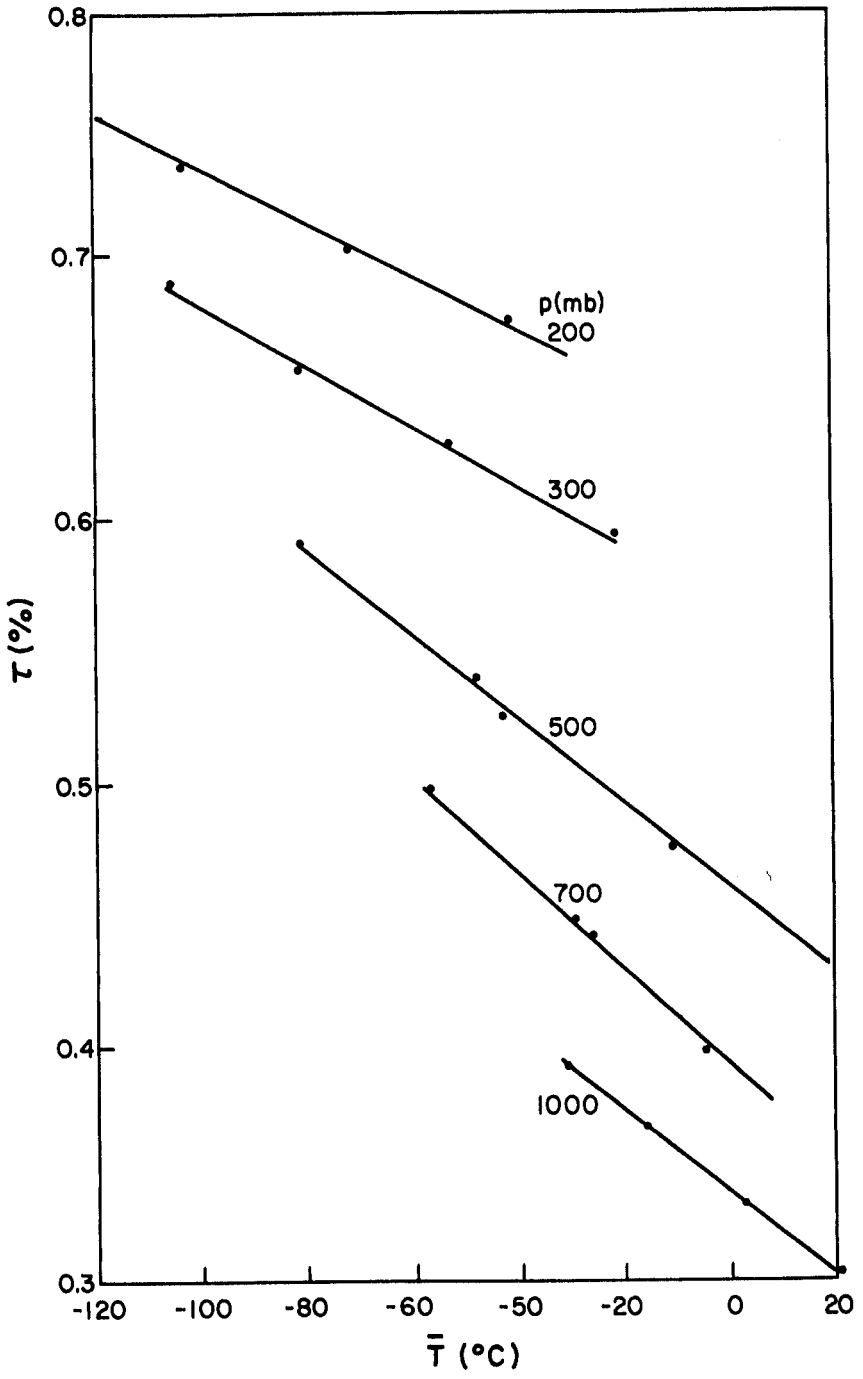

FIG. 8 THEORETICAL TRANSMISSIONS FOR 15μ CO_2 BAND AS A FUNCTION OF A WEIGHTED TEMPERATURE $\bar{T}$.

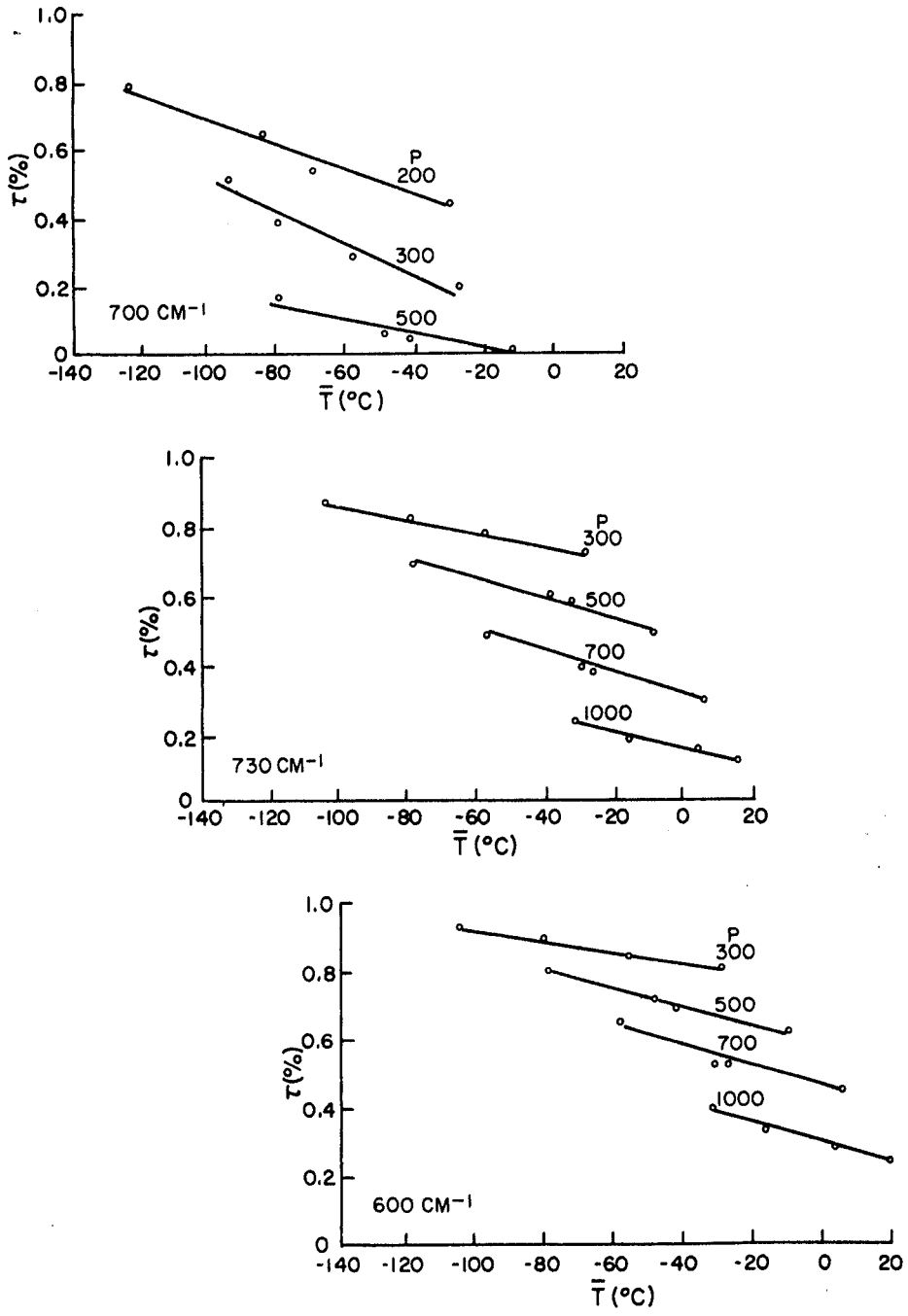

FIG. 9 THEORETICAL TRANSMISSIONS AS A FUNCTION OF $\bar{T}$ FOR 5 CM^{-1} INTERVALS CENTERED AT THE INDICATED WAVE NO.

4.5 Comparison of Theory with Observation

4.5.1 General

The only source of data now available for comparison of theoretical transmission of the infrared through the atmosphere with actual transmission is the balloon observations in Alamogordo, New Mexico, reported by Strong, (1959). His observations were made with a balloon-borne grating spectrometer which recorded, as a function of wave length, the difference in the power received in fairly narrow beams from two directions, one centered at about 60° above the horizontal, the other at 60° below the horizontal. It was calibrated in flight periodically by recording the spectrum of radiation power difference in the same beam widths from two black body radiation sources at the temperatures of dry ice and of water and ice. Thus the ratio of the radiation difference from the atmosphere to the radiation difference from the black bodies effectively eliminated instrumental parameters, and the data could be interpreted in terms of the well-known theoretical black body radiation density functions. The published calibrated data gave the power difference over wide spectral bands, as obtained by an approximate integration over the original detailed spectral data.

4.5.2 Comparison with Strong's Measurements

Figure 10, taken from Strong, shows the variation of radiation flux (upward minus downward) with altitude for different balloon flights at Alamogordo, New Mexico, on 6 March and 29 April 1959. The units in the ordinate, which are in terms of hemispheric radiation, is a factor of π greater than the equivalent units of Figure 4.

To determine representative soundings for the flights, interpolation was made between the 1200Z El Paso and Midland radiosondes. Calculations of the upward radiation were made for an air mass of 1.15 (cosecant 60°).

For the 6.3 to 8.2 μ region (1220 - 1587 cm^{-1}) the K values of Table 2 were used to obtain an average transmission as a function of mP. No humidity data were available above 500 mb but standard values of the specific humidity were assumed above that level (see Volume I). No temperature correction was made, since it is presumed that for a full half of the 6.3 μ H_2O band such correction would be small (see Section 3.3).

For the 8.2 to 11 μ and 9 to 12 μ regions the standard O_3 distribution of Paetzold was assumed, as discussed in

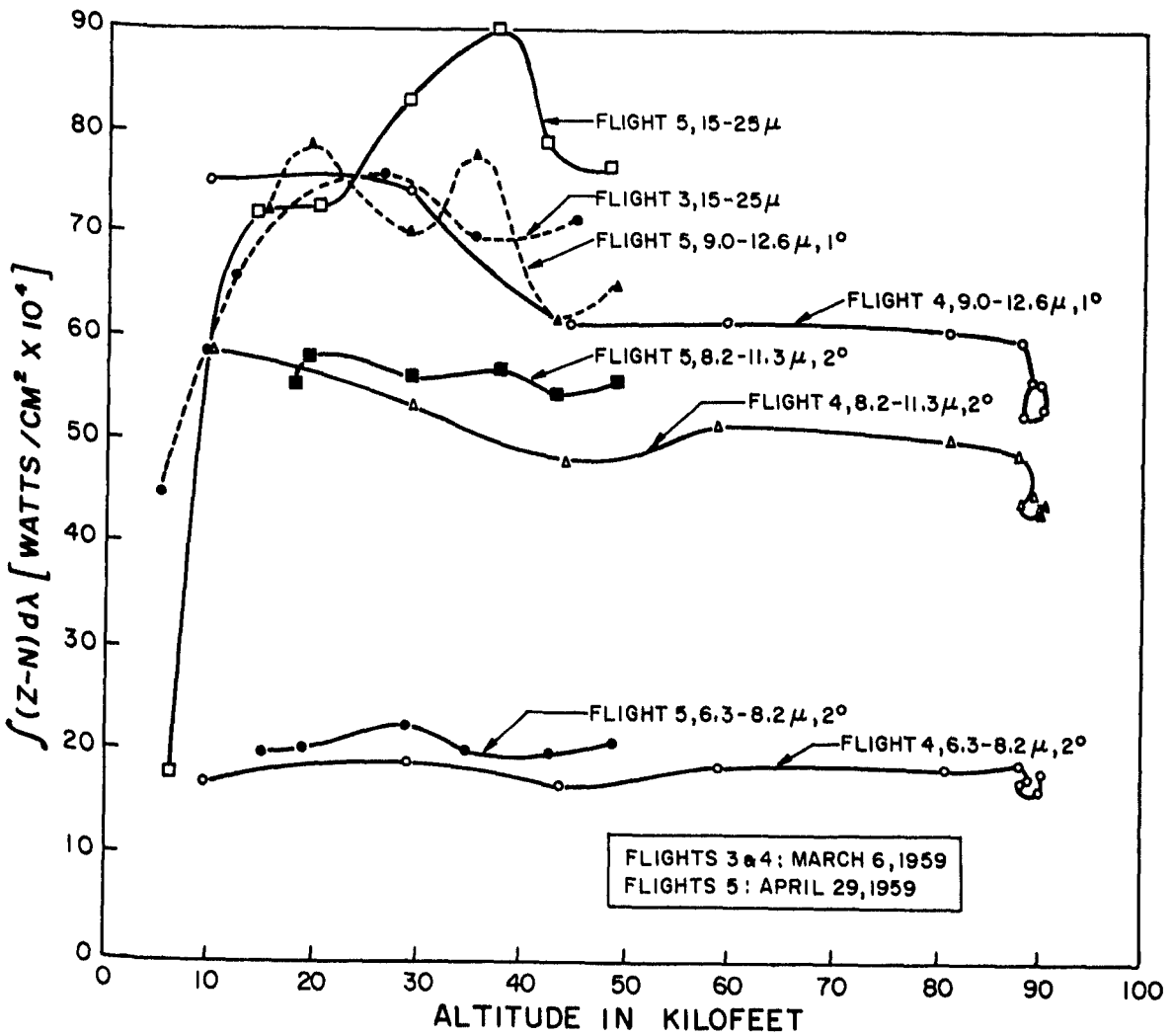

FIG. 10 VARIATION OF UPWARD MINUS DOWNWARD RADIATION WITH ALTITUDE (AFTER STRONG).

Volume I. Since most of the ozone lies above the 100 mb region, sample calculations of the downward radiation were made, but because of the nearly isothermal conditions at these altitudes it was found to be essentially negligible compared to the upward. These regions also envelop portions of the "window" region in which absorption due to water vapor occurs. The transmission in these regions was assumed to be (see Volume I):

$$\tau = e^{-\frac{4}{3} \times 10^{-4} mP} \tag{9}$$

where m is in cm and P in mb. Because of the dryness of the soundings the correction due to this effect is relatively small.

The 15 to 25μ region covers half of the CO_2 band and a portion of the rotational water region. For CO_2 it was assumed that the 12.5 to 17.9μ absorption band is completely symmetric so that the theoretical transmissions of Figure 6 with temperature dependence could be used for the 15 to 17.9μ region. K values of Table 1 and the y values of Figure 1 (for temperature dependence) could be used directly for the rotational water region. Results of the computations and comparison with the observed radiation amounts are shown in Table 5.

TABLE 5

COMPARISON OF COMPUTED AND OBSERVED RADIATION AMOUNTS

(10^{-2} cal cm^{-2} min^{-1})

FOR 6 MARCH AND 29 APRIL 1959

Date	Spectral Region (μ)	Computed	Observed
6 March	6.3 - 8.2	2.9	2.7
29 April		2.7	2.9
6 March	8.2 - 11.3	7.9	7.2
29 April		10.8	8.2
6 March	9.0 - 12.6	9.2	9.0
29 April		12.5	10.3
6 March	15 - 25	11.2	10.4
29 April		12.1	11.2

All regions except the 6.3 to 8.2μ region show consistently larger computed outgoing radiation than actually observed. Larger deviations appear to be in the window and ozone regions 8.2 to 11.3μ and 9.0 to 12.6μ, which may be partly due to dust layers, too low ozone contents assumed for the troposphere, or to departures of ground temperature from that read in the instrument shelter. The 15 to 25μ region

shows computed values to exceed observed by about 8%. Better agreement would have been obtained taking into account the overlapping of the rotational water region with the 15μ CO_2 band or by increasing the absorption in the 15μ CO_2 region by about 6%, thus bringing Kaplan's theoretical values more in agreement with Howard's experimental values. Nevertheless, the agreement of theoretical calculation with the observations made by Strong are perhaps better than might have been anticipated from the known shortcomings of the radiosonde data. It is to be noted that a 10% error in the first three spectral regions involve an error in the equivalent temperature of 4 to 5°C; in the 15 to 25μ region, it amounts to about 7°C.

4.6 Infrared Maps for 9, 10 and 11 February 1959

4.6.1 General

Since any broad spectral region gives a similar radiation pattern, it will suffice to display a "clean window" map for comparison with synoptic patterns. A clean window map shows the actual temperatures of the surface for clear conditions or of the cloud top for overcast conditions. For partial cloudiness the radiation from cloud top and surface is

prorated and an equivalent temperature computed. Although it is realized that the infrared windows: 8.3 - 9.1μ and 10 - 12.5μ are essentially "dirty windows", nevertheless, considering the tremendous contrast between warm surface areas and the cold high overcast areas, the reduction in contrast by the slight absorption is relatively small.

The case discussed in Volume I involves a deep cyclonic storm with the circulation extending to stratospheric levels. Under such conditions it was shown that an infrared map gave a pattern which could be interpreted in terms of the flow pattern associated with the storm. In this section, a high index situation, involving relatively shallow pressure systems and extremely rapid motion is analyzed. Surface maps and "clean window" maps at 24 hour intervals for 3 days indicate the association of surface pressure patterns with infrared patterns which would be observed by a satellite.

4.6.2 Maps for 9 February 1959

Figure 11 shows the surface map for 1200Z, 9 February 1959. A weak storm has entered the Pacific Northwest and another somewhat deeper storm is located over southwestern Colorado. A wavy warm frontal system extends eastward to the

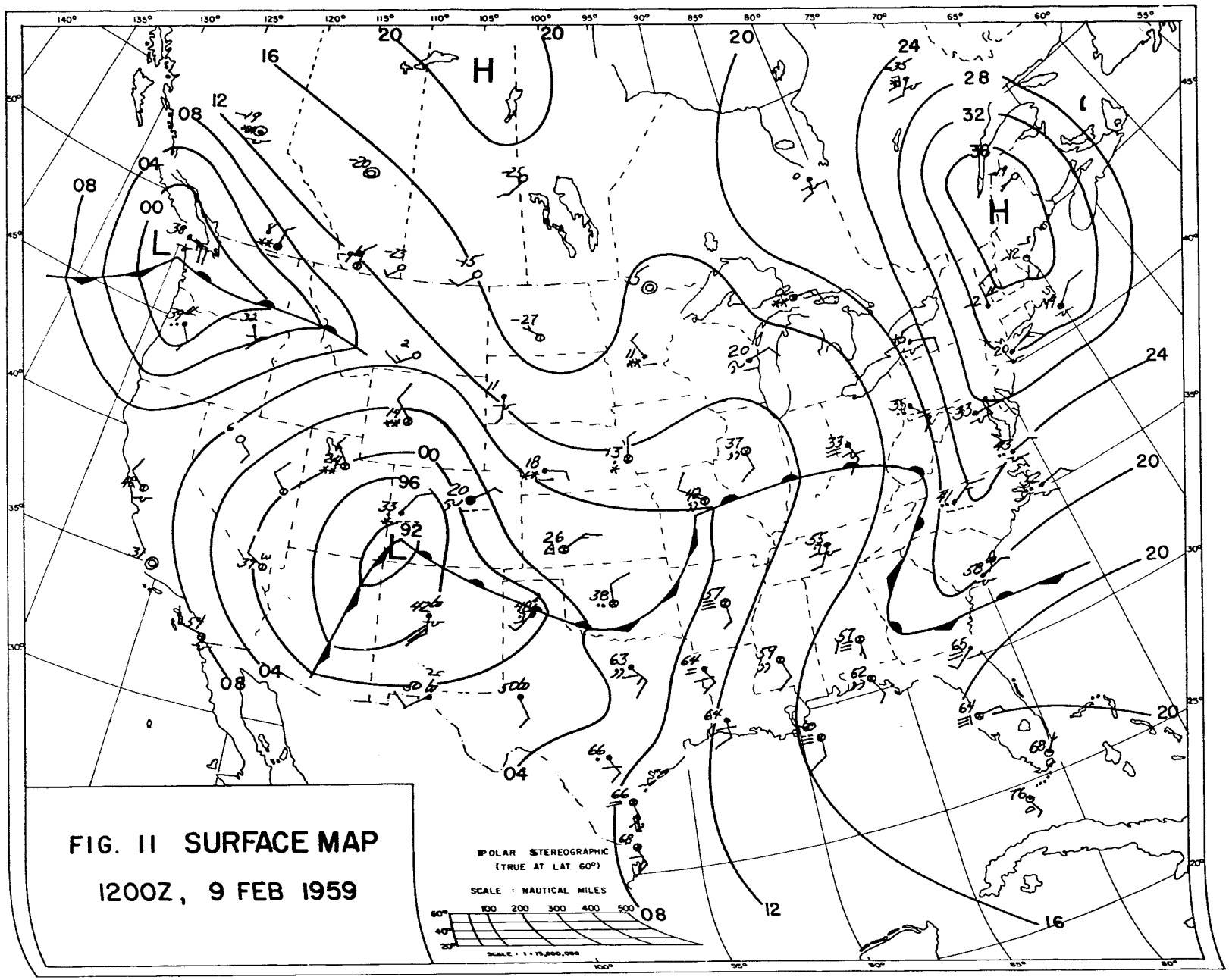

FIG. 11 SURFACE MAP

1200Z, 9 FEB 1959

Atlantic. Warm tropical air with widespread fog and drizzle extends northward as far as southern Illinois. Widespread snow cover with cold clear radiation conditions prevailed over most of Canada. It is of interest to determine whether these very cold surface conditions can be distinguished from the cold temperatures associated with high clouds.

Figure 12 shows the window map for this day. The high clouds of the Pacific northwest storm show up as a cold area of -40°C. Another cold area of -40°C over Utah is associated with the Colorado storm. Somewhat surprisingly a vast cold area of -60°C extends from Texas to the Atlantic and northward to New England which cannot be immediately interpreted as being associated with the synoptic pressure pattern. This vast cirrus overcast is not observed at the surface because of the widespread drizzle but is fairly evident from the radiosonde plots which show nearly saturated conditions extending to the highest levels reported (generally about 400 mb) and unstable lapse rates above almost to the tropopause. The wave on the surface map over Missouri may be interpreted on the window map as a northward protrusion of the cold area into this region. A relatively warm area, due to low cloud tops

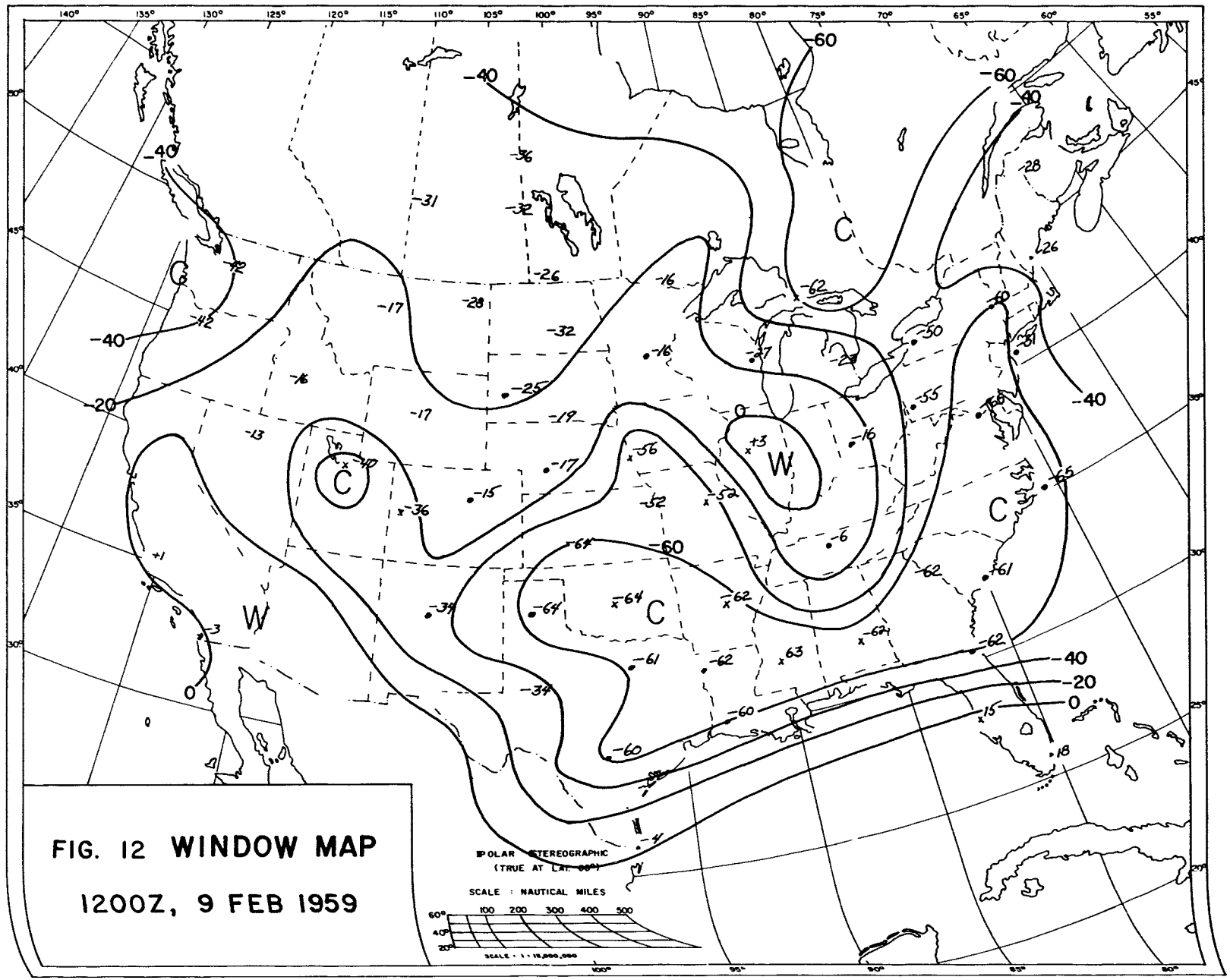

FIG. 12 WINDOW MAP

1200Z, 9 FEB 1959

evident in the Peoria and Nashville radiosondes, is located to the east and northeast of the wave.

The clear cold snow-covered area of southern Canada with temperatures of -30 to -40°C is seen as a relatively flat region on the infrared map and is readily distinguishable from the -60°C high cloud region north of Lake Huron.

This window map for 9 February 1959 gives considerable information concerning the large scale field of vertical motion not readily apparent from a study of surface or upper air maps.

4.6.3 Maps for 10 February 1959

The rapid motion of the Colorado storm carried it to central Illinois in 24 hours (Fig. 13). Cold dry air to the west of this storm has penetrated to northern Texas. The Pacific storm, being blocked by the southward penetration of the Canadian high, shows little motion.

The window map (Fig. 14) shows a core of cold cloud top over Minnesota associated with the surface low pressure area over Illinois. This cold core is connected in the form of an occlusion to the vast cold (high cloud) region extending from

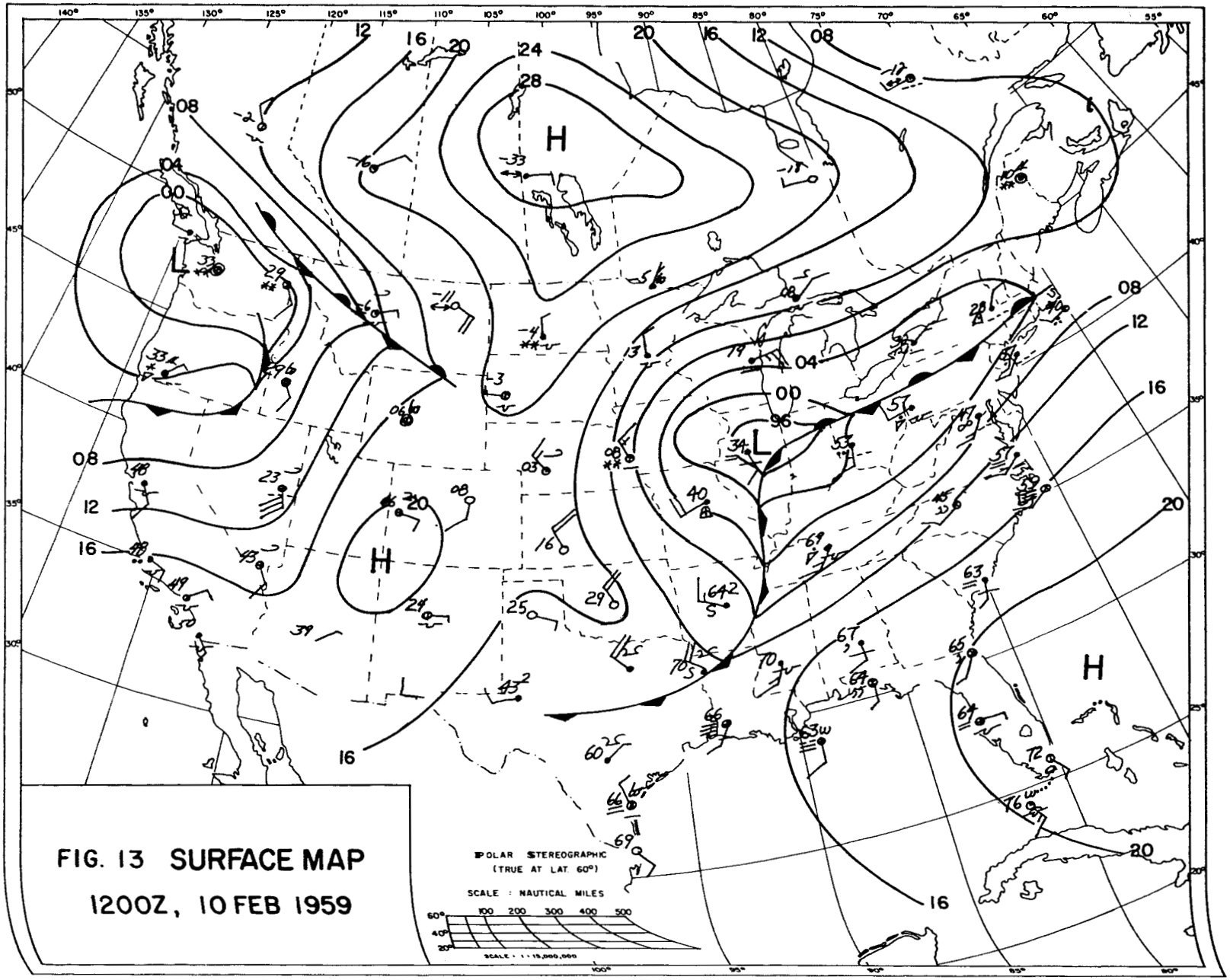

FIG. 13 SURFACE MAP
1200Z, 10 FEB 1959

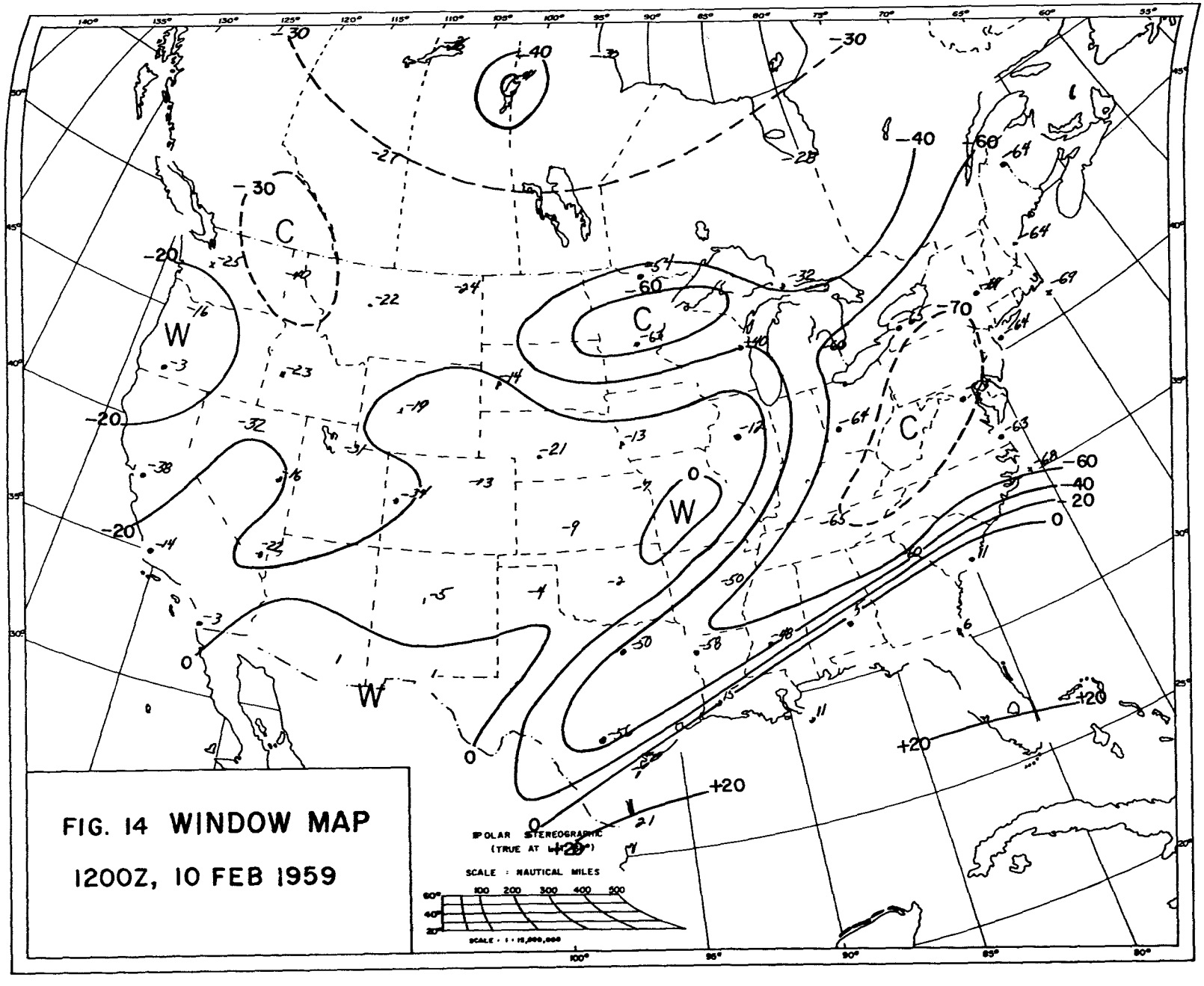

FIG. 14 WINDOW MAP

1200Z, 10 FEB 1959

New York to southern Texas ahead of the advancing cold front. Relatively warm clear conditions (but cold air for the surface) extend from Missouri to New Mexico west and southwest of the surface low. A steep gradient in the equivalent temperature occurs through South Carolina to Mississippi and marks the disappearance of the high cirrus ahead of the cold front.

The weak cold core of -40°C over northern Idaho is associated with the Pacific storm. It may be difficult to differentiate this area from the vast cold clear snow-covered area of nearly the same temperature over southern Canada.

It is evident that the window map for 10 February 1959 gives supplementary information concerning the Illinois storm, showing that most of the rising motion is occurring well ahead of the surface position of the cold front and indicating an occlusion process north of the surface position of this low pressure center.

4.6.4 Maps for 11 February 1959

With the cold front having pushed eastward to the Atlantic, a low pressure area is located southeast of Nova Scotia (Fig. 15). A disturbance on the cold front in the

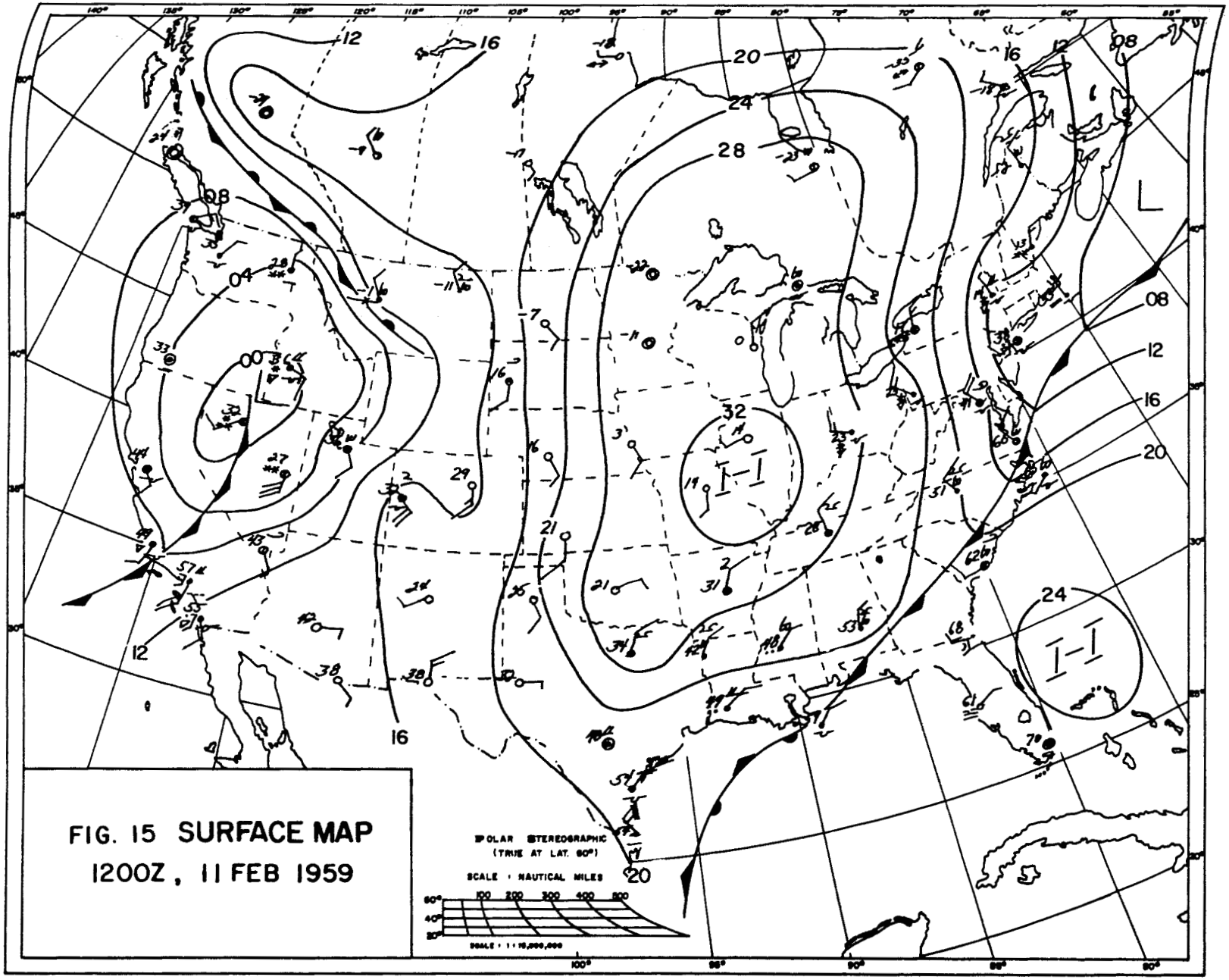

FIG. 15 SURFACE MAP
1200Z, 11 FEB 1959

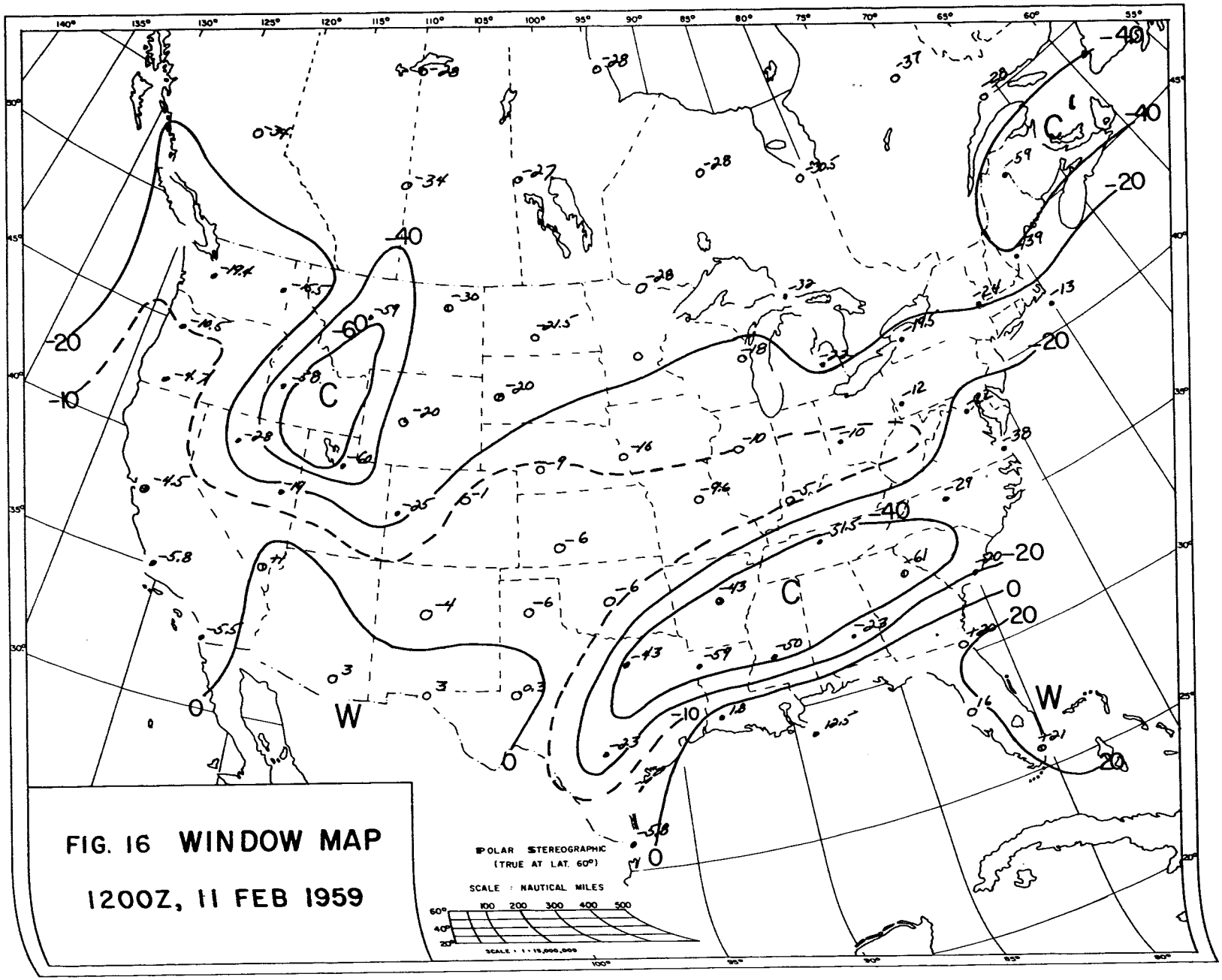

FIG. 16 WINDOW MAP

1200Z, 11 FEB 1959

Gulf of Mexico is causing some rain and extensive high cloudiness over the Gulf states. The western storm is now located over Nevada with snow extending northward through Idaho to western Montana.

The window map shows the cold high clouds over the Gulf states associated with the disturbance to the south. A belt of relatively warm equivalent radiation temperatures extends from Kansas to West Virginia. The cold region over Maine is the remnant of the high cloudiness associated with the Atlantic storm. The western storm, showing development of a more extensive and colder cirrus region, is centered in Idaho northeast of the developing storms in Nevada. A flat featureless pattern represents the vast snow covered area over Canada.

The pattern of vertical motion represented in the window map of 11 February 1959 is in excellent agreement with the synoptic pattern of the surface weather map (Fig. 16).

4.6.5 Characteristic Circulation Patterns

The cold and warm area of the window maps mark the location of large scale ascending and descending motion. The patterns also give indications of horizontal flow patterns.

Various characteristic patterns are associated with different stages of a cyclonic storm. In the early stages a relatively small area of high cloud with top near -40°C is located generally to the north of the cyclonic center at the surface. As the storm develops a more widespread cloud deck with top near -60°C develops, which extends in a band some 200 to 300 miles wide ahead of the cold front, and is joined to a vaster area ahead of the storm center. The occlusion process shows up as a separate small cold area with a narrow connection to the widespread cold area. Finally in the very deep storms, areas of ascending and descending motion are interspersed into a spiral circulation pattern. Similar patterns have been observed in the TIROS photographs.

The deeper the storms the better the association between infrared maps and surface weather maps. In high index situations, widespread cloudiness may appear which has no apparent connection with surface pressure patterns. In low index situations, the patterns of the infrared maps show a more direct association with surface features.

4.7 Summary and Conclusion

The analysis of the rotational H_2O, $6.3\mu H_2O$ and $15\mu CO_2$ regions makes it possible to calculate the outgoing radiation in any portion of these regions for an atmosphere of known properties.

For rotational water, at wave numbers smaller than 560 cm^{-1}, absorption increases with decreasing wave number. Temperature correction is made by modifying the Curtis approximation by a factor y which is related to the intensity and half width of the absorption lines. The factor y is chosen as unity for the temperature of the experiments but decreases with decreasing temperature. Thus, temperature dependence for rotational water results in higher transmission at colder temperatures.

For the $6.3\mu H_2O$ region temperature dependence is also taken into account by use of a factor y. Within 100 cm^{-1} of the band center y decreases with temperature, so that the transmission increases with temperature. However, since the central region is so opaque anyway, even for small atmospheric layers, temperature dependence in the central region is relatively unimportant. Outside of this central region the

transmission decreases as the temperature increases. As a result, for the entire 6.3 μ H_2O region, the transmission decreases as the temperature increases but its effect is relatively small.

The caluclations of the transmission for small intervals in the 6.3 μ H_2O band were made somewhat roughly from published graphs of Howard's empirical relationships. More detailed experimental transmissions in this region are desirable and will soon be available from experiments conducted at Ohio State University.

Calculations by Kaplan of the absorptions at small intervals in the 15 μ CO_2 region give values which are about 6% smaller than the empirical value of Howard at approximately the same temperature. The theoretical transmission from a given pressure p to the 100 mb level was found to vary linearly with a pressure weighted temperature. This result enables a relatively simple determination of temperature dependence for the entire CO_2 band. A similar linear relationship was found for 5 cm^{-1} intervals outside of the central region of the band. The variations of absorption with temperature in the CO_2 region amounts to about 20% of the absorption between -50 and $0^{o}C$.

From theoretical considerations it may be shown that temperature dependence in the 9.6 μ O_3 band is relatively unimportant. Calculations of the outgoing radiation involving the O_3 band are at best uncertain without measurements of distribution of the O_3 in the atmosphere.

Empirical relations may be used to determine the transmissions in the window regions 800 - 1000 cm^{-1} and 1100 - 1200 cm^{-1}. Theoretical calculations will be necessary to determine transmissions over small intervals in these regions.

Theoretical outgoing radiation in four different spectral regions was found to be relatively high compared to balloon observations of infrared radiation in these regions on two separate days over Alamogordo, New Mexico. A good fit was found in the 6.3 - 8.2 μ H_2O region. This may indicate that our assumptions of the water vapor content above 500 mb and the empirical transmissions for the 6.3 μ H_2O band are reasonably valid. Calculations involving the window and O_3 regions give agreement within 10% of the observed values on one day, but are about 20% too large on the other day. The discrepancy may be due to dust layers, an incorrect assumption concerning the distribution and amount of ozone, and to departures of ground emissivity from that of a black body.

For the 15 to 25μ region calculated radiations are about 10% higher than observed. The discrepancy may also be due to dust layers, and to overestimation of transmissions in the CO_2 band. This latter possibility should be looked into more carefully.

Nevertheless, considering the type of measurements, overall agreement is good. More comparisons of this type are desirable. Another source of data which may soon become available is the measurements of the total earth-emitted radiation from Explorer VII. Patterns of the measured radiation over a portion of the earth's surface would be most useful for comparison with theory.

With empirical methods available for the computation of the outgoing radiation from an atmosphere of known properties, the reverse problem of determining atmospheric characteristics from measurements of the radiation in selected spectral regions is more difficult. Kaplan (unpublished) has shown that it is possible to determine the temperature distribution from radiation measurements using six different wave lengths in the 15μ CO_2 region and one in the window region. The distributions are computed by a perturbation method from a best fit using layers of

different model atmospheres. Future research could well turn to simplified methods for estimating atmospheric temperature distributions and in addition the distributions of water vapor and ozone in the atmosphere.

The use of patterns of infrared radiation to give information concerning the macroscale field of vertical motion appears very promising. Maps of this nature may give supplementary information not apparent from surface or upper air measurements. The development of cyclonic storms can be followed by a sequence of such maps. A circulation pattern, involving the cold areas of high cloud tops and the warm areas from near the surface, is generally apparent in the area surrounding a deep storm. Such circulations in the form of spiral patterns have been observed photographically from TIROS I. Infrared maps give information on the heights of cloud systems not apparent in TIROS photographs. The preparation of infrared window maps from observations of an infrared sensor on a future TIROS should therefore add another dimension to the interpretation of these spectacular photographs.

Blank page retained for pagination

CHAPTER III

CLOUD STUDIES

ABSTRACT

Ten mid-United States composite radarscope pictures are presented in Section 1, showing radar precipitation echoes, frontal positions, and total cloud cover. These are accompanied by analyses of the low, middle and high cloud shields. Three strip composites using radarscope pictures, taken during aircraft reconnaissance flights over the eastern Pacific, are included with their corresponding cloud and frontal analyses. The ten cloud-analyzed continental composites and the reconnaissance composites are discussed in the text with respect to the cloud-precipitation relationships. Characteristics of the cloud patterns which seem, from the composite analyses, to be associated with precipitation or storm systems are discussed in terms of the likelihood that they could be discerned from satellite photographs.

In Section 2, a number of operational conclusions and tentative research results are listed and described relative to the immediate operational use program. The post launching preparations for an analysis and use of satellite pictures in tropical meteorology are outlined. Phenomena of particular interest in these and the future studies are commented upon briefly.

Through the use of TIROS I photographs, a frontal system is studied and followed for a period of nine days in its movement across

the Pacific Ocean in the last Section of Chapter III. The series of TIROS I pictures show that it is possible to maintain a day-to-day surveillance of mid-latitude storms with a meteorological satellite. The rectified pictures show the movement and the day-to-day changes in the cloud patterns of the frontal system which could be an indicator of the future development in a storm.

CHAPTER III

SECTION 1

CLOUD SHIELD AND RADAR PRECIPITATION ECHO RELATIONSHIPS WITH SATELLITE APPLICATIONS*

1.1 Introduction

This Section attempts to indicate those relationships which might exist between cloud cover, as observed from the ground and aircraft; and precipitation, as indicated in radarscope photography. These results are then studied to determine their usefulness when applied to cloud cover observations which might be expected from a satellite.

In the process of selecting suitable storms for analysis, the U. S. Weather Bureau's daily weather maps for the years 1957, 1958, and 1959 were studied. From this study a number of situations which seemed typical of various storm types were selected. The number of promising situations was reduced by study of radarscope films and by discarding the storms occurring on days of insufficient or poor radar film coverage. Most of the storms selected by this method were in the Mid-West.

Cases involving cloud and precipitation data obtained by airborne observers and instruments were limited to the three Pacific weather reconnaissance flights during which the aircraft's radarscope was photographed.

*The material in this Section was taken from Scientific Report 1, "Cloud Shield and Radar Precipitation Echo Relationships with Satellite Applications", by F. L. Ludwig and R. E. Nagle, Stanford Research Institute. The work was sponsored under Contract No. AF 19(604)-5982, under ARPA Order No. 26-59. In addition, the reader's attention is invited to the aforementioned report for a discussion of four additional continental storms plus thirteen other composites from West Coast and picket ship radarscope pictures.

1.2 Data Sources

1.2.1 Radarscope Photographs

The radar pictures used in the construction of the composites shown in this study were made from an extensive collection of radarscope film taken at various Air Defense Command stations during the International Geophysical Year, 1957-1958. Stations whose film was used in the construction of the composites of this report and its appendix are shown in Fig 1, * with areas of 150-mile-radius coverage indicated. In no one instance are films from all the sites shown used. The flight tracks and area of radar coverage of the composites made from weather reconnaissance flight radarscope films are shown in Fig. 2.

1.2.2 Cloud Data

Cloud data recorded by surface observers has been obtained primarily from microfilm copies of the weather records at Asheville, N.C. Generally, these are copies of the original forms filed by the stations. U. S. Weather Bureau forms WBAN 10-A, B and D were used by most of the stations shown in Fig. 3. The cloud information used in the analysis of the storm of November 17-19, 1957, was obtained directly from the stations shown in Fig. 4.

Cloud observations taken during the weather reconnaissance flights were recorded on Air Weather Service form 35; copies of the forms—from the three flights on the days radarscope photographs were taken—were graciously supplied to the authors by the 55th Weather Reconnaissance Squadron.

---

* Illustrations appear at the end of each sub-section.

1.2.3 Frontal Analyses

The frontal analyses shown in Figs. 6-35 of this chapter are those of the U. S. Weather Bureau. In some instances, slight adjustment of frontal positions to better correspond with the radar echo patterns is indicated. These adjustments are usually obvious, but have not been made because it was felt that the use of completely independent analyses was more important than achieving perfect compatibility. The agreement between radar echoes and frontal analysis is usually very close and adjustments in either would have dulled the significance of this agreement.

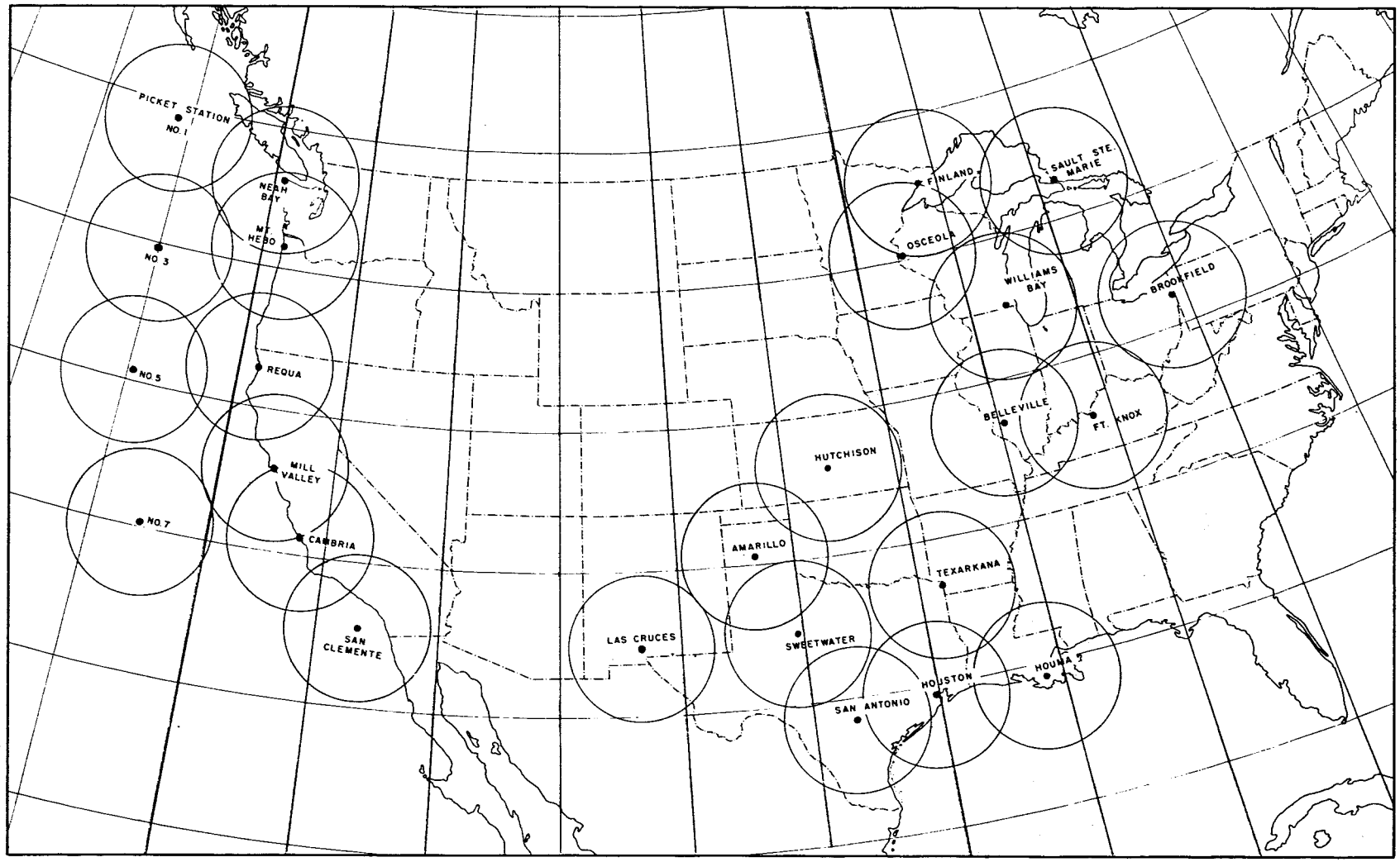

FIG. 1

RADAR STATION NETWORK

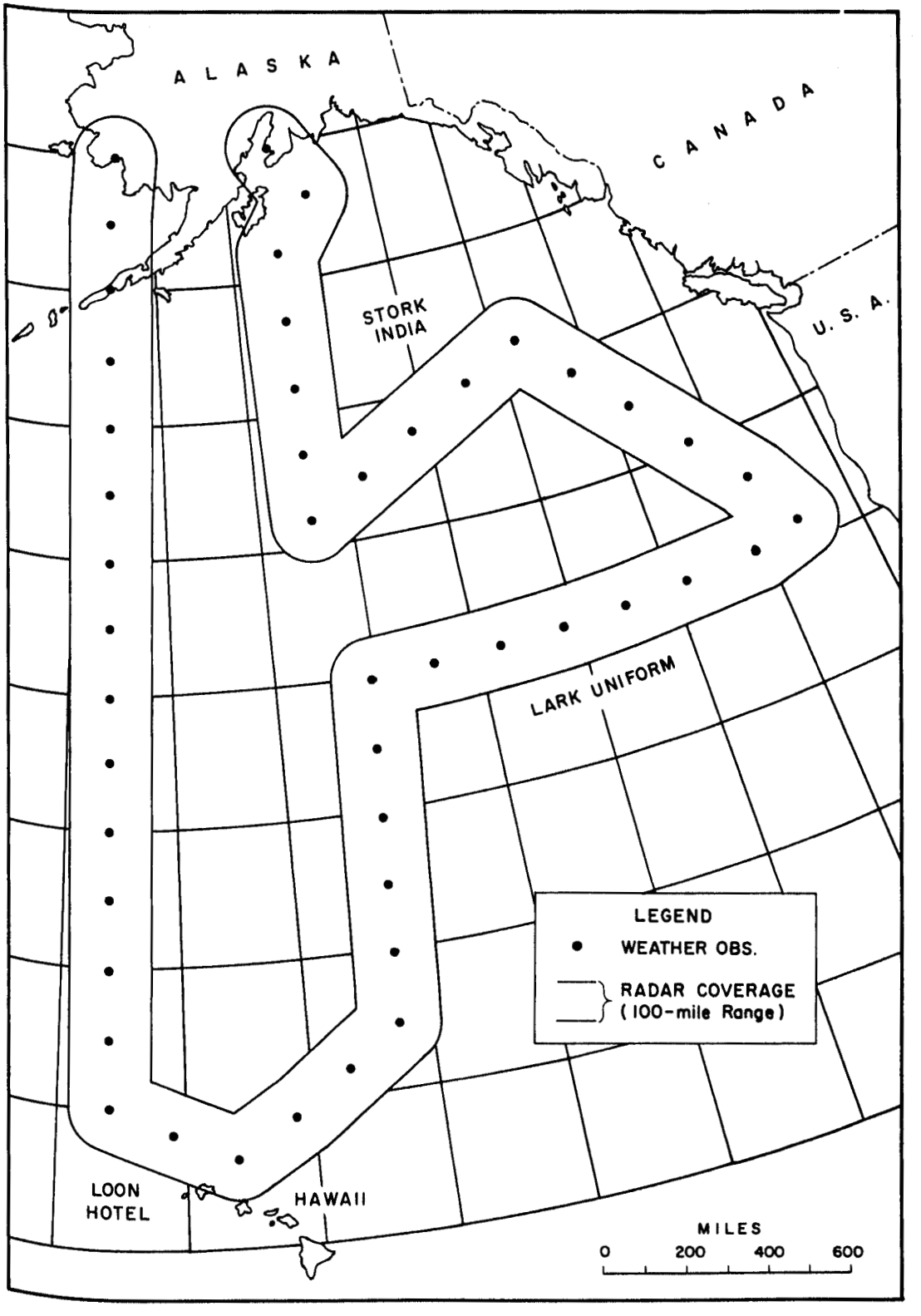

FIG. 2

RECONNAISSANCE FLIGHT TRACKS AND RADAR COVERAGE

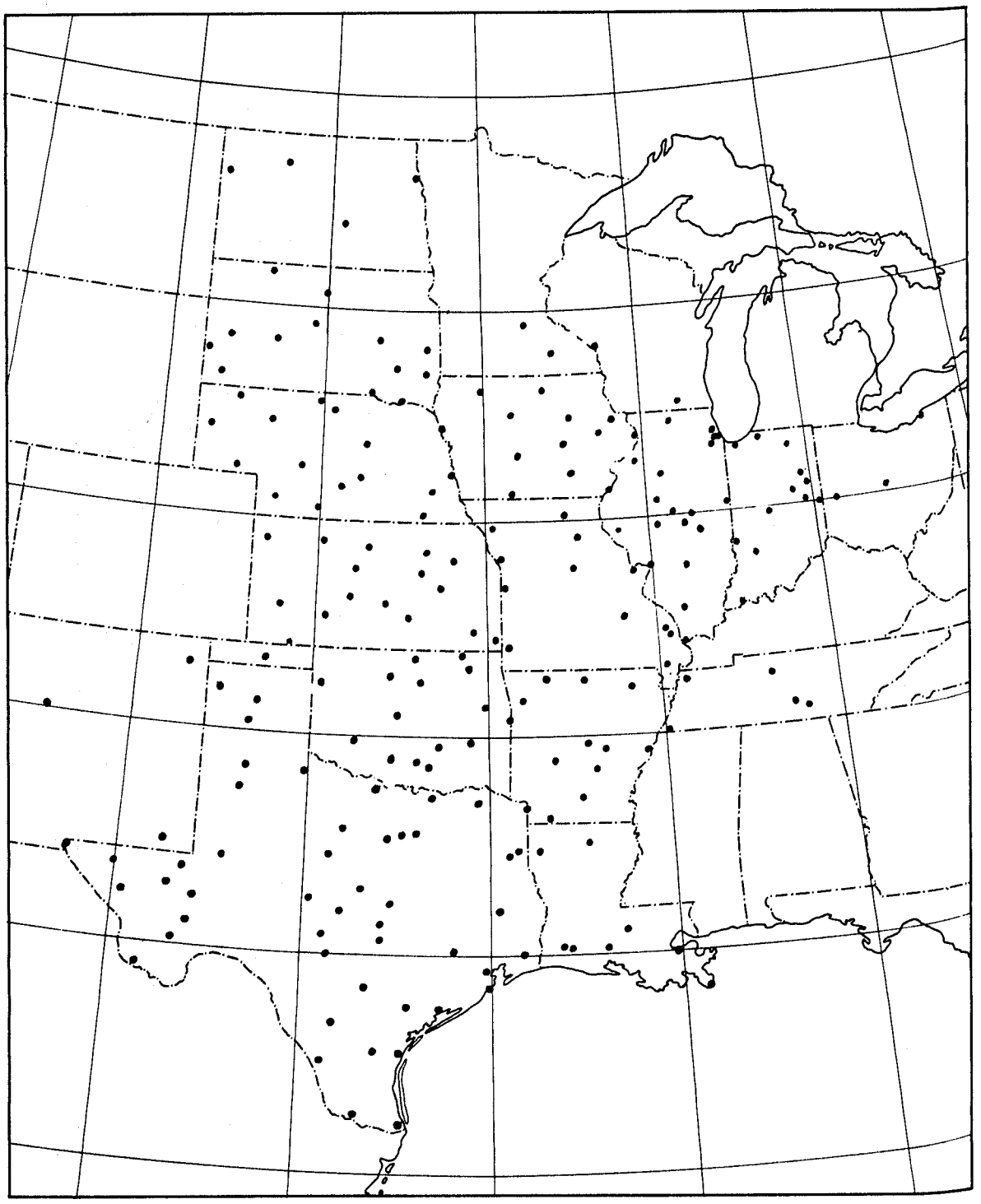

FIG. 3
CLOUD DATA NETWORK

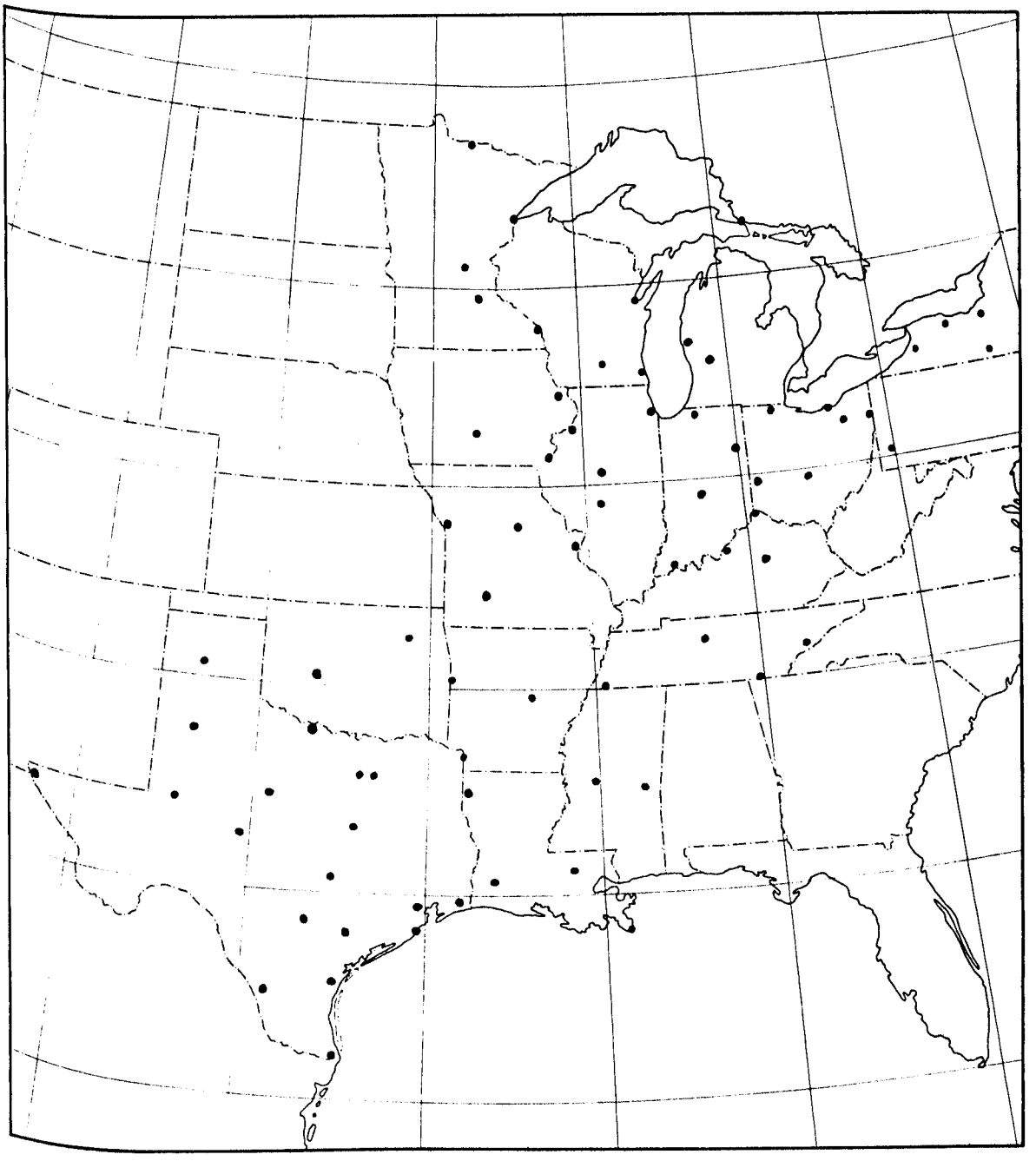

FIG. 4

CLOUD DATA NETWORK USED IN ANALYSIS OF 17-19 NOVEMBER 1957 STORM

1.3 Methods of Analyses

1.3.1 Continental Data

1.3.1.1 Radar Composites

The analyses of storms over land were made as follows. After a storm was selected, prints of the radarscope pictures were made to a scale of 100 nautical miles to the inch. These pictures were then properly placed and aligned on the base map. They were cut and pasted to the map to form the final composites. To prepare illustrations for this report, overlays were made on clear plastic. These overlays showed frontal position and the distributions of total sky cover. The ground echo patterns were also blocked out with the overlay. The composite-overlay combination was then photographed, and these pictures were used for the illustrations of this report.

1.3.1.2 Cloud Analyses

The cloud analyses, accompanying the continental composites, have proceeded strictly from the point of view of the reports of ground based observers. This approach leads to the representation of the cloud cover as a continuous field although the actual cloud formation itself may be discontinuous. For example, in the exaggeration shown in Fig. 5, the observer at A has total sky cover, the observer at E has none; and the intermediate observers see varying amounts of partial sky cover even when the actual cloud sheild ends abruptly. Thus, it is quite possible that, where the isopleths of reported cloud cover are closely packed, the cloud sheet may have a sharp boundary. However, such information was not available in the data. The nature of the

analysis and their possible relation to the actual cloud field should be remembered when attempting to visualize what a cloud observation satellite might have seen in the situation.

The total sky cover and low cloud cover analyses are straightforward, but, due to the large amounts of low cloud, the analysis of middle and high cloud cover usually had to be based on sparse data. Ground based cloud observations suffer from the fact that the "summation principle" is utilized in reporting multiple cloud layers on WBAN form 10B. The cloud amount reported at any particular level is based on the percentage of the total sky covered by clouds up to the level of interest. If low clouds exist, then the fraction reported for the amount of a higher cloud layer does not necessarily represent the true cloud cover at the higher altitude. In such cases the data were altered so that the higher-cloud-covered fraction of that part of the sky which was not obscured by the lower layer was assumed to apply over the entire sky. For example, if the fraction of the sky reported covered by low cloud is 4/10, and the fraction reported covered by middle cloud is 3/10, then it is assumed that the total fraction of the sky by middle cloud, N_M, is given by:

$$N_M = \frac{3/10}{1-4/10} = 5/10.$$

Of course, the larger the fraction of the sky covered by lower clouds, the less reliable the technique becomes.

Certain parts of the analyses, indicated by dashed lines, are considered doubtful either because of lack of data or because of uncertain data. Dashed lines mark those areas which were overcast by clouds at the level represented by the particular analysis.

Cloud cover was not investigated for times corresponding to periods of total darkness in the area, because of the doubtful accuracy of nocturnal cloud observations and of the lack of pertinence to the problem of satellite cloud observations.

To facilitate the comparison of the radar echoes with the cloud distribution figures, the principal radar echoes seen in the composites and the area of radar coverage available in each case were entered on the cloud analyses.

In considering the validity of the cloud distribution charts, mention also must be made of the scale of both the cloud systems and the observing network. The intent of the analysis is to determine relationships, if present, between precipitation areas and cloud shields associated with synoptic scale weather phenomena.

The observations utilized in the nephanalysis of the November 1957 series were obtained from a synoptic scale network of stations while those used in the remainder of the continental composites were obtained from a network which approached the meso-scale. It is now recognized that meso-scale systems exist within synoptic patterns. Such systems generate clouds which may not show any definite relationship with the over-all large scale pattern (Fujita, et al, 1956). Obviously, it is not possible to completely define mesoscale systems with a synoptic scale observational network; nor can the cloud structure

associated with these mesosystems be completely separated from the larger scale features. There is the distinct possibility, too, that mesoscale cloud patterns are uniquely associated with more violent weather conditions and in their uniqueness may be more readily detected by satellite observations.

1.3.2 Reconnaissance Flight Oceanic Data

1.3.2.1 Radar Strip Composites

The construction of the strip composite photographs from airborne radarscope pictures was similar to the construction of the continental composites. The construction was complicated though, by the large number of individual pictures used and the difficulties involved in the orientation of the pictures. After the pictures had been taken and developed, prints were made for specific intervals along the track.* These prints were made to the same scale as the continental prints of the U. S., i.e., 100 miles to the inch. Positioned along the flight track, the prints were then aligned by using echoes on successive prints as a guide. Afterwards, the prints were cut and fitted together to reveal as completely as possible the detected precipitation echo pattern.

Initially, a spacing of 50 miles was used between successive prints. However, when the aircraft was in clouds a considerable attenuation was observed in the radar. As a result, this attenuation required a reduction in the print intervals to 25 miles for the composites constructed

*The position at which a picture was taken is obtained from information contained in the aircraft log, and the time and frame numbers recorded with the radarscope pictures.

for the Loon Hotel and Stork India tracks. This permitted a greater display of the echoes detected. Even with this reduced interval, all the echoes visible in the film record could not be presented in the composites.

A graphical representation of the total echo, as detected on each flight, is shown in the overlays to the composites. These overlays are felt necessary due to the loss of detail in reproduction of the strip composite. The information in these overlays is not an exact positioning of the echoes. Instead, the information is provided as a guide to the actual data contained in the original film.

The weather reconnaissance squadrons' WB-50D aircraft are all equipped with AN/APS-23 radars. This is an X-band, 3-cm radar with peak power output of 44 kw. Its antenna is mounted in a bubble beneath the fuselage, allowing 360° scan operation. The radiational pattern is cosecant squared and has 55.0° vertical and 1.50° horizontal beam angles.

With the antenna tilt at zero degrees, the radar is capable of detecting clouds and precipitation areas from the flight level down to the surface. Consequently the echoes seen in the strip composites at the range of 100 miles originate from energy reflected from precipitation generally below 24,000 feet.

1.3.2.2 Cloud Analyses

Observations taken from weather reconnaissance positions were used as the primary information on which the cloud analysis was conducted.

In the RECCO code (AWSM 105-34), the aircraft is considered to be located at the center of a cylinder of air, 30 nautical miles in radius. "From this position, present weather, cloud types and amounts, flight conditions, and other observational elements are observed as occurring within the cylinder. Outside the cylinder, the quadrantal concept is used to report prevailing conditions in the four major quadrants."

If no obstruction to visibility exists, at the 500-mb level the most distant point on earth visible from the aircraft is approximately 160 miles away. Thus, when the flight altitude is relatively cloud free, the 500-mb level provides complete visual observation of clouds over the area of radar coverage; when clouds or other obscuring phenomena exist at the flight level, or slightly below, the slant range visibility is greatly reduced.

The cloud type, amount, bases and tops, at each observation position were plotted. Contour lines for cover of equal cloud amounts, from 0-25%, 25%-50%, 50%-75%, and greater than 75% at low, middle, and high levels, were drawn from this plotted data; cloud reports from surface ships, when available, were used to supplement the reconnaissance data. After the total sky cover at each level had been analyzed, the observed cloud types were entered in the areas where they were reported.

The total visible "top view" cloud amount charts were prepared in the following manner. The high cloud distribution was overlaid on the middle cloud chart and a composite cloud cover chart was drawn from these two layers. This composite distribution was then overlaid

on the low cloud amount chart and added to give the total cloud amount visible from above.

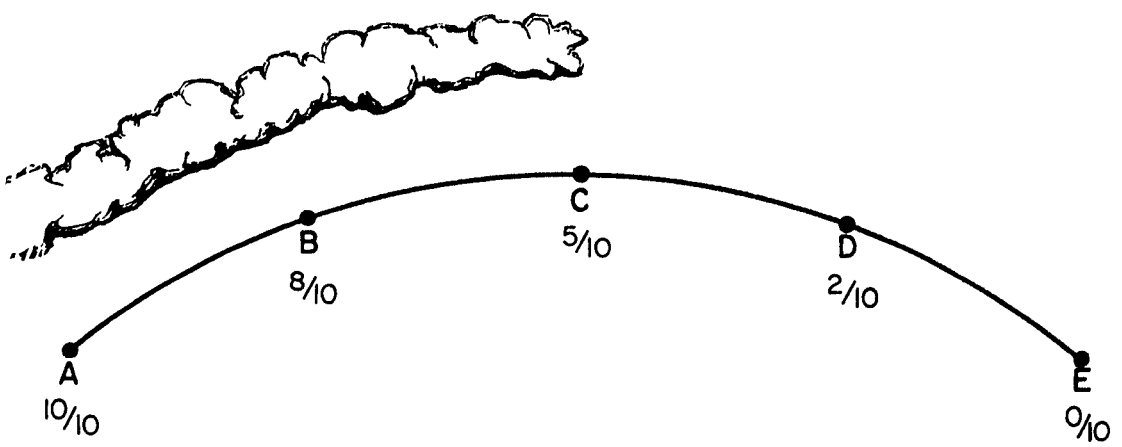

FIG. 5
SCHEMATIC REPRESENTATION OF CLOUD SHIELD

1.4 Discussions of a Continental Storm

1.4.1 17-19 November 1957 Storm

1.4.1.1 17 November 1957, 1200Z (Fig 6)

On 17 November 1957, at 1200Z, there was a stationary frontal system extending across the southern United States. Associated with this front were minor areas of precipitation in Tennessee, Kentucky, and southern Illinois. The precipitation was probably more extensive than shown; but, it was not detected because it was either too light or was below the radar horizon.

In addition to the area of rainfall associated with the front, there were several areas of showers. One of these shower areas was in the warm air mass in southern Arkansas. It seemed to have a linear pattern which suggested a meso-scale system such as a squall line. A very thin line of precipitation was detected in the Texas Panhandle. This line and the showers in Kansas were probably indicators of local convective activity in the cold air mass, with the former possibly taking its configuration due to a local asymptote of confluence in the streamline field. Such features are generally too small for identification in a synoptic scale analysis.

The sky was generally overcast throughout most of the area shown on the maps. This overcast area began 200-300 miles from the front in the warm air and extended well behind the front--with the exception of the small areas of broken sky cover in Texas and Mississippi. The termination of the overcast in the cold air was not shown because it extended outside the area of data coverage.

The low clouds accounted for most of the total sky cover near the southern boundary of the cloud shield, as can be seen by comparing the low cloud and total cloud analyses in Fig. 6. In the warm air mass, these low clouds were mostly stratus becoming strato-cumulus at the boundary. There was one notable exception and that was an area of cumulo-nimbus, corresponding to the showers in Arkansas. The northeastern part of the analysis consisted primarily of strato-cumulus. The rest of the low cloud area featured mixed reports of stratus and strato-cumulus with some reports of fracto-cumulus.

The decreasing low cloudiness and increasing middle cloudiness in Tennessee, Kentucky, and Illinois suggested that the precipitation in this area was caused by general upslope motion.

Most of the stations reporting middle cloud indicated alto-cumulus, while the high cloud was reported as cirro-stratus.

1.4.1.2 17 November 1957, 1800Z (Fig. 7)

The situation at this time was little changed. The front was in approximately the same position indicated six hours previously. Taking direction of flow into consideration, the area of total overcast generally began in the warm air and conformed roughly to the shape of the front. Unlike six hours previously, the line marking the beginning of the area of total overcast sky now had become closer to the front, more nearly 75 miles than 200 to 300 miles.

There still existed the area of up-glide rainfall in Kentucky. Cold air mass showers were still evident in Kansas. Warm air mass shower activity could be found in Texas and Louisiana.

The low cloud distribution is shown in Fig. 7. Except in an area on the cold air side of the front in Texas, where stratus and fracto-stratus predominated, this distribution consisted mostly of strato-cumulus. The overcast low cloud isopleth was found on the cold air side of the front in the Oklahoma-Arkansas area. The gross configuration of the isopleths of the low cloud cover suggest the possible formation of an area clear of low cloud, next to one totally overcast by low cloud. The patterns shown are generally oriented north-south with the clear area east of the overcast. This configuration became quite pronounced six hours later.

Again, the upglide nature of the rain in Kentucky was suggested by the low and middle cloud patterns.

The middle and high cloud shields very nearly conformed to the front except over the eastern part of the map. They also exhibited a tendency toward alternate areas of overcast and clear, as did the low cloud pattern. The middle clouds were generally alto-cumulus at the edge, becoming alto-stratus deeper in the overcast area. The high clouds were distributed similarly, varying from cirrus to cirro-stratus.

1.4.1.3 18 November 1957,0000Z (Fig. 8)

At this time a very small wave on the front could be found near the Oklahoma-Arkansas-Texas junction. Precipitation was found near this wave. Cold mass showers in Kansas and western Texas and warm mass precipitation in Mississippi were other precipitation features at this time.

The total sky cover pattern reflected the trends which were becoming apparent in the low, middle and high cloud shields six hours previously. An area of broken sky cover was found east of the overcast area which protruded into the warm mass.

The low cloud cover at this time markedly exhibited the characteristics of adjacent overcast and clear areas which had begun six hours earlier. Low cloud cover in the warm air consisted mostly of strato-cumulus and cumulus or cumulo-nimbus. Along the eastern part of the front were found double layers of low cloud, featuring stratus and strato-cumulus. Along the western part of the front stratus and fog were observed. The rest of the low clouds were primarily strato-cumulus becoming stratus toward the west.

The tendency toward decreasing low cloud coincident with increasing middle cloud was less than shown at the first two times. As would be expected, the precipitation over Kentucky, which was assumed to be caused by upgliding over the cold air, had either ceased or moved out of radar range.

The middle and high cloud patterns also exhibited the areas of clear or scattered cloud east of the areas of heavier cover. It appears as if this may be a precursor of the frontal wave formation. Were such a development generally characteristic of wave formation, it could be quite useful in the analysis of satellite cloud observations. It is not safe to generalize from the one case, though, and further study is warranted.

The middle clouds were generally alto-cumulus, with a few stations reporting alto-stratus. High clouds were cirro-stratus, becoming cirrus in the southeast corner of the map and along the southern edge. Some cirrus was also reported in Iowa and Nebraska.

1.4.1.4 18 November 1957, 0600Z (Fig. 9)

The wave in the front had become more pronounced. The precipitation was organized into lines along the cold front and an area of rainfall in Kentucky, southern Illinois, and Missouri, behind the warm front. Other areas of precipitation shown in this figure include those in the cold mass in Texas, along the Gulf Coast in Mississippi, and the snow over Lake Superior.

The cloud cover is not shown because of darkness in the area of observation.

1.4.1.5 18 November 1957, 1200Z (Fig. 10)

At this time, the wave in the polar front over southern Missouri was still more pronounced, and the cold front was extremely well marked by radar precipitation echoes. Warm frontal precipitation was strongly evident. Precipitation was also taking place in the Great Lakes region. Most of the area of interest was overcast, but part of the warm sector indicated broken cloud to within 100 miles of the cold front. Clearing began about 300 miles behind the cold front.

The edges of the overcast layers of all three levels of cloud conformed reasonably well in shape and location with the southern part of the cold front. The low cloud layer deviated from this pattern more widely than did the other two levels, with a small area of overcast

about 150 miles ahead of the cold front. The low clouds along the cold front were mostly cumulus and cumulo-nimbus. Strato-cumulus were ahead; stratus, fracto-stratus and strato-cumulus, behind. The central part of the area shown was covered with stratus, fracto-stratus and fog. Strato-cumulus clouds were found along the northern and eastern borders of the map.

The middle clouds were mostly alto-cumulus. The high clouds were reported as cirrus. Away from the edges of the high cloud deck, cirro-stratus was probably found but due to the overcast lower layers, such a supposition can not be confirmed.

1.4.1.6 18 November 1957, 1800Z (Fig. 11)

The frontal wave was still more pronounced at this time and had moved into central Illinois. There were strong radar precipitation echoes along the cold front and at the apex of the wave. There was also much precipitation well back of the frontal system in the cold air. The area of total sky cover extended about 200 miles into the warm air south of the warm front. General clearing began about 200 miles behind the southern part of the cold front. The remainder of the analysis was overcast.

The area of low cloud cover was distributed similarly to the area of total cloud cover. However, the low cloud cover area conformed more closely to the warm frontal position than did the total cover pattern. There was an area of broken low cloud just north of the frontal wave.

The predominant low cloud-type within the warm sector was strato-cumulus. Cumulo-nimbus predominated along the cold front.

These gave way to fracto-stratus, then to strato-cumulus and cumulus in the cold air mass behind the cold front. Preceding the warm front by 200 to 300 miles fracto-stratus was found, with one report of a cumulo-nimbus at the surface position of the warm front. Much of the remaining area shown had a low cloud covering of stratus.

Due to the uncertainties in the analysis of the middle and high cloud fields, it would be unjustified to attempt a detailed description of them. However, they do seem to conform generally to the frontal shape while extending some distance into the warm air.

1.4.1.7 19 November 1957,0000Z (Fig. 12)

At this time the front had occluded. It was accompanied by snow over Lake Michigan, Minnesota and Wisconsin. The low cell associated with this system was located near Chicago, Illinois, at this time with a minimum pressure of 983 mb. There also appeared to be precipitation in the warm sector. The line of total sky cover preceding the cold front was outside the area of data coverage. Behind the front clearing began within 100 miles, in the southern portion; in the rest of the area total cloud cover extended deep into the cold air.

The area of total low cloud cover had as a boundary, a line which very nearly coincided with the surface location of the warm front. Low cloud (as well as high and middle cloud) clearing began abruptly behind the cold front in Mississippi and Alabama. The distribution of low cloud types was much the same as for the previous observation time. However, lack of data along the cold front leads to some uncertainty in this region.

Again, lack of data makes detailed comment on middle or high cloud distribution unjustified. A general idea of the configuration of these fields can be obtained from Fig. 12.

1.4.1.8 19 November 1957 0600Z (Fig. 13)

The system had occluded further and the low center was found over central Wisconsin with the central pressure still 983 mb. Where radar coverage was available, there appeared to be no precipitation associated with the cold front. Warm frontal precipitation was present, however, and the snow over Lake Superior may also have been associated with this system.

1.4.1.9 19 November 1957, 1200Z (Fig. 14)

The deeply occluded system had nearly passed from the data region by this time. Little cloudiness seemed to be associated with the southern part of the cold front. Clearing did not begin over the remainder of the area until about 500 miles behind the system.

Apparently low cloudiness accounted for most of the total sky cover. This low cloudiness was generally strato-cumulus. It thoroughly obscured the sky above, making middle and high cloud discussion virtually impossible.

1.4.1.10 19 November 1957, 1800Z (Fig. 15)

On this, the last map of the series, the front had passed almost entirely from the field of interest. Little or no precipitation was evident in the available radarscope pictures. The area of clearing skies began 200 to 500 miles behind the front in the north, while the

southern end of the front probably had only scattered to broken sky cover.

The low clouds had much the same array as the total sky cover, except that there was little or no low cloud coverage in Louisiana and eastern Texas. The low clouds were primarily strato-cumulus.

The middle clouds were alto-cumulus at the edge of the area of total coverage. Their nature north of this is unknown due to low cloud obscuration.

The high cloud coverage over Louisiana, Arkansas and Texas was cirrus, while the area to the northeast of this was cirro-stratus according to the one available report.

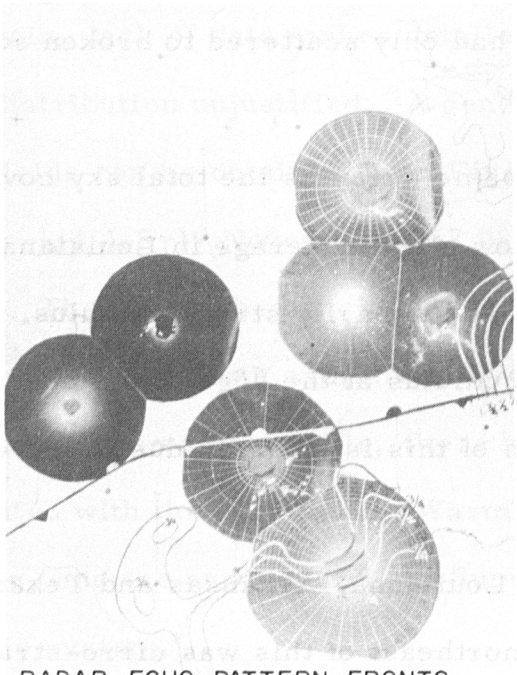

RADAR ECHO PATTERN, FRONTS AND TOTAL SKY COVER

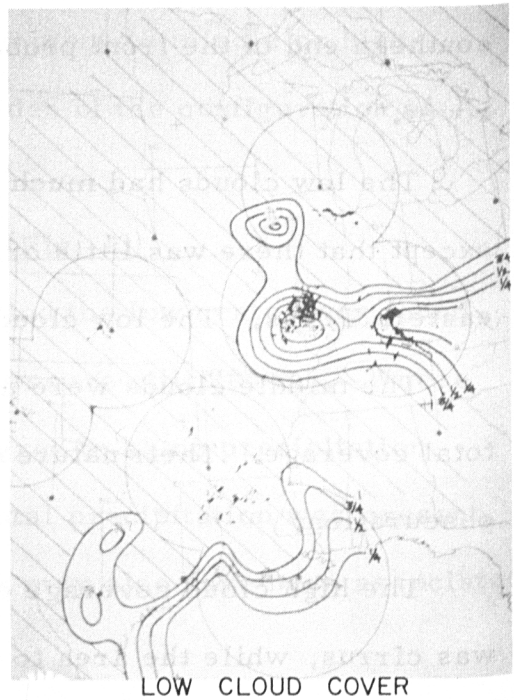

LOW CLOUD COVER

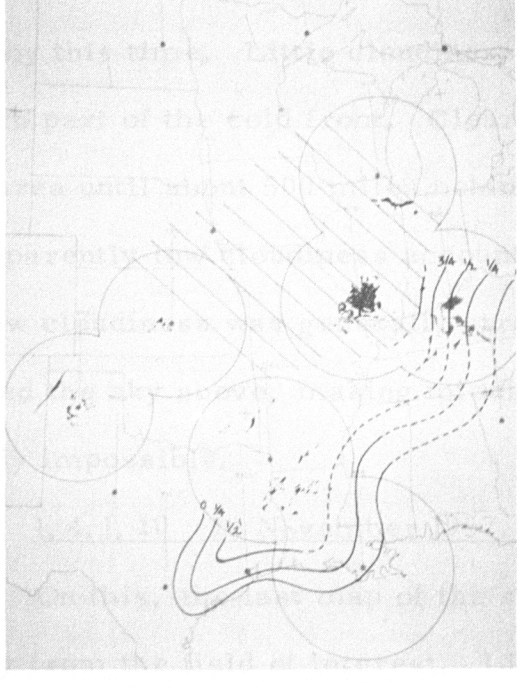

MIDDLE CLOUD COVER

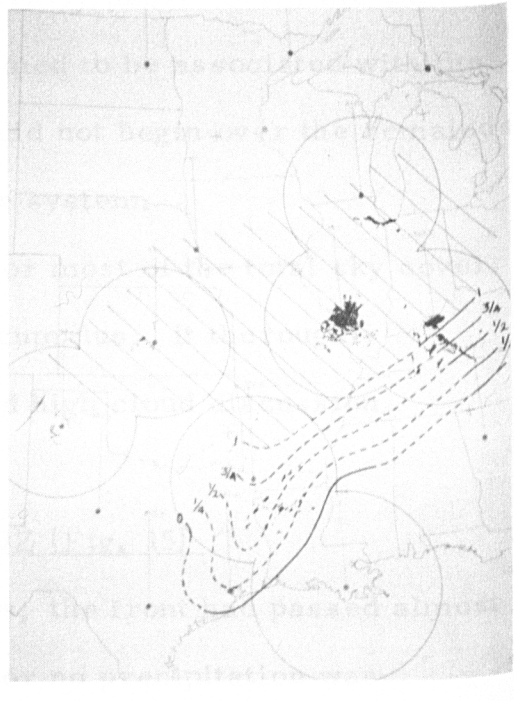

HIGH CLOUD COVER

FIG. 6

17 NOVEMBER 1957, 1200Z

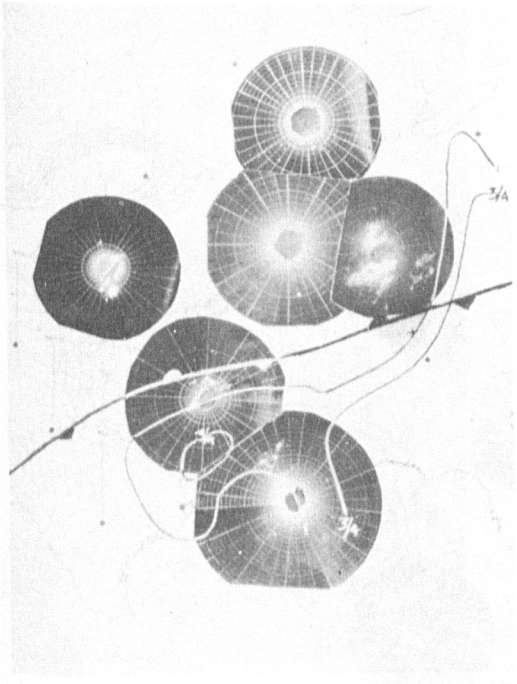

RADAR ECHO PATTERN, FRONTS AND TOTAL SKY COVER

LOW CLOUD COVER

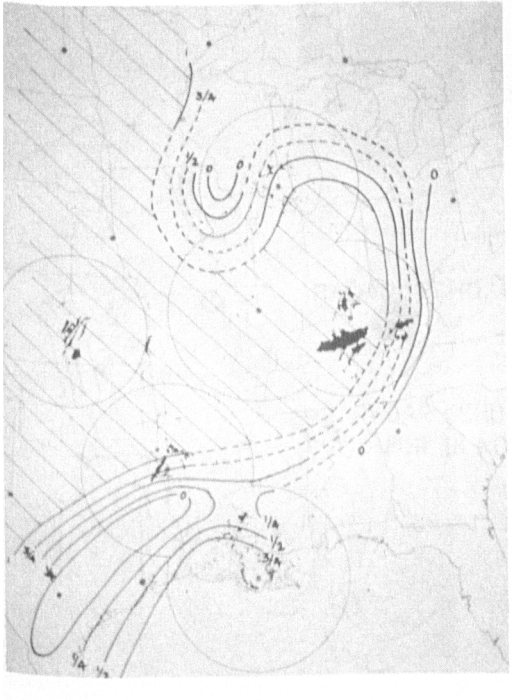

MIDDLE CLOUD COVER

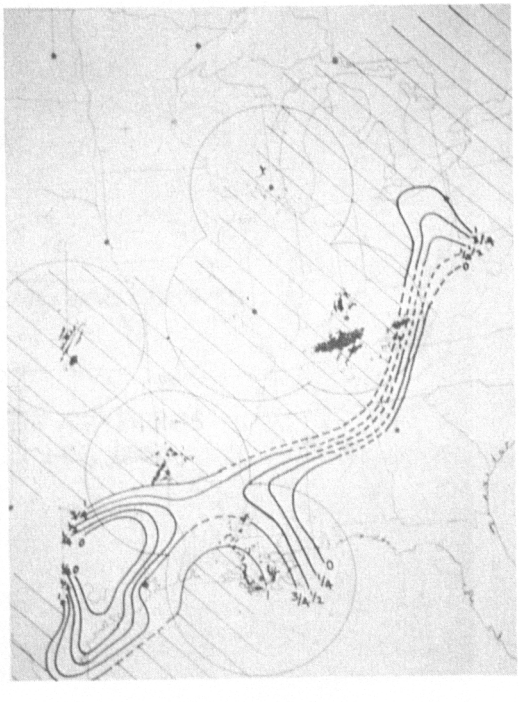

HIGH CLOUD COVER

FIG. 7

17 NOVEMBER 1957, 1800Z

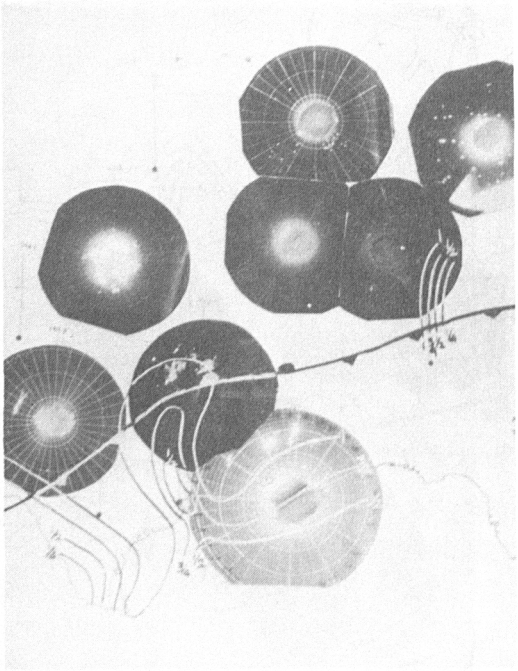

RADAR ECHO PATTERN, FRONTS AND TOTAL SKY COVER

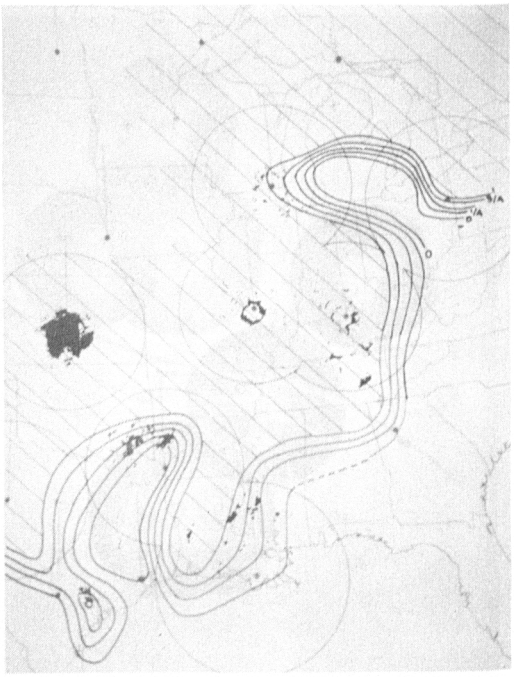

LOW CLOUD COVER

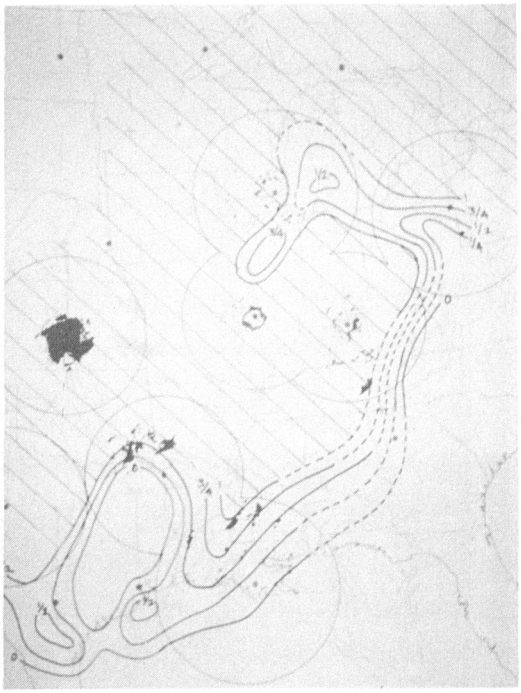

MIDDLE CLOUD COVER

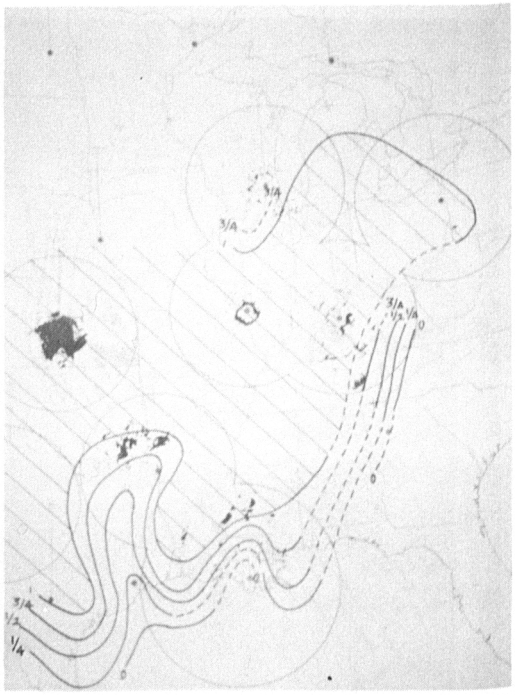

HIGH CLOUD COVER

FIG. 8

18 NOVEMBER 1957, 0000Z

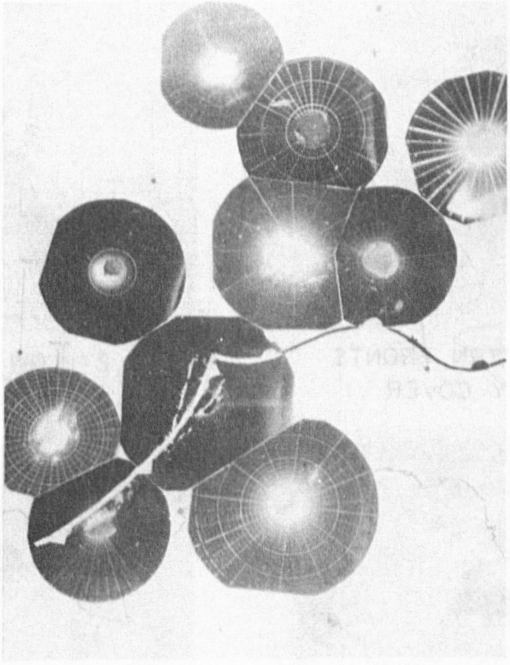

RADAR ECHO PATTERN AND FRONTS

FIG. 9

RADAR ECHO PATTERN AND FRONTS
FOR 18 NOVEMBER 1957, 0600Z

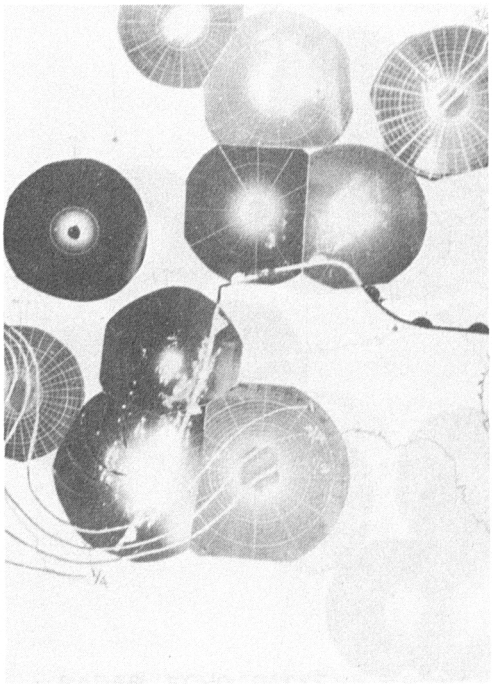

RADAR ECHO PATTERN, FRONTS AND TOTAL SKY COVER

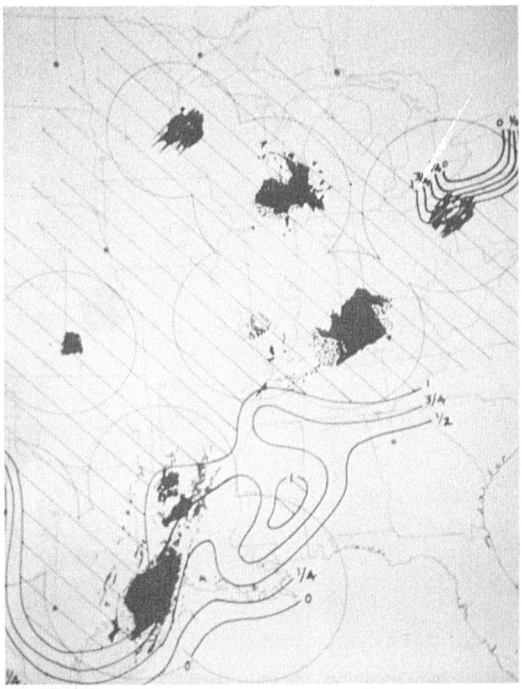

LOW CLOUD COVER

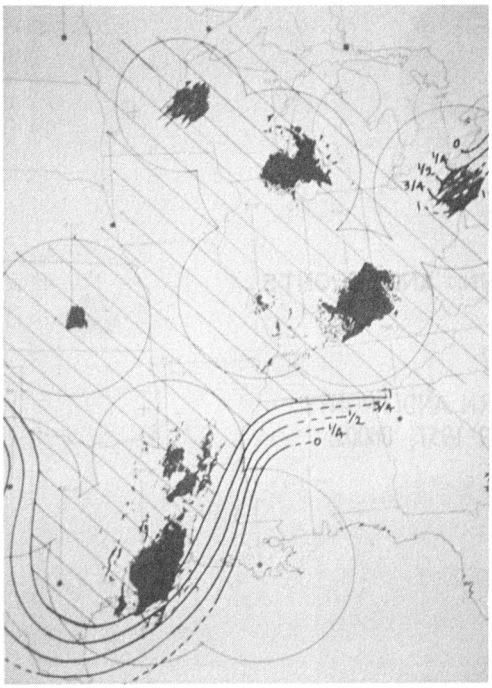

MIDDLE CLOUD COVER

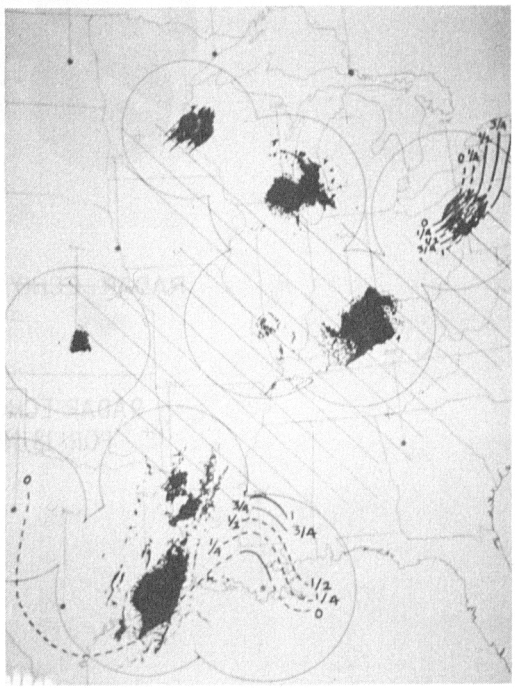

HIGH CLOUD COVER

FIG. 10

18 NOVEMBER 1957, 1200Z

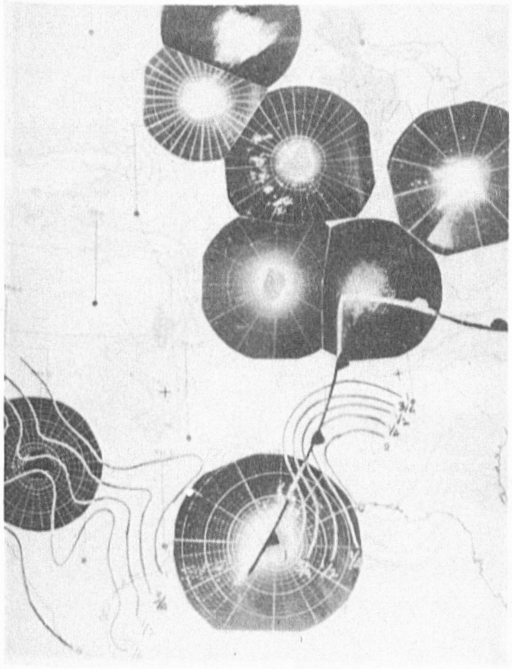

RADAR ECHO PATTERN, FRONTS AND TOTAL SKY COVER

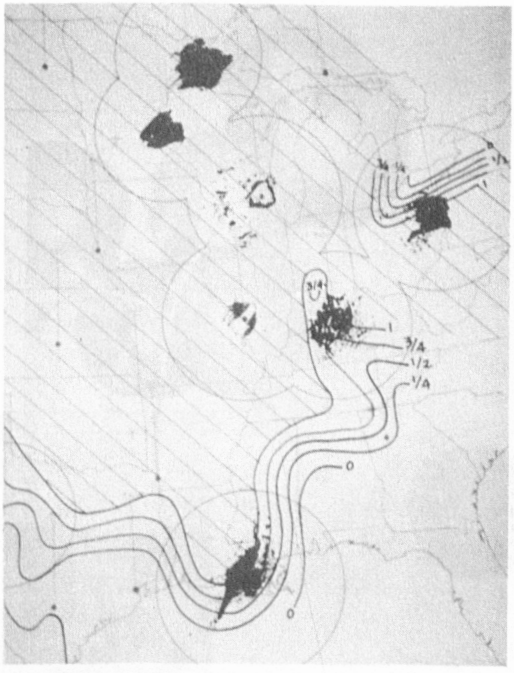

LOW CLOUD COVER

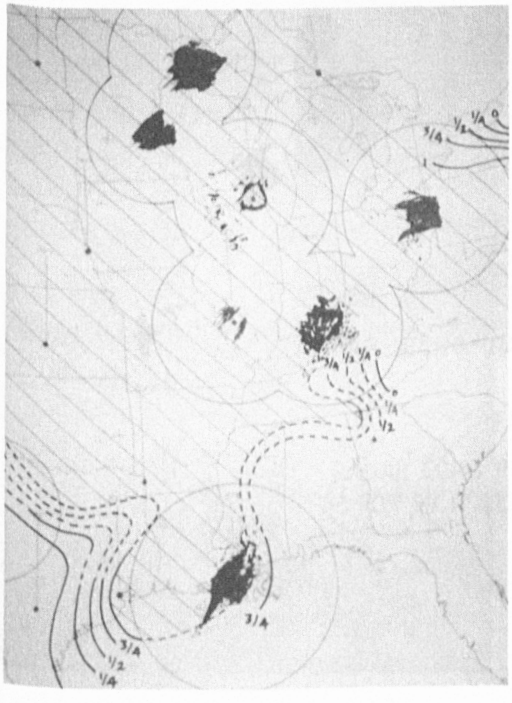

MIDDLE CLOUD COVER

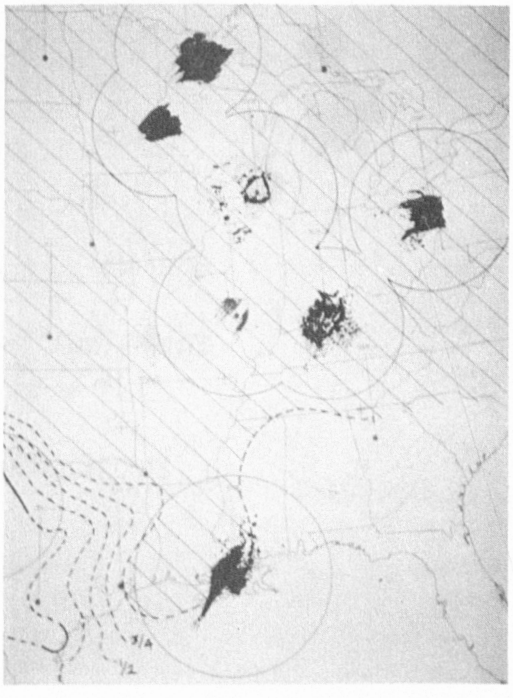

HIGH CLOUD COVER

FIG. 11

18 NOVEMBER 1957, 1800Z

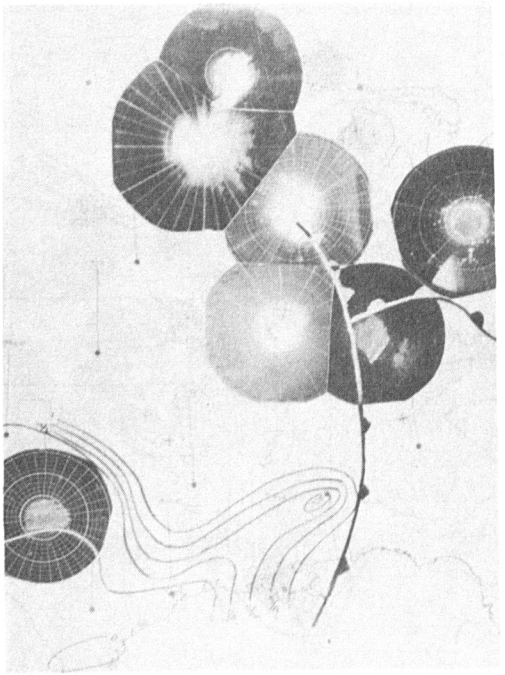

RADAR ECHO PATTERN, FRONTS AND TOTAL SKY COVER

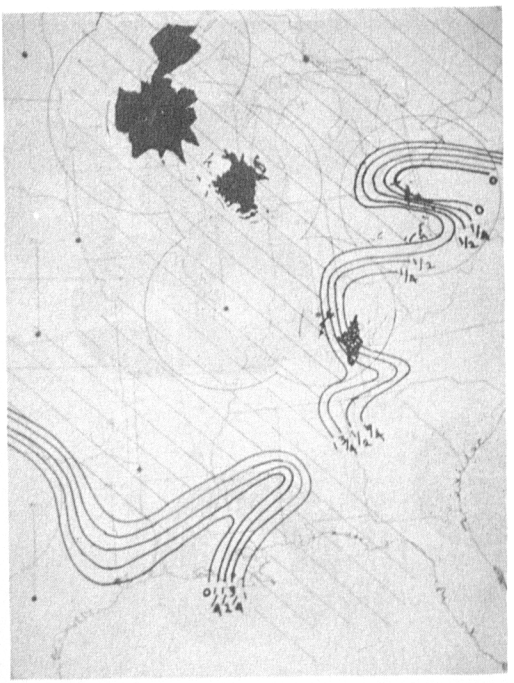

LOW CLOUD COVER

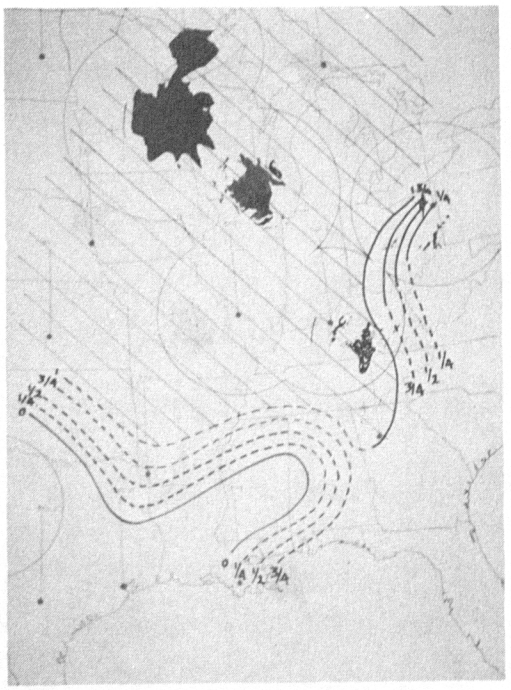

MIDDLE CLOUD COVER

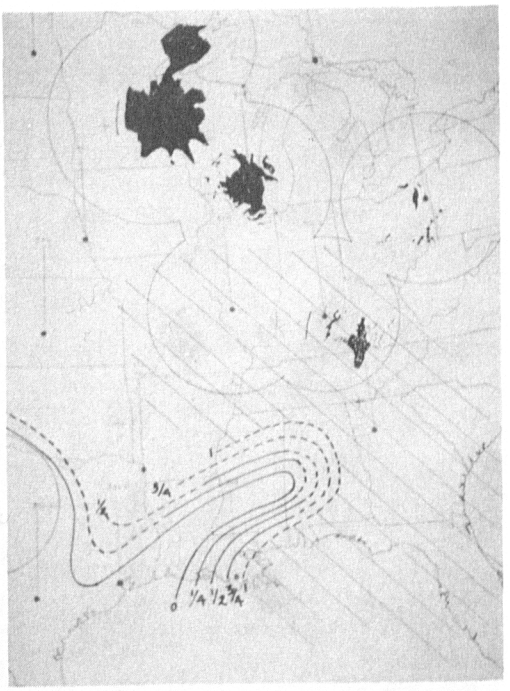

HIGH CLOUD COVER

FIG. 12

19 NOVEMBER 1957, 0000Z

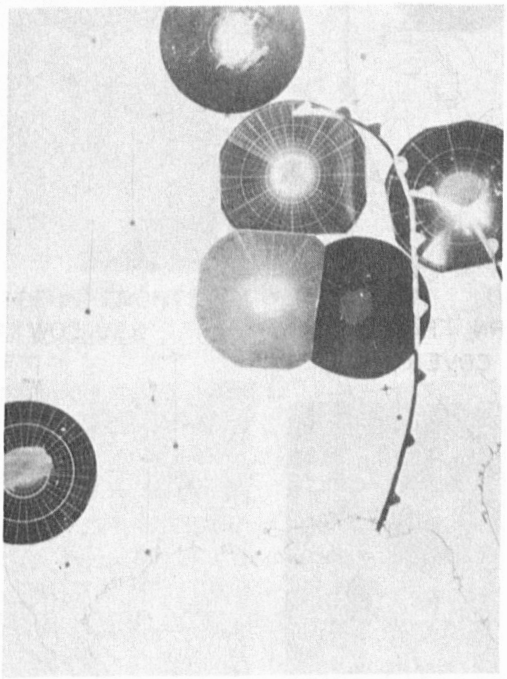

RADAR ECHO PATTERN AND FRONTS

FIG. 13

RADAR ECHO PATTERN AND FRONTS
FOR 19 NOVEMBER 1957, 0600Z

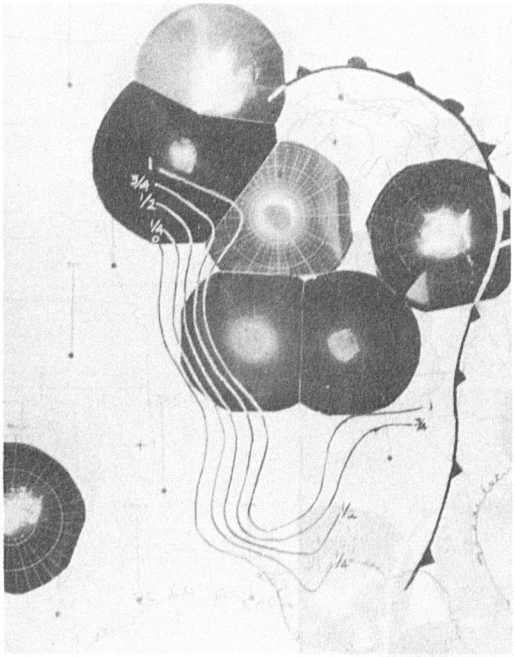

RADAR ECHO PATTERN, FRONTS AND TOTAL SKY COVER

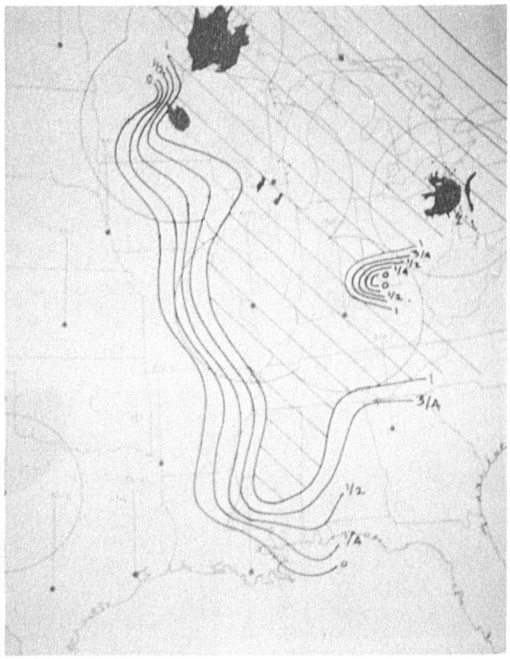

LOW CLOUD COVER

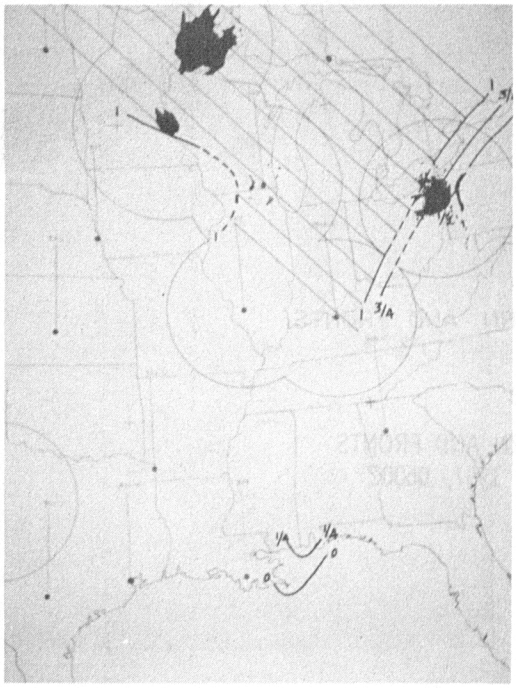

MIDDLE CLOUD COVER

INSUFFICIENT DATA FOR ANALYSIS

HIGH CLOUD COVER

FIG. 14

19 NOVEMBER 1957, 1200Z

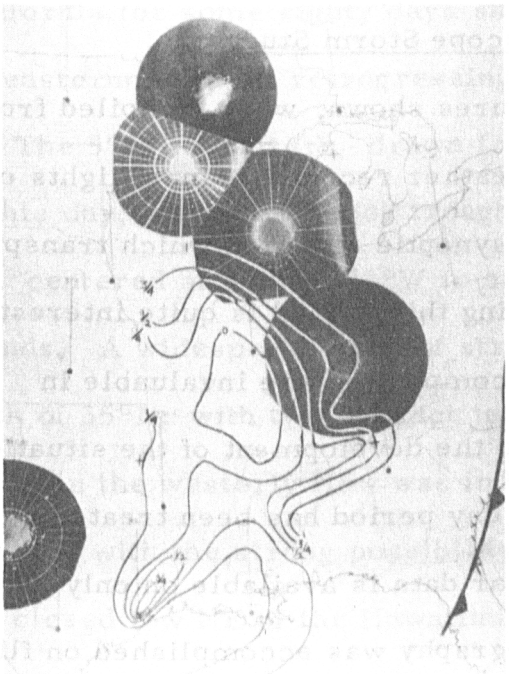

RADAR ECHO PATTERN, FRONTS AND TOTAL SKY COVER

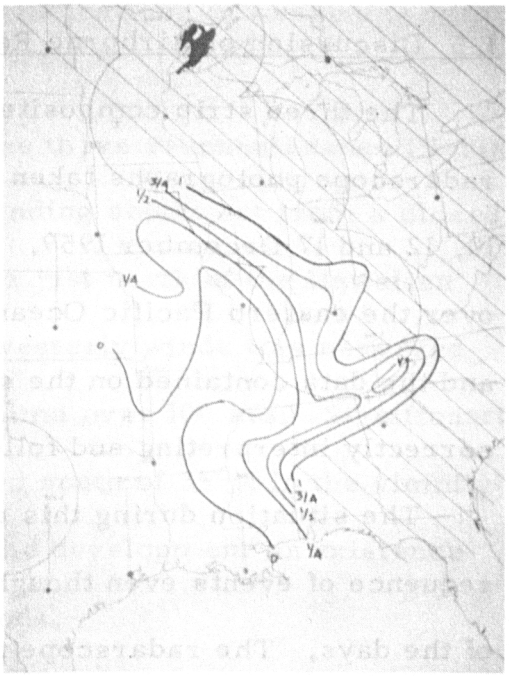

LOW CLOUD COVER

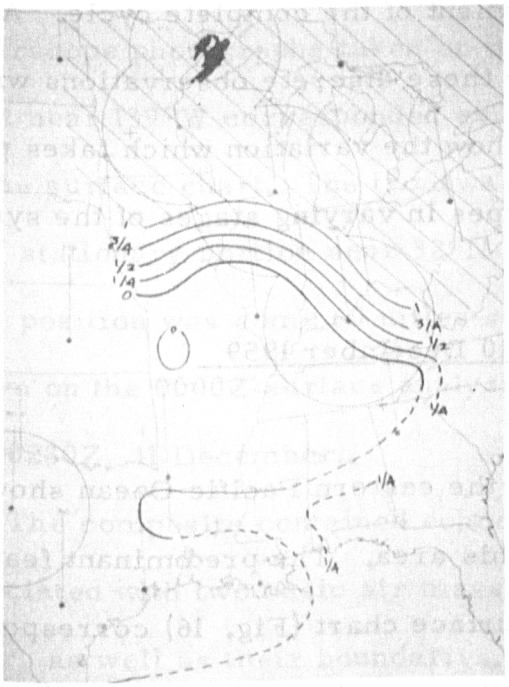

MIDDLE CLOUD COVER

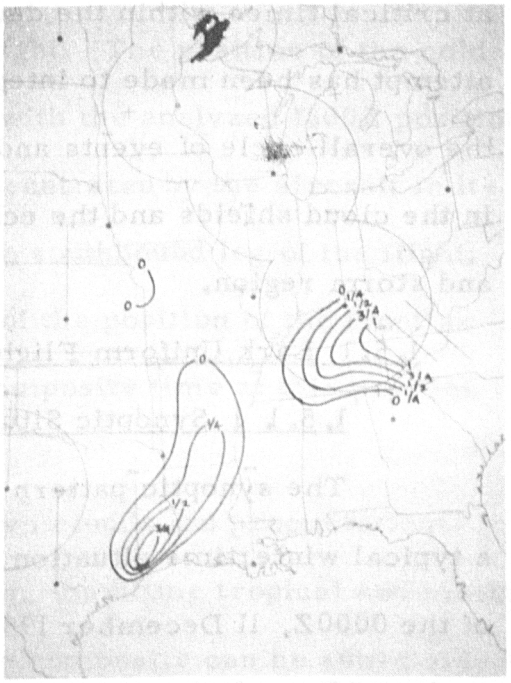

HIGH CLOUD COVER

FIG. 15

19 NOVEMBER 1957, 1800Z

1.5 Discussion of Airborne Radarscope Storm Study

The three strip composite pictures shown, were compiled from radarscope photographs taken on weather reconnaissance flights on 10, 12 and 17 December 1959. The synoptic situation which transpired over the eastern Pacific Ocean during this period is quite interesting and the data contained on the strip composites are invaluable in correctly interpreting and following the development of the situation.

The situation during this eight day period has been treated as a sequence of events even though radar data is available on only three of the days. The radarscope photography was accomplished on flights which traversed significant areas of the synoptic pattern and occurred at critical times within the development of the complete cycle. An attempt has been made to integrate these discrete observations with the overall cycle of events and to show the variation which takes place in the cloud shields and the echo types in varying stages of the system and storm region.

1.5.1 Lark Uniform Flight of 10 December 1959

1.5.1.1 Synoptic Situation

The synoptic pattern over the eastern Pacific Ocean showed a typical wintertime situation for this area. The predominant features of the 0000Z, 11 December 1959, surface chart (Fig. 16) corresponding to the mid-track time of the aircraft, were the two cold frontal systems and the strong zonal flow in evidence between 40°N and 50°N. The

sub-tropical high pressure ridge which had been stationary over central California for some eighty days showed indications of weakening with the easternmost cell retrogressing.

The 500-mb pattern, drawn from the three reconnaissance flights on this day, showed a major trough extending southwest from a closed low, centered at 45°N, 138°W to an area just north of the Hawaiian Islands. A widespread band of strong westerly winds was observed north of 35°N, with two distinct jet maxima over 100 kts. Significantly, a split in the westerly flow was indicated south of 35°N in the vicinity of 143°W with the strong possibility of the development or existence of a closed low NE of the Hawaiian Islands.

1.5.1.2 Radar Data

Figure 17 shows the strip composite constructed from the radarscope photographs taken on this flight. The position of the cold front near 139°W corresponded exactly with the analyzed 1800Z position on the surface chart. The front was repenetrated by the aircraft in its E-W stationary portion near 32°N on the southbound leg of the flight. This position was some 60 miles south of the position of the front as shown on the 0000Z surface analysis (composite time at this position was 0230Z, 11 December).

The composite contained echoes from clouds and precipitation associated with two basic air mass types, maritime tropical and maritime polar, as well as their boundaries. The composite can be sub-divided into the following five areas along the flight track, each of which contained a specific echo type associated with the stability of the air masses:

Area I--A stable, maritime tropical air mass, extending from the West Coast to 139°W, contained a large number of small, weak, convective echoes and several moderate bands oriented NW-SE.

Area II--The frontal zone and the unstable mP air behind it, extending from 139°W to 152°W, contained echoes from the frontal precipitation band and from the post-frontal shower activity.

Area III--A stable subsidence region in the mP air mass, extending from 152°W to 36°N on the southbound leg of the flight track displayed no echoes.

Area IV--A stable region with the mT overriding the mP air existing between 36°N and 32°N, contained weak stratiform echoes which terminated in a scattered line of convective echoes at the southern boundary of the cold air mass.

Area V--An unstable mT air mass south of 32°N latitude was characterized by scattered, moderate to strong convective echoes.

1.5.1.3 Cloud Distribution and Comparison with Radar Data

Figures 18, 19 and 20 show the distribution, amount and type of the low, middle and high clouds that existed over the entire analysis area on 10 December.

The total "top view" cloud distribution, Fig. 21, shows that the cloud shield associated with the low cell in the southern Gulf of Alaska region was quite extensive and covered practically the entire eastern portion of the analysis area. In the area of radar coverage seen on the composite, the shield extended some 150 miles west of the 0000Z surface frontal position and paralleled the boundary of the cold air in the vicinity of the low cell.

Cloud data and the associated radar echoes in the various composite areas were as follows:

Area I-- A dense cirro-stratus overcast covered this entire region and extended over the northwestern states into northern California. In addition to this cloud layer, a solid strato-cumulus undercast (with tops to 6000 ft) and a scattered alto-cumulus deck (with bases at 7000 ft and tops at 8000 ft) were reported in this area. The cellular type echoes, seen in the composite, were undoubtedly reflections from small buildups in the strato-cumulus or alto-cumulus cloud layers. The bands of moderate convective echoes in the composite were oriented generally normal to the lower level wind flow and were indicative of the scattered shower activity reported by several ships.

Area II--The pre-frontal cirro-stratus shield extended 150 miles into the cold air. The frontal band, itself, consisted of moderate to heavy showers some five miles wide while the shower intensity and amount decreased with distance into the cold air. Convective cloud tops were reported between 18,000 and 22,000 ft just west of the frontal bands. The vertical extent of these cumulus clouds decreased gradually to 6000 ft at the western extreme of the area.

Area III--The cloud types in this area typify the upper level stability that was developing in association with the rapid building of the high cell in the post-frontal cold air mass. Scattered cumulus with little vertical extent and broken strato-cumulus were the predominant cloud types observed. This area appeared to have been quite extensive with similar cloud conditions reported up to 600 miles to the west and 400 miles to the north.

Area IV--This area commenced with a thin alto-stratus layer reported between 22,000 and 23,000 ft; the broken strato-cumulus clouds reported in Area III were also observed in the region. The scattered alto-stratus clouds increased rapidly to overcast and the bases lowered to a level beneath the aircraft's flight altitude. At the southern boundary of this area, a weak E-W line was in close agreement with the 0000Z surface frontal position and the change in cloud forms to the south of this line was further evidence of the existence of the front at this position.

Area V--The visual cloud observations in this area were limited, due to darkness overtaking the aircraft, but the radar data gave an excellent indication of the cloud amounts and types present.

This area was characterized by scattered cumulus activity and a high broken alto-stratus layer in its northerly extreme. The cumulus activity increased south of 30°N latitude and could be seen in the composite as scattered, moderate to strong echoes. This typical trade-wind cumulus activity, that is characteristic of the region, appears to have been intensified by the presence of cold air at the 500-mb level.

1.5.2 Loon Hotel Flight of 12 December 1959

1.5.2.1 Synoptic Situation

The synoptic situation in the next 48 hours changed markedly from that of 10 December. The 0000Z 13 December surface chart, Fig. 22, shows an "Omega" blocking pattern over the analysis area with a strong N-S ridge along 139°W longitude. The rapid development of the high pressure region was coupled with the retrogression and

vast increase in cyclonic circulation around the semi-permanent Gulf of Alaska low.

The breakdown of the eastern cell of the Pacific sub-tropical high pressure region permitted the occluding frontal system, seen in Fig. 16, to continue its southeasterly movement at approximately 20 kts. This system later passed the San Francisco Bay Region as a line of moderate showers bringing the first precipitation to the California area in 83 days.

The primary polar front regenerated in the tight gradient between the two major pressure systems and an occluded portion of this front advanced rapidly northeastward into the Gulf of Alaska.

The 500-mb pattern on this day showed a major ridge oriented NE-SW from Sandspit Island, B.C., to an area some 300 miles NW of the Hawaiian Islands. Major troughs were situated along the West Coast and west of the Loon Hotel flight track. Northwesterly flow and a marked warming tendency could be observed over the entire eastern portion of the analysis area, indicating strong subsidence and intensification of the surface high cell.

The wind and 500-mb height values northeast of the Hawaiian Islands still indicated a depression in the area with a slight displacement eastward. In general, the position of a low in this area is quite characteristic of the formation of blocking action over the eastern Pacific Ocean. The appearance of this system on 10 December was indicative of the subsequent rapid development of the surface high cell and the temporary return to a summertime type situation in this area.

1.5.2.2 Radar Data

Figure 23 shows the radarscope strip composite constructed from photography accomplished on the Loon Hotel flight of 12 December 59. The position of the surface front is verified almost exactly by the radar data. The wave on the primary polar front, as seen on the strip composite, was some 400 miles northeast of the position indicated on the 0000Z surface chart. The radar data revealed that the wave was quite well developed and had considerable weather associated with it.

Again the flight track of the aircraft was through two air mass types, mT and mP; the echoes detected could be associated with the relative stability of each.

The composite has also been subdivided into areas characterized by specific echo types which are associated with the varying stability of the two air masses. Some of these areas are of the same type as those described in the Lark Uniform track and in these cases the classification numbers are retained in this description.

The flight started from Hickam Air Force Base, Hawaii and traversed Area V type conditions up to 26°N latitude. The echoes in this area were similar to those detected at the same latitude of the Lark Uniform flight with the exception that the convective cells were aligned in parallel bands. Of particular interest were the two concentric bands detected in the vicinity of 25°N, 163°W. Both these bands had sharp curvature to the northwest. They appear to be associated with low level wind shear between the two cells of the sub-tropical high pressure region.

Echo character in the remaining composite areas was as follows:

Area VI--Between 26°N and 35°N, is an area of stable mP air containing few or no echoes.

Area VII--Between 35°N and 40°N, contains echoes from clouds associated with a developing wave on the primary polar front. Continuing further north the echoes between 46°N and 51°N are from clouds associated with unstable mP air and are comparable to those detected in Area II of the Lark Uniform composite.

Area VIII--Between 51°N and the Aleutian Islands, contains intense convective echoes associated with the deep trough and occluded front.

1.5.2.3 Cloud Distribution and Comparison with Radar Data

Figures 24, 25 and 26 show the distribution, amount and type of low, middle and high clouds in existence over the entire analysis area on 12 December. The shift in the total "top view" cloud shield distribution, Fig. 27 from that of 10 December was quite striking. The entire central and northern portions of the analysis area were covered by this shield. Breaks in the "top view" could be seen off the west coast of the United States and south of the central and western Aleutian Islands.

Significantly, an area of widespread middle and high cloudiness was observed NE of the Hawaiian Islands which could not be traced to any surface system. These clouds were believed to be associated with a high level low cell whose presence was indicated at the 500-mb level.

The comparison between the clouds observed and the radar echoes in the various areas of the composite is as follows:

Area V--Scattered to broken strato-cumulus and cumulus clouds were reported extensively in this area with bases at 2000 ft and tops to 4000 ft with occasional buildups to 8000 ft. The echoes seen in the composite were undoubtedly from the occasional cumulus buildups oriented in parallel bands. No precipitation was reported as occurring from these clouds at the time of the radar pictures.

Area VI--This area began with an abrupt end to the cumulus activity in Area V, and was reported as relatively cloud free over some 125 miles. The northern extreme of this area contained strato-cumulus in increasing amount with bases at 2000 ft, tops at 4000 ft. These conditions were indicated by the lack of echoes on the composite in this area.

Area VII--The echoes in this area showed the complete precipitation structure of an unstable wave on the primary polar front. A cirro-stratus shield covered the entire area with multiple cumulo-type cloud layers that were reported beneath it. The frontal portion of this wave extended SW out of the circulation center and could be seen as echoes from a solid line of thunderstorms just west of the flight track. The diffuse echoes north of this area were associated with warm frontal overriding. The predominate cloud, reported in advance of the cold front, was cumuliform with tops initially at 15,000 ft and increasing rapidly to a height above the flight level of the aircraft. The total cloud shield across the flight track extended for some 600 miles.

Area II--This was a narrow region in the area of large pressure gradient south of the major low cell. Cold mP air had moved over the warm Japanese current, creating unstable conditions in the lower layers of the atmosphere. A solid cumuliform undercast with tops to 12,000 ft was observed throughout the region. The echo characteristics were ill-defined due to a malfunction of the radar in the region.

Area VIII--This area contained intense convective cloud forms with tops to 20,000 ft and numerous cumulo-nimbus towers extending to 26,000 ft. This activity was oriented along the "back bend" trough extending south out of the Alaskan low. That the aircraft was forced to circumnavigate these cells attested to the cells' severity, for normally these aircraft fly through such storms unless it is thought that structural damage might be sustained. Several of these echoes had a spiral appearance of approximately thirty miles in diameter, which was indicative of the intense wind shear in this trough.

1.5.3 Evolution of the Synoptic Situation During the Period from 0000Z, 13 December to 18 December 1959

Figures 28 and 29 show the 0000Z surface charts for 15 and 17 December respectively. The large high cell off the west coast of the United States sustained its central pressure of 1036 mb through 0000Z 15 December and drifted slowly southeast. The ridge existing in the Gulf of Alaska on 12 December, had dissipated to bring about a gradual southerly movement in the primary polar front. Numerous intensifying, unstable waves moved rapidly eastward along this front and curved

sharply into the Gulf of Alaska before reaching the coast. The occlusions associated with these lows moved northeast into British Columbia rather consistently, bringing extended periods of cloudiness and intermittent moderate to heavy precipitation to this area.

The situation persisted for another 48 hours with the high cell continuing its southerly drift and weakening. By 0000Z on 17 December the central pressure had fallen to 1019-mb and the primary polar front was now found along 40°N latitude. Successive waves still formed along the front and moved into the Gulf of Alaska but the occlusions were now moving in a more easterly direction bringing a renewal of the wet season to Washington and Oregon.

1.5.4 Stork India Flight of 17 December 1959

1.5.4.1 Synoptic Situation

By 17 December the easternmost cell of the sub-tropical high pressure region had retrogressed westward and was replaced by a weak trough off the west coast. The 0000Z 18 December surface chart, Fig. 30, shows a deep low cell that centered 600 miles NNW of Vancouver Island with an occluded frontal system extending out of it. The cold air behind this front had dipped below 35°N and strong westerly surface winds along 40°N indicated this system would continue a southeasterly trajectory onto the Northern California and Oregon coasts.

The 500-mb pattern had returned to a wintertime regime with a long wave trough extending south out of the Gulf of Alaska. Strong

westerly winds were found north of 35°N, with an 85 kt jet core along 40°N.

1.5.4.2 Radar Data

Figure 36 shows the strip composite constructed from the radarscope photographs taken on the Stork India flight. Unfortunately, the camera equipment became inoperative at the southern extreme of the flight and little data was available in the vicinity of the occluded front. The data shown in this composite were obtained entirely in cold mP air which was predominately unstable.

Two distinct echo types can be seen in the following areas:

Area IX--A relatively stable mP air mass, extending from the coast of Alaska to 49°N, is characterized by numerous weak echo bands.

Area II-- The remainder of the composite contains echoes in the Area II category. Commencing at 49°N and extending south and east are numerous moderate to strong convective type echoes. Along the eastern edge of the composite are several strong bands of echoes associated with the occluded front.

1.5.4.3 Cloud Distribution and Comparison with Radar Data

Figures 32, 33 and 34 show the distribution, amount and type of low, middle and high clouds which were in existence over the entire analysis area on 17 December 1959.

The total visible "top view" cloud distribution is shown in Fig. 35. The total cloud shield over this area was quite extensive with the

land masses in advance of the frontal systems having the heaviest cover. The two relatively clear spots in the cold air, positioned the open wave in the center of the analysis area quite well.

The middle and high cloud shields associated with the frontal systems quite closely approximated those specified by frontal models, especially in regard to the open wave. The tongue of broken cirrus NW of the open wave apex appears to be associated with a strong jet stream. Little explanation for the extensive area of scattered to broken cirrus north of the Hawaiian Islands was found from the available data.

The clouds reported and echoes associated with them within the area of radar coverage were as follows:

Area IX--An extensive undercast cumuliform cloud layer extended from the Alaskan coast to 49°N. Weak, mostly stratiform echoes can be seen in this segment of the composite.

Area II --This area began at 49°N with scattered to broken cumuliform clouds having bases at 8000 ft and tops to 15,000 ft. This cloud type and amount was typical of the cold area between the two surface cells. The cirro-stratus shield from the open wave extended some 650 miles north and northeast from the surface position of the low center and was overlying the cumulus activity up to 45°N.

The cloud shield from the occlusion extended westward in the "back bend" trough, creating a narrow, 100-mile break between the cloud shields associated with the two systems. The echoes seen in

the composite west of 145°W longitude clearly showed the cumulus activity as observed in this region. East of this longitude the echo had a more stratified appearance, which is indicative of the alto-stratus clouds in the "back bend" trough. Paralleling the northern segment of the southeast portion of the flight track several strong convective lines can be seen. These lines are post-frontal bands associated with the occlusion which had moved rapidly to the east.

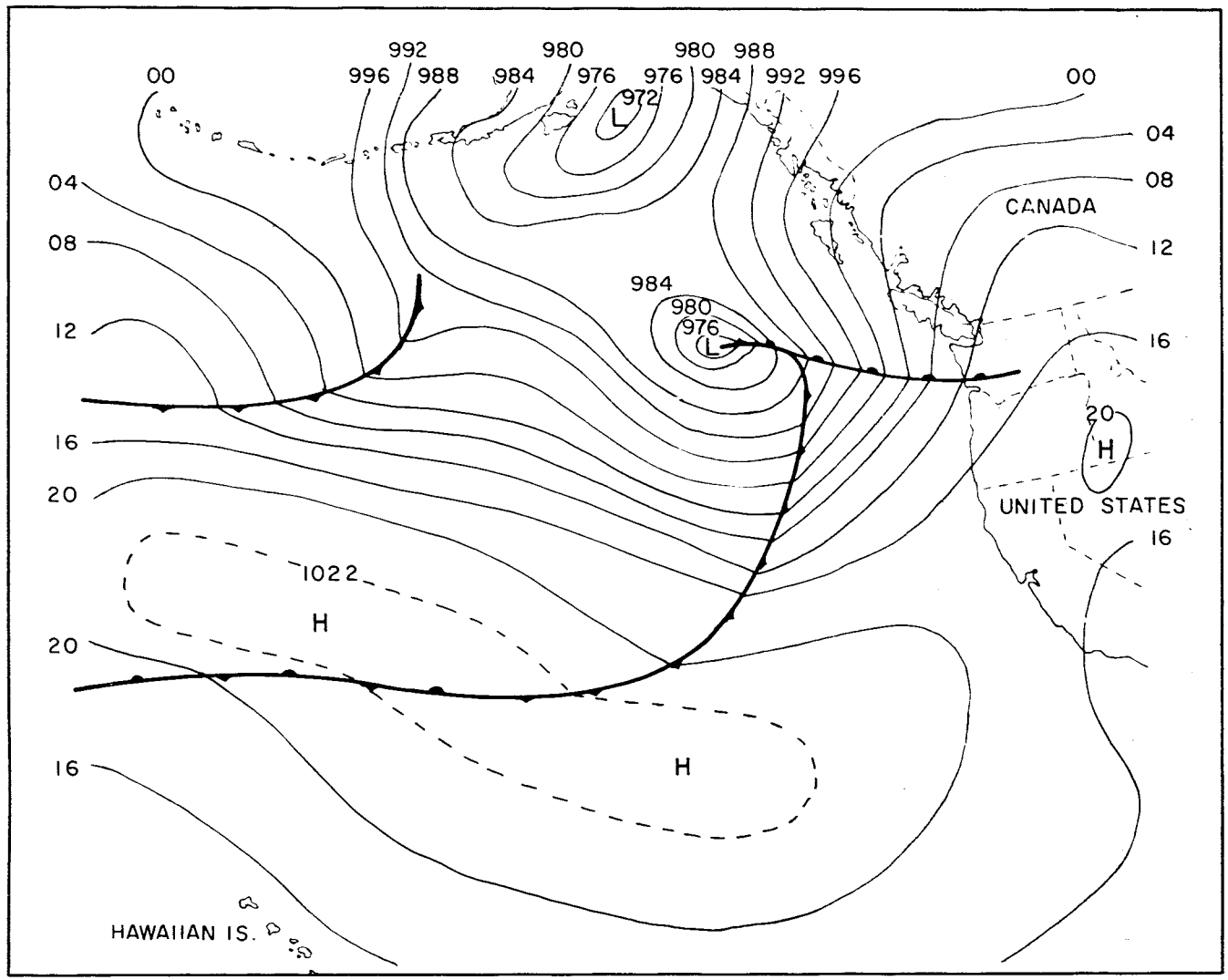

FIG. 16

EASTERN PACIFIC SURFACE CHART, 11 DECEMBER 1959, 0000Z

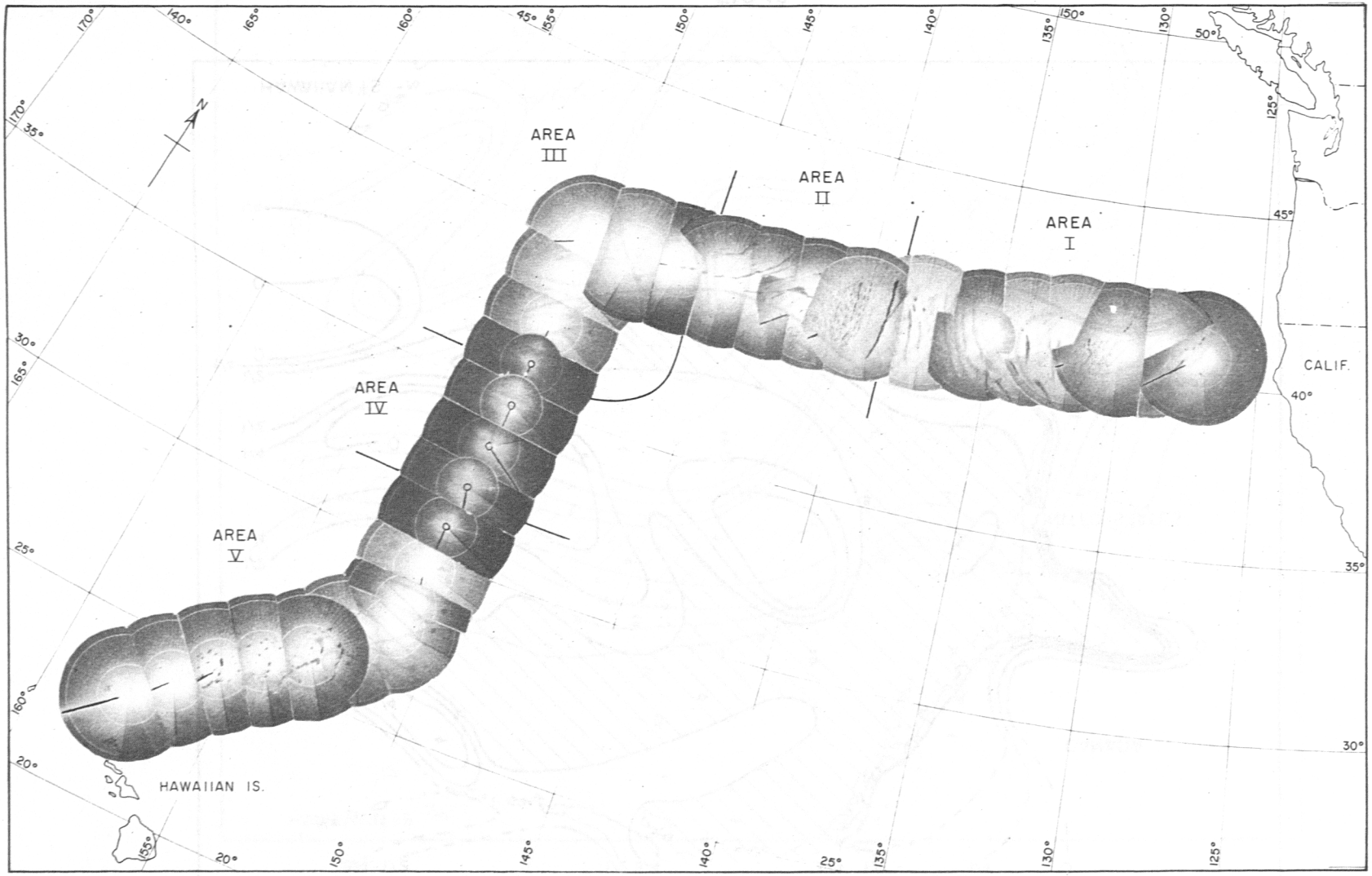

FIG. 17

RADARSCOPE STRIP COMPOSITE FOR LARK UNIFORM FLIGHT OF 10 DECEMBER 1959

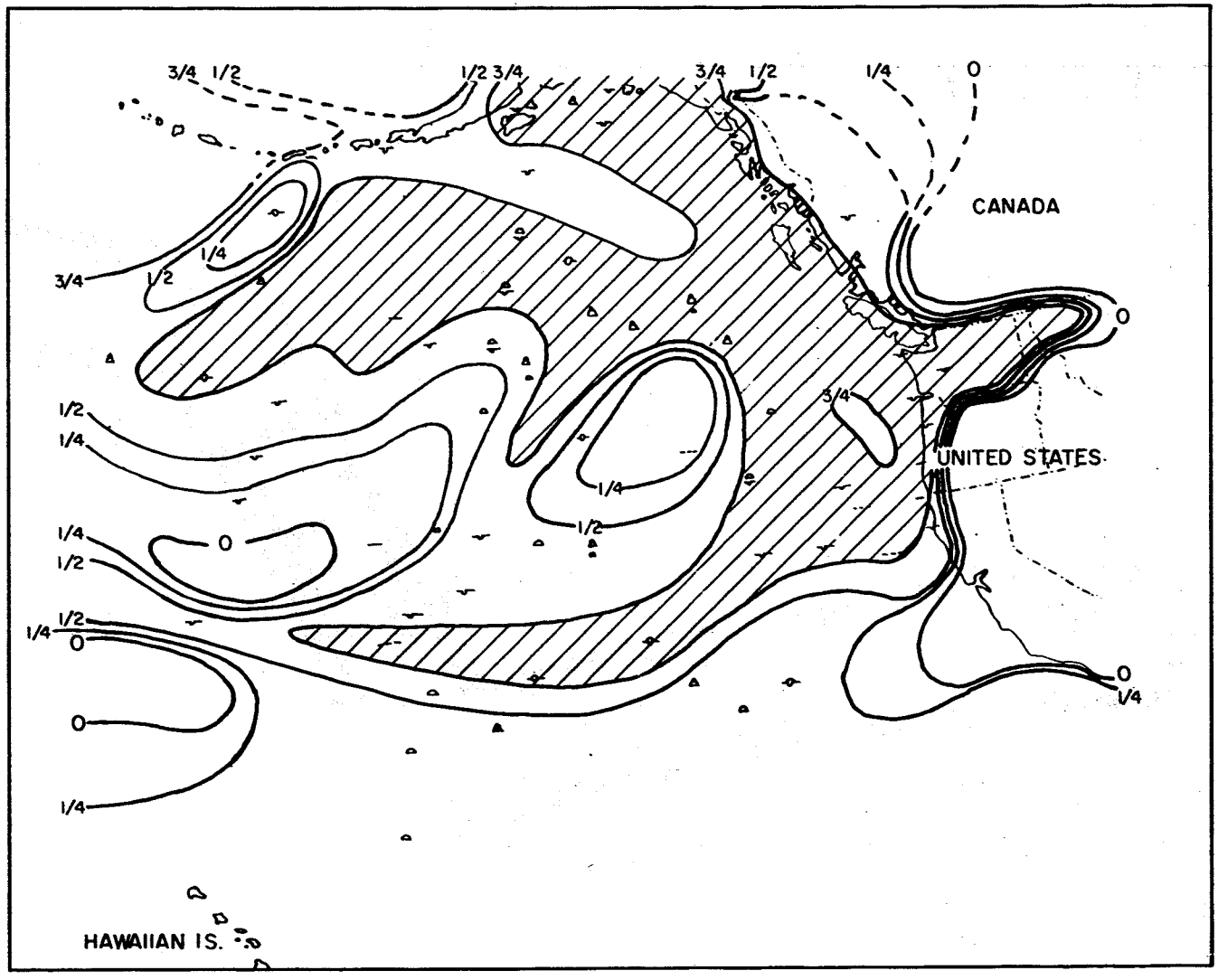

FIG. 18

LOW CLOUD DISTRIBUTION AND TYPE OVER EASTERN PACIFIC ON 10 DECEMBER 1959

FIG. 19

MIDDLE CLOUD DISTRIBUTION AND TYPE OVER EASTERN PACIFIC ON 10 DECEMBER 1959

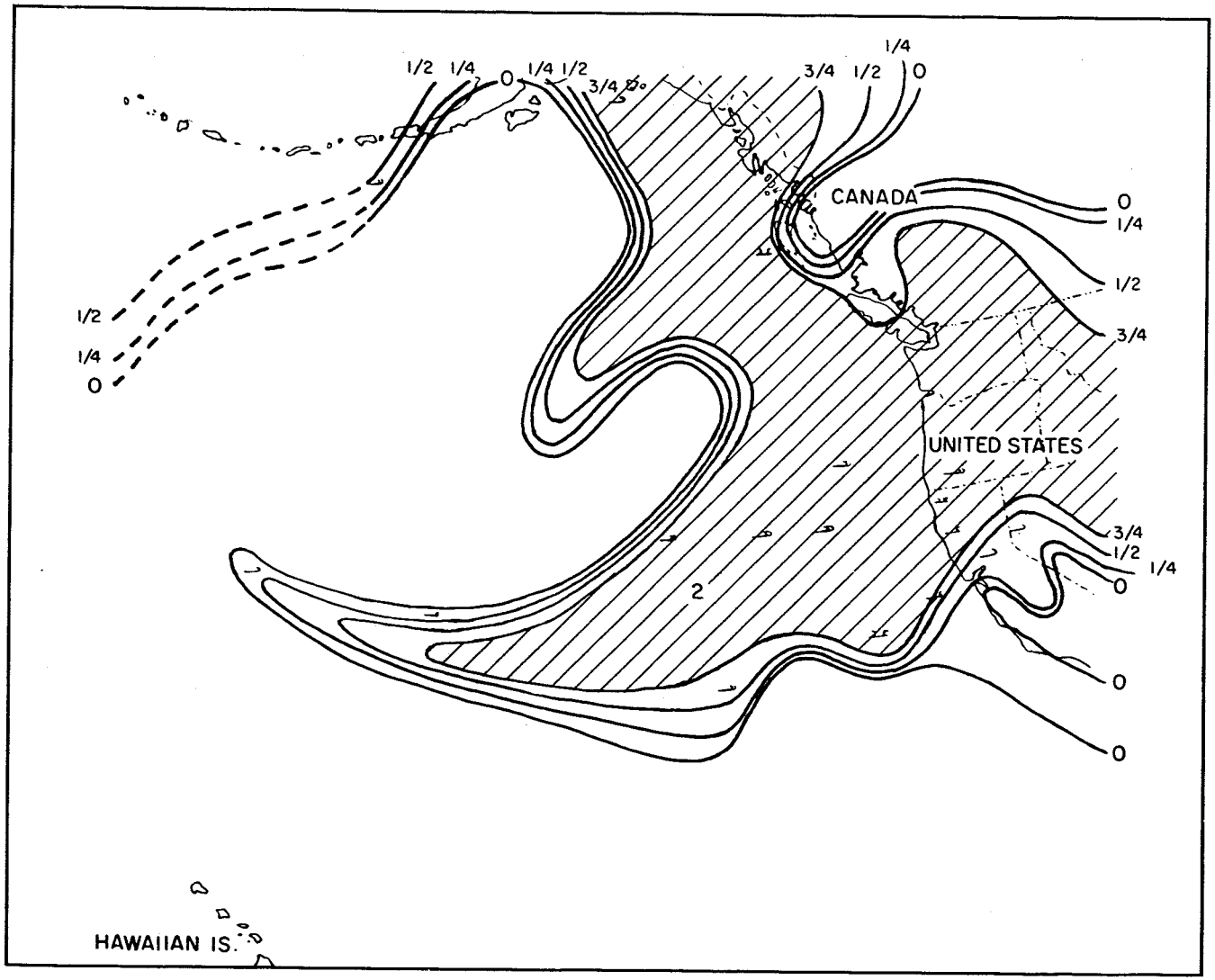

FIG. 20

HIGH CLOUD DISTRIBUTION AND TYPE OVER EASTERN PACIFIC ON 10 DECEMBER 1959

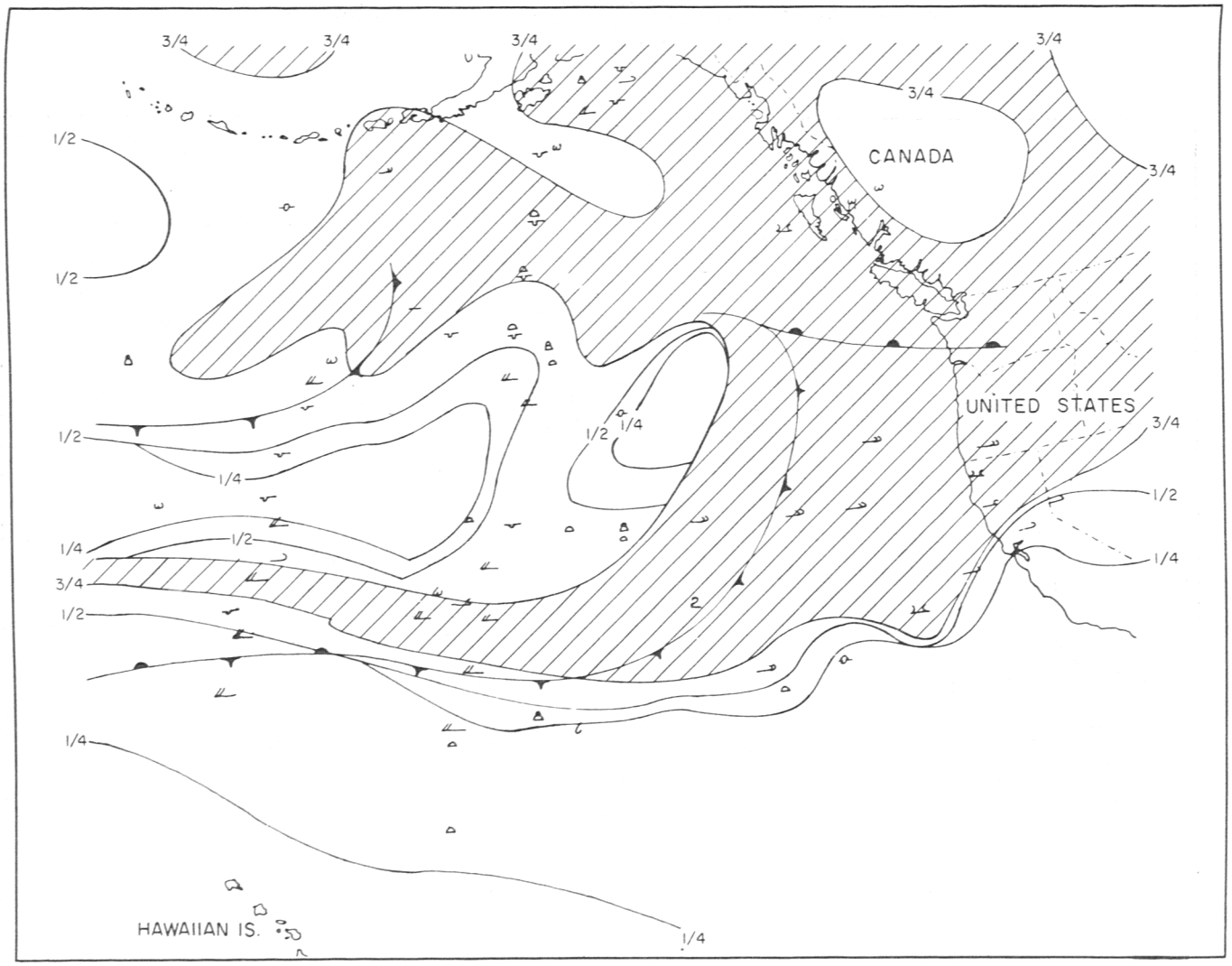

FIG. 21

TOTAL "TOP VIEW" CLOUD DISTRIBUTION AND TYPE OVER EASTERN PACIFIC ON 10 DECEMBER 1959

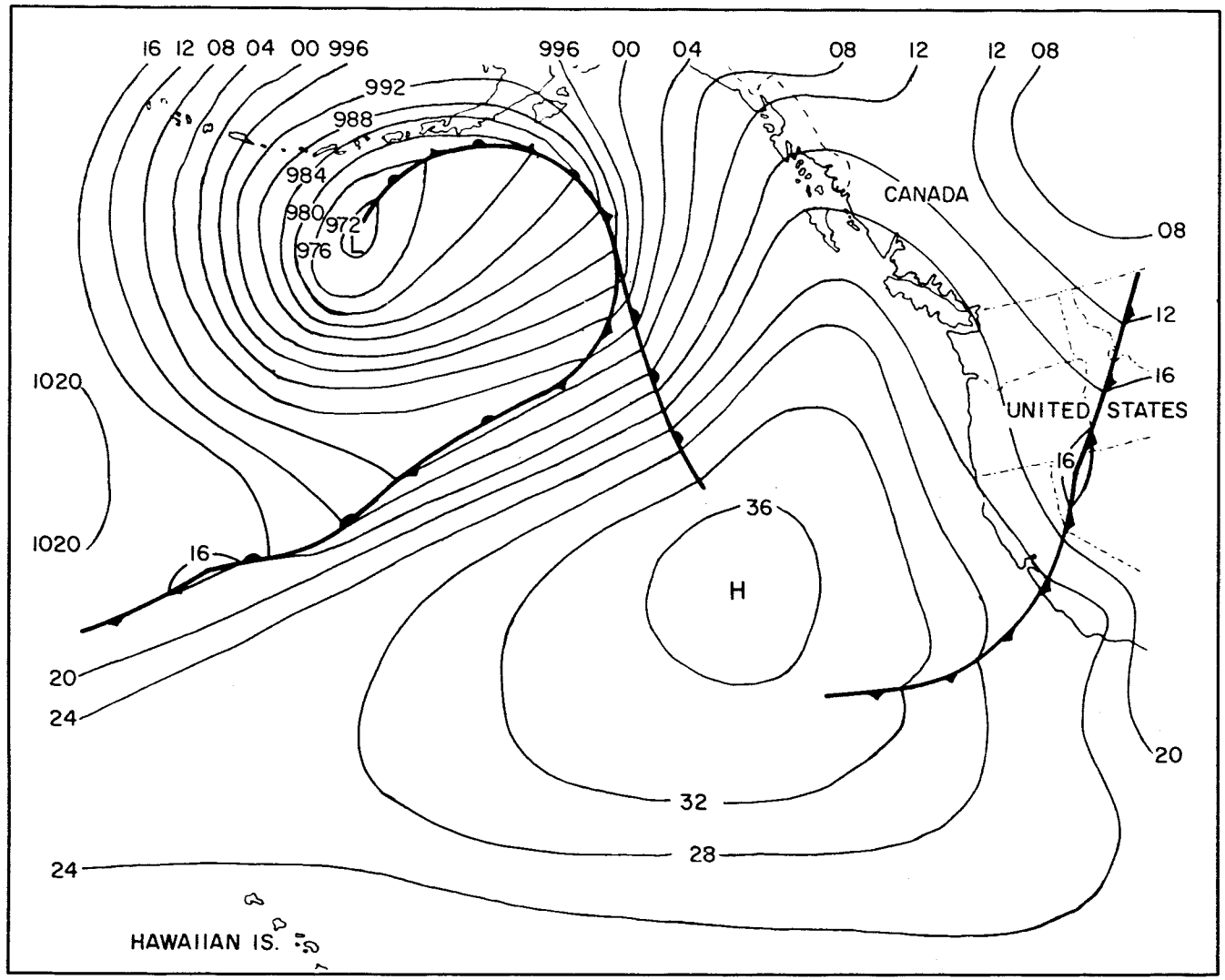

FIG. 22

EASTERN PACIFIC SURFACE CHART, 13 DECEMBER 1959, 0000Z

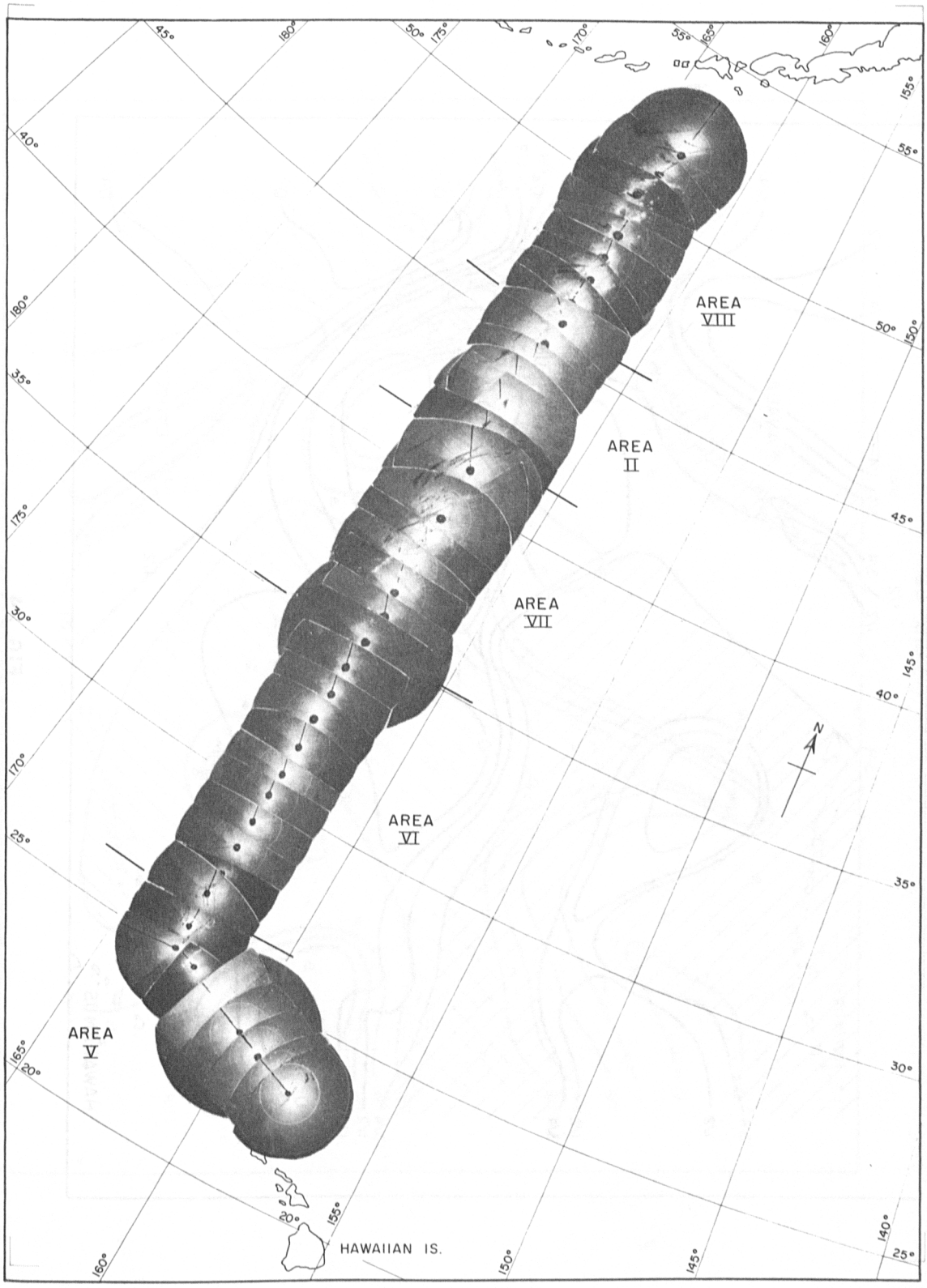

FIG. 23

RADARSCOPE STRIP COMPOSITE FOR LOON HOTEL FLIGHT OF 12 DECEMBER 1959

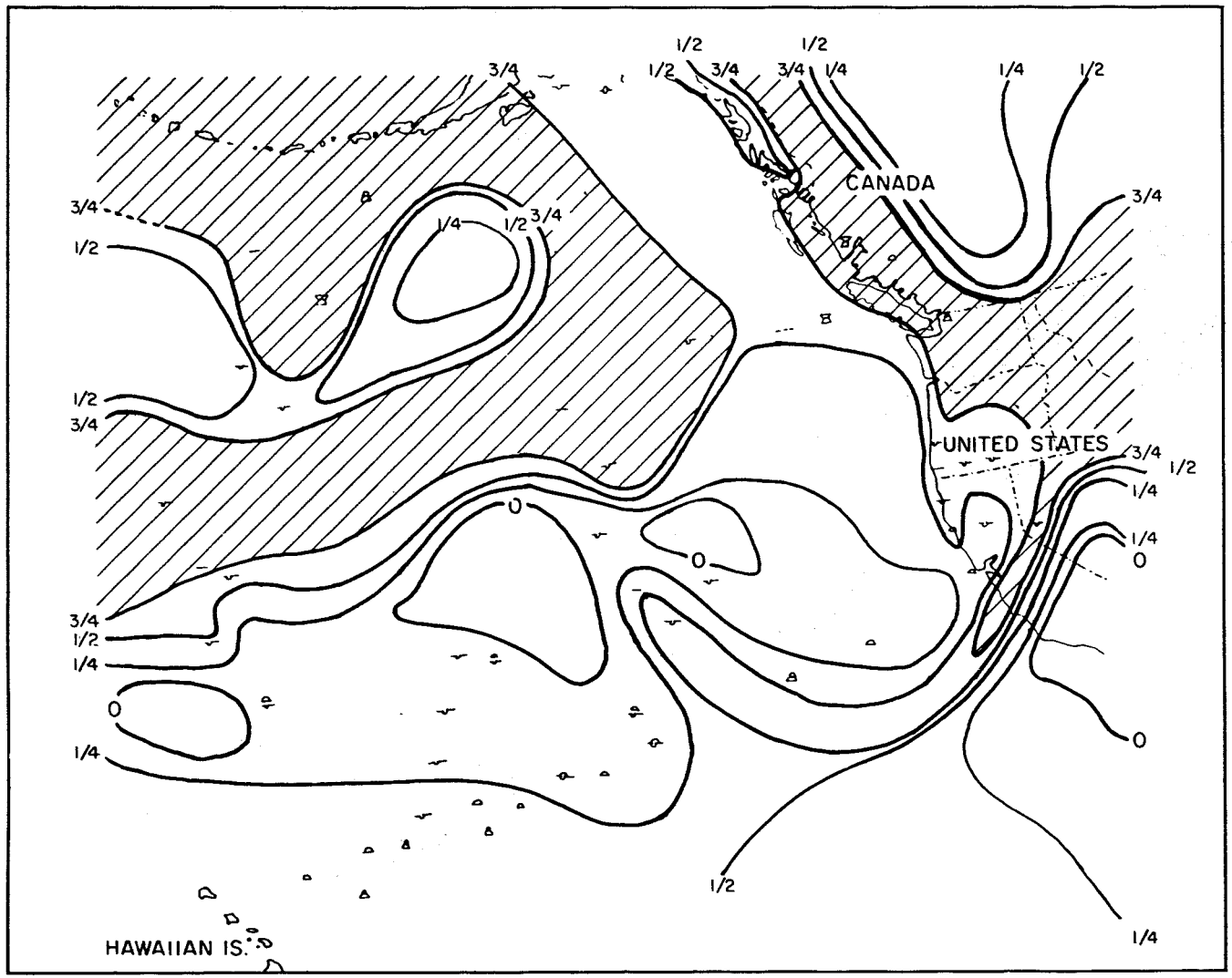

FIG. 24

LOW CLOUD DISTRIBUTION AND TYPE OVER EASTERN PACIFIC ON 12 DECEMBER 1959

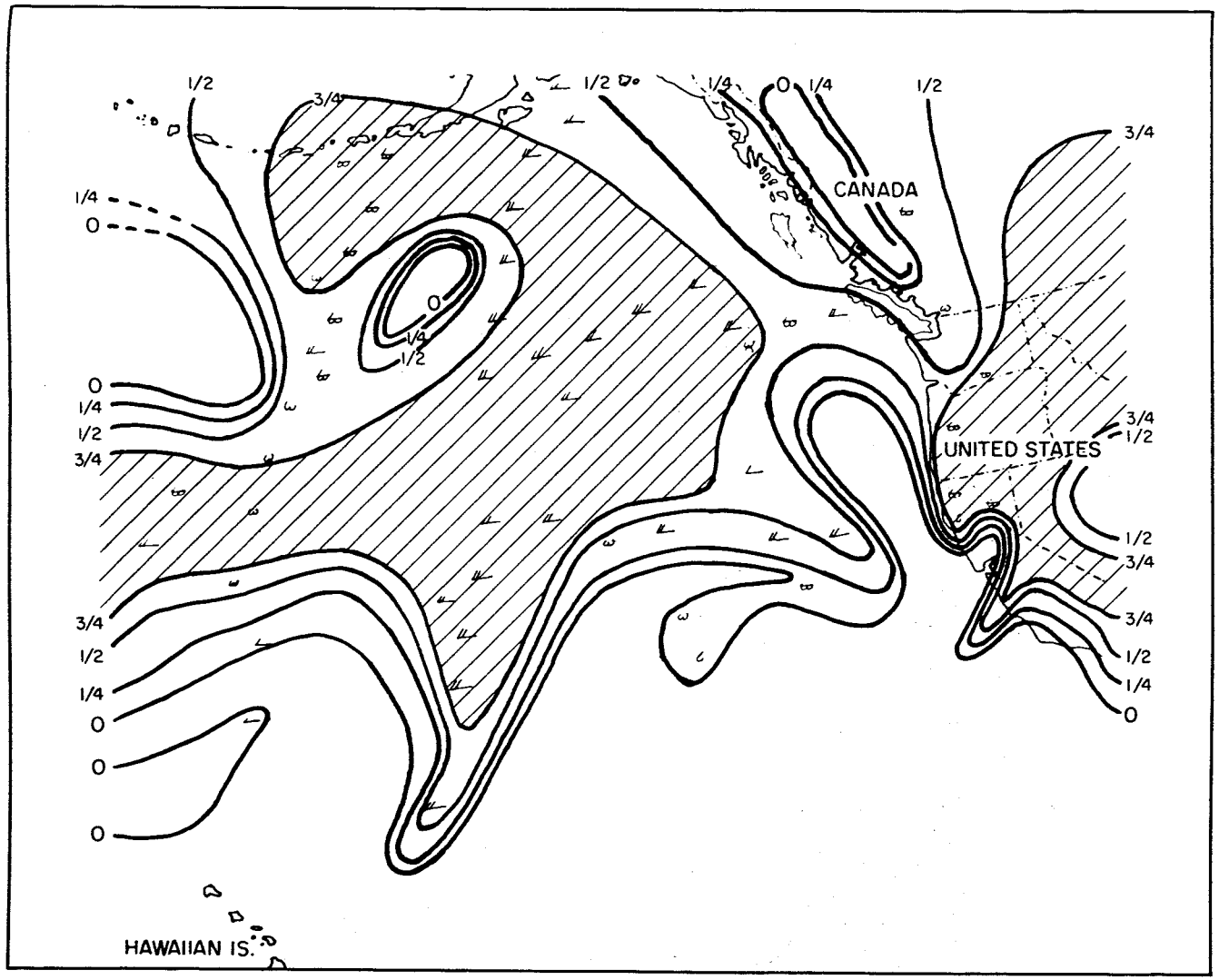

FIG. 25

MIDDLE CLOUD DISTRIBUTION AND TYPE OVER EASTERN PACIFIC ON 12 DECEMBER 1959

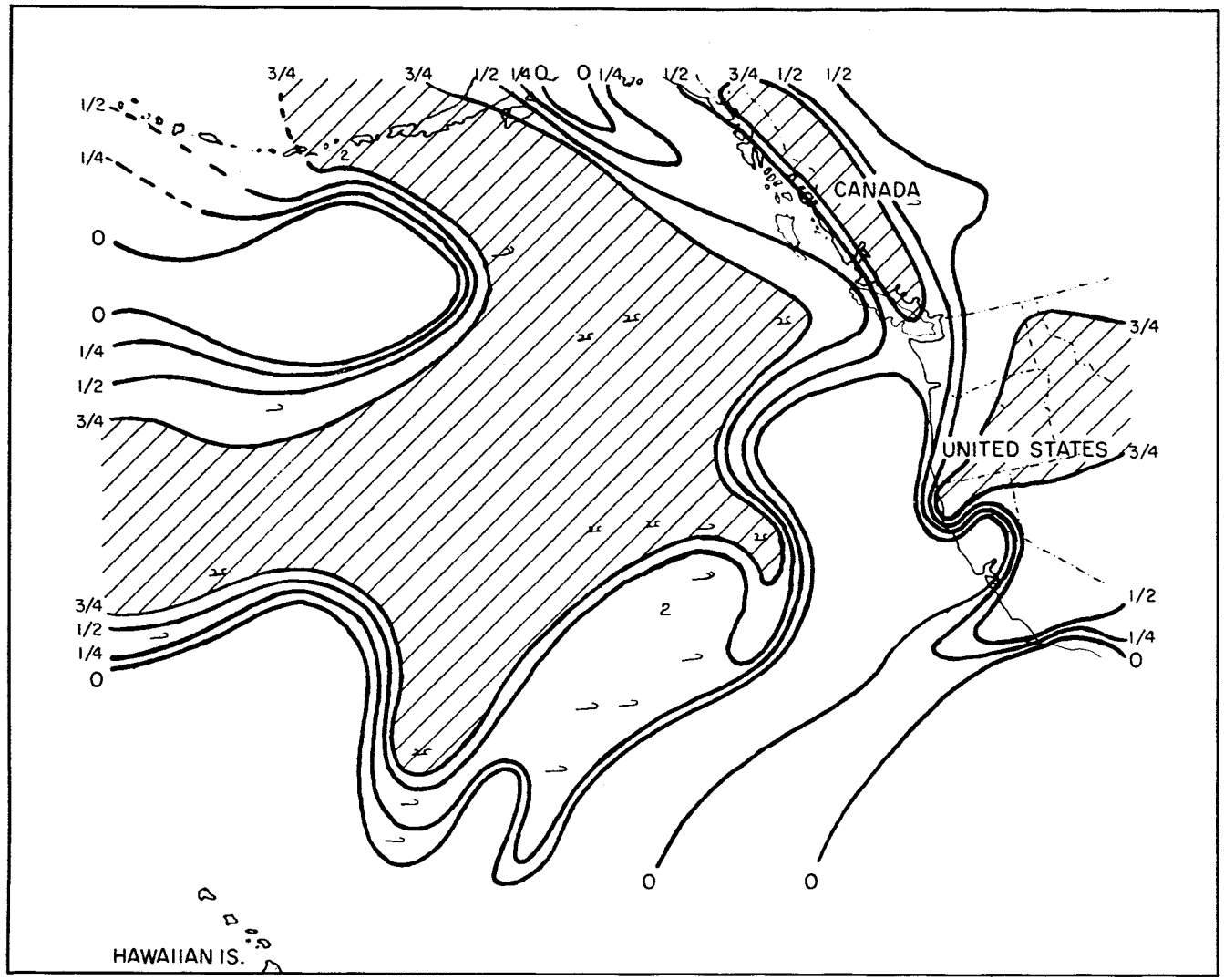

FIG. 26

HIGH CLOUD DISTRIBUTION AND TYPE OVER EASTERN PACIFIC ON 12 DECEMBER 1959

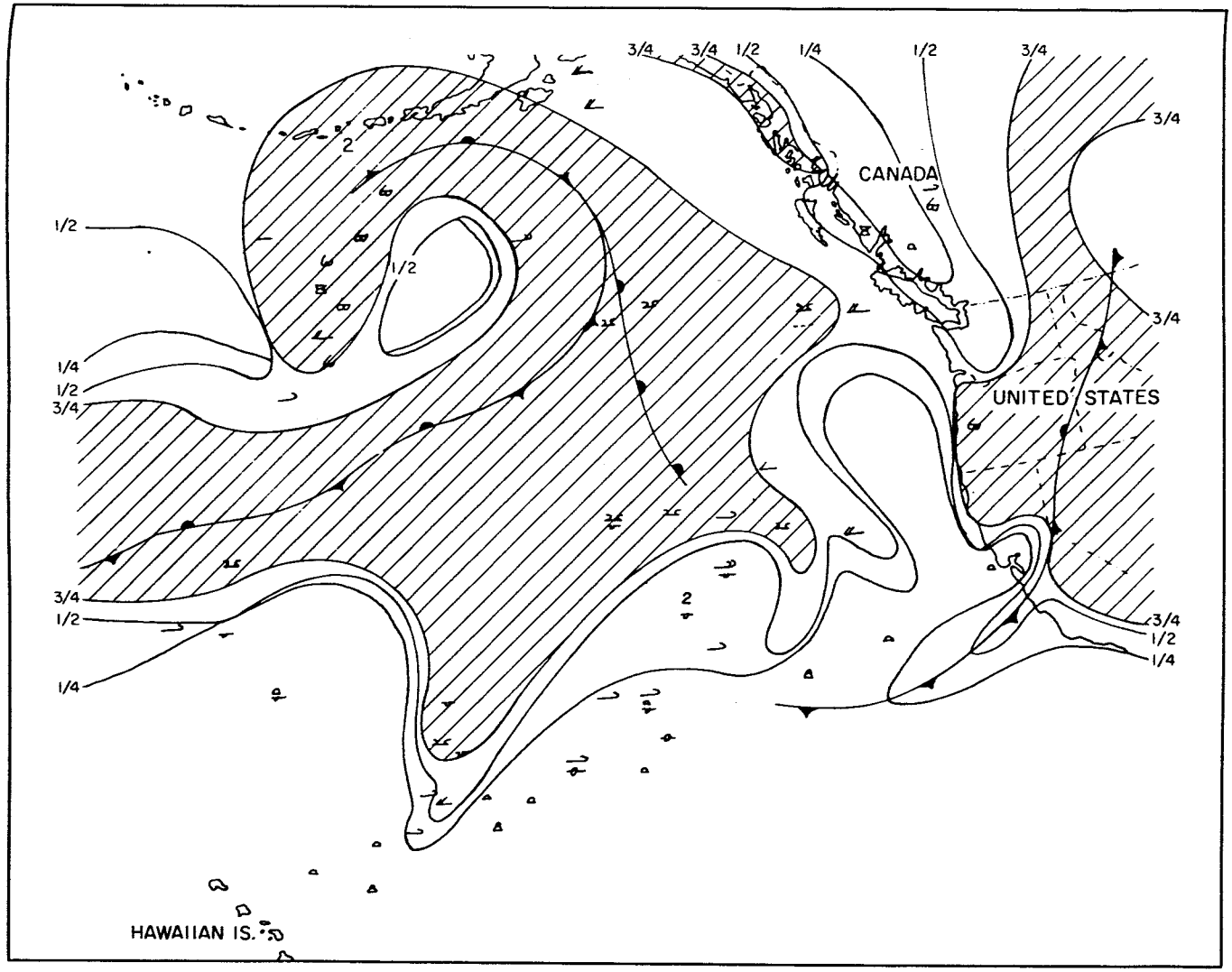

FIG. 27

TOTAL "TOP VIEW" DISTRIBUTION AND TYPE OVER EASTERN PACIFIC ON 12 DECEMBER 1959

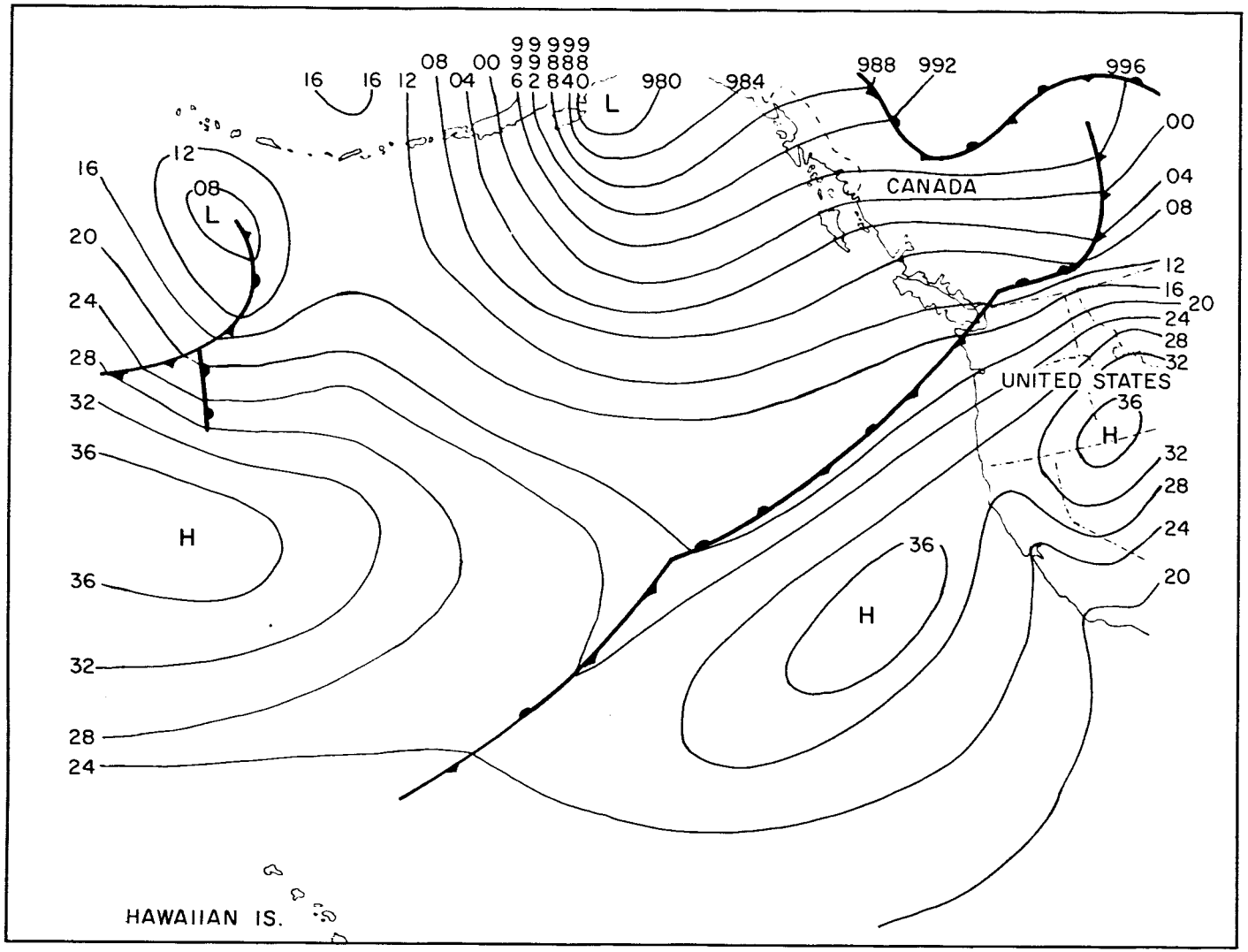

FIG. 28

EASTERN PACIFIC SURFACE CHART, 15 DECEMBER 1959, 0000Z

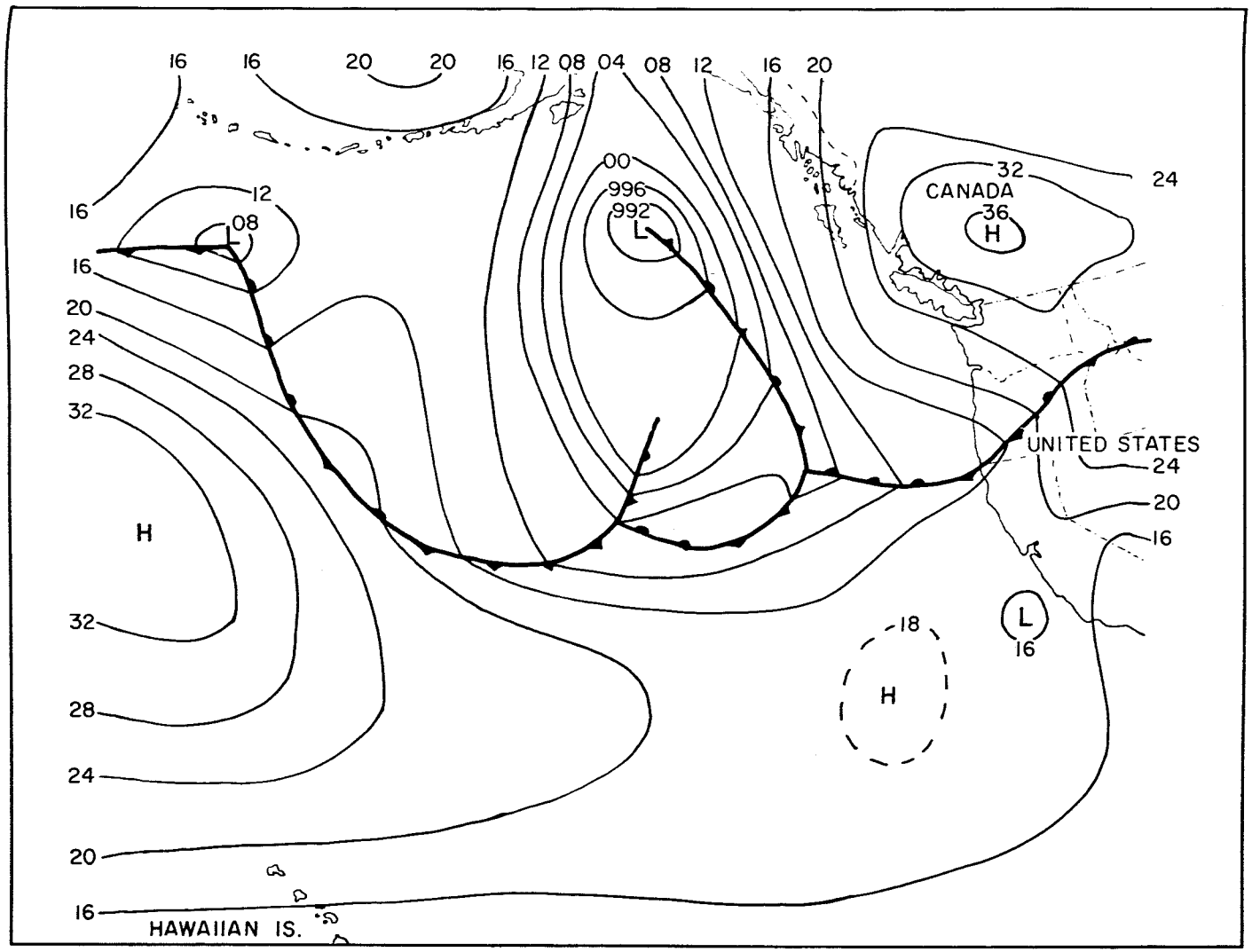

FIG. 29

EASTERN PACIFIC SURFACE CHART, 17 DECEMBER 1959, 0000Z

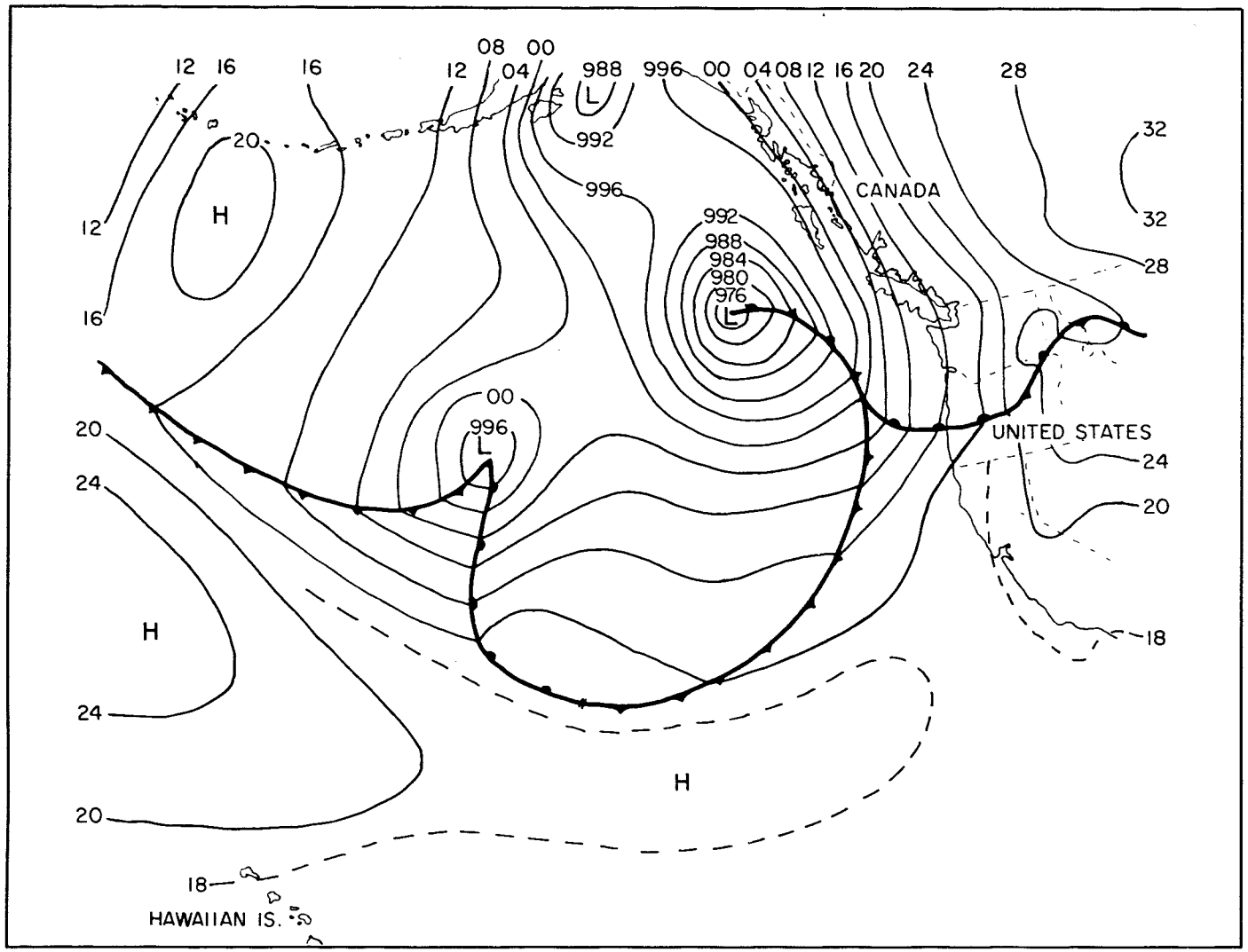

FIG. 30

EASTERN PACIFIC SURFACE CHART, 18 DECEMBER 1959, 0000Z

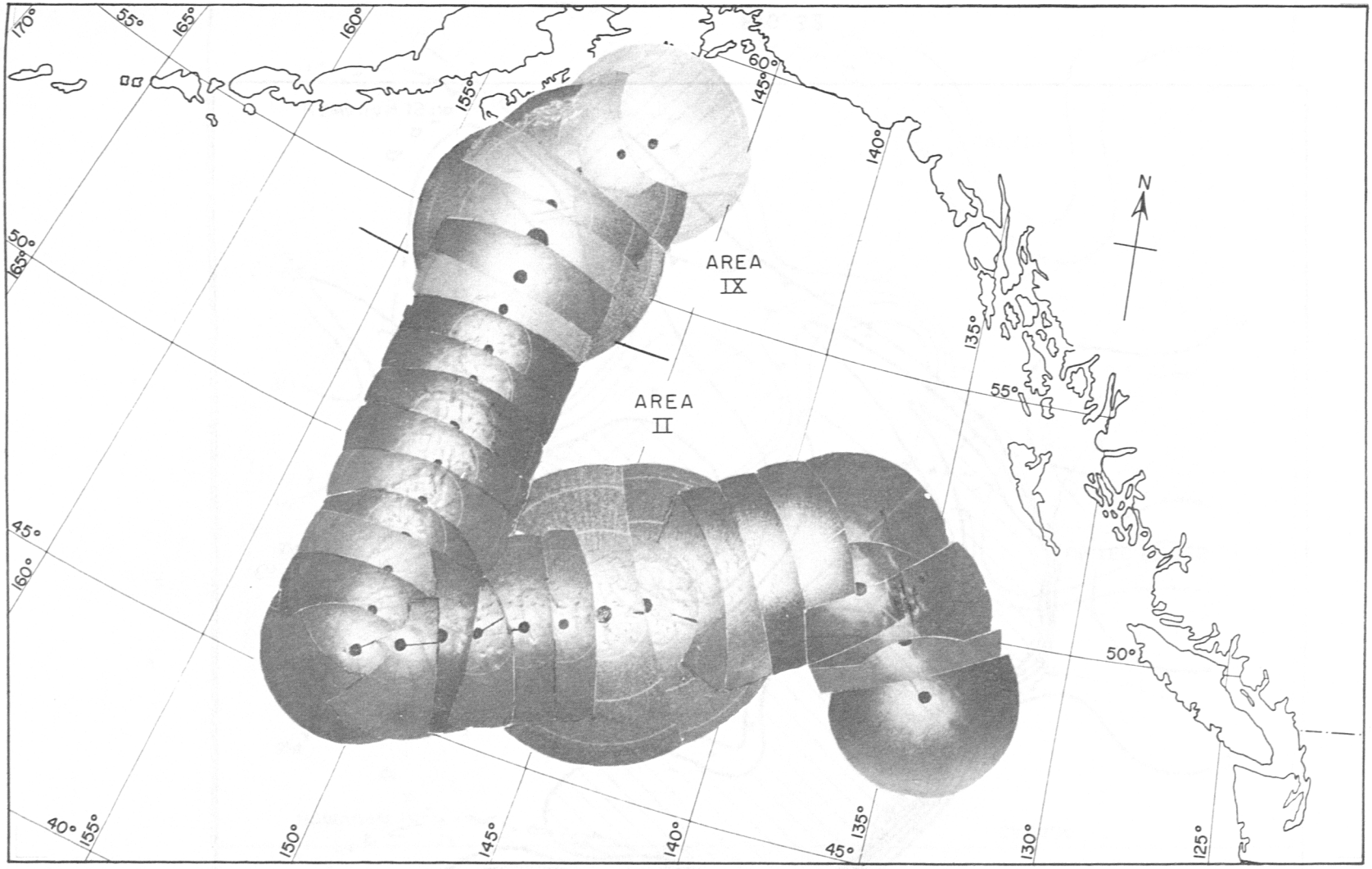

FIG. 31

RADARSCOPE STRIP COMPOSITE FOR STORK INDIA FLIGHT OF 17 DECEMBER 1959

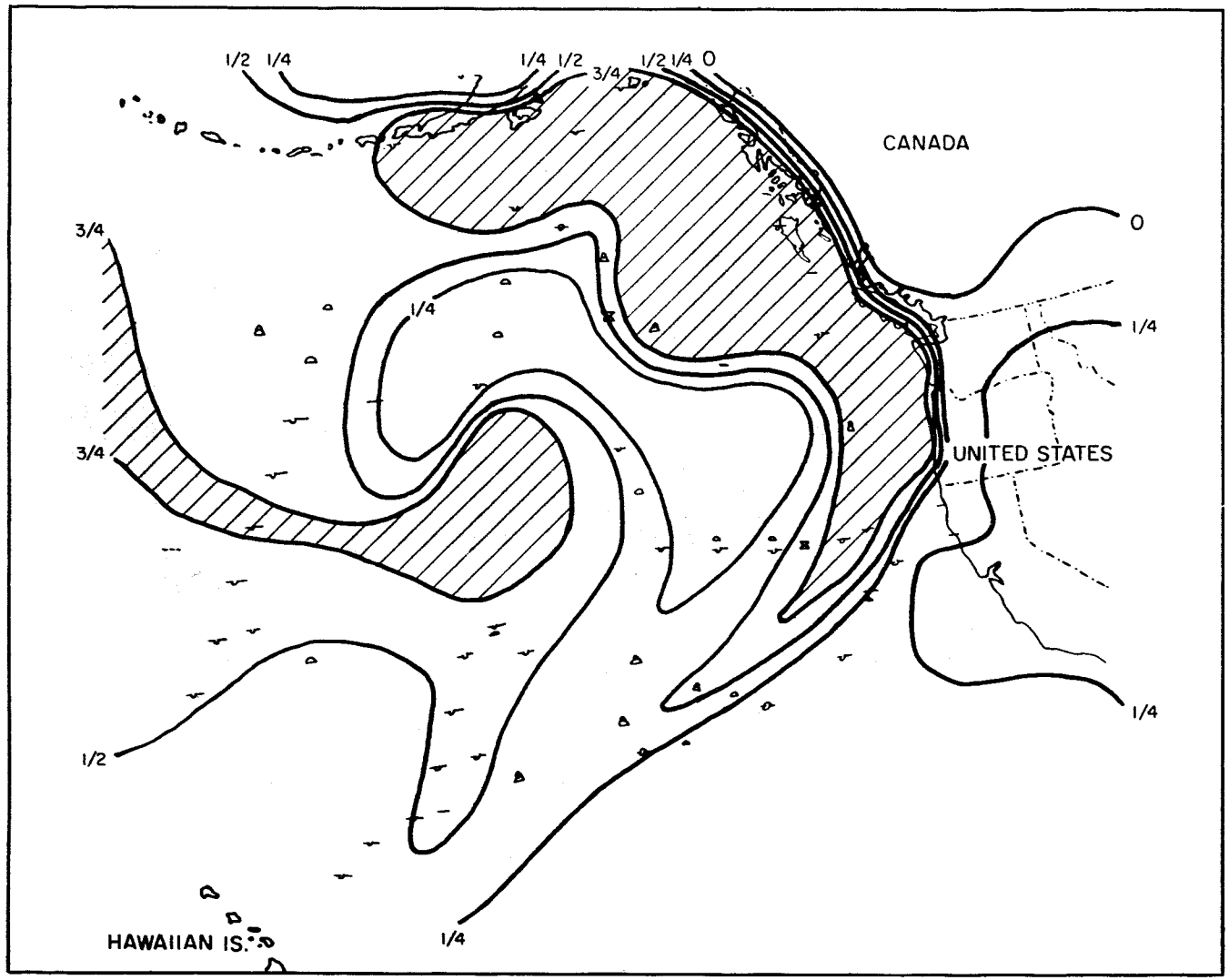

FIG. 32

LOW CLOUD DISTRIBUTION AND TYPE OVER EASTERN PACIFIC ON 17 DECEMBER 1959

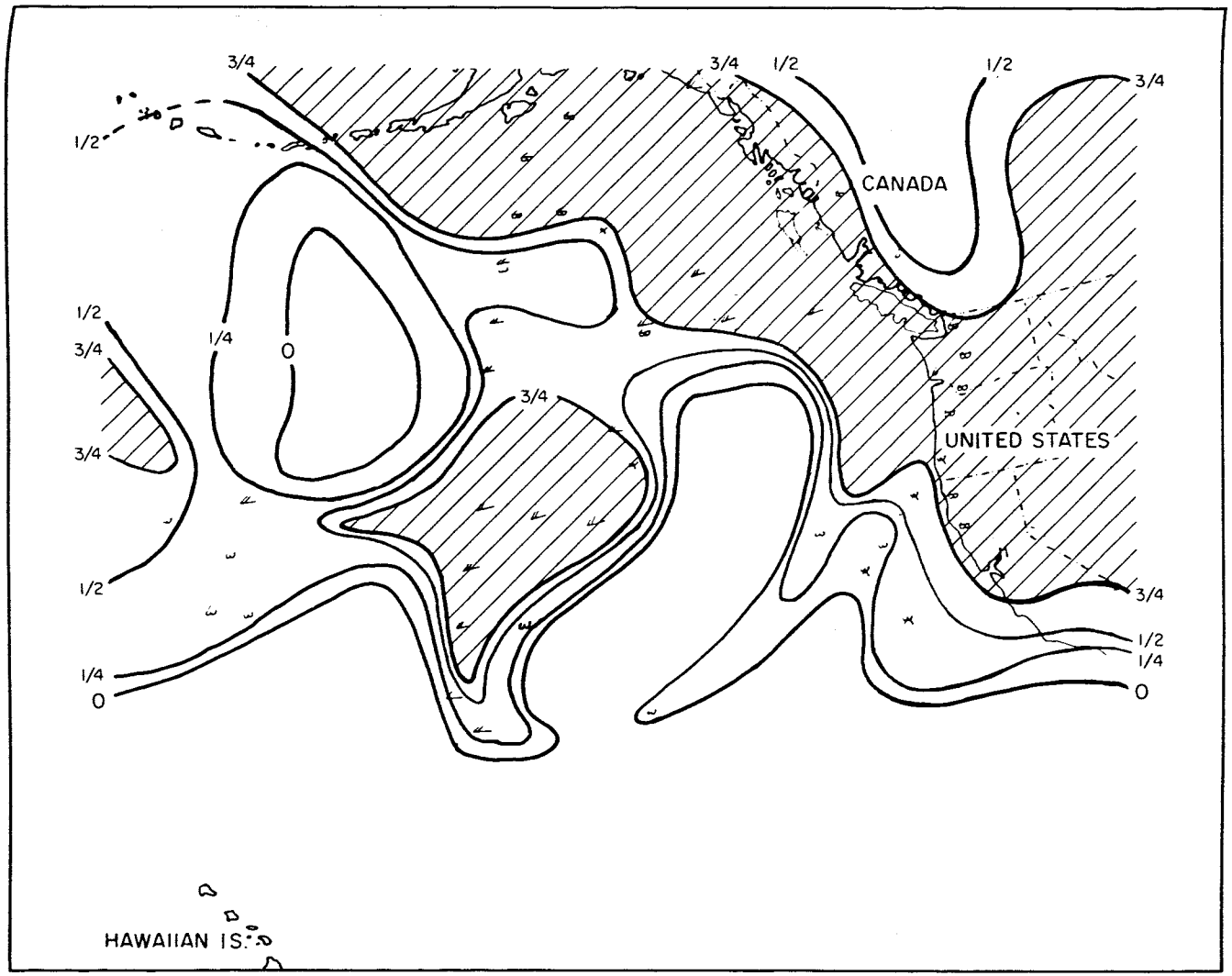

FIG. 33

MIDDLE CLOUD DISTRIBUTION AND TYPE OVER EASTERN PACIFIC ON 17 DECEMBER 1959

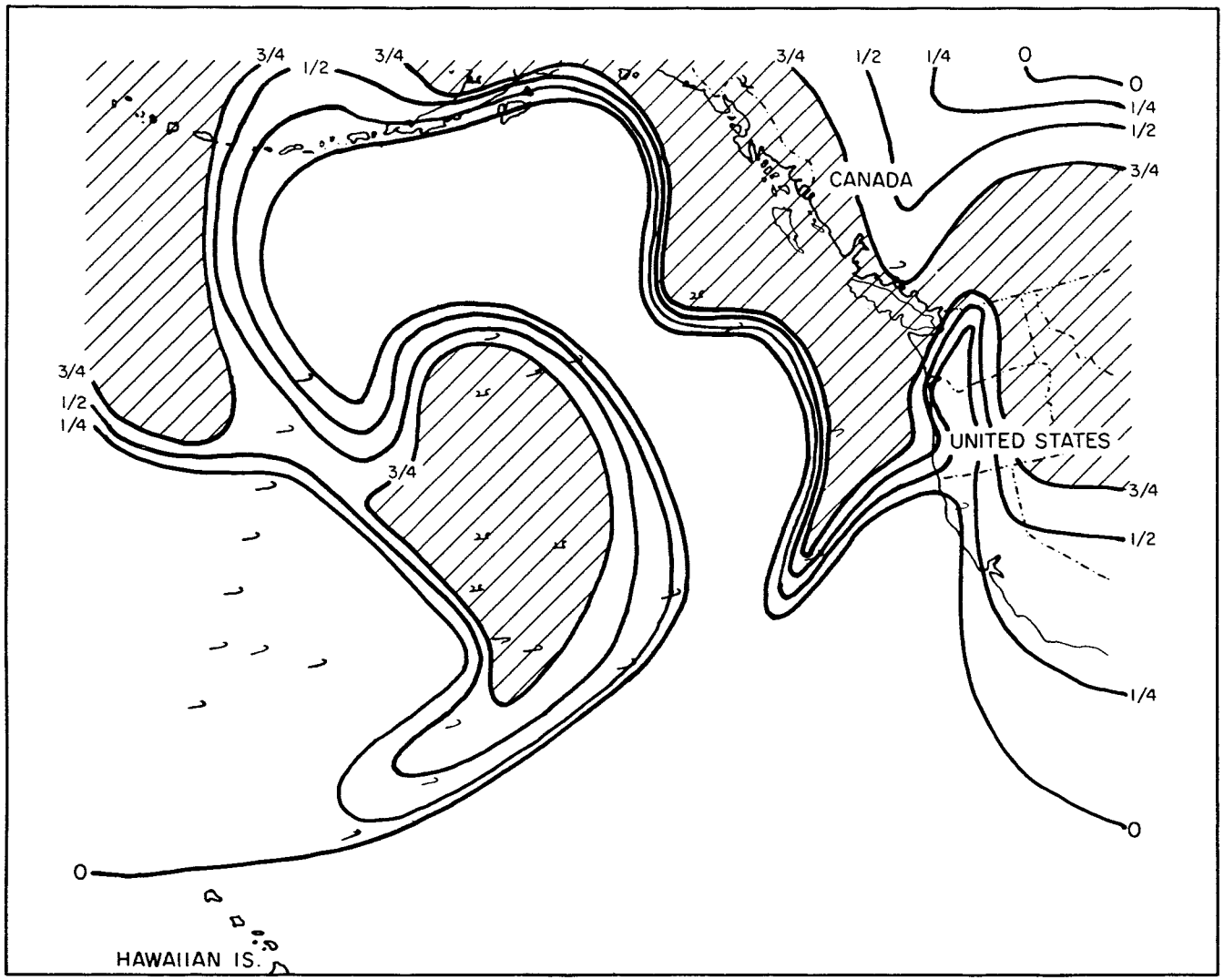

FIG. 34

HIGH CLOUD DISTRIBUTION AND TYPE OVER EASTERN PACIFIC ON 17 DECEMBER 1959

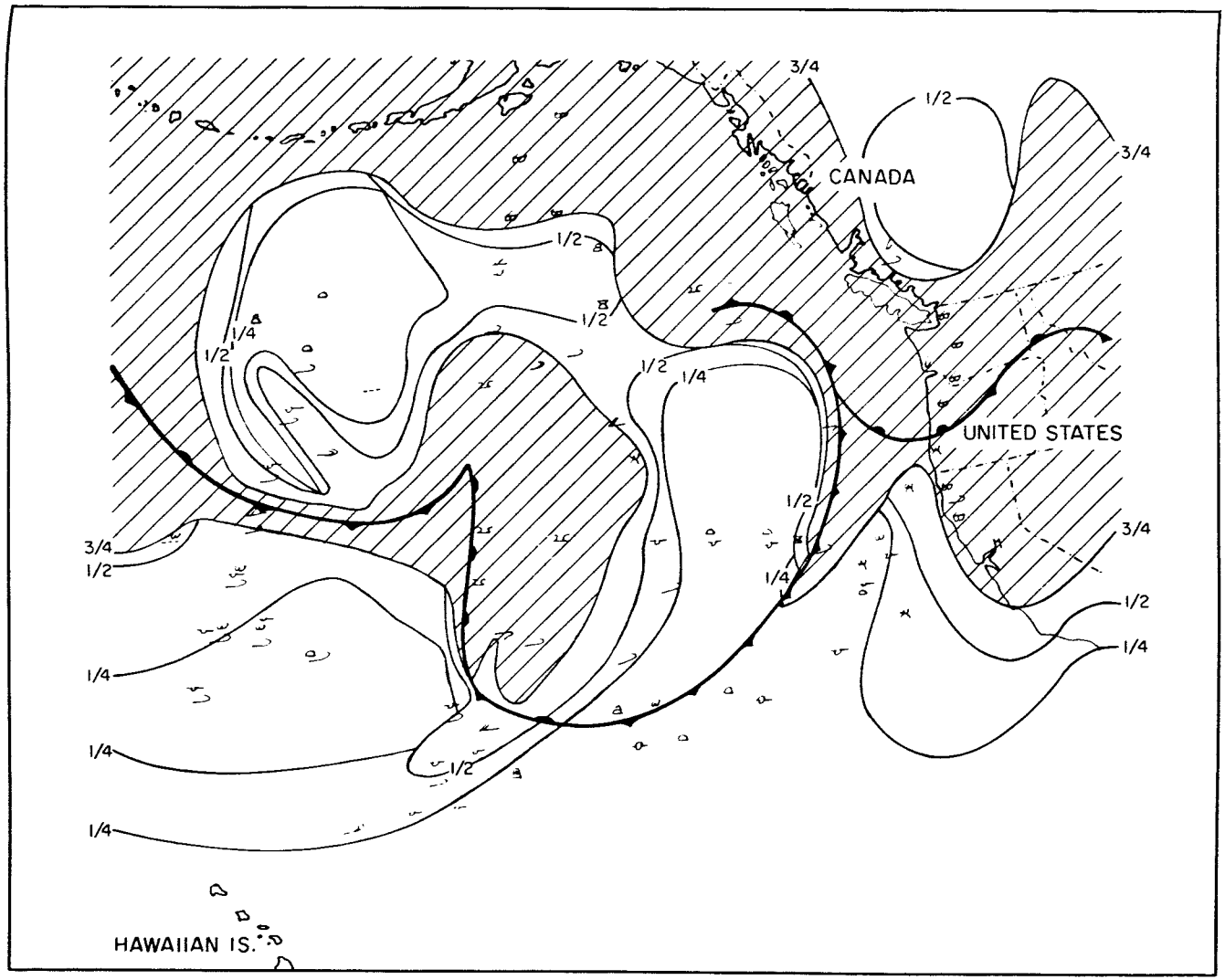

FIG. 35

TOTAL "TOP VIEW" CLOUD DISTRIBUTION AND TYPE OVER EASTERN PACIFIC ON 17 DECEMBER 1959

1.6 Conclusions

From the analyses presented, a number of promising clues for the detection of precipitation areas in synoptic scale cloud systems have appeared. The precipitation which seems to be most acceptable to nephanalysis detection is to be found in advance of clear or scattered cloud areas--areas, as noted, appearing behind the trailing cold front. This clear area is more apt to be valuable as an indicator of a cold front's presence and intensity than of its exact position. The analyses have indicated that the cold front model is reasonably descriptive of the actual conditions. The motions of this clear area and the area of cumulus activity will provide an indication of the movement of the cold air mass and of the front. The amount of cumulus activity may also be an indicator of the low level stability of the air mass. The variability of the clear area's distance behind the front will make this an imprecise method to locate the fronts. Nevertheless, even approximate location represents considerable improvement over the present capabilities in "silent areas."

In contrast to cold fronts where the precipitation occurs primarily along the front, the precipitation associated with warm or with stationary fronts may occur well away from these fronts in the cold air. The cloud shields associated with the warm and stationary fronts are often quite extensive and the rainfall patterns are usually less organized. Thus, for such a situation, locating warm and stationary frontal precipitation can become difficult.

As mentioned in the discussion of the 17-19 November 1957 storm, the formation of adjacent overcast and partially overcast areas may signal the development of a wave. If this assumption were generally true, satellite observations would provide a valuable tool for the forecaster. The feature, in the example studied, seems large and pronounced enough for ready detection. The presently planned satellite system has one major drawback in this respect: it may not be in the right place at the right time to detect developments, such as the wave formation, which last less than the twenty-four hour intervals between satellite observations of the same area. Furthermore, these developments might occur on the dark side of the earth.

The pictorial presentation of cloud cover that the satellite provides may be useful in calling attention to developments or features which might otherwise be missed in ordinary operational analyses. The eastern Pacific situation discussed in the report provides an example. The upper-level cold low cell NE of the Hawaiian Islands did not appear in the daily analyses. However, had this cloud information been readily available in pictorial form, the extensive cirrus clouds in this region might have signalled the need for a closer scrutiny of the data in this region.

There is much uncertainty about the obscuring effect of high cloud. If no lower layers can be discerned through this overcast, then most or all of the precipitation-associated details of low clouds will not be seen. Location of fronts, squall lines, and hurricanes

is apt to be quite difficult, for these phenomena are often overcast by layers or veils of cirrus or cirro-stratus.

The discussion of reflectivity from multiple layers indicates the possibility that low clouds under a high layer may be detectable as brighter areas in the high clouds. But there are other known factors which cast a doubt upon this possibility--i. e., inhomogeneities in the high cloud layer may be mistaken for low cloud; inadequate brightness resolution may make brighter areas undetectable; or the assumptions, on which the expression for the combined reflectivity of two layers is based, may not be entirely valid.

Although there exists the strong possibility that low clouds may not be detectable below higher clouds, it does seem worthwhile discussing certain features in cloud patterns which might be quite useful, should it develop that low clouds will appear as bright areas in the higher cloud shield.

Most of the precipitation in the examples studied is associated with low cloudiness. The converse is not necessarily true, of course; but brighter bands or areas in cloudy areas should be considered as suspect locations for precipitation. This agrees well with the work of Glaser (1957) who has prepared a number of brightness charts for various weather situations. In these charts the precipitation areas, as indicated on Weather Bureau analyses, were generally marked as being brighter than the surroundings.

The precipitation areas shown by radar often display definite patterns of organization. This is particularly true of the linear arrays

associated with squall lines and cold fronts. It is not unreasonable to suppose that the cloud formations attending these precipitation areas may be distinct from the surrounding cloud in some way. These cloud formations may actually form a line separate from the other clouds in the area or they may be thicker and more reflective than the surroundings. The size of these features should be generally large enough to be resolved by the satellite, as indicated by the radarscope degradation examples. The detectability of these features then hinges upon the brightness resolution of the system.

Ordinary meteorological data do not provide the information necessary for the location of cloud features whose scale is of the order of tens of miles. Therefore, it is not known from the cloud analyses if features of this size exist and can be used in the location of storm systems. However, the radar composites and some high altitude photographs do indicate the existence of systems of tnis size. While it cannot be accurately specified at this time how such patterns might be used in precipitation location, it can be stated that with the availability and study of satellite pictures these patterns may be exceedingly useful in analysis.

Of course, the interpretation of satellite pictures will require the analyst to include information beyond that contained in the individual picture. For instance, in determining whether a given cloud pattern is producing significant precipitation at the surface, the age of the system may be relevant; an extended squall line may develop

and produce intense storms from cloudless skies in a few hours, but an old, stagnant, cloud area of large extent may be pretty well "rained out."

As is true with more conventional types of analysis, the topography of the area under study will be important in identifying precipitating clouds. In many cases, surface reports will supplement the satellite pictures, helping to identify the areas of precipitation which are caused by orographic lifting. None of the cases studied in this report covered this type of precipitation. However, it is hoped that future work with actual satellite pictures will indicate the character of orographically precipitating clouds.

It is obvious that satellite observations are not soon apt to aid analysis materially in areas of good data coverage. That forms of data already available to the analyst are used in the search for cloud patterns of significance indicates this fact. Additionally, analysts do not generally use all the information presently available. For instance, only limited use is presently made of radar reports. It is clear from the composite radarscope pictures presented that some improvement in frontal placement could often be achieved by use of this information.

In areas where meteorological observations are widely spaced or non-existent, satellite photography holds great promise as an aid to better analysis. Subjective analysts may require time to gain the

experience necessary for the most efficient usage of the material. However, present models and knowledge should be sufficient to show immediate improvement in the analyses, and hence the forecasting in the "silent areas." Much research will probably be necessary to discover significant new relationships between weather and cloud patterns as shown by a satellite.

Research directed toward full operational use of satellite pictures will need to catalog cloud patterns and attendant weather. It will have to develop new models which better fit the new information and which will serve as a guide to the analyst. This research should develop statistical relationships between reflectivity patterns and other atmospheric fields. In addition, numerical models capable of assimilating satellite information--perhaps as an indicator of the moisture or net radiation fields--would be desirable.

SECTION 2

USE OF SATELLITE DATA IN TROPICAL METEOROLOGY*

2.1 Introduction

With the successful launching on 1 April 1960 of the weather satellite TIROS I, its placement, well spin-stabilized, in a nearly perfect, very nearly circular orbit, and the excellent functioning of the cameras and the electronic power, storage, and readout systems, production began of what proved to be a long series of sequences of excellent informative satellite pictures of cloud patterns and associated weather phenomena. The detail, both of cloud formations and of terrestrial landmarks, that the pictures revealed, and the abundance and general high quality of the pictures, exceeded most expectations and provided the meteorological analysts with a wealth of information-filled material to interpret, chart, describe, summarize, and make available for immediate operational use. Teams of meteorologists high on windy Kaena Point, Oahu, Hawaii, and at Fort Monmouth, New Jersey, performed these tasks on a current real time basis, and were the fortunate few who first saw and studied in detail the remarkable and informative large-scale cloud patterns of the pictures. Many of the patterns seen represented an atmospheric scale so large that

*Originally prepared as a Semi-Annual Technical Summary Report under Contract No. AF 19(604)-6156, under ARPA Order No. 26-59. This Section was written by H. M. Johnson, University of Hawaii.

(excepting the results of a few rocket shots) it had not been seen before, thus many new features appeared, some quite unsuspected.

A notable example is the vast scale on which combined cyclone-anticyclone systems integrate the cloud patterns of the adjoining regions of the atmosphere. Another is the wide range of scales of banding, which is largely without explanation in the theory of the present time. Another is the apparent variety and complexity of the smaller scale, but still relatively large, features in the low latitude regions. A final example is the unexpected appearance, often in extensive arrays, of cloud formations long observed from the ground. Many others could be listed here.

Although some real progress was made in the area of tropical meteorology and the use of satellite pictures in the study of low latitude cloud patterns and the related atmospheric phenomena during the initial essentially operational phase of the project, the subsequent gains were chiefly in the form of preparations for an intensive analysis to be based upon the use of special synoptic charts. This section will summarize the early findings, including the results of continued studies of picture sequences, and will outline the preparations completed for the next phase of the use of satellite data in Tropical Meteorology. This phase will include studies of the relations of the satellite photographic representations of major and lesser atmospheric systems, and the use of synoptic information in the further interpretation of satellite picture features.

2.2 Cloud Pattern Analysis

The cloud patterns of the satellite pictures were considered to represent a large amount of information, but in a form not easily interpreted. These patterns, and their details, sequences, and changes, comprise a complex, interesting and important natural "story," and it is most unfortunate that very little of it can be correctly read by anyone as yet. The immediate operational meteorologists were mostly too busy with their pressing operational tasks to take much time to investigate the meaning of cloud pattern details or to search for answers by comparing current pictures with pictures obtained during the earlier orbits. Dr. Johnson believed that one of the important ways in which he could contribute to the project and its ultimate success was through such interpretive investigations carried out on a current basis, concurrently with the operational phases of the project. He had such investigations as one of his major objectives, and thus was able to devote more time to investigations of this type. Some of the results of this work, mainly preliminary and tentative, will be touched upon in the brief general comments which follow.

Activities and progress in this phase of the project included the following:

a. The synoptic meaning of the largest scale cloud pattern features, and of the similar but smaller features, was determined or tentatively determined, particularly for the mid-latitudes. Among

the features identified were cyclones, anticyclones, cold frontal bands, vortex centers, vortex center cloud shields, warm sectors, cold air advection areas, possible waves, cyclone-anticyclone combined systems, cyclone families, other vortices, convergence zones, and other features. Relatively few low latitude systems were surely identified.

b. Different stages in the development of major features were observed. For example, new cyclones, developing cyclones, old occlusions, fresh strong cold fronts, old weak cold front, frontolyzing fronts, and others were identified.

c. The relationships of these systems to lower latitude and tropical systems were sought. Modifications occurring in typical mid-latitude systems as they moved or extended to lower latitudes were observed. Cold fronts were particularly interesting in this regard. They appear to undergo a series of changes which is neither simple nor well understood. Much more should be done with these transformations and relationships.

d. Types of cloud patterns and atmospheric systems which were distinctive (though varying in detail and in degree of development) and which occurred repeatedly, and therefore appeared on several or on many picture sequences, were given special attention. These included most of the systems mentioned under "a" above, but also others not satisfactorily identified or well understood. These

contrasted with patterns and systems which appeared to occur rarely or only once in the set of satellite picture sequences.

e. A wide variety of patterns, representing a notable complexity, was observed in the tropical regions particularly over the oceans. Some of these were of distinctive recurring types, mostly poorly understood, but many presented a chaotic appearance and possibly represented much randomness and thermodynamic disorder, or possibly represented an unusually complexly ordered greater system. Very likely turbulence effects, of several of the many scales of turbulence, were dominant in these patterns.

f. Day to day time changes in cloud patterns and system development were observable, and were usually considerable. In many cases continuity could be followed; in many other cases the changes were too great and continuity was lost. Longer period time changes were easily observed, and were very interesting. Hour to hour time changes and changes of similar time scale could usually not be determined effectively. One important exception occurred during the periods when pictures were taken at the southernmost limits of successive orbits, where several subpoint paths crossed. At such times appreciable short period changes were noted.

g. Many smaller scale patterns in mid- and low-latitude areas, and in the transition zones between them, were given special attention. Others deserved much more attention than they received. Those studied include: cloud types, only a limited number of which were

satisfactorily identified; fog areas; low stratus decks; coastal local effects; orographic effects, including lee waves; island effects; cloud subsystems in cyclones and anticyclones; banded cloud systems; extensive repetitive cloud patterns; parallelism and other types of oriented formations; recurring tropical formations; and others.

h. By the use of narrow angle lens pictures which represented known areas within wide angle lens pictures, when such pairs were available, a number of clouds were properly identified. In general, in the wide angle pictures, cirrus clouds of several types are clearly recognizable, as also are cumulus and towering cumulus cells or groups of cells. Low latitude cloud streets are highly distinctive, and show elements of a rather wide range of sizes. Some middle cloud formations were identified tentatively. Many cloud elements in each sequence of pictures were not surely identified. Many unidentified types and patterns may well be middle cloud formations.

i. The low level air flow patterns were often well revealed by groups of relatively numerous cloud streets, which showed extensive parallel flow areas, distinct and at times extensive zones or lines of convergence, and other details. Cloud elements at more than one level at times clearly revealed different flow directions at the different levels. Flow patterns characteristic of cyclone and anticyclone systems were assumed, and were at times confirmed by oriented cloud elements in the system cloud patterns.

j. A highly distinctive, often recurring, mottled or speckled pattern which occurred typically in the western, or southwestern (in the Southern Hemisphere, northwestern) sector of oceanic well developed cyclone systems, and often extended into the associated anticyclone system, and which represented equatorward flow and cold air advection, was found to consist of towering cumulus elements, isolated and clustered, often with spreading tops. Areas with this convective pattern, and the associated low level instability were at times very extensive, having dimensions of many hundreds of miles. Large scale banding was sometimes apparent in such areas.

k. An attempt was made to relate "small" cloud elements (which were still rather large) of the satellite wide angle pictures to what is observed and recorded by ground observers. Special cloud observations were made at Kaena Point at the times of satellite passes to help establish the relationships, but because readouts were usually being made when the satellite was nearest or overhead, few pictures were taken near enough to include the clouds observed from the ground. In fact, pictures of the Hawaiian Islands with clouds near or above the islands proved to be very rare. Nevertheless, large formations observed but not well seen from the ground, because of distance and perspective, and therefore very difficult if not impossible to visualize correctly from ground observations (as has certainly been the case for many years), were recognized in a limited number of cases to be the same as or closely similar to certain of the "smaller" elements which were newly seen in the satellite pictures. More

progress was made in the interpretation of these relationships by the use of the narrow angle pictures. These pictures provided the needed intermediate scale detail, and provided the key to the solution of many aspects of this problem. Details seen in these pictures often relate directly to what has long been seen from the ground.

l. In one exceptional case a dense (highly reflective overcast) largely north-south band, which had associated cloud areas and other features, and was not clearly "frontal," was observed from above in current satellite pictures while it was over the island of Oahu and there causing extraordinary very heavy rainfall and several remarkable occurrences of hail. Much middle cloud was present at this time.

m. While not easy, in many cases, it proved to be possible to relate narrow angle picture cloud elements in one to one correspondence with elements in a small portion of the related wide angle picture. The outline details of many small scale cloud elements often remained distinct in the wide angle lens picture, although the difference in resolution generally caused substantial changes in the appearance of the elements and their patterns. It is, therefore, most unfortunate that the narrow angle camera system was inoperative through much of the productive period of the satellite. In some sequences of narrow angle pictures certain distinctive features appeared twice (at times more than twice) appearing in one picture and then again in the following picture (or pictures). The successive picture pairs thus linked the

sequence and provided continuity, but lacking horizons did not permit orientation in the same manner that it was obtained for the wide angle pictures. When large and small angle pictures alternated, orientation was possible for both. Thus the relationships between pictures from the two cameras not only facilitate the recognition and identification of cloud types and ground observed formations, but also provide orientation information (and information on satellite motions including the spin axis motion or wobble).

2.3 Picture and Cloud Pattern Orientation

In the absence of useful landmarks, and also of good computing center positional data, orientation can be achieved quantitatively by a method which provides a close approximation. This method requires a sequence of closely related pictures, and uses the information contained in the apparent motion of distinctive cloud features which is seen in successive pictures as the satellite moves along its path. The time rate of change of the apparent positions, with respect to the principal line, of the cloud features provides a measure of the angle between the principal line and the subpoint path, hence of the azimuth, at each point or time. When this method was used nadir angles were obtained quickly and with sufficient accuracy by interpolation from the rectification grids. Subpoint to principal point earth surface distances corresponding to the nadir angles were taken from curves (or tables) based on the geometry involved. A family of curves which takes into account the latitudinal and azimuthal variations of this relationship when the distance is measured in degrees would be very helpful. Good satellite data from the computing center,

which were always available, were also required. With the subpoint as one known point and the azimuth as a known direction, the known earth surface distance from subpoint to principal point established the picture center position, and the pricipal line established the direction to the picture center, thus orientation was achieved. Results obtained by this method when checked against those obtained by the use of landmarks, when both methods were used on picture sequences which had good landmarks, showed very good agreement. This method for obtaining orientation was used routinely during the last week of full scale operations, was used effectively and intensively later during the reduced operation (particularly by careful weather bureau personnel), and has been used routinely in the research studies.

2.4 Data Collection

This activity commenced shortly after TIROS I was launched, and increased as data arrived in increasing abundance from an increasing number of sources, and as the pictures and other materials became available. A gradual tapering off is anticipated, but the end is not yet in sight. The data collected were of several main types:

2.4.1 Synoptic Data

After the successful launching of TIROS I, when its ability to produce detailed informative pictures became known, telegrams and letters were sent to the weather services which were making continental and sub-continental synoptic collections in the tropics and subtropics, requesting copies of the data for a period from 30 March on (estimated

to continue for about three months). When TIROS I became non-productive, letters were sent to request that no data be sent after 24 June. Thus data were requested for the period from 30 March to 24 June 1960.

The broadcasts requested, the organizations contacted, and the responses (at the present time) are listed below:

(1) Data requested: AXM (Canberra), sub-continental broadcasts.

L. J. Dwyer, Director of Meteorology
Commonwealth Bureau of Meteorology
Box 1289 K G. P. O.
Melbourne, Australia

Data received for: 3 April - 9 June (except 3 days), also 17-21 June.

(2) Data requested: New Zealand Daily Weather Bulletin

Director, New Zealand Meteorological Service
P. O. Box 722
Wellington, New Zealand

Data received for : 30 March - 19 June (complete)

(3) Data requested: JMG RTT broadcasts from Tokyo

Commander, First Weather Wing
Wheeler Air Force Base
Oahu, Hawaii

Data received for: 26 April - 6 July (except 10 days)

(4) Data requested: AIE RTT broadcasts from Guam

Commander, First Weather Wing
Wheeler Air Force Base
Oahu, Hawaii

Data received for: 6 May - 23 June (except 3 days)

(5) Data requested: SE Asian CW intercepts made at Clark Field

Commander, First Weather Wing
Wheeler Air Force Base
Oahu, Hawaii

Data received for: 10 May - 21 June (except 1 day)

(6) Data requested: Receptions made at WBAS Honolulu

Honolulu Airport Station
U. S. Weather Bureau
Honolulu, Hawaii

Data received for: 30 March - 31 May (over 30 large cartons)

(7) Data requested: Indian Daily Weather Report

High Commission of India
Establishment Dept., Publications Branch
India House, Aldwiych, London, W.C. 2

No data received for period of request. Data scheduled for delivery.

(8) Data requested: AFMET SIX, African subcontinental broadcasts

A. Rowe, Director
Meteorologique de la Metropole et de l'Algerie
2 Avenue Rapp
Paris 7^{e}, France

Data received for: 30 March - 24 June (complete)

(9) Data requested: AFMET FIVE, African subcontinental broadcasts.

Monsieur M. Brouquet-Laglaire, Director
Service Meteorologique de l'Afrique
Occidentale Francaise
Dakar, French West Africa

Data received for: 30 March - 31 May (complete)

(10) Data requested: AFMET FOUR, African subcontinental broadcasts

Director
British W. Africa Meteorological Service
Lagos, Nigeris

Data received for: 7 May - 31 May

(11) Data requested: AFMET THREE, African subcontinental broadcasts

Director of Union Weather Bureau
Department of Transport
Weather Bureau
P. O. Box 1135
Pretoria, Union of South Africa

No data received. Data scheduled for delivery.

(12) Data requested: AFMET TWO, African subcontinental broadcasts

B. W. Thompson, Deputy Director
Meteorological Department
Dagoretti Corner, Private Post Bag
Nairobi, Kenya, British East Africa

Data received for: 30 March - 31 May (complete)

(13) Data requested: AFMET ONE, African subcontinental broadcasts

M. F. Taha, Director General
Meteorological Department
Koubry El Quobba P. O.
Cairo, United Arab Republic

No data received. No data scheduled for delivery

(14) Data requested: AMERSUD, South American continental broadcasts

Director, Meteorological Service
Praca
5° Andar
Rio de Janeiro, Brazil

No response

The data received from these services have all been sorted, checked, logged in, put in good order, and organized and stored for easy accessibility and quick retrieval. Additional data arrive several times each week.

2.5 Analysis and Use of Satellite Data in Tropical Meteorology

In this part of the program the work and progress has consisted largely of preparations for the intensive study which has just commenced.

TIROS positional data, cloud charts, weather summaries, and the films have received considerable use in the selection of orbit passes and tape picture sequences to be studied first in this new phase.

Surface and upper air synoptic charts will be plotted first for sequences known to be of unusual interest. Then others will receive attention. The plotting of a limited number of surface charts has been completed. This work has not progressed further primarily because of the fact that until recently not enough data were on hand to permit completion of even one synoptic chart. Since only those charts can be plotted for which full sets of data are available, many important orbits, and picture sequences with phenomena known to be of unusual interest, have not yet received the attention they deserve. The plotting continues for those charts which can be completed. The data for the others are on their way. Clearly, the delays in data reception have determined to a large extent what could be done in this part of the program.

The analysis of the plotted charts is at its earliest stages, but has commenced. This work includes both contour and streamline analyses, and, of course, cloud analyses, and will soon progress at a greatly accelerated rate.

In the present phase of this work particular attention is being given to tropical formations and systems and tropical conditions, and to oceanic phenomena, especially at the lower latitudes. Phenomena and problems now under study include the following examples:

a. Large low latitude cloud patches, which appear repeatedly, may be relatively stable, occur fairly frequently, and seem to be at least partly cirriform.

b. Low latitude formations and systems which appear to be derived from mid-latitude systems.

c. Cloud streets and the convergence, convection patterns, and other processes and patterns which they reveal.

d. Cloudless or relatively cloud free areas, particularly when associated with unusually cloudy areas, and particularly when at the lower latitudes.

e. Land-sea cloudiness and cloud pattern differences.

f. Cloud pattern small element identification, particularly in those cases where narrow-angle pictures of conditions shown in known areas of wide angle pictures are available, and when the photographic conditions are unusually favorable. Entire patterns, and the large elements are also under study.

g. The relationships of satellite picture cloud pattern elements to cloud types and other information found in the standard synoptic reports and reported by ground observers.

h. Unusual conditions and systems in the Southern Hemisphere, and over the southern seas.

i. Typhoon occurrence, and typhoon development.

j. And many others.

For these studies, which so far represent only a good start, and which require good analyzed synoptic charts, it is too early to give technical summaries or to give tentative conclusions.

SECTION 3

THE LIFE-CYCLE OF A PACIFIC FRONTAL SYSTEM

3.1 Introduction

The ability to photograph large-scale cloud cover has been amply demonstrated by the TIROS meteorological satellite. Another useful aspect of this satellite is found to be the ability to see the day to day variations and developments in the large-scale meteorological systems as shown by changes in cloud cover and patterns.

The orbital period of TIROS I is such that on the South to North leg in the Northern Hemisphere, orbit (N+14) is approximately 23 hours later than orbit (N) and the path lies approximately 7.6 degrees longitude to the east. The change of 7.6 degrees longitude to the east in 23 hours can be used to advantage in attempting to follow the day to day development and easterly movement of a large scale system such as an extra-tropical cyclone. As a demonstration of this technique, a frontal system which was first photographed in the western Pacific on 18 May 1960 was followed in its movement across the Pacific until it entered the west coast of the United States on 26 May 1960.

Attitude data for TIROS I was of such a nature as to make the exact location of pictures doubtful in regions without suitable landmarks. Since these pictures were all rectified without the use of any landmarks, no attempt has been made to make any detailed comparisons between the cloud patterns and the pressure analysis over these areas.

*This Section was written by J. A. Leese, Geophysics Research Directorate

Such comparisons would be of little or no value even with good attitude data since the analysis could also be doubtful in this region of little or no data. The rectifications were performed as follows: a series of frames with good horizons were rectified on a blank paper to get the relation between the sub-point and the principal point lines. It was then assumed the starting time was as programmed, and the sub-point track was correct. From this it was possible to get a fixed location on the surface of the earth as a starting point. It was found this assumption led to no gross errors in location, at least, in a study of large-scale cloud patterns such as this.

3.2 Discussion and TIROS Rectification of a Pacific Frontal System

Orbit 677, 0230Z, 18 May 1960

The Northern Hemisphere Surface Analysis for 0000Z 18 May 1960 (Fig. 36A) shows a new wave cyclone developing near 35N 160E after the occlusion has been "washed out" and the low pressure area associated with the occlusion has begun to fill. The rectification of orbit 677 (Fig. 36B) has a relatively narrow band in the region of the cold front but otherwise exhibits little in the way of an organized cloud pattern around the frontal system. The large overcast area in the vicinity of 40N is probably associated with the old occlusion. Scattered cumuliform clouds to the northeast show a tendency to be organized into lines parallel to the flow around the anticyclone.

Orbit 691, 0145Z 19 May 1960

The Surface Analysis for 0000Z 19 May 1960 (Fig. 37A) located the center of the low pressure area near 38N 173E and shows a drop

in the central pressure of nearly 15 millibars in 24 hours. The frontal system is already well into the occluded stage. The rectification of orbit 691 (Fig 37B) shows a much more organized cloud pattern than was seen nearly 23 hours earlier on orbit 677 (Fig. 36B). The band of clouds in the vicinity of the cold front is now much broader. The brighter reflectivity indicated by the heavier shading shows the cloud cover now extends through a greater depth than previously. A broad band has also developed ahead of the warm front. The cloud band associated with the occlusion is now moving around the northern periphery of the low and on into the northwest quadrant indicating an increase in circulation around the storm. At this stage the center of the vortex is not well defined by the cloud patterns. Evidence of drier air being drawn into the system in the southwest quadrant is shown by the presence of only a few cumulus clouds in this area. The relatively small bright reflective areas along 175W, above 35N, indicate the presence of bands within this region of general overcast. These bright bands could indicate the presence of buildups in those areas, or if the cloud cover is in layers, the sum of the depth of these layers is greater in the brighter reflective areas than the surrounding overcast.

Orbit 705, 0100Z, 20 May 1960

The center of the low pressure area was located near 50N 176E on the Surface Analysis for 0000Z 20 May 1960 (Fig. 38A) and shows a further deepening of eight millibars in the past 24 hours. The circulation shows a further intensification while the frontal system

has continued to occlude. One of the most striking features of the rectification of orbit 705 (Fig. 38B) is the clarity of the definition of the center of the vortex by the cloud pattern. The ability of the relatively dry air entering the system from the southwest and the frontal band spiraling around from the northwest to maintain their separate identities in the form of a logrithmic spiral into the center of the vortex is certainly an outstanding feature. Such a feature would appear to be a characteristic reserved for a slow moving system or at least a system which maintains a wind speed around it many times greater than the speed of its horizontal movement in order to prevent the mixing of these two air masses. The lack of agreement between the surface analysis and cloud rectification on the exact location of the center of the vortex cannot be accounted for solely by the time difference. This lack of agreement could be the result of an inaccurate location of the center in the analysis due to lack of data, or could result from an inaccurate location of the rectification. In any case, it is felt the vortex of an intense slow-moving system such as this should be nearly vertical through the atmosphere and the center as shown by the cloud pattern should show good agreement with the center of the vortex on the surface. The cold front was placed without any data in the region and therefore could be displaced at least five degrees to the west to show better agreement with the band of clouds in that region. The band of clouds associated with the warm front is now better defined than it was approximately 23 hours earlier on orbit 691.

The region from 40N to 45N and 150W to 160W has a thin cirrus cover but more notably it has a complete lack of low cumulus clouds. This feature of a sharp cut-off of the low cumulus clouds well ahead of the warm front cloud band has been seen in other pictures of systems similar to this, and could be an indication of the line where the difference between the sea water temperature and the free air temperature changes sign together with the different physical processes involved with this change. It should also be noted that although there has been a complete change in the organization of the cloud pattern in most of this frontal system, the warm sector has remained generally broken with an appearance indicating multiple layers of clouds.

Orbit 720, 0145Z, 21 May 1960

The movement of the low pressure area in the past 24 hours has shifted to a more northerly direction, and the center is shown to be near 48N 176W on the 0000Z 21 May 1960 surface analysis (Fig. 39A). A comparison of this analysis with the analysis 24 hours previously (Fig. 38A) would indicate there has been little change in the system during this period. However, when the rectification of the cloud patterns of orbit 720 (Fig. 39B) is compared with the rectification of orbit 705 (Fig. 38B), changes can be noticed, especially in the vicinity of the center of the vortex. One reason for this change in pattern near the center of the vortex could be that the occluded system reached its peak of development near the time of orbit 705 and by the time of orbit 720 the system had begun to decay. This together with a weakening

in the intensity of the circulation would allow the air masses to become more homogeneous resulting in cloud cover all around the center of the vortex rather than the two separate air masses as appeared near the center 24 hours previously. The region to the southwest of the center of the vortex has shown a significant increase in cloud cover in the 24 hour period. These clouds are predominately cumulus and stratocumulus with a large overcast patch in the center of this region. These cumuliform clouds show a sharp cut-off near 170E or approximately at the ridge line between the two systems. The band of clouds associated with the cold front still exhibits a reflectivity which is brighter than the surrounding overcast, while the bright reflective band associated with the warm front on orbits 691 and 705 has completely disappeared. This would indicate the cold front has had no noticeable change in intensity while the warm front has significantly decreased in intensity.

Orbits 733 and 734, 0000Z, 22 May 1960

The low pressure center has continued to move toward the north-northeast during the past 24 hours, and is centered near 54N 172W on the surface analysis for 0000Z, 22 May 1960 (Fig. 40A). It also shows a filling of approximately 16 millibars. The frontal system has moved eastward and out of the low. The rectification of orbits 733 and 734 (Fig. 40B) shows a band of brighter reflectivity which is probably associated with the frontal system. However, this band is located from five to ten degrees west of the position of the front, shown on the surface analysis, in the region above 40N. As in the previous rectifications, the reason for this lack of agreement

cannot be determined accurately. If the rectification is located accurately, then the front above 40N has not moved as rapidly as was indicated by the surface analysis. It is doubtful that a small wave such as the one developing near 36N 165W would ever show a cloud pattern of such organization as to be able to determine its presence from cloud pictures alone. The region to the west of the frontal band is still dominated by scattered cumuliform clouds. The tendency to organize into lines parallel to the flow is not as strong at this stage as it was in the earlier stages. This would indicate a further weakening in the intensity of the circulation. The reflective pattern to the east of the frontal band would suggest the presence of cumuliform clouds with a wide sheet of cirrus above. However, the few ship reports available in this area are reporting low stratus clouds and fog together with the cumuliform clouds and illustrates one of the problems of cloud identification in TIROS pictures.

Orbits 747 and 748, 2300Z, 22 May 1960

The low pressure area has moved northward into the Bering Sea while the cold front has moved eastward as seen on the surface analysis for 0000Z, 23 May 1960 (Fig. 41A). The rectification for orbits 747 and 748 (Fig. 41B) shows little in the way of organized large-scale cloud patterns. A band of brighter reflectivity is distinguishable in the vicinity of the cold front north of 40N. The large overcast area west of the cold front and north of 45N is in the general vicinity of an upper air trough, but lack of upper air data

in this region precludes any attempt at direct association of the cloud cover with the trough. The vortex off the west coast of the United States, centered near 42N 127W (Fig. 41A) is indicated in the cloud pattern by the lines of cumulus clouds spiraling into the center of the vortex. The western U. S. north of 40N was dominated by buildups and thunderstorm activity. This is indicated on the TIROS photographs as relatively small masses of bright reflective overcast and serves as another illustration that the brightness of the clouds is an indicator of the depth of the clouds.

Orbits 762 and 763, 0000Z, 24 May 1960

The surface analysis for 0000Z, 24 May 1960 (Fig. 42A) shows the frontal system has continued to move eastward with a new wave beginning to develop in the vicinity of 51N 150W. Evidence for this wave development is not immediately apparent in the cloud pattern at this time as shown in the rectification of orbits 762 and 763 (Fig. 42B). The cloud patterns in the region 50N to 55N and 150 to 155W indicate a vortex centered near 52N 154W which could be an indicator of an upper air low over this region. The band of clouds in the vicinity of the front as well as the clouds to the east shows a more organized pattern than was seen nearly 25 hours earlier on orbits 747 and 748 (Fig. 41B). The band of clouds in the vicinity of the cold front would suggest that the front does not go south of 40N. Relatively narrow bands to the east of the frontal band, oriented in a north-south direction, show the circulation

aloft has changed and become stronger in this direction. One interpretation of this overall pattern could be that the upper level trough is moving into a position with reference to the cold front so as to set up favorable conditions for the development of a wave on the surface front, but had not reached that position at the time these pictures were taken.

Orbits 775 and 776, 24 May 1960, 2200Z

The wave has gone through a period of rapid movement and development during the 24 hour period as seen by comparing the surface analysis for 0000Z 25 May 1960 (Fig. 43A) with the analysis 24 hours previously (Fig. 42A). These analyses show that the wave developed to the occlusion stage quite rapidly with a low associated with the occlusion centered near 48N 145W and another low centered at the vortex of the wave at 42N 134W. The rectification of orbits 775 and 776 (Fig. 43B) shows that the cloud band associated with the cold front to the west of 140W has assumed an east-west orientation along 35N. The extensive area of scattered low cumuliform clouds to the north of the cold front band indicates a new injection of cold dry air into the frontal system from the northwest. Relatively narrow bands of bright reflectivity are seen embedded in the band of clouds ahead of the warm front with an orientation parallel to the front. The area in the vicinity of the occlusion shows no organized band structure. An upper air trough oriented northwest-southeast extends northwest from the occlusion and probably accounts for the

extensive cloud cover in this region. An area of buildups, with many of the stations reporting cumulonimbus type clouds, existed in the coastal area of the northwest United States and southwestern Canada. These clouds showed up as relatively small areas of bright reflectivity on the TIROS pictures.

Orbit 791, 2300Z, 25 May 1960

The surface analysis for 0000Z, 26 May 1960 (Fig. 44A) shows the frontal system has continued to occlude and has entered the west coast of the United States. The center of the low pressure area associated with this frontal system is now near 47N 135W or approximately in the same position as it was 24 hours previously (Fig. 43A). The cloud patterns associated with this system are shown in the rectification of orbit 791 (Fig. 44B). Evidence of the occlusion advancing out of the center of the low is shown by the cloud band having its western edge along 125W. This band appears to circumscribe the periphery of the low pressure area although the changes in the reflective pattern indicate the cloud band is not distributed uniformly around the low. The area of scattered cumuliform clouds to the west of the frontal band has now become oriented approximately north-south below 40N in agreement with the orientation of the flow to the south of the low pressure area. The region of cumulonimbus activity has also moved eastward during the past 24 hours and is now located mostly to the east of 120W in the region 50N to 55N.

3.3 Conclusion

This series of rectified pictures has shown it is possible to maintain a day to day surveillance of mid-latitude storms with a satellite such as TIROS I. The pictures show the day to day changes in the cloud patterns and thus give an indication of the stage of development of the storm. The clouds and the patterns into which they organize should be an indicator of future developments in a storm since they are visible evidence of the physical processes at work in the atmosphere. When it becomes possible to interpret these cloud patterns in terms of future developments, then the satellite will become, in addition to a unique observation platform, a tool to be used as an aid in forecasting.

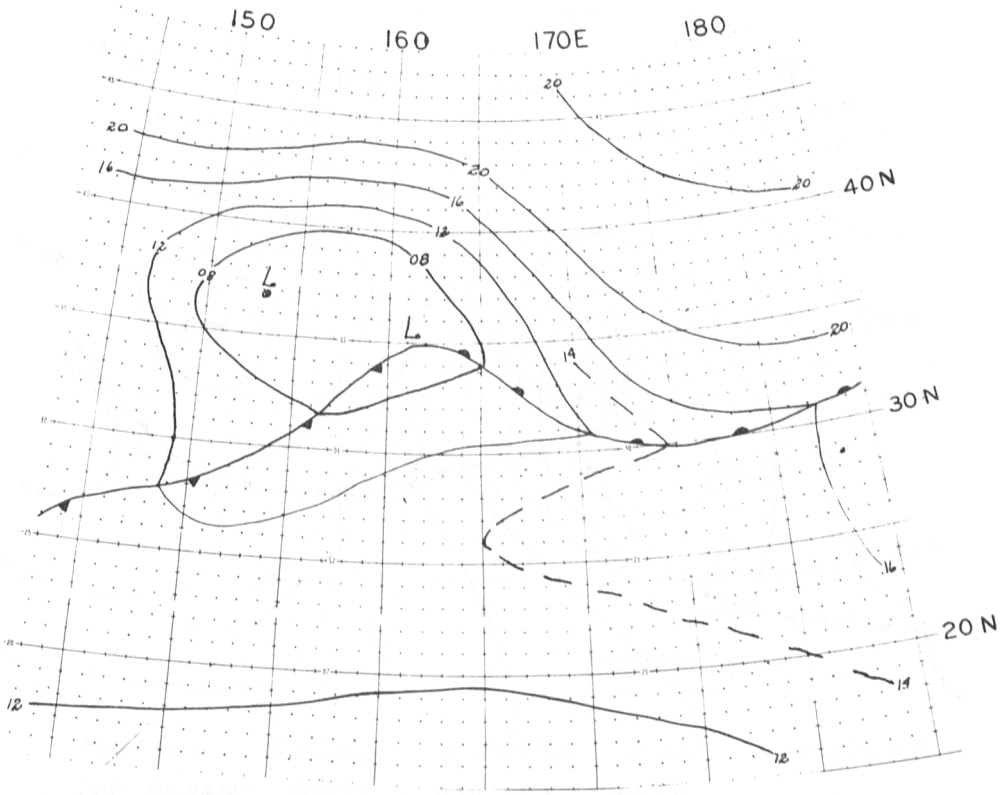

FIG. 36A SURFACE ANALYSIS 0000Z MAY 18, 1960

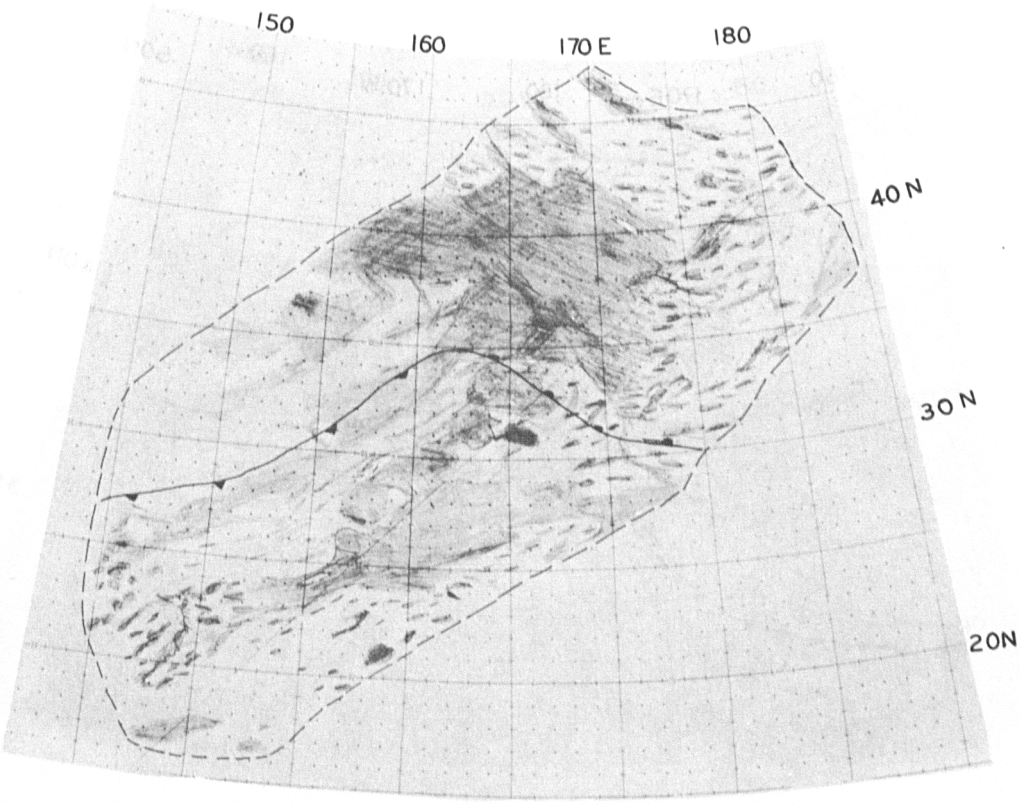

FIG. 36B ORBIT 677 0230Z MAY 18, 1960

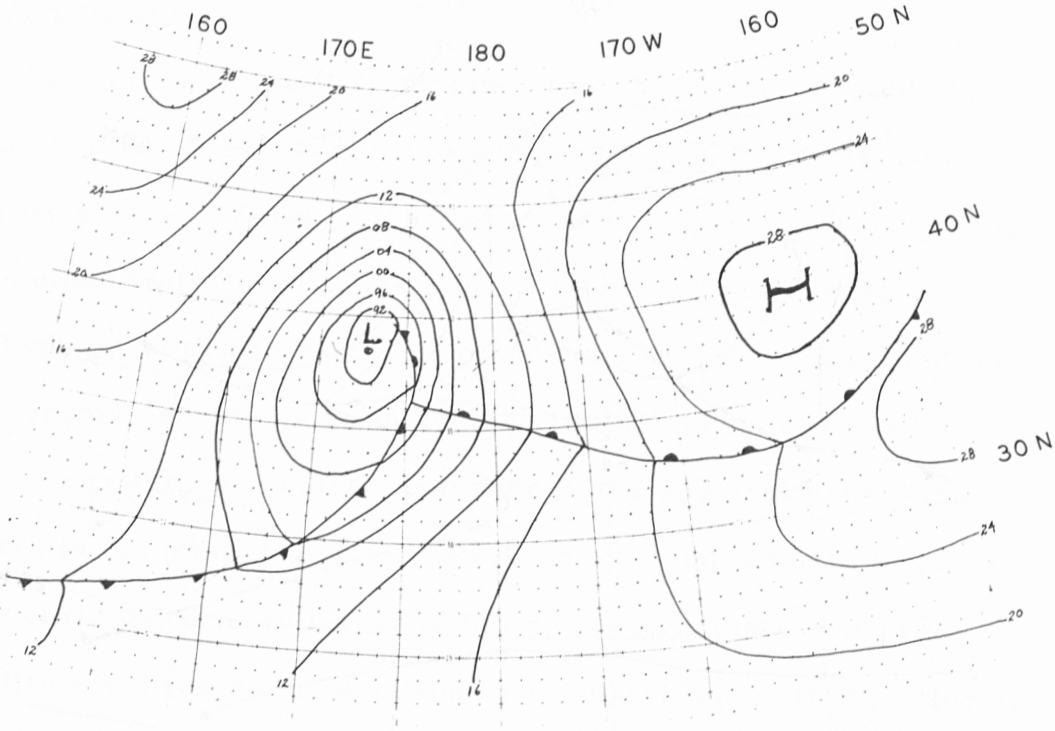

FIG. 37A SURFACE ANALYSIS 0000Z MAY 19, 1960

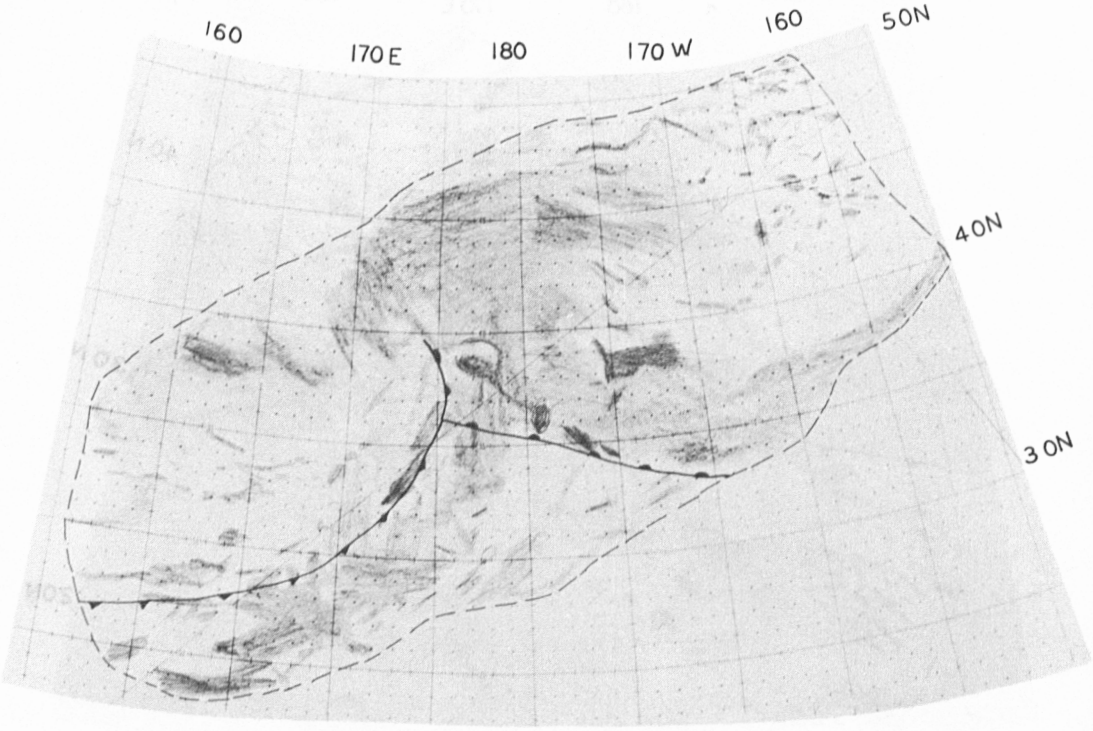

FIG. 37B ORBIT 691 0145Z MAY 19, 1960

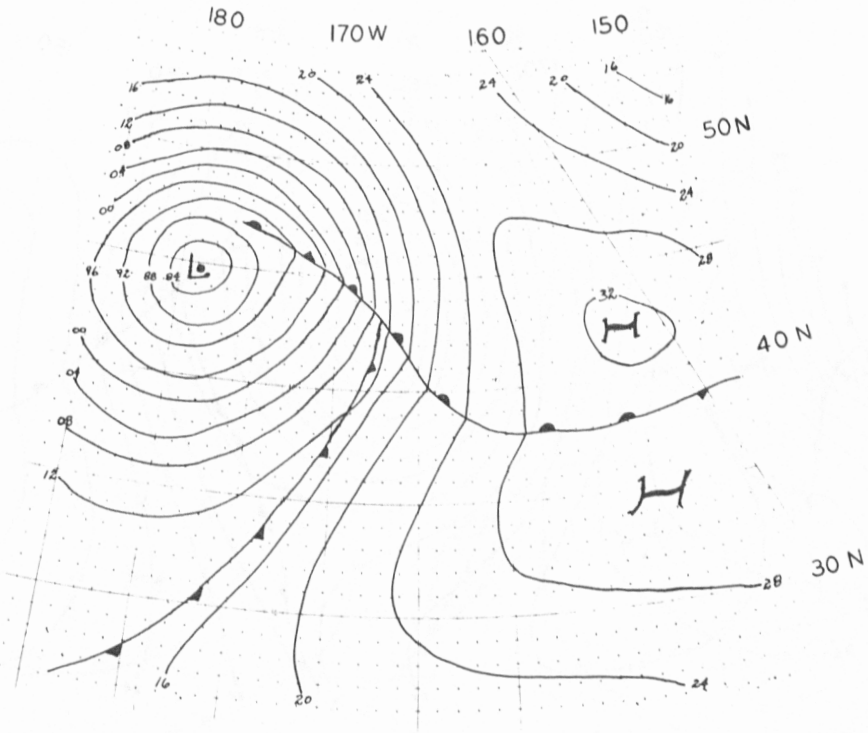

FIG. 38A SURFACE ANALYSIS 0000Z MAY 20, 1960

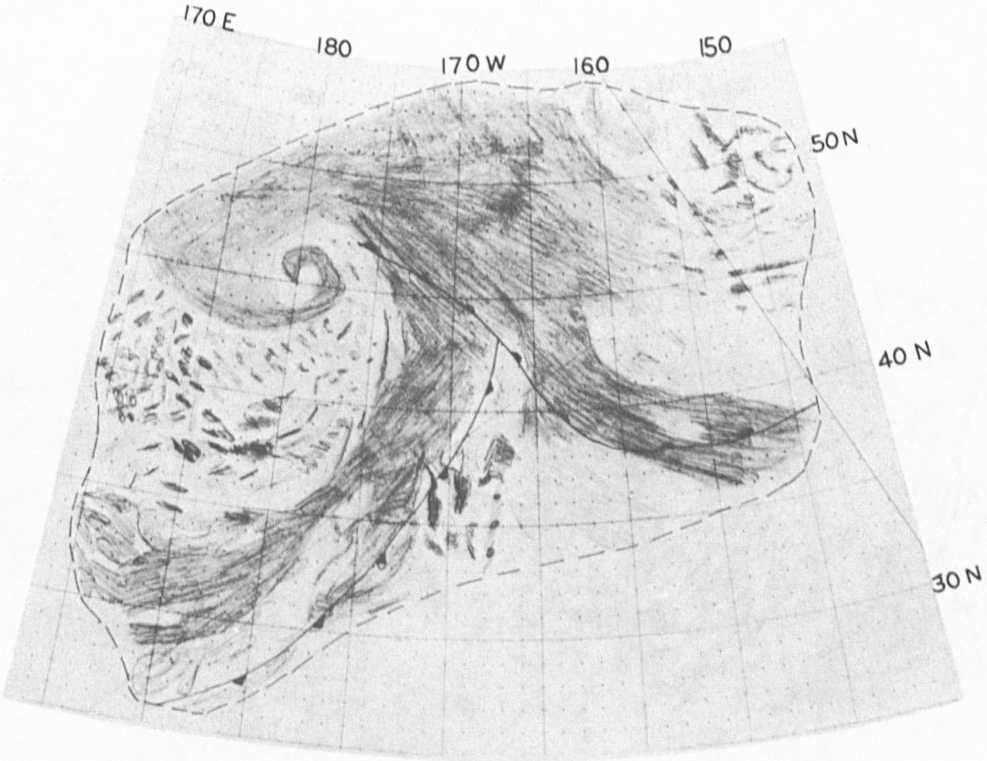

FIG. 38B ORBIT 705 0100Z MAY 20, 1960

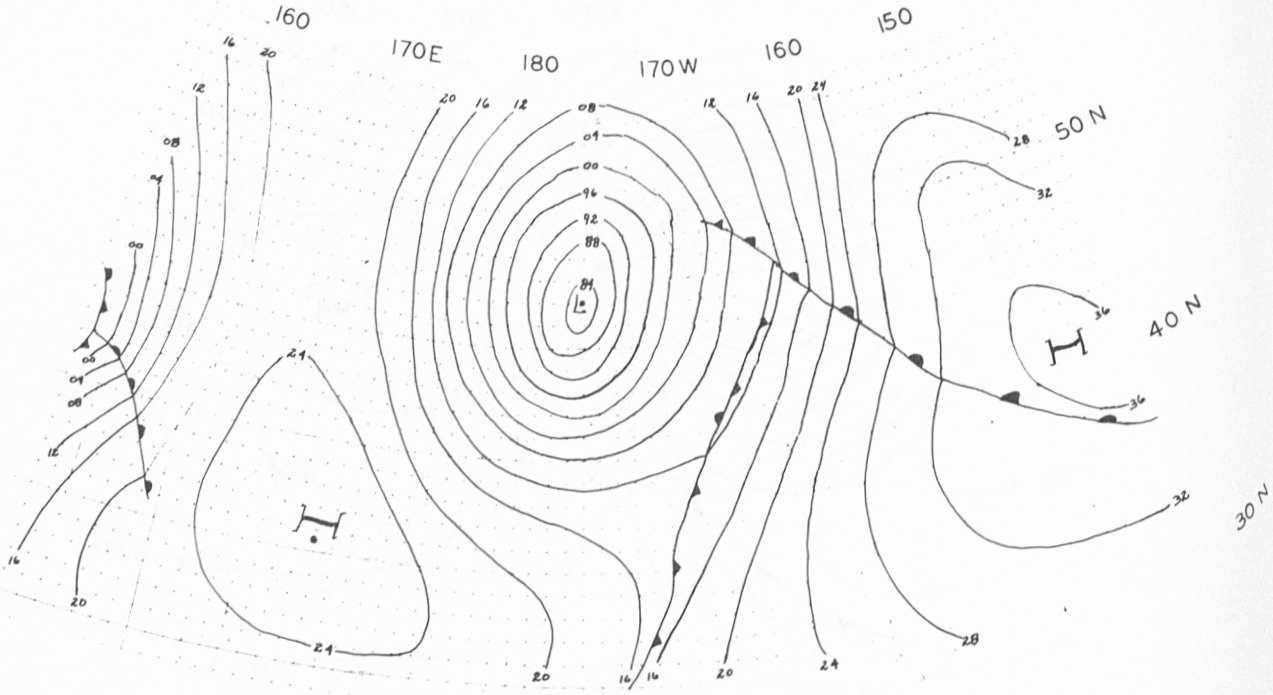

FIG. 39A SURFACE ANALYSIS 0000Z MAY 21, 1960

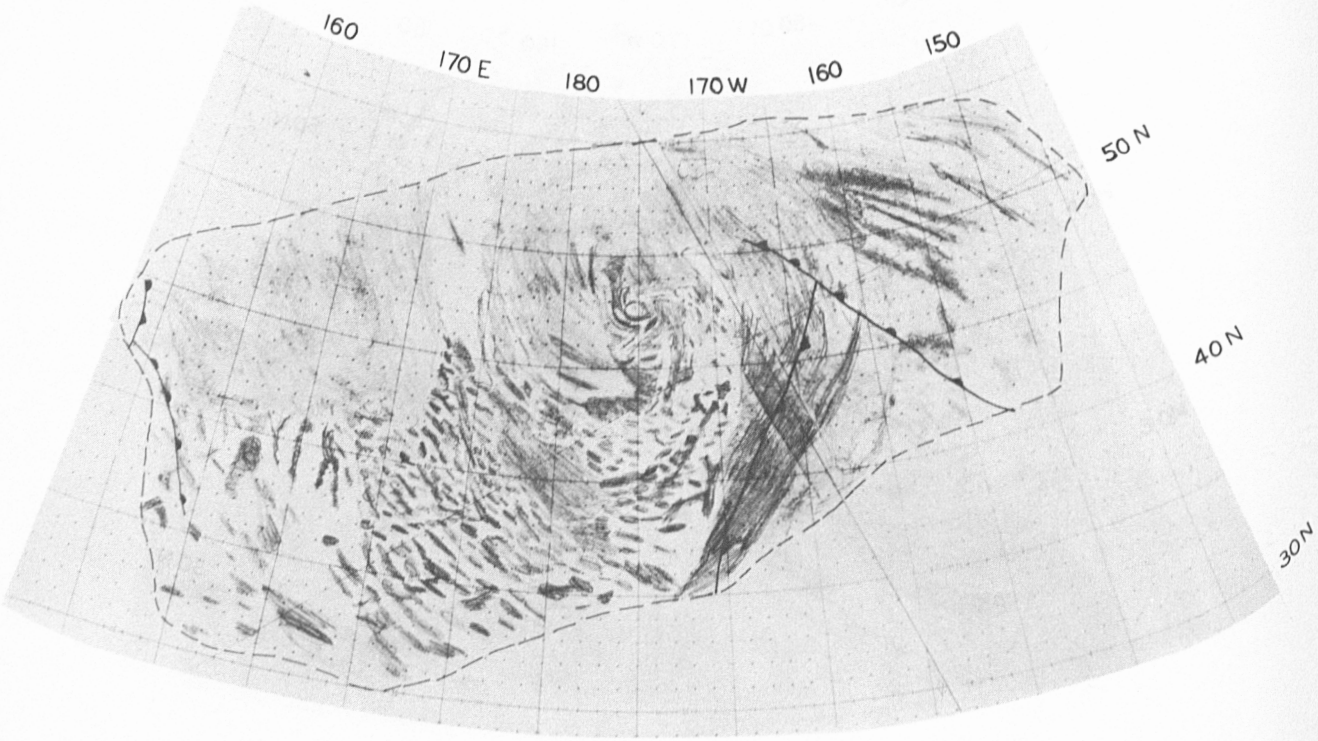

FIG. 39B ORBIT 720 0145Z MAY 21, 1960

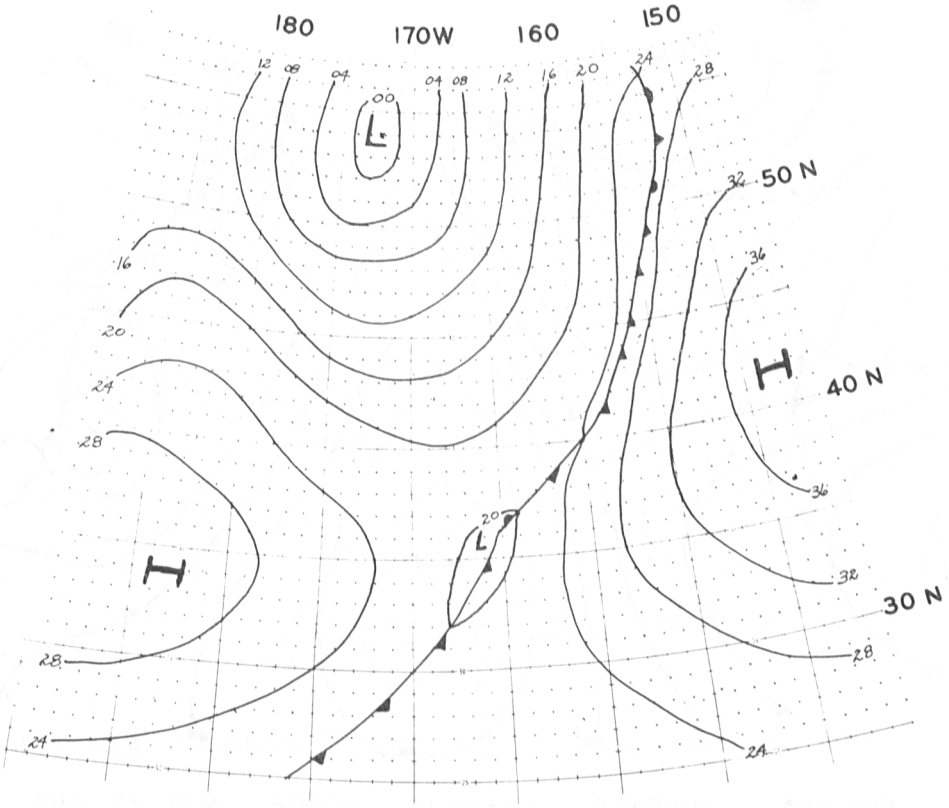

FIG. 40A SURFACE ANALYSIS 0000Z MAY 22, 1960

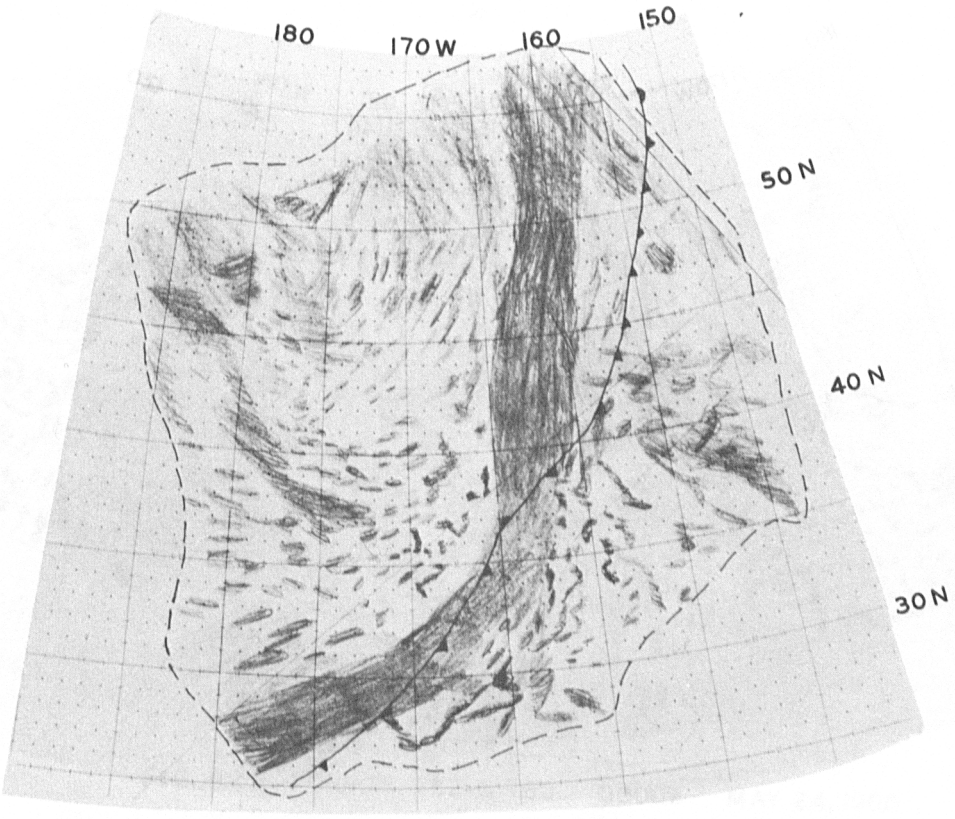

FIG. 40B ORBITS 733 & 734 0000Z MAY 22, 1960

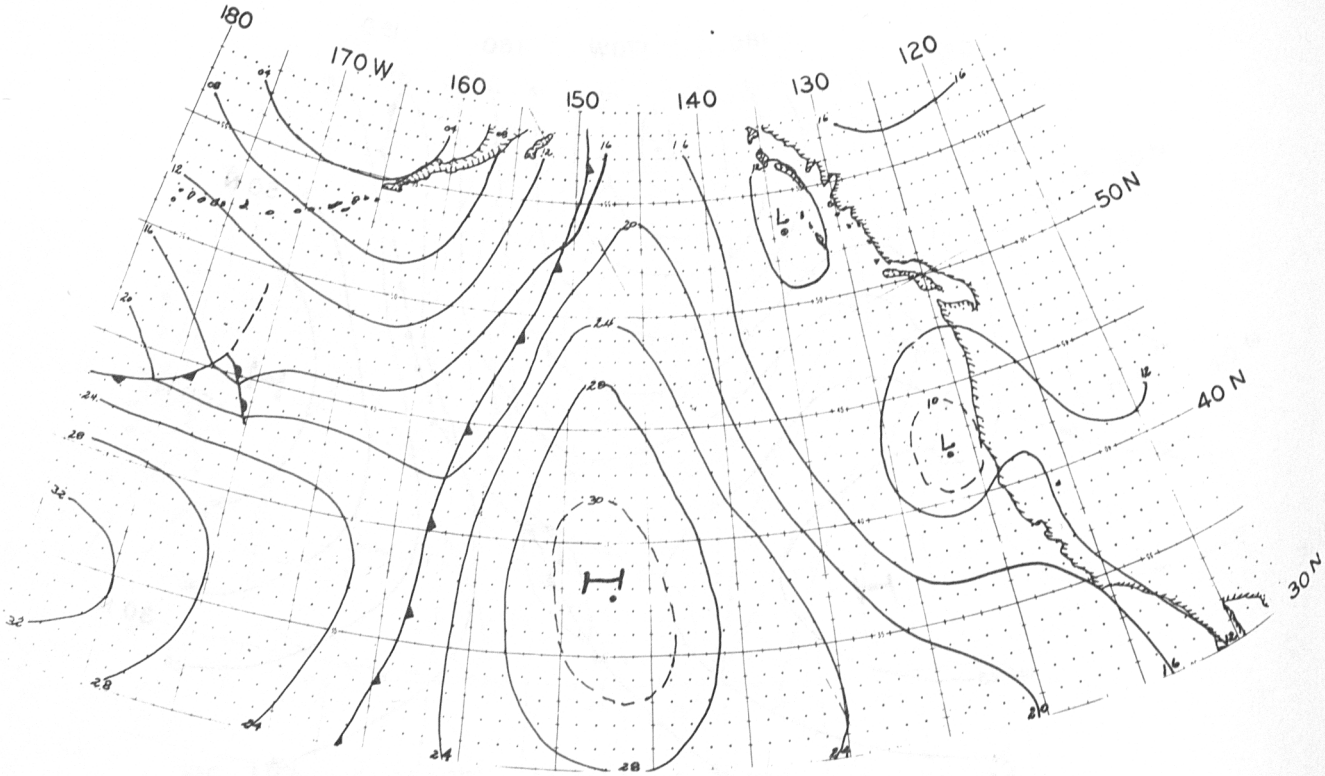

FIG. 41A SURFACE ANALYSIS 0000Z MAY 23, 1960

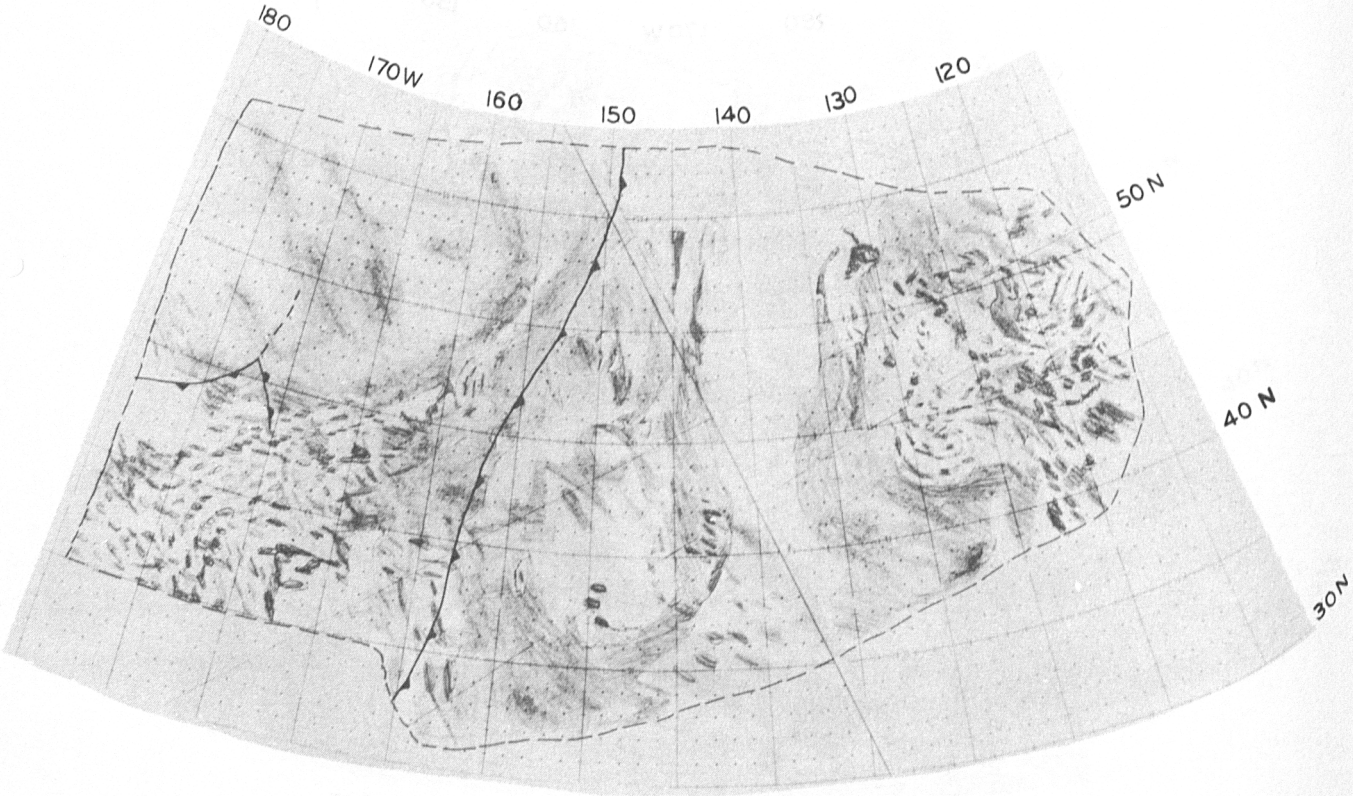

FIG. 41B ORBITS 747 & 748 2300Z MAY 22, 1960

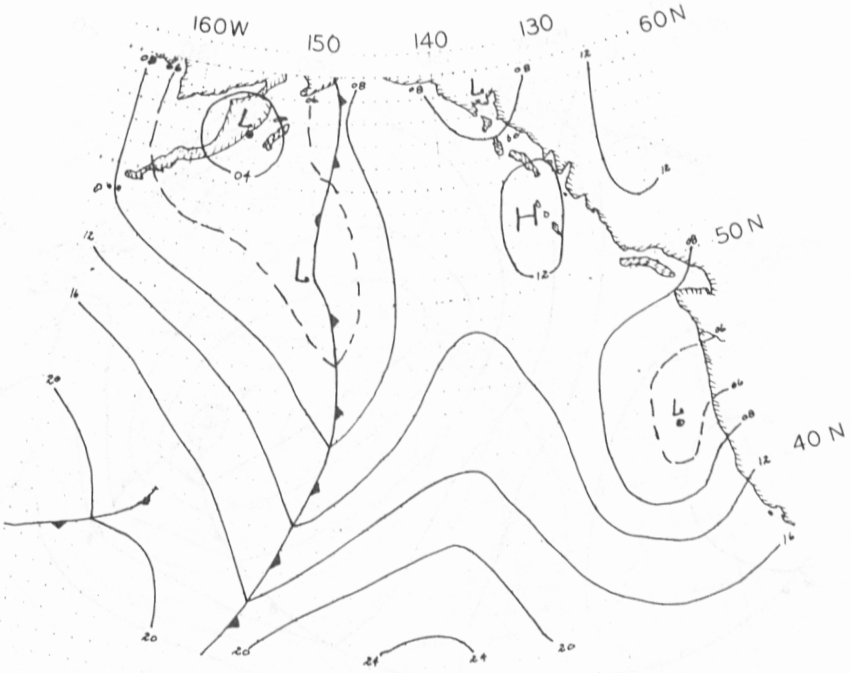

FIG. 42A SURFACE ANALYSIS 0000Z MAY 24, 1960

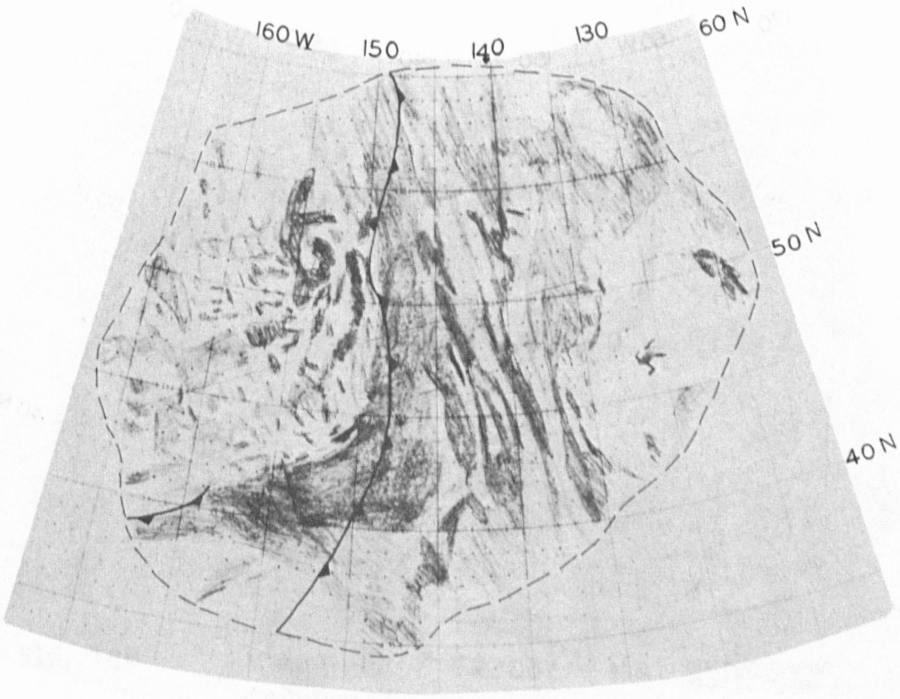

FIG. 42B ORBITS 762 & 763 0000Z MAY 24, 1960

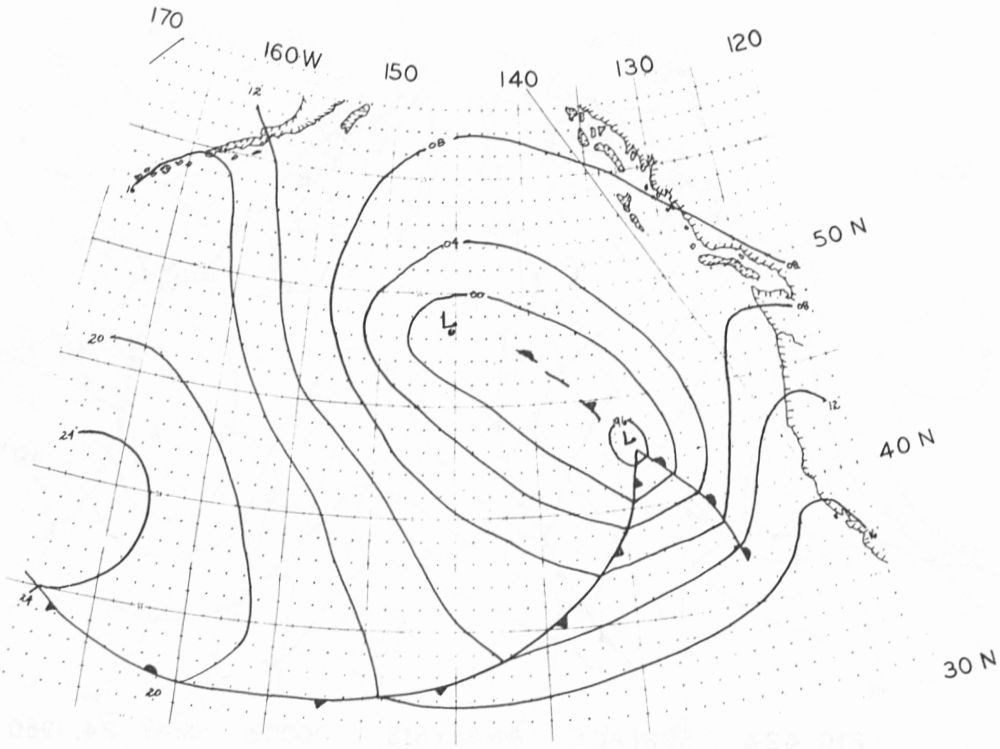

FIG. 43A SURFACE ANALYSIS 0000Z MAY 25, 1960

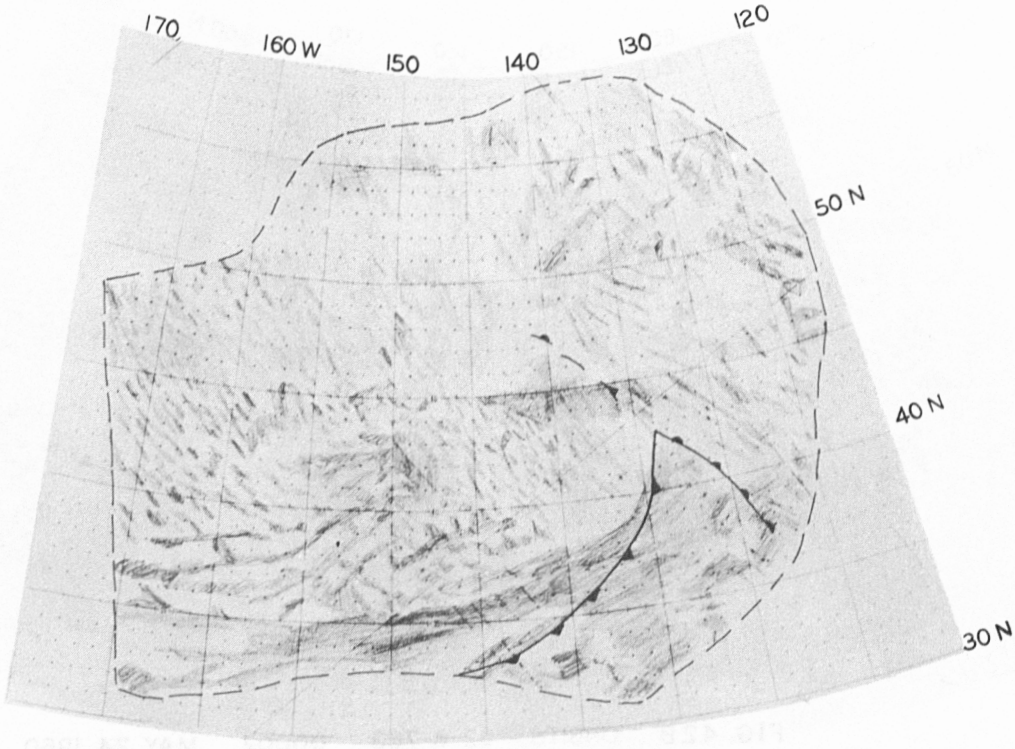

FIG. 43B ORBITS 775 & 776 2200Z MAY 24, 1960

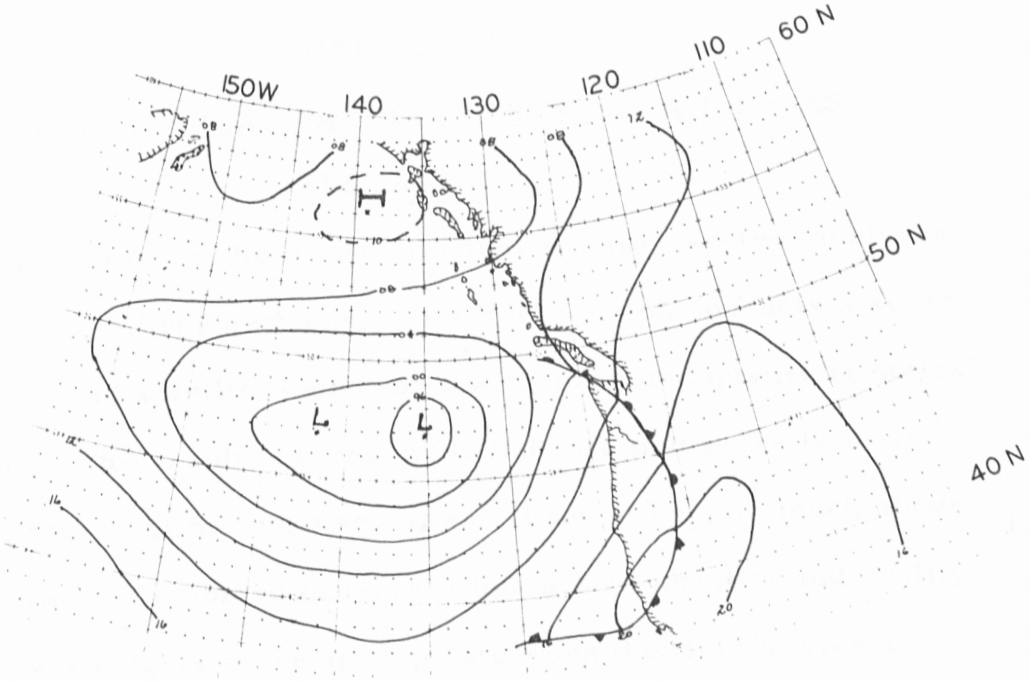

FIG. 44A SURFACE ANALYSIS 0000Z MAY 26, 1960

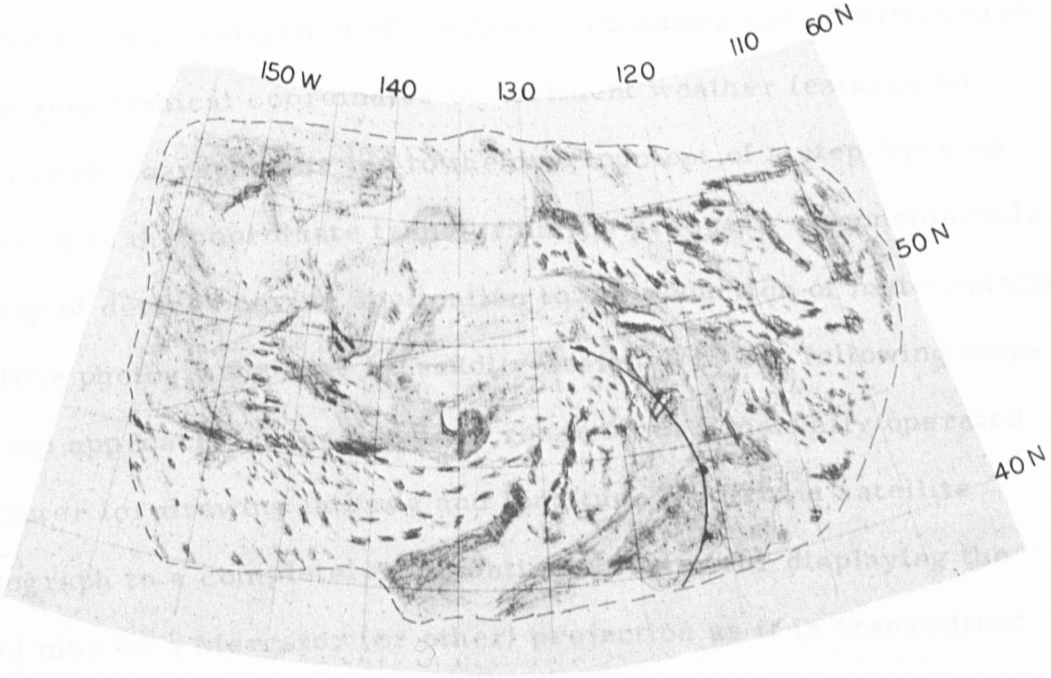

FIG. 44B ORBIT 791 2300Z MAY 25, 1960

Blank page retained for pagination

CHAPTER IV

METEOROLOGICAL SATELLITE SYSTEM ANALYSES

ABSTRACT

This chapter on the meteorological satellite system analyses is divided into three Sections. The first section conducts a study of the effect of satellite height on the quantity and quality of optical coverage. The results of this study indicate that there is little point in operating meteorological satellites at heights much above 4,000 miles. Combined consideration of both quantity and quality make lower heights more appropriate when the field of view is limited. When resolution at the center of the image is relatively more important than the area covered, lower heights are again more appropriate.

Next, an investigation of methods facilitating the determination of the geographical coordinates of pertinent weather features on satellite photographs has led to the development of a step-by-step approach to the coordinate transformation process. A considerable variety of devices having application to the reduction of meteorological satellite photographs may be readily designed by the following step-by-step approach. These devices range from a manually operated computer for drawing latitude and longitude grids on a satellite photograph to a completely automatic computer for displaying the cloud map on a Mercator (or other) projection as it is transmitted from the satellite.

Finally, an experiment for studying the optimum interval between satellite meteorological observations is described and discussed in Section 3.

SECTION I

ORBITAL SAMPLING CHARACTERISTICS*

The size of the area viewed in a single observation, the frequency with which a given area of this size can be observed, and the resolution which can be achieved over this area are clearly important properties of a meteorological satellite system. These and other data gathering properties of a meteorological satellite system depend on its orbital parameters, as do the required telemetering parameters (e.g., transmitter power and bandwidth). A quantitative understanding of the effects of orbital parameters on meteorological satellite system performance is therefore essential to the intelligent design of such systems. The following material is an examination of the effects of satellite height on a limited, but important, aspect of meteorological satellite system performance: the size of the area viewed in a single observation and the resolution which can be achieved over this area.

1.1 The Effect of Satellite Height on Optical Coverage

1.1.1 Introduction

There is a rather obvious qualitative statement that can be made about the variation of optical coverage with satellite height: the greater the satellite height, the larger the area that can be viewed, but the poorer the resolution over this area. In order to render such a statement more precise and, therefore, more useful in the

*Sections I and II of Chapter IV were originally prepared as a Semi-Annual Technical Summary Report under Contract No. AF 19(604)-5582, under ARPA Order No. 26-59 and GRD-TN-60-609, dated 30 June 1960. This section was written by G. Cooper, Allied Research Associates, Inc.

design of meteorological satellite systems, it is necessary to introduce quantitative definitions of coverage and resolution. Such quantitative definitions must be physically significant and, ideally, should lend themselves to convenient mathematical analysis. Accordingly, in this section, coverage is defined in terms of the maximum "useable" area that can be viewed at one instant, and resolution is defined in terms of the scale factor relating distances on the ground to distances on the image.

This definition of total coverage is independent of satellite attitude and the optical field of view but is dependent on the meaning of "useable". Two quantitative definitions of "useable" are employed in this study. The first definition is based on the assumption that the grazing angle (angle above local horizontal) of a ray must be above a certain minimum value in order for it to be in the useable portion of the image. In this first approach, the minimum value of this angle above horizontal is taken as the parameter defining "useable" coverage. The second definition of "useable" is based on the assumption that there is a maximum tolerable decrease in scale factor from its value at the subpoint. In the second approach, this allowable scale factor deterioration is taken as the parameter defining "useable" coverage. Other arbitrary definitions of "useable" are possible, but it is believed that the use of these two parametric definitions provides sufficient insight into the effect of satellite height on total optical coverage to permit intelligent meteorological satellite system design. Only these two definitions are treated in this section.

Another aspect of coverage that may be of interest to the consumer of meteorological satellite data concerns the effect of satellite height on the resolution or scale factor attainable with a specified coverage. This matter is also treated in this section, but in somewhat less detailed fashion than total coverage.

1.1.2 Total Coverage--Grazing Angle Parameter

Figure 1 shows the geometry pertinent to the computation of total "useable" coverage based on the definition of "useable" in terms of the grazing angle parameter, θ. The covered area is completely described by the central angle γ, which for convenience, is termed the "radius of coverage" (in degrees of equatorial latitude). Applying the Law of Sines to Figure 1 yields

$$\frac{R}{\sin \alpha} = \frac{R+h}{\sin (90^\circ + \theta)} \tag{1.1}$$

where

α = angle subtended at the satellite

R=earth radius

h=satellite height.

Substituting

$\alpha = 180^\circ - \gamma - (90^\circ + \theta)$ into Equation (1.1) and solving for γ yields,

$$\gamma = \cos^{-1} \left(\frac{\cos \theta}{1 + \frac{h}{R}} \right) - \theta \tag{1.2}$$

FIG. 1

GEOMETRY PERTINENT TO GRAZING ANGLE COMPUTATIONS

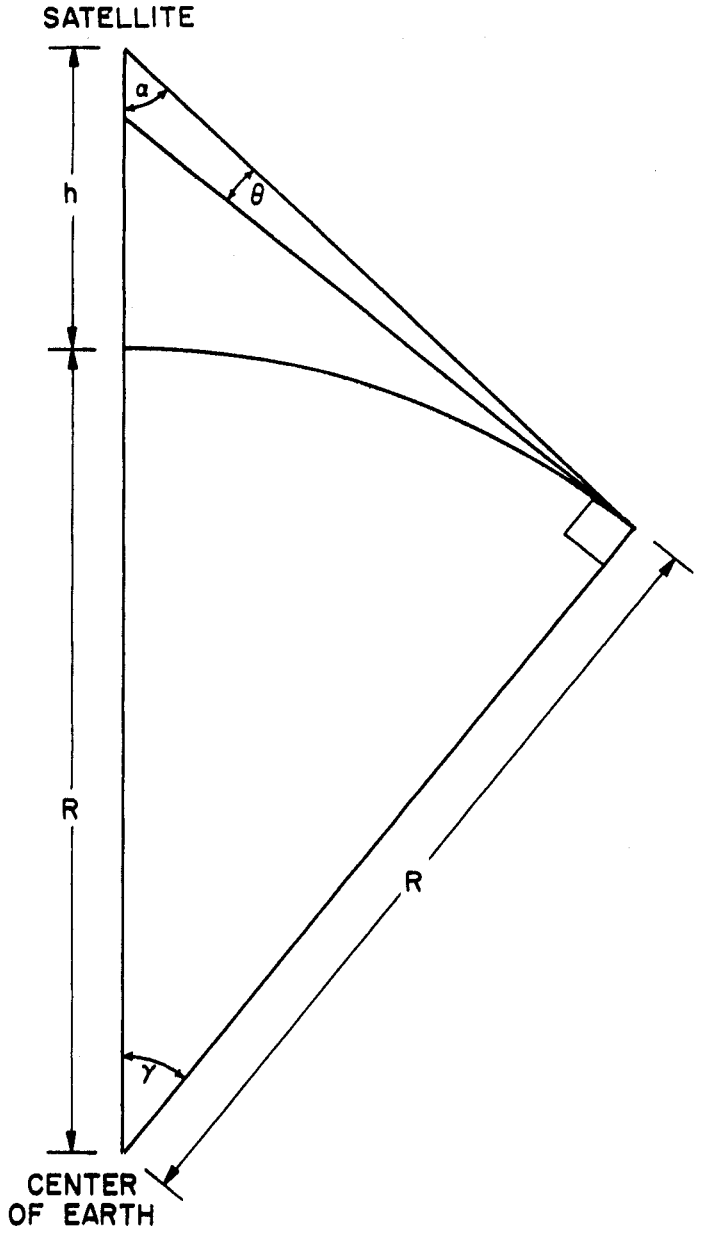

Figure 2 is a plot of γ vs. h/R for various values of the grazing angle parameter θ. Inspection of Figure 2 indicates that the total "useable" coverage increases with satellite height regardless of the value of θ which is chosen to define "useable". Of course, the larger θ, the smaller is the total "useable" coverage. The curve for $\theta = 0$ represents the coverage that would be obtained if the entire region within the horizon were considered "useable". For satellite heights greater than about 10 earth radii (about 40,000 miles), there is no appreciable increase in coverage for increased satellite height. In fact, "diminishing returns" sets in at satellite heights of about 1 earth radius (about 4000 miles), regardless of the choice of the grazing angle parameter. This implies that, from the point of view of coverage, there is an optimum satellite height of about 1 earth radius. Further discussion of this point is contained in Section 1.1.3.

1.1.3 Total Coverage--Scale Factor Parameter

Figure 3 shows the geometry pertinent to the computation of scale factor as a function of distance from the satellite subpoint. Scale factor is defined as the differential increment in angle subtended at the satellite produced by differential increment in position on the earth, or, referring to Figure 3, $d\alpha/d\gamma$. From Figure 3 it is seen that

$$\alpha = \tan^{-1}\left(\frac{R \sin \gamma}{R + h - R \cos \gamma}\right) \tag{1.3}$$

where the symbols have the same significance as in Section 1.1.2.

FIG. 2

RADIUS OF COVERAGE vs. SATELLITE HEIGHT
(GRAZING ANGLE AS PARAMETER)

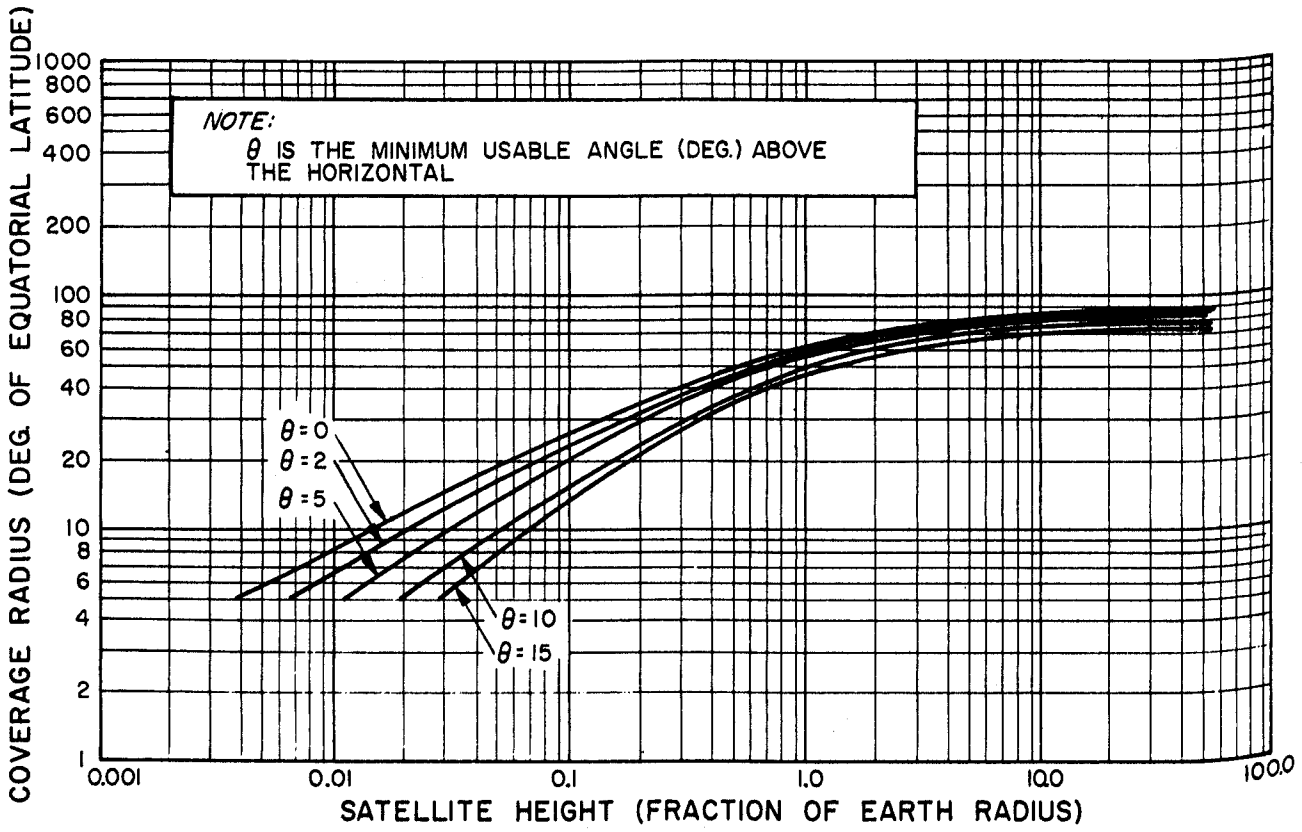

FIG. 3

GEOMETRY PERTINENT TO SCALE FACTOR COMPUTATIONS

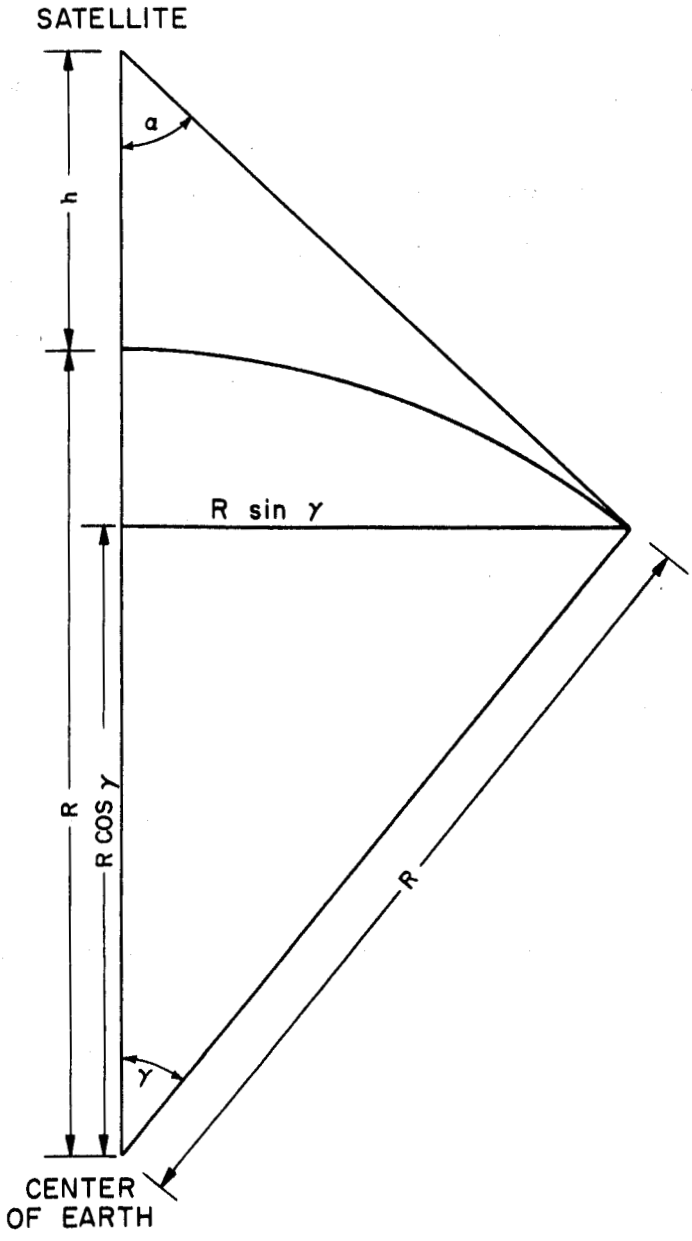

Differentiating Equation (1.3) yields

$$\frac{d\alpha}{d\gamma} = a = \frac{\left(1 + \frac{h}{R}\right) \cos \gamma - 1}{\left(1 + \frac{h}{R}\right)^2 - 2\left(1 + \frac{h}{R}\right) \cos \gamma + 1} \tag{1.4}$$

where a = scale factor (differential angle subtended at the satellite per differential angular change in position on the earth).

Figure 4 shows the behavior of the scale factor as a function of distance from the satellite subpoint, with satellite height as parameter. It is seen that the scale factor is a maximum (resolution is greatest) at the subpoint and it decreases monotonically, eventually reaching 0 (at the horizon). Because of the monotone behavior of the scale factor, the "useable" coverage may reasonably be defined as that region for which the scale factor is greater than a fraction K of the scale factor at the subpoint. From Equation (1.4), the scale factor at the subpoint is $a_o = R/h$. Therefore,

$$K = \frac{a}{a_o} = \frac{h}{R} \frac{\left(1 + \frac{h}{R}\right) \cos \gamma - 1}{\left(1 + \frac{h}{R}\right)^2 - 2\left(1 + \frac{h}{R}\right) \cos \gamma + 1} \tag{1.5}$$

Solving Equation (1.5) for γ yields

$$\gamma = \cos^{-1} \left[1 + \left(\frac{h}{R}\right)^2 \frac{(K - 1)}{\left(1 + \frac{h}{R}\right)\left(2K + \frac{h}{R}\right)} \right] \tag{1.6}$$

Again, γ is the "radius of coverage" (degrees of equatorial latitude).

Figure 5 shows a plot of γ vs. h/R for various values of the scale factor parameter, K. The similarity between Figures 2 and 5

FIG. 4

SCALE FACTOR vs. DISTANCE FROM SUBPOINT

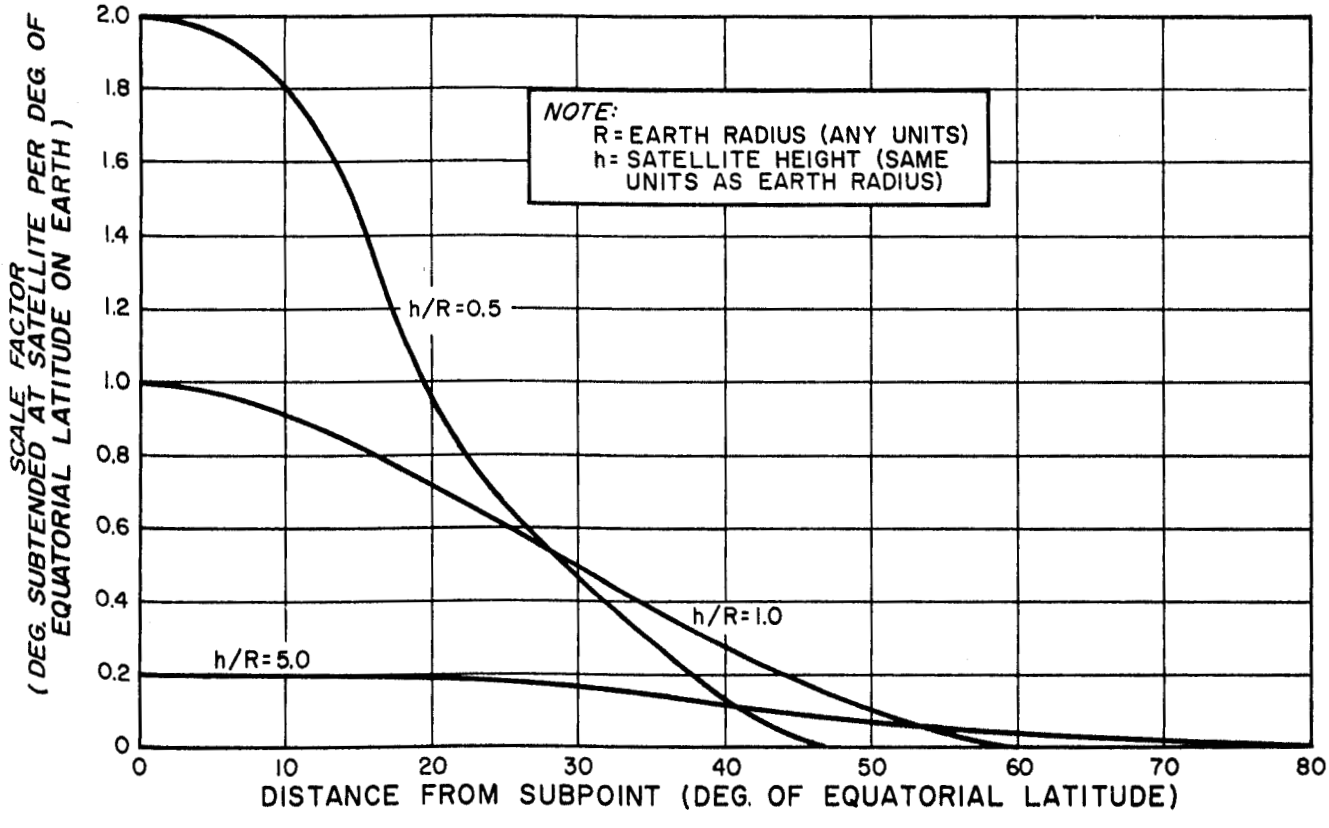

FIG. 5

RADIUS OF COVERAGE vs. SATELLITE HEIGHT
(SCALE FACTOR AS PARAMETER)

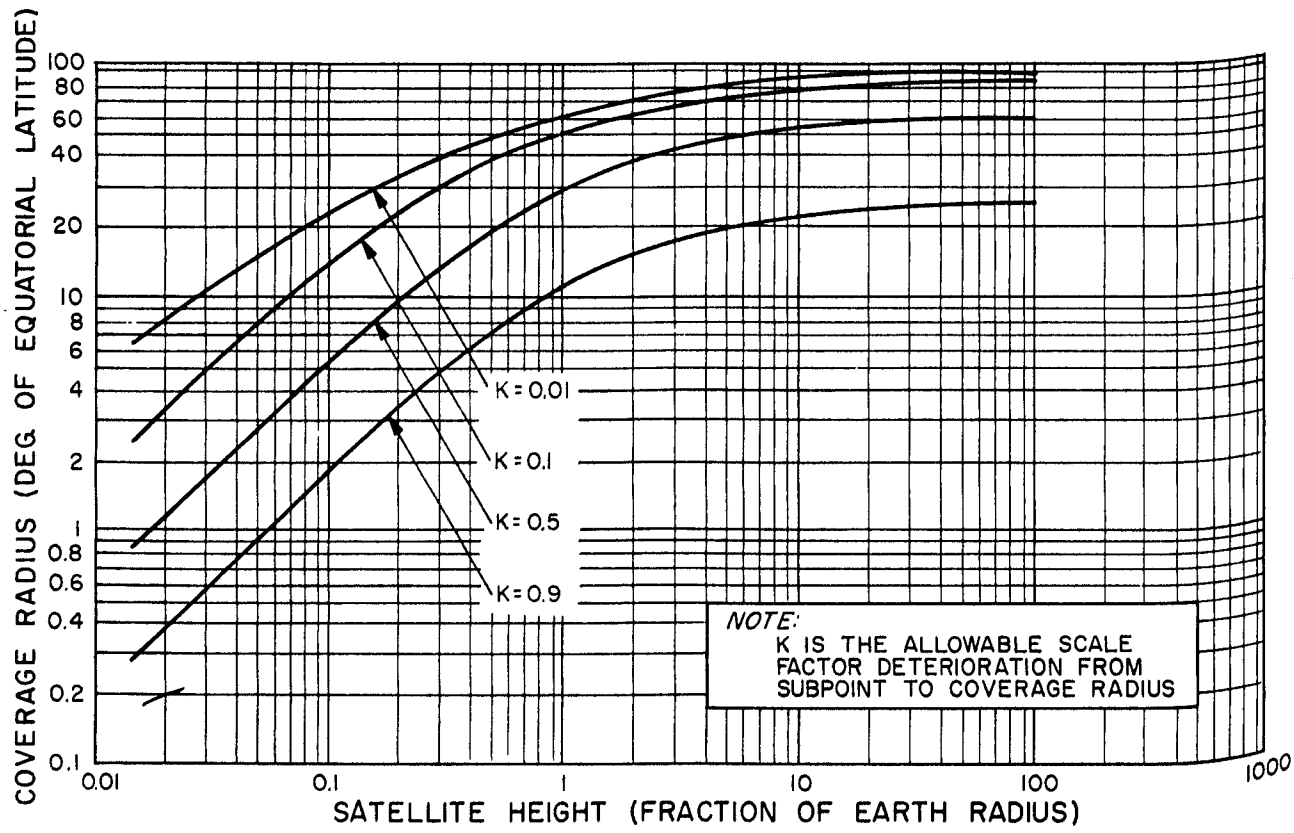

is readily apparent. "Diminishing returns" in coverage sets in at satellite heights of about 1 earth radius (about 4000 miles), regardless of the parameter chosen to define "useable". Quite naturally, the more deterioration allowed in the scale factor, the larger the "coverage radius" at a given satellite height.

The appearance of the "diminishing returns" effect in Figures 2 and 5 suggests the existence of an optimum satellite height with respect to coverage in the vicinity of about 4000 miles. Indeed, since scale factor decreases with increasing satellite height, there is little reason to increase the satellite height beyond the point of "diminishing returns" in coverage. To quantitatively determine this point, it is necessary to introduce some coverage figure of merit which takes into account the attainable scale factor as well as the "useable" area covered. There are many ways to define such a figure of merit; perhaps the simplest definition weighs the scale factor and covered area equally by taking the product of the surface area covered and the scale factor at the subpoint. Using this definition, with the surface area normalized to a fraction of the surface area of a hemisphere, the coverage figure of merit, F, is given by

$$F = a_o \int_o^{\gamma} \frac{2\pi (R \sin \gamma)(R\, d\gamma)}{2\pi R^2} \tag{1.7}$$

or

$$F = a_o (1 - \cos \gamma) = \frac{R}{h} (1 - \cos \gamma) \tag{1.8}$$

Combining Equations (1.6) and 1.8) yeilds

$$F = \frac{h}{R} \frac{(1 - K)}{\left(1 + \frac{h}{R}\right)\left(2K + \frac{h}{R}\right)} \tag{1.9}$$

Figure 6 shows a plot of F vs. h/R for various values of the scale factor parameter, K. It is seen that for values of K greater than about 0.5, the maximum value of F is attained for satellite heights of about 1 earth radius. This implies that the optimum satellite height is about 4000 miles if relatively uniform image quality is required over the covered area. Should wider tolerances be placed on the uniformity of image quality (K less than 0.5), this figure of merit indicates a lower optimum satellite height. It should be recalled that the figure of merit has been defined somewhat arbitrarily, so that conclusions drawn from Figure 6 should not be dogmatic. However, the conclusions do appear quite reasonable.

1.1.4 Specific Coverage

As indicated in Section 1.1.1, there may be applications of meteorological satellite systems for which the resolution at a specified distance from the subpoint is of more interest than the total coverage. This is particularly true where the field of view is limited by the viewing optics or the satellite attitude. Figure 7, based on Equation (1.4), shows the variation of a scale factor with satellite height for various distances from the subpoint.

Examination of Figure 7 shows that there is an optimum satellite height which produces the maximum scale factor associated with each

FIG. 6

COVERAGE FIGURE OF MERIT vs. SATELLITE HEIGHT

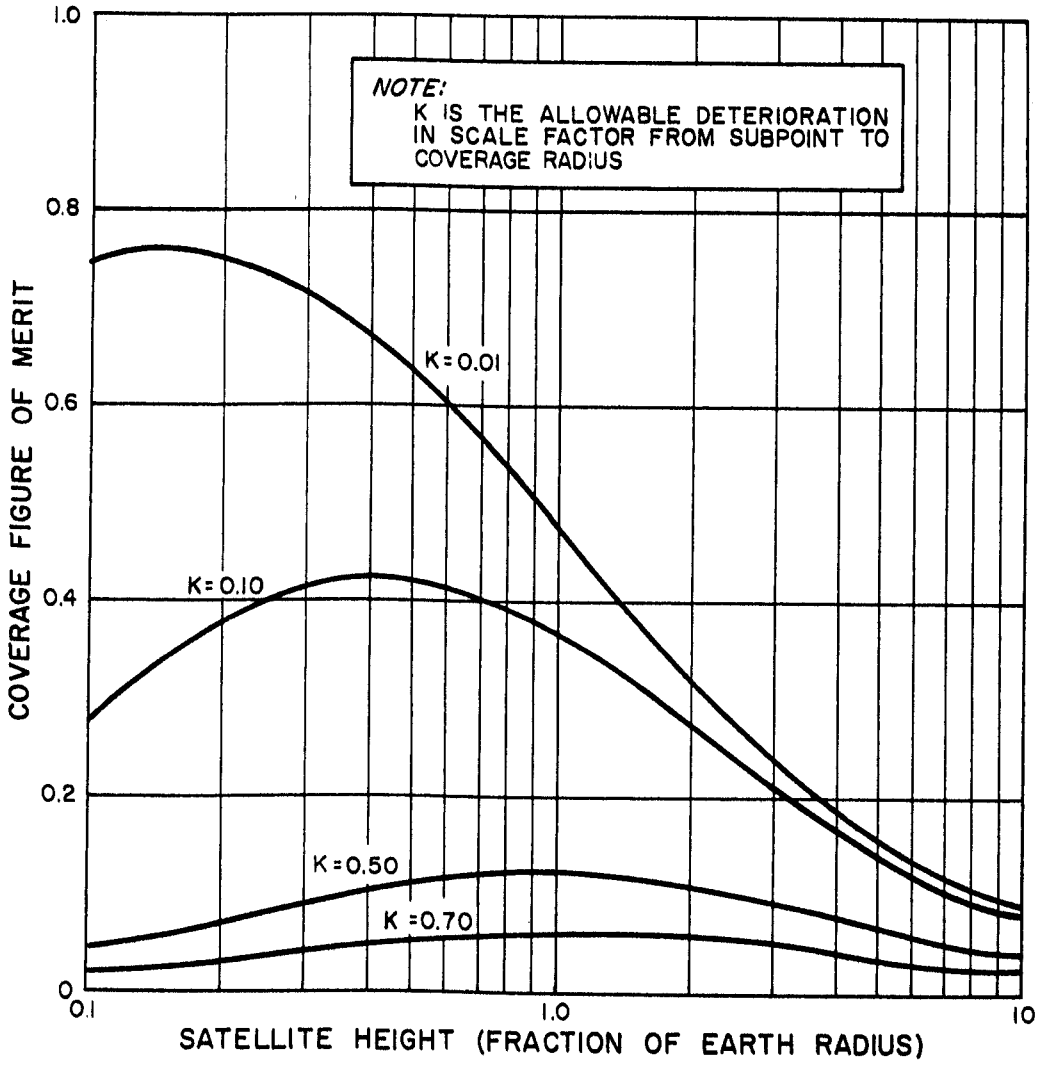

FIG. 7

SCALE FACTOR vs. SATELLITE HEIGHT

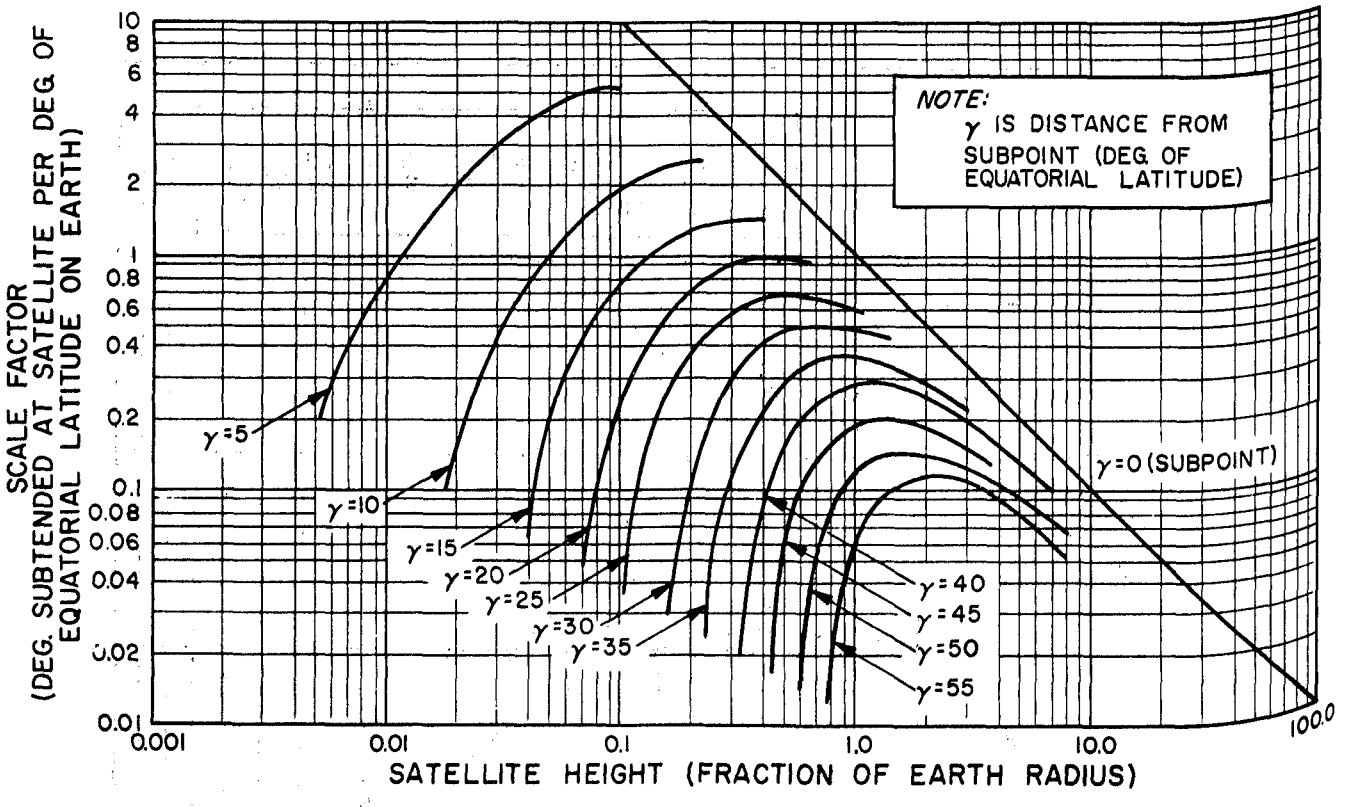

distance from the subpoint. This optimum height is obtained by differentiating Equation (1.4) with respect to height, setting the derivative to zero, and solving for height. In detail,

$$\frac{da}{dh} = \frac{1}{R}\frac{da}{du} = \frac{1}{R}\frac{d}{du}\left(\frac{u\cos\gamma - 1}{u^2 - 2u\cos\gamma + 1}\right) \tag{1.10}$$

where $u = 1 + h/R$

$$\frac{da}{dh} = \frac{-1}{R}\frac{u^2\cos\gamma - 2u + \cos\gamma}{(u^2 - 2u\cos\gamma + 1)^2} \tag{1.11}$$

Setting $da/dh = 0$ in Equation (1.11) and solving for u_m

$$u_m = \left(1 + \frac{h}{R}\right)_m = \frac{1 + \sin\gamma}{\cos\gamma} \tag{1.12}$$

or

$$\left(\frac{h}{R}\right)_m = \frac{1 + \sin\gamma}{\cos\gamma} - 1 \tag{1.13}$$

where $(h/R)_m$ is the satellite height for maximum scale factor.

Substituting $(h/R)_m$ from Equation (1.13) into Equation (1.4) yields

$$a_m = \frac{\cos^2\gamma}{2\sin\gamma\,(1 + \sin\gamma)} \tag{1.14}$$

where a_m is the maximum scale factor. Figure 8 shows $(h/R)_m$ and a_m vs. distance from subpoint. For comparison purposes, a plot of the subpoint scale factor, a_o, at the optimum satellite height for the given distance from subpoint is also included in Figure 8.

FIG. 8

OPTIMUM SCALE FACTOR AT GIVEN DISTANCE FROM SUBPOINT
(WITH CORRESPONDING SATELLITE HEIGHT AND SCALE FACTOR AT SUBPOINT)

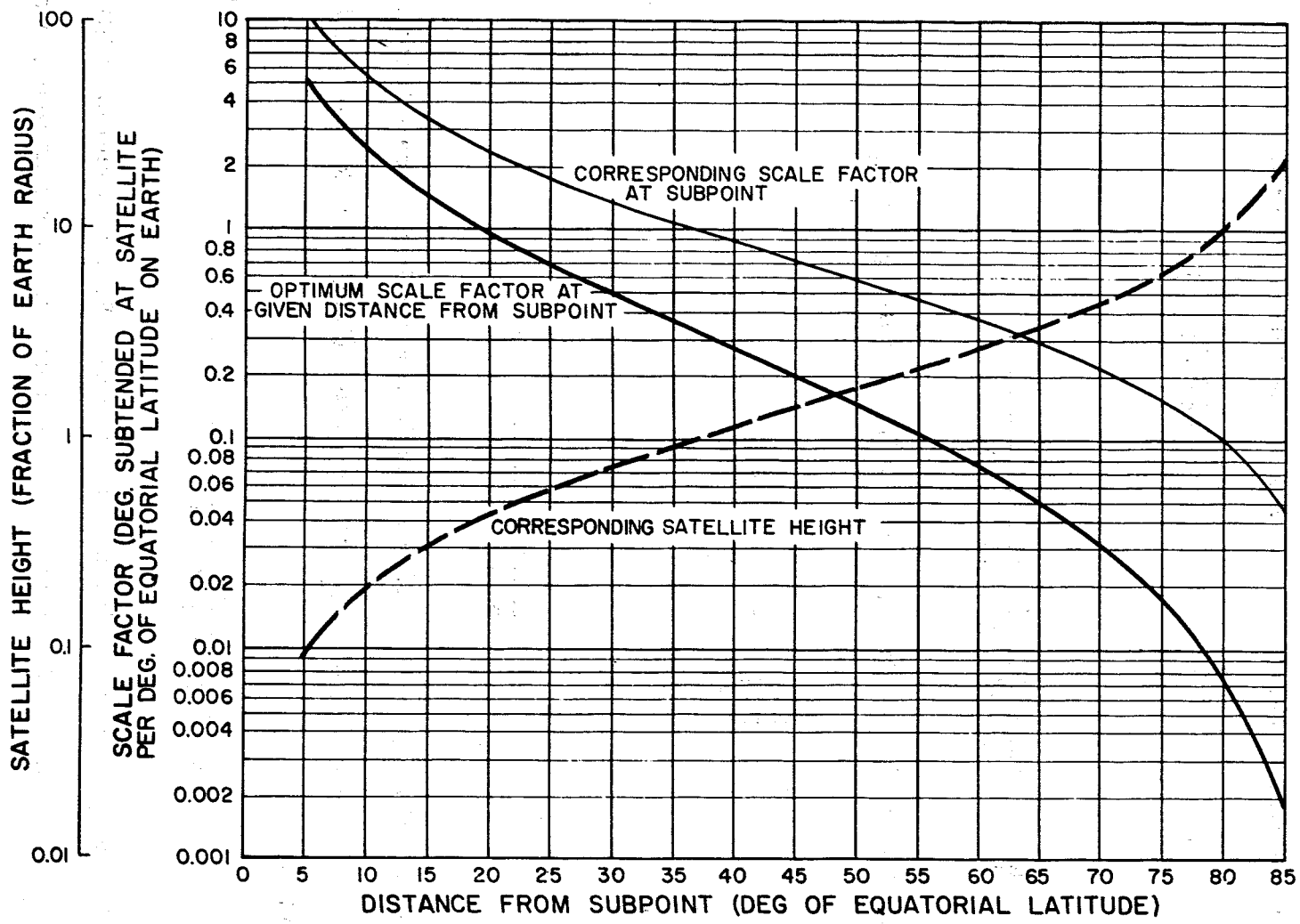

Examination of Figure 8 indicates that the maximum attainable scale factor decreases as distance from the subpoint increases. Furthermore, the satellite height required to attain the maximum scale factor increases with distance from the subpoint. As an example of the significance of these results, consider a satellite whose field of view is limited by the optics to about 10° from the subpoint (this corresponds to about the field of view of TIROS I). To achieve the maximum scale factor at this distance from the subpoint, the satellite height should be about 800 miles. The scale factor at the edge of the field of view would be about 2.5, while the corresponding scale factor at the subpoint is 5.0.

1.1.5 Conclusions

It appears that insofar as optical coverage is concerned, there is little point in operating meteorological satellites at heights much above 4000 miles. Lower heights are more appropriate when resolution at the center of the image is relatively important. Lower heights are also appropriate when the field of view is limited, either by satellite attitude or viewing optics. This investigation was primarily concerned with satellite systems with unlimited fields of view; further investigation of systems with limited view is required for the intelligent design of such systems.

Factors other than optical coverage may exercise the controlling influence on the choice of orbital height for a meteorological satellite system. Perhaps the most important of these factors is the telemetering system requirements as a function of satellite height.

CHAPTER IV (Continued)

SECTION 2

DATA PROCESSING AND INTERPRETATION*

Actual operating experience with data processing for the TIROS I photographs has shown that present methods require a great deal of time to determine the geographical coordinates of the pertinent weather features. An investigation of methods of facilitating this processing has led to a re-examination of the mathematical relations between photographic and geographic coordinates. A convenient visualization of these relations has been developed. It may be applied in various ways to provide practical devices for partially or wholly automating photographic rectification. Such devices should result in considerable time savings in actual operation. The following material describes this visualization and a possible electromechanical device for partially automating photographic rectification whose design is based on this visualization.

The device to be described in Section 2.1.3 was designed to automate as fully as possible the cloud analysis procedure that has been used with TIROS pictures. In that procedure a meteorologist draws a pencil sketch of the principal cloud masses on a standard map projection, adding words and descriptive symbols to describe the finer details that are apparent in the pictures. The input of the

*This section was written by G. Cooper, Allied Research Associates, Inc. The work was sponsored under Contract No. AF 19(604)-5582, under ARPA Order No. 26-59.

new machine would be derived from the motion of a pointer with which he would trace on the original photograph the outlines of the cloud masses; the output of the machine would be an x-y recorder which would correctly plot out those outlines on any chosen map projection. Thus, the device would eliminate the error and the time consumed in the present procedures in which the transformation from picture to map is a task which the meteorologist must perform with only simple graphical aids, in addition to his task of cloud analysis.

The study of the transformation has also suggested several related devices which could be used with modified cloud analysis procedures. Each appears to have merit for specific applications. These are outlined briefly in Section 2.1.4.

2.1 Photographic Rectifiers for Satellite Applications

2.1.1 Introduction

A photograph of the earth's surface taken from a satellite is a two-dimensional projection of an appreciable portion of a nearly spherical surface. As a result, the picture is seriously distorted. With a non-stabilized satellite, the projection generally has a skew orientation with respect to the usual latitude-longitude earth coordinate system. This combination of distortion and skew coordinate systems makes the problem of determining the geographic location of weather features seen on a satellite photograph rather difficult.

In order to deal with this problem, it is convenient to introduce two right-handed Cartesian coordinate systems. The earth coordinate

system has its origin at the center of the earth, its X-axis in the equatorial plane at 90° West Longitude, its Y - axis in the equatorial plane at 0° Longitude (in the plane of the Greenwich Meridian), and its Z-axis along the earth's rotational axis, pointed towards the North Pole. The satellite coordinate system has its origin at the satellite, its X'-axis in the film plane in a direction defined by fiducial marks on the photograph, its Y'-axis in the film plane in a direction orthogonal to the X'-axis, and the Z'-axis perpendicular to the film plane, pointing down towards the earth (along the principal axis).

Any point on the earth's surface may be represented by its coordinates in either of these two systems. Furthermore, the X', Y' coordinates of a point in the satellite coordinate system, when multiplied by the appropriate scale factor (focal length divided by the projection of slant range on the principal axis), are the photographic positions of that point. Thus, the problem of photographic rectification can be mathematically described as the problems of determining the transformation equations between the two coordinate systems.

The nature of the coordinate transformation equations is discussed in Section 2.1.2. A relatively simple electromechanical analog computer for performing the operations described by these equations is described in Section 2.1.3. Other methods of solving these equations are described in Section 2.1.4, along with some discussion of particular features that might be desirable in an actual operational photographic rectifier.

2.1.2. The Nature of the Coordinate Transformation Equations

The key point of this approach is to recognize that the satellite coordinate system may be related to the earth coordinate system by a

sequence of translations and rotations corresponding to the degrees of freedom of the satellite. Since, in general, the satellite has six degrees of freedom, there must be six independent parameters involved in the coordinate transformation equations. While there are a variety of ways of defining these parameters, it is convenient to use satellite height, h_s; latitude of satellite subpoint, Φ_s; longitude of satellite subpoint λ_s; nadir angle of the principal line, n; geographical azimuth of the principal line measured from local North, θ; and the azimuth of the projection of the principal line on the photograph relative to a fiducial line on the photograph (the angle from the satellite X'-axis to the projection of the principal line), ψ. An earth-stabilized satellite is a special case of the general satellite, having fewer degrees of freedom and requiring fewer parameters (i. e., $n = 0°$ and $0 = \psi$).

The actual process of coordinate transformation may be visualized as a sequence of three translations to move the origin from the center of the earth to the satellite followed by three rotations to align the axes of the translated coordinate system with those of the satellite coordinate system. The three translations are governed by the parameters h_s, Φ_s, and λ_s while the three rotations are governed by the parameters n, θ, and ψ. Since the rotational parameters n and 0 have been defined with respect to local vertical and geographic reference, it is necessary to take Φ_s and λ_s into account in performing the three rotations. Conceptually, it is most

convenient to accomplish this by first rotating the translated coordinate system to align one axis with the local vertical and a second axis with the geographic reference. These preliminary rotations are governed by the parameters Φ_s and λ_s. Thus, for ease in visualization, the three rotations have become five rotations, although there are still only three rotational degrees of freedom.

It is now appropriate to be specific about the transformation equations. The coordinates of the origin of the satellite coordinate system relative to the earth coordinate system are given by Equations (2.1) to (2.3).

$$X_s = (R + h_s) \cos \Phi_s \sin \lambda_s \tag{2.1}$$

$$Y_s = (R + h_s) \cos \Phi_s \cos \lambda_s \tag{2.2}$$

$$Z_s = (R + h_s) \sin \Phi_s \tag{2.3}$$

where

R is the earth's radius

λ_s is positive for West Longitude, negative for East Longitude

Φ_s is positive for North Latitude, negative for South Latitude.

The three translations require the coordinates of a point (X, Y, Z) in the earth coordinate system to be expressed in terms of an (X'', Y'', Z'') coordinate system which is parallel to the earth coordinate system but whose origin is at the satellite. These transformations are given by Equations (2.4) to (2.6).

$$X'' = X - X_s \tag{2.4}$$

$$Y'' = Y - Y_s \tag{2.5}$$

$$Z'' = Z - Z_s \tag{2.6}$$

Two preliminary rotations, as described above, are required to transform the (X'', Y'', Z'') coordinate system into an (X''', Y''', Z''') coordinate system which is aligned with local vertical and the geographic reference (assumed to be local North). The first of these is about the Z''-axis by an amount equal λ_s; the resulting Y-axis lies in the same meridional plane as the satellite. The second preliminary rotation is about the resulting X-axis by an amount $90° - \phi_s$; the resulting Z-axis (which has been denoted as Z''') coincides with the local vertical directed away from the earth while the resulting Y-axis (which has been denoted as Y''') coincides with the local South.

The final three rotations of the(X''', Y''', Z''') system are required to make it coincide with the(X', Y', Z') satellite coordinate system. The first of these rotations is about the Z'''-axis by an amount $\theta + 180°$, the resulting Y-axis lies in the plane of the principal axis. The second rotation is about the new X-axis by an amount $180°-n$; the resulting Z-axis (which has been denoted as Z') coincides with the principal axis. After this second rotation, the projection of the principal axis on the resulting XY plane (the film plane) coincides with the negative Y-axis. To align the resultant X-axis with the X'-axis, so that it will be at an angle of ψ from the negative Y-axis, a third and final rotation about the new Z'-axis (the principal axis) by an amount $\psi - 90°$ is required.

The equations for transforming the (X^{II}, Y^{II}, Z^{II}) coordinates into the (X^{I}, Y^{I}, Z^{I}) satellite coordinates are therefore determined by five successive applications of the equations for rotation of coordinates. In general, the coordinate transformation equations for the rotation from a (ξ, η, ζ) coordinate system to a (ξ^{I}, η^{I}, ζ^{I}) coordinate system about the ζ - axis through an angle γ are:

$$\xi^{I} = \xi \cos \gamma - \eta \sin \gamma \tag{2.7}$$

$$\eta^{I} = \xi \sin \gamma + \eta \cos \gamma \tag{2.8}$$

$$\zeta^{I} = \zeta \tag{2.9}$$

It is not necessary to perform all the substitutions in detail, since a device to perform these operations may be synthesized in terms of the individual steps involved in this visualization. Actual detailed substitution would result in extremely lengthy expressions which would be quite subject to typographical errors and contribute practically nothing to the comprehension of the operations.

2.1.3 A Possible Electromechanical Photographic Rectifier

Most of the elegance that can be claimed for the foregoing visualization of the transformation from geographic to satellite coordinates lies in treating the transformation as a sequence of relatively simple basic steps. However, coincidence, in the form of an equally simple electromechanical device known as a resolver, enhances the elegance of this visualization by providing a natural mechanization for the basic step. The resolver, which is shown schematically in Figure 9, is a device which produces an internal

magnetic field which is proportional to the vector sum of two electrical inputs. Its two electrical outputs are proportional to the components of the internal magnetic fields along two orthogonal axes determined by a shaft position. This operation is mathematically identical to rotation of coordinates as described by Equations (2.7) and (2.8). Thus, the sequence of rotation required to perform the coordinate transformations may be mechanized with a series of interconnected resolvers.

To be specific about the application of resolvers to the problem of photographic rectification, assume that it is desired to design a device which will produce a line drawing on a Mercator projection corresponding to a line traced on a satellite photograph. This particular device has been chosen because it illustrates an interesting difficulty in the application of this step-by-step approach together with its solution. This difficulty arises from the fact that the coordinate transformation requires the knowledge of all three coordinates of a point in the satellite (photographic) coordinate system, whereas only two coordinates (which have been designated as X' and Y') are known: the solution to this difficulty is somewhat analogous to a successive approximation procedure, although the actual mechanization of this solution is, in reality, a closed form, single step procedure.

In essence, the solution is based upon performing the coordinate transformations using an assumed value of Z'. The resultant (X, Y, Z) coordinates are then converted into polar coordinates (latitude,

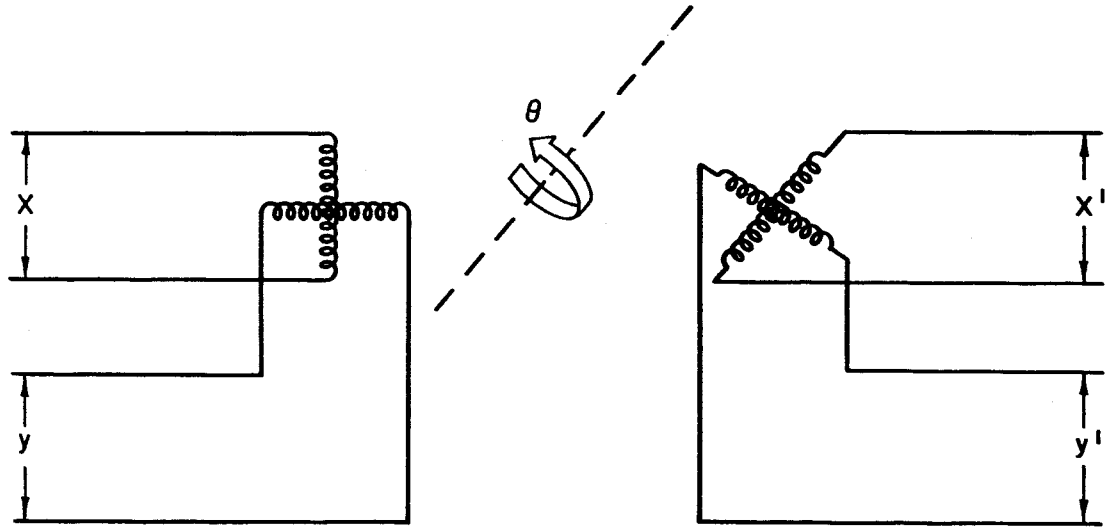

$$X' = X \cos\theta - y \sin\theta$$
$$y' = X \sin\theta + y \cos\theta$$

NOTES:

1. *THE VOLTAGES X AND Y MUST BE IN PHASE, AS MUST THE VOLTAGES X' AND Y'.*
2. *THE BROKEN LINE REPRESENTS THE SHAFT OF THE RESOLVER.*

FIG. 9

THE RESOLVER AND ITS OPERATION

longitude, and radial distance from the center of the earth). The difference between this computed radial distance and the known (or estimated) radial distance of the point is then determined. A feedback circuit may be used to reduce this difference to zero by appropriate adjustment of the assumed value of $Z^{\prime}$.

The known (or estimated) radial distance of the point under consideration is the earth radius plus the height of the point. Usually, the height of any point of meteorological interest may be taken as zero, with negligable resulting error, but this restriction is not essential.

With the foregoing as background, the electromechanical computer shown in Figure 10 is nearly self-explanatory. It is implicit in Figure 10 that the photographic coordinates ($X^{\prime}$, $Y^{\prime}$) are available as electrical voltages and that the output Mercator map coordinates are supplied as electrical voltages. There are a number of commercially available plotting tables which can perform the actual input and output functions.

As indicated in Figure 10, the first step in the transformation is to provide the proper scaling from photographic distance to true distance as determined by the $Z^{\prime}$ coordinate and camera focal length. Although not shown in Figure 10, this picture magnification control can also allow for compensation of lens distortion and unequal electronic gain in the vertical and horizontal channels of the transmission system. Non-linear electronic gain effects can also be compensated at this point if their nature is known.

Following the picture magnification control, the five coordinate transformations are performed in the reverse of the sequence described in Section 2.1.2, since the problem here is to transform from satellite coordinates to earth coordinates. The required signal is introduced at the nadir angle resolver as shown. Zero positions and direction of shaft rotation for the resolvers are chosen so as to provide the actual angle required by the transformation equations.

After completion of the rotational transformations, the translations are performed in the summing circuits, which are actually three separate summing amplifiers. The other inputs to the summing amplifiers, namely Cartesian coordinates of the satellite, are readily generated through the use of resolvers which are mechanically coupled to the other satellite latitude and longitude resolver shafts. The zero positions of the two latitude resolvers differ by 90°, but the two longitude resolvers are aligned to have the same zero positions. As indicated in Figure 10, one of the electrical inputs to each of these satellite coordinate computing resolvers is zero.

The signals at the output of the summing circuits are the Cartesian coordinates of the point in the earth coordinate system. It is necessary to convert these Cartesian coordinates into polar coordinates to provide the required feedback for the unknown third coordinate (Z') in the satellite coordinate system. It is also convenient to perform this conversion as a preliminary to the computation of the Mercator coordinates. The conversion from Cartesian to polar coordinates

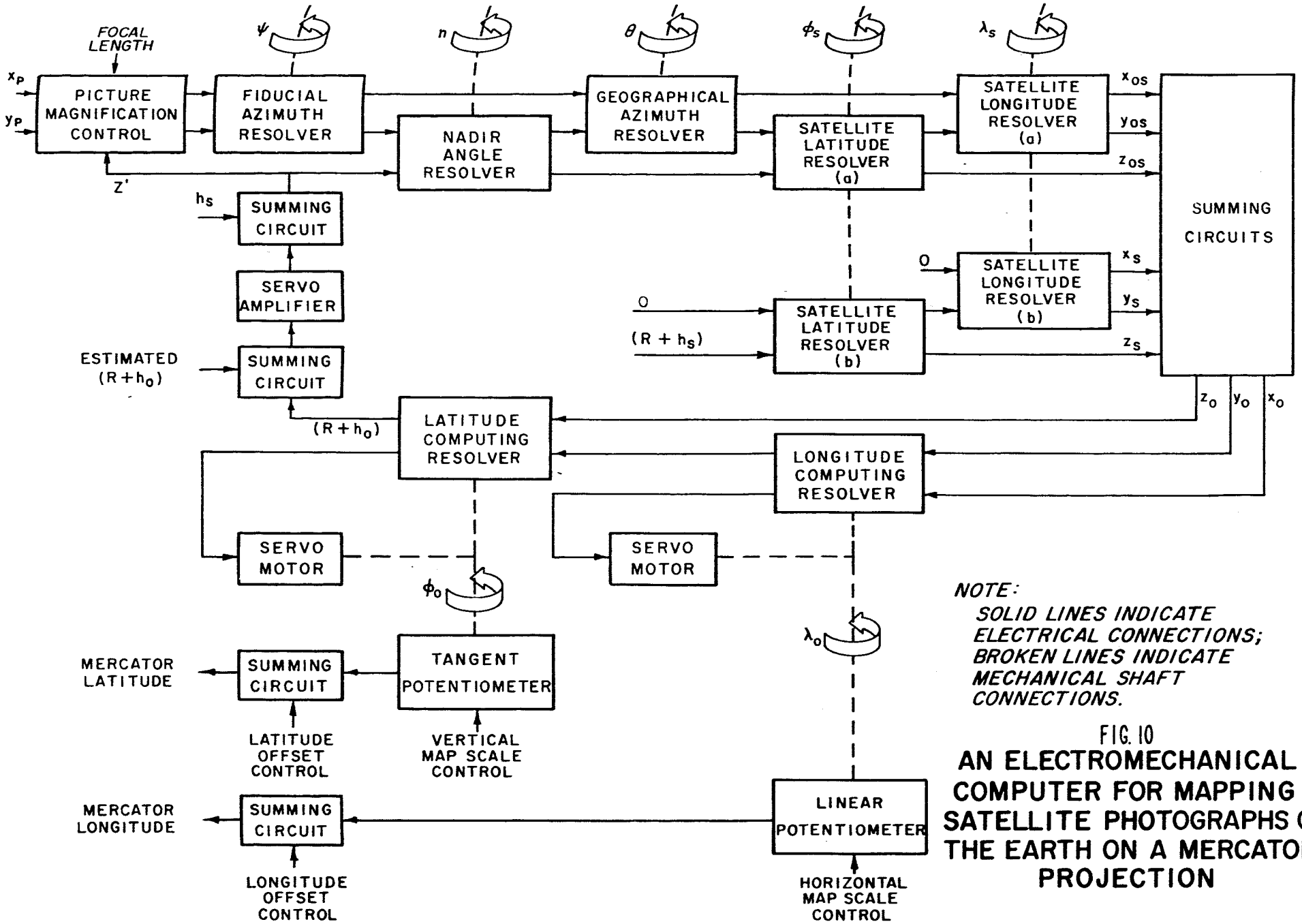

NOTE:
SOLID LINES INDICATE ELECTRICAL CONNECTIONS; BROKEN LINES INDICATE MECHANICAL SHAFT CONNECTIONS.

FIG. 10

AN ELECTROMECHANICAL COMPUTER FOR MAPPING SATELLITE PHOTOGRAPHS OF THE EARTH ON A MERCATOR PROJECTION

can also be accomplished with resolvers by the use of a feedback technique. A servo motor is used to drive the shaft of the resolver until one of its outputs is zero. The other output is then proportional to the vector sum of the inputs, while the shaft angle is the angle whose tangent is the ratio of the two inputs. This is precisely the relation between Cartesian and polar coordinates in two dimensions, as expressed in Equations (2.10) and (2.11):

$$\rho = \sqrt{x^2 + y^2} \tag{2.10}$$

$$\theta = \tan^{-1} \frac{y}{x} \tag{2.11}$$

The corresponding transformation from polar to Cartesian coordinates is given by Equations (2.12) and (2.13)

$$x = \rho \cos \theta \tag{2.12}$$

$$y = \rho \sin \theta \tag{2.13}$$

The non-zero electrical output of the latitude computing resolver is the radial distance of the point from the center of the earth. It is compared with estimated radial distance of the point in a summing circuit and the difference is amplified to provide a portion of the feedback signal for the third coordinate, Z' of the satellite coordinate system. Another summing circuit is shown to add in the other portion of this feedback signal, namely, the satellite height, h_s. This latter signal is the quiescent point of the servo amplifier, indicated in this way for conceptual convenience. The summing circuit is not required in an actual device.

The relation between the latitude and longitude of a point and its Mercator coordinates are given by Equations (2.14) and (2.15):

$$x_m = K_H \lambda \tag{2.14}$$

$$y_m = K_v \tan \phi \tag{2.15}$$

where

x_m = horizontal Mercator coordinate (longitude)

y_m = vertical Mercator coordinate (latitude)

K_H = horizontal scale factor

K_v = vertical scale factor

λ = longitude of point

ϕ = latitude of point.

A potentiometer is a straightforward means of converting shaft position into electrical voltage. A linear potentiometer (i. e., one whose output is proportional to shaft positions) whose supply voltage is adjusted to provide the desired scale factor is, therefore, shown in Figure 10 to provide the horizontal Mercator output. A tangent potentiometer (i. e., one which is wound in such a way to provide an output which is proportional to the tangent of shaft position) is shown providing the vertical Mercator output. Again, the supply voltage is adjusted to provide the desired scale factor. The potentiometer outputs are then fed to summing circuits to provide control over the latitude and longitude corresponding to the center of Mercator projection. This feature, together with the scale factor controls, permits the tracing of several successive photographs on a single

Mercator projection. Such mosaics are obviously useful in studying weather systems which are larger than the field of view of a single photograph.

The accuracy of the device described herein has not been investigated in detail. It is believed that it can be made sufficiently accurate for meteorological satellite photographic rectification applications, since resolvers with accuracies of better than 0.1° are available. Indeed, devices built with resolvers whose accuracy are from 0.25° to 0.5° would probably prove to be quite useful.

2.1.4 Other Applications and Configurations

The device described in Section 2.1.3 is not the only application of the visualization of coordinate transformations described in Section 2.1.2. A far simpler device would result if it were merely desired to trace a latitude and longitude grid on the satellite photograph. The feedback of the third coordinate would not be required since it would actually be known (i.e., the earth's radius itself). Furthermore, the computing servos for latitude and longitude would not be required, nor would the Mercator potentiometers. However, the picture magnification control would still be necessary with the required Z' coordinate being directly available. Manual control of the desired latitude and longitudes would yield the simplest device, but it would also be possible to incorporate a computer to automatically generate a specified latitude and longitude grid.

A slightly more complex device than that of Figure 10 could be designed to permit tracing of satellite photographs onto Mercator grids and the tracing of latitude and longitude grids on the satellite photographs. Switches (both mechanical and electrical) would have to be added to provide this flexibility. Other map projections can also be provided either as alternatives to or replacements for the Mercator projection.

It is not even necessary to employ resolvers to perform the coordinate rotation, although some of the elegance of the approach would then be lost. Completely electronic computing devices may be used instead of resolvers. This would result in an increase in computing speed because of the absence of moving parts. Such an all electronic version of the device of Figure 10 could conceivably be designed to operate in real time using the television scan voltages as the input signals and a cathode ray tube output. The output display would then be a television photograph on a Mercator projection (or other projection if desired).

2.1.5 Summary

A visualization of the transformation from satellite coordinates to earth coordinates as a step-by-step process consisting of translations and rotations has been developed. The mechanization of this transformation following this step-by-step approach simplifies the design of aids for rectification of meteorological satellite photographs. Considerable flexibility is possible in the type of devices

that may be designed. For example, one device may trace latitude and longitude grids on a satellite photograph. Another device may permit the tracing of satellite photographs on a Mercator or other projection. A fairly straightforward design results from the use of electromechanical resolvers in performing the basic operation of coordinate rotation. Greater operating speed can be attained through the use of completely electronic computing components. Real-time operation, providing a TV display which is a cloud map on a Mercator or other projection, is possible with the completely electronic device.

SECTION 3

AN EXPERIMENT FOR STUDYING THE OPTIMUM INTERVAL BETWEEN SATELLITE METEOROLOGICAL OBSERVATIONS*, [1]

3.1 Introduction

A problem which has as yet been given little consideration with regard to meteorological satellites is that of the desirable frequency of observation. Doubtless this will be dependent on the types of observations to be made and on their expected utilization. While there will certainly be some reasons for desiring, in at least some cases, continuous or very frequent observations, it may not be possible to justify them on economic grounds.

3.2 Experiment Description

The following is a description of a possible experiment which, using two satellites placed in constantly varying synchronized orbits, should provide sufficient data to permit significant study of this problem over time intervals between observations in the range of one to six hours. (A single satellite itself provides the twelve hour interval, assuming observations in the dark hemisphere are provided for through proper instrumentation.) Since the experiment would require only two satellites, it would appear to be much more economic than other possible approaches to the problem, which would

---

* This Section was written by W. K. Widger, Jr., Geophysics Research Directorate.

[1] Present Affiliation: National Aeronautics and Space Administration

probably, for a thorough study, require a minimum of four vehicles, the second, third, and fourth of which would be spaced, respectively, one, three, and six hours after the first.

It is anticipated that most future meteorological satellites (after the TIROS series) will be placed in quasi-polar, retrograde orbits with a precession of the plane of the orbit of one degree per day, thus maintaining essentially a constant local time of observation over the useful life of the payload. According to p. 19 of King-Hele (1960), the rate of precession of the plane of the orbit is given by the equation:

$$X = 9.97\ (R/R + h)^{3.5} \cos i$$

where

X = the precession in degrees per day

R = the earth's radius

h = the average altitude of the orbit

i = the inclination of the orbit to the equator

For a retrograde (east to west) orbit, the precession is from west to east. Based on this equation, Table One indicates possible combinations of orbit inclination and altitude for a one degree per day precession, ranging from 82.6° at 300 miles to 77.3° at 1000 miles.

Consider that a meteorological satellite has been placed in such an orbit with a one degree per day precession. As a specific example, assume the orbit altitude to be 700 (statute) miles and the inclination

79.7°. Then let a second satellite be launched one hour (15°) before or after the zenith passage of the first, with such an orbit altitude and inclination that the orbit precessions cause the orbit planes to rotate away from each other at a rate of 0.4° per day. Then, at the end of six months, the satellites will be executing the daylight portions of their orbits 90° or six hours apart. Over the six month period, samples will be provided of intervals between observations gradually increasing from one hour to six hours. Because of the comparatively slow rate of relative precession, there will be at least one month of data for each integral hour interval to a time accuracy within plus or minus one-half hour. A sample of this length, covering the entire earth on a substantially continuous basis, should be sufficient to permit significant deductions to be possible as regards the value of increased frequency of observation.

Two classes of 0.4° per day relative precession exist. In the first, the launch of the second satellite is made one hour before the zenith passage of the first satellite and the absolute precession rate of the second satellite is 1.4° per day. Possible combinations of orbit altitude and orbit inclination for this case are given in Table One, ranging from 300 miles and 79.6° to 1000 miles and 72.0°. For the second class, the launch of the second satellite would be one hour after the zenith passage of the first; the second satellite's absolute precession rate would be 0.6° per day. Table One also

gives the possible combinations for this case, ranging from 85.6° at 300 miles to 82.4° at 1000 miles.

No exhaustive study has been made of the relative merits of the two cases or of the optimum altitude within each of them. In the present state of launch technology, desired orbit inclinations can be obtained far more exactly than can orbit altitudes. The effect of orbit altitude error on desired precession rate varies from about 0.04° per day per 100 miles at 85° inclination to about 0.14° per day per 100 miles at 72° inclination. Thus a high inclination angle would seem very desirable. It would also seem logical to keep the inclinations of the two orbits approximately equal, although the value of this would require further study to be sure it exists. High orbit altitude has the value of increased coverage and increases the probability of achieving an orbit with a significant life in the event the desired altitude, or orbit circularity, is not attained. These considerations would seem to favor launching the second satellite one hour after the zenith passage of the first on a 1000 mile altitude, 82.4° inclination orbit. Should equal orbit inclination be found to be a factor of significant value, consideration could be given to some reduction in orbit altitude of the first satellite concurrent with increased orbit inclination. This would, however, increase the difference in relative coverage of the two satellites, and, if the same sensor systems were used, the difference in resolution of the observable features.

TABLE 1

Orbit Inclinations, as a function of orbit altitude, for precession rates (of the plane of the orbit) of 1.4, 1.0 and 0.6 degrees per day.

Orbit Altitude (Statute Miles)	Precession Rates (Degrees per day)		
	1.4	1.0	0.6
300	79.6	82.6	85.6
400	78.6	81.9	85.2
500	77.6	81.2	84.7
600	76.7	80.5	84.3
700	75.6	79.7	83.9
800	74.3	78.9	83.4
900	73.3	78.1	82.9
1000	72.0	77.3	82.4

Blank page retained for pagination

APPENDIX A

ATTITUDE DETERMINATION FROM PICTURE DATA*

A.1 Introduction

TIROS I is equipped with special sensors to telemeter the sun and horizon positions. With good data from these sensors the satellite Computation Center can calculate the attitude, i.e., the orientation of the TIROS camera at the time of each picture. It was expected that the Center could furnish predicted attitude for future orbits that would be accurate enough to be used in rectifying the cloud photographs as they were received. For several reasons the predicted attitudes were not sufficiently accurate, and throughout the real-time I. O. U. experiment it has been necessary to rely exclusively on attitudes that were deduced directly from the photographs. Provisions had already been made for emergency procedures to use in this situation (Conover and Sadler, 1960). However, under the pressure of this constant "emergency," the procedures have evolved into a somewhat different form, in order to make their use feasible on a real-time basis by the personnel whose primary concern is necessarily that of a rapid and efficient meteorological analysis.

The purpose of this appendix is to summarize and to systematize these developments. One particular concern is to insure that data from a complete sequence of pictures can be incorporated into a single self-consistent attitude analysis, and that it can be related to the results for preceding orbits so as to provide a reasonably

*This Section was written by Dr. C. Dean, Allied Research Associates, Inc. The work was sponsored under Contract No. AF 19(604)-5581, under ARPA Order No. 26-59.

accurate smoothed interpretation from the rather inaccurate individual bits of data. A second concern is to permit useful short-term extrapolations to be made by the meteorological personnel, when needed for the initial analysis of a new sequence of pictures.

A. 2 Attitude Nomograms

To interpret each picture we must know the direction in which the camera was looking, in addition to the location of the satellite at that instant. The TIROS design places the optical axis of the camera in line with the symmetry axis of the vehicle and with its axis of spin. Thus in the unperturbed calculations this direction (the attitude of the camera) is a constant vector in space, which we shall denote by the unit vector $\underline{N}$.

For convenience in the meteorological interpretation $\underline{N}$ should be described in a local coordinate system that is suitably aligned relative to the earth's surface at the satellite sub-point, i. e., the point on earth directly beneath the vehicle. We use the nadir angle, n, the angle between $\underline{N}$ and the line from the satellite through the center of the earth. To combine operational expediency with simple mathematics we take ξ, the azimuth angle of $\underline{N}$, to be positive clockwise (as seen looking down at the earth) from a reference direction which is tangent to the projection of the orbit onto the earth's surface at the subpoint, and which points in the direction opposite to the motion of the satellite. These variables describe $\underline{N}$ in terms of a polar coordinate system which travels with the satellite, as shown in Figure A-1.

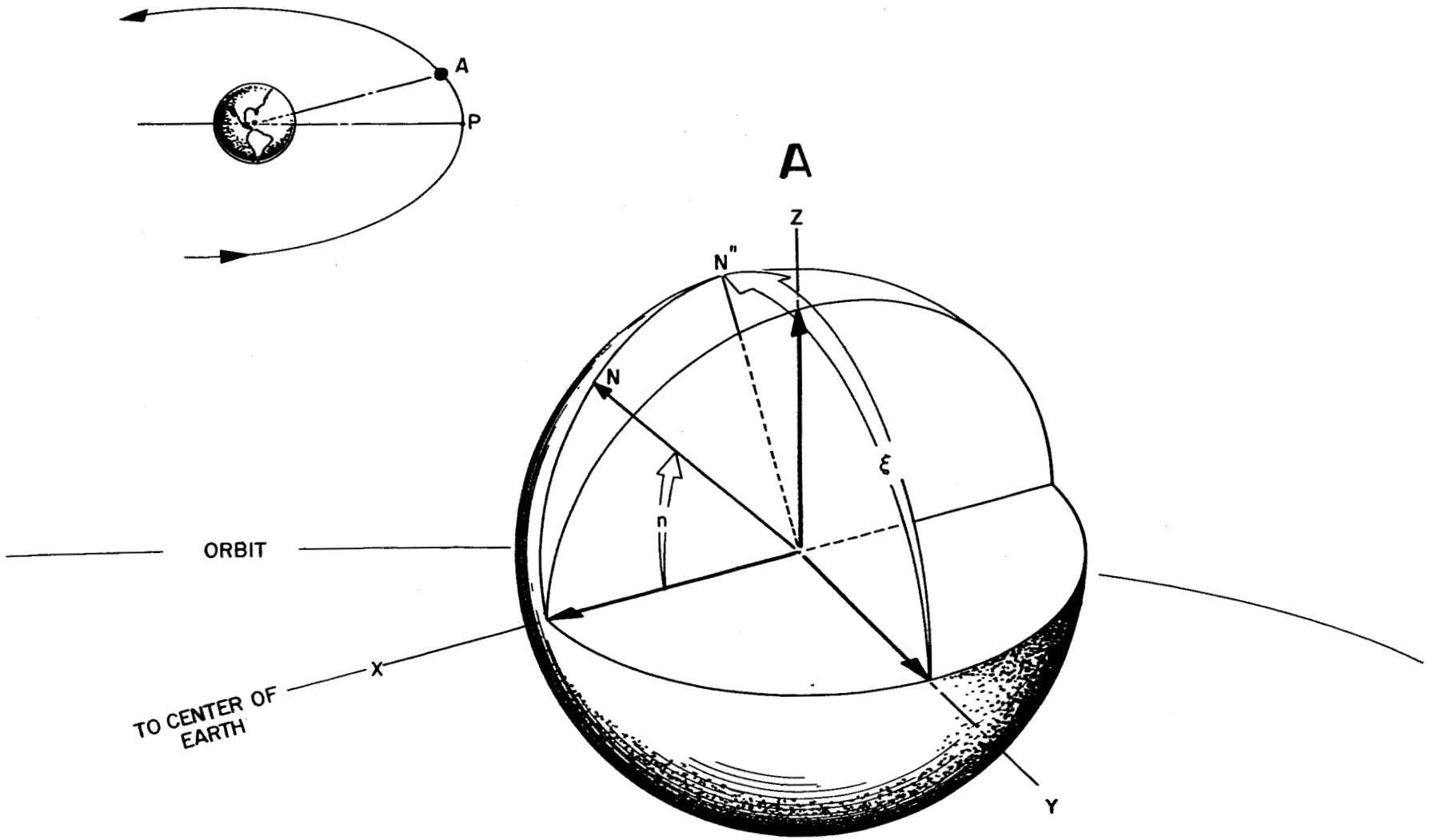

Fig. A-1 LOCAL ATTITUDE COORDINATES

We need expressions for ξ and n as functions of time, the orbital elements, and the spin direction in space, since this is the basic information which is currently available at the meteorological interpretation center. These expressions are simple for circular orbits, but to include the case of elliptical orbits we first derive them as functions of the true anomaly, w, i. e., the angle beyond perigee of the satellite in its orbit. The vector $\underline{N}$ makes a fixed angle, α, with the unit vector normal to the orbit, $\underline{z}$ (we take + $\underline{z}$ in the direction of the orbital angular momentum of the satellite). As seen from the viewpoint of the moving satellite, therefore, $\underline{N}$ appears to describe a circular cone about $\underline{z}$. The nadir angle varies with the position of the satellite, and has the minimum value $n_o = |90° - \alpha|$ at a particular true anomaly which we shall denote by w_o. The parameters n_o and w_o, together with the sign of $(90° - \alpha)$, constitute a complete description of the direction of $\underline{N}$ in space relative to the orbit. Since according to this definition we would necessarily have $0 \leq n_o \leq 90°$, it is useful to incorporate the sign by re-defining $n_o = 90° - \alpha$, that is, $\sin n_o = \underline{N} \cdot \underline{Z}$. The geometry for this set of variables is shown in Figure A-2.

The functions ξ and n are found by considering the two different sets of polar angle variables relative to a moving right-handed cartesian frame whose z axis is normal to the orbit, as above, and whose x axis is in the direction from the satellite to the center of the earth. Denoting the components of $\underline{N}$ in this frame as (X, Y, Z), we have

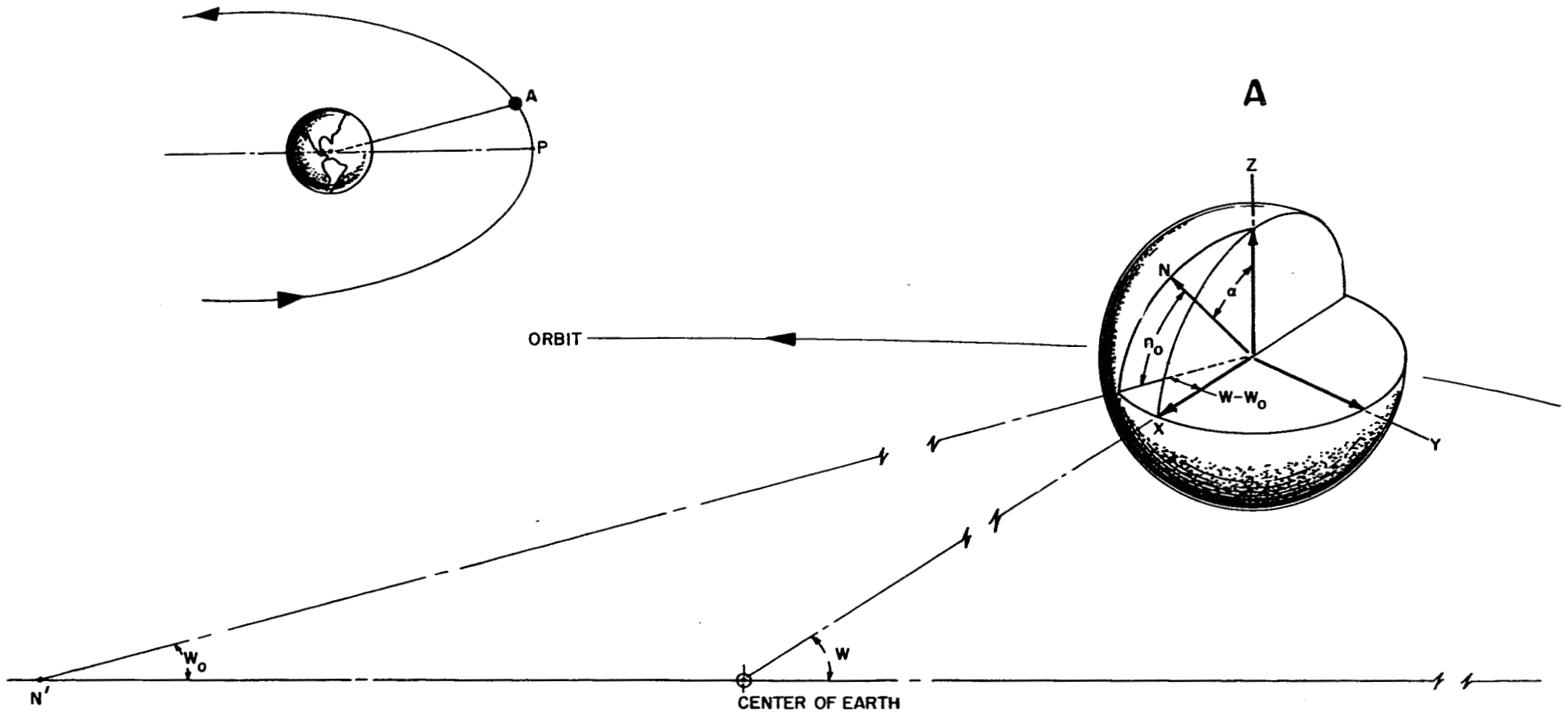

Fig. A-2 ORBITAL ATTITUDE COORDINATES

$$X \quad \begin{cases} = \cos(n) \\ = \sin\alpha \cos(w - w_o) = \cos(n_o) \cos(w - w_o) \end{cases}$$

$$Y \quad \begin{cases} = \sin(n) \cos(\xi) \\ = -\sin\alpha \sin(w - w_o) = -\cos(n_o) \sin(w - w_o) \end{cases}$$

$$Z \quad \begin{cases} = \sin n \sin \xi \\ = \cos\alpha = \sin n_o \end{cases}$$

Equating the two expressions for each component, we arrive at the computational formulae:

$$\cos n = \cos n_o \cos(w - w_o) \qquad (1)$$

$$\operatorname{ctg} \xi = -\operatorname{ctg} n_o \sin(w - w_o)$$

For circular orbits we may measure w from the ascending node of the orbit. Since w varies linearly with time in this case, we can write

$$(w - w_o) = 360\,(t - t_o)/T \text{ degrees,} \qquad (2)$$

where t is the time elapsed since the ascending node, t_o is the value of t at which the minimum nadir angle occurs, and T is the period of the orbit. For elliptical orbits the non-linear relation between t and w is that between mean anomaly and true anomaly, as described in texts on celestial mechanics (Moulton, 1914).

The preceding discussion is for unperturbed orbits. With sufficiently small perturbations on either or both the orbit and the satellite spin direction, n_o and w_o (or t_o) may be taken as constant throughout any single orbit, but there will be a slow cumulative change in these parameters with successive orbits. To within the current accuracy of the picture rectifications, this seems to be the

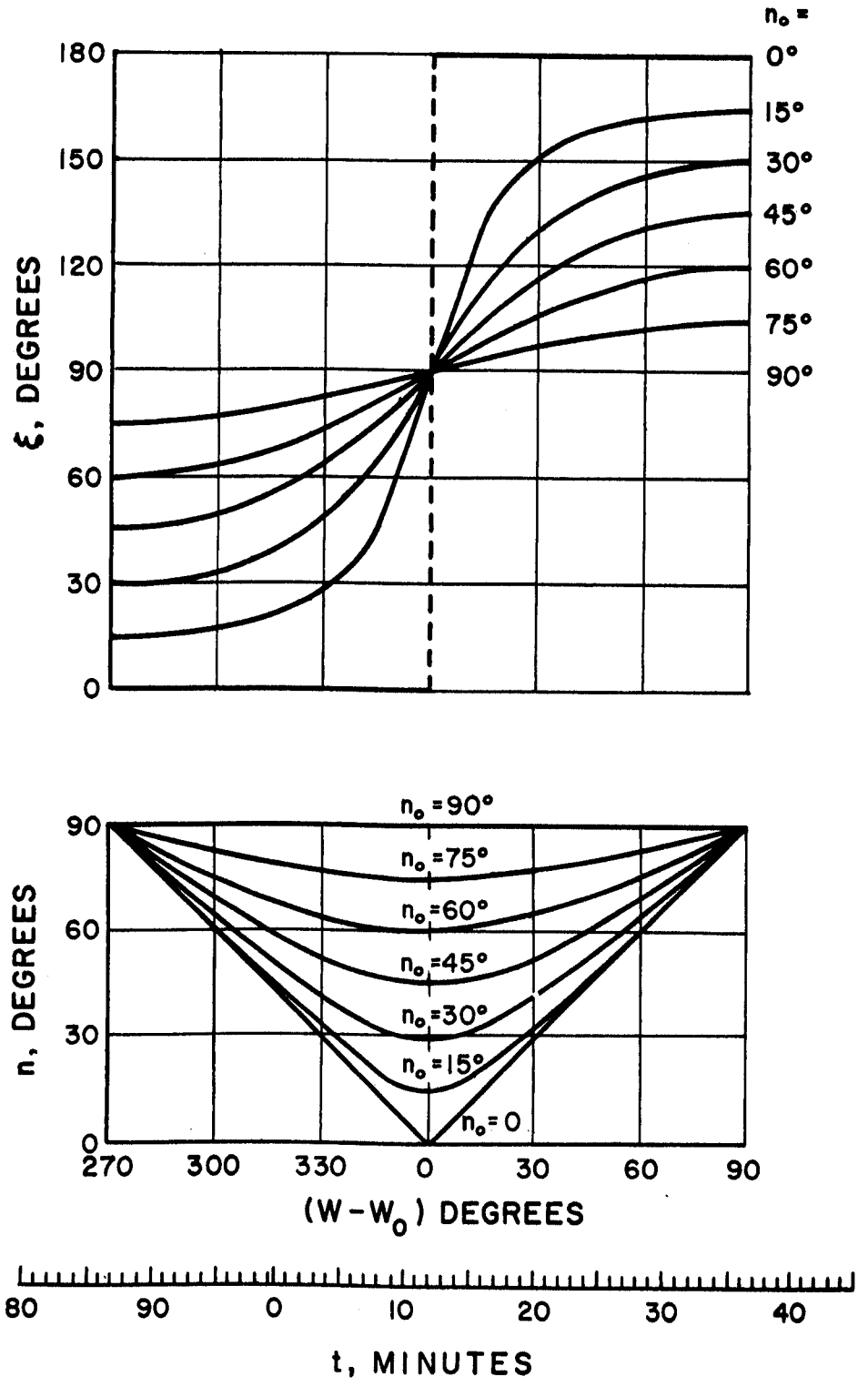

Fig. A-3 ATTITUDE NOMOGRAM

case with the TIROS I pictures, although the changes do become appreciable for this work in the order of ten orbits. Thus the aspect for any given picture in any orbit can be calculated from (1) if n_o and w_o or t_o are known as, say, functions of orbit number.

For the TIROS picture rectifications the accuracy of graphical attitude computations is ample. To permit a simple procedure the functions of Equation (1) are plotted in Figure A-3 for selected values of n_o; these can be considered as universal curves. Both graphs are drawn for positive n_o only. For negative values of n_o the same curves are used, the only change being to interpret ξ as negative, i. e., angle counter-clockwise from the path of the orbit. For a circular orbit a linear time scale is to be related appropriately to the angular abscissa, w, the scales being adjusted according to (2) to make the time interval of one period, T, match the angular interval of 360°. For convenience the time scale can be laid off on a separate strip of paper. In use, then, the value $t = t_o$ for a given orbit is aligned with the graph position $(w - w_o) = 0$, so that n and ξ can be read off for any value of t during the orbit by using the curves for the proper value of n_o. A separate scale in Figure A-3 illustrates the time scale aligned properly for the case $t_o = 12$ min, for a circular orbit with the period T = 99.2 minutes.

Although the curves of Figure A-3 also apply to elliptical orbits, the proper non-linear time scale must be laid off on the separate

strip of paper, and t = 0 must always be taken as perigee rather than the time of ascending node. If it becomes necessary to take the eccentricity of the orbit into account it will be necessary to construct a running graph of perigee times after ascending node, as a function of orbit number, since only the ascending node times are currently received for each orbit at the meteorological analysis sites. This graph can be made from the orbit elements which are received every two weeks or so. New time scales would be required from time to time to correspond to the gradually changing eccentricity of the orbit.

A. 3 Determination of Attitude Parameters from Satellite Photographs

In this section the discussion will be limited to the case of circular orbits, since this case is a good approximation for the TIROS I experiment. The discussion for elliptical orbits is essentially the same except for the additional complication needed to distinguish between the use of t and w as the independent variable.

A. 3. 1 The Uses of Nadir Angle Data

The nadir angle can be measured directly from nearly every photograph which shows the horizon (Conover and Sadler, 1960). Although this can be done by measuring the shortest distance in the picture from the principal point to the horizon, it is helpful to do so by trial and error with a selection of perspective grids, since the horizons on the grids have been drawn to conform to the rather queer distortions in the TIROS I lens. In fact, if the amount of rotation of the horizon within the picture borders from picture to picture has been checked

carefully, or the sun angle data can be deciphered, it is possible to determine the nadir angle fairly well from only a short section of horizon in the corner of a picture, even when the horizon point nearest to the principal point actually lies outside of the picture itself.

The set of nadir angles for a sequence of pictures taken at known times will determine values for $|n_o|$ and t_o; only the sign of n_o remains to be found. The first of the formulae in (1) is used for this. With ideal nadir angle measurements only two pictures would be needed to fix the two parameters. However, the uncertainty of the individual measurements makes it preferable to use all the nadir values that have been obtained for a sequence, and to choose $|n_o|$ and t_o for the best fit to a curve from Figure A-3. This is done quite easily by plotting nadir angles against time on a separate sheet, and using a copy of Figure A-3 which has been prepared on a transparent overlay. This apparatus can of course be used also in place of that described in the preceding section to predict n and ξ .

It is a particular virtue of this method of aspect determination that it involves no picture analysis of consequence. The measurements and the curve fitting can be accomplished in the first few minutes of the routine analysis of a picture sequence. It is expedient to measure the nadirs for all possible pictures in a sequence, even though some frames will not be needed for the subsequent cloud analysis. By doing this it is possible to determine a surprisingly convincing curve fit in spite of fairly appreciable errors in the individual measurements.

It is obvious that the individually measured nadir angles are useful in themselves, since they can be applied directly in the rectification of the individual pictures. However the practice of fitting the values to a curve at the beginning of a cloud analysis provides a guide for questionable frames, and a rapid and logical extrapolation for frames in which no horizon is visible. In addition, the fit of the nadir angle curve prescribes a particular n_o, and thereby prescribes the azimuth angles, aside from the question of sign. Although the fit is somewhat insensitive to n_o for the higher nadir angles for which the horizon data are fairly exact, and the derived azimuths are consequently only approximate, this can be a useful guide in special cases.

An unexpected but very useful application of the nadir angle data in the station has been to check the time of the first picture in a sequence, particularly for the tape-recorded remote pictures. By relying heavily on nadir angle data from the accurately timed direct picture sequences it has been possible to obtain values of t_o which fall with relatively little scatter around a smooth curve against orbit number. Freehand extrapolations of this curve for ten orbits or so beyond the last such data have been found accurate to within about a minute. Therefore, such an extrapolated value can be taken as a reference against which the indicated t_o from a remote sequence can be checked; any major discrepancy indicates the approximate error in the timing of the first of the remote pictures.

This technique has been particularly helpful for sequences in which considerably fewer than the expected number of pictures (32) were

received. In these cases it appears that the existing pictures usually correspond to either the beginning or the end of the intended full sequence (presumably the tape recorder sticks part way through either the recording or the playback). The choice of a picture timing which reproduces the predicted t_o generally settles this question.

Clearly distinguished landmarks are of course better than nadir angle for settling timing questions. On occasion, however, the use of nadir angles to determine approximate timing has led to the subsequent recognition of faint landmarks with sufficient certainty to permit a final accurate timing check.

A. 3. 2 Azimuth Determinations

An independent determination of azimuth angle can be made whenever a known vector on the surface of the earth can be located relative to the principal axis in the photographs. The line from the subpoint to a landmark point is such a vector. Two landmark points in one picture provide an independent vector, and of course an extended landmark is a congeries of such vectors. The use of landmarks to determine the azimuth for an individual picture is essentially automatic in the TIROS rectification procedure, since the analyst is logically forced to orient his sketch map properly in order to have the landmarks correspond to what he sees in the atlas by his side. Unfortunately good landmarks are rare, so that only occasionally can this procedure be used directly.

Sharply distinguishable and precisely located cloud features are usually found in some pictures of every sequence. Since their location is unknown apart from the pictorial evidence itself, the clouds in a

single picture cannot specify its orientation. On the other hand, the fact that there is considerable overlap between the areas viewed in successive TIROS pictures means that the velocity vector of the satellite can be deduced relative to the principal axis, from the apparent motion of the cloud features from one picture to the next. Since the velocity vector is in fact known precisely from the orbit data, the azimuth of the principal axis can be determined.

Let us consider the distinctive cloud features to be rectified onto a blank map, i. e., onto a blank sheet of paper, from one particular picture. (It is assumed here that the proper perspective grid and its orientation are known.) Let the subpoint and the direction of the principal line from it also be indicated on the map. If the pictorial data were ideal, the rectification of the same clouds from adjacent picture frames would be identical, since the time lapse between the pictures is trivial relative to that needed for significant cloud developments on the scale of the resolution of the pictures. Therefore let us consider the original rectified sketch to be moved to make the cloud pictures appear correctly on the transfer grid according to the next picture, and then enter the subpoint and the direction of the principal line for it for that picture. The pair of subpoints is obviously parallel to the projection onto the earth of the velocity of the satellite relative to the earth. (It is considered obvious that the cloud velocities relative to the earth are negligible in this context.) The projection of the true velocity is obtained after a minor correction for the velocity of the earth's surface,

that is, for the amount that the earth has rotated during the time between the two pictures. Since the satellite velocity vector in space is precisely known (all we really need is the path of the subpoints, corrected for the earth's rotation), the azimuth as defined in the preceding section is immediately read off the rectified map.

It seems reasonable to claim that an azimuth determination from cloud features can approach the accuracy of a determination from landmarks. Clearly recognizable points in the cloud structure are frequently found and the effect of distortions in the pictures is similar in the two cases. In addition, the determination from cloud features characteristically involved at least two pictures in a sequence, and it is often possible to use several cloud features to derive an over-all azimuth determination that is based on quite a number of the pictures in a sequence. Consequently the use of cloud features permits a form of averaging over the various distortions in the pictures, with the somewhat surprising result that one may at times claim even a better determination from clouds than from a landmark clearly seen but usable in only one or two pictures. In any case the fact that cloud features can be used much more often than landmarks makes the technique quite important.

The procedure is described in detail above to illustrate its theoretical basis. In the real-time operations a trial value of azimuth is often chosen by intuitive extrapolation from the analyst's recollection of a sequence from a prior orbit. The principles outlined above then guide the choice of azimuth for subsequent pictures, and trial and error

adjustments are made if necessary. The use of the relatively direct sequence of steps outlined in the preceding paragraphs is precluded at present, since the rectification is done onto a map on which the string of subpoints has already been marked. The exigencies of real-time operation rule against separate trial maps and also against completely new starts if a minor discrepancy appears.

It is recommended that the curves of Figure A-3 and the running charts of n_o and t_o be used fully to supplement the above procedures. As stated earlier, the sequence of nadir angles for a given picture sequence prescribes a particular n_o and thus the azimuth angles, although the prescription is not necessarily very precise. (It should be noted that this is true even with an incorrect choice for the time of the initial picture of the sequence; n_o and t_o are orthogonal in this sense.) Whatever good determinations can be made from landmarks or from cloud features can be used to guide the choice of the best value for n_o. In any event, it should be thoroughly understood by the analyst that the choice of both nadir and azimuth angles for an entire sequence should be considered as a single simultaneous curve-fitting operation. Initially there was some belief that the aspect was in fact wobbling, so that deviations from the curves of Figure A-3 should be expected. At present, however, it appears that if such wobbling occurs its amplitude is too small to be important relative to the present uncertainties in the rectification process.

The curve-fitting that is described above could be done by an automatic computer. However, the over-all uncertainty of the data and

the use requirements make the accuracy of the graphical method perfectly adequate, and the time needed to perform it is scarcely more than that needed to record the observed angles. In addition to this, an automatic program for use with these highly redundant bits of data, each of which is subject to a wide variety of random and accidental error, would require elaborate provisions to test for every possible data flaw, if its answers were to compare favorably with what can be done by human judgment. As future satellite systems are progressively refined much more accurate predictions of attitude will be possible from the Computation Center, so that the present need for emergency provisions will all but disappear. It is unlikely that a significant saving of man-hours would have been realized by that time through the development and use of a separate automatic computer program for use in the satellite meteorological interpretation center.

APPENDIX B

IMMEDIATE OPERATIONAL USE (I. O. U.) PROGRAM OF TIROS I*

B. 1 Introduction

TIROS I was in operation for about 78 days. Its creation and operation has been an unqualified success from the technological point of view and its televised pictures are demonstrating the greatest advance in weather observing and mapping since the telegraph made possible the first "real time" synoptic weather map.

The remarks contained in the following paragraphs are intended as a review of the operational procedures used during the I. O. U. program for TIROS I.

B. 2 Operational Procedures

B. 2. 1. Rectification of Pictures

B. 2. 1. 1. General

The rectification techniques underwent a period of experimentation and evaluation at Belmar out of which emerged a rather dependable working procedure. During the first few days of operation, the pictures were carefully monitored for quality and information content and obvious landmarks were noted. Later, rectifications were attempted for passes having recognizable landmarks, as this enabled obtaining accurate fixes to permit positive picture location and to determine the azimuth of the principal line. At this point

*This section was written by R. J. Boucher, Allied Research Associates, Inc. The work was sponsored under Contract No. AF 19(604)-5581 under ARPA Order No. 26-59.

in the operation there was no positive knowledge regarding the behavior of the satellite's optical axis and there was considerable doubt about the accuracy of the picture timing mechanism. For these reasons it was considered impractical to attempt rectification of picture sequences having no landmarks.

In time it was realized that the azimuth of the principal line changed very slowly from day-to-day at the same latitude. Hence it was possible, having established the azimuths on one orbit, to use these same values for successive orbits at the same latitudes. Errors in the timing system ("clock") were run down and the given time of start of remote pictures became quite reliable. Thus it became possible to rectify a large number of the remote passes. Another simple but very useful technique was to determine the image rotation rate in that portion of the picture sequence having a horizon for fitting the perspective grid. Since this rate changed very slowly from day-to-day, it was possible, knowing it, to continue rectification down to low nadir angles even after losing the horizon, by continuing to apply the same rate of image rotation to locate the principal line in the picture. This technique worked very well. However, as the minimum nadir angle position was reached, the azimuth of course rotated very quickly by a large angle and it was necessary to fit the cloud patterns very closely to avoid confusion.

B. 2. 1. 2 The procedure

Prior to receiving the first film positive, subpoints for all possible pictures from all of the day's passes as given in the program

were plotted on transverse mercator maps. The pertinent geography outlines were also traced on these from a previously prepared library of outlines. Status reports for each orbit were checked for possible changes from programmed times. Having received the film, it was first checked for consistency with the program and, if direct, with the events recorder data to establish the actual time of start of pictures sequences. In this inspection landmarks were identified and a decision made as to feasibility of rectification. Having decided on rectification, the film was placed in one of the two Simmon-Omega enlargers and projected onto a master focus sheet which had been prepared from lens calibration data for the wide angle camera. Having obtained a "best fit" of the fiducial marks on the film to those of the focus sheet, a blank sheet was laid down and the film fiducial marks traced exactly. This eliminated the necessity of "fitting" each picture thereby saving considerable time.

Rectification then proceeded. If landmarks were available, it was customary to use these as a starting point, giving a good check on the time of the pictures. If no landmarks were available, rectification began with pictures having horizons somewhere near the middle of the picture. This provided a reliable horizon for fitting the perspective grid and for establishing the principal line. An estimate of the principal line azimuth was then obtained from the latest available reliable rectification covering the latitudes of interest. The principal point location on the map was determined by scaling off the distance

along the azimuth from the plotted sub-point which is a function only of nadir angle, assuming a constant altitude of 450 miles. This scale was laid off on the transfer grid for convenience and labelled in terms of the nadir angle.

In the rectification, which was performed directly onto the transverse mercator map, major cloud features were located as precisely as possible. Smaller scale features were indicated schematically. If no serious timing error developed the sub-point locations were quite accurate and the rectification proceeded smoothly--one picture "dovetailing" into the next with a minimum of compromise necessary. However, because of the presence of some lens distortion, not known at the time the perspective grids were computed, the fit of individual cloud features from one picture to the next was not perfect--the largest departures occurring near the picture edge where presumably the uncompensated distortion was greatest. In general the distortion problem was not serious--simply another undesirable feature which "had to be lived with."

The end product of this process was a transverse mercator map on which were sketched, in more or less crude form, the cloud features and distribution of cloud cover as abstracted from the picture by the analyst. In carrying out this one step there is considerable room for differences in interpretation. However, it is also quite apparent to those who partook most extensively in the analysis, that after a sufficient amount of experience has been acquired by a competent analyst, differences tend to become rather insignificant--to use an

analogy: the shape of the letters may differ between analysts--but the words of the message and even the spelling of the words are the same.

Regarding the requirements of the analyst, he should be a professional meteorologist of research calibre with a considerable background in synoptic analysis of hemispheric scope and at least some forecasting experience. Such a person will have the tools necessary to grasp the significance of cloud patterns and abstract their essence--and acquaintance with forecasting problems will give him a means of evaluating the usefulness of the information and assist him in presenting it effectively to the user. Because so much abstraction and, to some degree, interpretation goes on during the rectification process, as described above, it would be a serious mistake to employ inadequately qualified personnel to carry out this most important single step in the data reduction process.

B. 2. 2 Transmission of Data

Having completed the rectification, two choices were available: (a) to transmit the transverse mercator map, and (b) to transfer the analysis to a smaller scale map and transmit. Both procedures were followed at various times at Belmar. Procedure (a) was the least time consuming. However, even this process required additional work on the map after the transfer of data to render it suitable for facsimile transmission. In some cases it necessitated tracing onto a clean map. Often the size of the rectified map precluded its transmission in a single section. Procedure (b) was utilized most frequently for two reasons;

(1) To reduce the map size and permit transmitting the entire rectification, in a single transmission

(2) To standardize the size and scale of maps transmitted.

The adoption of half-scale grids and maps during the latter part of TIROS I operation made it possible to transmit the original map. However, it was still found desirable to transfer the data to a 1:20,000,000 mercator map with printed geographical outlines. This became more or less the adopted standard base map for transmitting rectifications from Belmar.

In addition to the transmitted rectifications, summaries were prepared for each readout of data and transmitted by teletype. These contained an evaluation of the number, quality and content of the pictures and a brief descriptive summary of cloud forms seen, their probable synoptic interpretation and locations and visible landmarks.

B. 2. 3 Utilization of Data

Rectification of TIROS I cloud data has been considered throughout the operation to be on a strictly experimental basis. Accordingly no commitments were made to provide any operational group with specific data. Moreover, the relay of TIROS I nephanalyses by facsimile was done on a contingent basis as circuit time was available. Yet, in spite of these serious limitations, there was positive evidence that the TIROS I data, limited as they were, were very useful. Several instances have been cited by Widger (1960) where the TIROS I data provided the only solution to a problem involving cloud cover.

The TIROS I data, when integrated with conventional nephanalyses, resulted in much improvement in cloud depiction over water areas. Even in regions of dense weather reporting networks, the TIROS I data frequently delineated cloud patterns not apparent from an analysis of the ground sequence observations.

Thus TIROS I observations served at both extremes: to supply meteorological information not available by other means, and to indicate the organization existing in the clouds even for a region having adequate ground observation.

All of the known feedback originated at military installations--hence there is at this writing no knowledge of the usefulness of the TIROS data in synoptic analysis and medium range general forecasting.

B. 2. 4 Operational Difficulties

B. 2. 4. 1 General

This section will enumerate only those problems which were not adequately solved during the first three months of TIROS I operation. As anticipated, the first few weeks of operation of the readout stations brought to light a number of difficulties due to the complete newness of the operation. The majority of these problems were minor and were solved by the meteorology teams on site. The more difficult problems requiring more elaborate techniques will be discussed below.

B. 2. 4. 2 Attitude Data

In the original TIROS plans, attitude data for each picture were to be predicted by the Computation Center and transmitted to

the meteorological picture analysis center, along with the sub-point data. This was done, but the predicted attitudes were quickly shown to be useless by incontrovertible landmark data. Emergency procedures had been prepared to cope with occasionally missing parts of the predictions, but the complete failure of the predictions throughout the TIROS I operations had not been anticipated.

The meteorological analysis teams quickly devised means of inferring attitudes directly from the photographs, and these methods were used throughout the I. O. U. program. These methods depended primarily on a visible horizon in each picture to determine its nadir angle, with simple interpolation or extrapolation being trusted for perhaps two or three picture frames. The overlap of the cloud areas seen in successive frames helped in the choice of azimuth directions, but with little time to survey the basic geometry involved, these methods were considered inherently inexact, and great reliance was placed on the occasional good landmarks that were seen. Nevertheless, it was recognized that the rectified nephanalyses were fairly accurate in general.

The Meteorological Satellite Section of the U. S. Weather Bureau began analyzing the attitudes deduced from the pictures and predicting future attitudes. Apparently they also placed major emphasis on landmark data. Although their predictions were quite good, each prediction reached far enough into the future to require an accuracy dynamic analysis for adequate precision, rather than a simple extrapolation of the perturbation parameters. However, this work would have furnished the foundation for accurate attitude data for all

of the incoming pictures if it had been possible to quickly and conveniently modify the extrapolated attitudes in the rectification process to take into account the new pictorial data as it became available.

Since it was apparent that both the in-station procedures and the MSS computations were giving valid results, Allied Research scientists turned to the question of possible revisions in the kinematic description which would permit a more unified and complete use at the data analysis site. The nature and the completeness of the pictorial attitude data was reviewed as well as the form of the perturbation parameters that would be the most convenient and meaningful for the analyst performing the rectifications. The result, described in Appendix A, is a nomogram in which the nadir and azimuth angles for the pictures as a function of time in a given orbit are shown as a two-parameter family of curves, the parameters being the value of the minimum nadir angle for that orbit and the time after perigee (or ascending node, for a circular orbit) at which it occurs. These two parameters are equivalent to a description of the satellite spin orientation in space, but they have a precise and obvious meaning in terms of the variables that are most directly used by the meteorological personnel in performing the rectifications and nephanalyses. By using these functions as a family of universal curves, the parameter values for a new sequence of pictures can be deduced by finding the best fitting curves for the set of all nadir and azimuth angles that can be deduced from that sequence. This provides an up-to-the-minute

check on the accuracy of the predicted parameters. Attitudes for orbits in the future can be read off the curves that are specified by the predicted parameters. Since the entire process is graphical, and involves only numbers which are used directly in the rectifications, the additional time required is trivial. The precision easily matches or exceeds the precision with which the individual pictures can be rectified.

It is believed that the failure of the original attitude prediction program occurred because the telemetered information from the sun and horizon sensors was considerably poorer than anticipated. It should be appreciated that the use of the pictures to deduce attitudes has the tremendous advantage of using human judgement in an effective way to screen the data for both expected and unexpected flaws, and to reject or occasionally validly modify it before using it in the computations. Such flaws in predicted data were found by the score, and included wrongly labelled data (e.g., obviously wrong orbit number), incomplete remote picture sequences for which the picture taking times could be established only by ingenuity, and a myriad of oddities generated by electronic noise. On the other hand it also should be appreciated that the computation center was committed to an experiment on the functioning of the satellite system as planned. Thus the unfortunate fact that the original attitude part of the system was inadequate in effect forced the institution of a <u>second</u> attitude program based on the pictures, to serve the nephanalysis center.

Both programs were needed in the total experiment, and there was considerable logic in the arrangement that evolved, in that the system experiment continued at the main computation center while the nephanalysis service computations were performed in close contact with the meteorology group.

Blank page retained for pagination

APPENDIX C

RADARSCOPE PHOTOGRAPHY PROGRAM FOR TIROS I*

C. 1 Introduction

A contract for research directed toward the use of synoptic radar observations in the interpretation of satellite cloud observations was negotiated with Stanford Research Institute in July 1959. The purpose of this appendix is to acquaint the reader with the location of stations, areal coverage afforded, dates and times for which radarscope photography was accomplished during the operation of TIROS I. Also included are the dates and times of fifteen composite radarscope charts that were constructed for simultaneous satellite cloud comparisons.

C. 2 The Radarscope Photography Program

C. 2. 1 Completion of Preparations

Early in 1960, eighteen Air Defense Command radar stations were visited by personnel of S. R. I. for the purpose of installing special equipment needed in the photography program and indoctrinating station personnel in the procedures to be followed during the operation. Six additional ADC stations were visited for the same purpose during the middle of March, 1960.

A flight test was arranged with the 55th Weather Reconnaissance Squadron to ascertain the usability of airborne radar data in the program.

---

*This material was taken from a report entitled "Research Directed Toward the Use of Synoptic Radar Observations in the Interpretation of Satellite Cloud Observations", by R. E. Nagle, R. H. Blackmer and M. G. H. Ligda, Stanford Research Institute. The work was sponsored under Contract No. AF 19(604)-5982, under ARPA Order No. 26-59.

The results indicated that this type of data would be of outstanding value in evaluating oceanic precipitation patterns. Therefore, the three existing worldwide based weather reconnaissance squadrons were integrated into this program.

Film, logs, manuals, and other supplies sufficient to maintain the photographic operation for approximately one month were mailed to all participating stations. Early in March, 1960, a test was conducted to determine if all the camera equipment was still in operational condition, and to evaluate adherence to the procedure outlined in the Weather Watch II Manual and in the airborne addenda. This test was quite fortuitous. All but two stations had experienced difficulties; consequently, it was possible to correct most malfunctions in time for the launching of TIROS I.

As of 31 March 1960, the following ground and airborne radar stations were in readiness to commence the photographic program:

25 Air Defense Command Stations

4 Research Groups

5 Weather Bureau Stations

5 Navy Picket Stations

12 Air Weather Service Stations

3 Airborne Weather Reconnaissance Squadrons.

The location and areal coverage afforded by these radar stations is shown in Fig. C-1*.

*The weather reconnaissance tracks shown are the regularly scheduled flights and are not necessarily the actual tracks flown on any particular day.

C. 2. 2 Phase I of the Photography Program

On 1 April 1960 the successful orbiting of TIROS I required that photography begin by stations that had been organized for the program. In anticipation of a successful launch, the participating ADC stations had previously been notified to begin photography at 0000Z, 31 March. Therefore, many of these stations were taking pictures at the time TIROS was launched. As a result of confusion about the "operational" status of the satellite, some delay was experienced in notifying the AWS stations of the beginning of the effort. However, on or before 5 April 1960 all stations had been notified and by then they were engaged in taking pictures.

When we were notified that the satellite was assuming an unfavorable attitude to take pictures in the area of our radar coverage, a message was sent to all participating stations that requested the stations to terminate photography. The first photography period (hereafter referred to as Phase I) ended about 19 April. The variation in termination dates was due to our notification of ADC stations by mail.

The film accumulated during Phase I is generally of good quality and almost continuous in areal and time coverage. Several widespread precipitation areas recorded by more than one station have been noted in reviewing the film.

The film received from the various organizations during the Phase I photographic period is as follows:

66 100-foot rolls from ADC stations

8 100-foot rolls from the Navy Picket Ships

18 100-foot rolls from Research Groups (2 of the 4 groups)

13 100-foot rolls from the Weather Reconnaissance Squadrons.

In addition to these rolls of 35mm film, some 8,700 polaroid pictures were received from Air Weather Service and Weather Bureau stations. A comprehensive listing of the time, dates, and locations for which film is available is given at the end of Appendix C.

All film has been reviewed for quality control and weather content. Evaluation sheets were sent to stations on each roll of film to indicate its general quality and to advise of any equipment malfunction or objectionable deviations in procedures.

C. 2.3 Phase II of the Photography Program

With notification that the satellite was again taking pictures north of the equator, the stations were requested to recommence photography on 5 May 1960.

Some changes in the participating stations were necessary in this phase of the program. Film from the Navy picket ships was no longer available due to the termination of the contract through which these data were being obtained.

Grounding of all Air Weather Service reconnaissance aircraft forced a termination of their efforts in the program. The loss of this unique and high-quality data is extremely regretable, especially in light of the amount of precipitation seen on the film acquired from this source during Phase I of the operation.

It was felt highly desirable to maintain some radar coverage over oceanic regions because of the interesting patterns seen over the oceans in the satellite cloud pictures. Arrangements were made with the 552nd AEW and C Wing Headquarters to use the facilities of the squadrons under their command in the remaining phases of Weather Watch II. This wing maintains four airborne radar stations, 24 hours a day, some 450 miles off the West Coast of the United States. Continuous radarscope photography began on 13 May 1960 during daylight hours on all four of their stations.

The location and coverage afforded by stations participating in Phase II of the Photography program is shown in Fig. C-1. Additional listings of the times and locations of film available will be prepared at intervals as the film is accumulated. As of the date of this report, the following 35mm film has been received from the various stations during Phase II of the program.

115 100-foot rolls from ADC stations

36 100-foot rolls from AEW and C stations.

We have also received some 8,900 polaroid pictures from the Air Weather Service, Weather Bureau, and Navy sites.

C. 3 Construction of Current Composite Radarscope Charts

Fifteen composite radarscope charts have been constructed from the film data collected in Phase I of the photography program. The dates and times of the composites were those requested by the contract sponsor and correspond to areas and times of simultaneous satellite

cloud and radar precipitation pictures. The dates and times of these composite charts are given below:

1 April 1960	1330Z
	1400Z
	1700Z
	1830Z
	2030Z
2 April 1960	1430Z
	1600Z
	1800Z
	1930Z
	2130Z
3 April 1960	1700Z
5 April 1960	1700Z
8 April 1960	1600Z
9 April 1960	1700Z
10 April 1960	1400Z

Copies of these composites were mailed to the Atmospheric Circulations Laboratory, Satellite Meteorology Branch, GRD; the originals have been retained for future analysis when rectified cloud pictures become available or when sufficient data are supplied for us to accomplish our own rectification.

A comparison of the direct sequence satellite cloud pictures from orbit number 0005 and the 2030Z radarscope composite chart of

1 April has been attempted. As no readily identifiable landmarks are visible in the cloud pictures, the positions of the cloud patterns are uncertain. We are awaiting additional aspect data before continuing with this analysis.

C. 4 Investigations Leading to Compatible Radar and Satellite Data

Considerable knowledge of the data-handling procedures and difficulties involved in rectifying cloud pictures from the satellite was gained during the week of 23-30 May when a Stanford Research Institute meteorologist spent the week working at the TIROS readout site at Belmar, N. J. Serious reservations are now felt concerning the ultimate ability to rectify entire cloud pictures to a projection comparable to that in the construction of our radarscope composite charts, with the accuracy and definition needed for analysis. Complete picture rectification (even graphical representations) to a map projection of commonly used meteorological charts will be difficult even if the only distortion were created by the earth's curvature: the added factors of lens distortion, uncertain position, and satellite attitude data imply that rectification of whole cloud pictures to a map projection and to the accuracy needed for ready comparison with the radarscope composite pictures will be difficult if not impossible to achieve.

The solution to this problem appears to be in utilizing only segments of the cloud pictures, where distortion is negligible in the rectification process. Certain aspects of the satellite's characteristics and the picture-taking interval are conducive to accurate rectification of segments, optically, without undue difficulty or expense.

Because the optical axes of the cameras are very nearly along the velocity vector of the satellite, segments of pictures in proximity to the principle point (±3 degrees along the principle line and 5-7 degrees laterally from it) and at nadir angles of 45 degrees or less are little distorted by the earth's curvature. This will allow the cloud pictures to be projected onto a section of a spherical shell from an angle corresponding to the nadir angle at which the actual pictures were taken. Re-photographing the projection from a position on the normal to a tangential plane through the principle point will accomplish an accurate rectification of the cloud patterns in proximity to the principle point. Composites could be constructed from successive segments of the individual picture to give an adequate areal rectification for analysis purposes.

The problem of accurately positioning the cloud pictures in relation to the radar stations is another difficulty which will have to be solved before very meaningful comparisons can be accomplished. In the operational experiment being conducted at the readout site placement of the pictures according to their position on the earth was achieved primarily by aligning landmarks displayed on the rectification grids with landmarks readily observable in the satellite pictures. Rectification using this technique was considered accurate to ±1 degree of latitude, and ±2 degrees when landmarks were not visible. Admittedly this accuracy may be slightly improved upon with the additional time available under research conditions, but accurate

placement of cloud features to at least 10-20 miles will be necessary for specific comparisons with the radar echoes. In this respect the radar echoes may be, in themselves, of considerable use in exactly positioning the cloud pictures. After a picture has been roughly oriented in its proper position by use of landmarks, satellite sub-point, nadir angle, and other ephemeris data, it may be possible to position certain pictures accurately by use of distinctive cloud features (bands, bright areas*, etc.) which were detectable and can be identified by the radar(s) echoes in the picture area. This would lead to a limited area type of analysis rather than a synoptic scale analysis. In light of the difficulty we experienced in finding extensive areas of precipitation in selecting storms for composite construction, the limited area analysis may prove to be not only simpler to accomplish but a more logical approach to the comparison.

C. 5 Conclusions

Work in preparation for the radarscope photography program was accomplished, and uninterrupted radar coverage was obtained over the continental U. S. and coastal waters during daylight hours, and at times when simultaneous satellite cloud pictures were collected. The data collection program was initiated. The film collected to date contains numerous instances for which simultaneous radar echoes and cloud pictures are available.

*Several very bright clouds which are thought to be located over the Mississippi Delta at 2030Z on 1 April have been tentatively identified by the shape of several echoes seen on the Houma AF Station radar.

Fifteen radarscope composite charts have been constructed from data obtained during Phase I of the photography program. They show the distribution of precipitation over as large an area as possible for periods when simultaneous cloud pictures are available. These composites are not included in this report, but will be published when comparisons can be made with rectified satellite cloud pictures.

Our limited experience with the procedures involved in rectifying the satellite pictures leads to the following assumption: it will not be feasible to rectify whole satellite pictures to projections comparable with those in the construction of our radarscope composites and to the accuracy necessary to make specific comparisons between the two data. The proposed optical and photographic rectification techniques for segments of successive satellite pictures offer a method by which the satellite data can be made compatible with our radar data. In addition, the radar echoes, themselves, may be useful in exactly positioning the cloud patterns in cases where identifiable features can be recognized in both data.

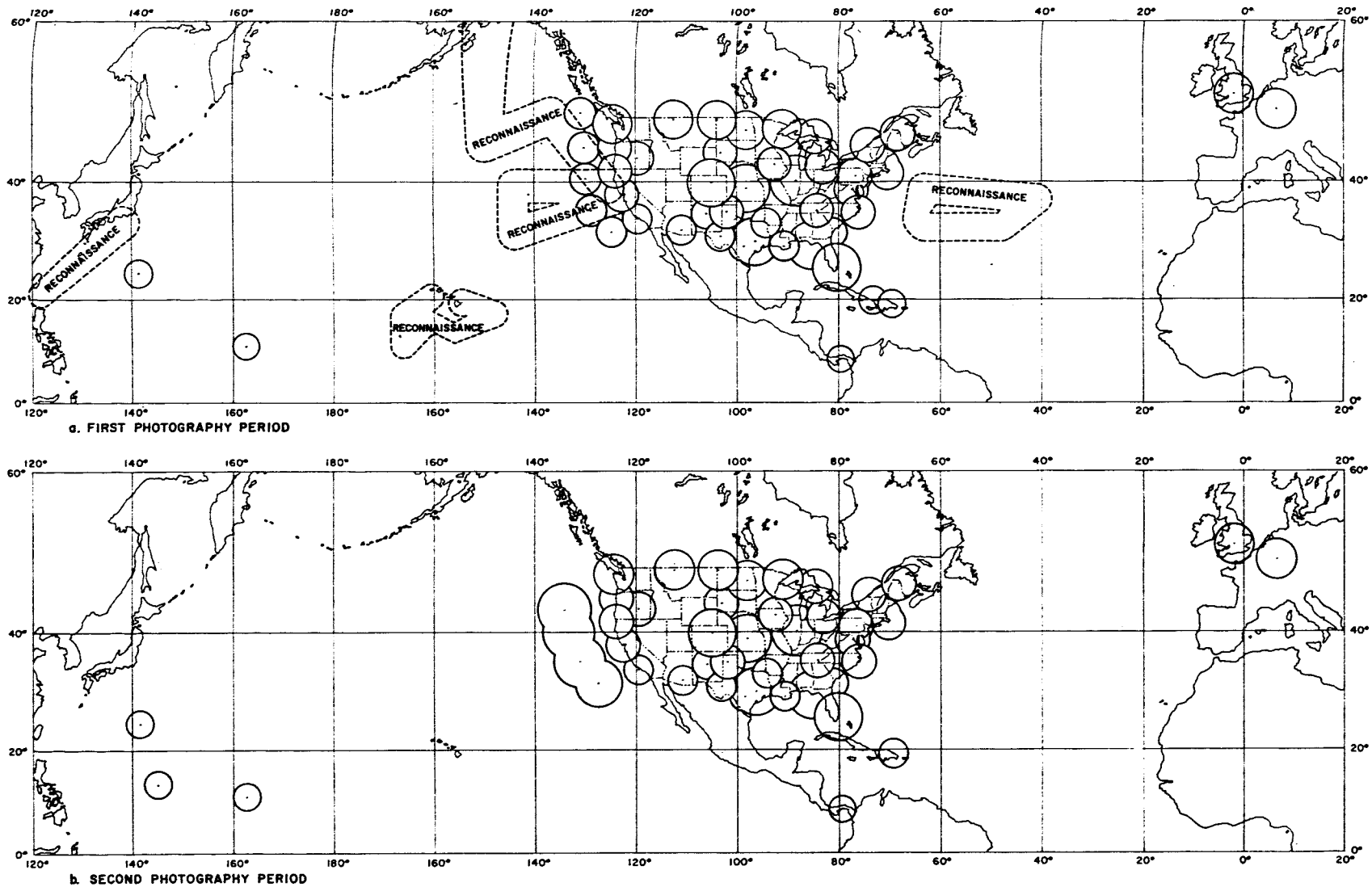

FIG. C-1. LOCATION OF RADAR STATIONS PARTICIPATING IN WEATHER WATCH II

Blank page retained for pagination

STATIONS TAKING ONE POLAROID PICTURE PER 15 MINUTES DURING DAYLIGHT HOURS

	APRIL 1	2	3	4	5	6	7	8	9	10	11	12	13	14	15	16	17	18	19	20
1. Lowry, Colorado	(All times GCT)				B1300	E0145 B1230	E0145 B1230	E0115 B1230	E0130 B1230	E0130 B1230	E0130 B1230	E0130 B1230	E0130 B1230	E0130 B1230	E0000					
2. Schilling, Kansas					B1745	E0115 B1200	E0100 B1215	E0100 B1200	E0100 B1200	E0100 B1200	E0100 B1200	E0100 B1200	E0100 B1200	E0100 B1145	E0100 B1145	E0115 B1145	E0115 B1145	E0155 B1145	E0115 B1145	E0115 B1145 E1645
3. Kadena, Okinawa					B0300 E0945 B2145	E0945 B2145	E0945 B2145	E0945 B2145	E0945 B2115	E0945 B2115	E0945 B2115	E0945 B2115	E0945 B2115	E0945 B2115	E0945 B2100	E1000 B2115	E1000 B2115	E0930 B2115	E0830	
4. Eniwetok					B0100 E0730 B1900	E0730 B1900	E0715 B1915	E0730 B1900	E0730 B1900	E0730 B1900	E0715 B1900	E0730 B1900	E0715 B1900	E0645 B1900	E0715 B1900	E0730 B1900	E0715 B1900	E0715 B1900	E0730 B1900	E0730 B1900 E1930
5. Brize Norton, England				B1200 E1845	B0545 E1845	B0500 E1845	B0529 E1845	B0530 E1845	B0534 E1845	B0649 E1900	B0530 E1900	B0515 E1815	B0533 E1900	B0515 E1900	B0518 E1900	B0522 E1900	B0515 E1900	B0500 E1130		
6. Hahn, Germany					B1133 E1815	B0615 E1815	B0445 E1815	B0445 E1815	B0445 E1830	B0500 E1830	B0445 E1815	B0430 E1830	B0430 E1830	B0430 E1830	B0430 E1830	B0430 E1830	B0430 E1830	B0430 E1830	B0430 E1830	B0430 E0700
7. Albrook, Canal Zone					B1315 E2300	B1100 E2330	B1100 E2330	B1200 E2215	B1200 E2330	B1100 E2330	B1100 E2315	B1215 E2315	B1115 E2300	B1115 E2300	B1100 E2315	B1200 E2030	B1200 E2330	B1145 E2330	B1130 E2230	B1215 E1245
8. Bermuda					B1300 E2230	B1145 E2230	B1000 E2245	B1000 E2245	B1000 E2245	B1000 E2245	B1000 E2245	B1000 E2245	B1000 E2245	B1015 E2245	B1000 E2245	B1000 E2245	B1000 E2230	B1000 E2230	B1000 E2245	
9. Ramey, Puerto Rico					B1411 E2230	B1030 E2230	B1029 E2230	B1030 E2230	B1030 E2230	B1030 E2230	B1030 E2232	B1033 E2230	B1030 E2230	B1030 E2230	B1030 E2230	B1029 E2230	B1030 E2230	B1030 E2230	B1030 E2230	B1030 E1330
10. Keflavik, Iceland					B0915 E2030	B0645 E2045	B0645 E2045	B0630 E2100	B0800 E2030	B0730 E2100	B0846 E2130	B0730 E2100	B0615 E2044	B0645 E2100	B0645 E2100	B0745 E2100	B0715 E2115	B0800 E2115	B0615 E2115	B0600 E0815
11. Apalachicola, Florida	B2045 E2400	B1230 E2400	B1145 E2400	B1145 E2400	B1145 E1500				B1130 E2400						B1130 E1315	B2145 E2400	B1300 E2400			
12. Guam						NO PICTURES FIRST PERIOD														

B - time photography began
E - time photography ended

Blank page retained for pagination

STATIONS EXPOSING 35mm FILM

ADC STATIONS (2 pictures per 15 minutes, 24 hours per day except as noted)

	MARCH										APRIL													
	31	1	2	3	4	5	6	7	8	9	10	11	12	13	14	15	16	17	18	19	20	21	22	23
	(All times GCT)																							
1. Texarkana, Ark.	B0001					E1500 B2230	E2005	B0500							E1957									
2. Lackland, Texas		B1428																E1809						
3. Amarillo, Texas		B2315														E1600								
4. Moriarty, New Mex.													B1525 E2235											
5. Houma, La.	B0001												(out of focus 12-18 April)							E1525				
6. Sault Ste. Marie, Mich.	B2348																			E1802				
7. Finley, N.D.	B0040		E1040 B1832																E2128					
8. Burns, Oreg.	(no film)																							
9. Benton, Pa.	B0001 E1204 B1620																	E1515 B2305	E1935					
10. Limestone, Me.			B1558																E2000					
11. Mt. Lemmon, Ariz.										B1630							E2215		B1530			E1500		
12. Mt. Hebo, Oreg.	Con't.					E1630 B1955	E1620	B0055			E1406 B1716	E1630	B0130	E1720										
13. Ellsworth, N.D.	B0015						E0513 B0804												E1420					
14. Lake City, Tenn.						B1207	(all out of focus)												E1734					
15. Hunter AFB, Savannah, Ga.	B1210		E0301 B1400																E1930					
16. Mill Valley, Calif.	Con't.									E0424 B0937		E1540 B2240					E2030		B1735 E1809					
17. Klamath AFS, Requa, Calif.		B1700					(all out of focus)													E1603				

Blank page retained for pagination

ADC STATIONS (Con't.)

	MARCH 31	1	2	3	4	5	6	7	8	9	10	APRIL 11	12	13	14	15	16	17	18	19	20	21	22	23
18. Neah Bay, Wash.	(all times GCT) B0549																			E0055 B0647				E1959
19. Cut Bank, Mont.	Con't.					E1700 B2215	E1618 B2300		E1304 B2307			E2200	B0600 E1319 E2252	E0100 B0833 E1500 B2226 E2320	B0550 E1511 B2207	B1200	B0115 E1722	B0115	E1506 B2400	E1505				
20. Finland, Minn.	B0001															E2220	B0040		E1758					
21. Santa Rosa Island, Calif.	Con't.				E1729 B2200	E1630	B0422 E2216	B0113 E1931 B2246							E1937 B2302	E1618 B2315	E0040 B0945	E1900						
22. Waverly, Iowa	B0001														E1601 B1915				E1900					
23. Selfridge AFB, Mt. Clemens, Mich.			B1930 E2130		B0030 E1730			B0900	E2300	B0800	E1800 B2216							E2100 B2400	E2017					
24. Pyote, Texas		B2050				E1430 B1715					E1630 B2230		E1300 B2200						E1430					
25. Fortuna, N.D.	B0001				E1400	B0001	E1800 B2145						E0301 B0600					E2004 B2400		E1900				
NAVY PICKET SHIPS (2 pictures per 15 minutes, 24 hours per day)																								
Station 1	no film (all times GCT)																							
3	B2100								E1400 B2300					E1430										
5	no film until 16 April																B1820							
7	Con't.																							E0330
9	Con't.																		E1600					

Blank page retained for pagination

OTHER INSTALLATIONS (Con't.)

	MARCH	APRIL																					
	31	1	2	3	4	5	6	7	8	9	10	11	12	13	14	15	16	17	18	19	20	21	22	23
		(all times CST)																						
Illinois State Water Survey		B1236	B0823	B1420	B1331		B1940		B0810	B0927		B0817	B0901	B0820	B1155	B0817								
		E2333	E1009	E1758	E2105		E2040		E2002	E1202		E1534	E1201	E1042	E2400	E0910								
										B1630		B2020	B1541	B1736		B1138								
										E1753		E2055	E1544	E2155		E2340								
McGill University	B2246	(all times EST)							E0555			E0845					E0745	E1230						
									B0630			B0945					B1605							

Blank page retained for pagination

WEATHER RECONNAISSANCE FLIGHTS (1 picture every 2 min. on 35mm film)

Date	Track	(GCT) Time Began	Time End	Total Footage	Classification	Remarks
4 April 60	Stock Juliett	2150Z	05/0425Z	34 ft	Confid.	Top of scope oriented to ACRFT Heading
6 April 60	Stock Juliett	2100Z	07/0410Z	28 ft	"	
7 April 60	Stock Juliett	1630Z	08/0040Z	17 ft	"	Excellent weather echoes
13 April 60	Stock Juliett	1720Z	14/0555Z	15 ft	"	Excellent weather echoes
9 April 60	Lark Special	2045Z	10/0545Z	35 ft	Confid.	Excellent weather echoes (Loc. Gulf of Alaska)
10 April 60	Stock Special	2025Z	11/0245Z	10 ft	"	Location: Northern Gulf of Alaska
11 April 60	Lark Special	0300Z	11/1200Z	42 ft	"	Location: Eastern Pacific near Calif.
7 April 60	Lark X-Ray Mod.	1840Z	08/0400Z	15 ft	Confid.	Location: Dogleg from Calif. to Hawaiian Islands
9 April 60	Loon Kilo	unk.	unk.	26 ft	"	(Clock Missing) Location: South of the Hawaiian Island
10 April 60	Loon Kilo	1930Z	11/0530Z	20 ft	"	" " " " "
12 April 60	Loon Kilo	unk.	unk.	21 ft	"	(Clock Missing) Location: South of the Hawaiian Island
13 April 60	Loon Kilo	2015Z	14/0415Z	17 ft	"	" " " " "
5 April 60	Loon Mike	2020Z	06/0230Z	15 ft	Confid.	Location: Southwest of Hawaiian Islands
2 April 60	Gull Sierra	1100Z	02/2045Z	16 ft	Confid.	(Out of Focus)
3 April 60	Gull Sierra	1440Z	03/1045Z	7 ft	"	
4 April 60	Gull Sierra	1405Z	05/0040Z	20 ft	"	(Misframed - film still usable)
5 April 60	Gull Sierra	1000Z	05/2100Z	34 ft	"	(Picture quality poor)
6 April 60	Gull Sierra	1100Z	06/2130Z	13 ft	"	(No radar pictures)
7 April 60	Fox Able	0200Z	Unk.	25 ft	"	(Poor picture quality) Location: Unknown
8 April 60	Gull Sierra	1120Z	08/1607Z	13 ft	"	
9 April 60	Gull Sierra	1110Z	09/2150Z	20 ft	"	
10 April 60	Gull Sierra	2340Z	11/0225Z	4 ft	"	(Excellent weather echoes)
11 April 60	Gull Sierra	1110Z	11/2130Z	14 ft	"	
12 April 60	Gull Sierra	1400Z	12/2045Z	14 ft	"	(Excellent weather echoes)
13 April 60	Gull Sierra	1300Z	13/2100Z	17 ft	"	
13 April 60	Gull Special	2355Z	14/0700Z	17 ft	"	(Excellent weather echoes) Location: Atlantic Ocean East of Bermuda
14 April 60	Gull Sierra	1840Z	14/1845Z	1 ft	"	
7 April 60	Buzzard India	2200Z	08/0700Z	25 ft	Confid.	
8 April 60	Buzzard Special #17	1040Z	08/2040Z	27 ft	"	Location: Sea of Japan
9 April 60	Buzzard Hotel	2230Z	09/2230Z	<1 ft	"	Only two frames available Location: Unknown
10 April 60	Buzzard Special #21	2240Z	11/0740Z	10 ft	"	Location: Sea of Japan - Yellow Sea
11 April 60	Buzzard Special #29	2215Z	12/0830Z	17 ft	"	Location: Sea of Japan - Yellow Sea

Blank page retained for pagination

APPENDIX D

THE PHOTOGRAPHIC AND PHOTOGRAMMETRIC ASPECTS OF TIROS I*

D. 1 Introduction

Since the successful 1 April 1960 launch, 1095 orbits have been made (15 June 1960, Kaena); 17, 449 and 5, 503 frames have been read out from the Fort Monmouth and Kaena Stations, respectively; total 22, 952 frames. Included are 51 orbits that were read out at both stations. Between 15, 000 and 17, 250 of the photo frames transmitted have been found to be usable.

The responsibility for the photographic handling and the photogrammetric aspects of all photo images received from TIROS I was assigned to the United States Navy Photographic Interpretation Center (hereafter NPIC).

The unprocessed film, obtained at both readout stations by photographing the cathode ray tubes during commanded transmissions from the satellite, was to be forwarded to NPIC regularly. NPIC was to direct the processing of the film which was to be undertaken by the Navy Photographic Center (hereafter NPC); distribute prescribed copies; analyze, catalog and maintain a library file of all film; photogrammetrically verify or correct the exact location of selected frames; and, in conjunction with the USWB computer equipment, prepare

*This section was prepared by the United States Navy Photographic Interpretation Center. The work was sponsored under MIPR 60-702, under ARPA Order No. 26-59.

latitude-longitude grid overlays for the selected frames, and produce a 35mm composite negative therefrom for distribution.

D. 2 Photographic Processing

NPIC received exposed, undeveloped film from readout stations at Kaena Point, Fort Monmouth and RCA, Hightstown. This film was first assigned a processing number which is consecutive with each roll of film from each station. Along with this number, a letter is prefixed to indicate the readout station: "K" designates original film from Kaena Point; "M" designates original film from Fort Monmouth, N. J.; "H" designates negatives made of re-run tapes of Kaena Point by RCA: "J" designates re-run tapes of Fort Monmouth by RCA. In the early phases of the program, NPIC received reverse polarity playback positives from each readout station. This film was identified "PK" or "PM". However, these playbacks were discontinued at an early date and no dissemination was attempted.

The unprocessed film (" Original") was sent to the Naval Photographic Center by messenger where it was programmed into their workload. This film was spliced chronologically by roll and orbit insofar as was identifiable and practical prior to processing. The original negatives were processed at 45 ft. per minute in an Eastman Capstaff negative developing machine that was designed for and installed at NPC by the Eastman Kodak Company. It was developed in NPC negative formula N8, which is slightly less active than D-76, to a gamma of 1.30. Processing temperatures are maintained at 70°F, controlled by Honeywell Temperature Control Units.

Next they went to the sensitometry section where densities were read by technicians utilizing Westrex RA-1100F Densitometers, examining areas of .01" by .15". The proper light value was assigned to each group of negatives with corresponding edge notches thereby preparing for printing. The printers used for printing "Master Positives", "Release Positives", and "Duplicate Negatives" are Depue Micro film printers. These are of tension-roller type with no sprocket registry. A program, furnished by the sensitometry section, was set up on Depue Automatic light control boards which control exposure voltage settings. An automatic selector, actuated by a microswitch along the film travel, selects these settings consecutively. The film, traveling at about 90 ft. per minute retains this switch in its open position. The microswitch closes as it drops into one of the recess notches along the edge of the film thereby adjusting the light intensity for the next series of negatives.

"Master" film positives are made from the original negative in a similar processing procedure to that of the original except that they are developed to a 1.15 gamma; they are used for making "Release" dupe negatives. The release positives and dupe negatives are developed in an Eastman Capstaff 35mm positive developing machine, to a gamma of 1.80. These are developed at a rate of 115 ft. per minute; the developer used is NPC-P9 formula.

D.3 Photographic Analysis

Upon receipt of the release positive for NPIC use, the analysts reviewed, edited and organized it. Analysis was restricted to numeric

identity, film quality in general and a brief consideration of frame content. Cataloging and initiation of an IBM card system for ultimate rapid recovery by frames was instituted. As more accurate and usable locational data became available, appropriate information was incorporated into the system.

In order to correct for image distortion, telereadex coordinate readings have been recorded from the photo negatives of the monitor display of the polar target made by the D3, wide angle camera. The monitor display calibration pattern was similarly recorded. From these and coordinate readings of registration marks on actual TIROS photography, a computational method has been established for determining and correcting the amount of stretching of horizontal dimensions relative to vertical dimensions from any two camera markers and their center crosses.

D. 4 Photogrammetric Aspects of TIROS I

The unavailability of accurate locational and attitude information introduced a major, confusing situation. However, after extensive message-search, liaison, calculations and interpolations, sufficient data has been acquired to virtually perfect the programming system for the IBM 704. Final testing and proving for grid production is currently well underway.

In order to prove the Church Method of tilt determination for location in space of the satellite and facilitate the problem of gridding TIROS photographs, all TIROS film for the first seven hundred orbits was screened for land area coverage including a minimum of three

well identified ground points. The identified ground points were located to the nearest minute of latitude and longitude on World Aeronautical Charts. These points were then read on the telereadex and the X-Y coordinates of points on the photograph were correlated with the known WAC ground positions. This information was then programmed into the 704 computer to establish the spacial location of the satellite and ground coverage of the photo frame.

Seven-hundred fifty nine (759) photographs were selected out of the 88 orbits for this computation. On completion of this phase, about 400 photographs will be computed on the 704.

Following this effort, the same photographs were used to prove accuracy using one well identified ground location and five horizon points. Similar telereadex computation and programmed input result in grid information in a tabular form.

From either or both methods, tabulated data concerning latitude and longitude were printed out from the 704. Although the grid drawing unit(to be used with the 704) is not yet available, the print-out data has been hand plotted, appropriate points connected and proper grids produced.

No difficulties are expected in the production of these items although somewhat time consuming. When a significant quantity of these products have been produced, distribution will be effected by NPIC. Meteorologically selected frames of interest will be similarly produced and distributed.

Blank page retained for pagination

APPENDIX E

WHOLE SKY CAMERA PROGRAM OF TIROS I*

E. 1 Introduction

A whole sky camera network was set up and operated during periods when TIROS I was scheduled to take pictures over the New England area. The stations which participated in this program were located at Bedford, Worcester and Woods Hole, Massachusetts and Bradley Field, Connecticut. The sky camera at Woods Hole used 16mm time lapse color film, while the others used TRI-X 620 film. A description of the sky cameras and the use of whole sky photos in the interpretation of cloud patterns is discussed by Conover (1959).

E. 2 Program Summary

During the operation of TIROS I, the whole sky camera network was alerted and picture taking times were coordinated between the stations by personnel of the Geophysics Research Directorate. At the conclusion of the operation, the film was forwarded to GRD. Examination of the film and comparison with TIROS I photos taken in the New England area show that simultaneous photos were obtained on 23 occasions. The results of this comparison of whole sky camera and TIROS I photos are shown in Table 1.

*This section was written by F. R. Valovcin, J. A. Leese, Geophysics Research Directorate

E. 3 Acknowledgments

Weather Bureau personnel at Worcester, Massachusetts and Bradley Field, Connecticut and Dr. William Von Arx and his group at Woods Hole, Massachusetts very kindly gave their time to operate the whole sky cameras upon request.

TABLE 1

SIMULTANEOUS PICTURE TAKING TIMES OF WHOLE SKY CAMERA AND TIROS I PHOTOS

Number	Date	TIROS I Orbit	Bedford	Worcester	Bradley Field	Woods Hole
1	6 Apr 60	75M - Direct	1549	None	1549	None
2	7 Apr 60	89M - Direct	1513	1513	1512	Reel 1
3	7 Apr 60	90M - Direct	1654	1655	1654	Reel 1
4	9 Apr 60	117M - Direct	1325	1325	1325	Reel 2
5	9 Apr 60	118M - Direct	1508	1507	1508	Reel 2
6	10 Apr 60	132M - Direct	None	1415	1415	Reel 2
7	10 Apr 60	133M - Direct	None	1557	1557	Reel 2
8	12 Apr 60	161M - Direct	1412	None	1413	Reel 3
9	16 May 60	658M - Direct	1911	1911	1911	Reel 4
10	16 May 60	659M - Direct	2052	2052	2052	Reel 4
11	17 May 60	673M - Direct	1958	None	1958	Reel 4
12	19 May 60	701M - Direct	None	1820	1820	Reel 4
13	19 May 60	701M - Direct	1855	1835	1835	Reel 4

TABLE 1 (Cont'd.)

SIMULTANEOUS PICTURE TAKING TIMES OF WHOLE SKY CAMERA AND TIROS I PHOTOS (Cont)

Number	Date	TIROS I Orbit	Bedford	Worcester	Bradley Field	Woods Hole
14	20 May 60	716M - Direct	1910	1910	1911	Reel 4
15	26 May 60	801M - Direct	1537	1541	1536	None
16	26 May 60	802M - Direct	1718	1718	None	None
17	26 May 60	803M - Direct	1904	1904	None	None
18	26 May 60	803M - Direct	1919;1920	None	1919	None
19	2 Jun 60	904M - Direct	1805	1805	1805	None
20	2 Jun 60	905M - Direct	2016	None	1945	None
21	3 Jun 60	918M - Direct	1743	1712	1712	None
22	3 Jun 60	919M - Direct	1835;1910	1855	None	None
23	6 Jun 60	962M - Direct	1758	1758	None	None

APPENDIX F

METEOROLOGICAL SUMMARIES OF TIROS I DATA--NORTHERN HEMISPHERE*

F. 1 Introduction

A vast number of satellite cloud photos came into being after the successful TIROS I operation. In order to alleviate potential researchers of the arduous task of examining some 23,000 satellite photos for interesting and provocative cloud features, a brief summary of those TIROS I orbits for which synoptic data were immediately available is presented in this Appendix. Consequently, the meteorological summaries are limited at this time to Northern Hemisphere coverage. The method used was to examine the pertinent satellite cloud photos without recourse to exact rectification of the photos and compare them with the most nearly concurrent synoptic map. This method could be described in general terms as a first approximation in the research of satellite cloud data.

F. 2 Form and an Explanation of the Abbreviations used in the Meteorological Summaries

1. Readout Orbit Number and Location of Readout Station
    a. K: Kaena Point, Hawaii
    b. M: Fort Monmouth or Belmar, N. J.
2. Approximate Greenwich Civil Time (GCT) that TIROS I began taking pictures

*This section was written by J. A. Leese and F. R. Valovcin, Geophysics Research Directorate

3. Mode of Operation

a. Direct: TIROS I was within a 1000 mile radius of a readout station and was commanded to take pictures and transmit same directly to the readout station.

b. Tape or P. B. Pix: TIROS I was commanded to take pictures and store same on magnetic tape for later relay to the readout station.

4. Camera Numbers

a. C1 or (1): Narrow Angle System or Camera 1

b. C2 or (2): Wide Angle System or Camera 2

5. Number of photos taken with each camera on direct and/or tape:

a. 37 Direct - 12(2) 25(1): Thirty-seven (37) pictures taken on Direct mode of operation. Twelve (12) Camera 2 frames and twenty-five (25) Camera 1 frames.

b. 38 Tape - 31(2) 7(1): Thirty-eight (38) pictures taken and put on tape. Thirty-one (31) camera 2 frames and seven (7) camera 1 frames.

6. General geographical area where pictures were taken

7. Summary of the operation during a particular orbit.

F.3 METEOROLOGICAL SUMMARIES OF TIROS I DATA

1 April 1960

1M 01/1336 - 27(2) Direct - Many Hi Nadir - Gaspe Peninsula and Western Atlantic

Band of clouds west toward Great Lakes. Clouds to east of Gaspe Peninsula associated with frontal system in this region.

2M 01/1518 - 10(2) Direct - Gaspe Peninsula and Western Atlantic

Path is just south of 1M and shows essentially same area.

3M 01/1658 - 23(2) Direct - Western Great Lakes, across NE US and Western Atlantic

Shows extensive cloud cover associated with vortex off coast of New England. Band extends S from this vortex associated with cold front. Generally scattered to SE of this system.

3K Blank

4M 01/1841? - 34 Direct - 28(2) 6(1) - N Central US SE to Virginia and Atlantic

Shows clouds to north of low centered over Eastern Nebraska. Band of clouds across Great Lakes between this low and low in Atlantic is also shown. Pix stop just off coast with Delaware and Chesapeake Bay shown as landmarks. Second set of direct taken SE of cold front and shows mainly scattered Cufm with some street patterns.

4K Blank

5M 01/2022 - 37 Direct - 12(2) 25(1) - Midwest and Gulf States, across Gulf of Mexico and Caribbean

Camera 2 pix show vortex centered in Iowa with band extending S from vortex and associated with cold front on Surface Chart. Also some clouds along Gulf Coast - Camera 1 pix taken over Gulf of Mexico and Caribbean show scattered Cu with some street formations.

7K 01/2200 - 38 Tape - 31(2) 7(1) - NE Pacific then SE to Baja, California

Appears to have started slightly earlier than programmed. First pix show vortex which would be located to west of large vortex shown on surface chart centered near 50N 150W. This larger vortex shows later along path. Scattered low Cufm to S of both of these vortices. Band associated with cold front shown SE of the larger vortex. Multiple layers of clouds present to SE of frontal band. Clear over Baja, Calif. and surrounding waters. This band could be Cifm to south of clear area.

7K 01/2340 - 7(2) Direct - Mid Pacific S of 7K Tape

Shows scattered Cu to S of vortices described in 7K tape along with Srn extension of frontal band.

7K 01/2346 - 26(2) Direct - Pacific about midway between US and Hawaii

Frontal band on horizon, same band as described in two previous series of 7K. Shows clear area SE of band with broken multiple layers SE of clear area.

2 April 1960

8K 02/0104 - 18 Tape - Rest Hi Nadir - NW Pacific and Eastern Asia

Mainly scattered over Asia with increasing clouds over Japan and East culminating in extensive cloud cover in vicinity of open wave with vortex centered near 46N 162E. Band associated with cold front extending from vortex.

8K 02/0123 - 7(2) Direct - Mid Pacific NW of Hawaii

Band of clouds probably associated with warm front of wave described in 8K remote. This band continues SE and appears to be continuous through the ridge of high pressure although it appears weak. The surface analysis has washed out any front through this ridge. The contents of pix can be fitted to some degree to surface analysis, but nadir angles seem quite low for this far north.

8K 02/0129 - 10 Direct - 1(2) 9(1) - Pacific S of Hawaii

Few cu; increasing clouds on last two frames.

9K 02/0250 - 31 Tape - Asia and Western Pacific

First few frames show band associated with front in Northern China. Clear to scattered along coast of China and sea of Japan. Increasing clouds toward Japan and East. Relatively broad band associated with cold front in Pacific. Mostly clear SE of this band. (Band and clear are missing from reruns but show on originals.) Also two direct are on originals but not on reruns. A sequence of 16 Camera 1 Tape is on this orbit but cannot determine location. Then a sequence of 2(2) 2(1) Direct which is apparently in vicinity equator shows scattered Cufm.

14M 02/0755 - Tape - Blank

15M 02/1105 - 32 Tape - Eastern Atlantic, Southern Europe, and Eastern Mediterranean

Pix show frontal system and circulation of deep vortex centered near 50N 20W with frontal band around Southern periphery of vortex. Alps "cloud" visible. Cloud mass over Southern Italy and Greece associated with low over this region. Band of clouds extends eastward from this area of low in region of cold front on surface chart.

16M 02/1249 - 46 Tape - 31(2) 15(1) - Eastern Atlantic, Spain, Western Mediterranean and N. Africa

View of same frontal system and vortex as described in 15M. Eastern Spain, Western Mediterranean and N. Africa mostly clear.

16M 02/1425 - 8(1) Direct - Gaspe Peninsula

Clear to scattered.

17M 02/1446 - 20 Tape - Remainder Dark

Pix started over Nigeria at approximately 10N. Shows mainly clouds associated with ITCZ in form of bright patchy overcast-scattered Cufm S of this zone.

17M 02/1602 - 6(2) Direct - N Central US

Nadir angles relatively high for any details but mostly clear area seen with increasing clouds to east probably associated with low over Minnesota.

17M 02/1610 - 16 Direct - 4(2) 12(1) - NE US and Western Atlantic

Gaspe Peninsula mostly clear with overcast band further S in vicinity of Mass. extending East in association with frontal system as shown on surface analysis.

17K None

18M 02/1631 - 25 Tape - 18(1) 7(2) - Remainder of Camera 2 Dark

Should be located in S Atlantic and Southern tip of Africa.

18M 02/1746 - 6(2) Direct - Mid West US

Extensive cloud mass associated with low over Minnesota as described in first direct sequence of 17M.

18M 02/1754 - 7 Direct - 3(2) 4(1) - Atlantic off coast of Southern US

Contents of pix would indicate a vortex; however, in region where pix were programmed to be taken there is no indication of a vortex on surface analysis. Doubtful this could be vortex over Minnesota.

18K None

19M 02/1912 - 12 Tape - Remainder Hi Nadir - Eastern Pacific

First distinguishable pix show scattered to broken Cufm S of an apparent vortex which may be vortex near 58N 140W. A bright band mainly E-W appears to be over lower Sc. For this reason the band does not appear to be a frontal band and could be a heavy band of Cifm clouds.

19M 02/1930 - 3 Direct - 1(2) 2(1) - Midwest US

Scattered to broken Cufm SW of edge of overcast associated with low over Minnesota.

19M 02/1937 - 10 Direct - 4(2) 2(1) - Caribbean SE of Florida

Noise throughout makes recognition difficult but appears to be mainly scattered Cufm.

19K No useable pix

21K 02/2101 - 55 Tape - 31(2) 24(1) - N Pacific SE to SW US and Mexico

First few frames show bands associated with occluded front in NW Pacific. East of these bands are scattered to broken Cufm and the vortex of Aleutian low described in 19M tape. The band in the Eastern Pacific described in 19M tape and thought to be dense Cifm appears on this sequence and must be associated with warm front on surface analysis although the appearance of a high band overriding lower clouds is still present. This may be good example of a strong warm front and if so differs from cold front by its ragged edges along the band. SW US is predominately clear with scattered clouds to east.

21K 02/2252 - 4 Direct - 2(2) 2(1) - Pacific between Hawaii and US

Shows band of clouds near horizon associated with cold front. Appearance of multiple layers of clouds to SE of this band.

3 April 1960

22K 03/0004 - Tape - Blank

22K 03/0029 - 24(1) Direct - Mid Pacific

22K 03/0038 - 10 Direct - 5(2) 5(1) - Pacific E of Hawaii

Mainly broken multiple layered clouds.

23K 03/0154 - Tape - None

23K 03/0213 - 12(1) Direct - Mid-Pacific

28M 03/0520 - 18 Tape - Location doubtful due to time of pix start but probably over China and Pacific

Extensive cloud cover shown on pix could be over China as data on surface map shows this region to be mostly overcast.

29M 03/1014 - 32 Tape - N Atlantic off coast of France, across Southern Europe to Persian Gulf

Vortex shown centered near 50N 20W. Another vortex with occluded front centered near 50N 5W. Alps "cloud" visible. Cloud cover over Greece and Turkey probably associated with low over Turkey. Cloud cover appears as bright band. Small band clouds over Northern Persian Gulf.

30M 03/1155 - Tape - Blank

30M 03/1331 - 27(2) Direct - Many Hi Nadir - Gaspe Peninsula and Western Atlantic

Extensive cloud cover over St. Lawrence, relatively small clear area over Newfoundland. Generally broken to overcast over Western Atlantic--no significant patterns.

31M approx 03/1515 - 10(2) Direct - No pix programmed for this time but contents of pix reveals they were taken in same area as 30M. Clear area vicinity Newfoundland also shows on these pix. Otherwise mostly overcast.

31K 03/1346 - 32 Tape - Eastern Atlantic off coast of NW Africa and Spain through NW and Central Africa

Contents of first frames indicates pix started approximately 3 min early. Shows band associated with warm front in Eastern Atlantic. Mostly clear over NW Africa. Clouds in region of ITCZ indicate a wide but relatively weak zone.

32M -3/1652 - 24 Direct - 12(2) 12(1) - North Dakota, across Great Lakes, NE US and Western Atlantic.

Band on first few frames probably associated with occluded front through N. D. Small separation between this band and beginning of extensive cloud cover over Eastern US. Western Atlantic generally broken Cufm, with some multiple layers.

32K 03/1524 - 32 Tape - Eastern Atlantic from approximately 35N 30W SE through Africa

Band of clouds toward horizon on first few frames probably associated with cold front in mid-Atlantic. Mainly scattered low Cufm cells SE of this band. Clear along coast of Africa and inland to region of ITCZ. The ITCZ generally patchy overcast and appears much stronger than the region seen in 31K.

33M 03/1710 - 32 Tape - No program for these pix but this is probably read-out of pix scheduled to be started at 1710Z in which case the location is the Mid-Atlantic from approximately 20N

First few frames show two narrow bands apparently Cifm in E-W direction with scattered Cufm below. ITCZ shows narrow band of bright patchy overcast-scattered low Cufm S of this zone. Region of mottled broken clouds mainly Cufm toward end of picture path. A "doughnut" shaped cloud appears in this region on eight different frames. Last two frames quite dark.

33M approximately 03/1840 - 9(2) Direct - Contents of pix indicates region of coverage to be in Atlantic off coast of Florida

Extensive cloud cover toward horizon of first few frames with remainder showing numerous Cu street formations.

36K 03/2014 - 31 Tape - Eastern Pacific off coast US, through SW US, Gulf of Mexico and Central America

Appears to have started late as band of clouds associated with cold front at surface is shown toward horizon of first frames. Bright band nearer center of these same pix could be stratus deck off W coast US. Few clouds over SW US. Bright band over Southern Gulf and Yucatan Peninsula associated with quasi-stationary front. Region in vicinity ITCZ shows bright patches.

36K 03/2335 - 6 Direct - 3(2) 3(1) - Mid-Pacific

Shows occluded system in mid-Pacific in region where cold and warm front join to form occlusion. Shows two distinct bands joining to form a combination.

36K 03/2344 - 12 Direct - 5(2) 7(1) - Pacific East of Hawaii

Shows band associated with cold front in this region. Multiple layers SE of this band. Further south shows region of relatively uniform Cu cells.

4 April 1960

37K 04/0101 - 23 Tape - Many High Nadir - Eastern Asia and Western Pacific

First frames of recognizable features show the clouds associated with front and vortex centered near 47N 135E. Large area with Cifm clouds to E of this vortex. Increasing Cufm clouds to E of high pressure area and approaching cold front. This region very mottled in appearance resulting from multiple layers of clouds. Frontal band does not appear on pix.

37K 04/0120 - 8 Direct - 4(2) 4(1) - Region NW of Hawaii SE from 30N 180

Frontal band appears toward horizon with area of mostly clear S of band. Increasing Cufm clouds south of clear area.

37K 04/0129 - 11 Direct - 5(2) 6(1) - SE from 5N 155W in mid-Pacific

Shows mainly clouds associated with ITCZ.

42M Blank

43M 04/0928 - 32 Tape - Rumania, Turkey, Persian Gulf and Arabian Sea

Patchy overcast over Southern Europe with band of clouds E-W across Mediterranean representative of frontal band. No front shown on surface analysis at this time although one was drawn on earlier analyses. Mostly clear over remainder of picture path.

44M 04/1104 - 31 Tape - Eastern Atlantic off coast of France and Spain, across Southern Europe, Mediterranean and Red Sea.

First frames show Cufm clouds to W of frontal system in Atlantic. Band of clouds in Atlantic associated with cold front. Another band appears to cross over frontal band and over Southern France ending abruptly on Mediterranean coast. 30 MB Chart shows high wind speeds in vicinity of band diminishing to about half at approximately the same place as cloud band ends. Vortex appears to N of point where bands apparently cross adding to complexity of situation already vividly displayed on surface analysis. Alps "cloud" visible. Weak band of clouds N-S across Italy and Mediterranean could be cloud position of front shown further W on surface analysis. Thin band Cifm across Northern Red Sea probably associated with jet stream.

45M 04/1414 - 9(2) Direct - NE US and Atlantic

All high nadir angles

45K 04/1246 - 32 Tape - Atlantic from 45N 25W across Southern Spain, NW and Central Africa

Extensive Cufm associated with some patchy overcast of probably Cifm clouds. Southern extension of cold frontal band and also crossing of two bands described in 44M visible. Mainly scattered clouds E of band with small region of overcast off coast of Portugal. Scattered clouds along Mediterranean coast of Africa. Clear until last few frames where streaks of Cifm appear and S of this the beginning of ITCZ.

46M 04/1559 - 21 Direct - 13(2) 8(1) - Northern US and Western Atlantic

Generally scattered on first few frames increasing to mostly overcast associated with secondary front vicinity Wisconsin. NE US also extensively overcast indicative of the complex primary and secondary fronts shown on surface analysis. Band of clouds extends SW from this massive overcast-broken Cufm with uniform cells E of this system. Narrow angle pix show that many smaller cells go together within these larger cells.

47M 04/1743 - 25 Direct - 12(2) 13(1) - South of track of 46M direct

Scattered clouds on first few frames. Weak band probably associated with front just E of Rockies. Relatively broad band associated with front in Southern U.S. Scattered Cu streets E of this band. Street goes through center of frame on Camera 1.

47K 04/1429? - 30 Tape - Pix programmed to start at 04/1515 but contents and location of pix reveal the starting time to be approximately 04/1429. Area covered from mid-Atlantic 40N 35W SE through NW Africa along Atlantic coast.

First few frames show extensive Cufm associated with anticyclone centered near 38N 54W. Band associated with cold front very sharply defined and bright reflectivity. Few clouds SE of cold front to African coast. Clear over Africa. Cloud cover associated with ITCZ begins in vicinity of Gulf of Guinea but does not show typical cloud cover of ITCZ.

48M 04/1928 - 15 Direct - 8(2) 7(1) - Texas and Gulf of Mexico

Mostly clear over land. Band of clouds in Gulf associated with quasi-stationary front.

50K 04/2243 - 17 Direct - 8(2) 9(1) Eastern Pacific

Orbit with widely publicized pix of banded patterns associated with extra-tropical cyclone near 35N 140W. Frontal bands also shown on these pix.

5 April 1960

51K 05/0008 - 19 Tape - Remainder high nadir and noisy - Far northwestern Pacific, Northern China, Southern Siberia

Reflective area over Siberia could be snow cover. Clouds associated with vortex centered near 55N 150E. Clear to East of this vortex and then increasing Cufm clouds in cold air of high pressure area to NW of cold front. Cold front appears as heavy bright band. Data on surface chart indicates strong front at surface. Scattered clouds S of front. Direct pix are continuation along path after remote; however, first direct picture falls between last two remote and therefore it appears remote pix started approx 3 minutes late.

51K 05/0026 - 9 Direct - 4(2) 5(1) - Continuation along path after remote

Shows front described in remote and scattered to broken clouds south of front.

51K 05/0035 - 12 Direct - 5(2) 7(1) - Continuation of first direct

Generally broken with noise in all frames making resolution difficult.

52K 05/0212 - 14 Direct - 7(2) 7(1) - Path from 20N 175E to Eq

Patchy overcast clouds with multiple layers resembling clouds of ITCZ. Cu streets south of this zone.

57M Blank

58M 05/1146 - 32 Tape - Atlantic off coast of France, across Italy, Eastern Mediterranean and Saudia Arabia.

Band associated with front in Atlantic visible but all nadir angles make any distinguishing features difficult to resolve. Alps "cloud" visible. Clouds over Southern Italy and Greece probably associated with low in Mediterranean. Cifm clouds over Saudia Arabia could be associated with jet stream. Remainder clear.

59M No useable pix

60M 05/1505 - 13 Direct - 11(2) 2(1) - Eastern US and Western Atlantic

High nadir angles and noise deter the quality of pix but large cloud mass probably associated with wave cyclone off coast of New England.

60K 05/1519 - 31 Tape - Atlantic off coast of Spain, across Spain, Western Mediterranean and Africa

Pix may have started earlier than programmed. Cufm clouds to West of cold front on first few frames. Cold front sharply defined by bright cloud mass. Pix show patches of Cu over Spain but does not show the Cifm clouds prevalent over Central and Eastern Spain as plotted on surface map. Few clouds along Mediterranean coast of Africa. Remainder mostly clear until last few frames which has scattered clouds which may be associated with low on surface chart.

61M 05/1650 - 18 Direct - 11(2) 7(1) - Eastern US from N Dakota to Md and Western Atlantic

Pix in Western sector show region scattered to broken--no significant patterns. Vortex centered vicinity Eastern Mass. shown. Frontal band extends from this vortex, south along coast. "Christmas tree" pattern appears in same relative pattern as on Orbit 75M. Predominately broken E of frontal band.

61K 05/1519 - 30 Tape - Path from mid-North Atlantic (35N 45W) SE to equator with African coast visible on last few frames

First few frames show mass of clouds associated with frontal system north of 40N. The high pressure area to S of this system has scattered Cufm bands increasing toward S. A band of clouds is shown which is probably associated with cold front shown on surface chart. This band differs from what might be termed a typical frontal band in that it has the appearance of broken multiple layers rather than a dense and bright reflective band. This could be an example of front in process of "washing out". Another weak band possibly Cifm appears south of this frontal band. Mostly clear between this band and ITCZ. The ITCZ appears as a very narrow band with bright patches.

62M 05/1704 - 29 Tape - Mid-Atlantic from vicinity 20N 50W SE across equator

Predominately Cufm with streets or narrow bands north of ITCZ. ITCZ appears to have two separate bands of patchy overcast. Mainly scattered Cufm S of ITCZ with some street formations.

62M 05/1833 - 4 Direct -2(2) 2(1) - Midwest US

Patches of clouds with no significant patterns.

62M 05/1840 - 6 Direct - 4(2) 2(1) - Southern US and Gulf of Mexico

Clear over land except large mass in vicinity where surface analysis shows secondary cold front. Band of clouds just east of Southern Florida associated with cold front.

62K None

64K 05/2006 - 2 Tape

64K 05/2153 - 5(2) Direct - From content and nadir angles these pix are probably of Eastern Pacific and W Coast of US

Shows broad frontal band with Cufm clouds to NW of this band.

64K 05/2153 - 4(2) Direct - 4 views of vortex centered near 34N 137W

65K 05/2316 - 9 Tape - Rest high nadir - Western Pacific

Large cloud mass associated with occluded front and vortex centered near 48N 156E. Large clear area to W of this system.

65K 05/2335 - 9(2) Direct - Central Pacific N of Hawaii

Scattered Cu asociated with high pressure area NW of front. Frontal band appears quite weak to S of center of high and increasing in brightness toward NE. Band of relatively clear except scattered Cifm to N of frontal band. Multiple layers of clouds S of band.

65K 05/2344 - 9(2) Direct - Pacific SE of Hawaii

Multiple layers of clouds with street formations in lower Cu

6 April 1960

66K 06/0100 - 23 Tape - Rest high nadir. Noise and partial blanks make many of the frames very poor. Coverage should include Eastern Asia between 45N and 50N, Northern Japan and Western Pacific to 30N 170E

Very broad band on last few frames in vicinity of warm front drawn on surface analysis. Path goes over Southern part of deep low pressure system but noise makes it difficult to determine presence of vortex on pix.

66K 06/0120 - 6(2) Direct - Region West of Hawaii from 20N 180 to 10N 168W

Multiple layers of clouds giving pix a mottled appearance. No significant patterns.

71M 06/0426 - 31 Tape - 45N 90E Southeast across China and Western Pacific to approximately 10N

Clouds associated with occlusion and vortex (centered near 65N 100E) are shown toward horizon on first few frames. Remainder of China mostly clear except for small vortex near Shanghai. Band of Stfm clouds at approximately 20N to 25N. Band, shown by data on surface chart, consists mainly of alto stratus. Mostly clear south of this band.

72M 06/0923 - 31 Tape - Southern Europe, Turkey, Persian Gulf and across Arabian Sea.

Alps "cloud" visible on first few frames. Bright cloud mass over Greece and Turkey. Small Cifm bands over Persian Gulf could be associated with jet stream. Remainder mostly clear.

73M 06/1103 - 31 Tape - Atlantic west of France and Spain through these countries, across Mediterranean and through Africa

Frontal system and vortex visible on first few frames. Clear between this system and front through France and Spain. Wisps of clouds mainly Cufm and some Cifm along African coast of Mediterranean. Remainder mostly clear.

74M 06/1412 - 14(2) Direct - Gaspe Peninsula and Western Atlantic

Band of clouds visible but due to intermittent pictures and high nadir it is difficult to give general location.

74K 06/1242 - 32 Tape - Eastern Atlantic across NW Africa through to Central Africa

View of frontal system and vortex from the Southeast side. Same system as seen on 73M. Other front seen on 73M through France and Spain shows as diffuse clouds near coast of NW Africa. Some Cifm trails extend into Africa remainder mostly clear until Southern most part of path of pictures where evidence of ITCZ appears in the form of broken Cufm.

75M 06/1557 - 23(2) Direct - N Dakota, Lake Michigan, New York and Western Atlantic

Mainly scattered to broken up to a band associated and ahead of occluded front through Wisconsin. Entire region reporting snow showers and band shows bright reflection--from Eastern Ohio to Atlantic stations report Sc and Cu. This shows on pix similar to an area of snow and forest cover. Band in Atlantic associated with front on surface map. This band contains the "Christmas tree" formation in same relative position as on 65M.

75K 06/1431 - 32 Tape - Atlantic from 30N 25W SE across W coast Africa.

Scattered to broken Cufm over Atlantic with band (apparently Cifm) running E-W from horizon of first pix to Africa. Predominately clear along coast and down to ITCZ. Bright patchy clouds within this ITCZ with fibrous veils extending from these bright patches.

76M 06/1614 - 31 Tape - Mid-Atlantic SE from 15N

Multiple layers of clouds with dense streets of low Cufm. Decreasing cloud cover to Eq and mainly scattered S of equator. Frames become dark at end.

76M 06/1741 - 6(2) Direct - Nebraska SE to Georgia

Cold front drawn on surface chart but pix show nothing resembling frontal band. Peculiar cloud formation over Nebraska with circular cloud mass and cloud mass at center. Low, mid and high clouds reported over this area could combine as random clouds to give this appearance.

76M 06/1749 - 10(2) Direct - Path from E Coast Florida to lee side of Windward Islands

SE clear. Increasing cloud cover from off coast Florida to frontal band over Cuba and Hispaniola.

78K 06/2057 - 2(2) Direct - NE Pacific - Wide Frontal band on one frame. Other Presumably Cufm clouds NW of frontal band.

79K 06/1916 - 23 Tape - Rest high naidr and noise - NE Pacific, SW US to vicinity Yucatan Peninsula

First frame of distinguishable quality shows decaying vortex centered on surface map near 38N 132W. Cloud bands indicate possibility of analysis somewhat different than shown on surface map and that front may not be washed out as completely as would be indicated by analysis. Clouds from above system extend into California. Scattered to broken over SW US and mainly clear over Northern Mexico. Cirrus band E-W with trailing bands to S probably associated with jet over Southern Mexico. Reflective area S of this band of indeterminate origin with possibility that it could be snow on mountains.

79K 06/2240 - 9(2) Direct - Mid Pacific 30N to 45N; 155W to 175W

Extensive overcast in region of occluded system in mid-Pacific. Broken Cufm to east of frontal system in ridge of high pressure.

79K 06/2249 - 7(2) Direct - Extension of previous direct to region east of Hawaii

Good view of cold front and occlusion with vortex near 45N 145W and also the extensive field of low Cufm in the cold air to NW of this system. Extensive cloud cover with the appearance of multiple layers to south of cold front.

7 April 1960

85M 07/0016 - 30 Tape - 8 Hi Nadir - Coverage 45N 155E to 0N 160W

Apparent frontal band on last few frames with extensive clear area to NW of band. No agreement with surface analysis and could mean pix started approximately 5 minutes early (after examination of 94K Tape, possibly 10 minutes early).

86M 07/0830 - 31 Tape - SE Europe, Iran, Persian Gulf and into Arabian Sea

Alps "cloud" on first few frames. Bright cloud mass over Turkey and Black Sea. Remainder mostly clear. Good agreement with surface map where data are present.

87M 07/1009 - 28 Tape - Atlantic just W of France across Mediterranean to Southern part of Red Sea

Clouds with no significant patterns over France. Alps "cloud" visible. Mostly scattered over Mediterranean. Cifm bands across northern part of Red Sea. Apparently associated with jet stream.

88M 3(2) Direct Hi Nadir

88K 07/1152 - 31 Tape - Atlantic west of Spain through Central Africa

Cloud mass part of occluded system in Atlantic. Band of clouds west of Spain to about 45N 15W. Surface chart 12 hours earlier shows cyclonic vortex in this vicinity but has filled by time of pix. This could be example of cold front aloft. Some bands partly Cifm over NW Africa. Remainder mostly clear to ITCZ on last few frames.

89M 07/1502 - 11 Direct - 8(2) 3(1) - Mainly NE Coast of US and surrounding Atlantic

Clouds associated with low off New Jersey coast but high Nadir angles make more detailed analysis difficult.

89K 07/1335 - 31 Tape - Central Eastern Atlantic through central coast of West Africa

Bright band on pix in approximate position of cold front at surface. Cufm bands around NE sector of Bermuda high. These bands better depict the streamlines of 700 and 500 MB than the surface which as in the previous orbit is difficult to reconcile the pictures with the surface chart in the extreme eastern Atlantic. Fibrous Cifm bands in West Central Africa. Mostly clear until the ITCZ of the last few frames. (Small ring shaped cloud at approximately 26N14W).

90M 07/1646 - 32 Tape - Track from 27N 43W SE across equator through mid Atlantic

Frontal band shown on surface chart in mid-Atlantic north of 35N visible on first few frames. Mainly scattered south of this frontal band with increasing cloud cover toward ITCZ. Wide band of relatively uniform Cufm to south of ITCZ. Small street formations south of this along with patches of fibrous clouds.

90M 07/1654 - 15 Direct - 8(2) 7(1) - SE US and surrounding ocean.

Front drawn on surface chart shows as weak band dissipating toward west on pix. Bright cloud mass vicinity of ship reporting rain showers on surface chart.

91M 07/1832 - 14 Direct 7(2) 7(1) - SW US and Gulf of Mexico

Front drawn on surface chart through Texas has practically no clouds associated with it as pix show this region to be mostly clear. Gulf of Mexico mostly clear at beginning with increase in cloud cover shown on last few frames. Some bands in last few frames.

93K 07/2015 - 31 Tape - Area covered from 30N 120W SE across equator with Baja, California, visible.

Cloud mass between two frontal systems along coast of California shows as bright area on pix with no significant pattern. Extensive clear area over Baja, California, and surrounding ocean. Clouds increase S of 150N with two separate areas along path featuring cloud patterns normally seen in vicinity ITCZ.

93K 07/2147 - 6 Direct - 4(2) 2(1) - Mid Pacific around 40N 160W

Complicated frontal system drawn on surface analysis. Pix exhibit this analysis in the form of some of the broadest overcast bands yet seen with a bright reflection in the same proportion.

93K 2157 - 6 Direct - 3(2) 3(1) - Area of coverage mainly to west of remote pix of 93K beginning in vicinity of 25N 140W

Band of cold front segregated from clouds of surrounding area by narrow clear areas on either side in such a manner that one is led to believe the development of this sytem was done in accordance with the textbook.

94K 07/2314 - 9 Tape - Rest high nadir. Western Pacific mainly of vortex with occluded front centered at 47N 152E

Analysis shows this occlusion to be washed out near center on surface chart. . Pix show frontal band wrapped around the eastern periphery and spiraling into center of vortex from NW quadrant. Pix of 85M covers same area approximately 23 hr earlier although it was difficult to correlate with surface due to high nadir and not starting as programmed.

94K 07/2330 - 4 Direct - 2(2) 2(1) - Extension of coverage from where tape stopped and shows band which was only partially visible on last of remote

Surface analysis shows a stationary front in this area.

94K 07/2337 - 7 Direct - 3(2) 4(1) - Coverage should include Hawaiian Islands but impossible to verify due to cloud cover

Patterns difficult to ascertain due to multiple layers of clouds.

8 April 1960

100M 08/0427 - 31 Tape - 41N to Equator

Extensive cloudiness over China mainland and Formosa from 105E to 125E, 20N to 45N--probably result of frontal system in this area not drawn on SFC Chart--data on SFC Chart outlines this cloudy area--South of 20° TIROS shows clear to scattered to 10N. Large patchy overcast from 10° to Equator--No data on SFC Chart South of 20°.

101M 08/0918 - 31 Tape - 47N to 11N

Alps "cloud" visible--another "hook-shaped" cloud between 40 and 45N. Band of clouds from Red Sea over Saudia Arabia probably associated with jet stream.

102M Appears to have started 7 min late - banded clouds over Ern Atlantic but nadir angles are high in this region. Band of clouds over N Africa similar to those in 101.

103M 08/1412 - 3 Direct - Probably over Nrn New England

103M 08/1242 - 3 Tape - Scheduled to take over NW Africa

104M 08/1554 - 21 Direct - 18(2) 3(1)

Nadir Angles high over U. S. Wide clear area over Atlantic not seen on any of the surface data.

104K 08/1427 - 30 Tape - Ern Atlantic South from 25N

Pictures show Brkn Cufm. The few surface Reports call it everything in the books with a predominant trade Cu (low 8) some Mid and Hi Clds.

105M 08/1740 - 10 Direct - 5(2) 5(1)

Band across Southern U. S. corresponds to front on Surface Map. Surface Reports show Ci visible from Central Florida (Tampa and Orlando) but pictures show this area to be clear. Could be seeing the band across Southern Florida corresponding to jet stream at 300 MB.

105M 08/1610 - 24 Tape - South from 15N

107K All noisy and dark

108K Tape - All dark and high nadir

108K 08/2237 - 6 Direct

Northern Direct shows overcast possibly frontal band of Surface Chart 2 frames 1(2) 1(1) - Southern Direct (S of 15N) shows little discernible patterns.

109K 08/2354 - Tape

Across Eastern China - High nadir angles and dark frames.

9 April 1960

109K 09/0022 - 6 Direct

Band on horizon corresponding to cold front on Surface Chart in Mid-Pacific. Remainder clear to scattered.

114M 09/0506 - 31 Tape - Southern China-Burma area mainly across Himalayas

Mountains mainly cloud covered. No data on Surface Map.

115M 09/0827 - 31 Tape - 45N to 10N; 15E to 60E

High nadir angles in Northern Mediterranean. Cloud cover over Turkey and Eastern Mediterranean. Cloud cover over Western Persian Gulf corresponding to 300 MB Jet (No Data on map).

116M 09/1007 - 31 Tape - Front over France and Spain corresponding to surface chart. Cifm clouds over Algeria corresponding to jet on 300 MB. Remainder clear except scattered clouds on last two frames.

117M 09/1317 - 4 Direct - High nadir and dark

117K 09/1149 - 31 Tape - 40N to 10N; 25W to 20E

Path runs SE of 116M and gives view of same features as 116M from different angles. Extensive cloud cover over Africa below 15N; Probably the Eq. Conv. Zone. Some data on surface map for this area.

118M 09/1502 - Direct - 3(1) 7(2)

Pictures taken intermittently, difficult to ascertain approximate location. Thin cloud band may be cold front on surface chart, if so, then it is clear over large area behind front, rare for this region in Western Atlantic.

119M 09/1517 - 31 Tape - South from 18N through Mid-Atlantic

Mostly scattered cufm clouds above 10N.

119M 09/1645 - 9(2) Direct - through ridge in Midwest U. S.

119M 09/1654 - 9 Direct 5(2) 5(1) - Over Caribbean

Scattered to broken over area.

121K 09/2002 - 6(2) Direct

Nadir angles are high but evidence of frontal system and vortex as shown on surface map (off Californian coast) can be seen in the pictures.

122K 09/1824 - 29 Tape

Excellent quality. Path is from Pacific. Just west of California-Oregon border through SW US, Mexico and Central America. Front as shown on surface map is a band of clouds on the pictures. Also shows stratus deck off coast of Baja, California. Clouds along Texas Gulf Coast part of weak front on surface map. Mainly scattered Cufm in lower part of orbit around Central America.

122K 09/2150 - 9(2) Direct - Mid-Pacific

Shows northern part of same frontal band seen in direct of 109K (09/0022). Wave on front shown on surface map not distinguishable in pictures, probably because of angle of view.

122K 09/2154 - 8 Direct - 4(2) 4(1) - Covers region from E to SE of Hawaii

Data on map shows presence of multiple layers of clouds not directly associated with any system. Pictures give alternating camera 1 and 2 shots of this area of excellent quality and relatively low nadir angle.

123K 09/2329 - 3 Direct - 2(2) 1(1) - Path between 109K and 122K

Band of clouds on horizon corresponding to front on surface map.

10 April 1960

128M 10/0254 - 31 Tape - SE from 12N, 145E - Mainly scattered to equator

129M 10/0738 - 6 Tape - remainder above horizon

6 pictures over Arabian Sea. No data on surface chart.

130M Nothing

131M 10/1234 - 3(2) Direct - Western Atlantic - High nadir angles

131K 10/1102 - 31 Tape - Path from Northwest Africa through center of it to south of Equator. Cloud mass along Mediterranean coast of Algeria as in Orbit 116M (09/1007) and 117K (09/1149). Cloud band further south corresponding to jet of 300 MB with different shape than in 116M and 117K. Mass of clouds on horizon of earliest frames corresponds to front NW of Spain.

132M 10/1408 - 15(2) Direct - Pictures cover Western Atlantic off coast of New England. Nadir Angles are high. Band of clouds corresponding to front on surface chart is seen, but data on surface map does not show clear area behind front as in pictures.

132K 10/1243 - 31 Tape - 30N to S of Equator; 25W to 10E

No data on surface map. Analysis by clouds would give much more complicated structure than big high pressure area shown on surface map for Eastern Atlantic. Clouds over water give appearance of a series of eddies in this area. Band of thin clouds between 10N and 15N could be associated with jet stream. Eq Conv Zone appears weak without any solid band of clouds. Coast of Africa visible throughout series except first few pictures. Area of coverage similar to 118K (09/1334Z)

133M 10/1425 - 31 Tape - Through Mid-Atlantic South from 20N

Streets of Cufm at beginning then more patchy overcast farther south toward Eq Conv Zone.

133M 10/1552 - 8(2) Direct - Atlantic off coast of SE US

Converging bands corresponding to cold front and wave cyclone drawn on surface map.

136K 10/1734 - 27 Tape - SW US, Wrn Gulf of Mexico, Yucatan Peninsula and Central America

Band of clouds could be front off west coast of U. S. Clouds probably low Stfm present all along Gulf Coast. Heavy cloud masses over Central America. See nothing in pictures similar to frontal system over Rockies on surface map.

136K 10/2051 - 5 Direct - Massive cloud bands in region of wave cyclone on surface map. Nadir angles high for any close determination of the validity of surface analysis by these pictures.

136K 10/2100 - 4(2) Direct

Massive cloud cover lacking any significant detail or pattern to east of Hawaii.

137K 10/2235 - 6(2) Direct - Through Mid-Pacific NW of Hawaii

Cold front drawn on surface map is depicted in pictures as one solid band of high reflective cloud mass. Small wave on surface chart is not in evidence in the pictures. Front is very sharply defined in pictures.

137K 10/2243 - 14 Direct - 8(2) 6(1) - Region S-SE of Hawaii from 15N

Starts with broken Cufm and changes to patchy overcast as it approaches Equator.

137K Remote was started south of 10N. Entire series including remote and two direct sequences have some of best quality pictures seen.

11 April 1960

143M 11/0159 - 31 Tape - Path SE from 21N 145E

Front on surface chart does not show on pictures except may be on horizon which is not in agreement with analysis location if picture time is correct. If what appears to be land in first few frames is either Guam or Saipan, then pictures probably started 3 or 4 minutes late.

144M 11/0824 - 28 Tape - Coverage across SE France, Mediterranean, Saudia Arabia along Red Sea, and Gulf of Aden

High nadir angles in first few frames. Clouds over Mediterranean in region of low pressure area without any significant pattern. Clouds over southern part of Red Sea in patches rather than banded or line pattern of previous days.

145M 11/1010 - 31 Tape - Coverage from Mediterranean coast of Algeria through Central Africa to about 4S.

Clouds toward horizon off Atlantic coast of Spain and Portugal. Clouds over Algeria and French West Africa show line or street pattern and could be associated with jet stream. Last 10 frames show heavy broken of equator conv. zone and this zone appears stronger from cloud pattern than on previous days. Located approximately 10N to 5S.

146M 11/1321 - 4(2) Direct - Very high nadir

146K 11/1149 - 32 Tape - NW coast of Africa through Africa to about 5S

Heavy broken to overcast off coast with some wisps of probably Cifm extending into Africa and could be associated with jet stream. Light streak or band extending beyond this Cifm farther into Africa could be reflection from very thin Cirrus. Clouds of equator conv. zone at approximately 15N and southward are heavy as in previous orbit. Also appears tc be much stronger than same area on previous days. Few data on surface map.

147M 11/1332 - 32 Tape - Coverage SE from 25N 35W

Heavy broken Cufm with a single line of Cifm clouds to about 10N. Decrease in cloud cover between 10N and equator conv zone. Odd features in equator conv zone include widening of band of clouds downstream and horse shoe bend in one of the bands. Prominent feature S of equator is area of Cufm clouds with very uniform cells.

147M 11/1506 - 6(2) Direct - Western Atlantic off coast of US

Shows developing wave with band of cold front. Center of vortex not readily discernible but evidence of circulation is apparent.

148M 11/1644 - 8 Direct - Spotty coverage from Colorado to Caribbean

Nadir angles high and pictures noisy.

150K 11/1822 - 25 Tape - Rest high nadir - Eastern Pacific just West of California coast from 50N to 5N

Broad band just west of San Diego is roughly in position of front on surface chart but appears two fronts have merged to form so broad a band. Last few frames could be into equator conv zone and if so this zone appears much weaker in cloud formations than in vicinity of Africa.

150K 11/1959 - 6(2) Direct - Mainly Pacific to NE of Hawaii

Bright cloud masses but nadir angles high for examination of details.

151K 11/2013 - 32 Tape - Mid Pacific S of 15N

Predominately broken clouds. No unusual features for this area.

151K 11/2142 - 7(2) Direct - Mid Pacific from 35N 175W to Hawaii

Frontal band appears more extensive on pictures and appears to be located farther east than shown on surface map. Banded Cufm behind front.

151K 11/2150 - 12 Direct - 6(2) 6(1) - SE of Hawaii S of 15N

Mottled suggestive multiple layers of clouds with strong band near end of series and probably connected with ITCZ. No data on surface map.

152K 11/2328 - 14 Direct - 8(2) 6(1) - Mid Pacific SW of Hawaii from 22N

Mass of cloud cover toward horizon of first few frames suggests cloud evidence of front which has been washed out on surface chart. ITCZ is shown as area of patchy overcast.

12 April 1960

157M 12/0245 - 28 Tape - Extensive cloud mass on first few frames located SE of Phillipines

Very little data on surface map in this area. Previous maps show suggestion of easterly wave through this area. Extensive cloudiness S of equator.

158M 12/0746 - 30 Tape - SE from off coast of Saudia Arabia from 15N 55E

Patchy overcast through ITCZ with one giving indication of small vortex. No data on surface map.

159M 12/0925 - 15 Tape - SE from 15N 30E - Mainly over E Central Africa

Mottled appearance along E coast undecided whether it is cloud, or land, or both.

160M Nothing

161M 12/1233 - 30 Tape - Central Atlantic (40N 50W) Southeast to W coast of Africa at 5N

Frontal band discernible on pictures but wave cyclone on front of surface map not clear on pictures. Extensive Cufm clouds to SE of front. Clear off W coast of Africa vicinity 15N. Last few frames get into ITCZ.

161M 12/1414 - 2(2) Direct - High nadir angles

162M 12/1423 - 31 Tape - Western S Atlantic from 15N

Predominate feature on this series is the ITCZ across Western Atlantic and entering South America.

162M 12/1551 - 6(2) Direct - Nadir angles high but extensive cloudiness over Gulf states due to southerly flow off Gulf is clearly visible.

164K 12/1907 - 7(2) Direct - High nadir angles

165K 12/1558 - 32 Tape - Florida, Hispaniola and into Northern part of S America

Clear over Southern states. Extensive cloud cover Southern Florida to Caribbean. ITCZ discernible over S. America.

165K 12/2049 - 6(2) Direct - High nadir angles but some banding is visible which may be front as shown on surface map.

165K 12/2057 - 3 Direct - 1(2) 2(1) - Band shown on picutre from Camera (2) probably frontal band shown on surface map N of Hawaii.

166K 12/2105 - 32 Tape - Mid Pacific from equator toward SE. No frame numbers.

166K 12/2234 - 11(2) Direct - Mid Pacific in same region as 152K Direct

Solid bright cloud mass still appears in region just after surface analysis shows cold front stops. Few ship reports in area. Aircraft recon plotted on 700 MB Chart. 500 MB Analysis shows trough cut off from main westerly flow.

166K 12/2242 - 8 Direct - 5(2) 3(1) - Mid Pacific south from 15N

Mainly scattered Cufm.

13 April 1960

171M 13/0201 - 31 Tape - S Pacific from 5N 145E

172M 13/0653 - 32 Tape - SE from Saudia Arabia

Few clouds over Persian Gulf. Thin clouds over Arabian Sea. Small vortex very close to equator probably associated with ITCZ. Some frames mislabeled direct.

173M 13/0832 - 32 Tape - Egypt along Red Sea crossing eastern coastline of Africa over Italian Somaliland and into Indian Ocean.

Clouds over Ethiopia may be associated with jet stream. ITCZ band relatively narrow and appears weak in the region of this path.

174M 13/1011 - 32 Tape - SE across Central Africa from 10E 20N

Clouds in early frames could be associated with jet stream. Clouds across ITCZ form relatively broad band of broken and patchy overcast.

175M 13/1150 - 32 Tape - W coast of Africa from 20N SE through Africa

Appearance of multi-layer clouds off W coast of Africa. No data on surface map over this area. ITCZ shows up brighter and more dense over SW coast and surrounding Atlantic than over W coast and Indian Ocean.

175 13/1314 - Direct - High nadir angles

176M 13/1329 - 31 Tape - Mid Atlantic

Difficult to tie in pictures with area with given starting time. From nadir angles and content it appears to have started at least six minutes late. This then puts large cloud band in vicinity of accepted location of ITCZ. Also moves large frontal band and vortex closer to 35S rather than 20S. Feathery type cloud band probably Cifm runs diagonally across this frontal band.

179K 13/1648 - 31 Tape - Yucatan Peninsula across Central America and into S America

Clouds along Gulf coast of Mexico. Dense cloud masses vicinity Panama. Broken clouds over Northern part S America with band probably giving outline of Andes.

179K 4(2) Direct - Time uncertain but obviously not as shown on program.

180K 13/2012 - 31 Tape - Eastern Pacific from 5N

ITCZ shown as relatively narrow band. Street formations further south.

180K 13/2140 - 6(2) Direct

Cold front of surface analysis shows as band toward horizon on pictures. Large mass of bright clouds discussed in 152K and 166K still present in this area.

180K 13/2148 - 9 Direct - 5(2) 4(1) - Area SW of Hawaii vicinity 10N 160W

Predominately Cufm with no well organized patterns.

5 May 1960

487M Direct - None

488K 05/0204 - 16(2) Direct - 2S to 20N; 150W to 135W

Mostly clear just S of ITCZ. The ITCZ presents an unusual pattern of two or three long E-W bands with more numerous bands running N-S. Possibly the E-W bands could be Cufm with a veil of N-S Cifm bands over top. Banded Cufm also present to N of ITCZ.

488M Tape - S of equator

489M Tape - S of equator

489K 05/0344 - 16(2) Direct - From equator NE to Hawaii

Relatively broad band broken to overcast vicinity ITCZ. Mainly lines of Cufm N of this zone.

490M 05/0512 - 31 Tape - Mid Pacific from 30S to 15N

Scattered Cufm N of ITCZ. The ITCZ shows broken clouds and appears relatively weak. Vortex in S Pacific appears at beginning.

490K Direct - Dark

491M 05/1653 - 31 Tape - Western Pacific from 25S to 20N

Last few frames in twilight. Mainly scattered Cu N of ITCZ. The ITCZ shows one large overcast patch and is otherwise quite dispersed and appears to have two branches. Frontal band S of equator and landmark on last two frames.

493K 05/0837 - 31 Tape - Western Pacific from 10S NE across Phillipines to 30N

Wide band broken to overcast vicinity ITCZ. Scattered Cufm N of this zone. Frontal band visible toward end of sequence but path of pix is toward darkness and hard to examine in any detail.

494K 05/1155 - 25 Tape - Rest in darkness - Indian Ocean from 12S NE across India 30N

Scattered Cu increasing northward toward ITCZ. The ITCZ appears as single bright band. Southern India has scattered to broken cloud cover and mainly clear toward north.

495 Blank

500M 05/1833 - 26 Tape - Rest in Darkness - Eastern Atlantic from 5S to 35N

First few frames show mainly broken Cufm vicinity ITCZ. Lines of Cu north of this zone off W coast of Africa. Mostly clear over Africa.

500M 05/2200 - 8(2) Direct - 15N 80W to 30N 65W

Lines of Cu in Caribbean. Pix N of Caribbean are dominated with patterns associated with vortex centered near 30N 70W. Remainder in twilight.

501M 05/2324 - 31 Tape - Eastern Pacific from 25S to 15N

Mainly scattered Cifm N of ITCZ. ITCZ appears as relatively narrow broken to overcast band. Apparent frontal band near 25S.

501M Direct - Dark

6 May 1960

502M 06/0108 - 31 Tape - Eastern Pacific from 12S to 30N

Scattered Cu S of ITCZ. This zone marks the beginning of extensive cloud cover for the remainder of the sequence of pix. The progressive changes in reflectivity is probably the result of NE movement toward twilight. The cloud cover to N of ITCZ appears as predominately Cufm.

503K Tape - All S of equator

503K 06/0251 - 9 Direct 5(2) 4(1) - Mid Pacific NE to 20N 150W

Mainly banded and multiple layered clouds of ITCZ.

503K 06/0301 - 6(2) Direct - Pacific between Hawaii and W coast of US

Scattered to broken Cufm with frontal band to N on last frames.

504K 06/0435 - 12(2) Direct - Mid Pacific from 10N 175E to 30N 165W

Mainly scattered Cufm with increasing cloud cover to N coverging into what may be frontal band near horizon but pix are in twilight so is difficult to ascertain.

505M 06/0608 - 27 Tape - Mid Pacific from 5S to 35N

Broken multiple layers vicinity ITCZ. Lines of Cufm and banded clouds N of zone converging in a vortex centered near 32N 157E. Remainder of pix in twilight.

508K 06/0927 - 26 Tape - Rest in twilight. Indian Ocean from 5S, across SE Asia to Korea.

Multiple layers with patchy overcast in vicinity ITCZ. Lines of Cu N of this zone. Extensive cloud cover over SE Asia probably associated with stationary front drawn on surface analysis. Remainder of picture sequence in twilight and darkness.

509K 06/1245 - Tape - 3 useable pix with 2 showing coast line along Indian Ocean. Rest noisy and blank.

514M 06/1743 - 24 Tape - Remainder in twilight and darkness. Eastern Pacific from 2S NE across Western Africa

The ITCZ appears to be dispersed over relatively wide area with mainly scattered to broken clouds. A small doughnut shaped cloud appears on frames 22-26. Scattered clouds along coast of Africa with interior mostly clear.

514M 06/2108 - 4 Direct - 2(2) 2(1) - Caribbean and SW Atlantic

Generally broken Cufm with increasing cloud cover to N in association with vortex centered near 30N 70W.

515M 06/2231 - 31 Tape - Eastern Pacific from 25S to 15N

ITCZ shows bright patches overcast. Frontal band vicinity 20S.

515M Direct - Pix in twilight and darkness

7 May 1960

516M 07/0015 - 27 Tape - Eastern Pacific from 15S to 25N ending at Baja, California

North of equator has broken to overcast multiple layers with an extensive cirrus cover extending to near coast of Baja, California.

517K Tape - All S of equator

517K Direct one - S of 10N

517 07/0207 - 12(2) Direct - Eastern Pacific between Hawaii and US from 20N to 35N

First frame has appearance of very small circulation near center with doughnut shaped cloud at center of circulation. Broken Cufm N of this small circulation with a band to N of Cu. This band probably associated with cold front shown on surface analysis.

518K Tape - All S of equator

518K 07/0342 - 5 Direct - 2(2) 3(1) Mid Pacific SW of Hawaii

Mainly scattered Cufm, some in street formations.

518K 07/0350 - 10(2) Direct - Last few in twilight. Eastern Pacific N of Hawaii from 30N to 40N

Goes over region of large high pressure area on surface. Scattered to broken but does not have Cu cells seen so often in the region to W of cold front in April. This could mean that the location of pix is off. Also the circulation at surface is not as strong as it was in April.

519K Direct - Twilight and darkness

519M Tape - S of 15N - Bright doughnut shaped cloud over SE Australia

522K 07/0831 - 31 Tape - SE Indian Ocean (15S) NE across SE Asia to just SW of Japan (28N)

Generally broken with bright patches in vicinity of Malaya. Stations on surface chart are all reporting Cb with Tstm so this may be good example of cumulonimbus. Lines of scattered Cu in S China Sea. Increasing clouds to N with extensive overcast vicinity Formosa and N. The appearance of this overcast might be interpreted as an overcast of Stfm with towering Cu protruding through overcast.

523K 07/1148 - 31 Tape - Few with noise. E Africa (18S) NE across Indian Ocean to India.

The traditional cloud patterns in vicinity of ITCZ are not present. Lines of scattered Cu appear in vicinity of equator with some bright reflections indicating buildups. There are a few lines of Cu N of this zone. Otherwise mostly clear.

529M 07/1648 - 31 Tape - SE Atlantic (8S) NE across Western Africa to 30N

The ITCZ has broken cloud cover and appears relatively weak and dispersed. Few low Cu N of this zone with remainder of Africa mostly clear to Mediterranean Coast which has scattered Cu.

529M 07/2157 - 6 Direct - 3(2) 3(1) - Atlantic off coast of SE US

Shows vortex centered near 28N 70W with lines of Cufm clouds converging toward center of vortex.

530M 07/2320 - 31 Tape - SE Pacific from 25S to 20N with SW Coast of Mexico visible on last frame.

Equator and north is featured by clouds of ITCZ which shows mainly broken with bright reflectivity. Coast of Mexico mostly clear.

530M 07/2340 - 5(2) Direct - Midwest and SE US

Midwest mostly clear with band of clouds in Eastern US associated with front on surface analysis. Pix are in twilight.

8 May 1960

531M Tape - All S of equator

531K 08/0107 - 18 Direct - 13(2) 5(1) - Eastern Pacific SE of Hawaii from equator to 20N

Scattered Cu streets S of ITCZ with ITCZ mainly broken. Extensive area of uniform Cu cells found North of equator.

532K Tape - All S of equator

532K 08/0248 - 10 Direct - 5(2) 5(1) - Pacific SW of Hawaii from equator to 20N

ITCZ is mainly broken and like 531K Direct looks relatively weak. Mostly scattered Cu with no significant patterns North of ITCZ.

532K 08/0258 - 6(2) Direct - Pacific N of Hawaii from 30N to 40N

Assuming a reasonable approximation to location of pix, a large band of clouds is associated with the vortex centered near 43N 150W. This band appears as a typical frontal band although no front is shown on the surface analysis. In the region where the front is drawn on the surface chart, the pix show scattered to broken with no resemblance to a frontal band.

533M Tape - All S of 15N

533K Direct - None

534M 08/0609 - 22 Tape - Western Pacific from 10N 140E NE to approximately 40N 180

Scattered to broken multiple layers decreasing to lines of scattered Cu. Extensive cloud cover associated with vortex centered near 32N 175E appears on middle 9 frames. Rest in twilight and darkness.

536 08/0740 - 31 Tape - SE Indian Ocean (10S 100E) NE across Sumatra, Northern Phillipines to just S of Japan (30N 135E)

Patchy broken with bright reflectivity at beginning. Scattered to broken Cufm at equator and to N with many bright clouds indicating cumulonimbus clouds. Surface map at 1200Z shows nearly all stations observing cus with lightning and tstms. Bright band vicinity Phillipines could be clouds of easterly wave. Broken to overcast band is associated with cold front shown on surface chart. Clouds indicate a relatively weak front.

537K 08/1059 - 31 Tape - Southern Indian Ocean (10S) NE across India to Himalayas at approximately 30N 85E

Few patches bright clouds on first few frames, otherwise mainly lines of scattered Cu throughout this part of Indian Ocean. Relatively small round bright cloud vicinity Bombay with scattered Cufm east of this cloud. Cbs observed in this vicinity on 1200Z surface map. Rest of India mostly clear until vicinity Himalayas which has some cloud cover and possibly snow cover.

538K 08/1238 - 31 Tape - Central Africa (10S) NE across Southern Red Sea, Saudia Arabia and Persian Gulf

Mostly scattered Cu until just S of Red Sea which shows many bright patches indicating a region of strong build ups with tstsms. No data on surface map to verify this. These bright clouds also extend into Southern Saudia Arabia. Northern Saudia Arabia and Persian Gulf have clouds in pattern suggesting some type of vortex. Scattered clouds N of Persian Gulf.

543M 08/1736 - 31 Tape - Mid Atlantic (8S) NE to coast NW Africa (35N 10)

Lines of scattered Cu S of equator. ITCZ has broken to overcast and appears relatively weak. Scattered Cu vicinity Cape Verde Islands. Clouds off W Coast of Africa give appearance of small vortices. Large "doughnut" shaped cloud appears along W Coast of Africa at approximately 30N.

543M 08/2104 - 8(2) Direct - Caribbean, across Cuba to Western Atlantic (30N)

Band of clouds on first few frames associated with cold front to W of path. Lines of Cu converging at center of vortex near 30N 70W. Same vortex as seen on 529M Direct in approximately same location. Fewer clouds than on previous day.

544M 08/2229 - 31 Tape - Western Pacific from 20S NE to coast of Mexico (20N). ITCZ appears quite strong with two bands of bright broken to overcast. Mostly scattered N of ITCZ.

544M 08/2247 - 7(2) Direct - SE US

Clear over Gulf Coast but coastline not distinguishable due to low sun angle. Extensive cloud cover associated with wave centered over North Carolina. The pattern is interpreted as being a large cloud mass with vortex visible then small clear band separating this from extensive overcast to NE.

9 May 1960

545M 09/0013 - 26 Tape - Labeled Direct - Western Pacific from 10S NE to Baja, California (30N)

Mostly broken multiple layers vicinity ITCZ. Low Cu with Ci above to north of this zone. Scattered clouds over Northern Baja, Calif.

546M All S of equator

546K 09/0155 - 26 Direct - 19(2) 7(1) - Mid Pacific from equator 170W NE to 35N 130W

Wide band of scattered to broken multiple layer clouds on first few frames. Scattered Cu with some street formations to approximately 25N. Broad band associated with cold front on surface chart. The position of sun and resultant illumination of this band shows there are at least three distinct lines of build ups located in leading half of this band. Small breaks occur between these lines. Relatively clear band (comparable in width to frontal band) appears ahead of frontal band with low Cu behind frontal band.

547K All blank

551K 09/0650 - 29 Tape - 8S 110E Vicinity Sumatra and Borneo NE across Phillipines to approximately 30N 145E

Generally broken first few frames becoming scattered to broken Cu with some bright clouds indicating build-ups over Phillipines. Lines of scattered Cu NE of Phillipines until region of 25N which shows weak band of broken clouds associated with cold front drawn on surface chart. Band is quite diffuse as compared to cold frontal bands previously seen. Widespread cloudiness may be result of vortex to west than frontal band.

552K 09/1148 - 30 Tape - Eastern Africa from 7S NE across Eastern Saudia Arabia to Himalayas.

Scattered to broken Cu S of 10N. Thin Ci bands over Gulf of Aden and Saudia Arabia. Mostly clear over remainder. Snow cover with drainage patterns over Himalayas quite clear.

557M 09/1645 - 31 Tape - Mid Atlantic from approximately 7S NE across NW Africa to approximately 35N

ITCZ shows bright patches of broken to overcast. Scattered Cu N of this zone. Few Stfm clouds over Africa. Remainder clear.

557M 09/2012 - 8 Direct - 4(2) 4(1) - Caribbean and Atlantic vicinity Hispaniola

Mostly broken multiple layers.

558M Tape S of 15N

558M 09/2154 - 13(2) Direct - Yucatan Peninsula NE across Florida and Georgia to Atlantic off coast of New Jersey at approximately 40N 70W

Patch of clouds appears to be emanating from near center of high on surface. Scattered over Georgia and Florida with increasing clouds to N associated with front in Atlantic and vortex centered over Eastern Great Lakes.

559M 09/2320 - 31 Tape - Eastern Pacific from 10S NE to Northern Mexico approximately 30N 110W

Broken with some bright patchy overcast vicinity ITCZ. Scattered to broken Cifm N of this zone just W of Baja, California. Few Cu over Mexico

559M 09/2338 - 6(2) Direct - Midwest US

Dark and noisy pix preclude any details other than extensive cloud cover apparently associated with system over Eastern Great Lakes.

10 May 1960

560M Tape - All S of equator

560K 10/0103 - 22 Direct - 15(2) 7(1) - Mid Pacific vicinity equator and 165W NE to approximately 30N 135W

Scattered to broken vicinity equator and mostly scattered N of this to 20N. Band of clouds vicinity 25N to NE associated with cold front on surface chart. This is same frontal band described in 546K Direct. The width of the band appears to be only half that seen in 546. The lighting effect indicates there are some build-ups but not the three distinct lines seen in 546. Band of clear ahead of front still present as well as Cu behind front.

561K Tape - S of equator

561K 10/0246 - 8 Direct - 4(2) 4(1) - Mid Pacific from 8N 180NE to approximately 25N 165W

Mostly scattered Cufm with some multiple layers in a few sections.

561K 10/0255 - 12(2) Direct - Pacific from 30N 155W NE to approximately 45N 135W

Gives fairly complete view of deep low on surface chart centered near 45N 140W with strong circulation around it. Cumulus clouds of most any size and shape can be seen on these pix. Cloud band comes into center of vortex NW indicating frontal band may be wrapped around outside of this strong circulation.

562M Tape - Blank

562K 10/0434 - 9(2) Direct - N Central Pacific from approximately 32N 180NE to 42N 165W

Two extensive cloud masses with band of clear between. One of these cloud areas is located in SW quadrant of high pressure on surface with the other associated with cold front to W of high pressure area.

571M 10/1921 - 13(2) Direct - Atlantic from approximately 17N 65W NE to 35N 45W

Scattered Cufm clouds at beginning of sequence with increasing cloud cover to N with appearance of broken to overcast multiple layers.

572M 10/0740 - 31 Tape - Indian Ocean near equator 95E NE across SE Asia to Japan

Scattered to broken predominately Cufm with some bright clouds indicating build-ups up to about 20N. Few surface reports in this area all report Cbs on 1200Z surface map. Band of clouds associated with cold front extends to NE culminating in vortex off coast of Southern Japan. Vortex not visible on pix.

572M 10/2101 - 6 Direct 3(2) 3(1) - Florida with surrounding Gulf of Mexico and Atlantic

Band of clouds SE and E of Florida could be associated with weak cold front in this area. Band of clouds in Northern Florida associated with squall line shown on 1800Z surface chart. Clear to scattered between these bands.

573M 10/2226 - 62 Tape - 31(2) 31(1) - First orbit after remote Camera 1 came back in - Eastern Pacific from 15S NE to Southern Baja, Calif. at 25N.

No significant patterns N of equator but a comparison of the two cameras which are easily matched gives a good illustration of how examining Camera 2 can be misleading in interpretation. A good example of this is frame labeled 6 (2+4) on both cameras. Camera 2 alone would have been interpreted as Stfm clouds but examining Camera 1 showed it to be definitely Cufm.

573M 10/2244 - 10(2) Direct - Eastern US from Texas to Great Lakes

Scattered over Midwest US increasing clouds to East associated with vortex centered over Northern Ohio. Vortex well defined on last two frames.

11 May 1960

574M Tape - All S of equator

575M Tape - All S of equator

576M Tape - All S of equator

577M 11/0506 - 62 Tape - 31(2) 31(1) - SW Pacific from 8S NE to 32N 160E

Bright patchy overcast vicinity equator. Predominately scattered Cu to N for remainder of sequence with some lines and streets of low Cu.

586M 11/0824 - 62 Tape - 31(2) 31(1) - Central Indian Ocean vicinity 10S NE to SE Asia vicinity 35N 110E

Bright patches broken to overcast from equator to 5N. Scattered Cu N of this zone with some bright clouds indicating build-ups. Increasing cloud cover vicinity 20N with appearance of multiple layers.

586M 11/2009 - 11(2) Direct - Caribbean just S of Cuba vicinity of 20N 80W NE into Atlantic vicinity of 35N 60W

Generally broken multiple layers with one large band apparently Cifm not associated with any surface front in vicinity but may be associated with jet stream.

587M 11/2151 - 62 Tape - 32(2) 30(1) - Mostly S of 15N

Very good pix of Cu cloud streets with Camera 1 and comparative view with Camera 2.

587M 11/2151 - 8(2) Direct - Eastern US

Shows two separate vortices with one centered over South Carolina and other over Northern New York. Band of clouds connects these two vortices with appearances of frontal band but not directly associated with any front shown on surface chart.

588M Tape - All S of equator

588K 11/2320 - 7(2) Direct - Eastern Pacific from equator to approximately 15N

Mainly scattered Cu with some lines of Cu. Thin band of relatively short length possibly Cifm although ship report in vicinity reports altocumulus translucidus.

12 May 1960

589M Tape - Programmed to start at minute 1.8, but the nadir angles and contents indicate a starting time of about orbit 588, minute 82.

590M 12/0241 - 60 Tape - 29(2) 31(1) - Mid Pacific from 8N 180NE to approximately 45N 140W

Scattered to broken multiple layers at beginning with scattered Cufm in streets to north. Scattered Cifm clouds about 25N. Increasing cloud cover N of 30N predominately Cufm associated with vortex centered near 45N 135W. Vortex visible on last few frames.

591M 12/0421 - 61 Tape - 30(2) 31(1) - Western Pacific from 10N 145E NE to 45N 165W

Mostly scattered Cu with lines and streets to about 30N - Large clear area located to E of cold front on surface. Extensive cloud cover associated with frontal system vicinity 30N 45N - No evidence of frontal band as is usual but rather almost complete overcast for last 8 frames - Data on surface map shows 10 ship reports of overcast through a ridge of high pressure.

600M 12/0558 - 61 Tape - 30(2) 31(1) - Northern Borneo approximately 5N 115E NE across Phillipines and Western Pacific to approximately 40N 160E

Scattered to broken Cufm with bright patches indicating build-ups over Borneo and Phillipines - Scattered low Cu over Pacific vicinity 40N to 25N. Band of clouds on last 10 frames associated with quasi-stationary front drawn on surface chart. This band is much wider than those normally associated with front especially a definite cold front.

600M 12/1916 - 3 Direct - 1(2) 2(1) - Vicinity Hispaniola

Scattered Cu probably build-ups to Cb.

600M - 12/1923 - 7(2) Direct - Western Atlantic vicinity 35N to 43N, 40W to 55W.

Band of clouds with a vortex within this band probably associated with surface front in this area. Reports available in this area do not indicate this vortex.

601M 12/2041 - 61 Tape - 31(2) 30(1) - Eastern Pacific from 20S NE to Southern Mexico at approximately 20N

Scattered Cu in street formations vicinity equator to 5N. Band of broken with bright patchy overcast north of 5N depicting the ITCZ.

601M 12/2058 - 13(2) Direct - Eastern US

Shows two vortices in Eastern US. One centered in South Carolina, the other just off the coast of New Jersey. The clouds associated with these vortices indicate the northern circulation to be the stronger of the two.

602M 12/2232 - 62 Tape - 31(2) 31(1) - Eastern Pacific from approximately 10N 120W NE across Baja, California, Northern Mexico, Midwest US to Great Lakes

Various patterns of Cufm in Pacific extending to coast of Baja, Calif. Mostly clear with few areas of scattered Cufm over Mexico and Midwest US. Vortex on last few frames apparently centered over Lake Ontario. This vortex appears to be distinct from vortex near New Jersey described in 601M Direct. A low is drawn on 1800Z surface map over Lake Ontario but is not shown on surface map of 13/0000Z.

13 May 1960

603M 13/0013 - 62 Tape - 31(2) 31(1) - Eastern Pacific from approximately 15N 150W NE across Northern California to Minnesota

Scattered to broken predominately Cufm over Pacific. Scattered Cu over California with coastline faintly visible. Increasing cloud cover in association with front to West of Rockies but without typical frontal band. Some bright clouds indicating buildups over mountains. Last few frames in twilight.

604M Tape - Mostly S of equator

604K 13/0150 - 23 Direct - 19(2) 4(1) - Mid Pacific from approximately 10N 180NE to 40N 145W

Bands of scattered Cu at beginning of sequence. Horseshoe shaped band on frames 10 and 11. Increasing cloud cover to NE predominately Cufm with appearance of multiple layers.

605M 13/0321 - 62 Tape - 31(2) 31(1) - Northern Australia, New Guinea, NE across Pacific to approximately 30N 175E

Mostly broken with some bright patchy overcast vicinity equator. Scattered Cu N of equator and remainder of sequence. "Ring" shaped cloud appears on last four frames.

605K 13/0339 - 10 Direct - 5(2) 5(1) - N Center Pacific

Shows frontal band and clouds associated with vortex centered near 50N 160W. Small clear areas on both sides of frontal band on first frame probably about 40N but remainder almost completely overcast including region to W of cold front. Cold front is distinguishable by brighter reflectivity illustrating relationship between depth of cloud and reflectivity.

608K 13/0827 - 59 Tape - 28(2) 31(1) - Southern India from 10N NE across Eastern Himalayas to Manchuria

Examination of pix reveals the first frames were taken at about 15N. Scattered with bright overcast patch on first few frames. Other smaller bright clouds further N probably Cb. Broken Cufm S of Himalayas extending over Himalayas. Snow cover can be seen through these clouds. Cloud cover N of Himalayas probably associated with cold front drawn on surface chart but no frontal band is distinguishable.

609K 13/1041 - 54 Tape - 29(2) 25(1) - Indian Ocean near Gulf of Aden approximately 10N NE across NW India and Western Himalayas

Few lines of scattered Cu of first few frames. Scattered Cu over India. Snow cover on Himalayas shows details of terrain especially on Camera 1. Scattered to broken mainly Cufm N of Himalayas.

614M 13/1824 - 13 Direct - 10(2) 3(1) - Caribbean from approximately 15N 70W NE to vicinity 35N 45W

Scattered to broken Cufm. No significant patterns.

615M 13/1326 - 62 Tape - 31(2) 31(1) - Central Africa approximately 15N 5E NE across Eastern Mediterranean and Caspian Sea.

Scattered Cu at beginning of sequence. Mostly clear over Northern Africa. Scattered Cufm over Mediterranean. Relatively weak band over Turkey probably associated with front shown on surface map. Last few frames in twilight.

615M 13/2005 - 4 Direct - 2(2) 2(1) - Florida and surrounding waters

Uniform Cu cells shown on camera 1 over Gulf of Mexico. Cifm clouds over Southern Florida with Western Florida mostly clear. Band of clouds to SE of Florida might be associated with cold front shown on surface chart.

615M 13/2013 - 6(2) Direct - Western Atlantic off Coast of New England

Extensive cloud cover associated with front in this region. Data on surface chart verify extensive overcast. Banding difficult to detect. Most of clouds give appearance of being covered by Cifm veil.

616M 13/2131 - 63 Tape - 32(2) 31(1) - Eastern Pacific from 8S NE to Southern Baja, California and Mexico. Relatively thin band Cufm vicinity 5N

Broken Cufm vicinity 15N with cyclonic and vortical organization. Probably a weak tropical depression. Uniform Cu cells revealed by Camera 1 off coast of Baja, California. Scattered Cu over Mexico.

616M 13/2148 - 12 Direct - 6(2) 6(1) - Midwest US from Central Texas NE to Lake Erie.

Scattered Cifm at beginning of sequence. Pix show mostly clear over Midwest but data on surface map shows scattered to broken cloud cover. This could be a case of seeing through cirrus. Vortex over Wisconsin similar to that seen on 602M remote.

617M Blank

617K 13/2315 - 19 Direct - 15(2) 4(1) - Western Pacific vicinity equator NE to approximately 25N 135W

Cu streets on first few frames. Narrow bright band to north of equator may be associated with ITCZ. Generally scattered to broken Cufm N of this band.

14 May 1960

618M No film

619M No film

619K 14/0243 - 18 Direct - 15(2) 3(1) - Mid Pacific from 25N 175E NE to 47N 140W

Scattered to broken Cufm at beginning with increasing cloud cover to north. Band of clouds in region of cold front on surface analysis ending in vortex near 52N 155W. Extensive area of scattered Cufm to west of this frontal band. Eastern (leading) edge of frontal band does not show on pix.

622K 14/0735 - 50 Tape - 27(2) 23(1) - Bay of Bengal NE across SE Asia, China to approximately 45N 135E

Bright overcast patch on first few frames with scattered Cu vicinity this overcast. Scattered Cu over SE Asia with some bright clouds indicating buildups. The data on 1200Z surface map shows many stations reporting Cb in this area. Broken to overcast over China probably associated with cold front shown on surface chart although frontal band is not apparent.

623K 14/0914 - 53 Tape - 30(2) 23(1) - Indian Ocean vicinity 10N 60E NE across India, Himalayas to vicinity 45N 110E

Broken to overcast at beginning with clouds appearing to converge in vortex indicated by very bright overcast. Band of Cifm S of Himalayas. Patterns of snow cover over mountains. Generally broken N of mountains with vortex centered near 45N 120E.

629M No film

630M 14/2038 - 56 Tape - 31(2) 25(1) - Eastern Pacific from 15S NE to Mexico approx 25N 105W

Generally scattered Cu. No significant patterns.

630M 14/2055 - 10 Direct - 5(2) 5(1) - U. S. from Texas to New York

Large patchy overcast probably over Okla. and Ark. Scattered fairly uniform Cu cells to NE with increasing cloud cover toward end of sequence probably associated with surface low over New England.

631M Tape - All S of equator

631M 14/2240 - 2 Direct - 1(2) 1(1) - Midwest U. S.

631M 14/2223 - 13 Direct - 6(2) 6(1) - Mid Pacific from 2S NE to 18N 135W

Scattered Cu on first frames. Narrow band vicinity ITCZ. Broken mottled clouds N of this band have appearance of multi-layers of clouds.

15 May 1960

632M All S of equator

632K 15/0004 - 24 Direct - 17(2) 7(1) - Mid Pacific near equator NE across Hawaiian Islands to approx 35N 140W

Scattered Cufm no definite pattern at beginning of sequence increasing to broken multiple layers over Hawaii. Upper clouds give bright reflection with lower clouds a dull gray resembling landmarks. These multiple layers extend NE to end of picture sequence.

633M 15/0133 - 30 (2) Tape - Mid Pacific from approximately 20S NE to 20N, 175E.

Band of bright Stfm clouds vicinity of equator associated with ITCZ. Remainder north of equator mainly scattered to broken Cufm.

633K 15/0150 - 19 Direct - 13(2) 6(1) - Mid Pacific vicinity 20N 175E NE to approximately 45N 150W

Mainly scattered Cufm at beginning of sequence with increasing clouds in multiple layers to NE. Band associated with cold front in vicinity 35N appears relatively diffuse and narrow. Scattered to broken low Cufm is quite prevalent in region NW of cold front and S of deep vortex centered near 53N 148W. This vortex does not appear on this sequence.

634M 15/0329 - 59 Tape - 29(2) 30(1) - Path across Northern Pacific from approximately 22N 156E NE to 48N 142W

Surface map for this time shows extensive frontal system N of 35N with two deep vortices located respectively at 50N 178E and 53N 148W. The region in this sequence S of 35N is characterized by predominately scattered Cufm. N of 35N has extensive cloud cover commencing in the Western part with a frontal band and broken Cu NW of this band. The Western vortex is not visible but the occlusion to SE of vortex is shown as a complete overcast. Scattered to broken low Cu is present in the ridge between the two vortices. The eastern vortex with its associated cloud bands is visible on the last few frames.

637K 15/0653 - 54 Tape - 27(2) 27(1) - Bay of Bengal near 10N 90E NE across SE Asia, China to Northern Japan

Scattered clouds over water and SE Asia with frequent bright clouds indicating Cu buildups. The data on 1200Z surface chart show many Cb in this region. Broken to overcast over Southern China probably the cloud remnants of washed out front. Mostly clear from 30N to 40N. Broken to overcast clouds associated with frontal system and vortex centered near 47N 125E.

638K 15/1002 - 53 Tape - 29(2) 24(1) - E Africa vicinity Gulf of Aden NE across Saudia Arabia, Himalayas to approximately 45N 95E

Scattered Cu S of Gulf of Aden with remainder of Africa mostly clear. Also clear over Persian Gulf. Patterns of snow cover on Himalayas visible. Diffuse band of clouds N of mountains probably associated with front shown on surface map in this area.

643M 15/1321 - 62 Tape - 31(2) 31(1) - Central Africa vicinity 15N 5W NE across Mediterranean, Southern Greece, Turkey to Northern edge of Caspian Sea.

Scattered to broken near horizon at beginning of sequence. Clear over Central Africa. Band of Cifm clouds in Northern Africa. Also few scattered Cu over Northern Africa. Mostly clear along African Coast of Mediterranean. Generally broken predominately Cufm over Southern Greece and Turkey with broken to overcast over Caspian Sea.

643M 15/1820 - 6 Direct - 3(2) 3(1) - Caribbean and Atlantic in vicinity Cuba and Hispaniola

Relatively diffuse band probably associated with weak cold front or may be partly associated with easterly wave shown on surface chart. Remainder mostly scattered.

643M 15/1829 - 5(2) Direct - Western Atlantic vicinity 40N 45W

Overcast with breaks mainly Stfm in region of warm front. No evidence of a definite frontal band.

644M 15/1944 - 42 Tape - 27(2) 15(1) - Some high nadir. Eastern Pacific from approximately 22S NE to Mexico at 20N 100W

Scattered to broken Cufm vicinity equator. Mostly clear N of equator.

644M 15/2002 - 14 Direct - 7(2) 7(1) - Western Gulf of Mexico Northeast across Southern US

Mostly clear in Western Gulf with scattered Cu along Gulf Coast of US. Increasing cloud cover at end of sequence in association with surface low in NE US.

645M 15/2130 - 62 Tape - 31(2) 31(1) - Eastern Pacific from 5S NE to SW US vicinity 35N

Scattered Cufm vicinity equator. Broken Cufm clouds N of equator to Baja, Calif. with large region of Cu with uniform cells. Mostly clear over Baja, Calif. and SW US.

645M 15/2147 - 6 Direct 3(2) 3(1) - Midwest US

Large overcast patches vicinity Kansas and Oklahoma. Scattered Cifm clouds in SW Great Lakes with Lake Michigan clearly visible as landmark.

646M All S of equator

646K 15/2311 - 16 Direct - 8(2) 8(1) - Eastern Pacific vicinity equator at 160W NE to approximately 20N 150W. Generally scattered to broken Cu with some Cu streets. Bright overcast patch at end of sequence.

16 May 1960

647M 16/0037 - 18 Tape - 9(1) 9(2) - 23 Pix high nadir - Majority of pix taken Southern Hemisphere

647K 16/0055 - 22 Direct - DCS1 - 7(1) 7(2) - DCS11 - 8(2) - Pacific - 12N 178E to 41N 147W.

Area generally clear. Few Cu bands. Sun glint (16-17 C2T). Increase of cloudiness after 30N - Warm front 35N.

648M 16/0234 - 64 Tape - 32(1) 32(2) - Pacific - 13N 153E to 42N 153W.

Widely scattered Cufm patches - up to about 27N. Edge of frontal band seen about 30N. Sun glint (19 C2T). Frontal band clouds hold up until you reach vortex. See vortical cloudiness with big clear area in center. Possible Cu streets on Camera 1 sequence.

651K 16/0553 - 56 Tape - 31(1) 25(2) - Cambodia, Canton, Yellow Sea, Sea of Japan, ending NW Pacific - 47N 157E

No synoptic data available. Some landmarks but difficult to locate. May be some rough looking landmarks (F19-22 C2T). Cufm variable scattered to overcast patches. Sun glint (F6-7 C2T). Frontal or vortical cloudiness (extensive) either in Sea of Japan or NW Pacific.

652K 16/0911 - 59 Tape 31(1) 28(2) - Arabian Sea - 13N 52E - across Southern tip of Saudi Arabia, Afghanistan, Tibet - ending vicinity of Irkutsk, USSR.

No synoptic data available for comparison. Possible jet stream cirrus off coast of East Africa, vortex South of Saudi Arabia. See 666K and 681K for additional comments regarding this vortex. It also appears on 623K. Aside from vortex Arabian Sea and Gulf of Onan generally clear. Cufm over Sulaiman Range in Pakistan. Clear south over Indian Desert - good pix of Indus River. Increase Cufm over mountains of Tibet - then decrease of Cufm activity over Mongolia. Possible snow cover over mountains. Good landmarks on Camera 1 sequence. Possible Cu streets (F22-23 C1T).

657M 16/1230 - 61 Tape - 30(1) 31(2) - Frame numbers missing on monitor; Central Africa, Mediterranean, Turkey, and Black and Caspian Sea

Few broken patches Cufm over Central Africa. Thin Cirriform cloudiness over Africa. Lakes seem to be obscured. Generally clear over Mediterranean. Sun glint in Mediterranean (F13-16 C2T). Broken Cufm over Turkey. Vortex slightly north of Caspian Sea.

657M 16/1735 - 4(2) Direct - Atlantic 34N 46W to 38N 44W

Pass parallel to cold - stationary front - good picture of dense overcast. Probably multi-layer of frontal cloudiness in Atlantic.

658M 16/1852 - 64 Tape - 32(1) 32(2) - First 18 pix high nadir - Broken to overcast Cufm SW of Mexico

658M 16/1909 - 11 Direct - 5(1) 6(2) - Yucatan across Florida - along east coast of US ending in Atlantic 38N 69W

Some Cufm bands vicinity Yucatan. Sun glint Gulf of Mexico. Thin bright band Cufm running along east coast of US.

659M 16/2036 - 64 Tape - 32(1) 32(2) - Pacific vicinity 25S - across Baja, Calif. and into Mexico - 12 pix high nadir

Cufm in rows and at right angles to other Cufm rows SW of Baja, California - sometimes broken, sometimes almost overcast, but still can see rows. See (F7 C2T). Pix end west of Baja, California.

659M 16/2053 - 10 Direct - 5(1) 5(2) - Panhandle of Texas - Great Lakes area - Quebec.

Pass along stationary front, warm sector,warm front. Stationary front generally cloudless. See clouds associated with warm sector - warm front. Possible vortex cloudiness.

660M 16/2222 - 59 Tape - 31(1) 28(2) - Pacific vicinity 5N 155W across Central California - ending in Wyoming

Cufm band vicinity 5N. Possibly ITC. On about 3 frames, have double exposures; however, numbering system remains correct - broken anticyclonic Cufm to about 25N. Sometimes unorganized, becomes more organized as you proceed north, generally clear near Calif. Coast - Cufm over mountains.

660K No film

17 May 1960

661M 17/0004 - 64 Tape - 32(1) 32(2) - Central Pacific - 16N 172W - to Eastern Washington.

Pass starts over SW part of High. Area generally clear with some scattered cloudiness. F15-16 C2T overlap. F12-13 C2T picks up frontal cloudiness around 40N 145W. Pass runs along cold front, across warm sector -across warm front. Extensive cloudiness in F1-13 C2T but does not have a good pattern.

661K No film

662K No film

662M No film

665K 17/0502 - 56 Tape - 32(1) 24(2) - South China Sea, Formosa, Japan and Pacific Ocean - 47N 169E

No data for pix. Difficult to locate pix. Sunglint on F25 C2T. Some banded Cufm along island and/or mountain. Extensive cloudiness F1-13. Using some imagination, believe possible wave F14 C2T. No good landmarks.

666K 17/0820 - 60 Tape - 32(1) 28(2) - Arabian Sea - India - Tibet - Manchuria.

Excellent landmarks of India. Excellent pix of vortex in Arabian Sea, generally clear to scattered along Indian Coast. Broken Cufm over mountains of Tibet. Clears up in Mongolia. Excellent pix on Camera 1 sequence. See clouds at different levels - lower clouds Cufm, upper clouds Stratiform - isolated Cufm patches with shadows on ground. Banded Cufm. Surprised not to see snow cover drainage. If it is there, then it is not well defined.

672M 17/1139 - 63 Tape - 32(1) 31(2) - Central Africa, Egypt, Cyprus, Turkey, and Caspian Sea - Ending vicinity Aral Sea and Lake Balkhash.

Pix quality thin. Clear over Africa. Possible jet stream Cirrus. Sunglint Mediterranean. Turkey coast clear. Excellent landmarks Egypt and Turkey. Cufm clouds over mountains of Turkey. Extensive cloudiness east of Turkey into Aral Sea area.

672M 17/1816 - 9 Direct - 4(1) 5(2) - SE of Yucatan, Cuba, Bahama, Atlantic - 33N 70W

Area generally scattered to broken Cufm over water and islands - scattered Cufm in Atlantic.

673M 17/1942 - 64 Tape - 32(1) 32(2) - 18 high nadir - Most of pix taken south of 20N in Pacific - Orbit ends in Mexico

Area generally clear. Scattered banded cloudiness in Pacific. Possible wave developing or Easterly wave SW of Mexico (F10-12 C2T).

673M 17/2000 - 13 Direct - 6(1) 7(2) - Texas to New England area

Overcast area SW Texas. Frontal band cloudiness in Midwest. Overcast area associated with vortex Great Lakes.

674M 17/2128 - 63 Tape - 31(1) 32(2) - Pacific Equator 152W - Utah - Possible ITC vicinity 5 to 10N

Extensive Cufm in Pacific SW of California. Large cloud mass with small V-shaped clear area off coast of California. Good pix of San Joaquin Valley with clouds and/or snow cover demarking the Sierra Nevada Mountains.

674M 17/2145 - 8(2) Direct - SE Colorado - Great Lakes area.

No horizon seen. Generally overcast Dakota area. Clear to scattered Great Lakes area.

675M 17/2312 - 64 Tape - 32(1) 32(2) - Pix are dark - 14 pix have high nadir angles - Suspect that start of pix taking may be in error. Was programmed to start in Pacific - 15N 165W - to Montana

No landmarks. Pix generally clear to scattered and unorganized in the Pacific. Synoptic map would indicate extensive cloudiness off coast of Oregon, but nothing like this is found in TIROS Pix.

18 May 1960

676M 18/0052 - 64 Tape - 32(1) 32(2) - Central Pacific, 16N 171E to NE Pacific, 47N 132W

Pretty clear to scattered. Sunglint (22-24 C2T). About F18 Pass parallel to cold front in Pacific. See band of broken to overcast - this goes for about 10 frames; extensive cloudiness northern portion of frontal system.

677M 18/0230 - 64 Tape - 32(1) 32(2) - Central Pacific, 18N 149E to NE Pacific, 48N 151W

Some banded cloudiness. Bands become thicker and wider as you approach vortex in Pacific. Vortex cloudiness seen - overcast with bands radiating out. Looks as if 3 major bands are radiating out from vortex. Get into an area with broken Cufm. F1-13 no horizon visible.

679K 18/0550 - 55 Tape 29(1) 26(2) - Thailand - China - Korea Kurile Islands

Broken cloudiness with large clear areas. Japan and Sea of Japan pretty much overcast. Broken to overcast Yellow Sea. Extensive cloudiness over China.

680K 61 Tape - 32(1) 29(2) - Monitor misnumbered Orbit 679 - Also monitor reads Direct mode - No synoptic data. Program to start west coast of India and ending NE USSR near sea of Okhotsk

Clear to scattered over India. Cufm over mountains of Tibet. Generally Cufm for rest of orbit. No apparent pattern.

681K 18/0910 - 63 Tape - 32(1) 31(2) - Saudi Arabia - Afghanistan - Mongolia

Vortex which appeared on Orbit 666K may be seen - appears that it moved into Saudi Arabia. Otherwise, generally clear over Arabia, snow cover over mountains with maybe some cloud cover. Generally clear over remainder of orbit. Camera pix show some good snow cover over mountains.

686M 18/1048 - 64 Tape - 32(1) 32(2) - Egypt - Syria - Caspian Sea to north of Lake Balkhash

Clear over Egypt - Africa. Jet stream Cirrus vicinity Suez. Excellent landmarks. Broken to overcast vicinity Caspian Sea to Aral Sea. Very bright sunglint F7 C2T possibly in Lake Balkhash. Interesting pix on Camera 1 sequence, especially F15-16.

686M 18/1725 - 11 Direct - DCS1 3(1) 3(2) - Pass over Cuba - Atlantic, 30N 66W. Entire area generally clear to scattered. Some sunglint. DCSII 3(1) 2(2) - Atlantic Ocean - 38N 54W to 44N 42W

Excellent pix of vortex centered around 40N 50W.

687M 18/1907 - 15 Direct - DCSI - 1(1) 1(2) - Pix taken vicinity Texas - La. in Gulf of Mexico. Generally clear over Mexico. Broken to overcast SE Texas. DCSII - 13(2) - No program available. Maybe taken over Midwest - Mid Atlantic States. Possible pass over cold front - warm front. Extensive cloudiness with large clear area which should be in vicinity of Ohio. Only 1 pix with horizon. 64Tape - 32(1) 32(2) - 21(1) pix looking into space - 21(2) pix high nadir. Program to read SE Pacific south of Equator to NE Mexico.

Large mass of bright cloudiness broken to overcast vicinity 10 to 15N. Banded Cifm near Mexico mainland, possible jet stream Cirrus. Quick look at 300 MB map shows a secondary jet in the area.

688M 18/2033 - 64 Tape - 32(1) 32(2) - SE Pacific across Baja, California, ending in Arizona

12 pix high nadir. Extensive broken -overcast Cufm associated with high SW of Calif. Cold front cloudiness off Baja, California. Good landmarks. Generally clear over NE Baja, Calif., and NW Mexico.

688M 18/2051 - 8 Direct - 3(1) 5(2) - Kansas across to Quebec

Extensive cloudiness associated with wave located Kansas area. Overcast goes up to Dakotas. Large clear area Great Lakes. Some scattered to broken Cufm along St. Lawrence River.

689M 18/2236 - 4(2) Direct - 62 Tape - 32(1) 30(2) - Pacific 11N 160W to Montana

Dark, noisy, no horizon, taken North Central US and Lake Superior area. Extensive cloudiness vicinity vortex located Dakota area. Possible ITC vicinity 10 to 15N (F29-30). Scattered to broken Cufm vicinity Hawaii. Banded Cufm - maybe along isobars 25N. Anticyclonic Cufm 30N to 40N. Big clear area vicinity 35N 135W vicinity anticyclonic center. Generally clear off coast of California. Some odd looking patterns F1-4 from Oregon to Montana.

19 May 1960

690M 19/0002 - 64 Tape - 32(1) 32(2) - Pacific 21N 176W to Montana

Generally clear wtih few Cu from 21N to 35N. At 35N pick up frontal band cloudiness F9-20. TIROS pass parallels front. At 45N getting near to wave disturbance and extensive cloudiness is seen - no apparent pattern. Cufm with fairly large breaks are seen near WestCoast of US and over Rockies. On Camera 1 sequence possible Cufm Streets F24-25.

691M 19/0141 - 64 Tape - 32(1) 32(2) - Pacific 20N 162E to NE Pacific 47N 140W

Frames (F 24-31 C2T) show banded Cufm. There appears a thin band (thickness of piece of thread) running alongside of banded Cufm - vicinity 30N pickup frontal band cloudiness. Band becomes thicker and brighter vicinity 35N. Vortex seen (F17 C2T). Extensive cloudiness seen associated with warm front and vortex 35 to 40N. Generally clear behind cold front vicinity 40 to 45N. Pick up some cloudiness associated with second vortex vicinity 47N.

694K 19/0642 - 57 Tape - 32(1) 25(2) - Tibet - Across China ending in Pacific 47N 173E

No synoptic data. Pix quality thin. Appears that clouds are over snow cover in mountains of Tibet. Clear in China - broken Cufm vicinity Manchuria. Vortex located near Sokhalin Islands.

695K 19/0815 - 43 Tape - 32(1) 11(2) - Bebbera Coast of Africa - Southern part Saudi Arabia - Afghanistan - Tibet - Mongolia.

Majority of pix are either blank or noisy. Pix may show possible vortex located vicinity Aden. Same vortex that appeared on 666K and 681K. Otherwise Saudi Arabia generally clear. No pix after Saudia Arabia.

700M 19/1320 - 58 Tape - 30(1) 28(2) - French Morocco - Sardinia - Italy - Yugoslavia - slightly north of Black, Caspian, and Aral Seas - ending vicinity Lake Balkhash.

Overcast NW Africa - Spain over land. West Mediterranean generally clear, area vicinity Sardinia generally overcast. Generally scattered over Yugoslavia - Hungary. Vortex vicinity Caspian Sea. Small Cufm patches in bands enter vortex.

700M 19/1630 - 9 Direct - DCSI 4(2) - across Dominican Republic ending Atlantic 24N 66W. Nothing significant - some scattered Cufm. 5 DCSII - 2(1) 3(2) - 1640Z.

Pix are noisy. Pix taken across warm front into low center. Some vortex alignment of clouds but not too extensive.

701M 19/1813 - 15 Direct - DCSI 8(2) - Gulf of Mexico to Carolinas - DCSII 4(1) 3(2) - North Atlantic - 42N 65W to 47N 47W - 10 Tape 5(1) 5(2) - 27 pix high nadir - Pacific - ending vicinity Veracruz, Mexico

Generally clear to scattered in Gulf - Cirriform overcast patches along coast of Louisiana - Mississippi. Extensive cloudiness vortex circulation SE of Newfoundland. Some Cufm off West Coast of Mexico appears to be multi-layered in the area.

702M 19/1958 - 16 Direct - DCSI 7(1) 5(2) - DCSII 4(2) - 29 Tape - 14(1) 15(2) - Texas Panhandle -across Great Lakes. Quebec

"Square cloud" (F 5C2D)

Extensive cloudiness associated with cold front. Warm sector area warm front located vicinity of Great Plains. North Atlantic pix quality thin, dark. Extensive cloudiness along Northern part of vortex - good clear area in the pix. 17 Pix taken have high nadir angles. Good landmarks on Cameras 1 and 2 of Baja, California anticyclonic Cufm clouds lined up in rows SW of Calif. Cloudiness stops abruptly at coastline of Baja, Calif. A band of clouds along southern tip of Arizona - possible jet stream cirrus.

703K 19/2123 - 6(2) Direct - All pix have high nadir angles

703M 19/2127 - 64 Tape - 32(1) 32(2) - First 7 pix have high nadir - Pacific Ocean across US ending in Western Dakotas

No synoptic data available. Map missing or misplaced. Anti-cyclonic Cufm in bands over Pacific. Vicinity 30N in Pacific Cufm becomes thicker and brighter possibly multi-layered. Vicinity 35N clouds become stratiform. Clear along coast of California. Cufm over mountains, may have picked up edge of frontal cloudiness in Dakotas.

703M 19/2144 - 7 Direct - 3(1) 4(2) - Dakotas - Quebec.

Area generally overcast due to frontal system located vicinity Minn. A clear area in the form of a band is seen vicinity Ohio.

704K 19/2306 - 12(2) Direct - Pacific around 10N 179W to 25N 165W

Area covered with scattered Cufm. Some broken to overcast Cufm bands vicinity 10 to 15N.

704M - 19/2314 - 64 Tape - 32(1) 32(2) - Pacific 30N 159W to Great Lakes area

Sun glint in Pacific (F27 C2T). A lot of banded cloudiness. Banded Cufm running parallel to 35N. Banded stratiform along NW US - last few frames are dark.

20 May 1960

705M 20/0055 - Direct - None - All pix too dark - 62 Tape - 31(1) 31(2) - Pacific 33N 180 to Dakotas

No synoptic map available to compare pix with data. Excellent pix of vortex in Pacific. Large area off West Coast of US is covered with mottled Cufm clouds - good pix on Camera 1 of Cufm. Monitor in error relative to Frame Numbering and mode of readout.

708K 20/0552 - 52 Tape - 29(1) 23(2) - China - North of Japan - Pacific 46N 179W

No data area to compare. See frontal band of clouds over China, then a big clear area over land. Then a big area of Cufm as you approach the coast. Then an increase of cloudiness over the water. No apparent pattern.

709K 20/0730 - 57 Tape - 32(1) 25(2) - Arabian Sea - across Indian Desert - Tibet - Mongolia - Manchukuo.

No data area to compare. Generally clear over Arabian Sea - India. Cufm clouds over Tibet, then clearing over China.

714M 20/1540 - 13(2) Direct - Virgin Islands - Atlantic 36N 43W

Clouds along islands. Big cloud mass in Atlantic vicinity of cold front on map. This cloud mass does not appear to be organized as a frontal band as would be expected from the map nor as a wave development or vortex on the front.

715M 20/1227 - 61 Tape - 31(1) 30(2) - Africa, Italy, Black Sea - Ends vicinity Lake Balkhash, USSR

Jet Stream Ci over Africa (F25-20). Otherwise generally clear over Africa. Broken-overcast in Mediterranean between Italy - Africa. Weak vortex vicinity Black Sea. Cufm bands or streets around Caucasus Mountains. May be another vortex vicinity Aral Sea.

715M 20/1720 - 13 Direct - DCSI - 7(2) - Yucatan - Southern tip of Florida - Atlantic Ocean 31N 74W. Appears that Cufm clouds are over land areas. Generally clear over water isolated hook patch of clouds over water. DCS II 4(1) 2(2) - 1729Z. North Atlantic 39N 61W to 46N 44. Pix show extensive cloudiness of back side of low.

716M 19 Direct - (I) Camera took 19 Frames - 9 Blank - 5(1) 5(2) - somewhat confusing. Big band of clouds but cannot say where located. DCS II 9(2) - No horizon - Overlap pix. Again extensive cloudiness probably associated with cold front Central US. 8 Tape - 3(1) 5(2) - Cannot tell where or when.

717M 20/2032 - 35 Tape - 20(1) 15(2) - Pix F 1-10 are dark

There is only one pix with horizon. This orbit may be hard to locate - pix indicate that orbit is going into the dark. Whereas the program calls for the pix to be taken mid-afternoon. Program impulses check out to 2032Z.

717M 20/2049 - 11 Direct - 5(1) 6(2) - Great Lakes - Newfoundland -

Appears that clouds associated with cold front located Central US (Minn. - Iowa - Missouri, etc) is seen.

718K 2(2) Direct - Pix taken vicinity Equator - 15N - High nadir - No data

718M 20/2234 - 6 Direct - 2(1) 4(2) - Across north Central US - Canada

No horizon. Pix taken across North of Low between stationary and warm front. It is a complicated system on the 00Z 21 May 60 Synop Map. PB Pix - None. All pix are dark.

21 May 1960

719M 21/0004 - 27 Tape - 12(1) 15(2) - All pix on Camera 2 have high nadir

Also Camera 1 Pix do not correspond to Camera 2 pix. Camera 1 pix that should be looking out into space have pix of clouds.

719K 21/2359 - 11 Direct - 8(1) 3(2) - Direct camera program read out 2C1 then C2 in sequence for 6 minutes. There is noise in the pix - C2 pix picked up frontal band in Pacific - Pix read out was in Pacific from 25N 177E to 39N 163W

There is an overlap of pix on 719K with PB Pix on 719M. There seems to be some overlap on Camera 1 sequence but Camera 2 sequence pix all had high nadir angles.

720M 21/0142 - 64 Tape - 32(1) 32(2) - Pix show edge of frontal system located in Pacific 35N 160E region.

Then little cloudiness associated with high. Anticyclonic Cufm on East Side of High. Excellent pix of vortex vicinity 45N 175W. Extensive cloudiness associated with frontal system. Then as you approach West Coast of US there appears a weak vortex that is made up of anticyclonic Cufm clouds.

722K 21/0500 - 55 Tape - 31(1) 24(2) - China - North of Japan - Pacific 46N 171W

No synoptic data. Pix show edge of frontal band in China near East Coast. Weird sun glint F20 C2 along shoreline may be Kamchatka Peninsula. Increase of cloudiness as you go over the Pacific. Appears to be a vortex F10 C2 but it sure is different from others that were located over water. F3-7 are interesting - have what appears as an overcast of Cirrus - embedded in this mass is a distinct line of Cufm, probably CB. Also some very interesting cloud pix taken on Camera 1. To say the least - A VERY INTERESTING ORBIT.

723K 21/0640 - 57 Tape - 31(1) 26(2) - Starts in Tibet - Northern part of Sea of Japan - Pacific 44N 169E

Pix very thin at the start. May be hard to tell where or when pix started. F21-27 cloudy. F15-20 fairly clear. Then increase of cloudiness F1-14 - F1-14 have extensive cloudiness but no apparent shape or form. Some interesting shapes of clouds vicinity Kurile Islands (maybe). C1 pix show some interesting Cufm. See F21 C1 small Cufm patches along with their shadows on the ground.

724K 21/0813 - 59 Tape - 31(1) 28(2) - Saudi Arabia - Iran - Afghanistan - Mongolia.

No synoptic data. Excellent landmarks Saudi. Clear over Arabia as usual. Clouds in the mountains of NW Tibet. Camera 1 Pix show Cufm buildups along mountains. Snow - Good pix of Qatar Peninsula.

729M 21/1637 - 10 Direct - DCSI 7 - 3(1) 4(2) 1628Z - DCS II 3(2) - 62 Tape - 31(1) 31(2) - 1315Z - DCSI Cuba - SE of Florida - Atlantic 32N 66W

Area generally clear. Some Cufm along islands. DCS II - Atlantic Ocean. May have picked up some frontal band cloudiness PB Pix - Eastern Atlantic - Spain - Central Europe SW USSR to North of Caspian Sea and Aral Sea area. Some banded Cufm in Atlantic where it is generally clear. Increase of cloudiness SW France. Sun glint Adriatic Sea. Clouds at two levels Eastward into USSR.

730M 21/1810 - 17 Direct - DCSI 12(2) - Texas to Connecticut

Excellent and striking pix on direct readout. Generally clear over SE US vicinity of Penna. Camera picks up a striking pix of clouds around a vortex - with a well defined clear area. Excellent comparison with 1800Z Nephanalysis. PB Pix - All Pix have nadir angles greater than 60 degrees. DCS II 5(2) - Taken off the Newfoundland Coast. Extensive cloudiness in the area with some good clear areas.

731M 21/1956 - 15 Direct - DCS I II - 5(1) 6(2) - Colorado - Great Lakes area - Cufm along mountains. Vortex band of clouds - large clear area - same vortex as seen on 730M, but taken one orbit later. Good landmark on Camera 1 of Green Bay area. 45 Tape - 13(1) 32(2) - F12-32 have nadirs greater than 60°, F1-8 show clouds at two levels, lower level of Cufm - upper level Cirroform.

732K 8(2) Direct - Pix taken from minute 0-4. All pix have nadir greater than 60 degrees. No PB Pix.

732M 21/2124 - 64 Tape - 32(1) 32(2) - first 7 pix have high nadir angles - Pacific 14N 160W - across Oregon into Montana

Pacific covered with Cufm bands. All sizes real small to large. Pass goes by Southern and Western side of big anticyclone cell. Cannot tell from pix when you reach west coast of US.

732M 21/2141 - 10 Direct - 5(1) 5(2) - DCSI Dakotas - N. Great Lakes - Ontario.

Some noise and distortion. However, pix taken of same vortex vicinity Great Lakes.

733K 21/2304 - 14 Direct - 7(1) 7(2) - Central Pacific 16N 177E to 34N 164W

Pix taken along a cold front - see some frontal band of cloudiness.

733M 64 Tape - 31(1) 31(2) - Monitor reads incorrectly. There is some diagonal lines in almost all the pix, also, there appears some horizontal shrinking or vertical elongation - pix taken from Central N. Pacific - Washington - Great Lakes area

May have trouble with rectification. Pass goes through center of high in Pacific. However there is an excess amount of cloudiness. Anticyclonic Cufm - Appears that it may have picked up a frontal band which does not appear nor give any indication on Synoptic Map. Some streaky clouds around F10 C2T.

22 May 1960

734M 22/0051 - 47 Tape - 15(1) 32(2) - Pix supposedly started in center of high - However, a bright circular frontal band appears in F27-32 C2T. Incidently pix taken in Pacific 35N 173E to West Coast of US (SW section of Montana).

Generally broken to overcast stratiform - sometimes Cufm over Eastern Pacific. F1-2 C2T show an excellent pix of vortex in US. However, pix are a little dark and thin.

737K 22/1547 - 54 Tape 31(1) 23(2) - Tibet, across China, North of Japan - Ends in Pacific 47N 168E

No data to compare, area north of Japan generally broken with Cufm and Stratiform. Generally clear to scattered over China. Camera 1 Pix monitor in error - numbering goes 1-5 - repeat - could get them in proper sequence. Camera 1 pix show banded Cufm - Cufm streets. Also excellent pix of a lake.

738K 22/0728 - 58 Tape - 31(1) 27(2) - East Afghanistan to China. Ends vicinity of Kurile Islands

Cloud free over Afghanistan. Snow cover in mountains possibly Hindu Kush Mountains. See some clouds over snow cover F21-23 C2T See some hook shaped type clouds. Possible vortex vicinity 50N 137E. Very little organization and cloud distribution; Camera 1 pix show some Cufm bands. Possible Cufm streets - snow cover on mountains.

743M 22/1223 - 60 Tape - 29(1) 31(2) - Casablanca - Across Corsica - Italy - Yugoslavia - Odessa - Slightly north of Caspian and Aral Sea

Generally clear over Fr. Morocco. Good landmarks. Interesting cloud shape off Coast of Fr. Morocco. Sun Glint in Mediterranean off North African Coast near Oran. Good pix of Balearic Islands. Generally scattered to clear in Mediterranean. Clouds increase as you reach Italy. Sun glint in Adriatic Sea. Did TIROS pick up another egg-shaped top type cloud off coast of Crimea (F9-10 C2T)? Also sun-glint Black Sea. Some good landmarks on Camera 1.

743M 22/1543 - 12 Direct - 7 DCS I - 6(1) 1(2) - C2 Pix N. G. nadir too high and noisy; DCS II - 2(1) 3(2) - Mid Atlantic 35N 54W to 41N 43W

Pix taken vicinity Low in Atlantic - pix show broken to overcast cloudiness in area.

744M 22/1721 - 10 Direct - DCS II - 5(1) 5(2) - Pix start vicinity Cape Hatteras - into North Atlantic vicinity Nova Scotia

Nice pix of vortex with possible wave. However pix seem to be out of phase - top of pix appears on bottom and vice versa.

745M 22/1725 - 59 Tape - 32(1) 27(2) - South of Nova Scotia across North Atlantic to Southern France, ending vicinity Sardinia

Pix show extensive cloudiness. Pass across frontal band in Atlantic - clouds decrease as you approach France. Last few pix (F 1-4) are thin and dark.

745M 22/1902 - 16 Direct - DCS I - 6(1) 6(2) - NW Oklahoma - Great Lakes

Generally clear in Central Plains. Good pix of vortex located over Great Lakes. DCS II 4(2) - Pass East of Newfoundland. Extensive cloudiness associated with North side of Low located in Atlantic.

746M 22/2029 - 64 Tape - 32(1) 32(2) - South Pacific to Northern California

First 20 pix have high nadir angles. Possible vortex or front shows up off coast of California. Some good size Cufm SW of Calif. along Southeast side of high. These Cufm are much larger than normally seen in the Pacific. Cufm also show up good on Camera 1 pix.

746M 22/2047 - 10 Direct - 5(1) 5(2) - Dakotas - Across North of Great Lakes to Northern Maine

Generally clear to scattered over Midwest. Vortex over Great Lakes area shows up well in the pix.

747M 22/2218 - 64 Tape - 32(1) 32(2) - Central Pacific 31N 160W across Northern US, ending in Great Lakes area

Frontal band clouds in Pacific are seen. Good well defined clear area F14-19 C2T. Outside of this area - find stratiform clouds. May have picked up vortex off Coast of Washington. Along with frontal band, broken to overcast Cufm over NW US. Passes over what seems to be a dry stationary front located in Dakotas. Generally clear to scattered in this area.

23 May 1960

748M 23/0000 - 64 Tape - 32(1) 32(2) - Central Pacific 37N 177W across NW US, ending in South Dakota

Clear in high in Pacific. NE edge of high have band of clouds. May be associated with vortex north of track. Extensive clouds associated with front vicinity 155W. Same clear area that appeared in Orbit 747M is seen off coast of Washington. Pix on this orbit are taken slightly north of the previous orbit. Clear area in anticyclonic flow. As you approach coast increase of Cufm. Broken to overcast; Cufm decreases to scattered to broken over Rockies. Pass again over relatively dry stationary front located in Dakota area.

758M 32(1) Direct - Misprogrammed - No program available to determine where or when taken. 64 Tape - 32(1) 32(2) - No program available. It may have been taken around 0500Z. This would be taken from China into Pacific. No synop data available to compare.

Generally clear to scattered over land. Generally overcast over water. Checking MSS nephanalysis indicates that pix were taken on Orbit 754 around 10Z.

759M 48(1) Direct - No program available. 64 Tape - 32(1) 32(2) - No program available. In addition all pix have high nadir angles - 57 pix 25(2) 32(1) are looking into space the 48 Direct pix are good. No status report filed. Manual operation indicated in Met Summary.

760M 23/1953 - 23 Direct - DCS I 13(1) 6(2) - Wyoming - Great Lakes area - Quebec.

The cloudless stationary front that has been seen on previous orbits is now developing a wave just East of Salt Lake. Clouds associated with wave are seen. Midwest is generally clear. Clouds increase vicinity Great Lakes area towards the end of this pass - 8 consecutive pix are taken on Camera 1. The area covered should be overcast but is not so indicated on the Camera 1 pix. Lots of Cufm scattered to broken in the Quebec area.

760M 23/2004 - 4(2) DCS II - Mid Atlantic 46N 49W to 43N 40W -

Pass over rear side of vortex. Stratiform at different levels are seen - some semblance of vortex cloud pattern; 8(2) Tape - majority of pix taken have high nadir angles. Last 8 pix taken are OK. General Cufm broken SW of Calif. Picks up cloudiness associated with low off coast of Northern Calif. All pix taken with Camera 1 are looking into space.

761M 23/2125 - 64 Tape - 32(1) 32(2) - Pacific 30N 154W across Northern US and ending vicinity Great Lakes area

See frontal band cloudiness - not too extensive - in Pacific vicinity 155W then becomes more extensive in Northern part of front. Streaky stratiform clouds seen associated with northern part of high in Pacific. Few good clear areas in between. Cufm clouds appear off and on coast of Washington associated with low off the coast. Extensive and bright clouds in Idaho - Montana - Dakotas; Great Lakes area generally clear but may be pix have taken some extensive cirrus. Cannot really see it but based on intuition.

762M 23/2306 - 9(2) Direct - Pix are thin, dark and not much good; 64 Tape - 32(1) 32(2) - Central Pacific 32N 178W across Northwestern US ending SW N Dakota

Anticyclonic Cufm in Pacific vicinity 175W. Good clear area. Pass over cold front. Extensive cloudiness. Appears that there are two lines of clouds at right angles (22-24 C2T). Another area of extensive cloudiness along with frontal band located vicinity 148W. Streaky stratiform anticyclonic type over Northern section appears off the coast of Washington. This is about the 3rd or 4th orbit that this type of cloudiness appears within the past 24 hours. Cufm appear off the coast of Washington - the stationary front which had been cloudless is now almost overcast with few breaks.

24 May 1960

763M 24/0050 - 64 Tape - 32(1) 32(2) - Central Pacific 40N 174E across NW US to NW Colorado

Pacific area mostly cloudy. Clouds associated with wave are shown. A clear spot north of wave and then more cloudiness north of clear spot - frontal bands associated with cold front in Pacific are seen - behind cold front appear Cufm mottled type clouds - vortex circulation may be seen. Clouds off coast of NW US make landmarks difficult to see. Generally banded Cufm over Rockies.

772M 24/1540 - 15(2) Direct - DCSI 8(2) - High Nadir - DCS II 7(2) - Direct Program DCSI Caribbean - DCS II Atlantic Ocean 40N 55W to 45N 44W

DCS I - All pix with high nadir. DCS II - Some random cloudiness appears. No patterns. Some bright clouds indicating possible precipitation.

772M 24/0400 - 32 Tape - 32(1) 32(2) - East China - North of Japan - to Pacific Ocean 45N 170W

Generally broken to overcast with clear areas interspaced. Appears to have picked up a vortex in China around 50N 135E. Also shows the vortex that is located in Pacific. Frames 5-7 2 shades of cloudiness. Clouds at 2 levels. One stratiform, the other Cufm.

773M 8 Direct - 4(1) 4(2) - Nadir High - Difficult to say on which DCS taken - could be Texas or Maine - Only 1 pix Camera 2 of any value

774M 24/1720 - 54 Tape - 27(1) 27(2) - Albany, N. Y. - Atlantic across Spain into Mediterranean Sea

F11-32 fuzzy (seems out of focus) F 1-10 show streaky filament type clouds in all directions. Also possible clouds at two levels.

774M 24/1905 - 15 Direct - DCS I 1(2) - DCS II - 14(2) - DCSI - Neb-Minn; DCS II Quebec - Atlantic 45N 37W

DCS I - Frontal clouds seen. DCS II - Extensive cloudiness in Quebec. F6-10 shows unique cloud - could be CB. Clouds of secondary low show up.

775M 24/2029 - 43 Tape - 11(1) 32(2) - Pacific 16N 161W - Montana

F 18-32 High Nadir. Good pix of warm sector and vortex located off West Coast US. After reaching US broken to overcast. Clouds at 2 levels. Odd appearing Cufm overcast with numerous breaks.

775M 24/2046 - 10 Direct - 5(1) 5(2) - North Dakota - Lake Superior - Quebec - Nova Scotia

Edge of cloudiness associated with stationary front located in Central N. Dakota. Broken - Overcast clouds over Great Lakes - St. Lawrence.

776M 24/2218 - 33 Tape - 1(1) 32(2) - Pacific 39N 157W - Across Northern US to Great Lakes area of West NW - Penna

Pix probably taken over a washing-out vortex in Pacific. Anticyclonic appearing Cufm surrounds detached vortex (F25-30). Near West Coast find streaky filament clouds. Clouds at 2 levels. Clear area off coast. Mountain Cufm over Rockies. Noise and darkening of film toward end of roll. Pix seem to indicate less cloudiness over North Central US than what is reported on the synoptic map.

25 May 1960

777M 25/2357 - 29(1) Tape - No Camera 2 Pix - Difficult to locate Camera 1 Pix

786M 25/1440 - 11 Direct - DCSI 3(2) - High nadir; DCSII 8(2) 1446 - High nadir - 51 Tape - 28(1) 23(2) - Focus or double exposure difficulty. Getting double horizon. Camera 1 pix show some Cufm cloud streets.

787M 25/1451 - 46 Tape - 27(1) 19(2) - Starts Atlantic 43N 30W across France - Europe. Ends in Turkey.

Frame numbers in error after pix 15. Pix quality poor. No landmarks. Difficult to locate pix. See some anticyclonic Cufm over water. Possibly frontal band off coast of Ireland.

787M 25/1628 - 12 Direct - DCS I 4(2) - All 4 pix have high nadir - DCS II 8(2) - 5 with high nadir - Pix taken East of New England

Frontal band cloudiness associated with vortex located SE of Nova Scotia is seen. Pix also noisy.

788M 25/1812 - 9 Direct - DCS I 1(2) - High nadir; DCS II - 8(2) - Great Lakes across Canada to Newfoundland - 56 Tape - 32(1) 24(2)

Generally broken - overcast over Great Lakes area and US. Generally clear on Canadian Side of Great Lakes. PB Pix quality poor. Double exposure. Double horizon. Also only 3 pix with horizon. Pix taking vicinity of verticality.

789M 25/1955 - 12(2) Direct - Montana, Great Lakes, Canada

Pix show good clouds broken, overcast band associated with stationary front which is located in N. Dakota. Clear area north of Great Lakes on Canadian side.

790M No program available. However by deduction, believe that pix were taken on 789M 29.8. 60 Tape - 32(1) 28(2) - 19 Pix (F1-19) dark. Remaining pix no horizon. Quality poor. Camera 1 pix show some good Cufm - may be some streets.

791M 25/2306 - 64 Tape - 32(1) 32(2) - Pacific 41N 170W across NW US to Northern Missouri

Pix quality poor. Same double exposure pix has previously been mentioned - generally broken - overcast over Pacific. No important shapes over land. Cloudiness becomes less over US.

26 May 1960

800M 26/0400 - 7(2) Direct - Pix NG High nadir and noisy - 57 Tape - 25(1) 32(2) - China - Pacific Ocean 40N 168W

Pix quality poor, double exposure or out of focus. Interesting cloud patterns. No data area. Bright sun glint (F 15-19 C2).

801M 26/1535 - 19 Direct - DCS I 2(2) - NG Noisy - Scalloped; DCS II 17(2) - 12 high nadir - Pix taken over secondary low off Carolinas. See frontal bands - 43 Tape - 22(1) 21(2) - Atlantic 43N 32W across Europe (France - Hungary) Black Sea, Turkey.

Difficult to locate pix taking. Pass is over two frontal bands, cannot say whether first or last 5 min were omitted. There is a landmark that may be the coast of France.

802M 26/1545 - 53 Tape - 30(1) 23(2) - First 20 pix quality poor.

See band of frontal cloudiness associated with cold front off west coast of Europe. Sun glint in Mediterranean near coast. Interesting in F4-5 C2T.

802M 17 Direct - DCS I 3(2) - NG High nadir - DCS II 7(1) 7(2) - Great Lakes across Northern Maine, Newfoundland - Atlantic Ocean 48N 43W

Pix show clouds associated with weak stationary front vicinity Newfoundland. Possible secondary low cloudiness SE of Newfoundland.

803M 7 Direct - DCS I 1(2) - DCS II 6 1(1) - Pix vicinity Newfoundland show stationary front and secondary low. See 802 DCS II. Pix taken same general area on previous orbit.

803M 26/1730 - 56 Tape - 32(1) 24(2) - First 15 Pix C1 are dark or blank - C2 Pix show some with poor quality. Frontal band cloudiness off coast of Spain. Sun glint in Atlantic F13-18 C2T. Another frontal band at start of pix taking in Atlantic.

804M 26/2030 - 2(2) Direct - Little or no horizon and noisy - Taken East of New England - 25(2) Tape - 11 high nadir - nothing on Camera 1

Cufm bands along Northern Calif coast. Broken over NW US in line with stationary front. Then a clear area in Eastern Montana - Western Dakotas. Pix pick up cloudiness of low vicinity East Dakotas.

805M 26/2210 - Direct - All pix either dark or noisy - 26 Tape - 4(1) 22(2) - Majority of Camera 1 pix are dark - Camera 2 pix 11 high nadir. Picture quality is improved for the first time. Pix pass over cold front in Pacific then across occlusion off the West Coast of US. May be some difficulty in rectification due to misnumbering of pix frames.

27 May 1960

806M No useful pix - dark - noisy. No horizon.

815M 6(2) Direct - None useful. Nadir too high.

816M 13(2) Direct - Possibly one pix of any use - 12 have high nadir

817M 32(2) Tape - Across Pacific 47N 164E to 32N 121W

May have taken pix of 2 vortices and associated fronts.

818M Not programmed - spin up; 76(2) Direct - No program to determine where or when pix were taken

Excellent pix of clouds, frontal bands (wide) - Cufm bands. Just general extensive cloudiness in most frames with good clear areas separating the cloudiness. Quick deduction appears that pix were taken every 10 sec on Direct. It was possible to get 13 min of readout on direct. Comparison with 18Z 27 May 60 seems to indicate that pix were taken on Orbit 818 approx M 23. See wide band of frontal bands in Mid US.

819M Not programmed - spin up; 68(2) Direct - 12 pix NG - Either blank or noisy. Again no program available

Quick deduction appears that pix were taken on 819 approx min 28. Pix of same cloud systems which appeared on 818M. Approx same area covered on this pass. Should be excellent orbit to study relation to frontal systems. Vortices and change of cloudiness associated with aforementioned in a time and distance change between two consecutive passes.

28 May 1960

829M 28/2310 - 31(2) Tape - 8 dark - Pacific Ocean, 48N to 147W - Across US into Gulf of Mexico

Pix show vortex off coast of US. Good landmarks of Oregon. Cufm over mountains. Good pix of Great Salt Lake. Cloud regime seems to change abruptly at F13. Large and I mean large bright. Cufm patch (3 per pix - may be 240 Mi diameter) - appear in vicinity of stationary front on right side of Rockies. Last 8 pix (F 1-8) are dark.

831M No program - Only 1 pix on Direct - No horizon - Manual program - Spin up - Clock overset to clear.

832M 28/1900 - 44 Direct - 31(1) 13(2) - Across SE Canada - Atlantic, 43N 50W

Extensive cloudiness broken - overcast. Stfm associated with stationary front vicinity Great Lakes. Clearing vicinity Nova Scotia. Then overcast band south of Newfoundland associated with wave.

833M 12(2) Direct - Program read DCS I C2 PI 30S ET 3.0M - Pix seemed to have been paired off - Area covered N. Dakota - Great Lakes

Pix show clouds associated with stationary front. Have the feeling that clouds seen may have indicated a secondary low forming on front - does not show for at least 12 hours later on synoptic map - generally cloudy over Great Lakes.

834M 28/2225 - 16(2) Direct - 3 Pix with horizon present - Nebraska - Across SE US into Atlantic

See clouds of stationary front. Clear area Ohio - W Va. area. Then increasing clouds off SE Coast of US.

29 May 1960

843M 29/0135 - 55 Tape - 28(1) 27(2) - North Central Pacific 48N 171E to South East Pacific 25N 122W

Bright circular cloud mass appears vicinity of secondary low - precip in area. Frontal zone clouds appear vicinity stationary front. F20-32 Nadir high.

846M 29/1800 - 11(2) Direct - N Dakota across Canada, New Brunswick, Atlantic Ocean

Area broken, overcast. F10-12 show large amount of cloudiness associated with low centered in Atlantic Ocean SE of Nova Scotia.

848M 29/2133 - 16(2) Direct - Ill. - North Carolina - Atlantic 24N 64W

Frontal zone cloudiness in F1-4; extensive cloudiness along coast. Possibly low developing along coast - Cape Hat.

30 May 1960

858M 30/022430 - 52 Tape - 20(1) 32(2) - NW Pacific 48N 166E - S. Pacific 20N 135W

Extensive cloudiness associated with vortex to SW of pass or East of Japan is seen. An excellent example of vortex vicinity 45N 73W is seen. Extensive cloudiness associated with frontal system appears south of vortex. This orbit is a good one to study frontal systems and/or vortices in the Pacific.

861M 30/1858 - 16(2) DCSI - Quebec, Maine, Atlantic 35N 45W

Large mass cloudiness broken - overcast associated with stationary front in Canada. Sharp clear area vicinity Maine, Nova Scotia, then dense overcast with circular banded Cufm. Bands stop abruptly at clear area.

862M 30/2041 - 16(2) DCSI - Mich., Maryland, Atlantic 25N 58W

Occlusion depicted. F5-6 shows 2 shades of cloudiness - one very bright - other dull gray. Fog bank or status off shore. Cape Hatteras, Cape May - broken, overcast SW of orbit. North and SE of orbit scattered thin patchy Cufm.

863M 30/2221 - 6(2) DCSI - Mid Central US, Colorado, Oklahoma, Louisiana, Gulf of Mexico, Cuba

Broken Cufm along mountains - clouds at two levels orient perpendicular to each other - another sharp clear area. Camera stopped pix taking after 3rd minute.

31 May 1960

872M 60 Tape - 29(1) 31(2) - Program not available - but check with MSS Nephanalysis shows that it was taken on Orbit 866 1925Z - East USSR, North of Japan - Pacific

Most cloudiness ever seen on any Orbit - completely overcast in many frames. Few clear areas. Some wispy cloud formations. Generally clear to scattered over Pacific. Starts off with a nice vortex.

874M No pix

875M Direct - 1 pix

876M No film

1 June 1960

886M No film

890M No film

891M No film

901M 1/2351 - 55 Tape - 24(1) 31(2) - Pacific 47N 161W to 15N 110W

See extent of clouds of vortex west of pass. Frontal clouds under Pass. Extensive clear area with a small cloud in the middle associated with high. Increase of cloudiness as you approach lower California. Clouds appear at two levels - Stratiform - Cufm; Cufm off coast.

2 June 1960

904M 2/1622 - 57 Tape - 26(1) 31(2) - Newfoundland, Across Atlantic, West Coast Africa vicinity Canary Islands

Pix probably started about 8 min late, shows frontal band cloudiness located 40N 30W. Banded Cufm along African coast. Patchy Cufm over Africa. Last 6 frames dark.

904M 2/1802 - 16(2) Direct - 4 Noisy - Maine - Atlantic 33N 45W

Shows vortex. Frontal clouds located in Canada. Clear over SE New England. Stratiform overcast to north of pass vicinity Nova Scotia - Newfoundland.

905M 2/1945 - 16(2) Direct - Chicago across Mid Atlantic States - Atlantic Ocean 25N 60W

Frontal clouds seen - broken Cufm off coast.

3 June 1960

916M 3/3830 - 51 Tape - 19(1) 32(1) - Pacific Ocean 46N 178W to 14N 126W

Generally overcast with few breaks through Low - occlusion. Extensive cloudiness in southern part of High. Banded Cufm starts around 30N. Secondary Low cloudiness vicinity 25N may have been picked up by TIROS.

919M 3/1710 - 55 Tape - 24(1) 31(2) - Northern Maine to East Coast of Africa 22N 50W

Curved dense banded cloudiness associated with low located in Canada. Appears to pick up frontal cloudiness vicinity 40W. As you get into High, get patchy Cufm - some bands - cloud regime remains like this to Africa.

919M 3/1854 - 16(2) Direct - SE Penna - Atlantic 22N 50W

Edge of frontal cloudiness seen vicinity of Great Lakes area. Broken to overcast Cufm off coast of US about 30 to 35N. North of Orbit pass generally clear.

920M 3/2036 - 16(2) Direct - SE US (Mississippi) across Florida, Haiti, Caribbean Sea

Generally overcast, broken vicinity of secondary low. Few Cufm bright patches vicinity Florida.

4 June 1960

929M 4/2212 - 59 Tape - 27(1) 32(2) - first 7 pix Fuzzy - Starts off coast of Northern California - Central Mexico

Unusual clouds off coast of Calif. Coastal stratus along Calif. Big clear area separates coastal stratus from frontal cloudiness. Overcast Cufm off Lower Calif. Patches of overcast Cufm over Mexico.

932M 4/1445 - 61 Tape - 29(1) 32(2) - Frame numbering may be in error - SW of Spain - across Central Africa

Broken to overcast Cufm over ocean. No apparent organization. Generally clear over NW Africa. Very bright Cufm activity (possibly Cb) in interior Africa vicinity 10N.

933M 4/1755 - 16(2) Direct - North Dakota across Great Lakes - New England Atlantic 25N 46W

High nadir angles and double exposures leave much to be desired. Possible frontal band cloudiness.

934M 4/1959 - Direct - DCSI - 3(1) - DCSII 16(2) - then 12(2)? S. Dakota, Georgia, Atlantic, 25N 71W

It appears that what was seen in Orbit 933M was really seen in PB Pix on Orbit 934M. No program available. This accounts for DCS II 16(2) - should read PB Pix 16(2). Assume 16(2) is PB Pix. Have interesting cloud streamers or protuberance. Direct 12(2) shows up a lot of bright Cu or Cb activity in broken or overcast patches. This does not show up on synop map.

5 June 1960

944M No pix

945M 27(2) Tape - Crete, Egypt, Red Sea, West Coast Saudi Arabia, Gulf of Aden

Jet stream Ci 25N. Few Cu along mountains on East Coast Africa and West Coast Arabia. Generally clear to scattered to Gulf of Aden. Cloudiness increases into Indian Ocean - possible ITCZ clouds depicted in Indian Ocean.

948M Direct DCSII 14(2) - 2 pix destroyed due to examiner - 43 Tape - 13(1) 30(2) - 2 pix destroyed - Mid Atlantic States to West Central Atlantic, 20N 62W; PB Pix - Azores to Nigeria

DCSII - Large mass bright cloudiness suggests that low is present vicinity 30N 67W - PB Pix: Cloudiness in Frames 25-30 seems to indicate possible wave along line of orbit. F16-21 possible jet stream Ci. West Coast Africa generally clear. Clouds appear central French West Africa and increase inland.

949M 15(2) DCS I - Texas, Gulf of Mexico, Caribbean

Pix show advance of cold front in Texas. Scattered clouds associated with high in Gulf. Scattered Cu buildups along Yucatan and Cuba Coasts. Increase of cloudiness in Caribbean.

6 June 1960

958M No pix

959M 6/1123 - 46 Tape - 16(1) 30(2) - Turkey, Cyprus, Mid Saudi Arabia

Donut shaped cloud 959-(28)-2; jet stream Ci 959-(18-22)-2 - Cu buildups along mountains. Clouds (1-4) indicate vortex in Indian Ocean.

962 6/1612 - 64 Tape - 32(1) 32(2) - Ontario, Maine Atlantic 20N 25W

Correlating pix with synop map would indicate that PB Pix started 8-10 min later than what was deduced from Program interpretation. Start of Orbit shows a lot of cloudiness which is associated with cold front in Nova Scotia. Last 13 pix (F 1-13) are dark.

962 6/1758 - 14(2) DCS II - Mid Atlantic States (Penn) - Atlantic Ocean 25N 55W

Pix show broken cloudiness in weak cold front along coast. Large mass bright cloudiness in Atlantic suggests that low is present. Not shown on synop map. Should be same cloud mass that showed on Orbit 948M - at least its in same approximate location, 30N 62W.

963M 6/1937 - 22(2) DCSI - Kansas, Nebraska, Florida, Cuba

Extensive cloudiness behind and up to cold front. Bright banded Cufm clouds vicinity Florida. Precip and tstms in area.

7 June 1960

972M No pix

974M 7/1033 - 64 Tape - 32(1) 32(2) - Iran, Persian Gulf, Arabian Sea

Extensive cloudiness Indian Ocean. Possible ITC - F(7-9) cloud streamers out of main cloud. Banded Cufm at right angle in same pix. Banded Cufm off Southern Coast Arabia. Cufm buildups over mountains SE coast Arabia. Clear Over Arabia.

976M 7/1351 - 64 Tape - 32(1) 32(2) - French Morocco, Central Africa

Mottley Cufm clouds over Atlantic Ocean (F28-32); banded Cufm along mountains vicinity Marrakech Resort Area; clear through F20; some clouds associated with low appear. Some bright Cufm vicinity Lake Shad. South Lake Shad increase in Cufm activity with 6 or more Cbs or large Cufm clouds randomly spaced (F10). Cloudiness increases as you go southward.

977M 24 Direct - 16(2) DCSI - 8(2) DCSII - DCSI - Rapid City, S. D. to S Atlantic 28N 75W; DCSII continuation of Orbit 977 - ends vicinity Puerto Rico

Extensive cloudiness in majority of pix.

8 June 1960

987M No pix

988M 8/1124 - 64 Tape - 32(1) 32(2) - Red Sea (25N) - West Coast Saudi Arabia, Gulf of Aden, Indian Ocean

Extensive cloudiness in Indian Ocean south of 5N. Heavy Cufm along mountains East Coast Africa. Cufm activity East Coast Africa away from mountains. Generally clear North 18N. Check time of pix, may be off by 2 minutes.

991M 8/1622 - 45 Tape - 27(1) 18(2) - Central Atlantic 25N 40W to S of equator

Most pix taken in Southern Hemisphere. Pix show extensive cloudiness. Possible vortex S. Hemisphere. Also possible ITC. Pix taken to 20S.

991M 8/1756 - 19 Direct - 3(2) DCSI - Hi Nadir, Pix NG; 16(2) DCSII - DCSI - S. Dakota, Iowa; DCSII - North Carolina, South Atlantic, 17N 57W

DCSII - Extensive cloudiness. First 8-9 pix Nadir Hi.

992M 16(2) DCSI - North Central Texas, Caribbean

Clouds to right of pass. First few pix high nadir - noisy. Cufm over islands and Yucatan. Extensive cloudiness over land vicinity Yucatan.

994K 8/2251 - 6(2) DCSI - Central Pacific 39N 160W to 32N 150W

Nadir angles high.

9 June 1960

995K 9/0037 - 16 Direct - DCSII - Central Pacific 25N 165W to 10S; 22(1) Tape - Indian Ocean, Northern India, Punjab, Mongolia

Typical oceanic cloudiness. Possible ITC. No landmarks. PB Pix - All pix from Camera 1. Some pix show cloud streets - some banded forms.

1003M No pix

1004M 9/1350 - 64 Tape - 32(1) 32(2) - Interior Africa

Pix show clouds over Atlantic. Clear over coastal Africa. Possible jet stream Ci - F24-27 increasing cloudiness inland. Interesting cloud mass vicinity F10-13. Sharp cloud features.

1006M 9/1709 - 64 Tape - 32(1) 32(2) - Central Atlantic 25N 57W to 20S.

Generally clear to scattered over ocean to about 5N. Extensive cloudiness possible vortex. Clouds at two levels appear 15S - F2-6.

1006M 9/1847 - 8(2) Direct - Gulf of Mexico, Cuba, Caribbean

Horse-shoe shaped cloud appears in Gulf of Mexico. Extensive cloudiness in Caribbean off Central America is in line with low center that appears on map.

1009K No pix

1010K 8(2) Direct - No program

10 June 1960

1017M No pix

1019M 10/1300 - 64 Tape - 32(1) 32(2) - Central Africa 22N 4E - Madagascar

Possible jet stream Ci F26-31. Clear to scattered, clouds appear 10-15N. Possible ITC. Wide circle quasi-banded F12. Interesting cloud patterns F1-10.

1020M 10/1617 - 51 Tape - 32(1) 19(2) - Central Atlantic 25N 50W to 20S 5W

Extensive cloudiness vicinity equator. Possible ITC.

1020M 10/1749 or 1753 - 14 Direct - 2(2) DCSI - High Nadir; 12(2) DCSII - SE US - Bahama Islands

Nadir too high on 9 pix on Direct for any use. 3 pix useful. F10 interesting cloud feature. Extensive cloudiness F12.

REFERENCES

Air Weather Service Manual 105-34, RECCO CODE, Air Weather Service, Washington, D. C. (1 August 1953)

Allied Research Associates, Inc., ARA-739, 1959: "Operational Plan for Project TIROS - Immediate Operational Use--Data Abstraction and Analysis System", Special Report, Contract No. AF 19(604)-5581, 30 November 1959

Conover, J. H., 1959: "Cloud Patterns and Related Air Motions Derived by Photography", Final Report, Contract No. AF 19(604)-1589, Harvard University, June 1959

Conover, J. H. and Sadler, J. C., 1960: "Cloud Patterns as Seen from Altitude of 250-850 Miles--Preliminary Results", Bull. of A.M.S., Vol 41, June 60

Cooper, G., 1960: "Meteorological Satellite System Analyses", reprinted in "Contributions to Satellite Meteorology", GRD Research Notes No. 36, W. K. Widger, Jr., Editor. AFCRC-TN-60-427, Air Force Cambridge Research Center (June 1960)

Cox, C. and Munk, W., 1954: "Measurement of the Roughness of the Sea Surface from Photographs of the Sun's Glitter", J. of the Optical Soc. of America, Vol. 44, November 1954

Fujita, T., Newstein, H. and Tepper, M., 1956: "Mesoanalysis; An Important Scale in the Analysis of Weather Data", USWB Res. Pap. No. 39

Glaser, A. H., 1957: "Meteorological Utilization of Images of the Earth's Surface Transmitted from a Satellite Vehicle", Contract No. AF 19(604)-1589, Phase II, Harvard University, October 1957

Glaser, A. H., 1960: "A System for the Meteorological Operational Use of Satellite Television Observations", reprinted in "Contributions to Satellite Meteorology", GRD Research Notes No. 36, W. K. Widger, Jr., Editor, AFCRC-TN-427, Air Force Cambridge Research Center (June 1960)

Holl, M. M., 1960: "The Utilization of Satellite Observations in the Theory and Practice of Numerical Weather Prediction", Stanford Research Institute, Project 2994, Tech. Prog. Report 1, Contract No. AF 19(604)-5965

Howard, J. N., Burch, D. L. and Williams, D., 1955: "Near Infrared Transmission through Synthetic Atmospheres", GRD Paper No. 40, pp. 244

Kaplan, L. D., 1959: "Inference of Atmospheric Structure from Remote Radiation Measurements", J. Opt. Soc., 49, 1004-1007

King Hele, Desmond, 1960: "Satellites and Scientific Research", Routledge and Kegan Paul, London or Dover, New York, 180 pp.

London, J., 1960: "Satellite Observations of Infrared Radiation", Reprinted in "Contributions to Satellite Meteorology", GRD Research Notes No. 36, W. K. Widger, Jr., Editor, AFCRC-TN-60-427, Air Force Cambridge Research Center (June 1960)

McLachlan, D., Jr. and Chamberlain, L., 1959: "SRI Memorandum on Photomosaics" (10 September 1959)

Moulton, F. R., 1914: "Celestial Mechanics", The MacMillan Company, New York.

Strong, J., 1959: "Balloon Observations of Earth Radiations in the Infrared III", Contract No. AF 19(604)-2238, John Hopkins University, pp. 26

Wexler, R., 1960: "Satellite Observations of Infrared Radiation", reprinted in "Contributions to Satellite Meteorology", GRD Research Notes No. 36, W. K. Widger, Jr., Editor, AFCRC-TN-60-427, Air Force Cambridge Research Center (June 1960)

Widger, W. K., Jr., 1959: "Summary of Briefing Given to the Committee on Meteorological Satellites, Chairmanned by Mr. W. Becker", AFDRQ, The Pentagon (19 March 1959)

Yamamoto, G. and Onishi, G., 1949: "Absorption Coefficients of Water Vapor in the Infrared Region", Sci. Rep., Tohoku Univ., Ser. 5, I, 5-15

GRD RESEARCH NOTES

No. 1. Contributions to Stratospheric Meteorology, *edited by George Ohring, Aug 1958.*

No. 2. A Bibliography of the Electrically Exploded Wire Phenomenon, *W. G. Chace, Nov 1958.*

No. 3. Venting of Hot Gases Through Temperature Inversions, *M. A. Estoque, Dec 1958.*

No. 4. Some Characteristics of Turbulence at High Altitudes, *M. A. Estoque, Dec 1958.*

No. 5. The Temperature of an Object Above the Earth's Atmosphere, *Marden H. Seavey, Mar 1959.*

No. 6. The Rotor Flow in the Lee of Mountains, *Joachim Kuettner, Jan 1959.*

No. 7. The Effect of Sampler Spacing on Basic Analyses of Concentration Data, *Duane A. Haugen, Jan 1959.*

No. 8. Natural Aerosols and Nuclear Debris Studies, Progress Report I, *P. J. Drevinsky, C. E. Junge, I. H. Blifford, Jr., M. I. Kalkstein and E. A. Martell, Sep 1958.*

No. 9. Observations on Nickel-Bearing Cosmic Dust Collected in the Stratosphere, *Herman Yagoda, Mar 1959.*

No. 10. Radioactive Aggregates in the Stratosphere, *Herman Yagoda, Mar 1959.*

No. 11. Comments on the Ephemerides and Constants for a Total Eclipse of the Sun, *R. C. Cameron and E. R. Dyer, May 1959.*

No. 12. Numerical Experiments in Forecasting Air and Soil Temperature Profiles, *D. W. Stevens, Jun 1959.*

No. 13. Some Notes on the Correlation Coefficient, *S.M. Silverman, May 1959.*

No. 14. Proceedings of Military Geodesy Seminar, December 1958, Air Force Cambridge Research Center *(U), edited by O. W. Williams, Apr 1959. (SECRET Report)*

No. 15. Proceedings of the First Annual Arctic Planning Session, November 1958, *edited by Joseph H. Hartshorn, Apr 1959.*

No. 16. Processes for the Production and Removal of Electrons and Negative Ions in Gases, *S.M. Silverman, Jun 1959.*

No. 17. The Approximate Analysis of Zero Lift Trajectories, *Charles Hoult, Aug 1959.*

No. 18. Infrared Measuring Program 1958 (IRMP 58) – Activities, Achievements, and Appraisal *(U), M.R. Nagel, Jul 1959. (SECRET Report)*

No. 19. Artificial Radioactivity from Nuclear Tests up to November 1958, *E. A. Martell, Sep 1959*

No. 20. A Preliminary Report on a Boundary Layer Numerical Experiment, *M.A. Estoque, Oct 1959.*

No. 21. Recent Advances in Contrail Suppression, *(U), S. J. Birstein, Nov 1959. (CONFIDENTIAL Report)*

No. 22. A Note Comparing One Kilometer Vertical Wind Shears Derived from Simultaneous AN/GMD-1A and AN/GMD-2 Winds Aloft Observations, *H. A. Salmela and N. Sissenwine, Oct 1959.*

No. 23. Atmospheric Refraction of Infrared Radiation, *T. P. Condron, Oct 1959.*

No. 24. Natural Aerosols and Nuclear Debris Studies, Progress Report II, *M. I. Kalkstein, P. J. Drevinsky, E. A. Martell, C. W. Chagnon, J. E. Manson, and C. E. Junge, Nov 1959.*

No. 25. Observations of Jupiter Missile Re-Entry, *(U), R. G. Walker, R. E. Ellis and R. E. Hunter, Dec 1959. (SECRET Report)*

No. 26. Space Probes and Persistence of Strong Tropopause Level Winds, *H. Salmela and N. Sissenwine, Dec 1959.*

No. 27. A Relativistic Treatment of Strong Shock Waves in a Classical Gas, *A. W. Guess, Dec 1959.*

No. 28. Measurements of Flux of Small Extraterrestrial Particles, *H. A. Cohen, Jan 1960.*

No. 29. Proceedings of the Second Annual Arctic Planning Session, October 1959, *edited by Vivian C. Bushnell, Dec 1959.*

No. 30. Atmospheric Pressure Pulse Measurements, *(U), Elisabeth F. Iliff, Jan 1960. (SECRET Report -- Formerly Restricted Data)*

GRD RESEARCH NOTES (Continued)

No. 31. A Discussion of the Calder Equation for Diffusion from a Continuous Point Source, *W. P. Elliott, May 1960.*

No. 32. Lagrangian and Eulerian Relationships in the Absence of Both Homogeneity and Time Steadiness, *M. L. Barad and D. A. Haugen, May 1960.*

No. 33. Thermal Radiation from Rocket Exhausts at Extreme Altitudes, *(U) R. G. Walker, R. E. Hunter, and J. T. Neu, Jun 1960. (SECRET Report)*

No. 34. Thermal Radiation Measurement from an Aerobee Hi Research Rocket *(U), R. G. Walker, and R. E. Hunter, (SECRET Report) (to be published)*

No. 35. Additional Note -- Strong Vertical Wind Profiles and Upper-Level Maximum Wind Speeds Over Vandenberg Air Force Base, *H. A. Salmela and N. Sissenwine, May 1960.*